ON THE ENERGETICS OF PRIMARY AND SECONDARY INSTABILITIES IN PLANE POISEUILLE FLOW

by

Joseph W. Croswell

Thesis submitted to the Graduate Faculty of the
Virginia Polytechnic Institute and State University
in partial fulfillment of the requirements for the degree of

MASTER OF SCIENCE
in
Engineering Mechanics

Approved:

Dr. T. Herbert, Chairman

Dr. C. Thompson

Dr. D. T. Mook

July 1985
Blacksburg, Virginia

ON THE ENERGETICS OF

PRIMARY AND SECONDARY INSTABILITIES

IN PLANE POISEUILLE FLOW

by

Joseph W. Croswell

Committee Chairman: Thorwald Herbert

Engineering Science & Mechanics

(ABSTRACT)

The phenomenon of transition in a laminar flow has been a topic of continued interest for many years. Recent experiments in shear flows have revealed a series of instabilities that lead to breakdown to turbulence. We have completed an analysis of the mechanisms which drive the primary (TS wave) and secondary instabilities in plane Poiseuille flow. This was accomplished by studying the solutions of linear primary and secondary stability theory with energy methods. We found that primary instability occurred when the viscous stresses overpowered dissipative forces near the channel walls. For the secondary instability, we saw that the TS wave catalyzes the instability and then mediates the transfer of large amounts of energy from the mean flow into the three-dimensional disturbance, thus driving the instability. In addition, we have compiled an extensive catalog of the local energy and vorticity field distributions which result from each instability.

Acknowledgements

The author offers his deepest appreciation and thanks to for inspiring and guiding this work, and for the opportunity to contribute to his research in this very stimulating field. Thanks are also due to and for serving as committee members. also provided invaluable assistance in the use of computing resources. In addition, contributed her expertise in aiding the preparation of this document.

Many thanks go to fellow students and for their helpful discussions and viewpoints. Special thanks go to for her contributions in preparing this document and also for her considerable patience and support over the months.

This work was supported by the Office of Naval Research under Contract N00014-84-K-0093, and by the Air Force office of Scientific Research under Contract F49620-K-0002.

Table of Contents

1. Introduction

1.1. General

It has been said the more that is learned about the physics of the world, the less that is actually known. Accordingly, the study of fluid motion has led to many important and useful developments, flight being among the most notable. However, the nature of many phenomena in fluid flow remains unknown. Transition to turbulence in a laminar flow is one such phenomenon.

The goal of basic research in fluid dynamics has been to quantify the transition process and thereby understand, and ultimately control, the mechanisms involved. Transition is characterized by a marked and lasting increase in wall shear stress and measured drag. However, a cascade of events leading to breakdown into turbulence has been revealed in carefully controlled experiments. Typically, the mean flow becomes unstable to small disturbances which grow out of the low background-noise environment as periodic, two-dimensional waves. The theory of primary instability successfully models this process, but these two-dimensional waves suffer a secondary instability of a three-dimensional nature which, after several cycles, leads to a periodic pattern of large scale Λ-shaped structures that indicate either fundamental or subharmonic resonance with the two-dimensional wave, depending on their arrangement. Fully turbulent flow quickly develops thereafter.

At present, a theory of secondary instability, as developed by Herbert (1981,1983d) and Orszag & Patera (1980a,1981), best models transition observed in experimental flows by admission of subharmonic and fundamental modes of motion. In addition, peak-valley splitting and streamwise vortex formation, characteristic of the breakdown to turbulence, are duplicated. However, the prediction of transition is not yet possible since an

understanding of the instability mechanisms involved remains incomplete.

This theory is not without its limitations. It seems that tertiary instabilities and non-linear effects begin to dominate at some point between the onset of secondary instability and complete breakdown to turbulence. Perhaps other mechanisms presently unknown also take over. In any event, the theory of secondary instability provides a definite first step toward a better understanding of the transition process.

1.2. Review of Research

From the start, research in hydrodynamic stability has been focused on clarifying the physical mechanisms that are key elements in the transition from laminar to turbulent flows. The physics of some flows, namely Bénard convection (Busse 1981) and rotational Taylor flow (DiPrima & Swinney 1981) seem, to some extent, well understood. Shear flows received only sporadic treatment until computing resources developed, which allowed theoretical investigations reflecting the complexity of these flows to occur. However, these preliminary studies, in conjunction with low-noise experiments, did manage to characterize basic qualities of the transition process, crucial to later work.

Hydrodynamic stability analysis began with the investigations of Osborne Reynolds and Lord Rayleigh in the late nineteenth century. Reynolds' experiments (Drazin & Reid 1981) led him to believe transition occurred due to the growth of small velocity fluctuations in the flow field. These ideas were quantified by Rayleigh in various theoretical treatments on the stability of jets (1878), shear layers (1880) and rotational flows (1916). Further theoretical advances occurred in 1906/07 when Orr and Sommerfeld independently developed an equation which described the stability of the shear layer including the effects of viscosity.

Solutions of the Orr-Sommerfeld equation for realistic velocity profiles were not found until the successful asymptotic analyses of Heisenberg (1924) for Poiseuille flow, and Tollmien (1929) and Schlichting (1932) for Blasius flow. They found the wavelength of the disturbances, rather than their amplitude, was the critical stability parameter. Consequently, waves in a specific band of frequencies could produce laminar oscillations of the fluid, reinforcing the idea of a critical Reynolds number Re_c. Also, energy considerations revealed viscosity to be driving the instability. The pioneering experiments of Schubauer & Skramstad (1947) substantiated the new linear stability theory and documented the growth of artificially introduced two-dimensional waves, now known as TS waves in honor of Tollmien, Schlichting, Schubauer and Skramstad.

Squire (1933) found a transformation whereby the linear stability problem for three-dimensional disturbances was equivalent to a two-dimensional formulation at a lower Reynolds number. His findings had the unfortunate consequence of virtually halting further investigation of the three-dimensional aspects of the problem, not to be taken up again for about fifty years, since most researchers felt that Squire's result greatly simplified stability analysis.

Experiments in plane Poiseuille flow by Davies & White (1928) and Kao & Park (1970) produced transition at Reynolds numbers of 1000, far below the critical value of 6000 predicted by linear stability. However, Nishioka, Iida & Ichikawa (1975) were able to obtain laminar flow up to Reynolds numbers of 8000 by reducing the background-noise level to 0.05%. This discrepancy can be partially explained by considering the lack of two-dimensionality of the mean flows in the experiments, in addition to high background turbulence levels. As regards the theory, Meksyn & Stuart (1951), Stuart (1960) and Reynolds

& Potter (1967) used perturbation methods to reveal the existence of periodic finite amplitude equilibria at both subcritical and supercritical Reynolds numbers where instability in the subcritical region was indicated for TS amplitudes above a certain threshold value. By numerically solving non-linear disturbance equations, Herbert (1977) calculated subcritical equilibria for Reynolds numbers as low as 2900. Such work led to the conclusion that non-linear distortion of the mean flow and modification of the Reynolds stress was driving the experimentally observed instability.

In the boundary layer, Klebanoff, Tidstrom & Sargent (1962) had measured the growth of TS waves and found that at large amplitudes, the flow was highly three-dimensional. The K-breakdown (for Klebanoff) is characterized by weak TS growth followed by peak-valley splitting leading to the formation of both spanwise periodic Λ-shaped three-dimensional structures and streamwise, counter-rotating vorticies as the TS amplitude exceeds a threshold value of about 1%. Peak-valley splitting refers to regions of enhanced and reduced wave amplitude where the Λ vorticies are aligned with the peaks and repeat with λ_x, the TS wavelength.

Initially, it was thought that the high frequency disturbances measured by Klebanoff, et al. were the direct result of an instability of the TS wave. Early models formulated by Benney & Lin (1960) and Craik (1971) based on the weakly non-linear interaction of resonant wave triads proved to be inadequate to fully explain experimental observations. Further investigations (Herbert & Morkovin 1980) suggested that the primary instability instead led to strong, rapid growth of spanwise periodic three-dimensional disturbances, arising due to resonance with the TS wave. Numerical experiments by Orszag & Patera (1980b) revealed strong exponential growth of an infinitesimal disturbance, indicating a

linear secondary instability associated with the TS wave.

As a result of these findings, Herbert (1981,1983d) and Orszag & Patera (1980,1981) developed a theory of secondary stability based on the Floquet theory for ordinary differential equations with periodic coefficients (Coddington & Levinson 1955, Nayfeh & Mook 1979). Formally, an oscillatory basic flow is selected consisting of a non-linear, two-dimensional equilibrium state that satisfies the Navier-Stokes equations. This basic state is then perturbed with small three-dimensional disturbances whose form is derived from the normal-mode concept and the Floquet theory.

From here, Orszag & Patera (1983) numerically studied the evolution of the instability with time at high TS wave amplitudes in order to evaluate the relative time scales of the two- and three-dimensional growth rates. They found vortex stretching and tilting due to the convective growth of the three-dimensional disturbances to be driving the instability.

Herbert (1983a,1983b) simplified the basic flow by assuming its shape to be proportional to the linear theory solution (Stuart 1958) and studied the resulting classes of solutions obtained from the eigenvalue problem for the growth rate and the phase speed of the three-dimensional disturbances. He obtained a fundamental solution, as measured by Klebanoff and Nishioka, in both plane Poiseuille flow where symmetric and anti-symmetric modes are possible, and in Blasius flow where only one mode exists. Most importantly, Herbert (1983c) found secondary stability theory duplicated both peak-valley splitting and longitudinal vortex structures, key elements of the K-breakdown. In addition, a subharmonic solution was also found at lower TS amplitudes than for the fundamental, suggesting dominance of this mode at low Reynolds numbers. The subharmonic mode is characterized by a staggered alignment of Λ-shaped structures repeating with $2\lambda_z$ and has no associated

longitudinal vortex system, which is consistent with the experiments of Saric & Thomas (1981) and Kachanov & Levchenko (1982). Thus, the secondary stability theory provides a viable model for the three-dimensional instability observed in experiments. In addition, the model also predicted the subharmonic class of solutions, which were heretofore undetected.

An analysis of various shear flows based on the numerical simulation of the Navier-Stokes equations at large TS amplitudes by Orszag & Patera (1983) displayed the universality of the secondary instability. In addition, it was shown the TS wave mediates energy transfer from the basic flow to the three-dimensional disturbance for the fundamental mode. However, it remains to study the fundamental and subharmonic modes at low amplitudes to extend the present theory.

1.3. Motivation

Historically, plane Poiseuille flow formed the heart of hydrodynamic research centered among the boundary layer, plane Couette, pipe and convection problems. This means that any insight gained into the instability mechanisms present in plane Poiseuille flow will have profound effect upon these other areas. This flow was selected as a prototype basic flow for this analysis because of its attractive mathematical properties. The viscous solution is of closed form and the existence of symmetry reduces computing requirements. Also, reliable experimental data exist for comparison, but only in the subcritical region of the neutral surface. These data are similar to measurements for the boundary layer, thereby allowing present results to be easily extended qualitatively.

Orszag & Patera (1983) and Herbert (1983b) have demonstrated the explosive nature of the secondary instability caused by resonant interaction between the TS wave and the three-dimensional disturbance. Herbert revealed that resonance could manifest itself in

either of two forms, depending on the amplitude of the TS wave. At low amplitudes, parametric excitation of the subharmonic disturbance was responsible for rapid growth, while at larger amplitudes, primary resonance occurred leading to the commonly observed K-breakdown.

This synchronization between the TS wave and the disturbance leads to optimal conditions for the direct transfer of energy from the basic flow to the disturbance, with the TS wave acting as a catalyst or mediator. Tracing the transfer of energy among the basic flow, the TS wave and the three-dimensional disturbances should reveal the interaction of the two-dimensional wave with the subharmonic and fundamental modes of the instability. Correlation of the energetics of the flow with vorticity calculations may aid in developing simpler models for theoretically predicting transition in shear flows than presently exist.

As an introduction, Chapter 2 contains a linear stability analysis of plane Poiseuille flow subject to infinitesimal two-dimensional disturbances, followed by a study of the energetics of the instability mechanism present. Results are presented for stable, neutral and unstable cases. Chapter 3 extends this analysis to the three-dimensional problem using present techniques in secondary instability theory. A summary of the stability analysis as it currently exists is followed by an energy analysis of the solutions obtained. Results are presented for both fundamental and subharmonic solutions. In Chapter 4, the results of the analysis of the primary and secondary instabilities are discussed and some conclusions are drawn concerning their nature.

2. Energy Analysis of Primary Instability

2.1. Problem Statement

We consider the steady flow of an incompressible fluid between infinite parallel plates driven by a constant pressure gradient in the streamwise direction x'. The y-direction lies normal to the channel wall plates, z normal to the $x'-y$ plane and t represents time. All quantities are non-dimensional with respect to the half-channel width h and the maximum centerline velocity U_0, as shown in figure 1.

The non-dimensional field equations governing fluid motion in this instance are

$$\nabla \cdot \mathbf{v} = 0$$
$$\frac{\partial \mathbf{v}}{\partial t} + (\mathbf{v}\cdot\nabla)\mathbf{v} = -\nabla p + \frac{1}{Re}\nabla^2 \mathbf{v} \qquad (2.1a)$$
$$\mathbf{v} = 0 \quad at \quad y = \pm 1$$

where

$$\mathbf{v} = (u,v), \quad Re = \frac{hU_0}{\nu} \quad . \qquad (2.1b)$$

Introducing vorticity ω, we have

$$\omega = \nabla \times \mathbf{v} \quad . \qquad (2.2)$$

The viscous solution for plane Poiseuille flow satisfies (2.1) for all Re and serves as the basic flow to be studied with

$$\mathbf{v}_0 = U(y)\mathbf{i} = (1-y^2)\mathbf{i} \qquad (2.3)$$
$$p_0 = -\frac{2}{Re}x \quad .$$

We introduce a small perturbation of the basic flow such that

$$\mathbf{v} = \mathbf{v}_0 + A\hat{\mathbf{v}}_1 \qquad (2.4)$$
$$p = p_0 + Ap_1$$

with A a very small parameter. We assume $\mathbf{v}_1$ and p_1 are periodic in x' with wavelength λ_x and steady in a Galilean frame moving with phase speed c in the x'-direction :

$$\begin{aligned} \mathbf{v}_1(x',y,t) &= \mathbf{v}_1(x,y), \qquad x = x' - ct \\ \mathbf{v}_1(x,y) &= \mathbf{v}_1(x+\lambda_x,y), \qquad \lambda_x = 2\pi/\alpha \end{aligned} \qquad (2.5)$$

$$p_1(x,y) = p_1(x+\lambda_x,y)$$

where α is the wavenumber. We now proceed to determine the stability characteristics of the flow. We then follow this with an energy analysis of the results to shed some light on the instability mechanism.

2.1.1. Stability of the Basic Flow $\mathbf{v}_0$

Following the procedure of classical linear stability theory (Drazin & Reid 1981), we substitute the perturbed basic flow (2.4) into the governing equations (2.1) to arrive at a linearized disturbance equation

$$\frac{\partial\hat{\mathbf{v}}_1}{\partial t} + (\mathbf{v}_0\cdot\nabla)\hat{\mathbf{v}}_1 + (\hat{\mathbf{v}}_1\cdot\nabla)\mathbf{v}_0 = -\nabla\hat{p}_1 + \frac{1}{\mathrm{Re}}\nabla^2\hat{\mathbf{v}}_1 \qquad (2.6)$$

where terms of order A^2 have been ignored. We allow $\mathbf{v}_1$ and p_1 in (2.4) to be complex in general, denoted by hat ($\hat{}$). We express the velocity $\hat{\mathbf{v}}_1 = (\hat{u}_1,\hat{v}_1,0)$ in terms of a complex streamfunction $\hat{\psi}(y)$ such that

$$\hat{u}_1 = \frac{\partial\hat{\psi}_1}{\partial y}, \quad \hat{v}_1 = -\frac{\partial\hat{\psi}_1}{\partial x} \quad . \qquad (2.7)$$

Substituting (2.7) into (2.6) leads to two equations in $\hat{\psi}_1$ given by

$$\frac{\partial}{\partial t}\frac{\partial \hat{\psi}_1}{\partial y} + U\frac{\partial^2 \hat{\psi}_1}{\partial x \partial y} - \frac{\partial \hat{\psi}_1}{\partial x}\frac{dU}{dy} = -\frac{\partial \hat{p}_1}{\partial x} + \frac{1}{Re}\nabla^2\left(\frac{\partial \hat{\psi}_1}{\partial y}\right) \tag{2.8a}$$

$$-\frac{\partial}{\partial t}\frac{\partial \hat{\psi}_1}{\partial x} - U\frac{\partial^2 \hat{\psi}_1}{\partial x^2} - \qquad = -\frac{\partial \hat{p}_1}{\partial y} - \frac{1}{Re}\nabla^2\left(\frac{\partial \hat{\psi}_1}{\partial x}\right) \tag{2.8b}$$

Adding $\frac{\partial}{\partial x}$ of (2.8a) to $\frac{\partial}{\partial y}$ of (2.8b) gives an expression for $\nabla^2 \hat{p}_1$, which when substituted into the result of ∇^2 applied to (2.8b) gives the Orr-Sommerfeld equation (OSE) for $\hat{\psi}_1$

$$\left\{\left(\frac{1}{Re}\nabla^2 - \frac{\partial}{\partial t} - U\frac{\partial}{\partial x}\right)\nabla^2 + \frac{d^2U}{dy^2}\frac{\partial}{\partial x}\right\}\hat{\psi}_1 = 0 \quad . \tag{2.9}$$

The structure of equations (2.1) and (2.9) allow separation of variables thereby suggesting a solution in the form of normal modes

$$\hat{\psi}_1(x,y) = \hat{\psi}(y)\,e^{i\alpha x}, \quad x = x' - ct \tag{2.10}$$

where $c = c_r + ic_i$. We substitute (2.10) into (2.9) to obtain

$$\left\{(D^2-\alpha^2)^2 - i\alpha \mathrm{Re}\left[(U-c)(D^2-\alpha^2) - (D^2U)\right]\right\}\hat{\psi} = 0 \tag{2.11a}$$

with boundary conditions

$$\hat{\psi} = D\hat{\psi} = 0 \quad at \quad y = \pm 1 \tag{2.11b}$$

where $D = d/dy$. Equations (2.11a,b) represent an eigenvalue problem with a characteristic equation of the form $f(\alpha, Re, c) = 0$ whose first even mode is known to be the most unstable.

Since we formulated the linear stability problem to allow both the eigenfunction $\hat{\psi}(y)$ and the eigenvalue c to be complex, we must also accept their complex conjugates ($\bar{\psi}(y)$

and $\tilde{c}$) as a solution. Addition of these two solutions enables the disturbance streamfunction ψ_1 to be written in real form, necessary since the Navier-Stokes equations are real. We have

$$\begin{aligned} \psi_1(x,y) &= A_0 \left[\hat{\psi}(y) e^{i\alpha(x-ct)} + \tilde{\psi}(y) e^{-i\alpha(x-ct)} \right] \\ &= 2A_0 e^{\alpha c_i t} \left[\psi_1^+ \cos\alpha x - \psi_1^- \sin\alpha x \right] \end{aligned} \tag{2.12}$$

by recalling Euler's formula for $e^{i\theta}$ and grouping terms accordingly. We have defined αc_i as the growth rate of the disturbance and the real functions $\psi_1^{\pm}$ are given by

$$\psi_1^+ = \mathrm{Re}\{\psi(y)\} \ , \ \psi_1^- = \mathrm{Im}\{\psi(y)\} \ . \tag{2.13}$$

Recalling (2.7), the total velocity field $\mathbf{v}(x,y)$, we have

$$\begin{aligned} \mathbf{v}(x,y) &= \mathbf{v}_0(y) + A\mathbf{v}_1(x,y) \\ &= \mathbf{v}_0(y) + 2A \left[\mathbf{v}_1^+ \cos\alpha x - \mathbf{v}_1^- \sin\alpha x \right] \end{aligned} \tag{2.14}$$

with $A = A_0 e^{\alpha c_i t}$ and $\mathbf{v}_1^{\pm}$ are, from continuity

$$\begin{aligned} u_1^+ &= D\psi_1^+ \ , \ u_1^- = D\psi_1^- \\ v_1^+ &= \alpha\psi_1^- \ , \ v_1^- = -\alpha\psi_1^+ \ . \end{aligned} \tag{2.15}$$

With appropriate normalization of the streamfunction $\psi_1(x,y)$, the disturbance amplitude A provides a direct measure of the r.m.s. fluctuation of the TS wave (Herbert 1977).

The vorticity of the disturbance is given by

$$\begin{aligned} \varsigma_1 &= (0,0,\varsigma_1) = \nabla \times A\mathbf{v}_1(x,y) \\ &= A\left(\frac{\partial v_1}{\partial x} - \frac{\partial u_1}{\partial y} \right) \ . \end{aligned} \tag{2.16}$$

The details of substituting solution (2.12) into (2.16) appear in Appendix I with calculations to follow. With the stability of the basic flow determined, we are now prepared to

study the energetics of these solutions.

2.1.2. Energy Analysis of Primary Instability

The physics of the viscous instability mechanism operating in plane Poiseuille flow should become clearer by studying the energetics of solution (2.14). Throughout, we neglect thermodynamic effects and consider only the transfer of kinetic energy, as defined for the i^{th} component of $\mathbf{v}$ by

$$E^{(i)} = \frac{1}{2}\int_{\Omega} \mathbf{v}_{(i)}\cdot\mathbf{v}_{(i)}\, d\Omega\,, \quad i = 0,1 \quad . \tag{2.17}$$

The region Ω is an arbitrary area between the channel walls one TS wavelength long. To begin, we substitute solution (2.14) into the momentum equation (2.1) and arrive at

$$\frac{\partial}{\partial t}(\mathbf{v}_0+A\mathbf{v}_1) + [\,(\mathbf{v}_0+A\mathbf{v}_1)\cdot\nabla\,](\mathbf{v}_0+A\mathbf{v}_1) = -\nabla(p_0+Ap_1) + \frac{1}{Re}\nabla^2(\mathbf{v}_0+A\mathbf{v}_1) \tag{2.18}$$

We now form the dot product of (2.13) with $\mathbf{v}_0$ and $A\mathbf{v}_1$ respectively, and integrate over region Ω to obtain two energy equations. The first describes the energetics of the basic flow,

$$\int_{\Omega}\left\{\frac{\partial}{\partial t}(\mathbf{v}_0+A\mathbf{v}_1) + [\,(\mathbf{v}_0+A\mathbf{v}_1)\cdot\nabla\,](\mathbf{v}_0+A\mathbf{v}_1)\right\}\cdot\mathbf{v}_0\, d\Omega \tag{2.19}$$

$$= -\int_{\Omega}\nabla(p_0+Ap_1)\cdot\mathbf{v}_0\, d\Omega + \frac{1}{Re}\int_{\Omega}\nabla^2(\mathbf{v}_0+A\mathbf{v}_1)\cdot\mathbf{v}_0\, d\Omega$$

and the other is for the disturbance,

$$\int_{\Omega} \left[\frac{\partial}{\partial t}(\mathbf{v}_0+A\mathbf{v}_1) + [\,(\mathbf{v}_0+A\mathbf{v}_1)\cdot\nabla\,](\mathbf{v}_0+A\mathbf{v}_1)\right]\cdot A\mathbf{v}_1 \, d\Omega \tag{2.20}$$

$$= -\int_{\Omega} \nabla(p_0+Ap_1)\cdot A\mathbf{v}_1 \, d\Omega + \frac{1}{Re}\int_{\Omega} \nabla^2(\mathbf{v}_0+A\mathbf{v}_1)\cdot A\mathbf{v}_1 \, d\Omega \quad .$$

Equations (2.19)-(2.20) can be simplified by utilizing the periodicity of $\mathbf{v}_1$ and p_1 which will force terms such as

$$\int_{\Omega} \mathbf{v}_1(x,y)\cdot f(y) \, d\Omega$$

to integrate to zero over region Ω. The divergence theorem is also of use in simplifying (2.20) by providing the following relations:

$$\int_{\Omega} \nabla p_1\cdot\mathbf{v}_1 d\Omega = \int_{\Gamma} p_1\mathbf{v}_1\cdot\mathbf{n} \, d\Gamma = 0$$

$$\int_{\Omega} \mathbf{v}_1\cdot\nabla\mathbf{v}_1\cdot\mathbf{v}_1 \, d\Omega = \int_{\Omega} \nabla\cdot[\mathbf{v}_1\mathbf{v}_1\cdot\mathbf{v}_1] \, d\Omega - \int_{\Omega} (\nabla\cdot\mathbf{v}_1)\mathbf{v}_1\cdot\mathbf{v}_1 \, d\Omega$$

$$= \int_{\Omega} \nabla\cdot[\mathbf{v}_1\mathbf{v}_1\cdot\mathbf{v}_1] \, d\Omega = \int_{\Gamma} \mathbf{v}_1\cdot\mathbf{v}_1\mathbf{v}_1\cdot\mathbf{n} \, d\Gamma = 0$$

where $\mathbf{v}_1$ is assumed to vanish on Γ, the boundary of Ω. Also, we define the power $P^{(i)}$ as

$$\int_{\Omega} \mathbf{v}_0\cdot\frac{\partial\mathbf{v}_0}{\partial t} \, d\Omega = \frac{d}{dt}\int_{\Omega} \frac{1}{2}\mathbf{v}_0\cdot\mathbf{v}_0 \, d\Omega \equiv \frac{dE^{(0)}}{dt} = P^{(0)}$$

and

$$\int_{\Omega} A^2\mathbf{v}_1\cdot\frac{\partial\mathbf{v}_1}{\partial t} \, d\Omega = \frac{d}{dt}\int_{\Omega} \frac{1}{2}A^2\mathbf{v}_1\cdot\mathbf{v}_1 \, d\Omega \equiv \frac{dE^{(1)}}{dt} = P^{(1)}$$

using (2.17). Then (2.19)-(2.20) become

$$\frac{dE^{(0)}}{dt} = -\int_{\Omega} A^2 \mathbf{v}_1 \cdot \nabla \mathbf{v}_1 \cdot \mathbf{v}_0 \, d\Omega + \int_{\Omega} \frac{2}{Re} \mathbf{i} \cdot \mathbf{v}_0 \, d\Omega + \frac{1}{Re} \int_{\Omega} \nabla^2 \mathbf{v}_0 \cdot \mathbf{v}_0 \, d\Omega \qquad (2.21)$$

$$= -\int_{\Omega} A^2 \left[u_1 \frac{\partial u_1}{\partial x} + v_1 \frac{\partial v_1}{\partial y} \right] U \, d\Omega + \int_{\Omega} \frac{2}{Re} U \, d\Omega + \frac{1}{Re} \int_{\Omega} U \frac{d^2 U}{dy^2} \, d\Omega$$

$$\frac{dE^{(1)}}{dt} = -\int_{\Omega} A^2 \mathbf{v}_1 \cdot \nabla \mathbf{v}_0 \cdot \mathbf{v}_1 \, d\Omega + \frac{1}{Re} \int_{\Omega} A^2 \nabla^2 \mathbf{v}_1 \cdot \mathbf{v}_1 \, d\Omega \qquad (2.22)$$

$$= -\int_{\Omega} A^2 u_1 v_1 \frac{dU}{dy} \, d\Omega - \frac{1}{Re} \int_{\Omega} A^2 \left[\left(\frac{\partial u_1}{\partial x} \right)^2 + \left(\frac{\partial v_1}{\partial x} \right)^2 + \left(\frac{\partial u_1}{\partial y} \right)^2 + \left(\frac{\partial v_1}{\partial y} \right)^2 \right] d\Omega$$

where $\mathbf{v} = (U(y),0,0) + A(u_1,v_1,0)$.

Note that all non-linear terms have vanished in these two equations and, as a result, (2.21)-(2.22) are at most quadratic in the disturbance velocity $\mathbf{v}_1$. The last term on the right hand side of equations (2.21)-(2.22) represents the dissipation of kinetic energy in the flow. The vector form of the dissipation in (2.22) was converted to the scalar form shown by using integration by parts in conjunction with the boundary conditions from the OSE (2.11). The middle term in (2.21) supplies energy to the basic flow through the constant pressure gradient characteristic of plane Poiseuille flow. Notice the perturbation pressure p_1 in (2.20) contributes no net energy to the disturbance. The first term in each equation ties the two equations (2.21)-(2.22) together since they are energy transfer terms. In (2.21), this term represents energy transferred into the basic flow from the disturbance, while in (2.22) this term, known as the Reynolds stress, represents energy transferred into the disturbance from the basic flow. It can be shown (Appendix I) that these two quantities are equal in magnitude and opposite in sign, thereby revealing their role as the link between the basic flow and the disturbance.

These simplifications allow (2.21)-(2.22) to be rewritten as

$$\frac{dE^{(0)}}{\partial t} = - T^{(10)} + D^{(0)} \tag{2.23}$$

$$\frac{dE^{(1)}}{\partial t} = T^{(10)} + D^{(1)} \tag{2.24}$$

where $T^{(01)} = - T^{(10)}$, and the pressure term in (2.21) has been lumped with the dissipation term in $D^{(0)}$. It remains to substitute solution (2.14) into (2.24), the details of which appear in Appendix I, and analyze the result numerically.

Now consider the definition of the kinetic energy for the TS wave

$$E^{(1)} = \frac{1}{2}\int_{\Omega} A^2 \mathbf{v}_1 \cdot \mathbf{v}_1 \, d\Omega$$

where $\mathbf{v}_1$ is given by (2.14). Differentiation of the above with respect to time gives

$$\frac{dE^{(1)}}{dt} = (2\alpha c_i)\left[\frac{1}{2}\int_{\Omega} A^2 \mathbf{v}_1 \cdot \mathbf{v}_1 \, d\Omega\right] = (2\alpha c_i)E^{(1)} \quad .$$

Consequently,

$$2\alpha c_i = \frac{1}{E^{(1)}}\frac{dE^{(1)}}{dt} \quad . \tag{2.25}$$

This relation allows the growth rate of the two-dimensional disturbance to be directly calculated from (2.24), providing a check of solution (2.14).

Qualitative conclusions concerning the stability of the TS wave can be drawn by looking at (2.24). The term $D^{(1)}$ is always stabilizing since it removes energy from the disturbance by way of viscous dissipation. The Reynolds stress then, determines the stability of the flow. If the Reynolds stress is positive and greater than the dissipation, then $P^{(1)} > 0$ and instability results. If both quantities are balanced, then $P^{(1)} = 0$ and we have either

neutral oscillations or no motion. Lastly, if the Reynolds stress is negative, then $P^{(1)} < 0$ and the flow is stable. Three solutions of the Orr-Sommerfeld equation are presented in the results, Section 2.2, which typify these three possible stability conditions.

2.2. Computational Method

The Orr-Sommerfeld equation resulting from (2.11) was solved using a local eigenvalue search to obtain the most unstable mode. Treatment of the y-direction in the local procedure depended on a highly accurate spectral collocation technique which converts differential equations into algebraic equations as described by Orszag (1971) and Herbert (1984b). This technique is based on expanding the OSE solution $\psi(y)$ in the form

$$\psi(y) = \sum_{m=0}^{M} a_m T_m(y), \quad y = \cos\theta \tag{2.26}$$

where the T_m's are Chebyshev polynomials. Discrete collocation points are selected in the channel according to

$$y_j = \cos\theta_j, \quad \theta_j = \frac{j\pi}{J}, \quad j = 0,...,J = M-2 \quad . \tag{2.27}$$

Substitution of the Chebyshev series (2.26) into the OSE then converts the differential equation plus the two boundary conditions into an $M \times M$ complex system of linear algebraic equations for the Chebyshev coefficients a_m. The resulting eigenvalue problem is solved using a form of Newton's method to find the eigenvalue c. Sufficient convergence is obtained with 25 polynomials.

The properties of the Chebyshev expansion (2.26) allow complex operations such as integration, differentiation and fast transformations between spectral and physical space to be easily accomplished using simple algorithms involving the coefficients a_m (Schumann,

Grötzbach, & Kleiser 1979). Integration of the energy equation (2.20) across the channel in the y-direction was performed using these algorithms. In the streamwise direction x', we define the average of the function $f(x)$ over one TS wavelength λ_x as

$$\bar{f} = \frac{1}{\lambda_x} \int_{x_0}^{x_0+\lambda_x} f(x)\,dx \quad . \tag{2.28}$$

The normal mode assumption (2.10) results in integrals of closed form in x (2.28) for the energy equation (2.24).

2.3. Results

The viscous instability mechanism driving primary instability has become well understood through the theoretical work of Tollmien, Prandtl and Schlichting, and the experiments of Schubauer and Skramstad. Its inclusion here is to present results in a new form to be used on subsequent, less well understood problems.

2.3.1. Results of the Stability Analysis

Given a reasonable initial guess from a global eigenvalue procedure or from the literature, the spectral collocation technique converged to the exact eigenvalue in three to four iterations. Three solutions were selected representing unstable, neutral and stable cases according to linearized stability theory. The unstable case has been widely studied (Orszag 1971, Drazin & Reid 1981) and provides a reliable basis for evaluating the results of the energy analysis. The neutral case was selected at the minimum critical Reynolds number and wavenumber as it is a point of interest, while the stable case provides a contrast to the first two solutions. In each instance, the first even mode of the OSE in terms of $\hat{\psi}(y)$ was

calculated, since it is the "most dangerous" mode. The eigensolutions, normalized according to $\hat{\psi}(0) = 1$, are shown in figures 2.2, 2.3 and 2.4 for the parameters in Table 2.1. The horizontal lines at $y = \pm 1$ represent the channel walls. The origin lies at the midpoint of the dashed channel centerline. The two small tick marks on the y-axis denote the position of the critical layers defined by the location of $U(y) = c_r$,

$$y_c = [1 - c_r]^{1/2} \tag{2.29}$$

for plane Poiseuille flow. The line connected by crosses is the imaginary part of the solution while the real part is represented by the plain line. Note that the similarity of all three solutions masks the vastly different stability properties of each.

Each of the solutions obtained from the linear stability analysis was then substituted into the energy equation for the two-dimensional disturbance, equation (2.24), to study the instability mechanism affecting plane Poiseuille flow. Results for the Reynolds stress $T^{(10)}$, the dissipation $D^{(1)}$ and the power $P^{(1)}$ are presented in three ways - contour plots of functions of two variables, plots of single variable functions and numerical results in tabular form.

2.3.2. Results of the Energy Analysis

The contour plots are the graphical representation of the Reynolds stress, the dissipation and the power as functions of both x and y , similar to those of Radbill & McCue (1970) for the boundary layer. In all instances, the "plotting window" corresponds to the integration region Ω with the channel walls at $y = \pm 1$ and the x-axis one TS wavelength λ_x long, figure 2.5 as an example. The tick marks on the y-axis define the critical layer position and the dashed centerline marks the middle of the channel. The contours of each

Table 2.1 - Solution of the OSE

	Case 1	Case 2	Case 3
Re	10000	5772.22	4000
α	1.000	1.02056	1.000
c_r	0.23752643	0.26400174	0.27854215
c_i	0.0037397146	0.0	-0.0049455388

quantity occur at 20 equally spaced intervals, including the zero level, which are scaled separately for each case. The narrow pen width indicates negative regions of power while the wide pen width denotes positive values and zero. The zero level can be found where any wide line lies closest to a narrow line. Pertinent flow and plot parameters are found in the block below each plot.

If (2.19) is integrated in the y direction only, a plot such as figure 2.8 results. Here, the Reynolds stress is plotted as a function of the streamwise variable x over one TS wavelength. Similarly, integration in the x direction only leads to a function of y, as in figure 2.12 for the dissipation. The channel walls lie at $y = \pm 1$, the tick marks designate the critical layer position and the origin lies at the midpoint of the channel centerline. These single variable plots are scaled to the maximum absolute value among these functions of either x or y for each case. Pertinent parameters are listed in the block below each figure, including the minimum and maximum values in the plot above.

The power transferred into the disturbance from the basic flow is presented in plots as described above beginning in figure 2.7 and continuing in every third plot thereafter, for each of the three cases considered. Similar results are presented for the Reynolds stress and the dissipation which begin with figure 2.5 and figure 2.6 respectively.

We notice the power, the Reynolds stress and the dissipation are all periodic in the streamwise direction, as shown in figures 2.7 and 2.10 for $P^{(1)}$. This confirms the results of Radbill and McCue and is expected owing to the periodic nature of the TS wave itself. Looking closely at figures 2.10, 2.20 and 2.30 we see evidence of the stability characteristics of the TS wave as Re decreases. In figure 2.10, a net positive transfer of energy is indicated by the slight upward shift of the curve. Figure 2.20 shows that the curve has no offset indi-

cating the neutral condition, while the function in figure 2.30 for the stable case is shifted downwards. This indicates that energy is transferred back to the basic flow as the TS wave attenuates. Also, in figures 2.7, 2.17 and 2.27, the power peaks are steepest in the unstable case, becoming flatter as Re decreases. The regions of negative power become larger as Re decreases and we see the contour plots are also shifting downwards as Re decreases since in figure 2.27 there are not quite enough levels to accommodate the lowest values of the function.

Prandtl, in his theory of primary instability (Drazin & Reid 1981), said that viscosity leads to the formation of fluid stress, caused by satisfying the no-slip boundary condition at the channel walls. Even though viscosity, in general, has a stabilizing effect on the flow by dissipating energy, the distribution of the Reynolds stress in the flow, created by viscosity, can lead to instability. Energy transfer into the disturbance is enhanced by synchronization between the basic flow and the TS wave near the viscous critical layer y_c. Therefore the Reynolds stress and the dissipation exist in a balance of forces to determine the stability of the flow.

Plots of the dissipation term as a function of y are given in figures 2.6 and 2.12 for the unstable case and show regions where viscous effects are most pronounced. These areas lie between the channel walls and the two planes defined by the critical layer y_c. Also notice from figures 2.16, 2.22, 2.26 and 2.32 that the nearly inviscid region between the two viscous layers widens as Re increases. For a given wavenumber α then, the viscous instability mechanism requires viscous effects to be confined to some sufficiently small region before instability occurs.

The distribution of the Reynolds stress across the channel for the unstable case is

apparent in figures 2.5 and 2.11, which show a net positive transfer of energy into the disturbance. In all cases, energy transfer is concentrated around the critical layer, confirming Prandtl's ideas. Also, comparison of figures 2.11, 2.21 and 2.31 reveals that all changes in the Reynolds stress distribution are concentrated in this region. In the unstable case, figure 2.11 shows the disturbance gains energy over a TS wavelength, while in figures 2.21 and 2.31, we see the Reynolds stress is transferring energy back to the basic flow.

Figures 2.8, 2.18 and 2.28 show the streamwise variation of the Reynolds stress. Compared with similar plots for the dissipation in figures 2.9, 2.19 and 2.29, the Reynolds stress is much more energetic than the dissipation over a portion of one TS wavelength. These two sets of plots, in conjunction with figures 2.10, 2.20 and 2.30 for the power, reveal the delicate balance between the Reynolds stresses and the dissipation. We see that small changes in the distribution of the Reynolds stress in either the x or y directions have significant effect upon the stability of the flow.

The result of integrating the energy equation (2.24), which describes the stability of the disturbance, appears in Table 2.2. Case 1 corresponds to an unstable flow while Cases 2 and 3 are neutral and stable cases respectively, of the OSE. The bar over each quantity indicates normalization with respect to the net kinetic energy of the disturbance, $E^{(1)}$. Normalization directly relates $T^{(10)}$, $D^{(1)}$ and $P^{(1)}$ to the growth rate αc_i, as in (2.25). Table 2.2 shows the calculated growth rate, per (2.25), is in good agreement with that obtained from the OSE solution.

These calculations were extended to reveal the dependence of the Reynolds stress, the dissipation and the power on the parameters Re and α. The result of this calculation for fixed $\alpha = 1$, with Re varying between 2000 and 10000 can be found in figure 2.35. Similar

results for fixed $Re = 10000$, with α between 0.60 and 1.25 are plotted in figure 2.36. In both figures, the quantities plotted all decrease as the parameter of interest decreases, indicating the TS wave is becoming less energetic. Since $\overline{P}^{(1)}$ is twice the TS growth rate, negative values indicate stability and positive values instability. The point where $\overline{P}^{(1)}$ crosses the ordinate corresponds to the critical point for neutral stability. In figure 2.35 this point is approximately $\alpha_c = 1$, $Re_c = 5816$ and in figure 2.36 two neutral points occur at $\alpha_c = 0.80$ and $\alpha_c = 1.10$ with $Re_c = 10000$. A preferred wavenumber of $\alpha = 0.95$ for maximum disturbance power is evident in figure 2.36, while in figure 2.35 we see that $P^{(1)}$ is also near a relative maximum at $Re = 10000$. A second neutral point at $\alpha = 1.00$ occurs at an infinite Reynolds number. These two figures clearly show that primary instability depends on the balance of relatively large viscous stresses and dissipative forces to ultimately determine the stability of the disturbance.

Turning our attention to (2.23), the energy equation for the basic flow, we realize results can be obtained analytically since the basic flow is known. It has been shown that the energy transfer terms are equal and opposite, $T^{(01)} = -T^{(10)}$ so it remains to determine the result of the $D^{(0)}$ term. Recall

$$D^{(0)} = \int_\Omega \frac{2}{Re} U \, d\Omega + \frac{1}{Re} \int_\Omega U \frac{d^2U}{dy^2} \, d\Omega \qquad (2.30)$$
$$= \frac{1}{Re} \int_\Omega U \left[2 + \frac{d^2U}{dy^2} \right] d\Omega \quad .$$

Substituting the expression for the basic flow $U = 1 - y^2$ into the above gives

Table 2.2 - Result of Integrating Energy Equation (2.19)

	Case 1	Case 2	Case 3
Re	10000	5772.22	4000
α	1.000	1.02056	1.000
c_r	0.23752643	0.26400174	0.27854215
αc_i	0.0037397146	0.0	-0.0049455388
$\overline{T}^{(10)}$	0.019614488	0.014802987	0.0062931786
$\overline{D}^{(1)}$	-0.012135060	-0.014802464	-0.016184256
$\overline{P}^{(1)}$	0.0074794288	0.00000052	-0.0098910776
αc_i	0.0037397144	0.00000026	-0.0049455388

$$D^{(0)} = \frac{1}{Re}\int_{\Omega} U \left(2 - 2\right) d\Omega = 0 \quad . \tag{2.31}$$

Therefore, we see the basic flow pressure gradient acting as an energy source and the dissipation as an energy sink. The pressure gradient supplies energy to the system, part of which is transferred to the TS wave with the remainder dissipated in the basic flow. Equation (2.23) becomes

$$\frac{dE^{(0)}}{dt} = - T^{(10)} \tag{2.32}$$

which, when compared with (2.24), reveals that energy is not conserved in the system. This indicates that non-linear terms, which have been been neglected, are required in order to restore this balance.

Lastly, vorticity contours of the disturbance for each case appear in figures 2.14, 2.24 and 2.34. These contour plots are set up identically to those previous and show that the viscous instability establishes an array of streamwise-periodic concentrations of vorticity, whose maxima lie near the channel walls, inside the viscous wall layers. Thus, stability arguments based on vorticity agree with results obtained from the energy analysis, showing the critical layer has a primary role in determining the stability of the two-dimensional disturbance.

3. Energy Analysis of Secondary Instability

3.1. Problem Statement

We consider the steady flow of an incompressible fluid between infinite parallel plates driven by a constant pressure gradient in the streamwise direction x' as in Section 2. The y-direction is normal to the channel walls, with z normal to the $x'-y$ plane and t represents time. All quantities are non-dimensionalized with respect to the half-channel width h and the maximum centerline velocity U_0, as depicted in figure 2.1. However, in this instance, we allow the flow to be three-dimensional, whereas we previously restricted ourselves to two dimensions. Then the non-dimensional field equations governing fluid motion are

$$\begin{gathered} \nabla \cdot \mathbf{v} = 0 \\ \frac{\partial \mathbf{v}}{\partial t} + (\mathbf{v} \cdot \nabla)\mathbf{v} = -\nabla p + \frac{1}{Re}\nabla^2 \mathbf{v} \\ \mathbf{v} = 0 \quad at \quad y = \pm 1 \end{gathered} \tag{3.1}$$

where

$$\mathbf{v} = (u, v, w), \quad Re = \frac{hU_0}{\nu} \quad .$$

Introducing the vorticity ω, we have

$$\omega = \nabla \times \mathbf{v} \quad . \tag{3.2}$$

We begin the study of the secondary instability by constructing a periodic basic flow, composed of an oscillatory wave superimposed on a mean flow which satisfies equations (3.1) for all Re, of the form

$$\mathbf{v}_2(x',y,t) = \mathbf{v}_0(y) + A\mathbf{v}_1(x',y,t) \qquad (3.3)$$
$$p_2(x',y,t) = p_0(x') + Ap_1(x',y,t) \quad .$$

The mean flow $\mathbf{v}_0$, p_0 is given by the viscous solution of plane Poiseuille flow, utilized as the basic flow in Section 2, such that

$$\mathbf{v}_0(y) = U(y)\mathbf{i} = (1-y^2)\mathbf{i} \qquad (3.4)$$
$$p_0(x') = -\frac{2}{Re}x' \quad .$$

The oscillatory part of the basic flow (3.3) is comprised of a two-dimensional, non-linear equilibrium state of finite amplitude A (Herbert 1977) which is steady in a Galilean frame x such that

$$\mathbf{v}_1(x',y,t) = \mathbf{v}_1(x,y), \quad x = x' - ct \qquad (3.5)$$
$$\mathbf{v}_1(x,y) = \mathbf{v}_1(x+\lambda_x,y), \quad \lambda_x = \frac{2\pi}{\alpha}$$

where α is the streamwise wavenumber. The disturbance amplitude A in (3.3) measures the r.m.s. fluctuation of u_1, typically 1-3% of the maximum centerline velocity U_0. At these low amplitudes, the shape assumption (Stuart 1958) allows us to neglect the weak growth of A and replace the non-linear equilibrium state in (3.5) with the linear solution of the Orr-Sommerfeld equation (OSE) multiplied by the finite amplitude $A = A_0 e^{\alpha c_i t}$ such that

$$\begin{aligned}\mathbf{v}_2(x,y) &= \mathbf{v}_0(y) + A\mathbf{v}_1(x,y) \qquad (3.6)\\ &= \mathbf{v}_0 + 2A[\ \mathbf{v}_1^+\cos\alpha x - \mathbf{v}_1^-\sin\alpha x\ ]\end{aligned}$$

where $\mathbf{v}_1$ is defined in terms of a streamfunction ψ_1 such that

$$u_1 = \frac{\partial\psi_1}{\partial y}\ , \quad v_1 = -\frac{\partial\psi_1}{\partial x} \quad . \qquad (3.7)$$

Therefore, $\mathbf{v}_1^{\pm}$ in (3.6) is given by

$$u_1^+ = D\psi_1^+ \ , \ u_1^- = D\psi_1^- \qquad (3.8)$$
$$v_1^+ = \alpha\psi_1^- \ , \ v_1^- = -\alpha\psi_1^+$$

where $\psi_1 = \psi_1^+ + i\psi_1^-$ is the eigenfunction associated with the first even mode $c = c_r + ic_i$ of the OSE for given α, Re.

Although the non-linearity in the governing equations (3.1) determines the equilibrium amplitude attained by (3.5) on the viscous time scale, these effects are negligible on the convective time scale of the secondary instability. Thus, the weak variation of $A(t)$ can be neglected in our analysis if we assume $|\alpha c_i| << |\sigma_r|$, where σ_r is the growth rate of the secondary instability. We now perturb the basic flow $\mathbf{v}_2$ by superimposing an arbitrary three-dimensional disturbance such that

$$\mathbf{v}(x',y,z,t) = \mathbf{v}_2(x',y,t) + B\hat{\mathbf{v}}_3(x',y,z,t) \qquad (3.9)$$
$$p(x',y,z,t) = p_2(x',y,t) + B\hat{p}_3(x',y,z,t)$$

where B is sufficiently small to allow linearization.

3.1.1. Stability of the Basic Flow $\mathbf{v}_2$

To determine the stability characteristics of the basic flow $\mathbf{v}_2$, we follow the procedure of classical stability analysis and substitute the perturbed basic flow (3.9) into the governing equations (3.1) and neglect terms of order ϵ^2 to obtain the following set of linearized disturbance equations

$$\nabla\cdot\hat{\mathbf{v}}_3 = 0 \qquad (3.10a)$$
$$\frac{\partial\hat{\mathbf{v}}_3}{\partial t} + \mathbf{v}_2\cdot\nabla\hat{\mathbf{v}}_3 + \hat{\mathbf{v}}_3\cdot\nabla\mathbf{v}_2 = -\nabla\hat{p}_3 + \frac{1}{Re}\nabla^2\hat{\mathbf{v}}_3$$

with homogeneous boundary conditions on $\hat{\mathbf{v}}_3$. We allow the velocity to be complex in general, denoted by $(\hat{\ })$. The vorticity generated by the disturbance is given by

$$\hat{\omega}_3 = \nabla \times \hat{\mathbf{v}}_3 = (\hat{\xi}_3, \hat{\eta}_3, \hat{\zeta}_3) \tag{3.10b}$$

A comparison of the disturbance equations (3.10a) and (2.6) for primary and secondary instability shows that they have similar form, but the basic flow in the secondary stability equations is periodic, which is significant. We now substitute the basic flow (3.6) into the disturbance equation (3.10a), take the curl of (3.10a) to eliminate the pressure $\hat{p}_3$, introduce the vorticity components of the TS wave ζ_1 and the disturbance ω_3 and eliminate the z-component of the velocity $\hat{v}_3$ through continuity to obtain the following two linear partial differential equations which are coupled in $\hat{u}_3(y)$ and $\hat{v}_3(y)$

$$\left(\frac{1}{Re}\nabla^2 - (U-c)\frac{\partial}{\partial x} - \frac{\partial}{\partial t}\right)\nabla^2\hat{v}_3 + \frac{d^2U}{dy^2}\frac{\partial \hat{v}_3}{\partial x} \tag{3.11a}$$

$$+ A\left[\left(\frac{\partial\psi_1}{\partial x}\frac{\partial}{\partial y} - \frac{\partial\psi_1}{\partial y}\frac{\partial}{\partial x}\right)\nabla^2\hat{v}_3 + \frac{\partial^2\psi_1}{\partial x^2}\left(\frac{\partial\hat{\zeta}_3}{\partial y} + \frac{\partial\hat{\eta}_3}{\partial z}\right) - \frac{\partial^2\psi_1}{\partial x\,\partial y}\left(\frac{\partial\hat{\zeta}_3}{\partial x} + \frac{\partial\hat{\xi}_3}{\partial z}\right)\right.$$

$$\left. - \frac{\partial\zeta_1}{\partial x}\left(2\frac{\partial\hat{u}_3}{\partial x} + \frac{\partial\hat{v}_3}{\partial y}\right) - \frac{\partial\zeta_1}{\partial y}\frac{\partial\hat{v}_3}{\partial x} - \left(\hat{u}_3\frac{\partial}{\partial x} + \hat{v}_3\frac{\partial}{\partial y}\right)\frac{\partial\zeta_1}{\partial x}\right] = 0$$

$$\left(\frac{1}{Re}\nabla^2 - (U-c)\frac{\partial}{\partial x} - \frac{\partial}{\partial t}\right)\frac{\partial\hat{\eta}_3}{\partial z} - \frac{dU}{dy}\frac{\partial^2\hat{v}_3}{\partial z^2} + A\left[-\frac{\partial^2\psi_1}{\partial y^2}\frac{\partial^2\hat{v}_3}{\partial z^2}\right. \tag{3.11b}$$

$$\left. + \left(\frac{\partial\psi_1}{\partial x}\frac{\partial}{\partial y} - \frac{\partial\psi_1}{\partial y}\frac{\partial}{\partial x} - \frac{\partial^2\psi_1}{\partial x\,\partial y}\right)\frac{\partial\hat{\eta}_3}{\partial z} + \frac{\partial^2\psi_1}{\partial x^2}\left(\frac{\partial^2\hat{u}_3}{\partial x\,\partial y} + \frac{\partial^2\hat{v}_3}{\partial y^2}\right)\right] = 0$$

subject to the boundary conditions

$$\hat{u}_3 = \hat{v}_3 = \frac{\partial\hat{v}_3}{\partial y} \quad , \quad at \quad y = \pm 1 \quad . \tag{3.11c}$$

Equations (3.11a,b,c) are linear in $\hat{u}_3$, $\hat{v}_3$ and both the boundary conditions and the coefficients of (3.11) are independent of z and t, allowing the normal mode concept to be applied in the form

$$\hat{\mathbf{v}}_3(x,y) = e^{\sigma t} e^{i\beta z} \hat{f}(x,y) \qquad (3.12)$$

with $\sigma = \sigma_r + i\sigma_i$ in general complex in this temporal growth formulation and the spanwise wavenumber β taken as real. We assume the disturbance $\hat{\mathbf{v}}_3$ is periodic in the z-direction with wavelength $\lambda_z = 2\pi/\beta$, and in addition, we note that the coefficients of equations (3.11) are periodic in x, a characteristic feature of Floquet systems. The Floquet theory of ordinary differential equations with periodic coefficients (Coddington & Levinson 1955, Nayfeh & Mook 1979) provides two classes of solutions $\hat{f}(x,y)$ which differ in their streamwise periodicity.

When $\hat{f}(x,y)$ is periodic in x with wavelength λ_x, fundamental resonance with the TS wave occurs. The solution can therefore be represented in a Fourier series of the form

$$\hat{\mathbf{v}}_f = e^{\sigma t} e^{i\beta z} \sum_{n=-\infty}^{\infty} \hat{\mathbf{v}}_{2n}(y) e^{in\alpha x} \qquad (3.13)$$

A second solution arises when $\hat{f}(x,y)$ is doubly periodic in x with wavelength $2\lambda_x$, corresponding to principal parametric resonance, or subharmonic resonance, with the TS wave and can also be represented in a Fourier series of the form

$$\hat{\mathbf{v}}_s = e^{\sigma t} e^{i\beta z} \sum_{n=-\infty}^{\infty} \hat{\mathbf{v}}_{2n+1}(y) e^{i(2n+1)\frac{\alpha}{2}x} \qquad (3.14)$$

The coefficients $\hat{\mathbf{v}}_\nu$ in (3.13) and (3.14) have the symmetry

$$(\hat{u}_\nu(-y), \hat{v}_\nu(-y), \hat{w}_\nu(-z)) = (-1)^s (\hat{u}_\nu(y), -\hat{v}_\nu(y), \hat{w}_\nu(z)) \qquad (3.15)$$

with $s = 0,1$ for any ν (Herbert 1983b). In addition, successive coefficients $\hat{\mathbf{v}}_\nu$ and $\hat{\mathbf{v}}_{\nu+2}$ have opposite symmetry. Two fundamental modes can be distinguished, symmetric $\hat{\mathbf{v}}_{f_s}$ and anti-symmetric $\hat{\mathbf{v}}_{f_a}$, according to the character of $\hat{u}_0$, the leading aperiodic term in (3.13).

Subharmonic modes of differing symmetry exist but they are complex conjugate pairs and are redundant. The behavior of the fundamental and subharmonic modes represented by (3.13) and (3.14) is fully consistent with experimental observation (Herbert 1983c). The streamwise periodicity of the fundamental mode with λ_x results in the ordered in-line pattern of large scale Λ-shaped three-dimensional structures which are characteristic of peak-valley splitting. The streamwise aperiodic term $\hat{u}_0$ creates a mean flow distortion, while the pair $\hat{v}_0$, $\hat{w}_0$ forms a longitudinal vortex system. Such terms are absent in the subharmonic mode (3.14) and these types of structures do not appear in the flow. However, the staggered pattern of Λ-shaped vorticies which are indicative of the subharmonic mode arise from its periodicity with $2\lambda_x$.

The numerical solution of the system of differential equations requires low order truncation of the Fourier series in (3.13) and (3.14) to reduce the problem to a manageable size. The lowest truncation $n = 1$ was selected and gives only three terms from (3.13) and (3.14), $\hat{\mathbf{v}}_{(0)}$, $\hat{\mathbf{v}}_{(-2)}$ and $\hat{\mathbf{v}}_{(2)}$ for the fundamental and only two terms, $\hat{\mathbf{v}}_{(-1)}$ and $\hat{\mathbf{v}}_{(1)}$ for the subharmonic. However, at the low TS amplitudes applicable to this linear theory, such drastic truncation is justified. We have then

$$\hat{\mathbf{v}}_f = e^{\sigma t} e^{i\beta z} [\, \hat{\mathbf{v}}_0(y) + 2(\hat{\mathbf{v}}_2^+(y)\cos\alpha x - \hat{\mathbf{v}}_2^-(y)\sin\alpha x)\,] \tag{3.16}$$

$$\hat{\mathbf{v}}_s = e^{\sigma t} e^{i\beta z} [\, 2(\hat{\mathbf{v}}_1^+(y)\cos\frac{\alpha}{2}x - \hat{\mathbf{v}}_1^-(y)\sin\frac{\alpha}{2}x)\,]$$

where we have written the resulting solutions in trigonometric form by introducing

$$\mathbf{v}_n^+ = \frac{1}{2}(\hat{\mathbf{v}}_{(n)} + \hat{\mathbf{v}}_{(-n)}) \quad , \quad \mathbf{v}_n^- = \frac{1}{2i}(\hat{\mathbf{v}}_{(n)} - \hat{\mathbf{v}}_{(-n)})$$

into solutions (3.13) and (3.14) and rearranging terms accordingly. The linear nature of

the disturbance equations (3.11) admits complex conjugate solutions ($\tilde{\mathbf{v}}_f$ and $\tilde{\mathbf{v}}_s$) , which when added to (3.16) yield real expressions for $\mathbf{v}_f$ and $\mathbf{v}_s$, given by

$$\mathbf{v}_f(x,y,z,t) = \hat{\mathbf{v}}_f(x,y,z) + \tilde{\mathbf{v}}_f(x,y,z) \tag{3.17a}$$

$$\begin{aligned} &= 2e^{\sigma t}\Big\{ [\, u_0^+ + 2(u_2^+ \cos\alpha x - u_2^- \sin\alpha x)\,]\cos\beta z\ \mathbf{i} \\ &\quad + [\, v_0^+ + 2(v_2^+ \cos\alpha x - v_2^- \sin\alpha x)\,]\cos\beta z\ \mathbf{j} \\ &\quad - [\, w_0^- + 2(w_2^+ \cos\alpha x - w_2^- \sin\alpha x)\,]\sin\beta z\ \mathbf{k} \Big\} \end{aligned}$$

with z-components w_0^- , $w_2^{\pm}$ calculated from continuity

$$w_0^-(y) = \frac{i}{\beta} D v_0^+(y) \ , \tag{3.17b}$$

$$w_2^+(y) = \frac{i}{\beta}[D v_2^+ - \alpha u_2^-] \ , \quad w_2^-(y) = \frac{i}{\beta}[D v_2^- + \alpha u_2^+]$$

for the fundamental mode and by

$$\mathbf{v}_s(x,y,z,t) = \hat{\mathbf{v}}_s(x,y,z) + \tilde{\mathbf{v}}_s(x,y,z) \tag{3.18a}$$

$$\begin{aligned} &= 4e^{\sigma t}\Big\{ [\, u_{11}^+ \cos\frac{\alpha}{2}x - u_{11}^- \sin\frac{\alpha}{2}x\,]\cos\nu\ \mathbf{i} - [\, u_{12}^+ \cos\frac{\alpha}{2}x - u_{12}^- \sin\frac{\alpha}{2}x\,]\sin\nu\ \mathbf{i} \\ &\quad + [\, v_{11}^+ \cos\frac{\alpha}{2}x - v_{11}^- \sin\frac{\alpha}{2}x\,]\cos\nu\ \mathbf{j} - [\, v_{12}^+ \cos\frac{\alpha}{2}x - v_{12}^- \sin\frac{\alpha}{2}x\,]\sin\nu\ \mathbf{j} \\ &\quad - [\, w_{11}^+ \cos\frac{\alpha}{2}x - w_{11}^- \sin\frac{\alpha}{2}x\,]\cos\nu\ \mathbf{k} - [\, w_{12}^+ \cos\frac{\alpha}{2}x - w_{12}^- \sin\frac{\alpha}{2}x\,]\sin\nu\ \mathbf{k} \Big\} \end{aligned}$$

for the subharmonic mode where $\nu = \beta z + \sigma_i t$. The z-components $w_{11}^{\pm}$ and $w_{12}^{\pm}$ of velocity were calculated from continuity, giving

$$w_{11}^{+} = -\frac{1}{\beta}[Dv_{12}^{+} - \frac{\alpha}{2}u_{12}^{-}] \quad , \quad w_{11}^{-} = -\frac{1}{\beta}[Dv_{12}^{-} + \frac{\alpha}{2}u_{12}^{+}] \tag{3.18b}$$

$$w_{12}^{+} = \frac{1}{\beta}[Dv_{11}^{+} - \frac{\alpha}{2}u_{11}^{-}] \quad , \quad w_{12}^{-} = \frac{1}{\beta}[Dv_{11}^{-} + \frac{\alpha}{2}u_{11}^{+}]$$

We have defined the functions $\mathbf{v}_{11}^{\pm}$ and $\mathbf{v}_{12}^{\pm}$ in terms of the complex function $\mathbf{v}_1^{\pm}$ and its complex conjugate $\tilde{\mathbf{v}}_1^{\mp}$ as follows:

$$\mathbf{v}_{11}^{+} = \frac{1}{2}(\mathbf{v}_1^{+} + \tilde{\mathbf{v}}_1^{+}) \quad , \quad \mathbf{v}_{11}^{-} = \frac{1}{2i}(\mathbf{v}_1^{-} + \tilde{\mathbf{v}}_1^{-})$$

$$\mathbf{v}_{12}^{+} = \frac{1}{2}(\mathbf{v}_1^{+} - \tilde{\mathbf{v}}_1^{+}) \quad , \quad \mathbf{v}_{12}^{-} = \frac{1}{2i}(\mathbf{v}_1^{-} - \tilde{\mathbf{v}}_1^{-})$$

The vorticity generated by the three-dimensional disturbance can be written in real form in a similar manner from (3.10b) by adding a complex conjugate, which results in

$$\omega_3 = \nabla \times \mathbf{v}_3 = (\xi_3, \eta_3, \zeta_3) \tag{3.19}$$

$$= \left(\frac{\partial w_3}{\partial y} - \frac{\partial v_3}{\partial z}\right)\mathbf{i} - \left(\frac{\partial w_3}{\partial x} - \frac{\partial u_3}{\partial z}\right)\mathbf{j} + \left(\frac{\partial v_3}{\partial x} - \frac{\partial u_3}{\partial y}\right)\mathbf{k} \ .$$

The details of substituting the fundamental and subharmonic modes (3.17)-(3.18) into the expression for the vorticity (3.19) appears in Appendix II, while calculations appear later. Having now formulated a solution procedure for determining the stability of the basic flow $\mathbf{v}_2$, we now wish to analyze the energetics of these solutions to gain additional insight into the instability mechanisms involved.

3.1.2. Energy Analysis of Secondary Instability

As in Section 2.1, we neglect thermodynamic effects and consider the transfer of kinetic energy only, as defined for the i^{th} component of $\mathbf{v}$ by

$$E^{(i)} = \frac{1}{2}\int_{\Omega} \mathbf{v}_{(i)}\cdot\mathbf{v}_{(i)}\, d\Omega\,, \quad i = 0,1,3 \tag{3.20}$$

Here the region of interest Ω, is an arbitrary volume between the channel walls which extends one wavelength λ_z in the spanwise direction z and either one or two TS wavelengths λ_x for the fundmental or subharmonic mode respectively, in the streamwise direction x.

We begin by substituting the perturbed periodic basic flow (3.9) into the momentum equation (3.1) to arrive at

$$\frac{\partial}{\partial t}(\mathbf{v}_0+A\mathbf{v}_1+B\mathbf{v}_3) + [\,(\mathbf{v}_0+A\mathbf{v}_1+B\mathbf{v}_3)\cdot\nabla\,](\mathbf{v}_0+A\mathbf{v}_1+B\mathbf{v}_3) \tag{3.21}$$
$$= -\nabla(p_0+Ap_1+Bp_3) + \frac{1}{Re}\nabla^2[\mathbf{v}_0+A\mathbf{v}_1+B\mathbf{v}_3]$$

where $B = B_0 e^{\sigma t}$ represents the amplitude of the disturbance. We now form the dot product of (3.21) with $\mathbf{v}_0$, $A\mathbf{v}_1$ and $B\mathbf{v}_3$ respectively, and integrate over region Ω to obtain three energy equations. The first describes the mean flow

$$\int_{\Omega}\left\{\frac{\partial}{\partial t}(\mathbf{v}_0+A\mathbf{v}_1+B\mathbf{v}_3) + [(\mathbf{v}_0+A\mathbf{v}_1+B\mathbf{v}_3)\cdot\nabla](\mathbf{v}_0+A\mathbf{v}_1+B\mathbf{v}_3)\right\}\cdot\mathbf{v}_0\, d\Omega \tag{3.22}$$
$$= -\int_{\Omega}\left(\nabla(p_0+Ap_1+Bp_3)\right)\cdot\mathbf{v}_0\, d\Omega + \frac{1}{Re}\int_{\Omega}\left(\nabla^2(\mathbf{v}_0+A\mathbf{v}_1+B\mathbf{v}_3)\right)\cdot\mathbf{v}_0\, d\Omega\,,$$

the second the TS wave

$$\int_{\Omega} \left\{ \frac{\partial}{\partial t}(\mathbf{v}_0+A\mathbf{v}_1+B\mathbf{v}_3) + [(\mathbf{v}_0+A\mathbf{v}_1+B\mathbf{v}_3)\cdot\nabla](\mathbf{v}_0+A\mathbf{v}_1+B\mathbf{v}_3) \right\} \cdot A\mathbf{v}_1 \, d\Omega \tag{3.23}$$

$$= -\int_{\Omega} (\nabla(p_0+Ap_1+Bp_3)) \cdot A\mathbf{v}_1 \, d\Omega + \frac{1}{Re}\int_{\Omega} (\nabla^2(\mathbf{v}_0+A\mathbf{v}_1+B\mathbf{v}_3)) \cdot A\mathbf{v}_1 \, d\Omega \quad ,$$

and the third the secondary disturbance

$$\int_{\Omega} \left\{ \frac{\partial}{\partial t}(\mathbf{v}_0+A\mathbf{v}_1+B\mathbf{v}_3) + [(\mathbf{v}_0+A\mathbf{v}_1+B\mathbf{v}_3)\cdot\nabla](\mathbf{v}_0+A\mathbf{v}_1+B\mathbf{v}_3) \right\} \cdot B\mathbf{v}_3 \, d\Omega \tag{3.24}$$

$$= -\int_{\Omega} (\nabla(p_0+Ap_1+Bp_3)) \cdot B\mathbf{v}_3 \, d\Omega + \frac{1}{Re}\int_{\Omega} (\nabla^2(\mathbf{v}_0+A\mathbf{v}_1+B\mathbf{v}_3)) \cdot B\mathbf{v}_3 \, d\Omega \quad .$$

Simplifications of (3.22)-(3.24) are possible by utilizing the periodicity of the basic flow and the disturbance over the region Ω which forces integrals of the form

$$\int_{\Omega} f(x,y,z) \cdot g(x,y) \, d\Omega$$

to vanish due to the spanwise periodicity of f. The divergence theorem is also of use in simplifying (3.22)-(3.24) by providing the following relations:

$$\int_{\Omega} \nabla p_1 \cdot \mathbf{v}_1 \, d\Omega = \int_{\Gamma} p_1 \mathbf{v}_1 \cdot \mathbf{n} d\Gamma \equiv 0 \tag{3.26a}$$

$$\int_{\Omega} \nabla p_1 \cdot \mathbf{v}_3 \, d\Omega = \int_{\Gamma} p_1 \mathbf{v}_3 \cdot \mathbf{n} \, d\Gamma \equiv 0 \tag{3.26b}$$

$$\int_{\Omega} \nabla p_3 \cdot \mathbf{v}_3 \, d\Omega = \int_{\Gamma} p_3 \mathbf{v}_3 \cdot \mathbf{n} \, d\Gamma \equiv 0 \tag{3.26c}$$

$$\int_\Omega \mathbf{v}_1 \nabla \mathbf{v}_1 \cdot \mathbf{v}_1 \, d\Omega = \int_\Omega \nabla \cdot [\mathbf{v}_1 \mathbf{v}_1 \cdot \mathbf{v}_1] \, d\Omega - \int_\Omega (\nabla \cdot \mathbf{v}_1) \mathbf{v}_1 \cdot \mathbf{v}_1 \, d\Omega \tag{3.27a}$$
$$= \int_\Omega \nabla \cdot [\mathbf{v}_1 \mathbf{v}_1 \cdot \mathbf{v}_1] \, d\Omega = \int_\Gamma \mathbf{v}_1 \cdot \mathbf{v}_1 \mathbf{v}_1 \cdot \mathbf{n} \, d\Gamma \equiv 0$$

$$\int_\Omega \mathbf{v}_1 \nabla \mathbf{v}_3 \cdot \mathbf{v}_3 \, d\Omega = \int_\Omega \nabla \cdot [\mathbf{v}_1 \mathbf{v}_3 \cdot \mathbf{v}_3] \, d\Omega - \int_\Omega (\nabla \cdot \mathbf{v}_1) \mathbf{v}_3 \cdot \mathbf{v}_3 \, d\Omega \tag{3.27b}$$
$$= \int_\Omega \nabla \cdot [\mathbf{v}_1 \mathbf{v}_3 \cdot \mathbf{v}_3] \, d\Omega = \int_\Gamma \mathbf{v}_3 \cdot \mathbf{v}_3 \mathbf{v}_1 \cdot \mathbf{n} \, d\Gamma \equiv 0$$

$$\int_\Omega \mathbf{v}_3 \nabla \mathbf{v}_3 \cdot \mathbf{v}_3 \, d\Omega = \int_\Omega \nabla \cdot [\mathbf{v}_3 \mathbf{v}_3 \cdot \mathbf{v}_3] \, d\Omega - \int_\Omega (\nabla \cdot \mathbf{v}_3) \mathbf{v}_3 \cdot \mathbf{v}_3 \, d\Omega \tag{3.27c}$$
$$= \int_\Omega \nabla \cdot [\mathbf{v}_3 \mathbf{v}_3 \cdot \mathbf{v}_3] \, d\Omega = \int_\Gamma \mathbf{v}_3 \cdot \mathbf{v}_3 \mathbf{v}_3 \cdot \mathbf{n} \, d\Gamma \equiv 0$$

where $\mathbf{v}_1$ and $\mathbf{v}_3$ are assumed to vanish on Γ, the boundary of region Ω. Also, we define the power $P^{(i)}$ as

$$\int_\Omega \mathbf{v}_0 \cdot \frac{\partial \mathbf{v}_0}{\partial t} = \frac{d}{dt} \int_\Omega \frac{1}{2} \mathbf{v}_0 \cdot \mathbf{v}_0 \, d\Omega \equiv \frac{dE^{(0)}}{dt} = P^{(0)} \tag{3.28}$$

$$\int_\Omega \mathbf{v}_1 \cdot \frac{\partial \mathbf{v}_1}{\partial t} = \frac{d}{dt} \int_\Omega \frac{1}{2} \mathbf{v}_1 \cdot \mathbf{v}_1 \, d\Omega \equiv \frac{dE^{(1)}}{dt} = P^{(1)} \tag{3.29}$$

$$\int_\Omega \mathbf{v}_3 \cdot \frac{\partial \mathbf{v}_3}{\partial t} = \frac{d}{dt} \int_\Omega \frac{1}{2} \mathbf{v}_3 \cdot \mathbf{v}_3 \, d\Omega \equiv \frac{dE^{(3)}}{dt} = P^{(3)} \tag{3.30}$$

With these simplifications, we may rewrite equations (3.22)-(3.24) as

$$\frac{dE^{(0)}}{dt} = -\int_{\Omega} A^2 \mathbf{v}_1 \cdot \nabla \mathbf{v}_1 \cdot \mathbf{v}_0 \, d\Omega - \int_{\Omega} B^2 \mathbf{v}_3 \cdot \nabla \mathbf{v}_3 \cdot \mathbf{v}_0 \, d\Omega \tag{3.31}$$

$$- \int_{\Omega} \nabla p_0 \cdot \mathbf{v}_0 \, d\Omega + \frac{1}{Re} \int_{\Omega} \nabla^2 \mathbf{v}_0 \cdot \mathbf{v}_0 \, d\Omega$$

$$= -\int_{\Omega} A^2 \left(u_1 \frac{\partial u_1}{\partial x} + v_1 \frac{\partial u_1}{\partial y} \right) U \, d\Omega - \int_{\Omega} B^2 \left(u_3 \frac{\partial u_3}{\partial x} + v_3 \frac{\partial u_3}{\partial y} + w_3 \frac{\partial u_3}{\partial z} \right) U \, d\Omega$$

$$+ \int_{\Omega} \frac{2}{Re} U \, d\Omega + \frac{1}{Re} \int_{\Omega} U \frac{d^2 U}{dy^2} \, d\Omega$$

$$\frac{dE^{(1)}}{dt} = -\int_{\Omega} A^2 \mathbf{v}_1 \cdot \nabla \mathbf{v}_0 \cdot \mathbf{v}_1 \, d\Omega - \int_{\Omega} AB^2 \mathbf{v}_3 \cdot \nabla \mathbf{v}_3 \cdot \mathbf{v}_1 \, d\Omega \tag{3.32}$$

$$+ \frac{1}{Re} \int_{\Omega} A^2 \nabla^2 \mathbf{v}_1 \cdot \mathbf{v}_1 \, d\Omega$$

$$= -\int_{\Omega} AB^2 \left(u_1 \left(u_3 \frac{\partial u_3}{\partial x} + v_3 \frac{\partial u_3}{\partial y} + w_3 \frac{\partial u_3}{\partial z} \right) + v_1 \left(u_3 \frac{\partial v_3}{\partial x} + v_3 \frac{\partial v_3}{\partial y} + w_3 \frac{\partial v_3}{\partial z} \right) \right) d\Omega$$

$$- \int_{\Omega} A^2 u_1 v_1 \frac{dU}{dy} \, d\Omega - \frac{1}{Re} \int_{\Omega} A^2 \left(\left(\frac{\partial u_1}{\partial x} \right)^2 + \left(\frac{\partial u_1}{\partial y} \right)^2 + \left(\frac{\partial v_1}{\partial x} \right)^2 + \left(\frac{\partial v_1}{\partial y} \right)^2 \right) d\Omega$$

$$\frac{dE^{(3)}}{dt} = -\int_{\Omega} AB^2 \mathbf{v}_3 \cdot \nabla \mathbf{v}_1 \cdot \mathbf{v}_3 \, d\Omega - \int_{\Omega} B^2 \mathbf{v}_3 \cdot \nabla \mathbf{v}_0 \cdot \mathbf{v}_3 \, d\Omega \tag{3.33}$$

$$+ \frac{1}{Re} \int_{\Omega} B^2 \nabla^2 \mathbf{v}_3 \cdot \mathbf{v}_3 \, d\Omega$$

$$= -\int_{\Omega} AB^2 \left(u_3^2 \frac{\partial u_1}{\partial x} + u_3 v_3 \left(\frac{\partial v_1}{\partial x} + \frac{\partial u_1}{\partial y} \right) + v_3^2 \frac{\partial v_1}{\partial y} \right) d\Omega - \int_{\Omega} B^2 u_3 v_3 \frac{dU}{dy} \, d\Omega$$

$$- \frac{1}{Re} \int_{\Omega} B^2 \left(\left(\frac{\partial u_3}{\partial x} \right)^2 + \left(\frac{\partial u_3}{\partial y} \right)^2 + \left(\frac{\partial u_3}{\partial z} \right)^2 + \left(\frac{\partial v_3}{\partial x} \right)^2 + \left(\frac{\partial v_3}{\partial y} \right)^2 + \left(\frac{\partial v_3}{\partial z} \right)^2 + \right.$$

$$\left. \left(\frac{\partial w_3}{\partial x} \right)^2 + \left(\frac{\partial w_3}{\partial y} \right)^2 + \left(\frac{\partial w_3}{\partial z} \right)^2 \right) d\Omega$$

where

$$\mathbf{v}(x,y,z,t) = (U(y),0,0) + A(u_1,v_1,0) + B(u_3,v_3,w_3) \quad .$$

For $B = 0$, (3.31)-(3.33) reduce to the system for two-dimensional linear primary instability, (2.21)-(2.22). As in Section 2, the last term on the right hand side of each equation represents the dissipation of kinetic energy in the flow. The scalar form of the dissipation in (3.32) and (3.33) was obtained by integration by parts. Note that only the mean flow pressure gradient contributes a net amount of energy to the system.

The remaining terms in (3.31)-(3.32) are responsible for transferring energy among the mean flow, the TS wave and the three-dimensional (3D) disturbance. In (3.31), the first term represents energy transferred into the mean flow $\mathbf{v}_0$ from the TS wave $A\mathbf{v}_1$, while the second term denotes energy transfer into the mean flow from the 3D disturbance $B\mathbf{v}_3$. In (3.32), we have the energy transferred into the TS wave from the mean flow in the first term and energy transferred into the TS wave from the 3D disturbance in the second term. Lastly, in (3.33), the first term represents energy transferred into the 3D disturbance from the TS wave and the second term represents energy transferred into the 3D disturbance from the mean flow. With these definitions, we can rewrite (3.31)-(3.33) as

$$\begin{aligned} \frac{dE^{(0)}}{dt} &= T^{(01)} + T^{(03)} + D^{(0)} \\ \frac{dE^{(1)}}{dt} &= T^{(10)} + T^{(13)} + D^{(1)} \\ \frac{dE^{(3)}}{dt} &= T^{(31)} + T^{(30)} + D^{(3)} \end{aligned} \tag{3.34}$$

Figure 3.1 diagrams the energetics in (3.34) to show how these equations are linked together. It can be shown (Appendix II) that the complimentary energy transfer terms $T^{(ij)}$ and $T^{(ji)}$ are equal in magnitude and opposite in sign, which yields

$$\frac{dE^{(0)}}{dt} = - T^{(10)} - T^{(30)} + D^{(0)} \tag{3.35}$$

$$\frac{dE^{(1)}}{dt} = T^{(10)} - T^{(31)} + D^{(1)} \tag{3.36}$$

$$\frac{dE^{(3)}}{dt} = T^{(31)} + T^{(30)} + D^{(3)} \quad . \tag{3.37}$$

As in Section 2, the mean flow pressure gradient p_0 has been lumped into the $D^{(0)}$ term for compactness. It now remains to substitute solution (3.17) for the fundamental mode and (3.18) for the subharmonic mode into (3.35)-(3.37), the details of which appear in Appendix II, and analyze the results.

It is possible to calculate the linear growth rate σ_r of the disturbance from the energy equation (3.37). Consider the definition of the kinetic energy for the disturbance from (3.20):

$$E^{(3)} = \frac{1}{2}\int_{\Omega} B^2 \mathbf{v}_3 \cdot \mathbf{v}_3 \, d\Omega \quad . \tag{3.38}$$

Differentiation of the above with respect to time gives

$$\frac{dE^{(3)}}{dt} = (2\sigma_r)\left(\frac{1}{2}\int_{\Omega} B^2 \mathbf{v}_3 \cdot \mathbf{v}_3 \, d\Omega \right) \tag{3.39}$$

recalling the exponential time dependence of both the fundamental and subharmonic modes. Continuing, we have

$$2\sigma_r = \frac{1}{E^{(3)}} \frac{dE^{(3)}}{dt} \tag{3.40}$$

thereby allowing the stability solutions (3.17) and (3.18) to be verified.

3.2. Results

We present here an extensive catalog of graphical results which describe in detail the energetics and vorticity dynamics of the linear secondary instability, intended as a future reference. Detailed plots of each term in the energy equation for the three-dimensional fundamental and subharmonic disturbances reveal the distribution of power throughout the channel and the interaction of the mean flow, the TS wave and the disturbance.

3.2.1. Stability of the Basic Flow v_2

Substitution of the basic flow (3.6) and either the fundamental (3.17) or the subharmonic (3.18) mode into the disturbance equations (3.11a,b,c) results in an eigenvalue problem for σ whose characteristic equation is of the form $f(\alpha,\beta,Re,A,c,\sigma) = 0$. This problem is solved by employing the spectral collocation technique outlined in Section 2 for the treatment of the y-direction.

The most unstable eigenvalues calculated for $\mathbf{v}_{f_s}$, $\mathbf{v}_{f_a}$ and $\mathbf{v}_s$ (Herbert 1983b) are given in Table 3.1 for conditions resembling the experiments of Nishioka, et al. (1980,1981) at the lowest Fourier truncation of (3.13) and (3.14). The associated eigenvectors for $\mathbf{v}_{f_s}$, $\mathbf{v}_{f_a}$ and $\mathbf{v}_s$ are found in figures 3.2, 3.3 and 3.4 respectively, where the curves connected by marks denote the imaginary part of the solution and the plain line, the real part. Notice that the fundamental solutions are either symmetric or anti-symmetric about the mid-plane of the channel, while the subharmonic mode is asymmetric. However, there is some correspondence between the real and imaginary parts of $\mathbf{v}_{(1)}$ and $\mathbf{v}_{(-1)}$. A plot of the eigenfunction of the TS wave at these conditions can be found in figure 3.5 for comparison with the solutions presented in Section 2. Notice the amount of activity concentrated in the vicinity of the critical layer in all four figures.

Table 3.1 - Most Unstable Eigenvalues of Basic Flow $\mathbf{v}_2$

Parameters:

$\alpha = 1.1200 \quad \beta = 2.0000 \quad Re = 5000.0$

$c_r = 0.281755 \quad A = 0.0250$

fundamental	subharmonic
sym: 0.0463259 + i0.0	0.04444923 ± i0.001926491
anti-sym: 0.04379846 + i0.0	

At sufficiently large amplitudes, Herbert found that the most unstable eigenmodes of the fundamental were perfectly tuned to the TS wave with $\sigma_i = 0$, whereas for the subharmonic mode he observed that $\sigma_i \to 0$ as $\beta \to \infty$. The asymmetric nature of the subharmonic cannot allow $\sigma_i = 0$, however. The growth rate σ_r of the disturbance was, in all cases, larger than the associated growth rate αc_i of the two-dimensional wave arising from viscous instability, which exemplifies the convective nature of the secondary instability.

The subharmonic and fundamental modes were found to strongly depend on the amplitude of the TS wave and also on the disturbance background. Three amplitude ranges could be distinguished:

$0 \leq A \leq A_s$: no 3D instability, flow is stable

$A_s \leq A \leq A_f$: subharmonic instability, growth rate increases with A

$A_f \leq A$: unstable to either mode

The appearance of either mode is contingent on the disturbance background level and its frequency content. These and other qualitative features of secondary instability, e.g. peak-valley splitting and longitudinal vortex formation - are in good agreement with observations. We conclude the low truncation order selected to keep the numerical problem manageable has negligible effect on predicting the onset of the secondary instability for a finite-amplitude TS wave in equilibrium.

The solutions for $\mathbf{v}_{f_s}$, $\mathbf{v}_{f_a}$ and $\mathbf{v}_s$ at the subcritical point indicated in Table 3.1 were then substituted into the energy equation for the disturbance (3.37) to examine the energetics of the secondary instability. As in Section 2, results were prepared for each term in (3.37) in the form of contour plots, plots of a single variable and the numerical results of

integrating the energy equation for the disturbance over region Ω.

3.2.2. Results of the Energy Analysis for the Fundamental Modes $\mathbf{v}_{f_s}$ and $\mathbf{v}_{f_a}$

To gain insight into the distribution of the power $P^{(3)}$, and each of the quantities $T^{(30)}$, $T^{(31)}$ and $D^{(3)}$ for each solution $\mathbf{v}_{f_s}$ and $\mathbf{v}_{f_a}$, throughout the region of interest Ω, we plotted contours of these functions at specific points. These figures resulted from selecting some x, y or z position in region Ω and then plotting in the remaining two variables. Steps in the x-, y- or z-directions were possible and desirable, in order to study the variation of the quantities of interest. Thus, steps in the z-direction give contours plotted in x and y, steps in x give contours in y and z and steps in y give contours in x and z. Examples of each type of plot for the power $P^{(3)}$ are found in figures 3.13, 3.25 and 3.37, respectively.

In figures 3.9, 3.13 and 3.17, we have the power $P^{(3)}$ of the symmetric mode $\mathbf{v}_{f_s}$ plotted near the origin at z positions $z =$ (-0.120830, -0.040277 and 0.040277). The "plotting window" is composed of the channel walls at $y = \pm 1$ on the vertical axis and by a horizontal axis, which is one TS wavelength λ_x long in the x-direction, forming a spanwise elevation view. The tick marks on the vertical axis define the positions of the critical layers $y = y_c$, as defined by (2.29).

In figures 3.21, 3.25 and 3.29, the contours are plotted at x positions of $x =$ (2.589225, 2.733071 and 2.876916), which corresponds to approximately $x = \lambda_x/2$, for the power $P^{(3)}$ of $\mathbf{v}_{f_s}$. Here, the "plotting window" is formed by the channel walls lying at $y = \pm 1$ on the vertical axis, and by a horizontal axis representing one wavelength λ_z in the z-direction, creating a streamwise elevation view. As before, the tick marks on the vertical axis represent the positions of the critical layers $y = y_c$.

A plan view of the power $P^{(3)}$ of the symmetric fundamental mode is shown in figures 3.33, 3.37 and 3.41, drawn at y positions of $y =$ (0.885456, 0.845190 and 0.799443) near the upper critical layer. The "plotting window" is formed by the vertical axis, representing one spanwise wavelength λ_z, and by the horizontal axis, which is one TS wavelength λ_x long.

The contours in each of these plots occur at 20 equally spaced intervals which are scaled to the minimum and maximum values calculated among $T^{(30)}$, $T^{(31)}$, $D^{(3)}$ and $P^{(3)}$ throughout region Ω, for both the symmetric and anti-symmetric modes of the fundamental solution. The narrow pen width indicates negative values of the quantity being plotted while the wide pen width denotes positive values and zero. Associated parameters are listed in the block below each plot.

Another set of contour plots was obtained by integrating $T^{(30)}$, $T^{(31)}$, $D^{(3)}$ and $P^{(3)}$ once in either the x-, y- or z-direction. The properties of Chebyshev polynomials (Schumann, Grötzbach and Kleiser 1979) were utilized for integration in the y-direction, defined over some interval $[y_0, y_1]$ as

$$f(x,z) = \int_{y_0}^{y_1} f(x,y,z)\, dy \quad . \tag{3.41}$$

An example of applying integral (3.41) to the energy equation for the disturbance (3.37) is found in figure 3.53, for the power of the symmetric mode, whose configuration corresponds entirely to that of the plan view in figure 3.37. For all plots of this type, the interval [0,1] was chosen for integral (3.41) to filter out the influence of the lower half plane from the result. In the x- and z-direction, we define the average of the function f

over one wavelength as

$$\bar{f}(y,z) = \frac{1}{\lambda_x} \int_{x_0}^{\lambda_x + x_0} f(x,y,z)\, dx \tag{3.42}$$

$$\bar{f}(x,y) = \frac{1}{\lambda_z} \int_{z_0}^{\lambda_z + z_0} f(x,y,z)\, dz \quad . \tag{3.43}$$

The points x_0 and z_0 are totally arbitrary and have no effect on the result. The normal mode assumption (3.12) gives rise to integrals in equations (3.35)-(3.37) of the form (3.42) and (3.43) which are of closed form thus requiring no numerical treatment. Averaging $P^{(3)}$ for the symmetric mode in either the x- or z-direction according to (3.42) or (3.43) results in figures 3.49 and 3.45 respectively, whose configurations are analogous to the streamwise and spanwise elevations of figures 3.25 and 3.13 .

When any two of the integrals (3.41), (3.42) or (3.43) are applied to the energy equation (3.37), a function in one of the variables x, y or z results, as in figures 3.57, 3.61 and 3.65 for the power $P^{(3)}$ of the symmetric mode. In figure 3.57, we have $P^{(3)}$ plotted as a function of the streamwise variable x over one TS wavelength λ_x. Similarly, $P^{(3)}$ is plotted over one spanwise wavelength λ_z in figure 3.61, with the origin at the midpoint of the horizontal axis. The distribution of $P^{(3)}$ across the channel as a function of y is found in figure 3.65. The origin lies at the midpoint of the dashed line which represents the center of the channel. All pertinent parameters are listed in the block below each plot, including the minimum and maximum values of the function in the figure.

The power $P^{(3)}$ transferred into the disturbance $B\mathbf{v}_3$ from the basic flow $\mathbf{v}_2$ is

presented in the various plots described, beginning in figure 3.9 and continuing in every fourth plot thereafter, for the symmetric and anti-symmetric mode of the fundamental solution. Similar results are presented for the three terms in the energy equation (3.37) $T^{(30)}$, $T^{(31)}$ and $D^{(3)}$ beginning with figures 3.6, 3.7 and 3.8, respectively, for the symmetric mode. Those for the anti-symmetric mode start with figures 3.66, 3.67, 3.68 and 3.69.

We notice from these plots that the power $P^{(3)}$ of both modes, in addition to the terms $T^{(30)}$, $T^{(31)}$ and $D^{(3)}$, is periodic in both the streamwise and the spanwise directions, which arises from the periodicity of both the disturbance and the basic flow. We see in the spanwise elevations in figures 3.37 and 3.97 for the two modes, highly localized areas of peak power, also evident in other views, that are of a different nature than in primary instability. A closer look at each term comprising equation (3.37), beginning with the symmetric mode, reveals further characteristics of the energetics affecting the secondary instability.

The energy transferred from the TS wave into the disturbance $T^{(31)}$ appears in figures 3.6, 3.18 and 3.30 at various locations in region Ω. We see in the spanwise elevation views of figures 3.6, 3.10 and 3.14 that the TS wave is drawing energy from the disturbance, indicated by the two small negative regions in the channel at $x = (0.3\lambda_x$ and $0.7\lambda_x)$ near the lower and upper critical layers, respectively. The plan views afforded by figures 3.30, 3.34 and 3.38 reveal these regions are somewhat larger near $y = y_c$ and that they are aligned periodically in the spanwise direction at an x position of $x = 0.7\lambda_x$. The once-integrated forms of $T^{(31)}$ found in figures 3.42, 3.46 and 3.50 also show the transfer of energy out of the disturbance and into the TS wave occurs in periodic, concentrated regions near the critical layers y_c.

When $T^{(31)}$ is twice integrated, figures 3.54, 3.58 and 3.62 result, corresponding to

functions of x, y or z. The streamwise distribution of $T^{(31)}$ in figure 3.54 is asymmetrical with a peak in the energy transferred to the TS wave occurring at $x = 0.7\lambda_x$. Plotted as a function of y in figure 3.58, we see that the maxima in $T^{(31)}$ are associated with the position of the critical layers y_c, while there is no activity in the center of the channel. We also notice a weak spanwise variation of $T^{(31)}$ in figure 3.62, with peaks lying at $z = (-\lambda_z/2, 0$ and $\lambda_z/2)$. Therefore, we see from these and previous figures that the small amount of energy transferred from the disturbance into the TS wave is confined to regions that are arranged periodically in the spanwise direction at an x position of $x = 0.7\lambda_x$, in the vicinity of the critical layers.

The transfer of energy from the mean flow into the disturbance $T^{(30)}$, the second term in (3.37), appears in figures 3.7, 3.19 and 3.31 at the points mentioned previously. In the spanwise elevation views of figures 3.7, 3.11 and 3.15, we see steep energy peaks lying near the critical layers which are centered at $x = (0, \lambda_x/2$ and $\lambda_x)$, in an alternating pattern in the upper and lower halves of the channel, which is out of phase with $T^{(31)}$. A streamwise view, as in figures 3.19, 3.23 and 3.27, confirms this alternating pattern since only the upper peak from the previous view shows up, while the streamwise average in figure 3.47 shows both peaks. The spanwise periodic arrangement of these regions is revealed in the plan views of figures 3.31, 3.35 and 3.39 and also in figure 3.51, where $T^{(30)}$ has been integrated in the y-direction. We also see in these plots that $T^{(30)}$ is symmetric in both the streamwise and spanwise directions, in contrast to $T^{(31)}$.

The twice integrated result of $T^{(30)}$ can be found figures 3.55, 3.59 and 3.63 and these show that the magnitude of the energy transferred into the disturbance from the mean flow is an order of magnitude greater than $T^{(31)}$. We also see that $T^{(30)}$ is symmetric in the x-

and z-directions in figures 3.55 and 3.63 respectively. In figure 3.59, the distribution of $T^{(30)}$ across the channel is strongly concentrated near the critical layers and reveals that this is the source of power in the secondary instability.

The dissipation $D^{(3)}$ of kinetic energy contained in the disturbance can be found in figures 3.8, 3.20 and 3.32 at selected points. We see in the spanwise views of figures 3.8, 3.12 and 3.16 that the peak in the dissipation coincides with the maxima of $T^{(30)}$ in figures 3.7, 3.11 and 3.15. Similar observations can be made concerning the streamwise views in figures 3.20, 3.24 and 3.28. From these two views, we also see the dissipation is confined to the vicinity of the critical layers, whereas the remainder of the channel remains nearly inviscid. This trend is also reflected in the plan views in figures 3.32, 3.36 and 3.40 at y positions near $y = y_c$, where we notice the dissipation decreases rapidly away from the wall. The distribution of $D^{(3)}$ across the channel in figure 3.60 also confirms this property. The remaining two single variable plots, figures 3.56 and 3.64, are distributionds of $D^{(3)}$ in the x- and z-directions respectively. They reveal the streamwise and spanwise periodicity of $D^{(3)}$ and also show that the magnitude of the dissipation lies between that of $T^{(30)}$ and $T^{(31)}$.

The graphical results for the power of the disturbance $P^{(3)}$, and each of the terms $T^{(30)}$, $T^{(31)}$ and $D^{(3)}$ for the anti-symmetric mode, begin with figure 3.66 and are qualitatively similar to those discussed previously for the symmetric mode. The energy transfer term $T^{(31)}$ is negative and considerably smaller than $T^{(30)}$, the two also being out of phase. In addition, both the maximum energy transfer and the dissipation are confined to the vicinity of the critical layer.

The result of integrating the energy equation for the disturbance (3.37) over region Ω

using the integrals defined by (3.41), (3.42) and (3.43) appears in Table 3.2 for both the symmetric and the anti-symmetric modes of the fundamental solution (3.17) at the conditions listed. In this instance, the limits of integral (3.41) were chosen to include both halves of the channel. The bar over each quantity in Table 3.2 indicates normalization of these quantities with respect to the kinetic energy of the disturbance, $E^{(3)}$. Such normalization directly relates $\overline{T}^{(30)}$, $\overline{T}^{(31)}$ and $\overline{D}^{(3)}$ to the growth rate of the disturbance σ_r, as in equation (3.40). We also have the results for equations (3.35) and (3.36) listed in Table 3.3, for the mean flow and the TS wave respectively with the amplitude of the disturbance selected such that $B = A$.

The results in Table 3.2 for the symmetric and anti-symmetric modes of the fundamental solution are quantitatively consistent with the observations drawn from the graphical results presented earlier and reflect the results of Orszag & Patera (1983). Consider the energy transfer terms first. Notice $\overline{T}^{(31)}<0$, which indicates that energy is transferred into the TS wave from the disturbance, while $\overline{T}^{(30)}>0$ reveals that the mean flow is supplying energy directly to the disturbance, and at a rate 14 times greater than $\overline{T}^{(31)}$. As in primary instability, the dissipation $\overline{D}^{(3)}$ is stabilizing and opposes the growth of the disturbance at a rate four times greater than $\overline{T}^{(31)}$. Also, the anti-symmetric mode is more stable, with a smaller growth rate σ_r, than the symmetric solution. Notice the growth rate calculated σ_{cal} as per equation (3.40), is in good agreement with that provided by the stability analysis.

We see that the results in Table 3.3 reflect the behavior of the primary instability discussed in Section 2. The TS wave draws a small amount of energy, compared to the secondary instability, from the mean flow v_0, and $D^{(1)}$ acts to balance this increase in available energy through viscous dissipation. However, the small amount of energy added by $T^{(31)}$

Table 3.2 - Results of Energy Equation (3.37) for v_{f_s} and v_{f_a}

Parameters:

$\alpha = 1.1200 \quad \beta = 2.0000 \quad Re = 5000.0$

$c_r = 0.281755 \quad A = 0.0250 \quad \sigma_i = 0$

σ_r	0.04379846 (anti-sym)	0.0463259 (sym)
$\overline{T}^{(31)}$	-0.01070059	-0.01093845
$\overline{T}^{(30)}$	0.1473161	0.1511337
$\overline{D}^{(3)}$	-0.04901898	-0.04754367
σ_{cal}	0.04379827	0.04632577

Table 3.3 - Result of Equations (3.35) and (3.36) for $\mathbf{v}_{f_s}$ and $\mathbf{v}_{f_a}$

Parameters:

$\alpha = 1.1200 \quad \beta = 2.0000 \quad Re = 5000.0$

$c_r = 0.281755 \quad A = B = 0.0250$

Case:	anti-symmetric	symmetric
$10^4 \cdot T^{(01)}$	-0.03397285	-0.03397285
$10^4 \cdot T^{(03)}$	-0.6607110	-0.7108149
$10^4 \cdot D^{(0)}$	0.0	0.0
$10^4 \cdot P^{(0)}$	-0.6946838	-0.7447878
$10^4 \cdot T^{(10)}$	0.03397285	0.03397285
$10^4 \cdot T^{(13)}$	0.04799194	0.05144587
$10^4 \cdot D^{(1)}$	-0.04841452	-0.04841452
$10^4 \cdot P^{(1)}$	0.03355031	0.03700424

upsets this balance, resulting in growth of the TS wave.

3.2.3. Results of Energy Analysis for the Subharmonic Modes v,

The numerical and graphical techniques which were outlined in the previous section containing the results of the energy analysis for the fundamental solution (3.13) were next applied to the subharmonic solution of our Floquet system of equations (3.14). The doubly periodic nature of this mode necessitates a minor but important modification to our methods by extending the integration region Ω one additional TS wavelength in the streamwise direction. Then, Ω measures one spanwise wavelength λ_z in width, two TS wavelengths λ_x in length and spans the entire channel from $-1 \leq y \leq 1$ in the y-direction. We prepared numerical and graphical results for the power of the disturbance $P^{(3)}$ and each of the terms in the energy equation, $T^{(31)}$, $T^{(30)}$ and $D^{(3)}$ for the subharmonic mode of secondary instability listed in Table 3.1.

The graphical results begin with contour plots, much the same as those previous, in figures 3.126-3.161 for the three-dimensional functions $T^{(31)}$, $T^{(30)}$, $D^{(3)}$ and $P^{(3)}$ in views along each coordinate direction x, y and z at selected points throughout the region Ω. These views have been denoted as streamwise elevation, plan view and spanwise elevation, respectively. The streamwise elevations in figures 3.138-3.149 are positioned at $x =$ (5.178450, 5.466141 and 5.753833) which corresponds to a mid-channel position of approximately $x = \lambda_x$. The spanwise elevations in figures 3.126-3.137 and the plan views in figures 3.150-3.161 were plotted at the same locations as for the fundamental solution, at $z =$ (-0.120830, -0.040277 and 0.040277) at the channel center and near the upper critical layer $y =$ 90.885456, 0.845190 and 0.799443), respectively.

If the three-dimensional functions in the views above are integrated in only one of the three coordinate directions, then the two-dimensional functions in figures 3.162-3.173 result for $T^{(31)}$, $T^{(30)}$, $D^{(3)}$ and $P^{(3)}$. We integrated over the upper half of the channel in this instance, to remove the effects of the lower half of the channel form the result, as defined in equation (3.41). In the x-direction, we modified the average defined in (3.42) to allow for the extended period of the subharmonic as follows:

$$\overline{f}(y,z) = \frac{1}{2\lambda_x} \int_{x_0}^{x_0+2\lambda_x} f(x,y,z)\, dx. \tag{3.44}$$

The average in the z-direction defined by (3.43) remains unchanged. Integration in any two of the three coordinates yields functions of the type presented in figures 3.174-3.185, which are streamwise, spanwise and cross-channel distributions of each term, respectively. The configuration of each type of plot discussed here is completely analogous to those for the fundamental solution, excepting of course, the inclusion of an additional TS wavelength in the streamwise direction where applicable.

The power $P^{(3)}$ exchanged between the subharmonic mode of the disturbance $B\mathbf{v}_3$ and the basic flow $\mathbf{v}_2$ is found in figures starting with 3.129 and continuing with every fourth plot thereafter. These plots confirm the periodic nature of the subharmonic solution (3.18) and also reveal highly localized regions of peak power distributed periodically throughout Ω . Further examination of the results for each of the three terms in the energy equation (3.37), $T^{(31)}$, $T^{(30)}$ and $D^{(3)}$, reveals more detailed information concerning the energetics of the secondary instability.

Looking at the energy transferred into the disturbance from the TS wave, denoted by

$T^{(31)}$, we first consider the spanwise elevations of figures 3.126, 3.130 and 3.134, the streamwise elevations of figures 3.138, 3.142 and 3.146 and the plan views of figures 3.150, 3.154 and 3.158 at discrete positions within Ω. Small, clearly defined regions of negative energy transfer, periodically arranged in the streamwise and spanwise directions are evident. Figures 3.162, 3.166 and 3.170 resulting from integrating $T^{(31)}$ once in each of the three spatial directions show that the negative regions in the upper half of the channel are about T/4 out of phase with respect to those in the lower half of the channel, in both the streamwise and spanwise directions, where we allow T to assume the period of $T^{(31)}$ in either the x- or z-directions. We also notice that $T^{(31)}$ is not symmetric about the x-axis in the plan views, indicating the imaginary part of the subharmonic solution (3.14) contributes a small phase shift. The importance of tuning the disturbance to the phase speed of the TS wave is clearly displayed in the concentration near the upper and lower critical layers of the energy transfer into the TS wave. The distribution of $T^{(31)}$ across the channel in figure 3.178, obtained by averaging in x and z, confirms that the TS wave extracts energy from the disturbance in the immediate vicinity of the critical layers, with virtually no activity in the channel center. Figures 3.174 and 3.182, the streamwise and spanwise distributions of $T^{(31)}$ respectively, reveal this energy extraction varies periodically in x and z, with peaks at $x = (0.3\lambda_x, 0.7\lambda_x, 1.3\lambda_x \text{ and } 1.7\lambda_x)$ and at $z = (-0.25\lambda_z \text{ and } 0.25\lambda_z)$.

$T^{(30)}$ is the second term in the energy equation (3.37) and the spanwise elevations in figures 3.127, 3.131 and 3.135, the streamwise elevations in figures 3.139, 3.143 and 3.147 and the plan views in figures 3.151, 3.155 and 3.159 show a much higher level of energy transfer from the mean flow into the disturbance than we saw for $T^{(31)}$. The results of integrating $T^{(30)}$ once in each of the three coordinate directions plotted in figures 3.163, 3.167 and 3.171 reveal very steep energy peaks with similar spanwise arrangement in Ω to

$T^{(31)}$. Again, the peaks in the upper half of the channel are approximately T/4 out of phase with those in the lower half of the channel, in both x and z directions, where T is the period of $T^{(30)}$. Plan views show that $T^{(30)}$ also is not symmetric about the x-axis, a direct result of the imaginary part of the subharmonic solution (3.14). The increase in the magnitude of $T^{(30)}$ over that of $T^{(31)}$ becomes readily apparent when we consider figures 3.175, 3.179 and 3.183, resulting from integrating $T^{(30)}$ in any two directions,where we see that $T^{(30)}$ is an order of magnitude greater than $T^{(31)}$. The importance of the critical layer in enhancing the transfer of energy into the disturbance from the mean flow is reiterated in the distribution of $T^{(30)}$ across the channel as depicted in figure 3.179. The streamwise and spanwise distributions of $T^{(30)}$ in figures 3.175 and 3.183 respectively, indicate that energy is drawn from the mean flow in a periodic fashion, with energy peaks occurring at $x = (0.80\lambda_x$ and $1.8\lambda_x)$ and also at $z = (-0.25\lambda_z$ and $0.25\lambda_z)$.

The dissipation $D^{(3)}$ of kinetic energy in the disturbance appears in spanwise elevations in figures 3.128, 3.132 and 3.136, in streamwise elevations in figures 3.140, 3.144 and 3.148 and in plan views in figures 3.152. 3.156 and 3.160. These views show periodically arranged, localized areas of peak dissipation that are coincident with $T^{(30)}$. The once-integrated results in figures 3.164, 3.168 and 3.172 confirm that viscous effects are limited to the two regions near the channel walls. The distribution of $D^{(3)}$ across the channel in figure 3.180, in conjunction with the plan views, reiterate the confinement of viscous effects in the regions defined by the upper and lower critical layers and the channel walls, with the channel center nearly inviscid. The streamwise and spanwise distributions of $D^{(3)}$ in figures 3.176 and 3.184 respectively, are negative and remain nearly constant over Ω.

The result of integrating the energy equation for the disturbance (3.37) in all three

coordinate directions according to the integrals defined in (3.41), (3.43) and (3.44) appear in Table 3.4 for the subharmonic mode listed in Table 3.1. An interval including both halves of the channel was necessary for applying integral (3.41), in this instance. The bar over each quantity in Table 3.4 indicates normalization with respect to the kinetic energy $E^{(3)}$ of the disturbance, which directly relates $\overline{T}^{(31)}$, $\overline{T}^{(30)}$ and $\overline{D}^{(3)}$ to the growth rate of the disturbance σ_r, as in equation (3.40).

We see the numerical results in Table 3.4 are quantitatively consistent with the graphical results discussed previously. Notice that the TS wave draws a small amount of energy from the disturbance which is comparable to that extracted from the mean flow by the Reynolds stress $T^{(10)}$. However, the mean flow supplies 9 times the amount of energy to the disturbance through $T^{(30)}$ than is lost via $T^{(31)}$. The dissipation $D^{(3)}$ is stabilizing and is twice as large as $T^{(31)}$, but the magnitude of the energy exchange term $T^{(30)}$ dominates, leading to an unstable condition with $P^{(3)} > 0$. Excellent agreement was obtained between the calculated growth rate σ_{cal} and the growth rate supplied from the stability analysis σ_r, thereby providing a check of solution (3.14).

The results listed in Table 3.5 complete the energy balance of the system of equations in (3.35)-(3.37) with $B = A$ and reveal additional details concerning the physics of the secondary instability. The mean flow terms $T^{(01)}$ and $T^{(03)}$ are both negative which suggests that the mean flow pressure gradient is the source of energy for the instability, by supplying $T^{(30)}$. Also, we see the TS wave draws a small amount of energy from the mean flow $\mathbf{v}_0$ via the Reynolds stress $T^{(10)}$ whereas the dissipation $D^{(1)}$ seeks to balance this increase in available energy through viscous dissipation. However, the energy added from the disturbance through $T^{(31)}$ upsets this balance, resulting in an unstable condition with $P^{(1)} > 0$. Plots of

Table 3.4 - Results of Energy Equation (3.37) for $\mathbf{v}_\theta$

Parameters:

$\alpha = 1.1200 \quad \beta = 2.0000 \quad Re = 5000.0$

$c_r = 0.281755 \quad A = 0.0250$

$\sigma = 0.04444923 \pm 0.001926491$

$\overline{T}^{(31)}$	-0.014347928
$\overline{T}^{(30)}$	0.1321063
$\overline{D}^{(3)}$	-0.02885990
σ_{cal}	0.04444923

Table 3.5 - Result of Equations (3.35) and (3.36) for $\mathbf{v}_s$

Parameters:

$\alpha = 1.1200 \quad \beta = 2.0000 \quad Re = 5000.0$

$c_r = 0.281755 \quad A = B = 0.0250$

$10^4 \cdot T^{(01)}$	-0.06794579	$10^4 \cdot T^{(10)}$	0.06794579
$10^4 \cdot T^{(03)}$	-0.6121409	$10^4 \cdot T^{(13)}$	0.6648399
$10^4 \cdot D^{(0)}$	0.0	$10^4 \cdot D^{(1)}$	-0.09682906
$10^4 \cdot P^{(0)}$	-0.6461137	$10^4 \cdot P^{(1)}$	0.03760074

the Reynolds stress and the dissipation for the basic flow $\mathbf{v}_2$ appear in figures 3.186-3.191 which are completely analogous to those in Section 2 for primary instability. As in Section 2, the Reynolds stress is concentrated near the critical layers. We also see a balance existing between the Reynold stress and dissipation, whose outcome determines the stability of the basic flow.

At this point, it is now possible to make some comparisons between the results obtained for the fundamental and subharmonic modes of the secondary instability. The graphical and numerical results presented for both solutions are similar in many respects, even though the subharmonic mode is doubly periodic with wavelength $2\lambda_z$ in the streamwise direction.

We saw in the various views of the two- and three-dimensional functions for the transfer of energy from the TS wave to the fundamental disturbance, denoted by $T^{(31)}$, that on the average, energy was actually drawn into the TS wave within clearly defined regions in the flow. A comparably small amount of energy also flowed into the TS wave from the subharmonic disturbance, but there were twice as many areas in which the energy transfer occurred, owing to the longer period of the subharmonic. In addition, these regions were arranged in phase with respect to the lower half of the channel in the spanwise direction for the fundamental mode, but were out of phase for the subharmonic mode. The phase difference is due to the contribution of the imaginary part of the subharmonic solution (3.18). In both instances, all energy transfer is concentrated in the immediate vicinity of the upper and lower critical layers.

The graphical and numerical results presented for the transfer of energy into the disturbance from the mean flow revealed that $T^{(30)}$ is roughly an order of magnitude greater

than $T^{(31)}$, indicating that it is $T^{(30)}$ which drives the secondary instability. This agrees in a qualitative sense with Orszag & Patera (1983). We also saw that there were twice as many peaks in $T^{(30)}$ in the x-direction for the subharmonic as for the fundamental, with comparable total amounts of energy transferred. These energy peaks are out of phase with respect to the lower half of the channel in the spanwise direction for the subharmonic, but are in phase for the fundamental. As for $T^{(31)}$, this is because the imaginary part of the subharmonic mode contributes a small phase shift. In both cases, all energy transfer is limited to the critical layers.

The dissipation for both fundamental and subharmonic modes exhibit similar characteristics. There are twice as many regions of peak dissipation in the streamwise direction for the subharmonic as for the fundamental. However, these peaks are arranged in phase in the spanwise direction for both modes, but they are not of similar shape in the two channel halves for the subharmonic because of the asymmetric nature of the subharmonic. For both modes, all viscous effects were seen to be limited to the regions between the critical layers and the channel walls, with the channel center remaining nearly inviscid. The similarity of these results for the fundamental and subharmonic modes on a local scale indicates that the mechanism affecting the stability of each mode is identical in nature.

The results compiled so far for the fundamental and subharmonic solutions have enabled us to trace the transfer of energy among the mean flow, the TS wave and the disturbance so as to characterize secondary instability. The viscous solution for plane Poiseuille flow tells us that the mean flow pressure gradient drives the flow, and the results in Tables 3.3 and 3.5 confirm this as the source of energy in the flow. However, the presence of infinitesimal disturbances in a specific band of wavenumbers leads to the slow growth of

small TS waves which are due to the formation of viscous stresses, known as the Reynolds stress, in the critical layer. It is the balance of these stresses and dissipative forces which then determine the stability of the flow. Interestingly, even at the subcritical point considered in this analysis, non-linearities in the Navier-Stokes equations, which are important on the viscous timescale of primary instability, allow finite-amplitude equilibrium states to exist.

When the amplitude of such an equilibrium state exceeds a threshold value of typically 1%, our knowledge of secondary instability (Herbert 1983b) tells us that resonance with the TS wave occurs, amplifying either fundamental or subharmonic three-dimensional disturbances from the background noise environment. The ability of the disturbance to tune itself to the speed of the TS wave is extremely important because we saw the critical layer provides optimum conditions for the transfer of energy. For the fundamental, where perfect tuning of the basic flow and the disturbance was achieved, and for the subharmonic, where the TS wave and the disturbance were only slightly mistuned, strong, direct energy transfer occurred in several small areas distributed periodically in the upper and lower critical layers. In addition, the TS wave draws a small amount of energy from the disturbance, leading to further growth of the basic flow and in turn, the disturbance, thus establishing a self-sustaining instability mechanism causing the flow to experience transition soon thereafter.

Clearly, the TS wave catalyzes the secondary instability through its ability to resonate with low level three-dimensional noise, and also to tune the disturbances to its phase speed, allowing energy transfer to easily occur. However, the TS wave also mediates the transfer of energy into the disturbance from the basic flow, propelling the instability from a viscous to

a convective timescale.

3.2.4. Vorticity Considerations

The primary viscous instability discussed in Section 2 establishes streamwise-periodic, two-dimensional concentrations of vorticity near the critical layer. However, the three-dimensional nature of the secondary instability creates three components of vorticity $\omega_3 = (\xi_3, \eta_3, \varsigma_3)$, for the disturbance which have been defined in equation (3.19). We have plotted each component of ω_3 in contour plots very similar to those for the energy, for the fundamental and subharmonic modes of the secondary instability. The symmetric and anti-symmetric modes of the fundamental solution appear in figures 3.192-3.200 and 3.201-3.209, respectively. Those for the subharmonic can be found in figures 3.210-3.218. Spanwise elevations, streamwise elevations and plan views of the vorticity were plotted at the same points selected for the plots of the energy, except for the streamwise elevations of ξ_3 and η_3, which were plotted at $z = 0.765260$ or $z = 0.25\lambda_z$.

We see from these figures that the vorticity is concentrated in the two viscous critical layers near the walls, whereas the remainder of the channel is nearly inviscid. Thus, the maxima in the vorticity and the energy coincide. reinforcing the importance of the critical layer. These figures also show that the secondary instability proceeds by lifting regions of concentrated spanwise vorticity ς_3 towards the channel center where they are convected downstream. The inherent stretching and tilting of the vorticity as it moves downstream is what gives rise to the explosive growth rates associated with secondary instability. In addition, the spanwise vorticity component ς_3, in conjunction with the streamwise component ξ_3 are responsible for the formation of the large-scale Λ-shaped three-dimensional structures which become evident following the onset of the instability. The normal component

appears to be too weak to make any noticable contribution. Notice the imaginary part of the subharmonic mode again contributes a phase shift, this time to the vorticity, as seen in the plan views of figures 3.216-3.218.

4. Conclusions

We have successfully completed a study of primary and secondary instability mechanisms in plane Poiseuille flow through the use of energy methods. Primary instability arises from classical, two-dimensional linear hydrodynamic stability analysis, while secondary instabilities occur when a periodic, two-dimensional basic flow becomes unstable with respect to fundamental and subharmonic classes of three-dimensional disturbances at some threshold amplitude of the basic flow. A spectral-collocation numerical technique, in conjunction with extensive plotting procedures, allowed us to characterize the energetics involved in each of these two instabilities.

In both the primary and secondary instabilities, we found that tuning of the disturbance with respect to the basic flow allowed optimum conditions for the transfer of energy to exist at the critical layer. This explains why the most unstable modes of the fundamental and subharmonic solutions have the smallest value of σ_i, the relative phase speed of the disturbance. The graphical results presented so far have revealed that all energy transfer, for both the primary and secondary instabilities, is concentrated in the critical layer. In addition, these regions of energy exchange are arranged periodically in the streamwise direction for primary instability, and in both the streamwise and spanwise directions for secondary instability. Vorticity calculations also showed that these peaks lie near positions of maximum vorticity.

We saw in Section 2 that the primary instability mechanism establishes viscous stresses by enforcing the boundary conditions at the channel walls. Consequently, the stability of the mean flow to two-dimensional disturbances depends directly on the balance of viscous stresses and dissipative forces. We see a similar balance of forces in secondary ins-

tability, but of a more subtle nature. Here, the instability is driven by the strong, direct transfer of energy from the mean flow into the three-dimensional disturbance, denoted by $T^{(30)}$, in periodic regions in the critical layer for both fundamental and subharmonic modes. However, the relatively small amount of energy drawn from the disturbance into the TS wave, denoted as $T^{(31)}$, was seen to initially catalyze and later mediate the exchange of energy via $T^{(30)}$, once a threshold TS amplitude of about 1% is reached. At the onset of the secondary instability, the addition of energy through $T^{(31)}$ causes the TS amplitude to grow even further, leading to more energy exchange between the mean flow and the disturbance, thus establishing a self-sustaining instability mechanism with the rapid growth rates which have been observed immediately prior to transition.

We conclude from this analysis that the TS wave catalyzes the instability by resonating with low-level noise at specific fundamental or subharmonic frequencies. Once the instability has been established, the TS wave then mediates the strong transfer of energy between the three-dimensional disturbance and the mean flow that leads to the explosive growth rates associated with the instability. We also saw that the critical layer plays an important role in both primary and secondary instability by providing conditions conducive to energy transfer. The similarity of the regions of energy transfer for the fundamental and the subharmonic modes on a local scale suggests that the secondary instability establishes an energy field in shear flows which varies only in the exact placement of these peaks in the flow. This explains the universal nature of the instability observed by Orszag & Patera (1983) in the various shear flows they studied, e.g. the boundary layer, plane Couette flow, pipe Poiseuille flow and plane Poiseuille flow. The numerical and graphical techniques developed for this analysis may be easily modified in order to study these other flows, because a similar catalog of the energy and vorticity fields present would certainly be

desirable for use in documenting the secondary instability.

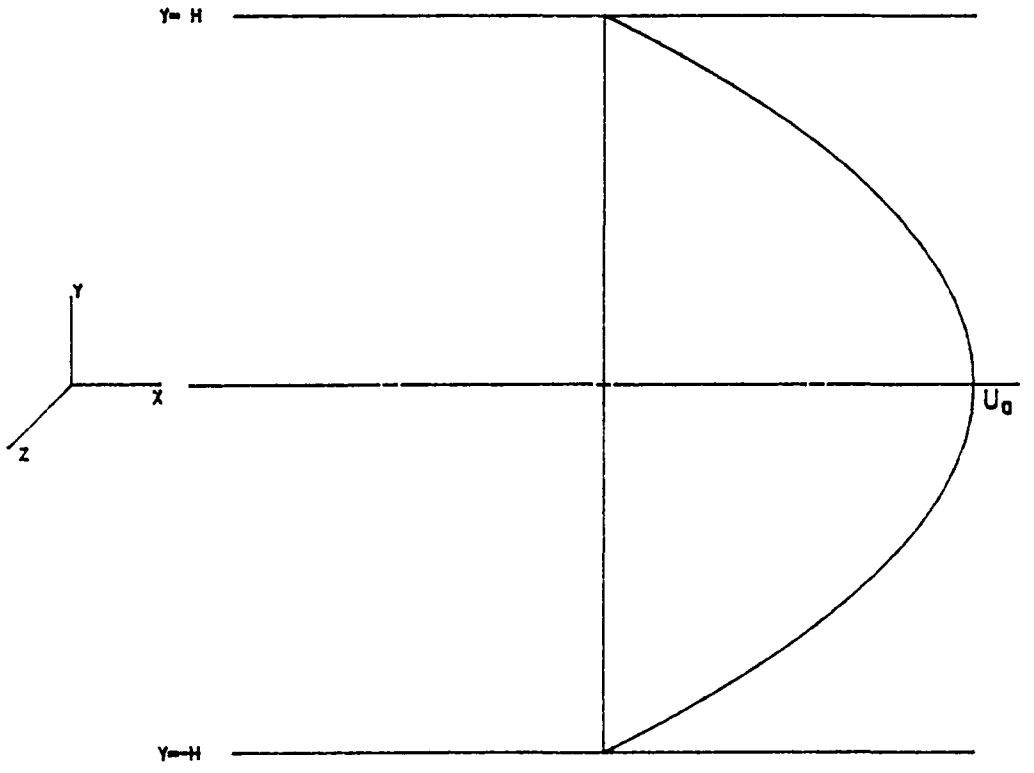

Figure 2.1- Schematic of plane Poiseuille flow.

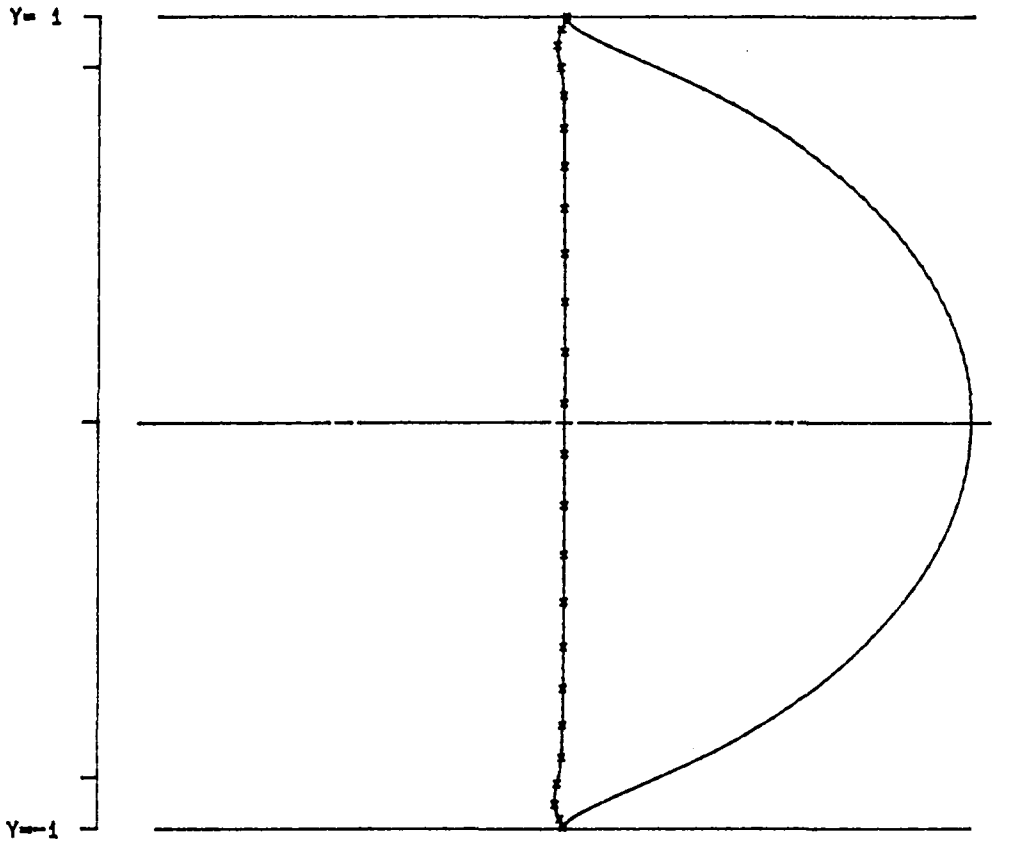

EIGENFUNCTION PSI(Y)

RE	10000.0	CR	0.237526
ALPHA	1.0000	CI	0.003740

PSI(0) = 1

Figure 2.2- Eigenfunction of OSE for $\alpha = 1.000$, $Re = 10000$.

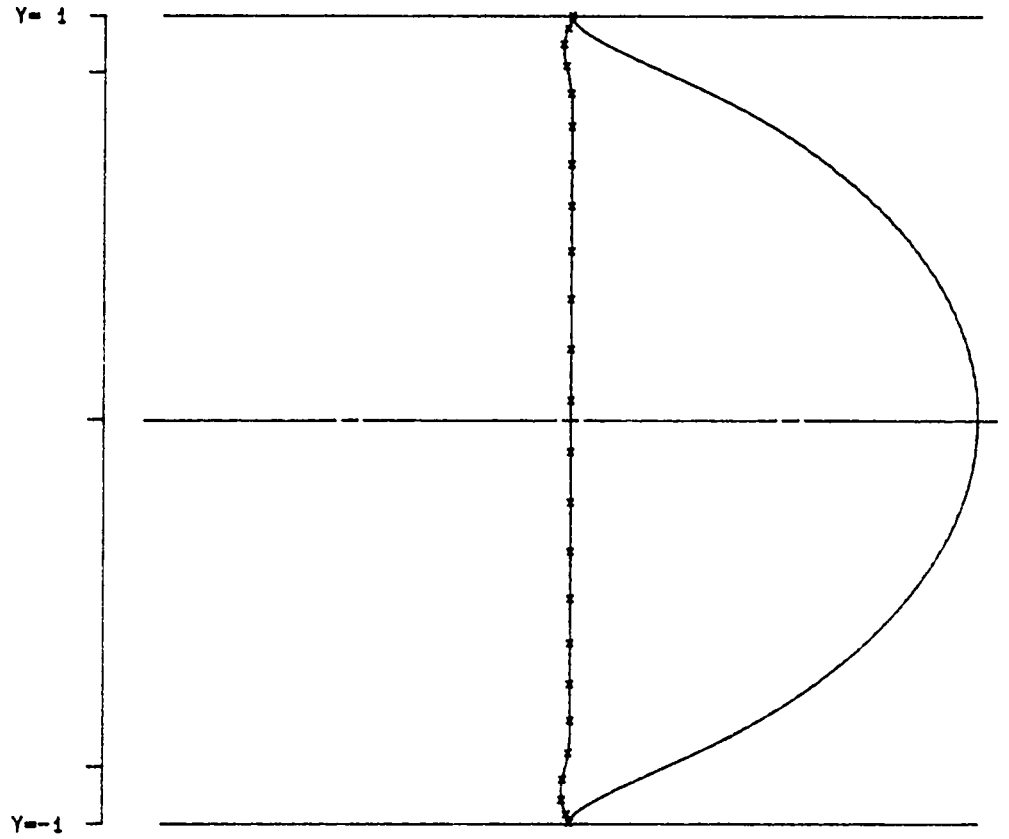

EIGENFUNCTION PSI(Y)

RE	5772.2	CR	0.264002
ALPHA	1.0206	CI	-0.000000

PSI(0) = 1

Figure 2.3- Eigenfunction of OSE for $\alpha = 1.02056$, $Re = 5772.2$.

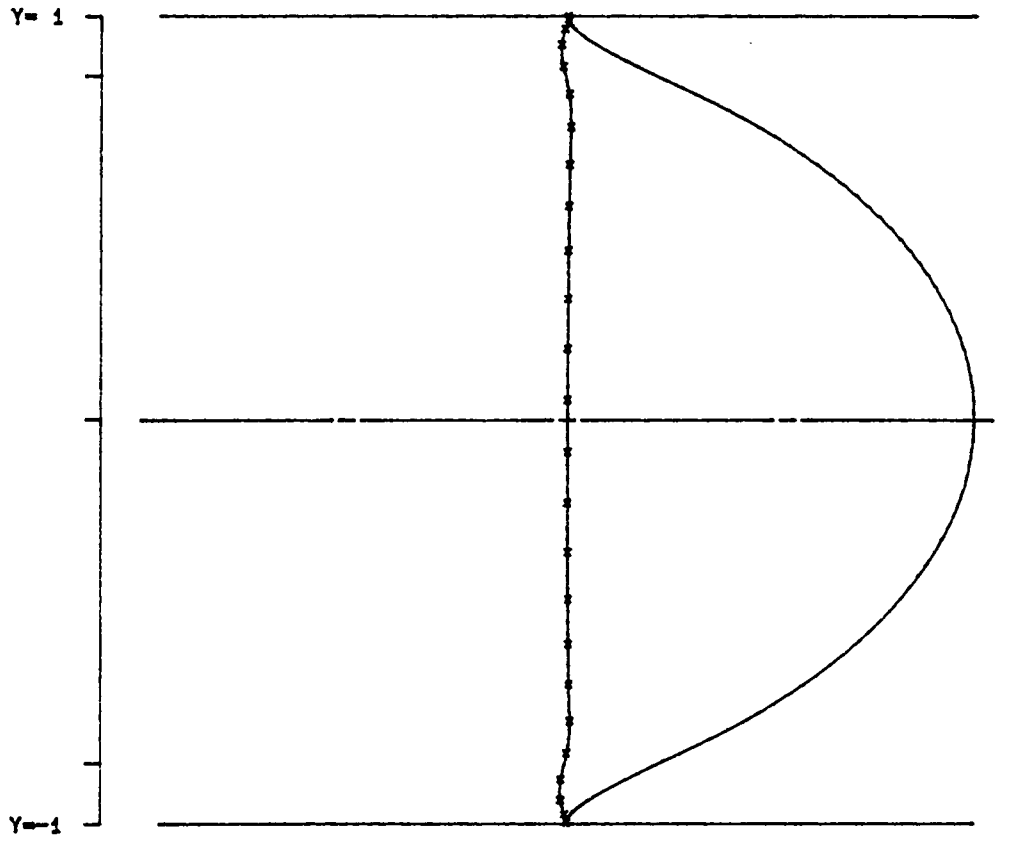

EIGENFUNCTION PSI (Y)

RE	4000.0	CR	0.278542
ALPHA	1.0000	CI	-0.004946

PSI (0) = 1

Figure 2.4- Eigenfunction of OSE for $\alpha = 1.000$, $Re = 4000$.

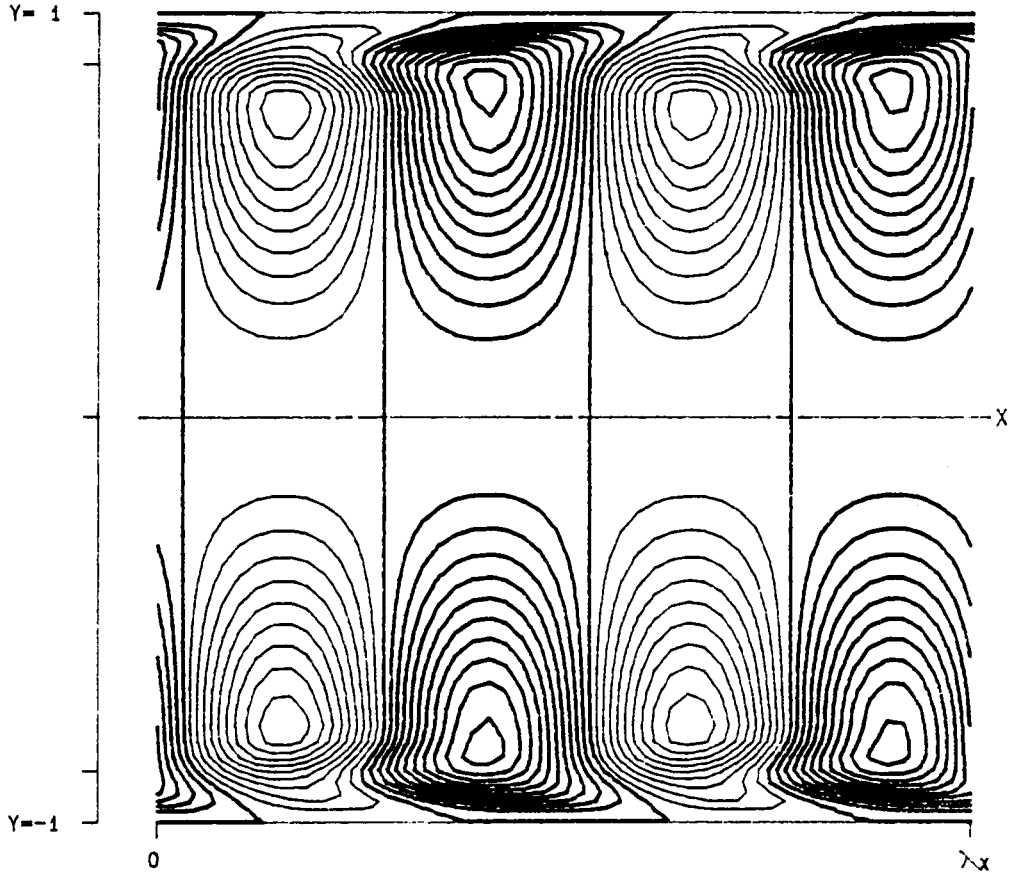

PPT 2-D T10 (X, Y)

RE	10000.0	LEVELS: MIN	-0.0000108
ALPHA	1.0000	DIF	0.0000012
RMS	0.010000	NO.	20
MAX	0.000013		

Figure 2.5- Reynolds stress as a function of x and y for $\alpha = 1.000$, $Re = 10000$.

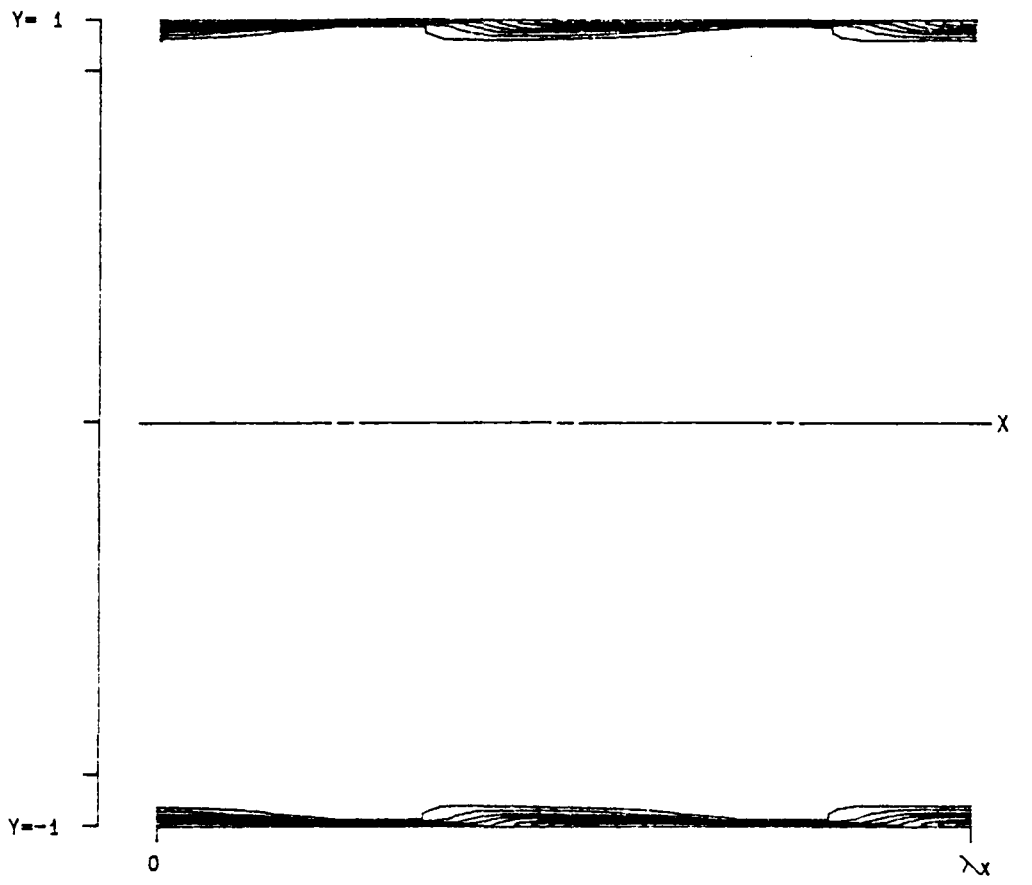

PPT 2-D D1 (X, Y)

RE	10000.0	LEVELS:	MIN	-0.0000108
ALPHA	1.0000		DIF	0.0000012
RMS	0.010000		NO.	20
MAX	0.000013			

Figure 2.6- Dissipation as a function of x and y for $\alpha = 1.000$, $Re = 10000$.

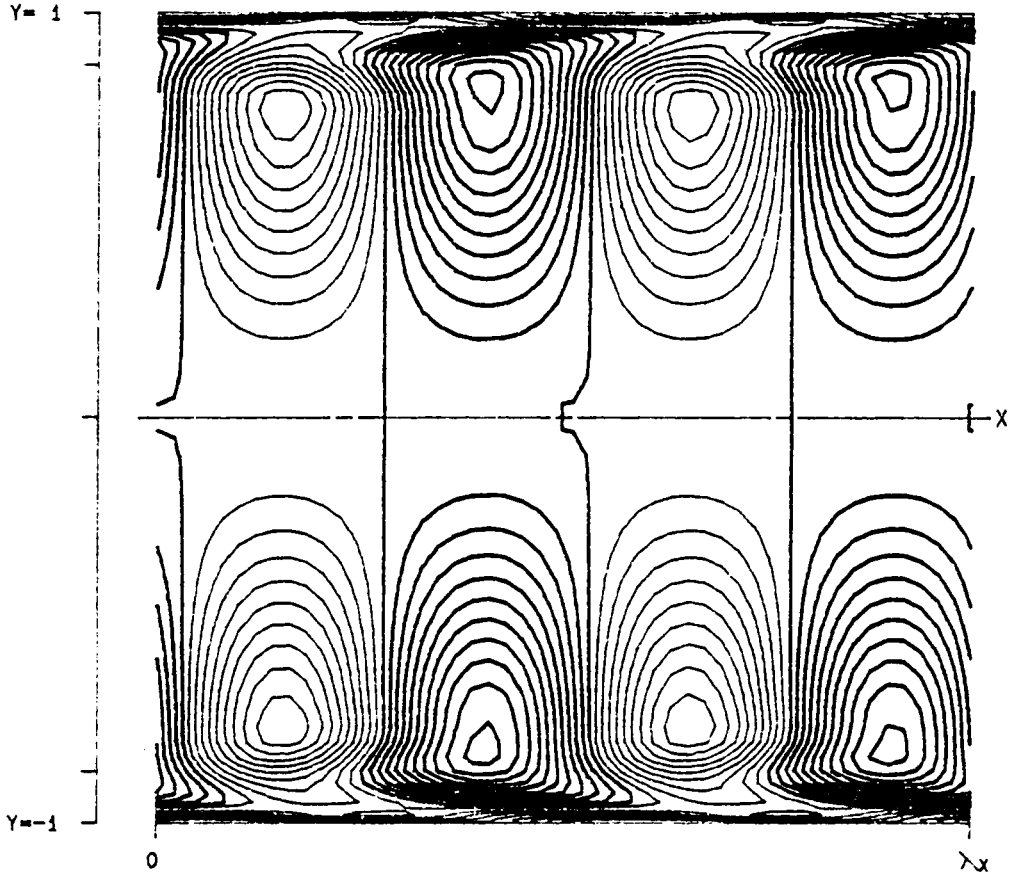

PPT 2-D P1 (X, Y)

RE	10000.0	LEVELS: MIN	-0.0000108
ALPHA	1.0000	DIF	0.0000012
RMS	0.010000	NO.	20
MAX	0.000013		

Figure 2.7- Power as a function of x and y for $\alpha = 1.000$, $Re = 10000$.

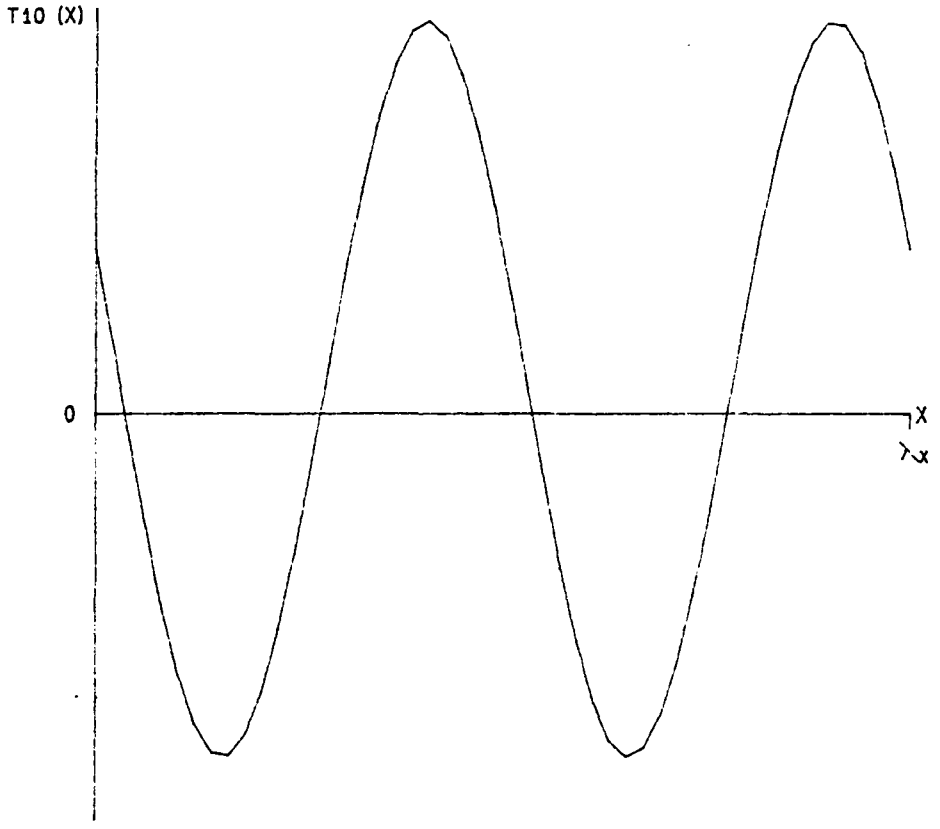

PPT 2-D T10 (X)

RE	10000.0	CR	0.237526
ALPHA	1.0000	MAX	0.0000120
RMS	0.010000	MIN	-0.0000104

Figure 2.8- Reynolds stress as a function of x for $\alpha = 1.000$, $Re = 10000$.

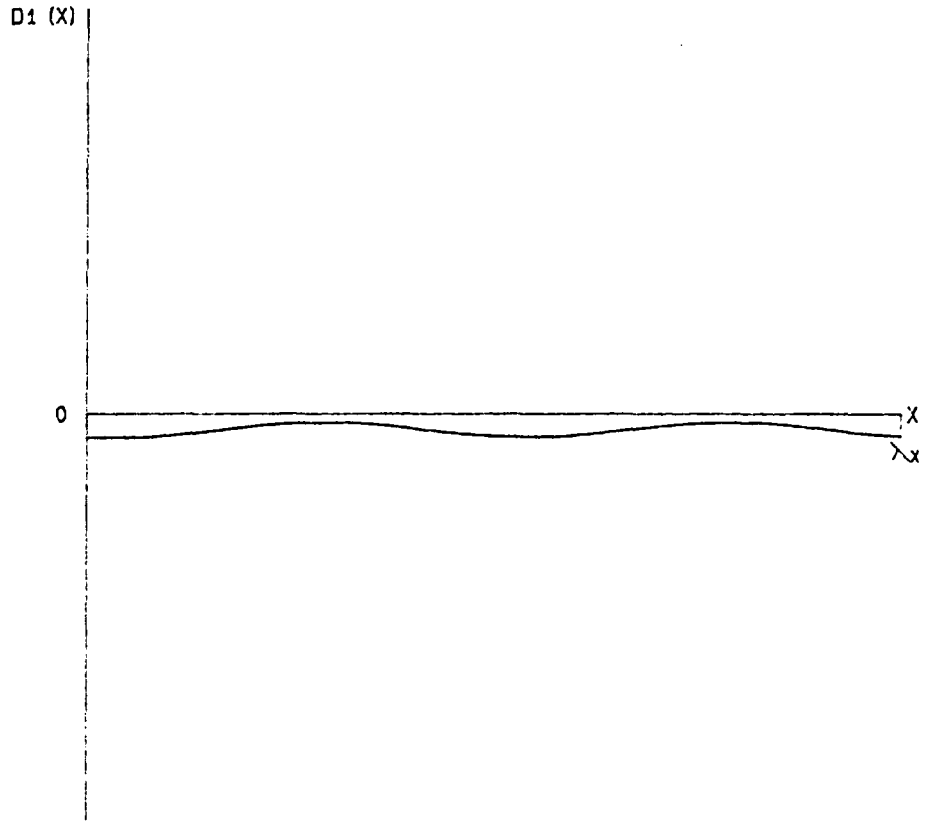

PPT 2-D D1 (X)

RE	10000.0	CR	0.237526
ALPHA	1.0000	MAX	-0.0000002
AMS	0.010000	MIN	-0.0000007

Figure 2.9- Dissipation as a function of x for $\alpha = 1.000$, $Re = 10000$.

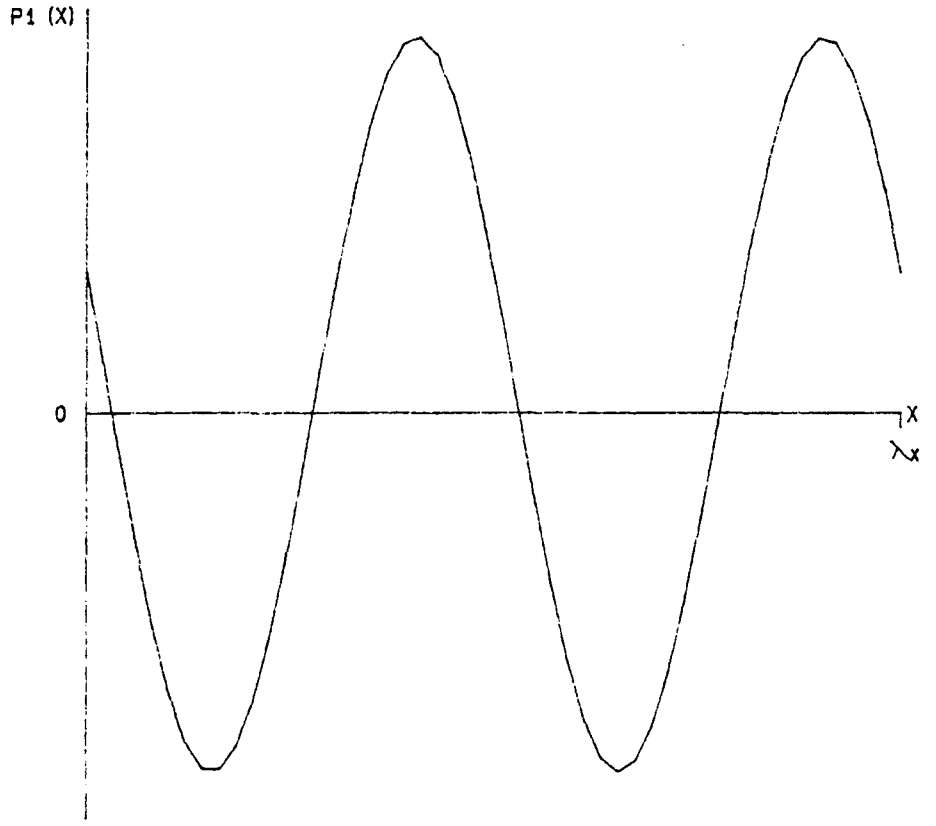

PPT 2-D P1 (X)

RE	10000.0	CR	0.237526
ALPHA	1.0000	MAX	0.0000115
RMS	0.010000	MIN	-0.0000109

Figure 2.10- Power as a function of x for $\alpha = 1.000$, $Re = 10000$.

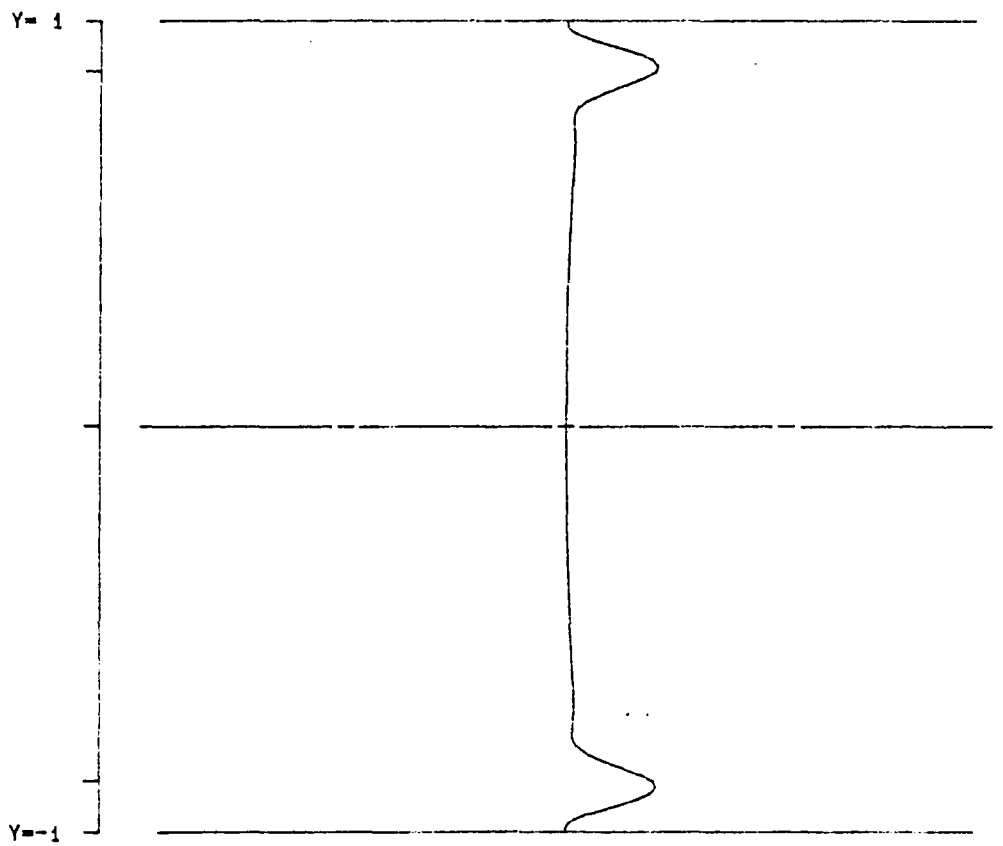

PPT 2-D T10 (Y)

RE	10000.0	CR	0.237526
ALPHA	1.0000	MAX	0.0000026
RMS	0.010000	MIN	0.0000000

Figure 2.11- Reynolds stress as a function of y for $\alpha = 1.000$, $Re = 10000$.

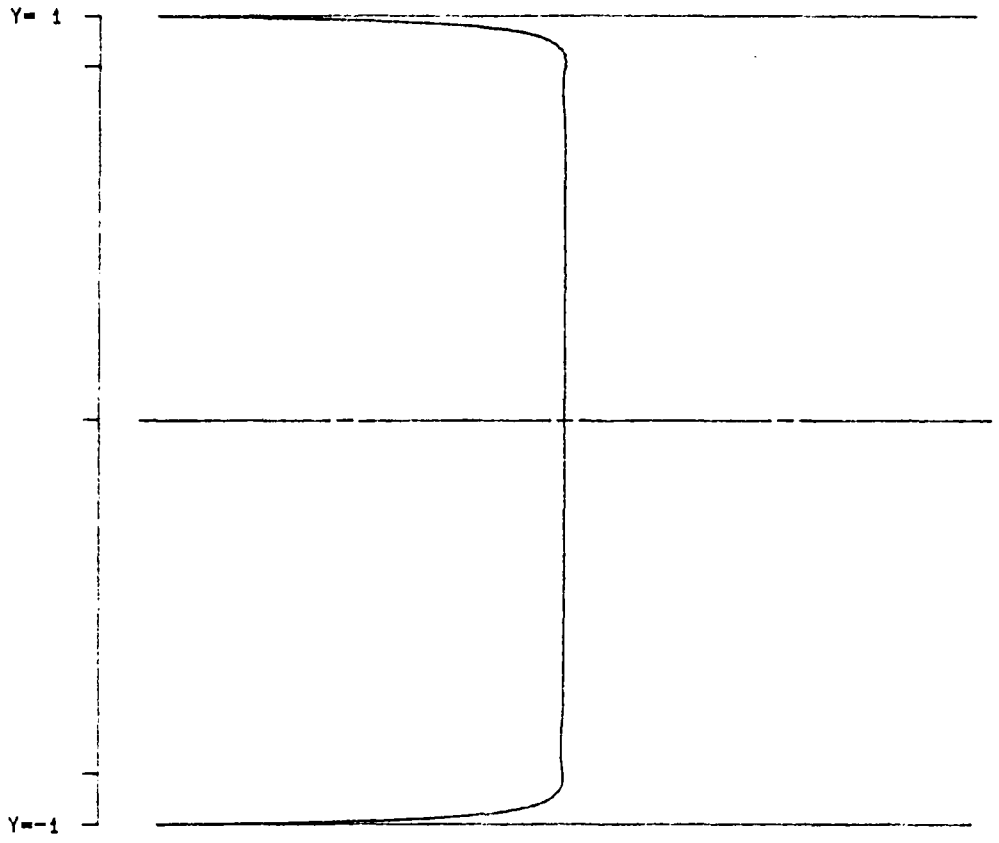

PPT 2-D D1 (Y)

RE	10000.0	CR	0.237526
ALPHA	1.0000.	MAX	-0.0000000
RMS	0.010000	MIN	-0.0000123

Figure 2.12- Dissipation as a function of y for $\alpha = 1.000$, $Re = 10000$.

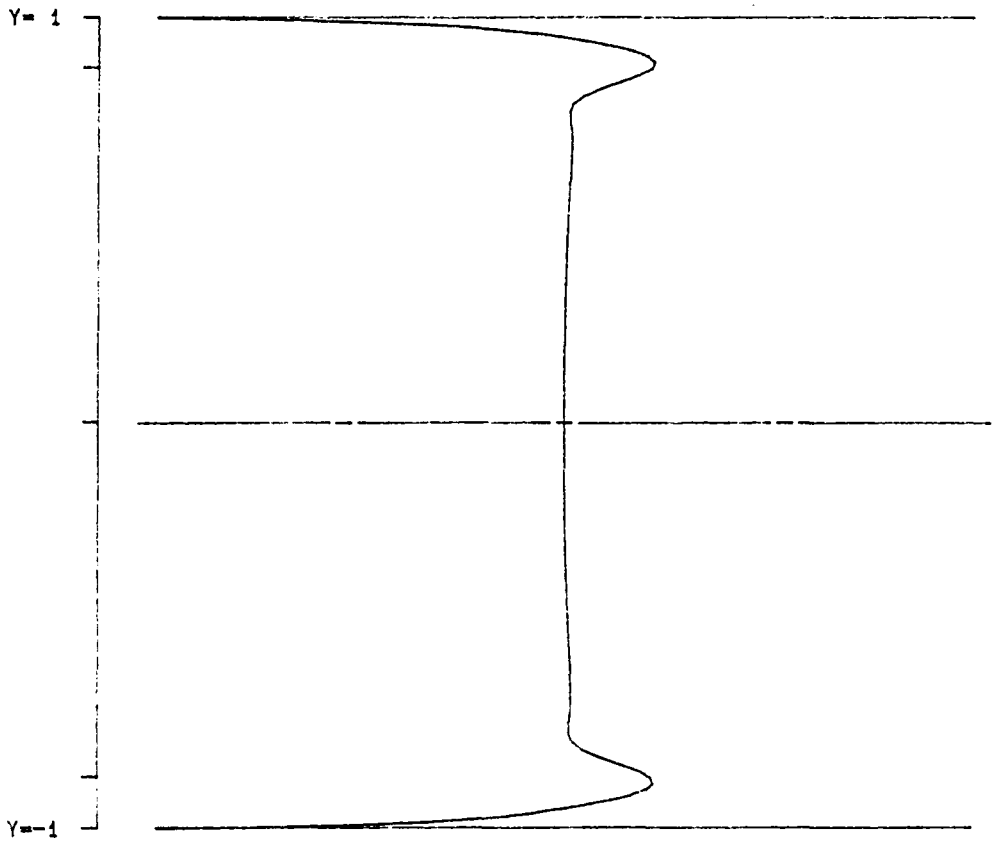

PPT 2-D P1 (Y)

RE	10000.0	CR	0.237526
ALPHA	1.0000	MAX	0.0000026
RMS	0.010000	MIN	-0.0000123

Figure 2.13- Power as a function of y for $\alpha = 1.000$. $Re = 10000$.

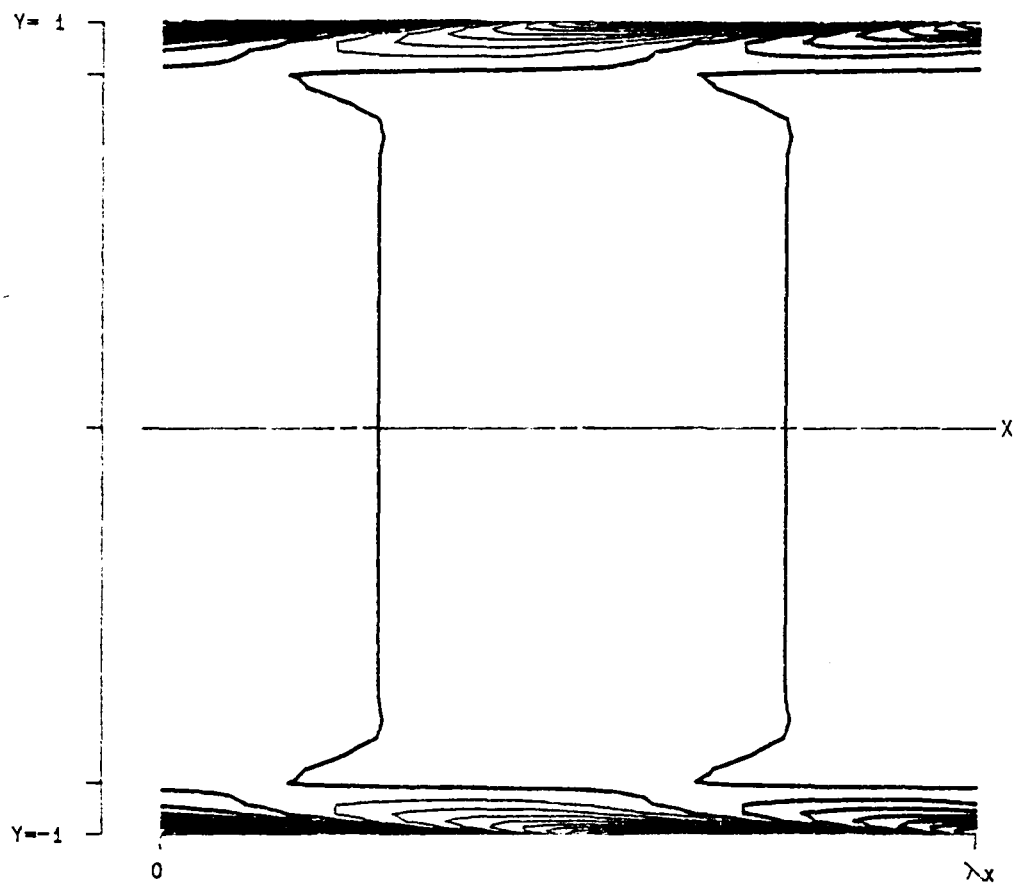

PPT 2-D VORTICITY-ZETA (X, Y)

RE	10000.0	LEVELS: MIN	-0.4253483
ALPHA	1.0000	DIF	0.0472609
RMS	0.010000	NO.	20
MAX	0.496240		

Figure 2.14- Vorticity of flow as a function of x and y for $\alpha = 1.000$, $Re = 10000$.

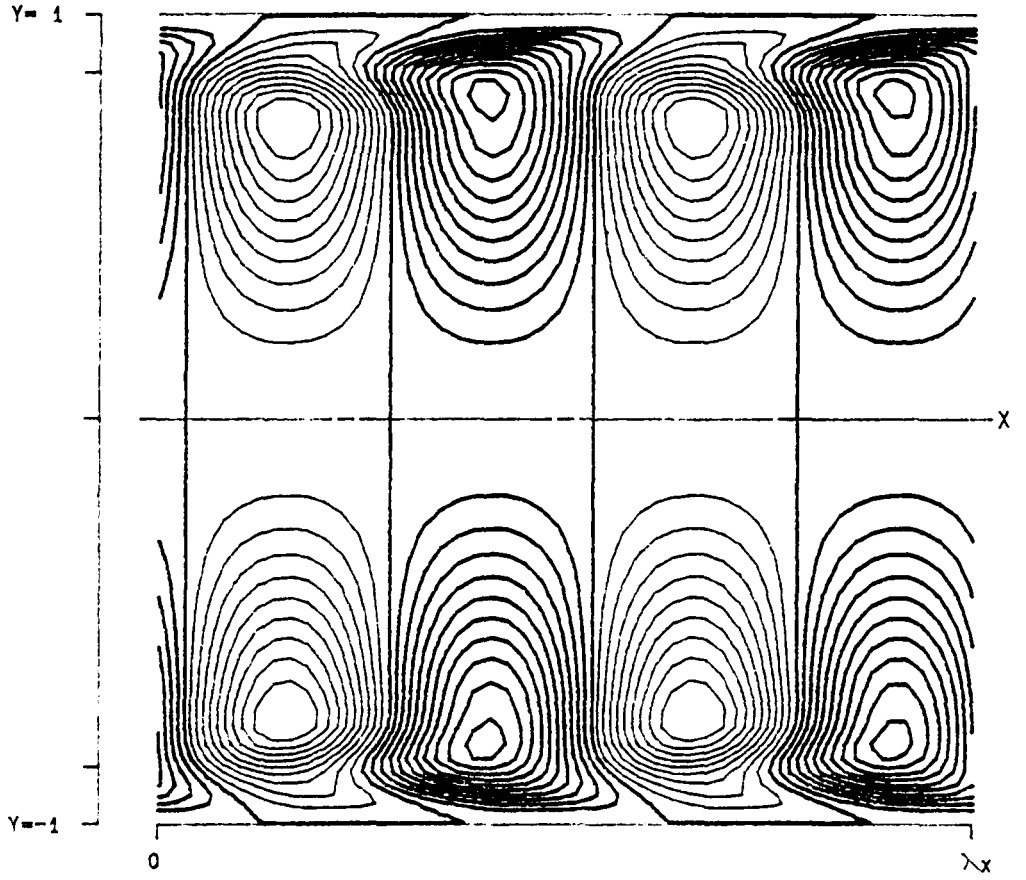

PPT 2-D T10 (X, Y)

RE	5772.2	LEVELS: MIN	-0.0000118
ALPHA	1.0206	DIF	0.0000013
RMS	0.010000	NO.	20
MAX	0.000014		

Figure 2.15- Reynolds stress as a function of x and y for $\alpha = 1.0206$, $Re = 5772.2$.

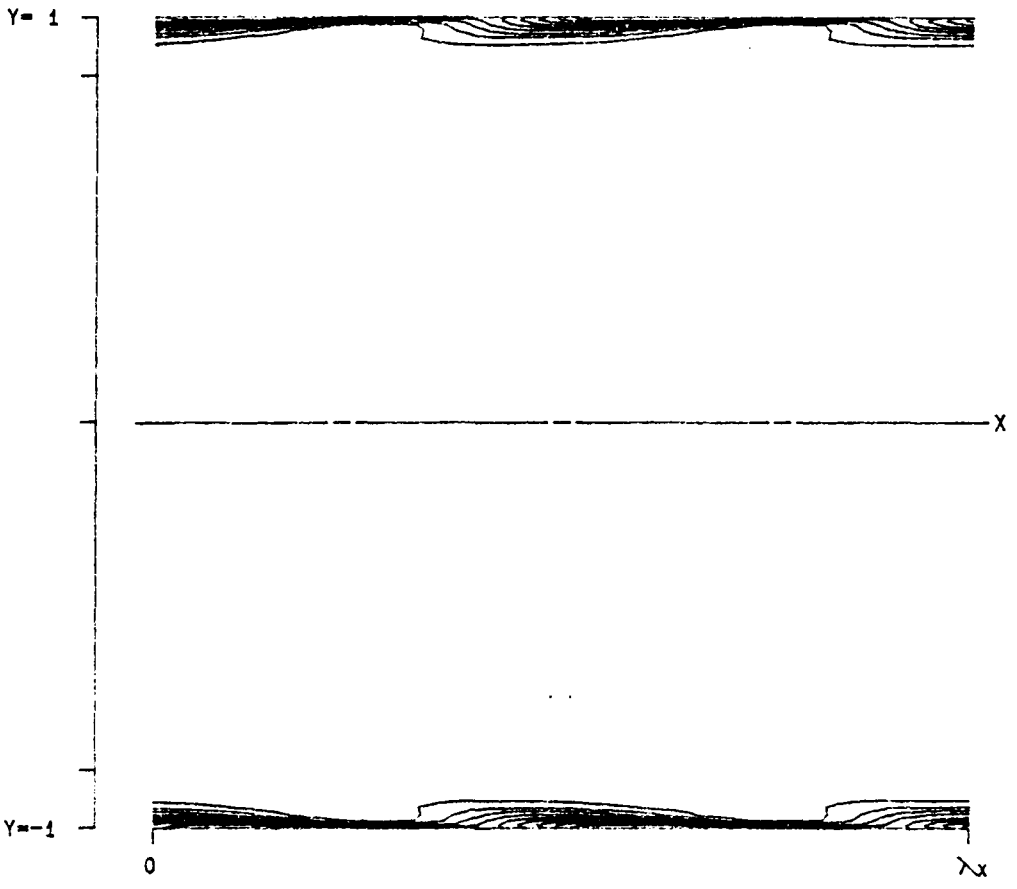

PPT 2-D D1 (X, Y)

RE	5772.2	LEVELS: MIN	-0.0000118
ALPHA	1.0206	DIF	0.0000013
RMS	0.010000	NO.	20
MAX	0.000014		

Figure 2.16- Dissipation as a function of x and y for $\alpha = 1.0206$, $Re = 5772.2$.

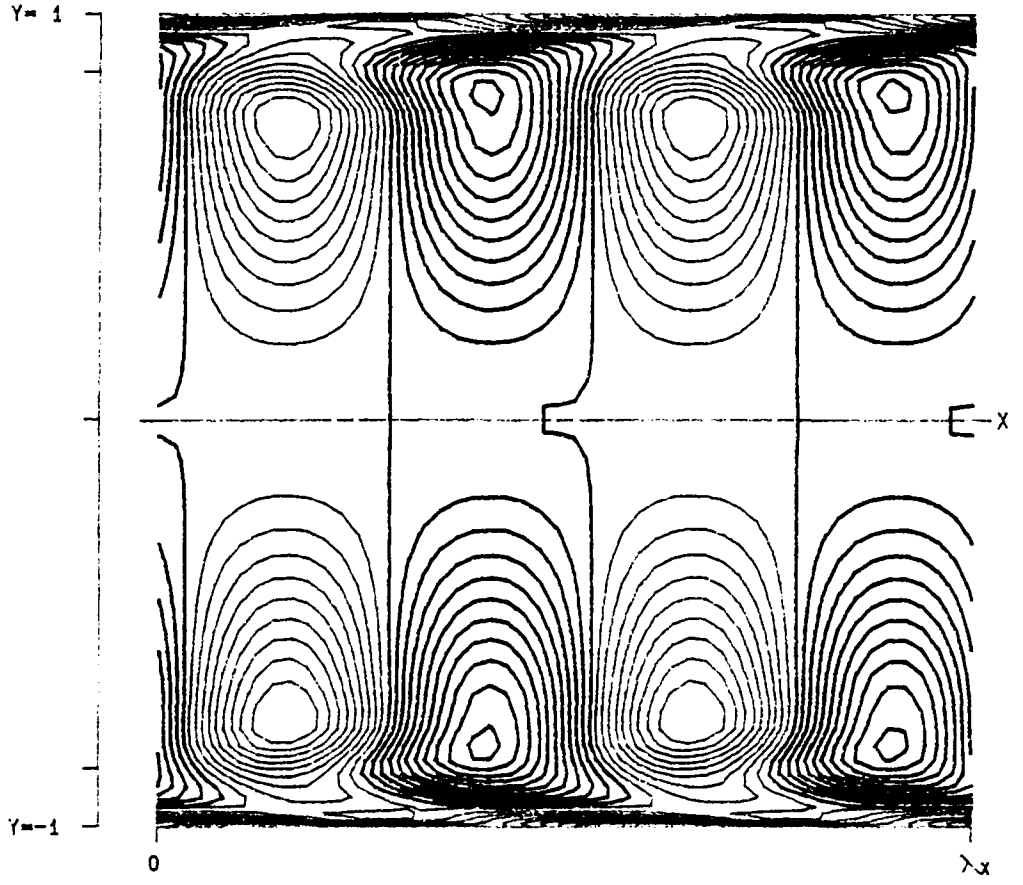

PPT 2-D P1 (X, Y)

RE	5772.2	LEVELS: MIN	-0.0000118
ALPHA	1.0206	DIF	0.0000013
RMS	0.010000	NO.	20
MAX	0.000014		

Figure 2.17- Power as a function of x and y for $\alpha = 1.0206$, $Re = 5772.2$.

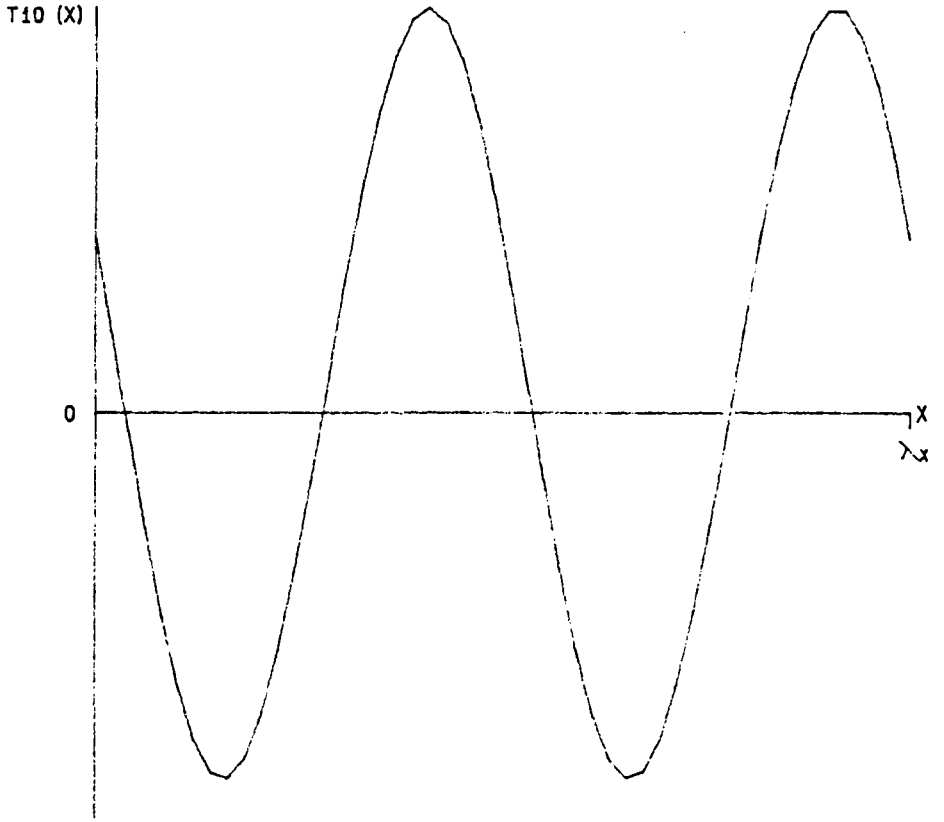

PPT 2-D T10 (X)

RE	5772.2	CR	0.264002
ALPHA	1.0206	MAX	0.0000129
RMS	0.010000	MIN	-0.0000116

Figure 2.18- Reynolds stress as a function of x for $\alpha = 1.0206$, $Re = 5772.2$.

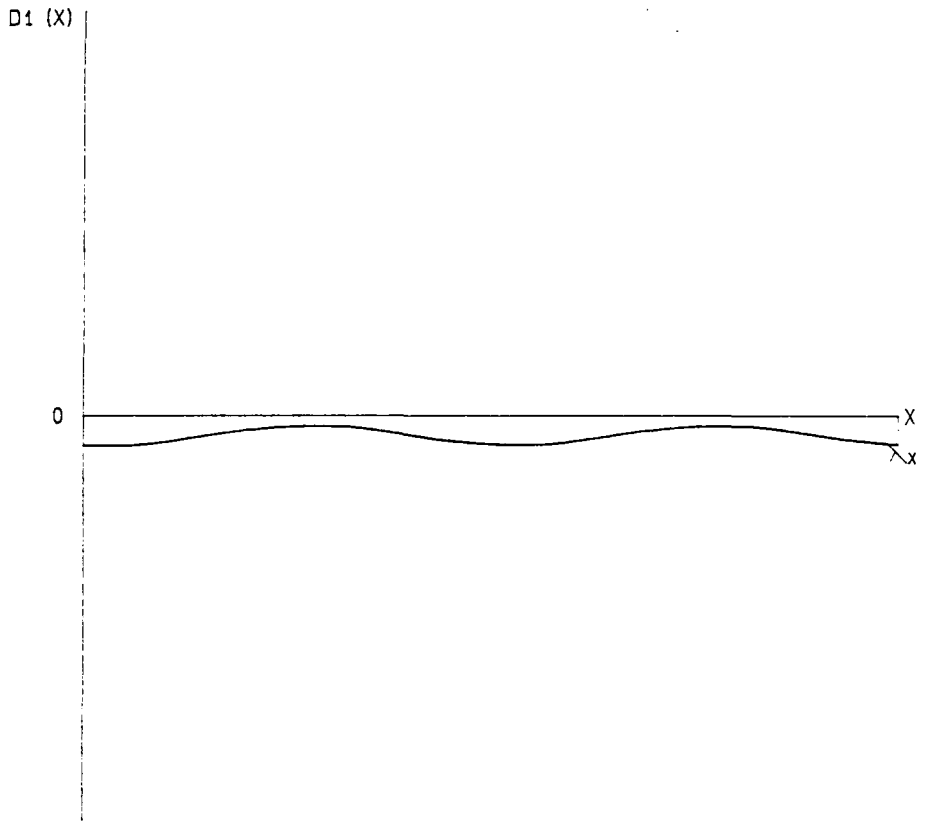

PPT 2-D D1 (X)

RE	5772.2	CR	0.264002
ALPHA	1.0206	MAX	-0.0000003
RMS	0.010000	MIN	-0.0000009

Figure 2.19- Dissipation as a function of x for $\alpha = 1.0206$, $Re = 5772.2$.

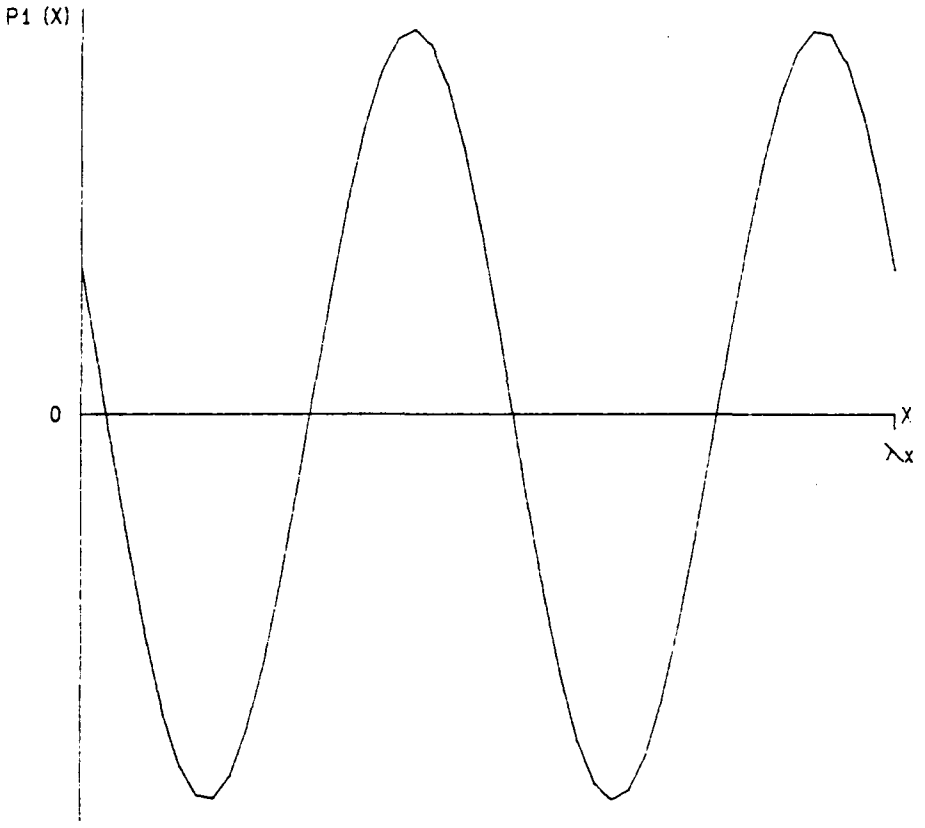

PPT 2-D P1 (X)

RE	5772.2	CR	0.264002
ALPHA	1.0206	MAX	0.0000123
RMS	0.010000	MIN	-0.0000122

Figure 2.20- Power as a function of x for $\alpha = 1.0206$, $Re = 5772.2$.

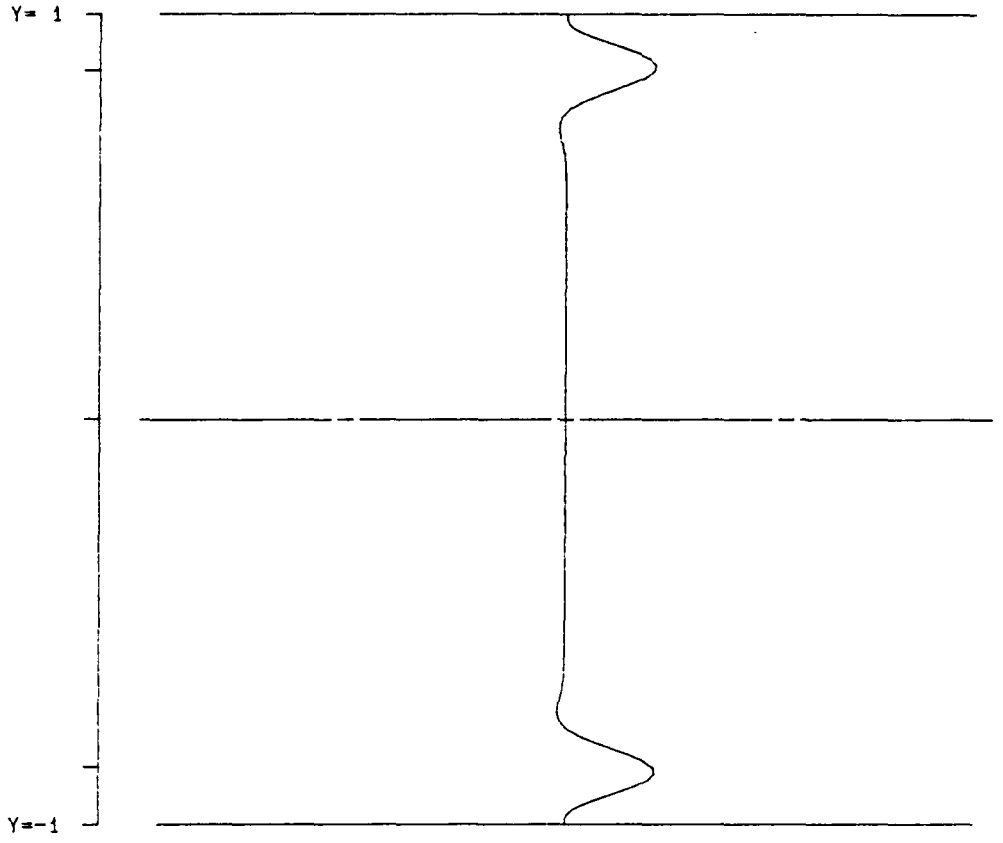

PPT 2-0 T10 (Y)

RE	5772.2	CR	0.264002
ALPHA	1.0206	MAX	0.0000028
RMS	0.010000	MIN	-0.0000002

Figure 2.21- Reynolds stress as a function of y for $\alpha = 1.0206$, $Re = 5772.2$.

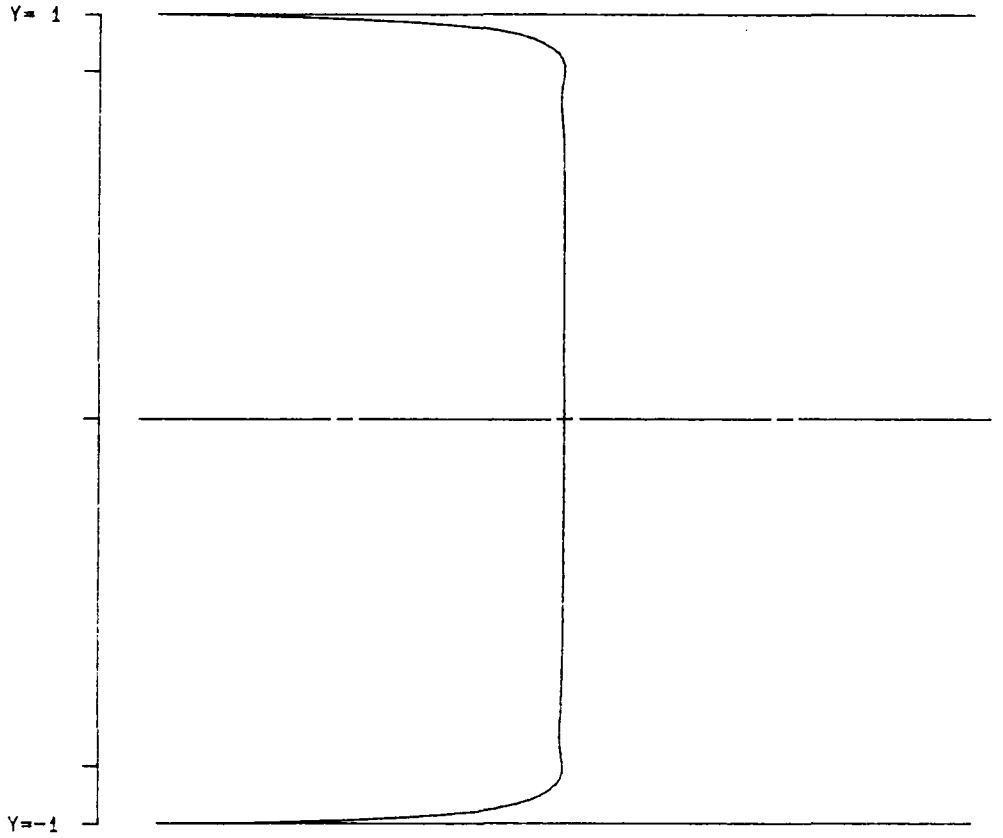

PPT 2-D D1 (Y)

RE	5772.2	CR	0.264002
ALPHA	1.0206	MAX	-0.0000000
RMS	0.010000	MIN	-0.0000120

Figure 2.22- Dissipation as a function of y for $\alpha = 1.0206$, $Re = 5772.2$.

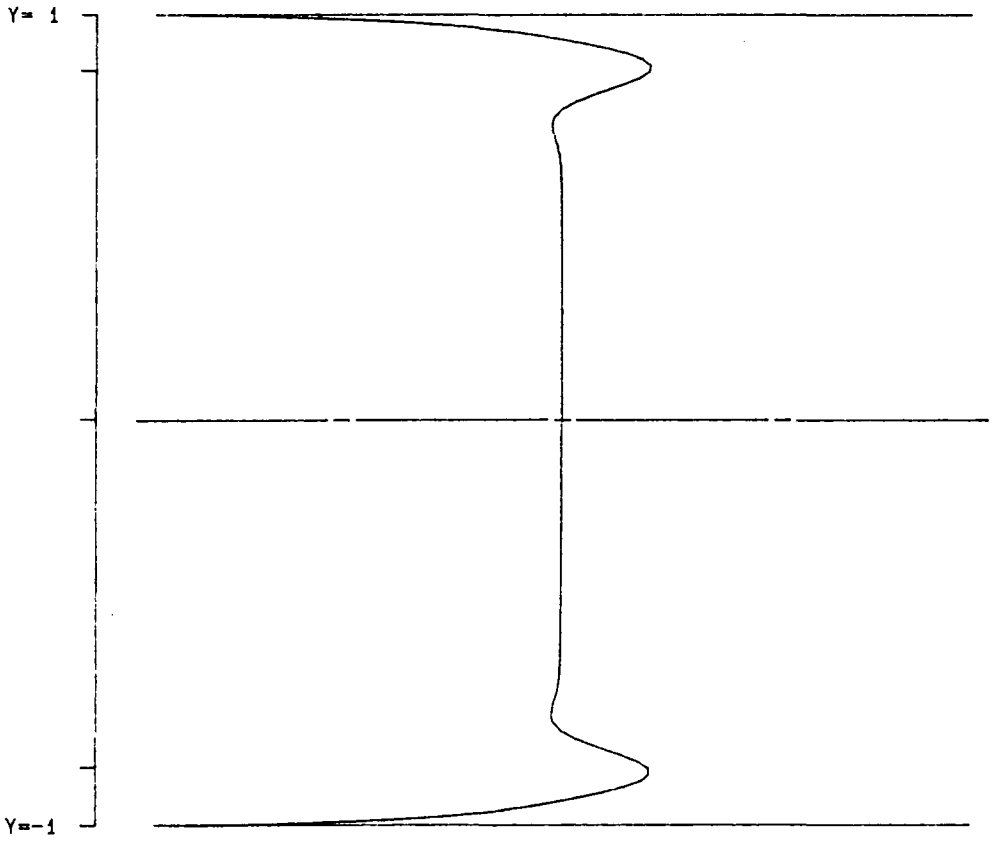

PPT 2-D P1 (Y)

RE	5772.2	CR	0.264002
ALPHA	1.0206	MAX	0.0000028
RMS	0.010000	MIN	-0.0000120

Figure 2.23- Power as a function of y for $\alpha = 1.0206$, $Re = 5772.2$.

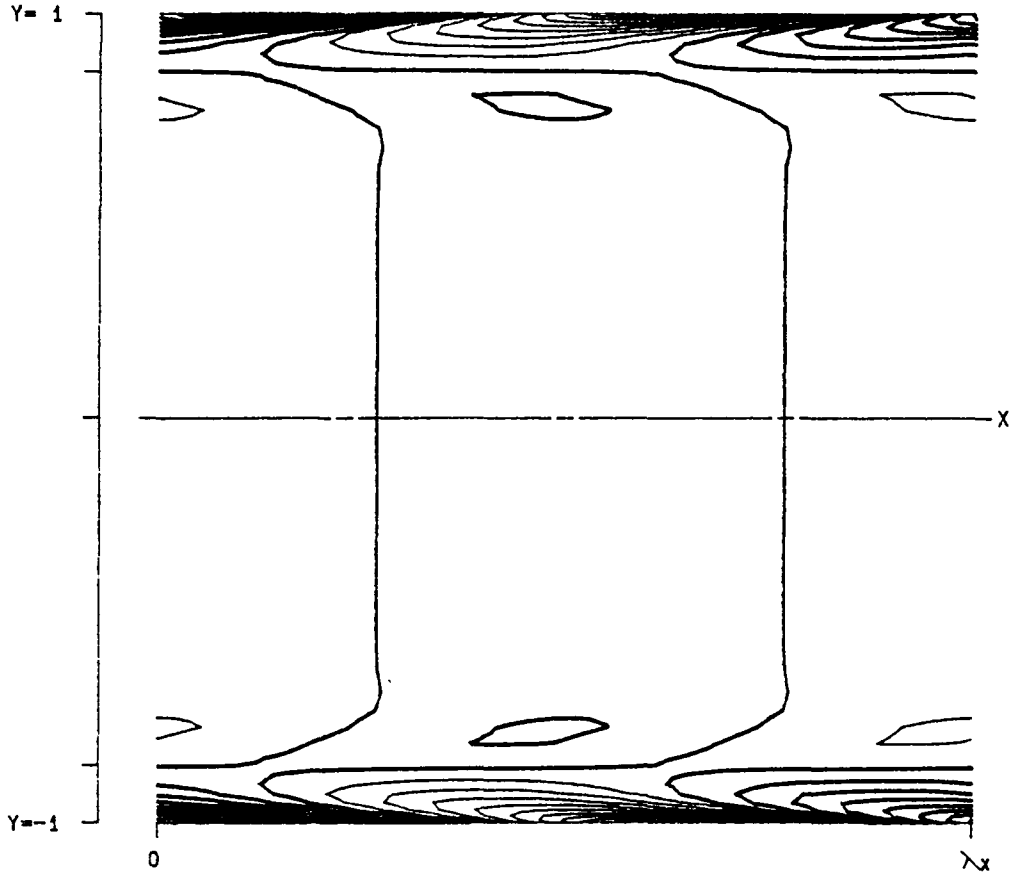

PPT 2-D VORTICITY-ZETA (X, Y)

RE	5772.2	LEVELS: MIN	-0.3180474
ALPHA	1.0206	DIF	0.0353386
RMS	0.010000	NO.	20
MAX	0.371055		

Figure 2.24- Vorticity of flow as a function of x and y for $\alpha = 1.0206$, $Re = 5772.2$.

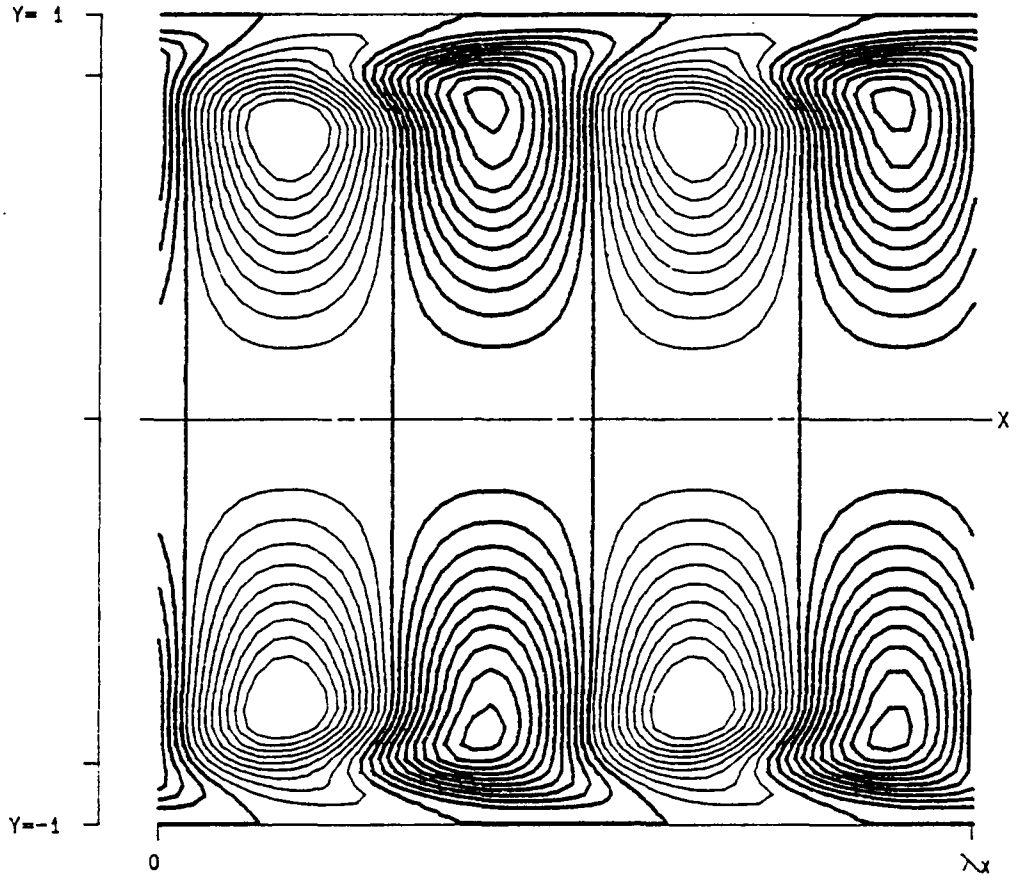

PPT 2-D T10 (X, Y)

RE	4000.0	LEVELS: MIN	-0.0000117
ALPHA	1.0000	DIF	0.0000013
RMS	0.010000	NO.	20
MAX	0.000014		

Figure 2.25- Reynolds stress as a function of x and y for $\alpha = 1.0206$, $Re = 4000$.

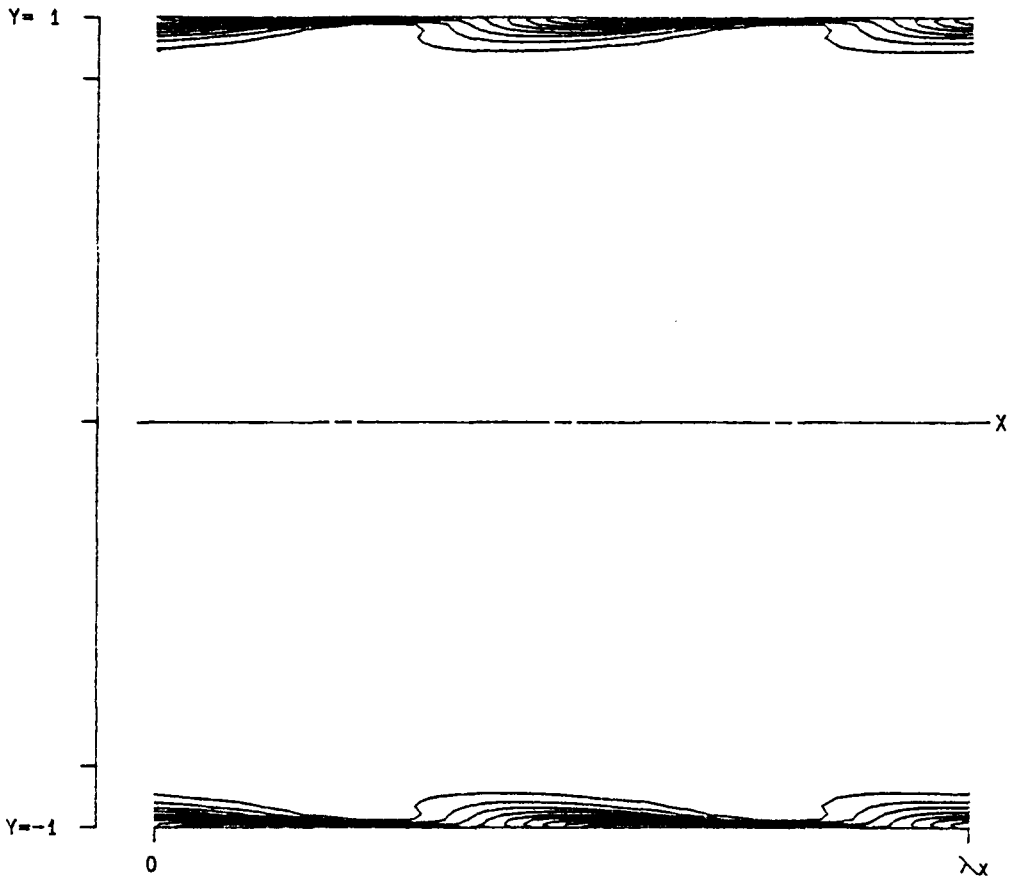

PPT 2-D D1 (X, Y)

RE	4000.0	LEVELS: MIN	-0.0000117
ALPHA	1.0000	DIF	0.0000013
RMS	0.010000	NO.	20
MAX	0.000014		

Figure 2.26- Dissipation as a function of x and y for $\alpha = 1.000$, $Re = 4000$.

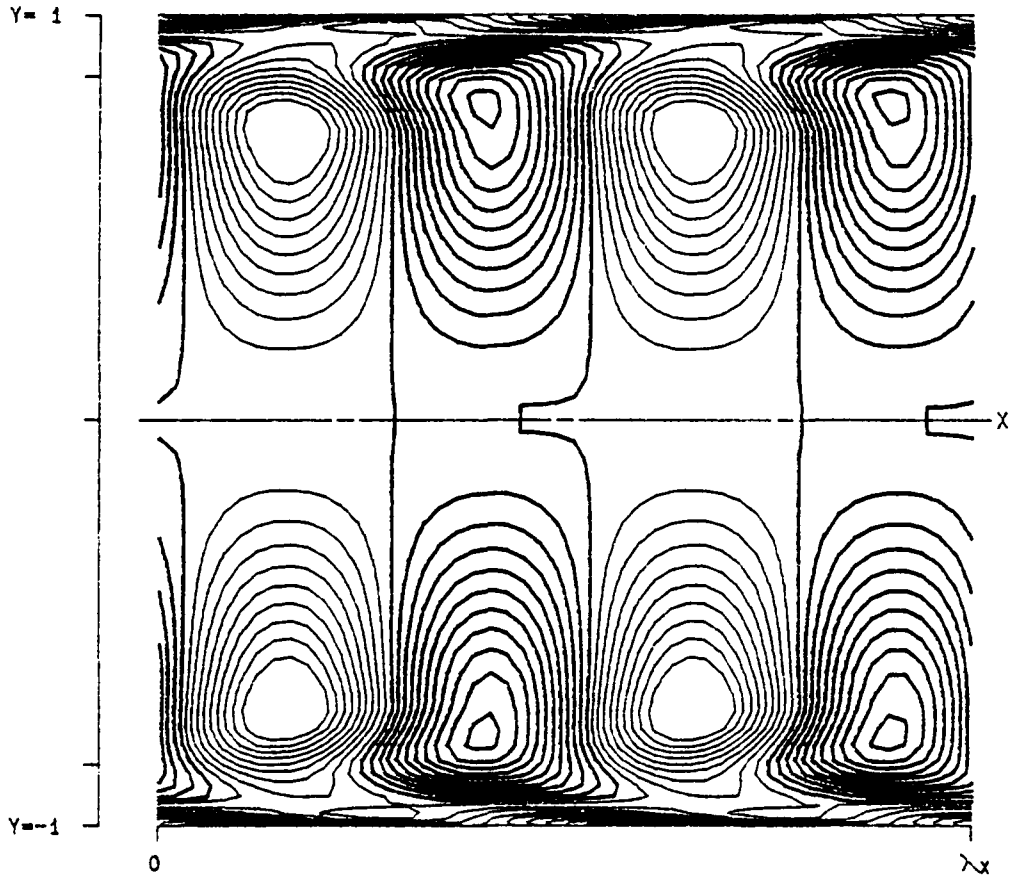

PPT 2-D P1 (X, Y)

RE	4000.0	LEVELS: MIN	-0.0000117
ALPHA	1.0000	DIF	0.0000013
RMS	0.010000	NO.	20
MAX	0.000014		

Figure 2.27- Power as a function of x and y for $\alpha = 1.000$, $Re = 4000$.

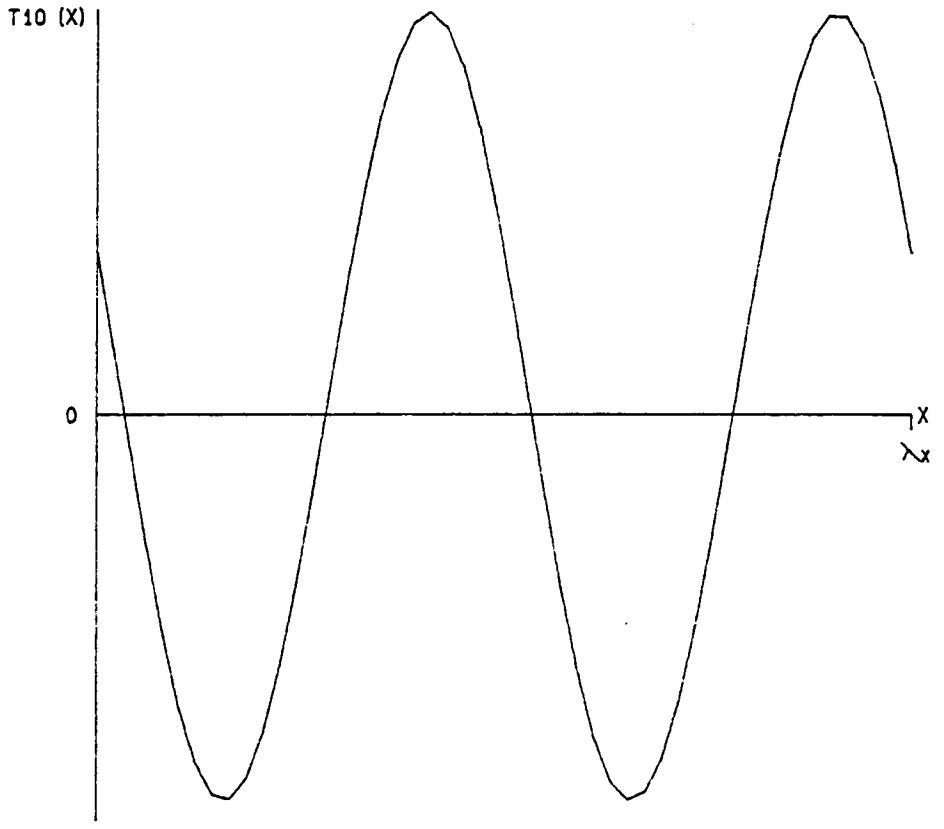

PPT 2-D T10 (X)

RE	4000.0	CR	0.278542
ALPHA	1.0000	MAX	0.0000129
RMS	0.010000	MIN	-0.0000124

Figure 2.28- Reynolds stress as a function of x for $\alpha = 1.000$, $Re = 4000$.

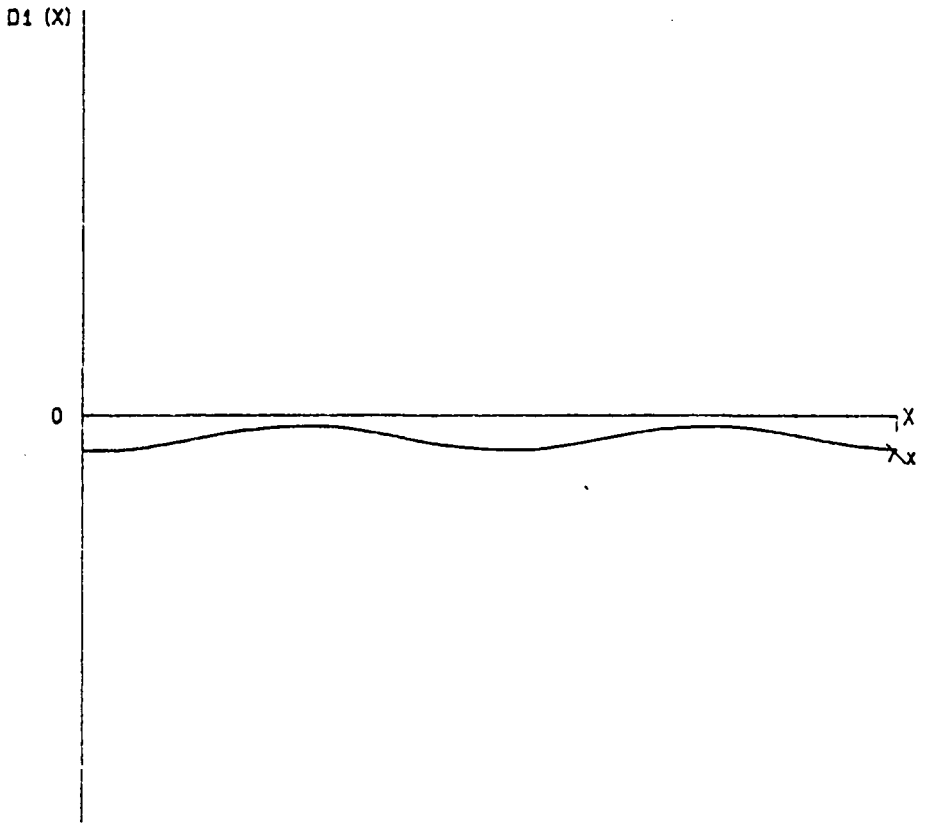

PPT 2-D D1 (X)

RE	4000.0	CR	0.278542
ALPHA	1.0000	MAX	-0.0000003
RMS	0.010000	MIN	-0.0000011

Figure 2.29- Dissipation as a function of x for $\alpha = 1.000$, $Re = 4000$.

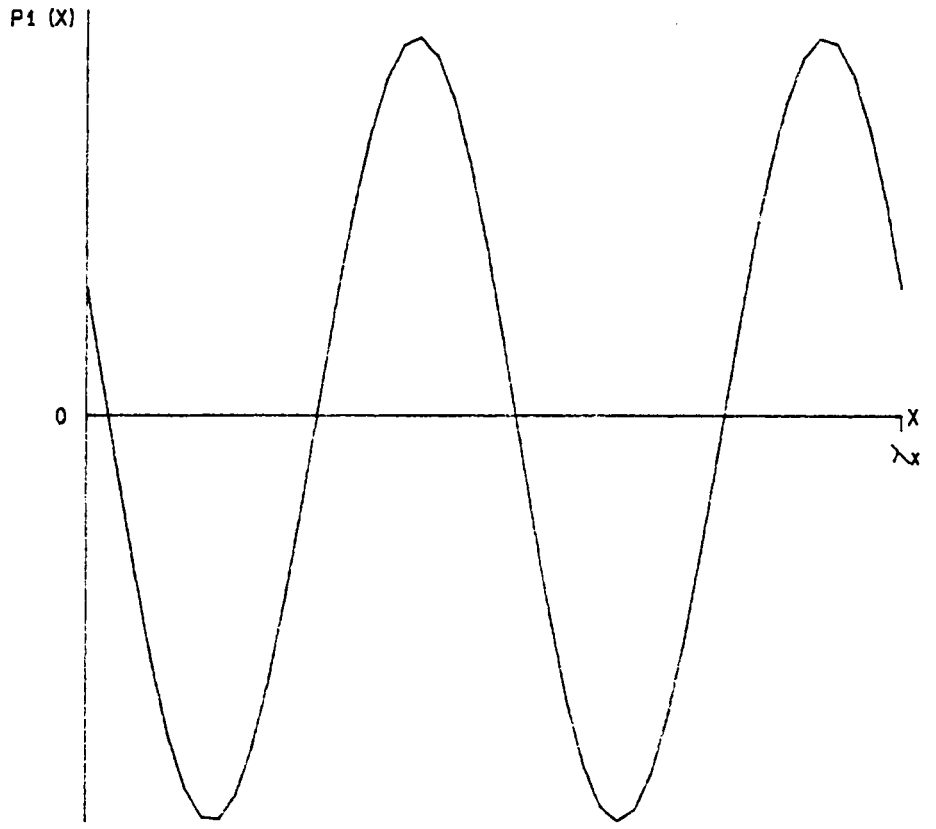

PPT 2-D P1 (X)

RE	4000.0	CR	0.278542
ALPHA	1.0000	MAX	0.0000121
RMS	0.010000	MIN	-0.0000130

Figure 2.30- Power as a function of x for $\alpha = 1.000$, $Re = 4000$.

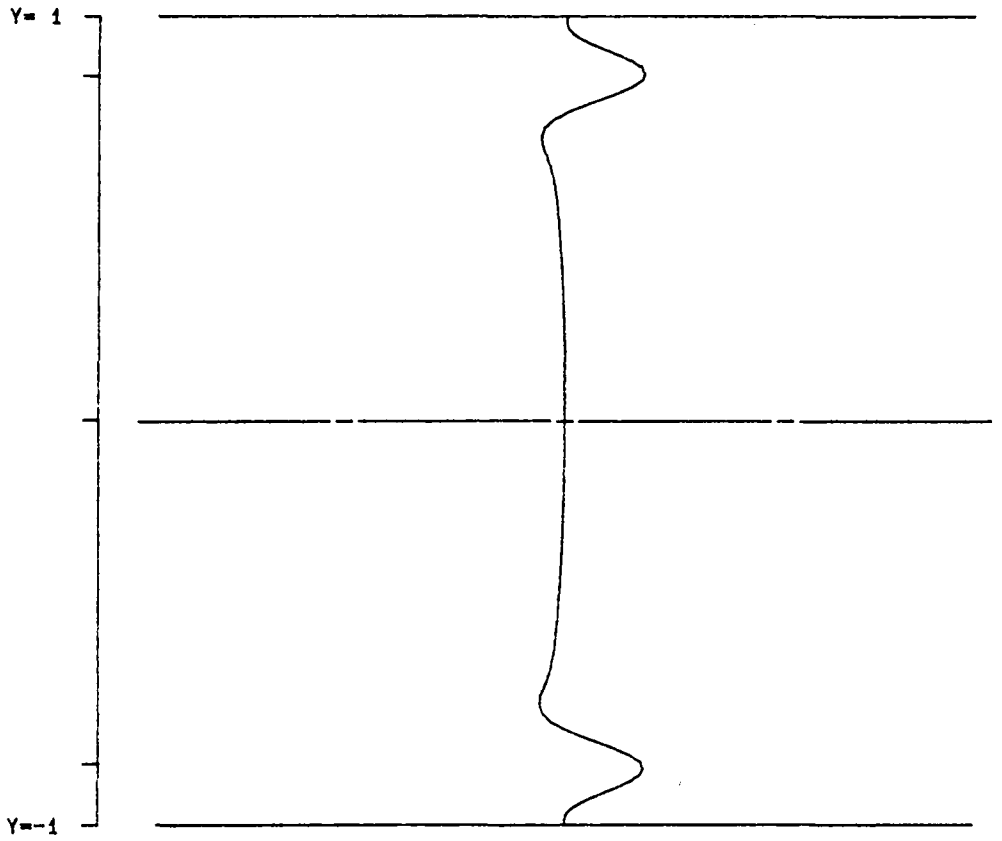

PPT 2-D T10 (Y)

RE	4000.0	CR	0.278542
ALPHA	1.0000	MAX	0.0000025
RMS	0.010000	MIN	-0.0000007

Figure 2.31- Reynolds stress as a function of y for $\alpha = 1.000$, $Re = 4000$.

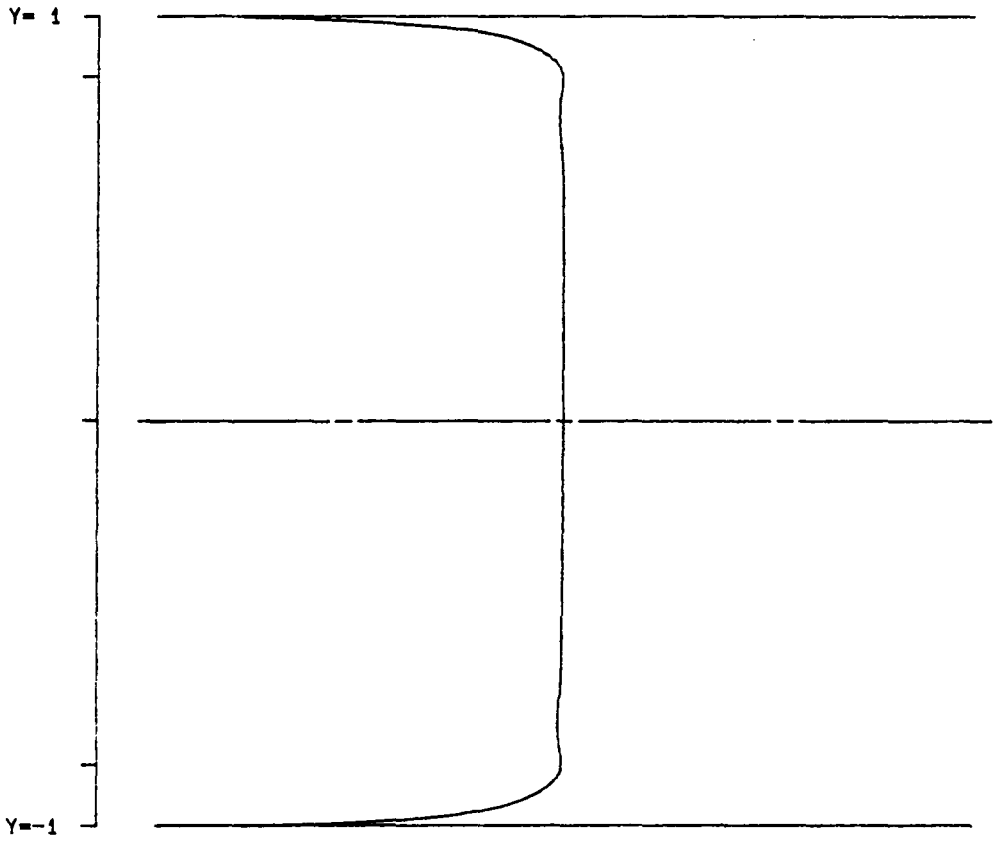

PPT 2-D D1 (Y)

RE	4000.0	CR	0.278542
ALPHA	1.0000	MAX	-0.0000000
RMS	0.010000	MIN	-0.0000103

Figure 2.32- Dissipation as a function of y for $\alpha = 1.000$, $Re = 4000$.

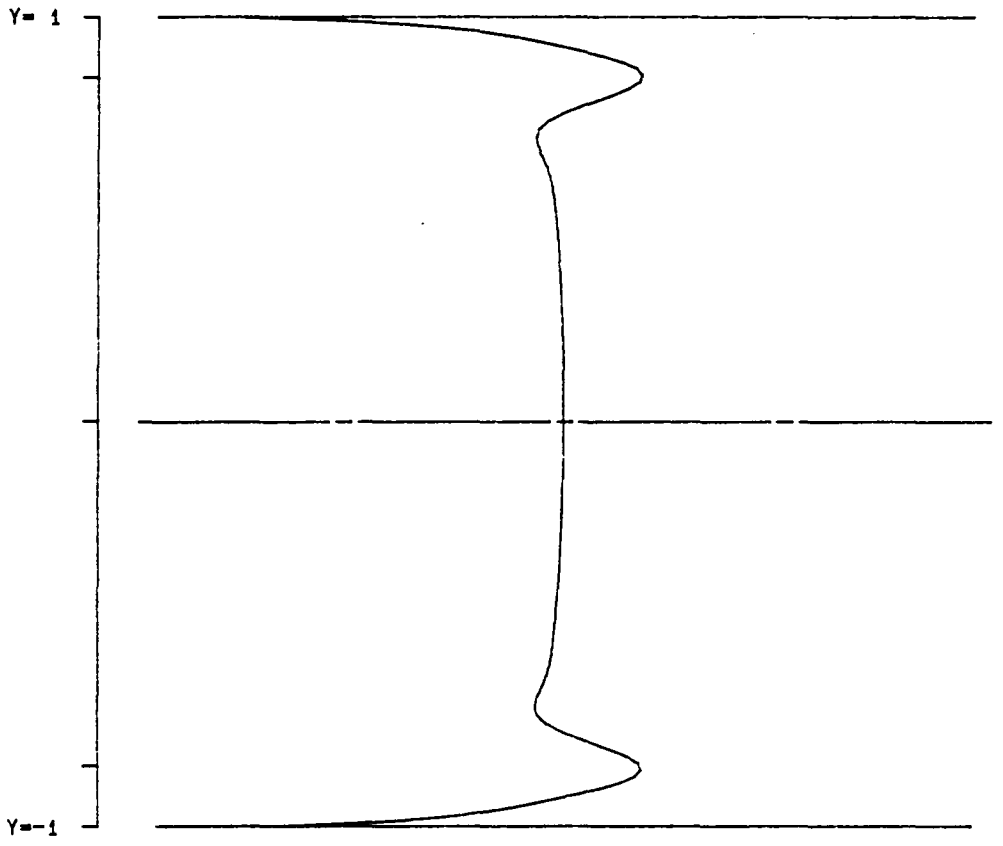

PPT 2-D P1 (Y)

RE	4000.0	CR	0.278542
ALPHA	1.0000	MAX	0.0000023
RMS	0.010000	MIN	-0.0000103

Figure 2.33- Power as a function of y for $\alpha = 1.000$, $Re = 4000$.

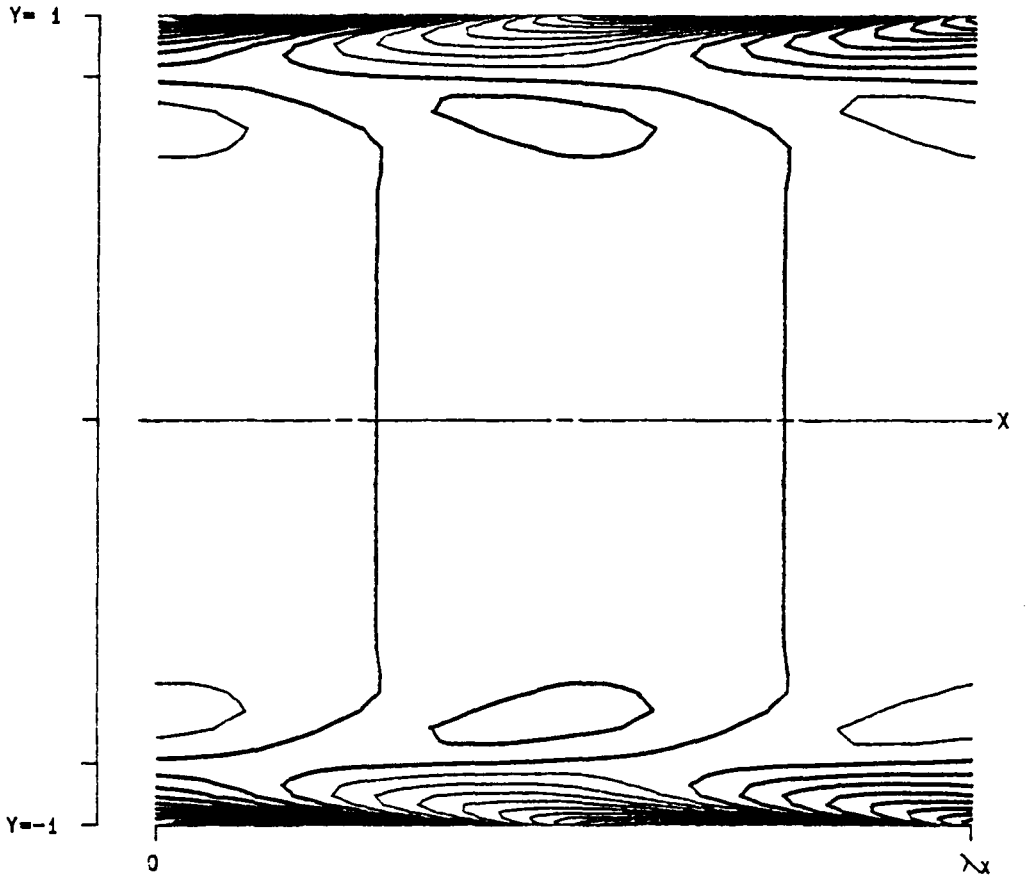

PPT 2-D VORTICITY-ZETA (X, Y)

RE	4000.0	LEVELS: MIN	-0.2457576
ALPHA	1.0000	DIF	0.0273064
RMS	0.010000	NO.	20
MAX	0.286717		

Figure 2.34- Vorticity of flow as a function of x and y for $\alpha = 1.000$, $Re = 4000$.

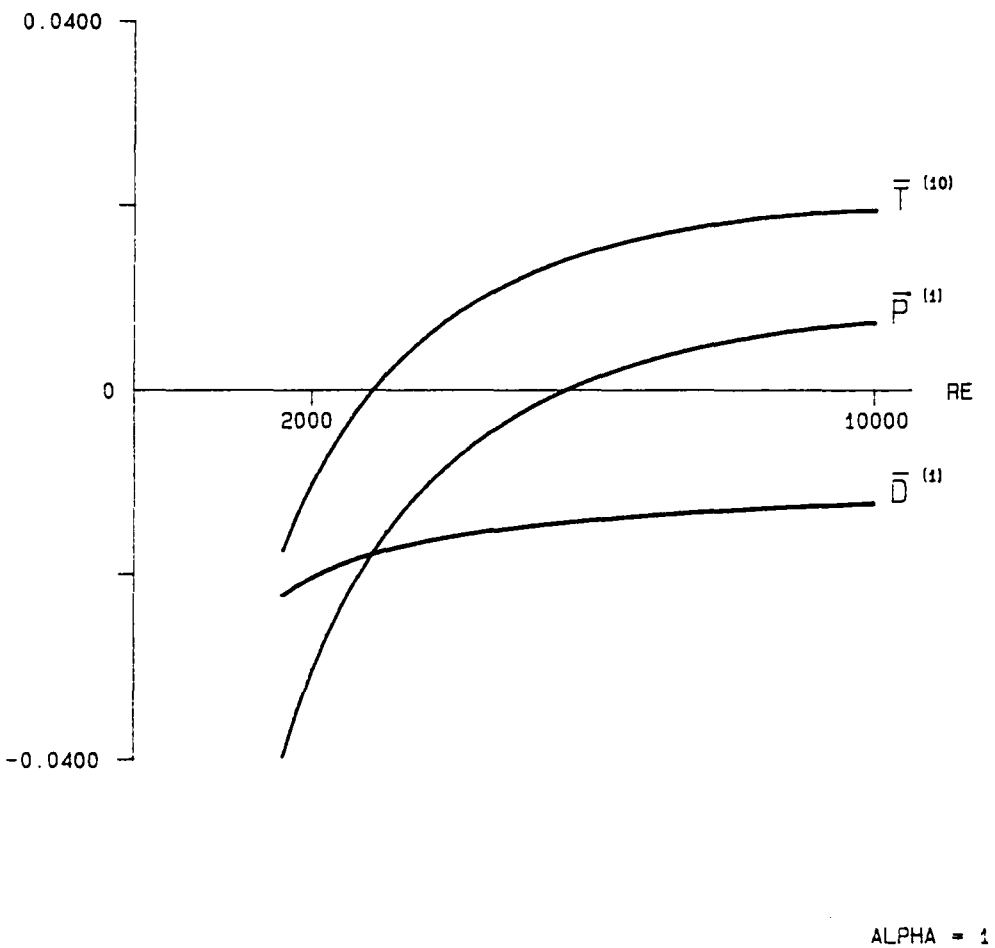

Figure 2.35- $T^{(10)}$, $D^{(1)}$ and $P^{(1)}$ as functions of Re at $\alpha = 1.000$.

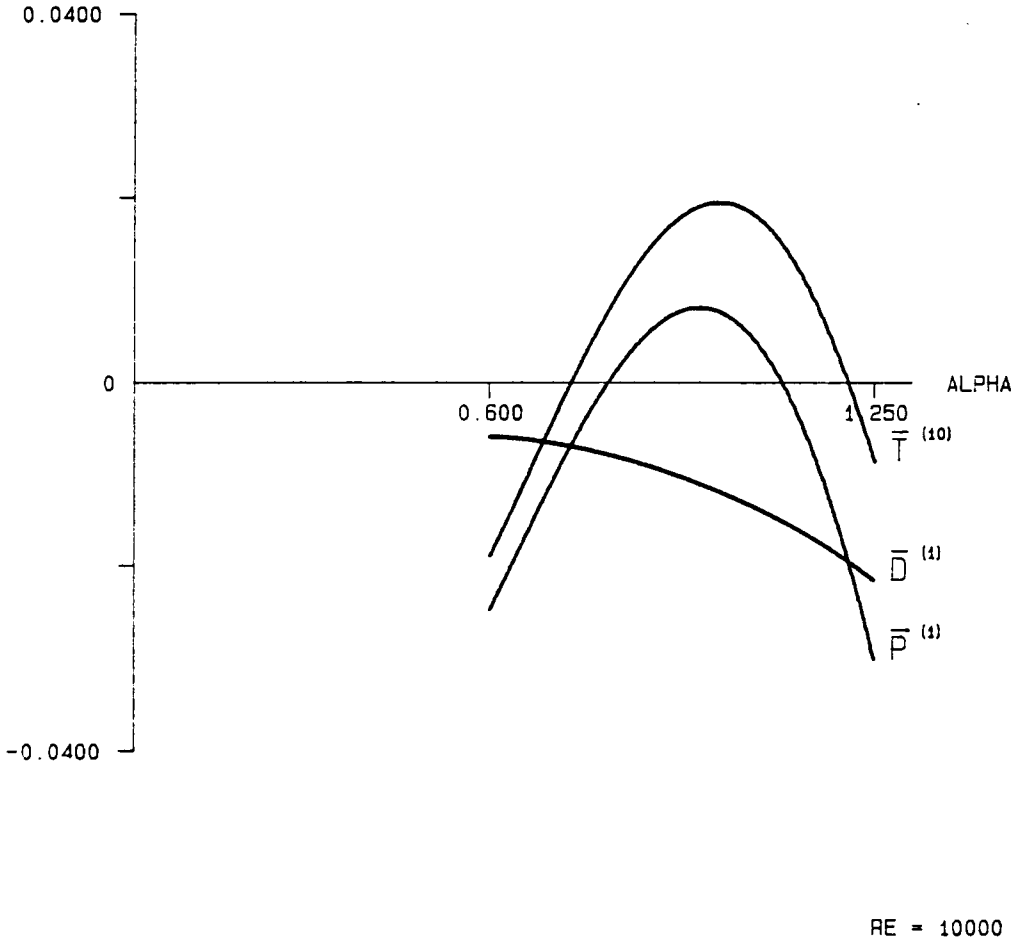

Figure 2.36- $T^{(10)}$, $D^{(1)}$ and $P^{(1)}$ as functions of α at $Re = 10000$.

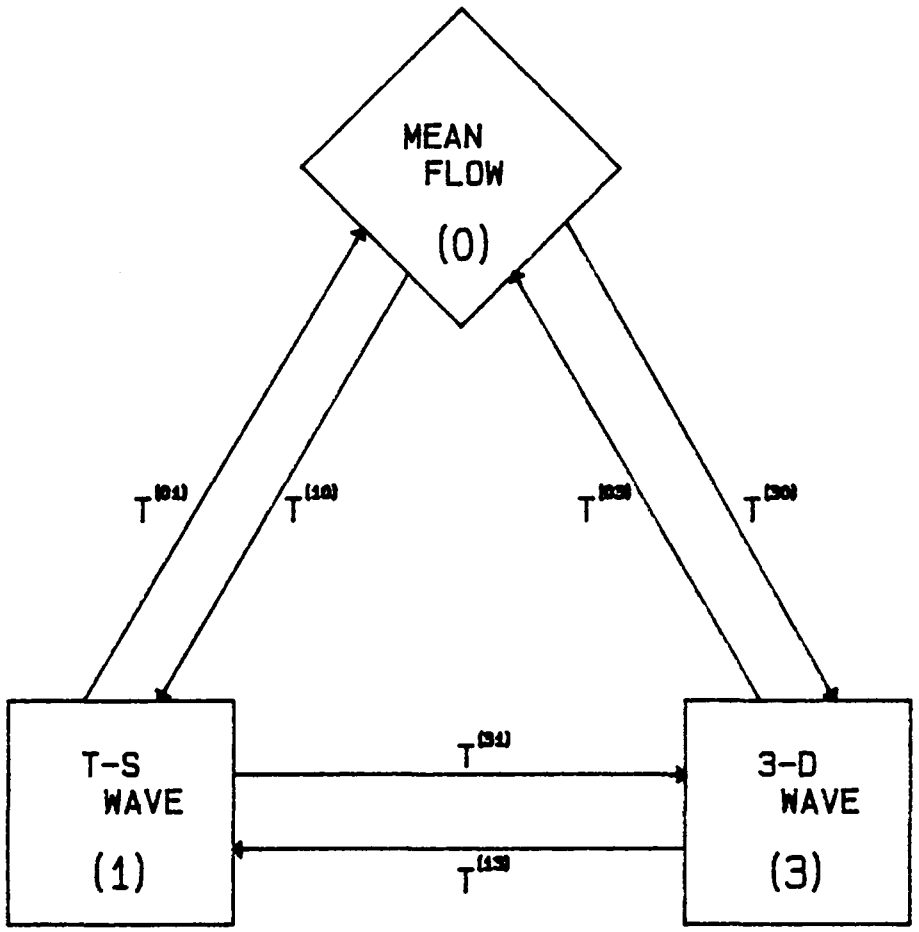

Figure 3.1- Diagram of energy transfer terms $T^{(ij)}$.

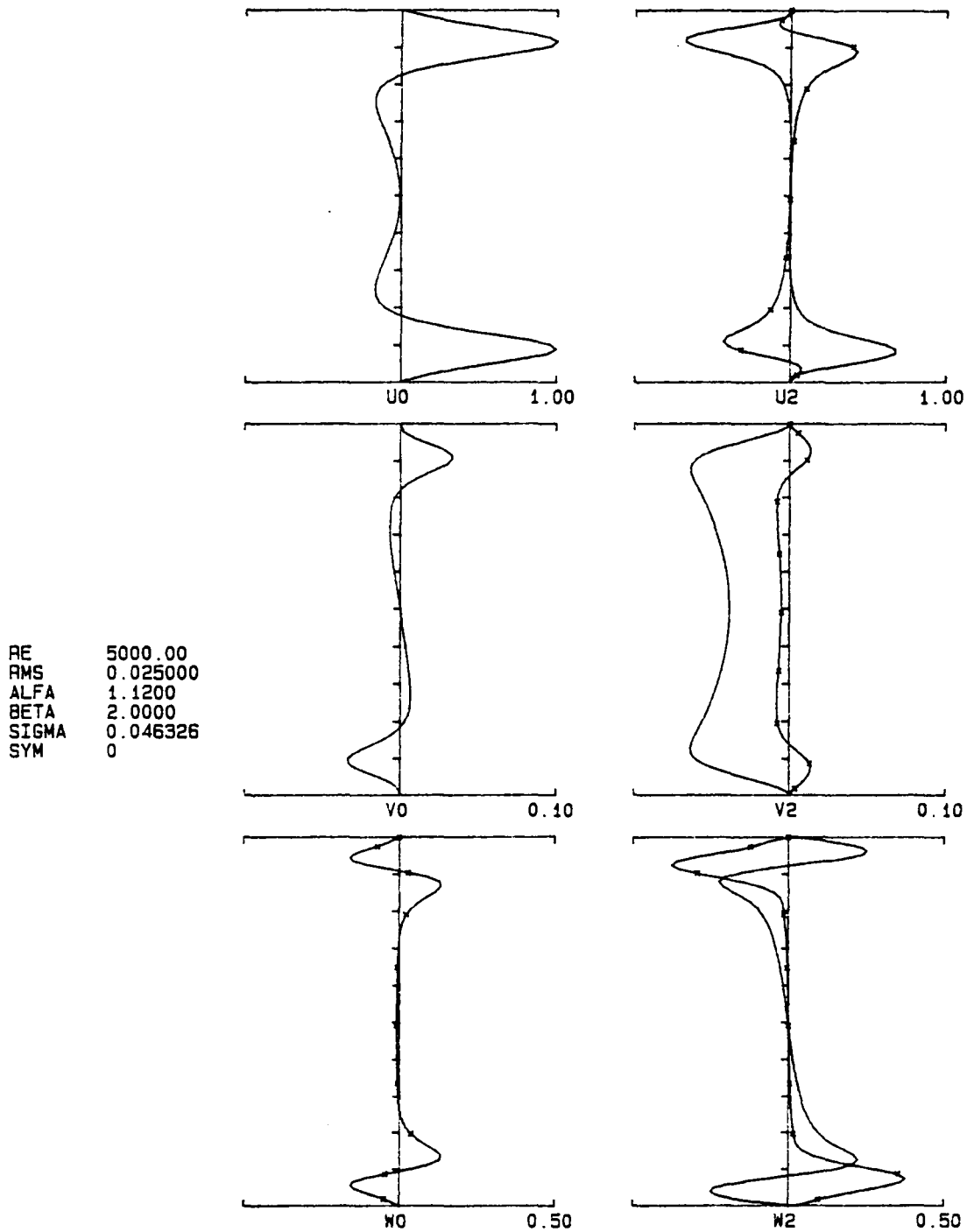

Figure 3.2- Eigenfunction for $\mathbf{v}_f$, at $\alpha = 1.12$, $Re = 5000$, $\beta = 2.0$, $A = 0.025$.

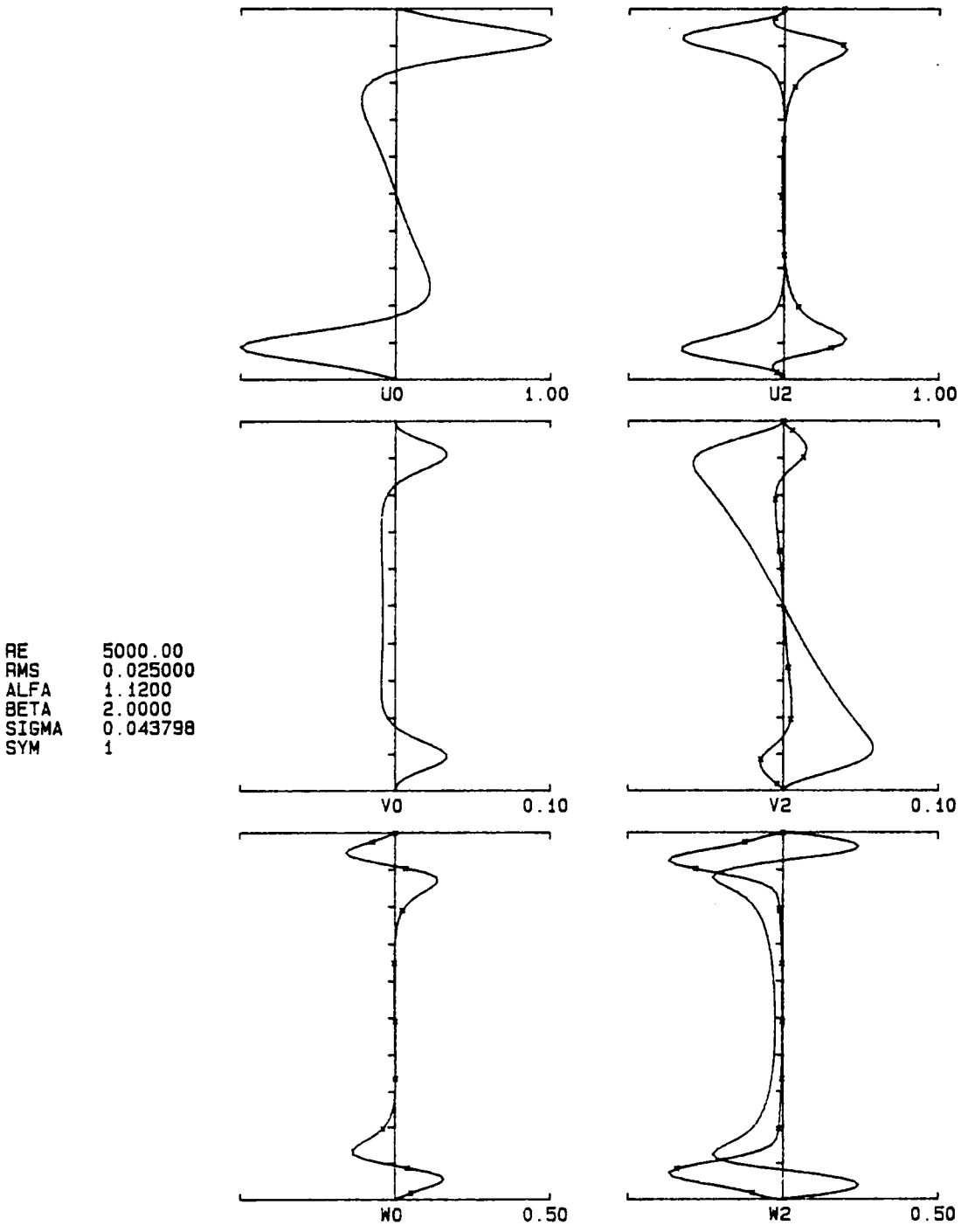

Figure 3.3- Eigenfunction for $\mathbf{v}_{fs}$ at $\alpha = 1.12$, $Re = 5000$, $\beta = 2.00$, $A = 0.025$.

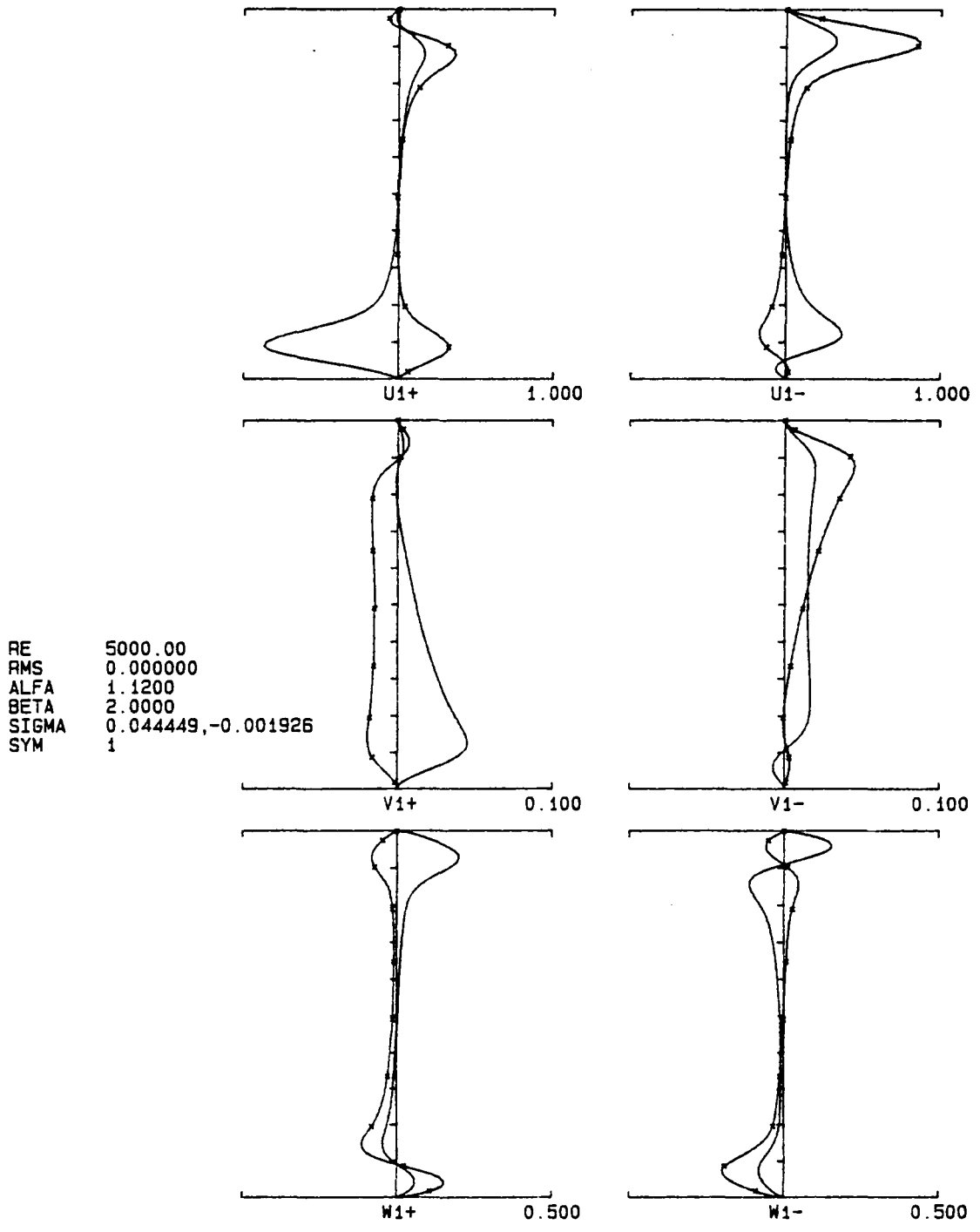

Figure 3.4- Eigenfunction for $\mathbf{v}_1$ at $\alpha = 1.12$, $Re = 5000$, $\beta = 2.0$, $A = 0.025$.

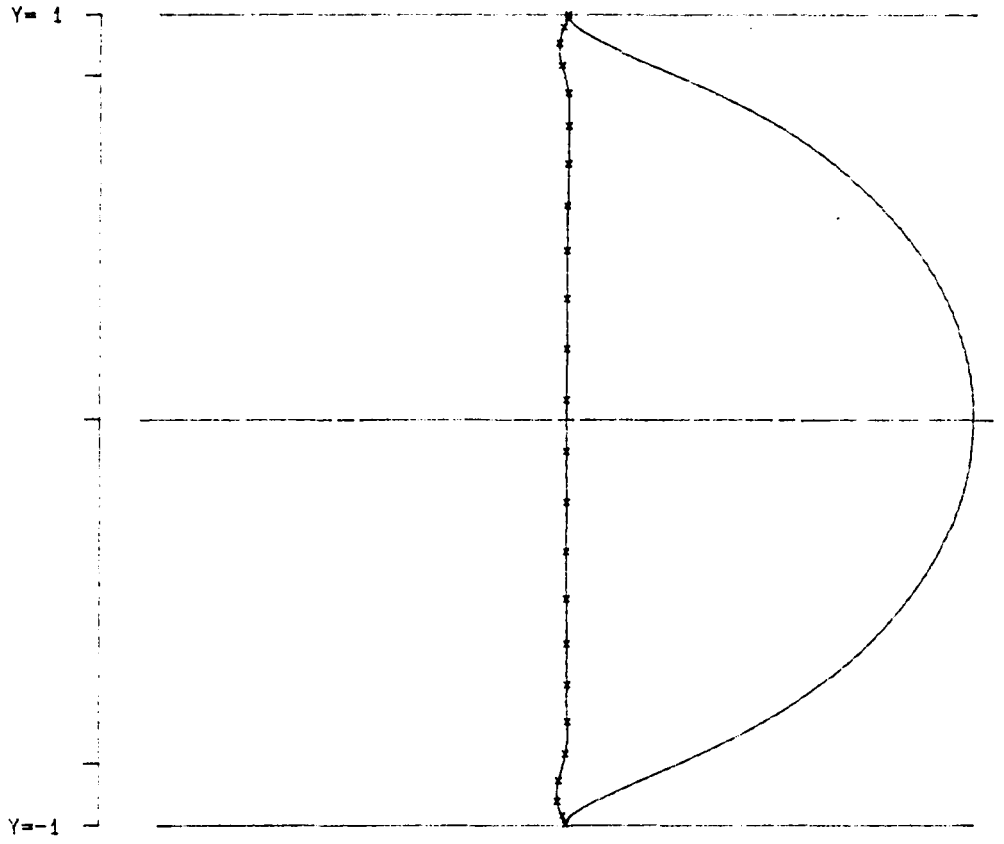

EIGENFUNCTION PSI(Y)

RE	5000.0	CR	0.281752
ALPHA	1.1200	CI	-0.002485

PSI(0) = 1

Figure 3.5- Eigenfunction of OSE for $\alpha = 1.1200$, $Re = 5000$.

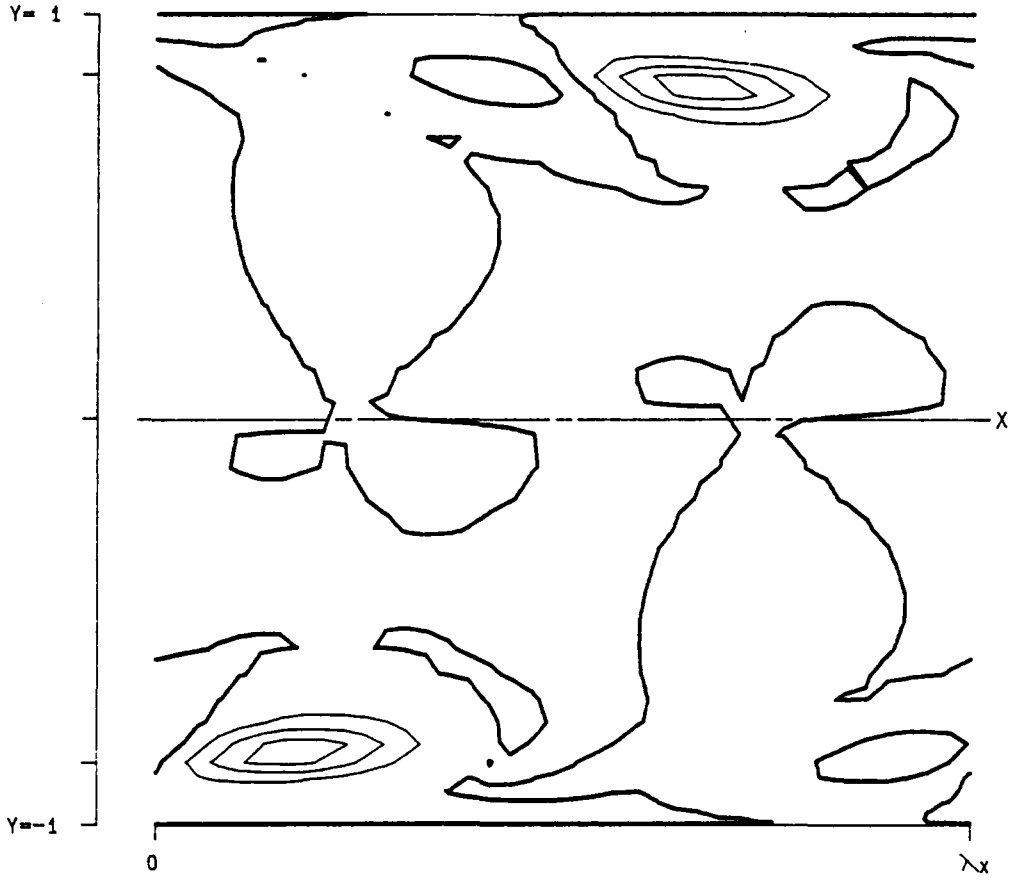

PPT 3-D F T31 (X, Y, Z)

RE	5000.0	LEVELS: MIN	-0.0005081
ALPHA	1.1200	DIF	0.0001016
BETA	2.0000	NO.	20
SIGMA	0.046326		
RMS	0.025000	Z =	-0.120831
MAX	0.001474		
SYM	0		

Figure 3.6- $T^{(31)}$ as a function of x, y and z at a position of $z = -0.120831$ for $\mathbf{v}_{f_\theta}$ at $\alpha = 1.12$, $Re = 5000$, $\beta = 2.00$ and $A = 0.025$.

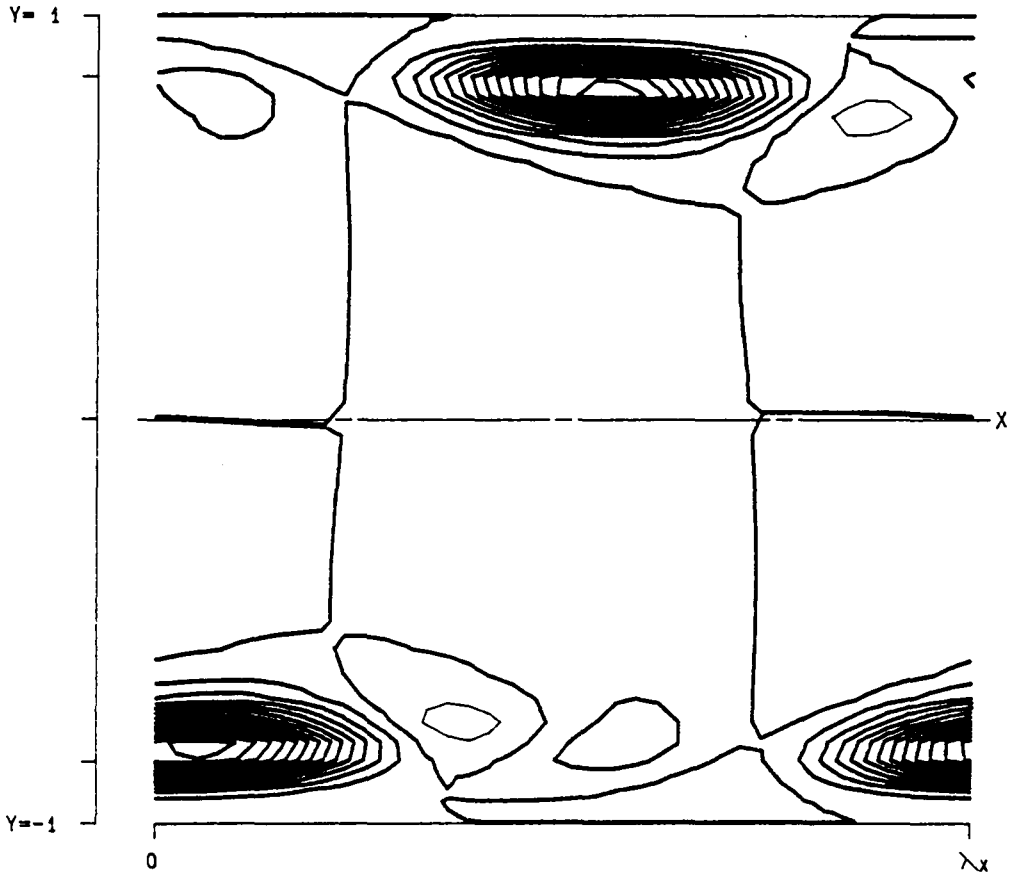

PPT 3-D F T30 (X, Y, Z)

RE	5000.0
ALPHA	1.1200
BETA	2.0000
SIGMA	0.046326
RMS	0.025000
MAX	0.001474
SYM	0

LEVELS:	MIN	-0.0005081
	DIF	0.0001016
	NO.	20
	Z =	-0.120831

Figure 3.7- $T^{(30)}$ as a function of x, y and z at a position of $z = -0.120831$ for $\mathbf{v}_{f_\bullet}$ at $\alpha = 1.12$, $Re = 5000$, $\beta = 2.00$ and $A = 0.025$.

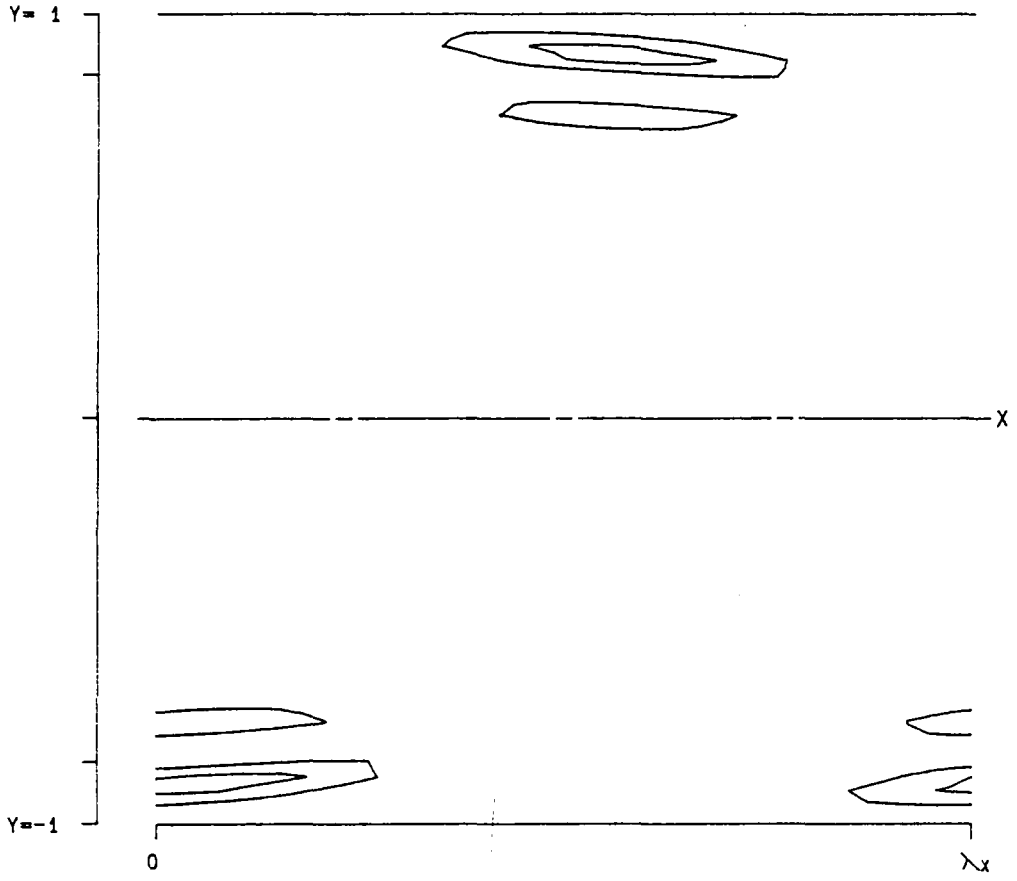

PPT 3-D F D3 (X, Y, Z)

RE	5000.0
ALPHA	1.1200
BETA	2.0000
SIGMA	0.046326
RMS	0.025000
MAX	0.001474
SYM	0

LEVELS:	MIN	-0.0005081
	DIF	0.0001016
	NO.	20
	Z =	-0.120831

Figure 3.8- $D^{(3)}$ as a function of x, y and z at a position of $z = -0.120831$ for $\mathbf{v}_f$, at $\alpha = 1.12$, $Re = 5000$, $\beta = 2.00$ and $A = 0.025$.

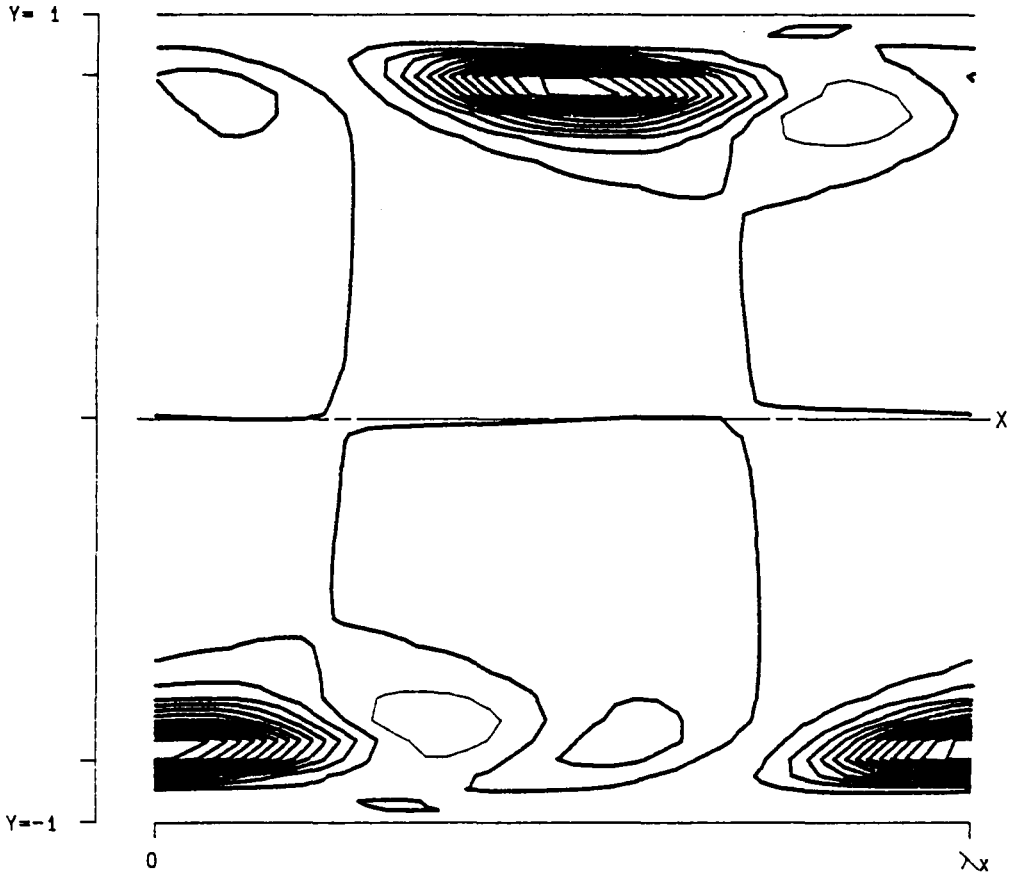

PPT 3-D F P3 (X, Y, Z)

RE	5000.0	LEVELS:	MIN -0.0005081
ALPHA	1.1200		DIF 0.0001016
BETA	2.0000		NO. 20
SIGMA	0.046326		
RMS	0.025000		Z = -0.120831
MAX	0.001474		
SYM	0		

Figure 3.9- $P^{(3)}$ as a function of x, y and z at a position of $z = -0.120831$ for $\mathbf{v}_{f_s}$ at $\alpha = 1.12$, $Re = 5000$, $\beta = 2.00$ and $A = 0.025$.

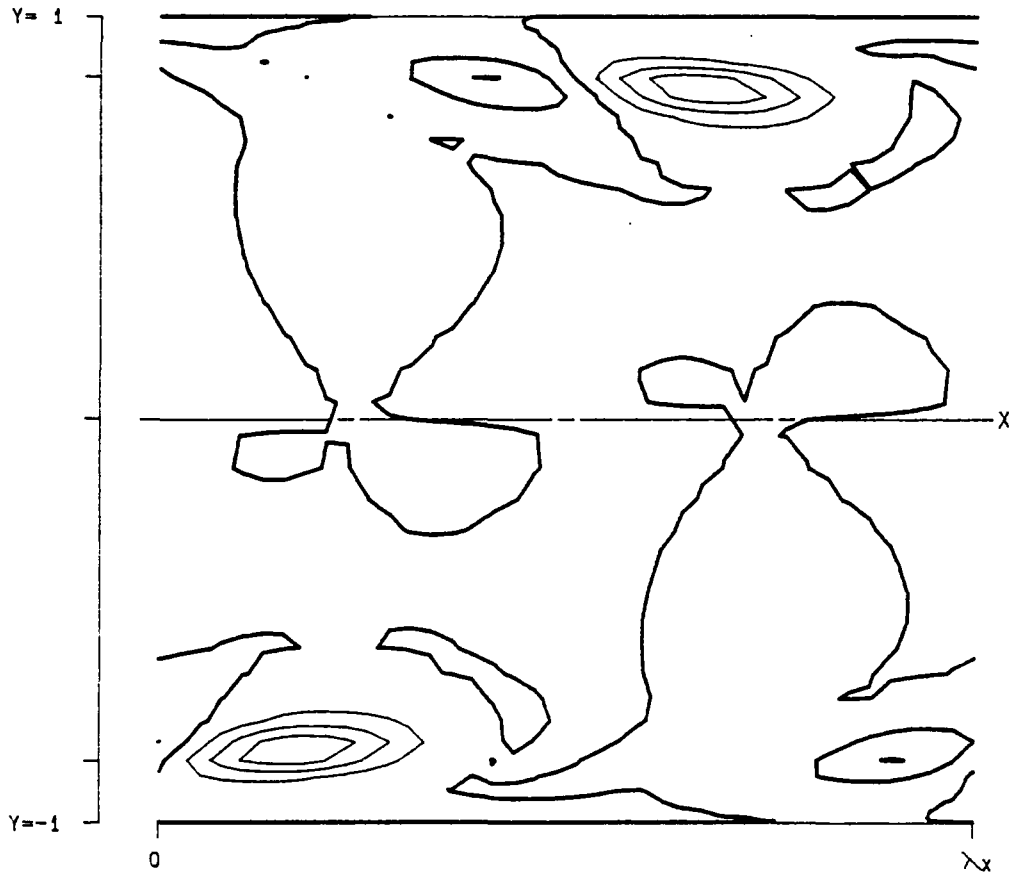

PPT 3-D F T31 (X, Y, Z)

RE	5000.0
ALPHA	1.1200
BETA	2.0000
SIGMA	0.046326
RMS	0.025000
MAX	0.001474
SYM	0

LEVELS:	MIN	-0.0005081
	DIF	0.0001016
	NO.	20
	Z =	-0.040277

Figure 3.10- $T^{(31)}$ as a function of x, y and z at a position of $z = -0.040277$ for $\mathbf{v}_f$, at $\alpha = 1.12$, $Re = 5000$, $\beta = 2.00$ and $A = 0.025$.

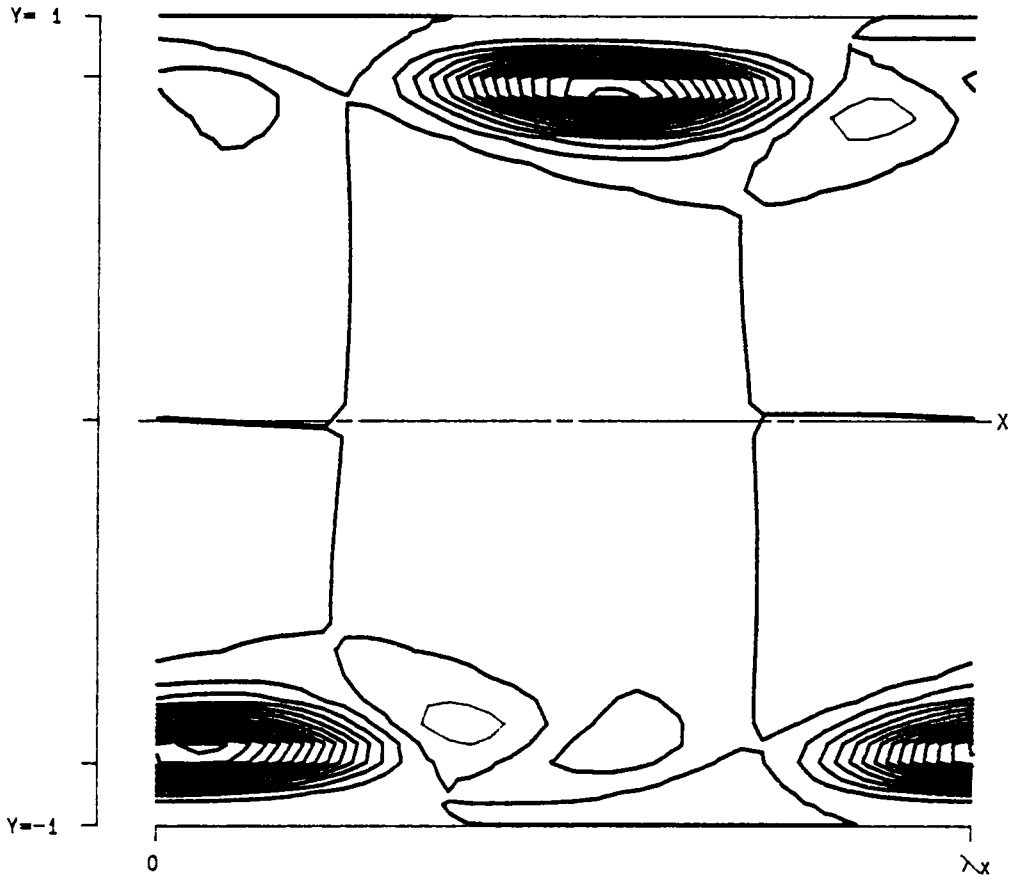

PPT 3-D F T30 (X, Y, Z)

RE	5000.0
ALPHA	1.1200
BETA	2.0000
SIGMA	0.046326
RMS	0.025000
MAX	0.001474
SYM	0

LEVELS:	MIN	-0.0005081
	DIF	0.0001016
	NO.	20
	Z =	-0.040277

Figure 3.11- $T^{(30)}$ as a function of x, y and z at a position of $z = -0.040277$ for $\mathbf{v}_f$, at $\alpha = 1.12$, $Re = 5000$, $\beta = 2.00$ and $A = 0.025$.

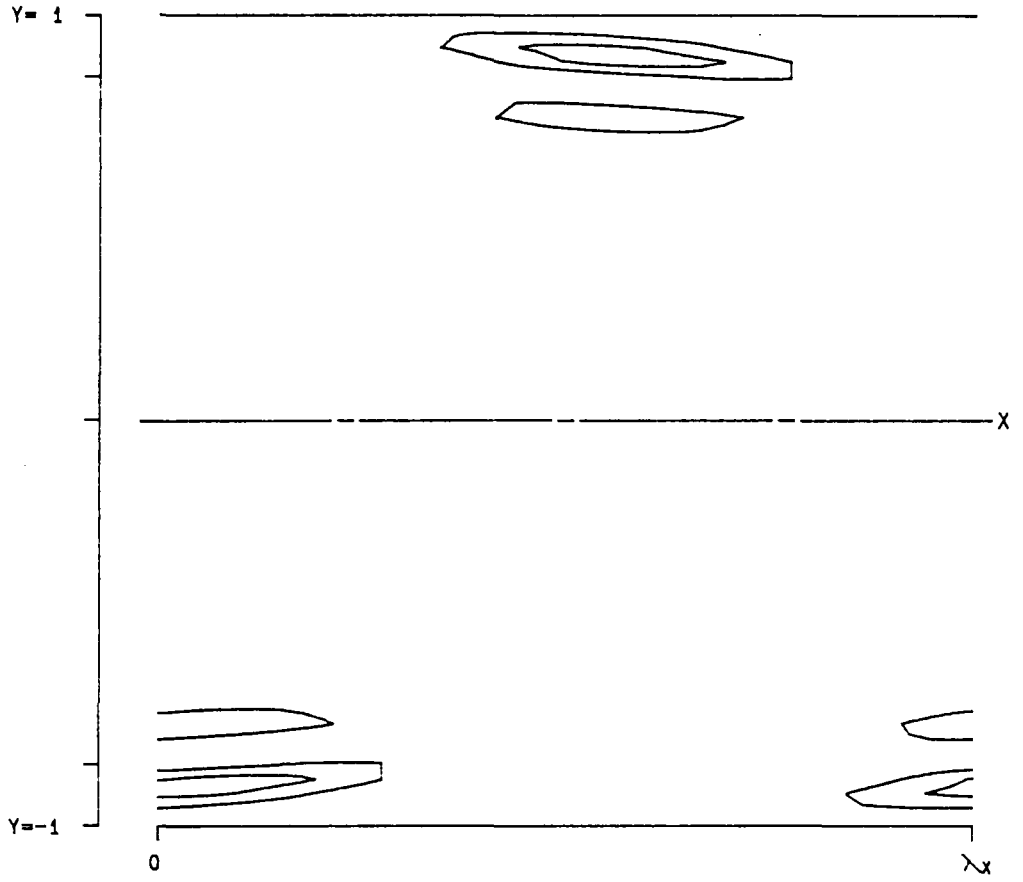

PPT 3-D F D3 (X, Y, Z)

RE	5000.0	LEVELS: MIN	-0.0005081
ALPHA	1.1200	DIF	0.0001016
BETA	2.0000	NO.	20
SIGMA	0.046326		
RMS	0.025000	Z =	-0.040277
MAX	0.001474		
SYM	0		

Figure 3.12- $D^{(3)}$ as a function of x, y and z at a position of $z = -0.040277$ for $\mathbf{v}_f$, at $\alpha = 1.12$, $Re = 5000$, $\beta = 2.00$ and $A = 0.025$.

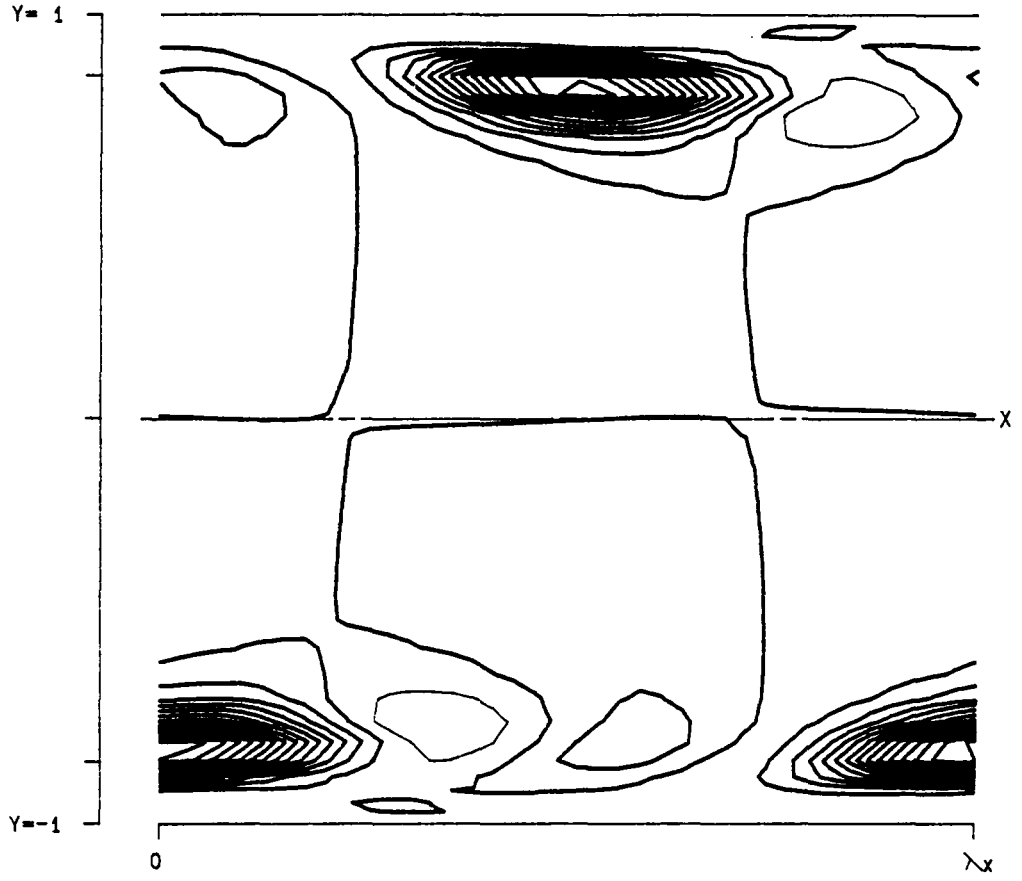

PPT 3-D F P3 (X, Y, Z)

RE	5000.0
ALPHA	1.1200
BETA	2.0000
SIGMA	0.046326
RMS	0.025000
MAX	0.001474
SYM	0

LEVELS:	MIN	-0.0005081
	DIF	0.0001016
	NO.	20
	Z =	-0.040277

Figure 3.13- $P^{(3)}$ as a function of x, y and z at a position of $z = -0.040277$ for $\mathbf{v}_{f_s}$ at $\alpha = 1.12$, $Re = 5000$, $\beta = 2.00$ and $A = 0.025$.

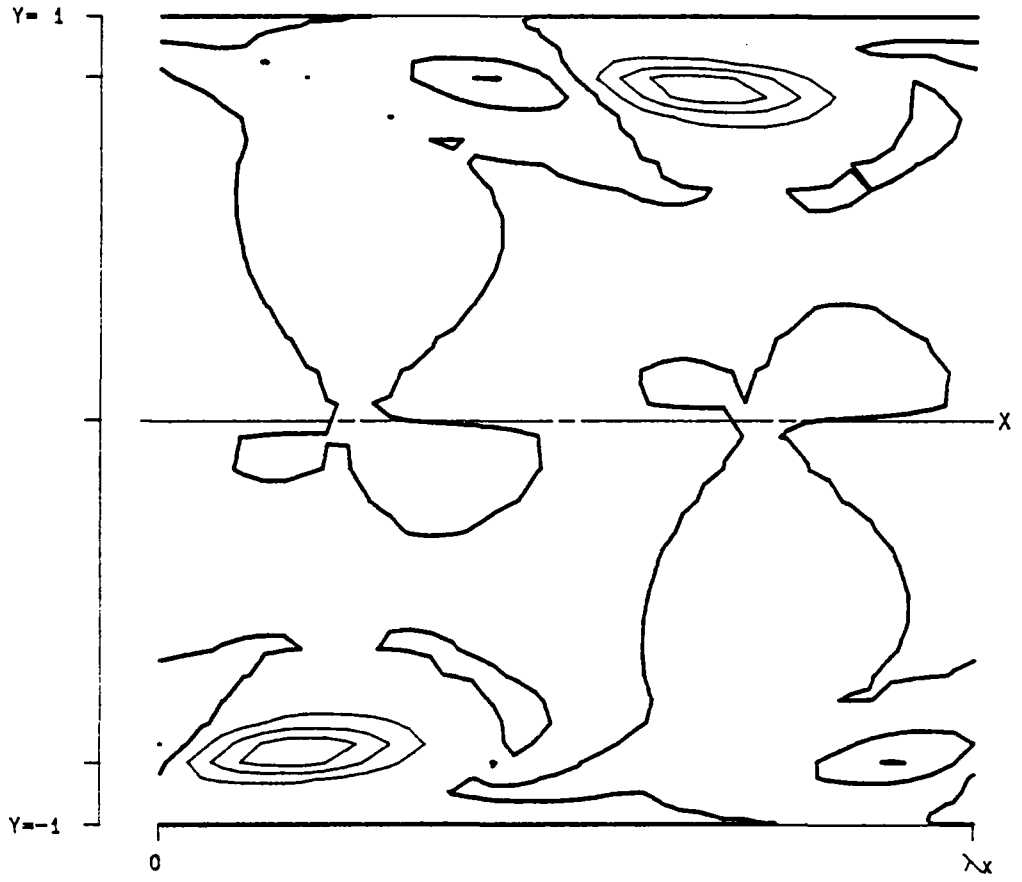

PPT 3-D F T31 (X, Y, Z)

RE	5000.0
ALPHA	1.1200
BETA	2.0000
SIGMA	0.046326
RMS	0.025000
MAX	0.001474
SYM	0

LEVELS:	MIN	-0.0005081
	DIF	0.0001016
	NO.	20
	Z =	0.040277

Figure 3.14- $T^{(31)}$ as a function of x, y and z at a position of $z = 0.040277$ for $\mathbf{v}_f$, at $\alpha = 1.12$, $Re = 5000$, $\beta = 2.00$ and $A = 0.025$.

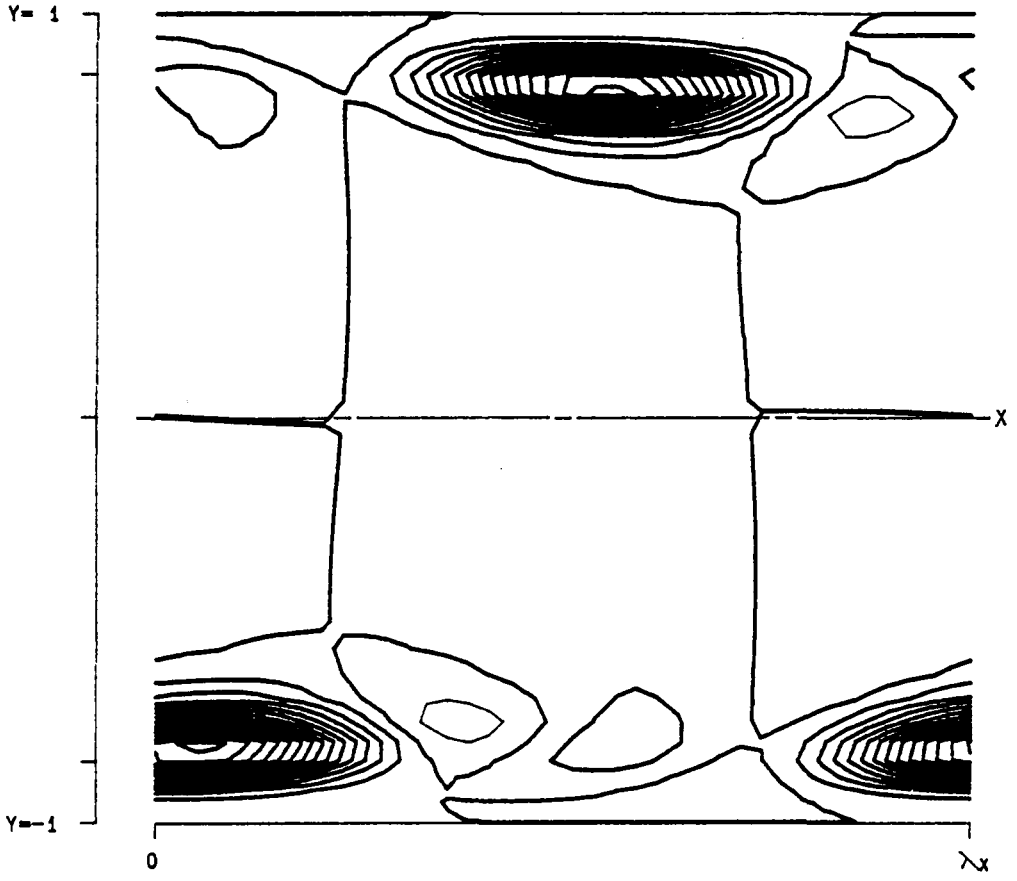

PPT 3-D F T30 (X, Y, Z)

RE	5000.0
ALPHA	1.1200
BETA	2.0000
SIGMA	0.046326
RMS	0.025000
MAX	0.001474
SYM	0

LEVELS:	MIN	-0.0005081
	DIF	0.0001016
	NO.	20
	Z =	0.040277

Figure 3.15- $T^{(30)}$ as a function of x, y and z at a position of $z = 0.040277$ for $\mathbf{v}_f$, at $\alpha = 1.12$, $Re = 5000$, $\beta = 2.00$ and $A = 0.025$.

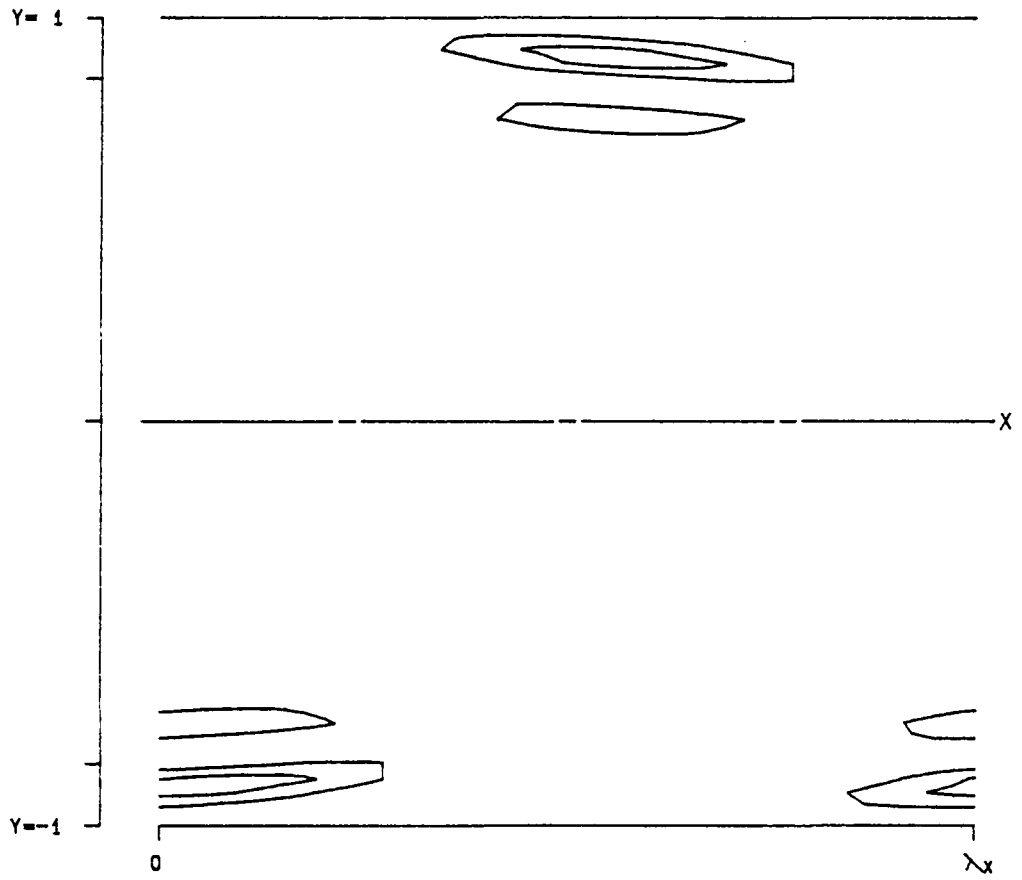

PPT 3-D F D3 (X, Y, Z)

RE	5000.0
ALPHA	1.1200
BETA	2.0000
SIGMA	0.046326
RMS	0.025000
MAX	0.001474
SYM	0

LEVELS:	MIN	-0.0005081
	DIF	0.0001016
	NO.	20
	Z =	0.040277

Figure 3.16- $D^{(3)}$ as a function of x, y and z at a position of $z = 0.040277$ for $\mathbf{v}_f$, at $\alpha = 1.12$, $Re = 5000$, $\beta = 2.00$ and $A = 0.025$.

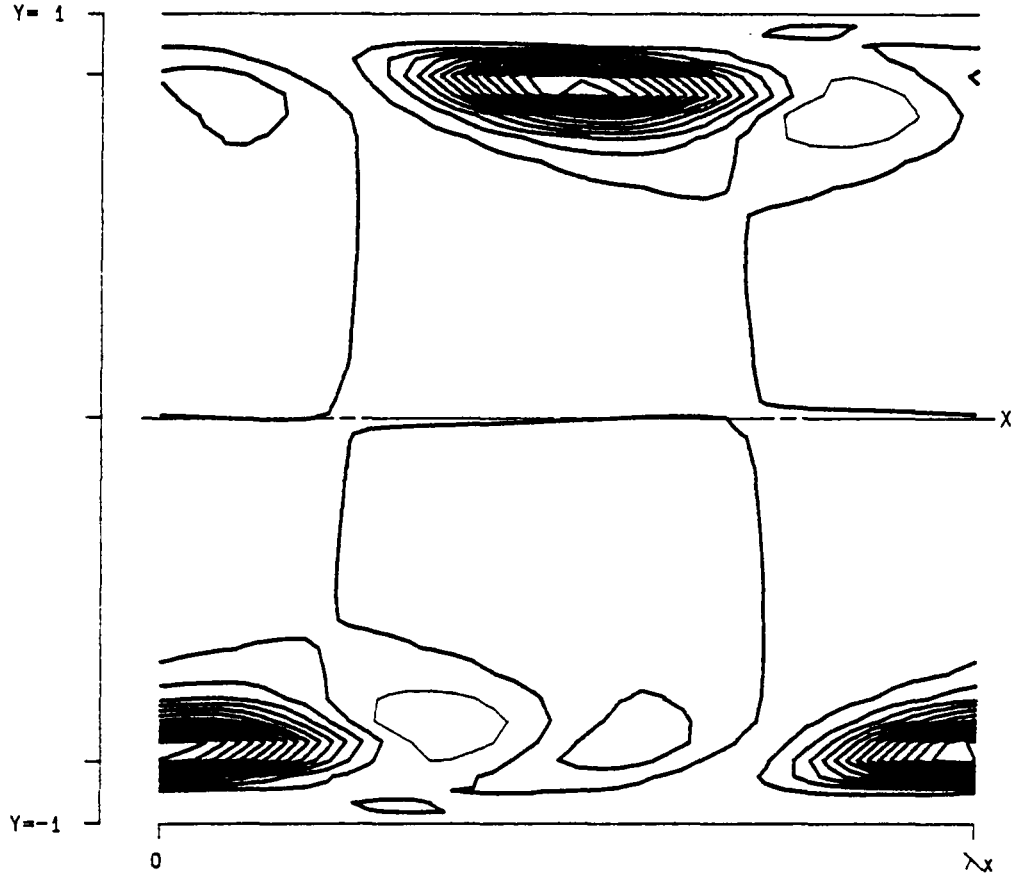

PPT 3-D F P3 (X, Y, Z)

RE	5000.0
ALPHA	1.1200
BETA	2.0000
SIGMA	0.046326
RMS	0.025000
MAX	0.001474
SYM	0

LEVELS:	MIN	-0.0005081
	DIF	0.0001016
	NO.	20
	Z =	0.040277

Figure 3.17- $P^{(3)}$ as a function of x, y and z at a position of $z = 0.040277$ for $\mathbf{v}_f$, at $\alpha = 1.12$, $Re = 5000$, $\beta = 2.00$ and $A = 0.025$.

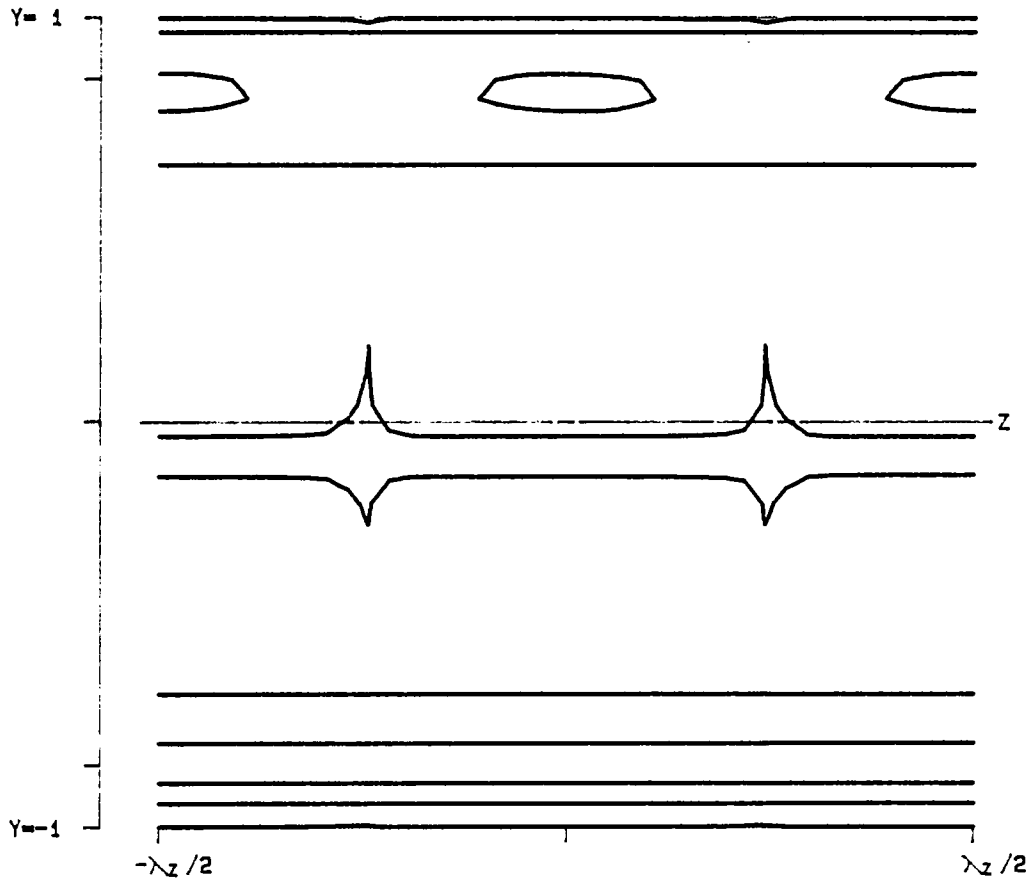

PPT 3-D F T31 (X, Y, Z)

RE	5000.0	LEVELS: MIN	-0.0005081
ALPHA	1.1200	DIF	0.0001016
BETA	2.0000	NO.	20
SIGMA	0.046326		
RMS	0.025000	X =	2.589225
MAX	0.001474		
SYM	0		

Figure 3.18- $T^{(31)}$ as a function of x, y and z at a position of $x = 2.589225$ for $\mathbf{v}_f$, at $\alpha = 1.12$, $Re = 5000$, $\beta = 2.00$ and $A = 0.025$.

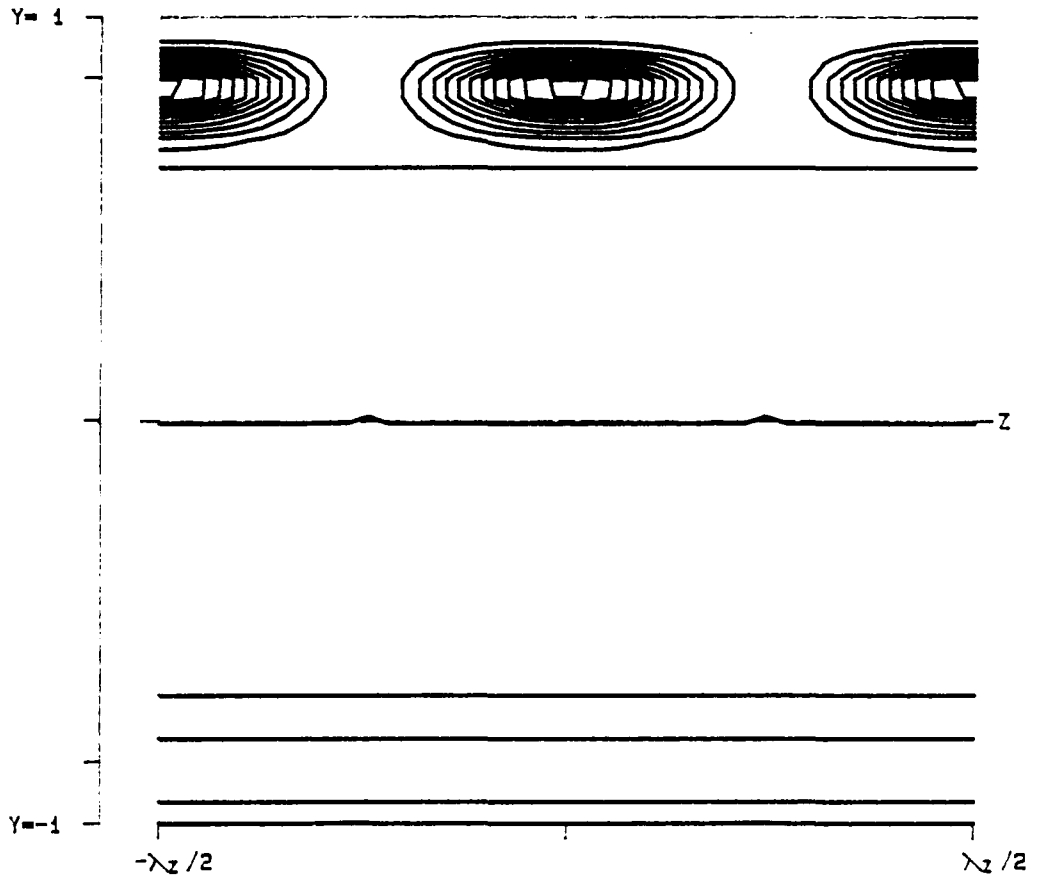

PPT 3-D F T30 (X, Y, Z)

RE	5000.0
ALPHA	1.1200
BETA	2.0000
SIGMA	0.046325
RMS	0.025000
MAX	0.001474
SYM	0

LEVELS:	MIN	-0.0005081
	DIF	0.0001016
	NO.	20
	X =	2.589225

Figure 3.19- $T^{(30)}$ as a function of x, y and z at a position of $x = 2.589225$ for $\mathbf{v}_f$, at $\alpha = 1.12$, $Re = 5000$, $\beta = 2.00$ and $A = 0.025$.

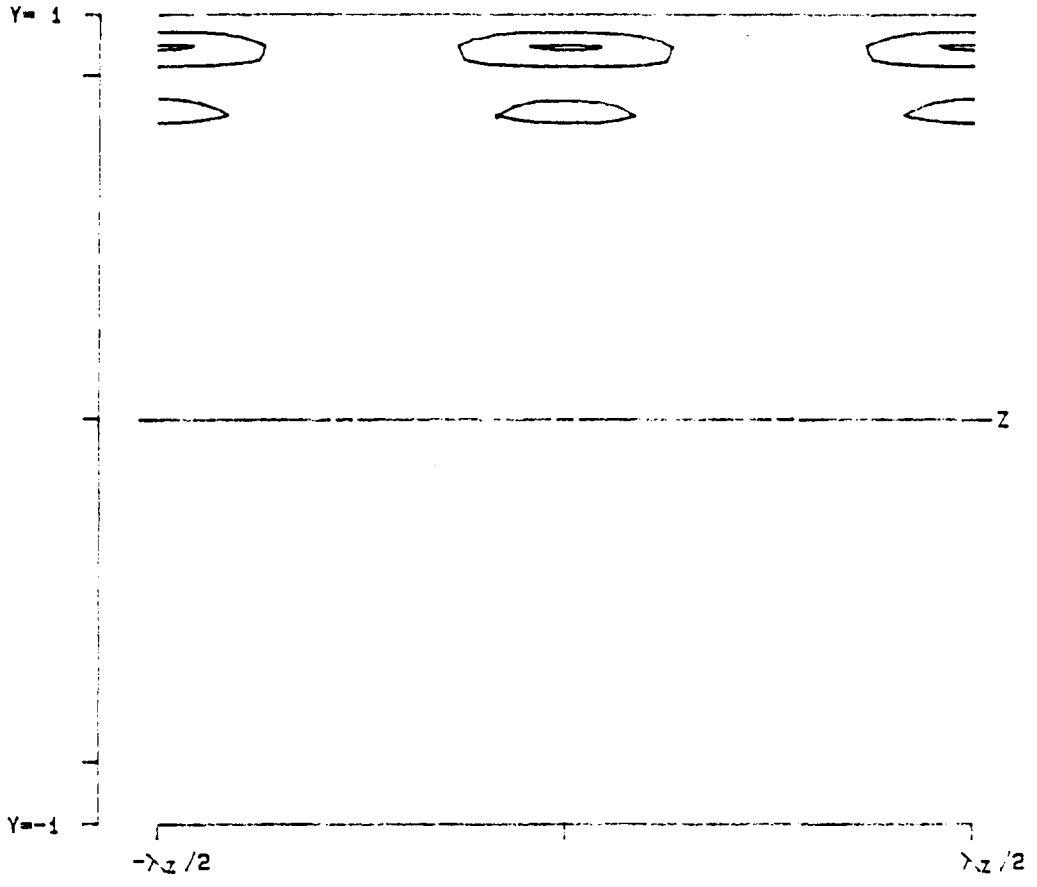

PPT 3-D F D3 (X, Y, Z)

RE	5000.0
ALPHA	1.1200
BETA	2.0000
SIGMA	0.046326
RMS	0.025000
MAX	0.001474
SYM	0

LEVELS:	MIN	-0.0005081
	DIF	0.0001016
	NO.	20
	X =	2.589225

Figure 3.20- $D^{(3)}$ as a function of x, y and z at a position of $x = 2.589225$ for $\mathbf{v}_f$, at $\alpha = 1.12$, $Re = 5000$, $\beta = 2.00$ and $A = 0.025$.

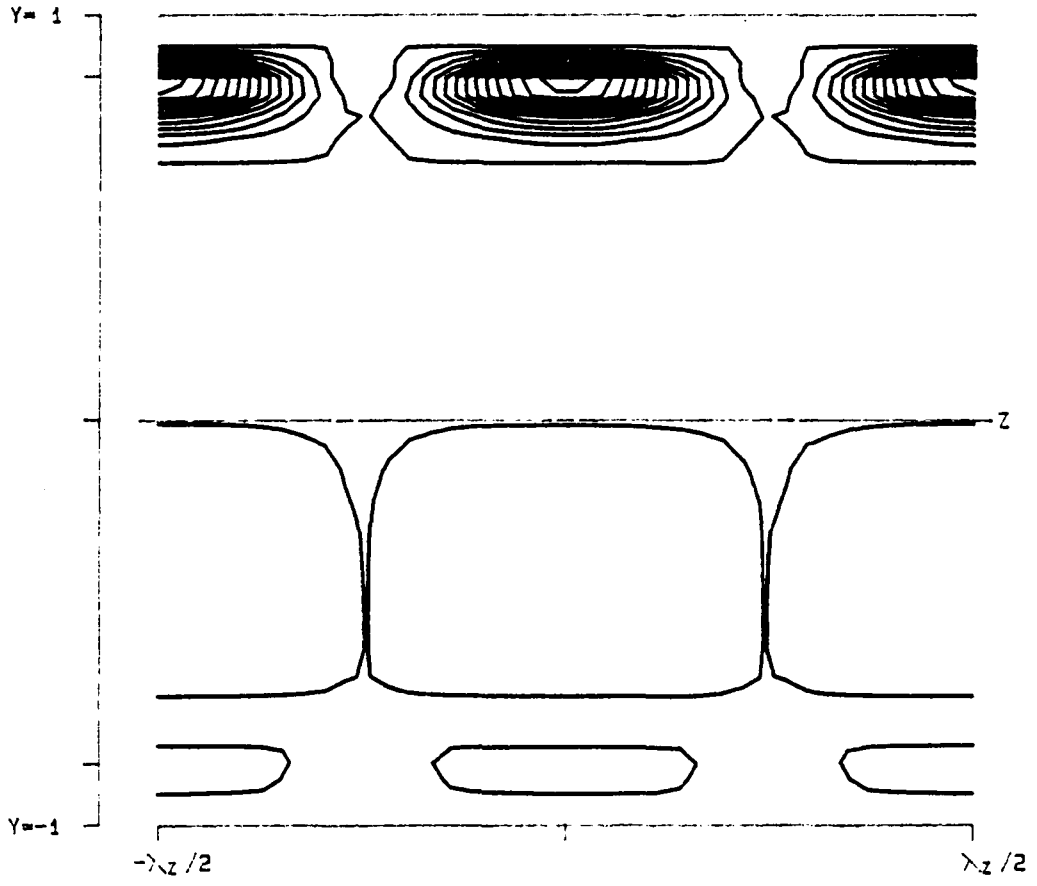

PPT 3-D F P3 (X, Y, Z)

RE	5000.0
ALPHA	1.1200
BETA	2.0000
SIGMA	0.046326
RMS	0.025000
MAX	0.001474
SYM	0

LEVELS:	MIN	-0.0005081
	DIF	0.0001016
	NO.	20
	X =	2.589225

Figure 3.21- $P^{(3)}$ as a function of x, y and z at a position of $x = 2.589225$ for $\mathbf{v}_f$ at $\alpha = 1.12$, $Re = 5000$, $\beta = 2.00$ and $A = 0.025$.

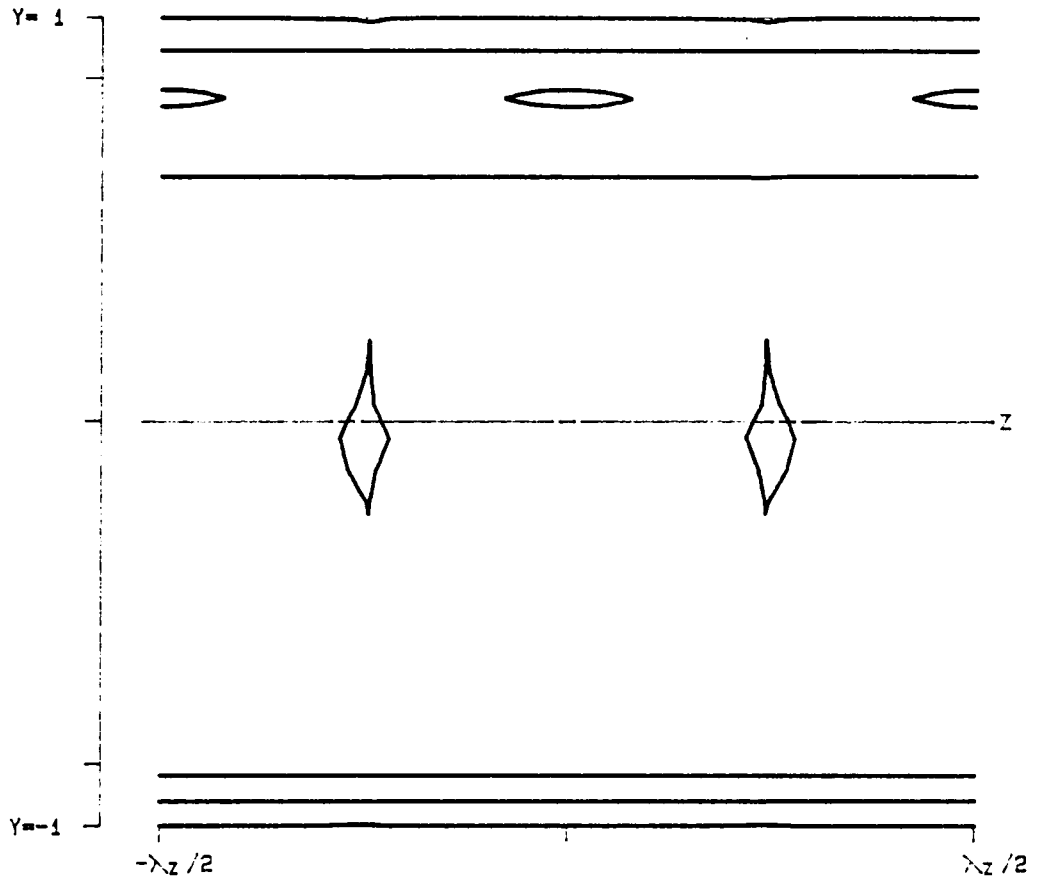

PPT 3-D F T31 (X, Y, Z)

RE	5000.0	LEVELS:	MIN	-0.0005081
ALPHA	1.1200		DIF	0.0001016
BETA	2.0000		NO.	20
SIGMA	0.046326			
RMS	0.025000		X =	2.733071
MAX	0.001474			
SYM	0			

Figure 3.22- $T^{(31)}$ as a function of x, y and z at a position of $x = 2.733071$ for $\mathbf{v}_f$ at $\alpha = 1.12$, $Re = 5000$, $\beta = 2.00$ and $A = 0.025$.

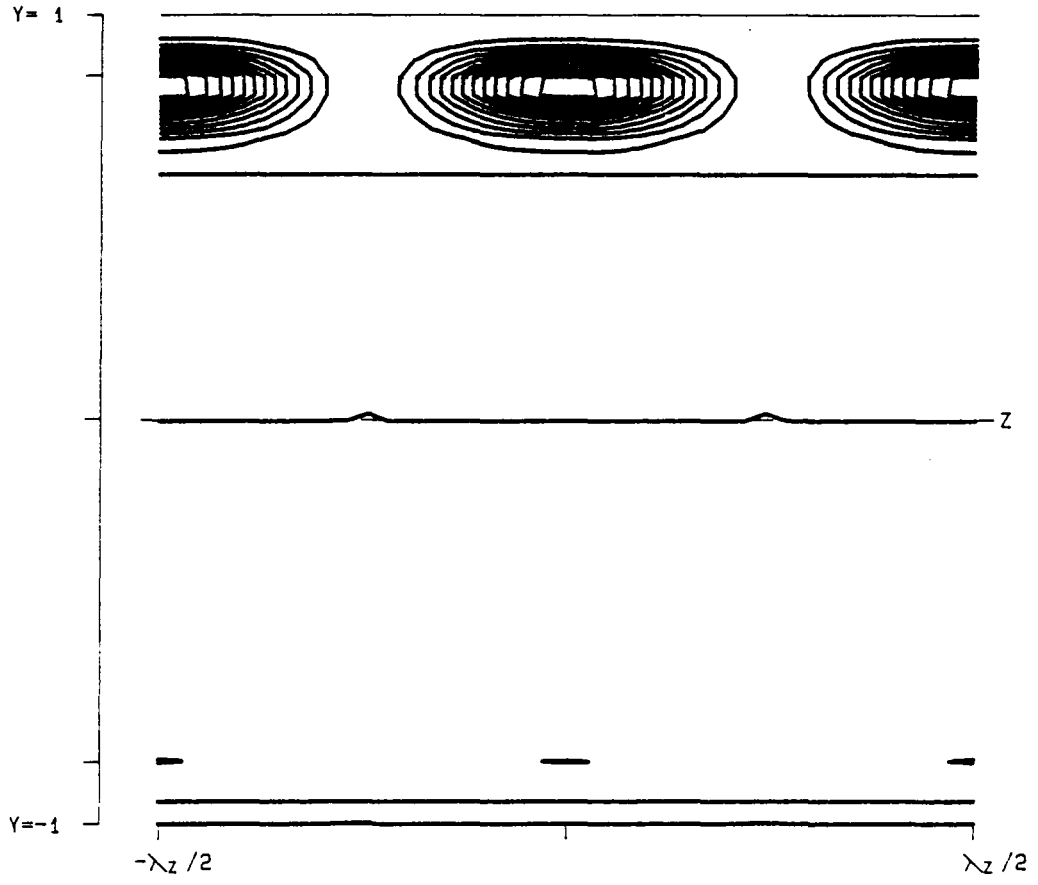

PPT 3-D F T30 (X, Y, Z)

RE	5000.0	LEVELS: MIN	-0.0005081
ALPHA	1.1200	DIF	0.0001016
BETA	2.0000	NO.	20
SIGMA	0.046326		
RMS	0.025000	X =	2.733071
MAX	0.001474		
SYM	0		

Figure 3.23- $T^{(30)}$ as a function of x, y and z at a position of $x = 2.733071$ for $\mathbf{v}_f$, at $\alpha = 1.12$, $Re = 5000$, $\beta = 2.00$ and $A = 0.025$.

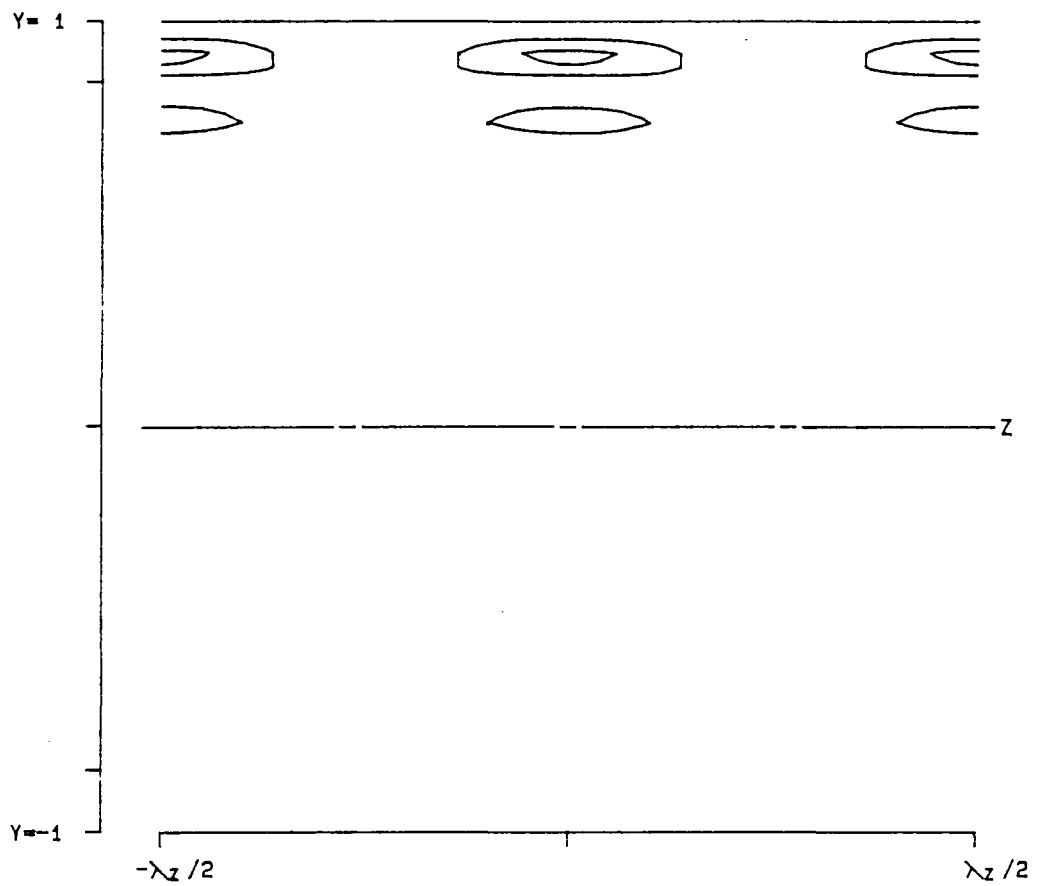

PPT 3-D F D3 (X, Y, Z)

RE	5000.0
ALPHA	1.1200
BETA	2.0000
SIGMA	0.046326
RMS	0.025000
MAX	0.001474
SYM	0

LEVELS:	MIN	-0.0005081
	DIF	0.0001016
	NO.	20
	X =	2.733071

Figure 3.24- $D^{(3)}$ as a function of x, y and z at a position of $x = 2.733071$ for $\mathbf{v}_{f_\theta}$ at $\alpha = 1.12$, $Re = 5000$, $\beta = 2.00$ and $A = 0.025$.

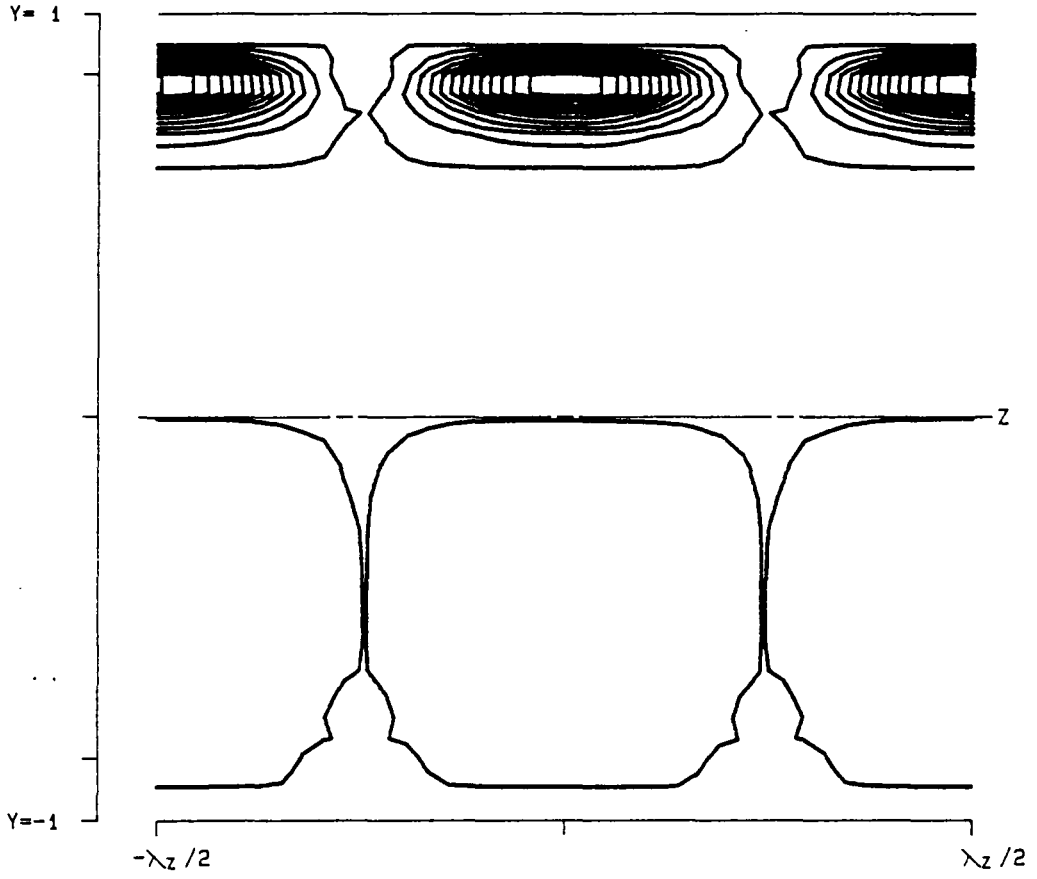

PPT 3-D F P3 (X, Y, Z)

RE	5000.0
ALPHA	1.1200
BETA	2.0000
SIGMA	0.046326
RMS	0.025000
MAX	0.001474
SYM	0

LEVELS:	MIN	-0.0005081
	DIF	0.0001016
	NO.	20
	X =	2.733071

Figure 3.25- $P^{(3)}$ as a function of x, y and z at a position of $x = 2.733071$ for $\mathbf{v}_f$, at $\alpha = 1.12$, $Re = 5000$, $\beta = 2.00$ and $A = 0.025$.

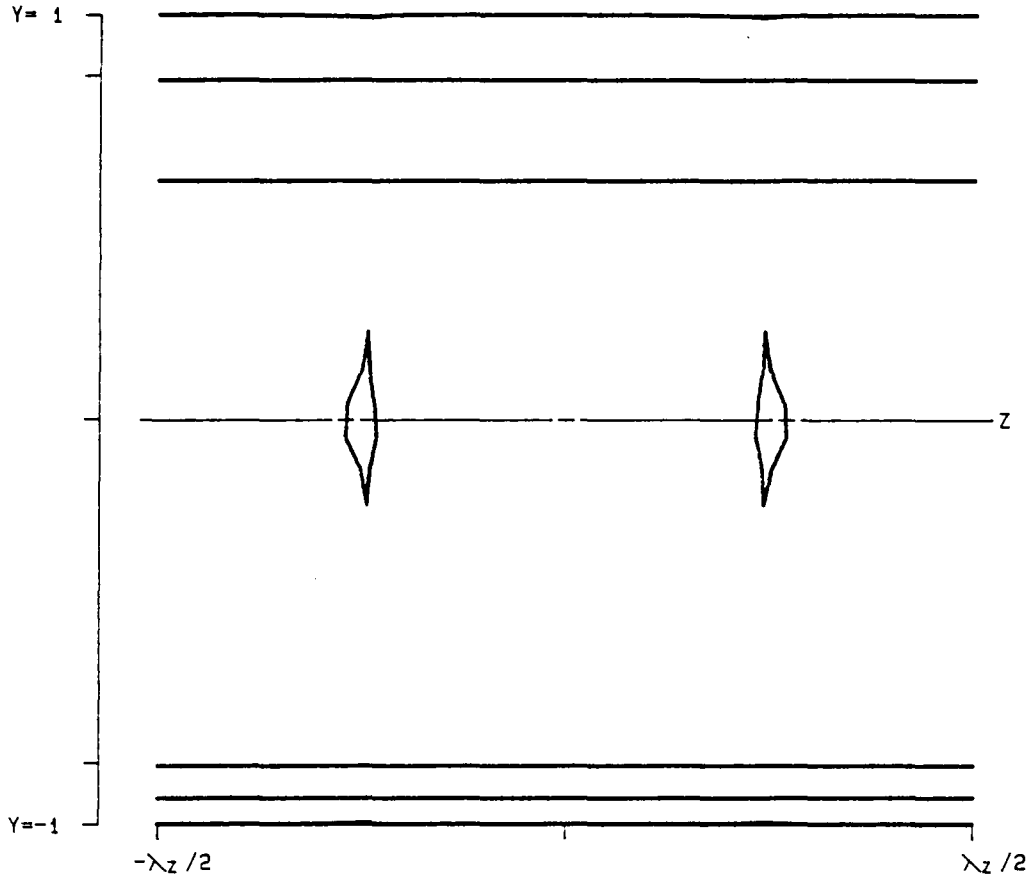

PPT 3-D F T31 (X, Y, Z)

RE	5000.0	LEVELS: MIN	-0.0005081
ALPHA	1.1200	DIF	0.0001016
BETA	2.0000	NO.	20
SIGMA	0.046326		
RMS	0.025000	X =	2.876916
MAX	0.001474		
SYM	0		

Figure 3.26- $T^{(31)}$ as a function of x, y and z at a position of $x = 2.876916$ for $\mathbf{v}_f$, at $\alpha = 1.12$, $Re = 5000$, $\beta = 2.00$ and $A = 0.025$.

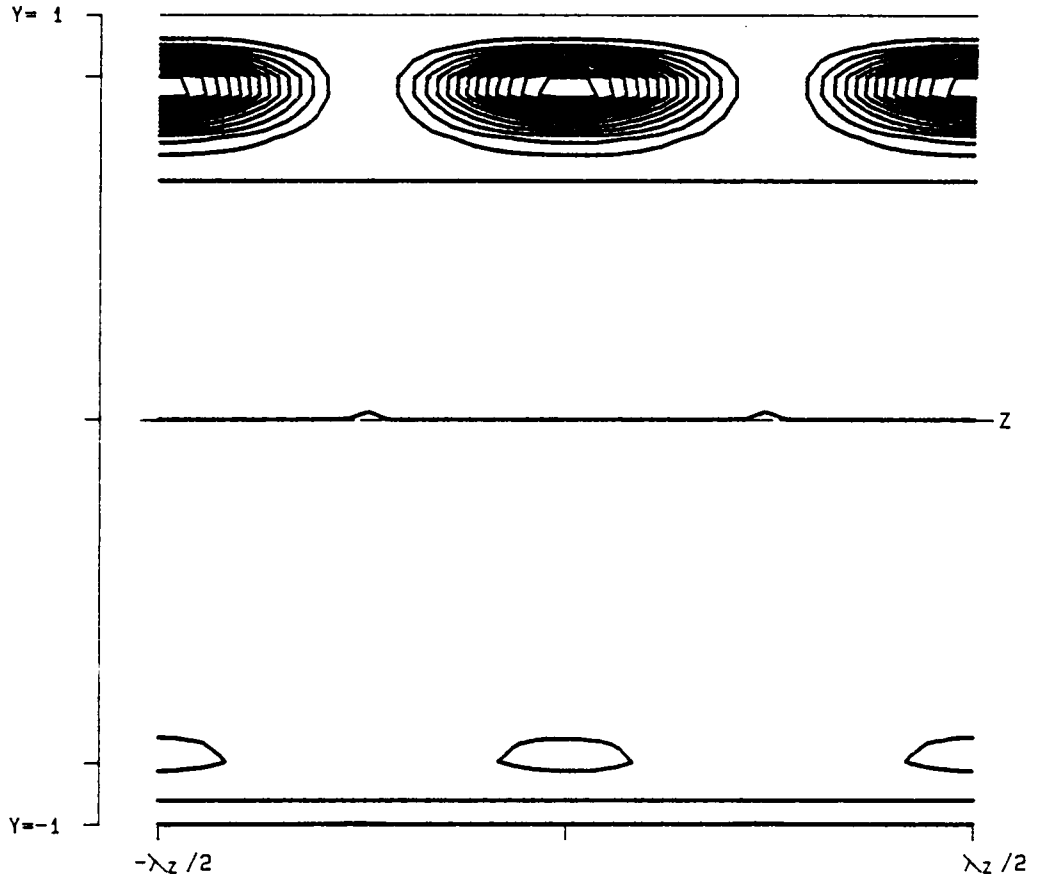

PPT 3-D F T30 (X, Y, Z)

RE	5000.0	LEVELS: MIN	-0.0005081
ALPHA	1.1200	DIF	0.0001016
BETA	2.0000	NO.	20
SIGMA	0.046326		
RMS	0.025000	X =	2.876916
MAX	0.001474		
SYM	0		

Figure 3.27- $T^{(30)}$ as a function of x, y and z at a position of $x = 2.876916$ for $\mathbf{v}_{f_s}$ at $\alpha = 1.12$, $Re = 5000$, $\beta = 2.00$ and $A = 0.025$.

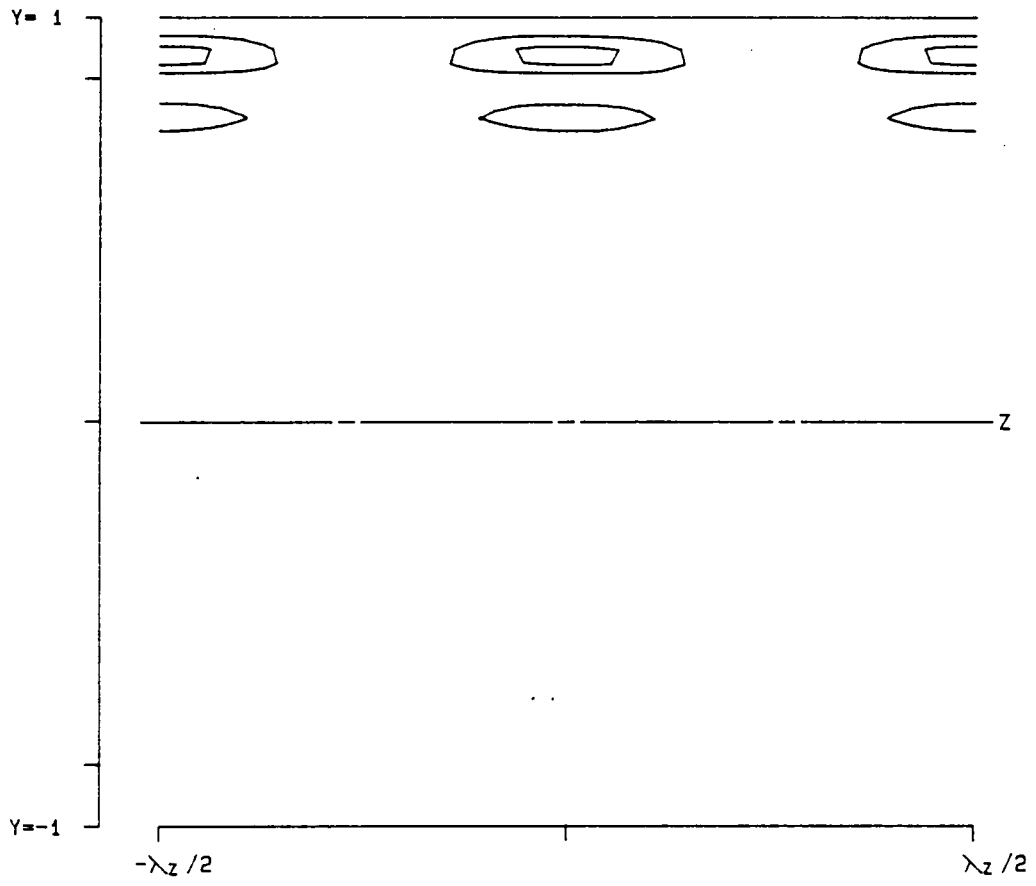

PPT 3-D F D3 (X, Y, Z)

RE	5000.0	LEVELS: MIN	-0.0005081
ALPHA	1.1200	DIF	0.0001016
BETA	2.0000	NO.	20
SIGMA	0.046326		
RMS	0.025000	X =	2.876916
MAX	0.001474		
SYM	0		

Figure 3.28- $D^{(3)}$ as a function of x, y and z at a position of $x = 2.876916$ for $\mathbf{v}_j$, at $\alpha = 1.12$, $Re = 5000$, $\beta = 2.00$ and $A = 0.025$.

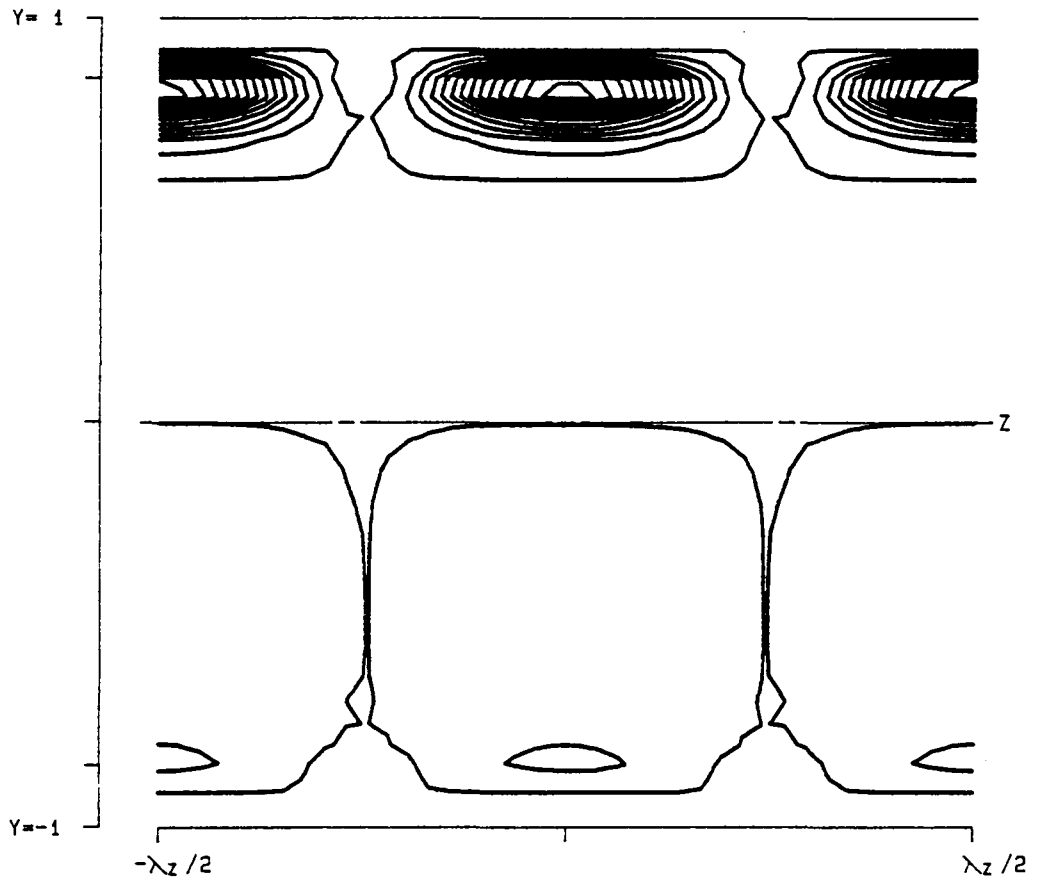

PPT 3-D F P3 (X, Y, Z)

RE	5000.0	LEVELS: MIN	-0.0005081
ALPHA	1.1200	DIF	0.0001016
BETA	2.0000	NO.	20
SIGMA	0.046326		
RMS	0.025000	X =	2.876916
MAX	0.001474		
SYM	0		

Figure 3.29- $P^{(3)}$ as a function of x, y and z at a position of $x = 2.876916$ for $\mathbf{v}_f$, at $\alpha = 1.12$, $Re = 5000$, $\beta = 2.00$ and $A = 0.025$.

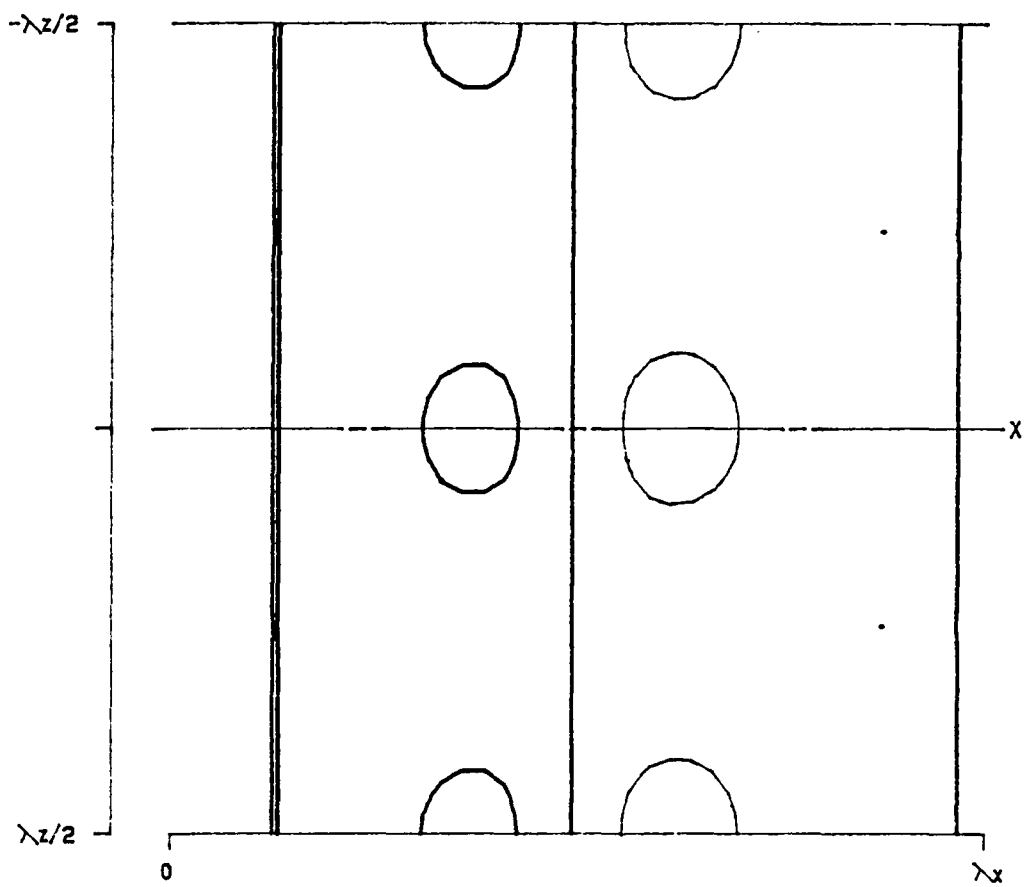

PPT 3-D F T31 (X, Y, Z)

RE	5000.0
ALPHA	1.1200
BETA	2.0000
SIGMA	0.046326
RMS	0.025000
MAX	0.001474
SYM	0

LEVELS:	MIN	-0.0005081
	DIF	0.0001016
	NO.	20
	Y =	0.885456

Figure 3.30- $T^{(31)}$ as a function of x, y and z at a position of $y = 0.885456$ for $\mathbf{v}_f$, at $\alpha = 1.12$, $Re = 5000$, $\beta = 2.00$ and $A = 0.025$.

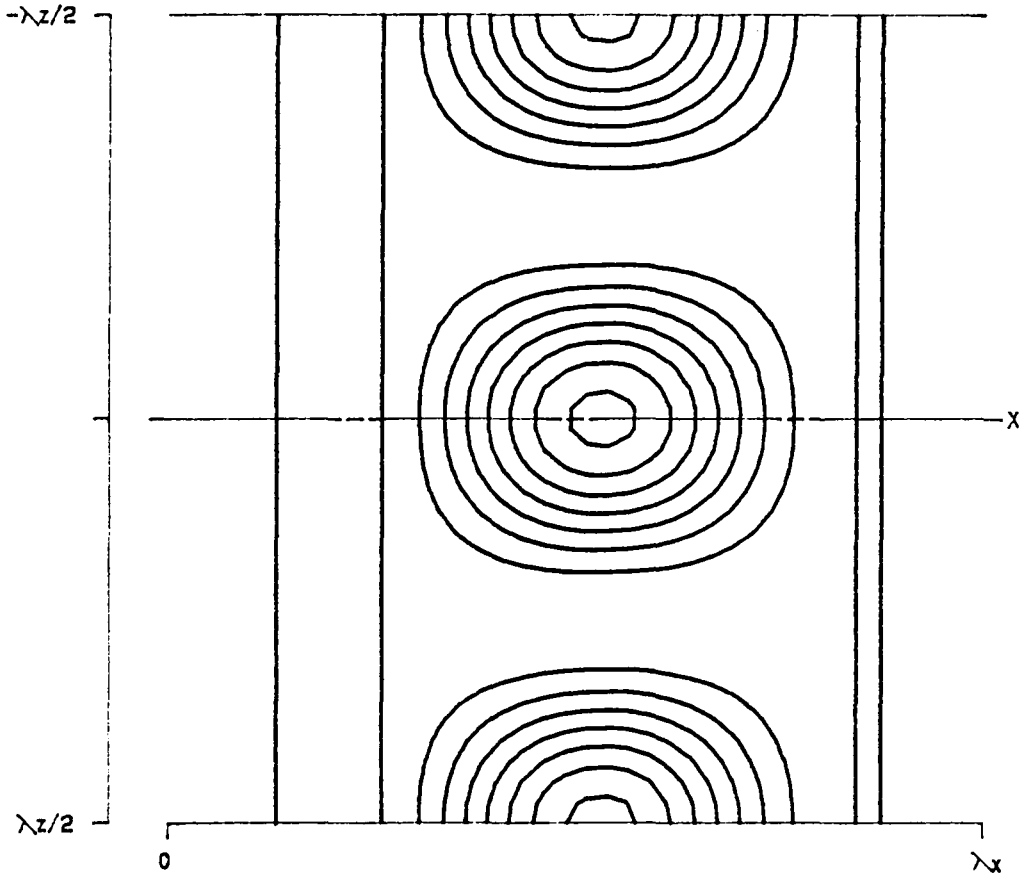

PPT 3-D F T30 (X, Y, Z)

RE	5000.0
ALPHA	1.1200
BETA	2.0000
SIGMA	0.046326
RMS	0.025000
MAX	0.001474
SYM	0

LEVELS:	MIN	-0.0005081
	DIF	0.0001016
	NO.	20
	Y =	0.885456

Figure 3.31- $T^{(30)}$ as a function of x, y and z at a position of $y = 0.885456$ for $\mathbf{v}_{f_\bullet}$ at $\alpha = 1.12$, $Re = 5000$, $\beta = 2.00$ and $A = 0.025$.

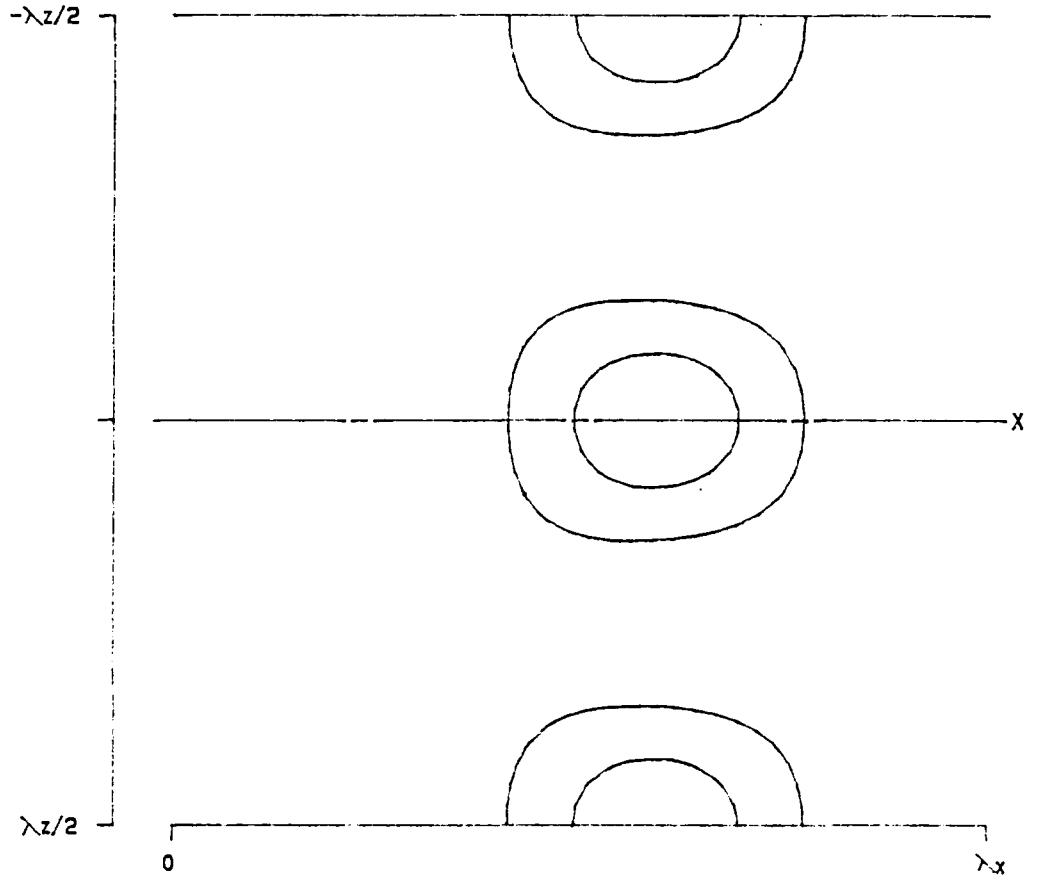

PPT 3-D F D3 (X, Y, Z)

RE	5000.0
ALPHA	1.1200
BETA	2.0000
SIGMA	0.046326
RMS	0.025000
MAX	0.001474
SYM	0

LEVELS:	MIN	-0.0005081
	DIF	0.0001016
	NO.	20
	Y =	0.885456

Figure 3.32- $D^{(3)}$ as a function of x, y and z at a position of $y = 0.885456$ for $\mathbf{v}_f$, at $\alpha = 1.12$, $Re = 5000$, $\beta = 2.00$ and $A = 0.025$.

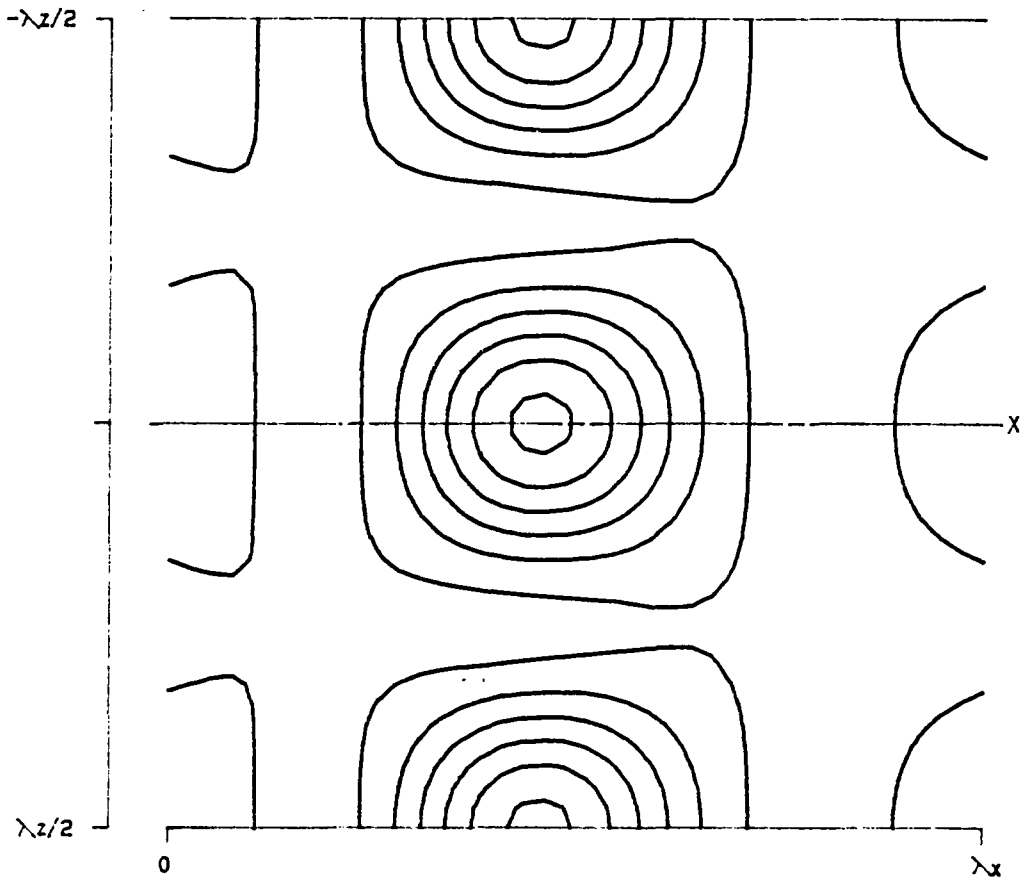

PPT 3-D F P3 (X, Y, Z)

RE	5000.0
ALPHA	1.1200
BETA	2.0000
SIGMA	0.046326
RMS	0.025000
MAX	0.001474
SYM	0

LEVELS:	MIN	-0.0005081
	DIF	0.0001016
	NO.	20
	Y =	0.885456

Figure 3.33- $P^{(3)}$ as a function of x, y and z at a position of $y = 0.885456$ for $\mathbf{v}_{f_s}$ at $\alpha = 1.12$, $Re = 5000$, $\beta = 2.00$ and $A = 0.025$.

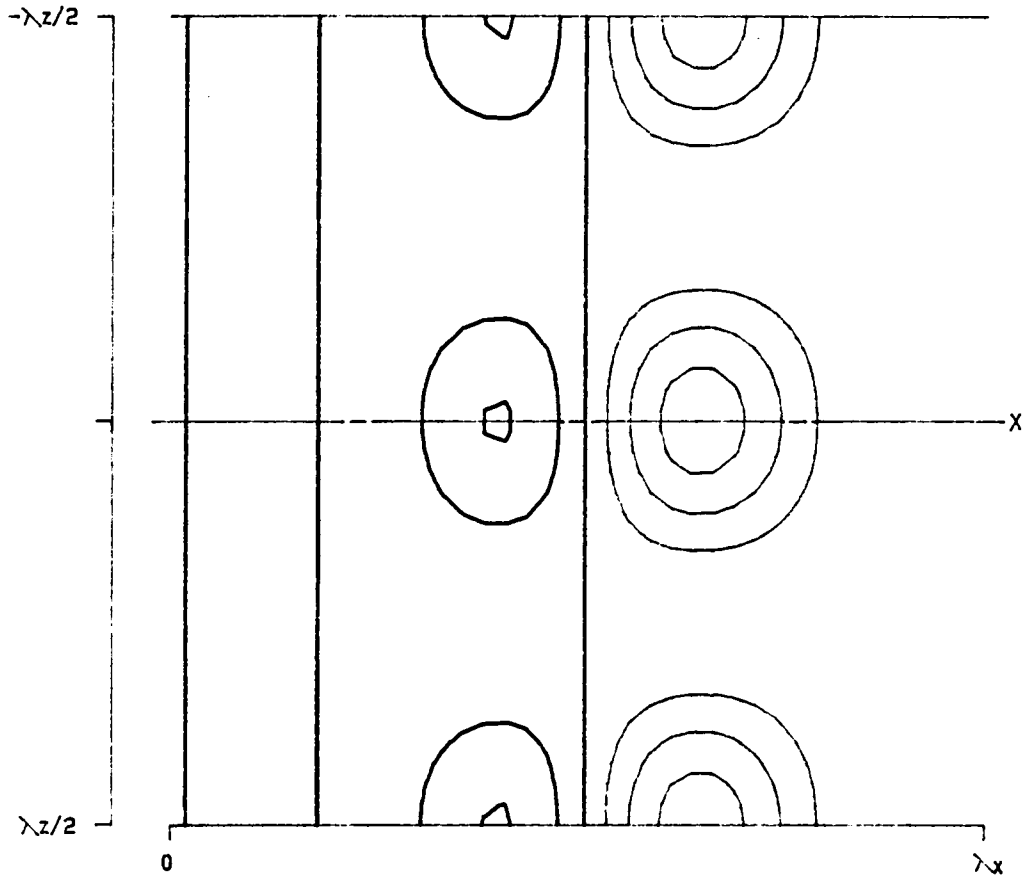

PPT 3-D F T31 (X, Y, Z)

RE	5000.0
ALPHA	1.1200
BETA	2.0000
SIGMA	0.046326
RMS	0.025000
MAX	0.001474
SYM	0

LEVELS:	MIN	-0.0005081
	DIF	0.0001016
	NO.	20
	Y =	0.845190

Figure 3.34- $T^{(31)}$ as a function of x, y and z at a position of $y = 0.845190$ for $\mathbf{v}_f$, at $\alpha = 1.12$, $Re = 5000$, $\beta = 2.00$ and $A = 0.025$.

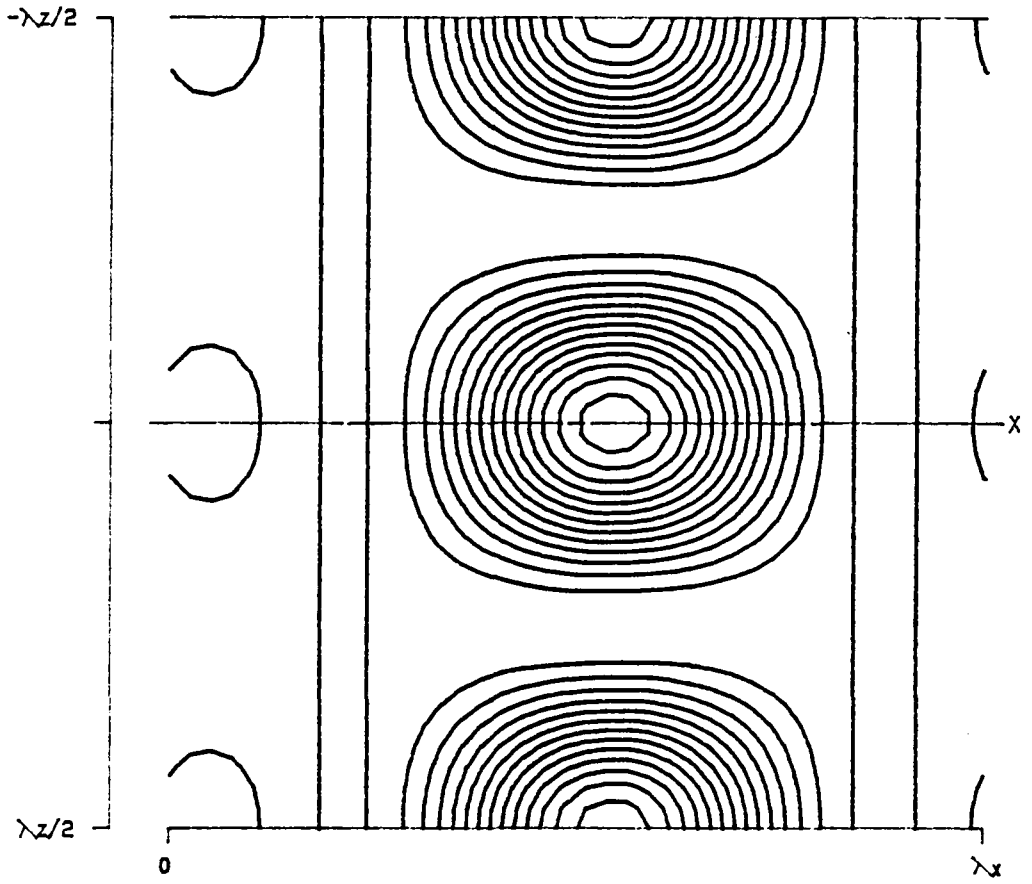

PPT 3-D F T30 (X, Y, Z)

RE	5000.0
ALPHA	1.1200
BETA	2.0000
SIGMA	0.046326
RMS	0.025000
MAX	0.001474
SYM	0

LEVELS:	MIN	-0.0005081
	DIF	0.0001016
	NO.	20
	Y =	0.845190

Figure 3.35- $T^{(30)}$ as a function of x, y and z at a position of $y = 0.845190$ for $\mathbf{v}_{f_s}$ at $\alpha = 1.12$, $Re = 5000$, $\beta = 2.00$ and $A = 0.025$.

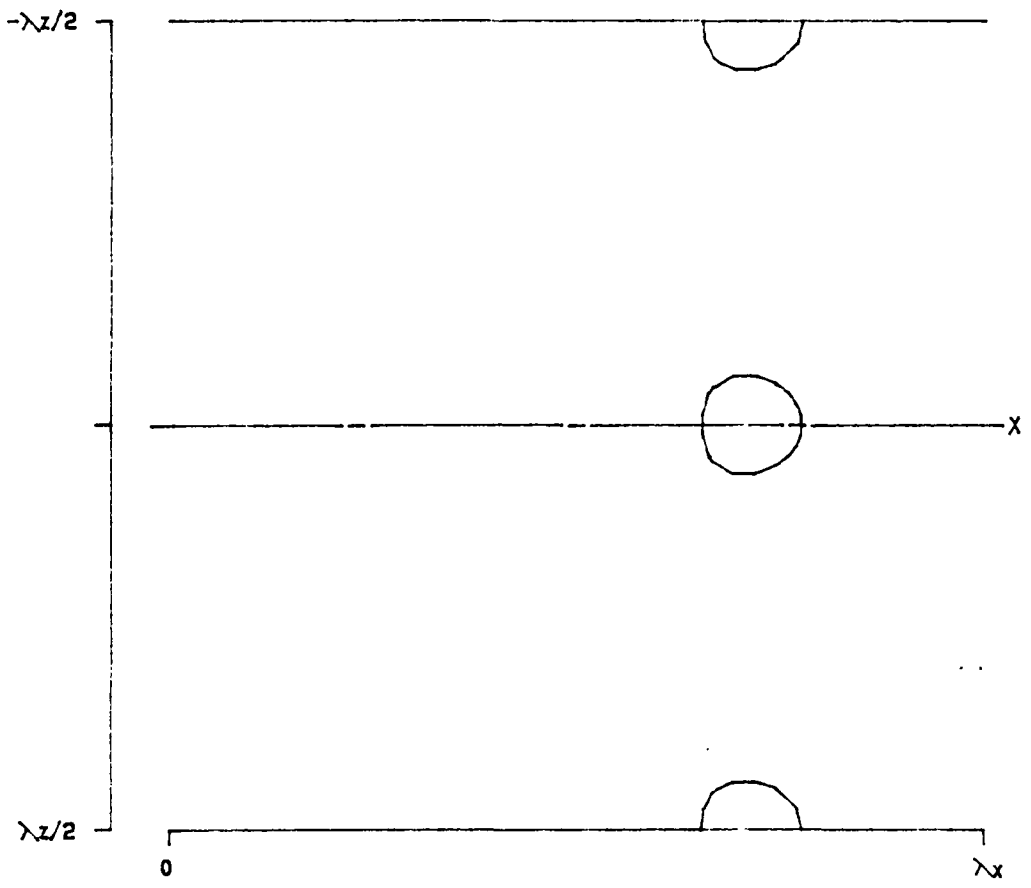

PPT 3-D F D3 (X, Y, Z)

RE	5000.0
ALPHA	1.1200
BETA	2.0000
SIGMA	0.046326
RMS	0.025000
MAX	0.001474
SYM	0

LEVELS:	MIN	-0.0005081
	DIF	0.0001016
	NO.	20
	Y =	0.845190

Figure 3.36- $D^{(3)}$ as a function of x, y and z at a position of $y = 0.845190$ for v_f, at $\alpha = 1.12$, $Re = 5000$, $\beta = 2.00$ and $A = 0.025$.

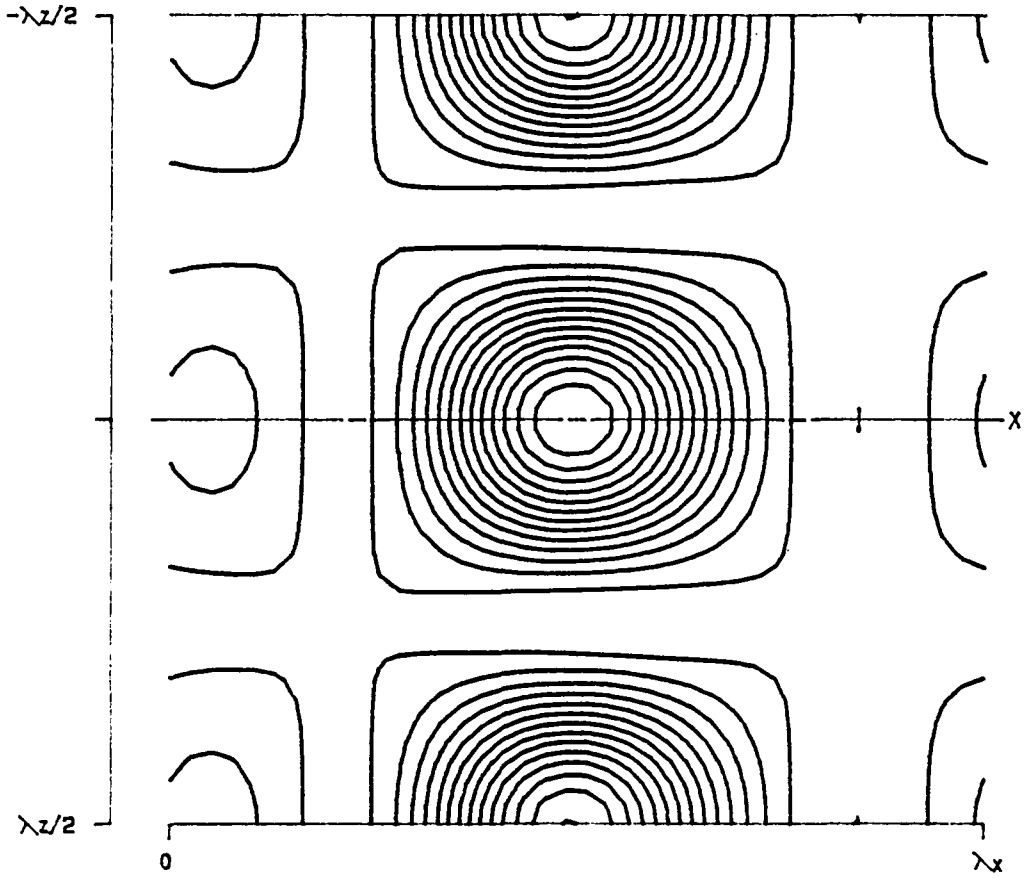

PPT 3-D F P3 (X, Y, Z)

RE	5000.0
ALPHA	1.1200
BETA	2.0000
SIGMA	0.046326
RMS	0.025000
MAX	0.001474
SYM	0

LEVELS:	MIN	-0.0005081
	DIF	0.0001016
	NO.	20
	Y =	0.845190

Figure 3.37- $P^{(3)}$ as a function of x, y and z at a position of $y = 0.845190$ for $\mathbf{v}_f$, at $\alpha = 1.12$, $Re = 5000$, $\beta = 2.00$ and $A = 0.025$.

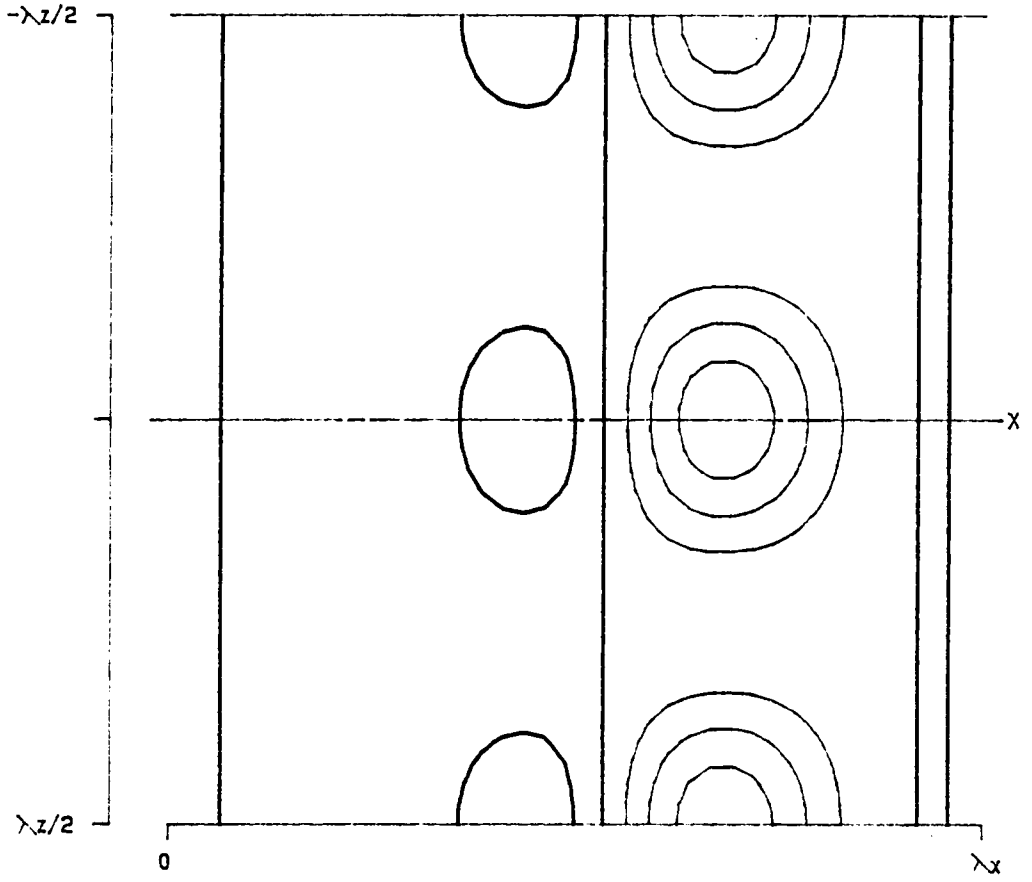

PPT 3-D F T31 (X, Y, Z)

RE	5000.0
ALPHA	1.1200
BETA	2.0000
SIGMA	0.046326
RMS	0.025000
MAX	0.001474
SYM	0

LEVELS:	MIN	-0.0005081
	DIF	0.0001016
	NO.	20
	Y =	0.799443

Figure 3.38- $T^{(31)}$ as a function of x, y and z at a position of $y = 0.799443$ for $\mathbf{v}_f$, at $\alpha = 1.12$, $Re = 5000$, $\beta = 2.00$ and $A = 0.025$.

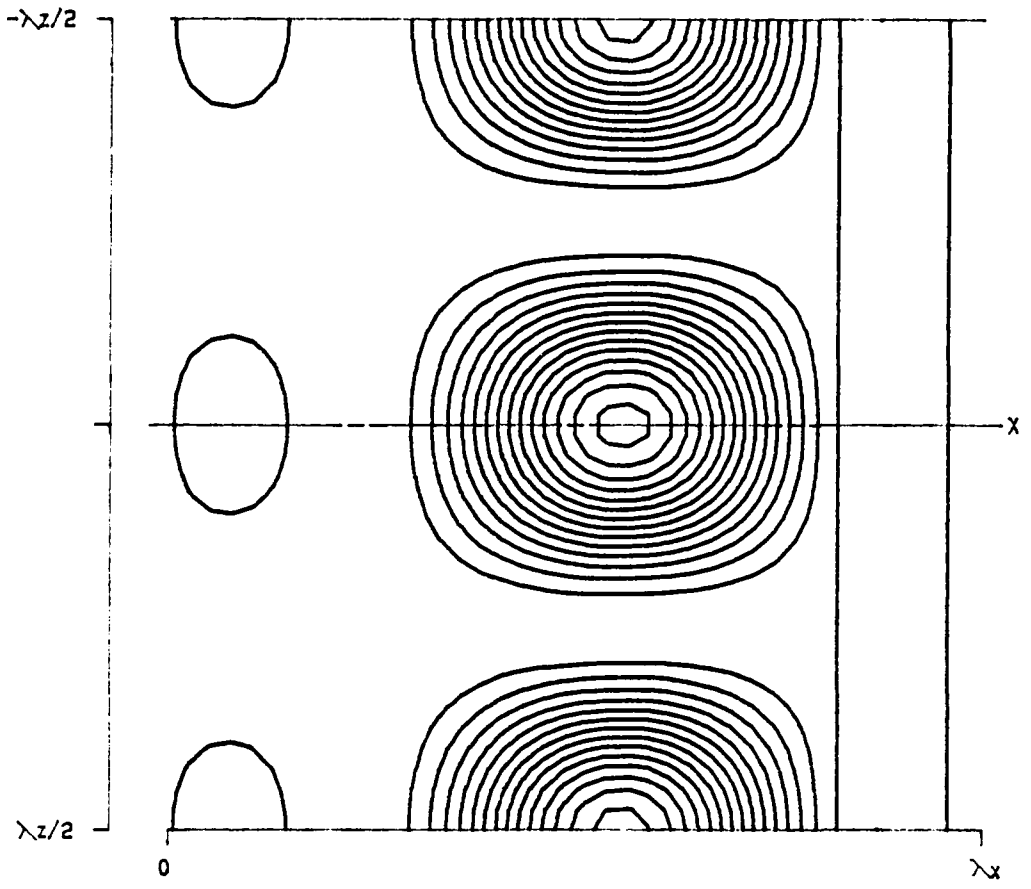

PPT 3-D F T30 (X, Y, Z)

RE	5000.0	LEVELS: MIN	-0.0005081
ALPHA	1.1200	DIF	0.0001016
BETA	2.0000	NO.	20
SIGMA	0.046326		
RMS	0.025000	Y =	0.799443
MAX	0.001474		
SYM	0		

Figure 3.39- $T^{(30)}$ as a function of x, y and z at a position of $y = 0.799443$ for $\mathbf{v}_{f_\bullet}$ at $\alpha = 1.12$, $Re = 5000$, $\beta = 2.00$ and $A = 0.025$.

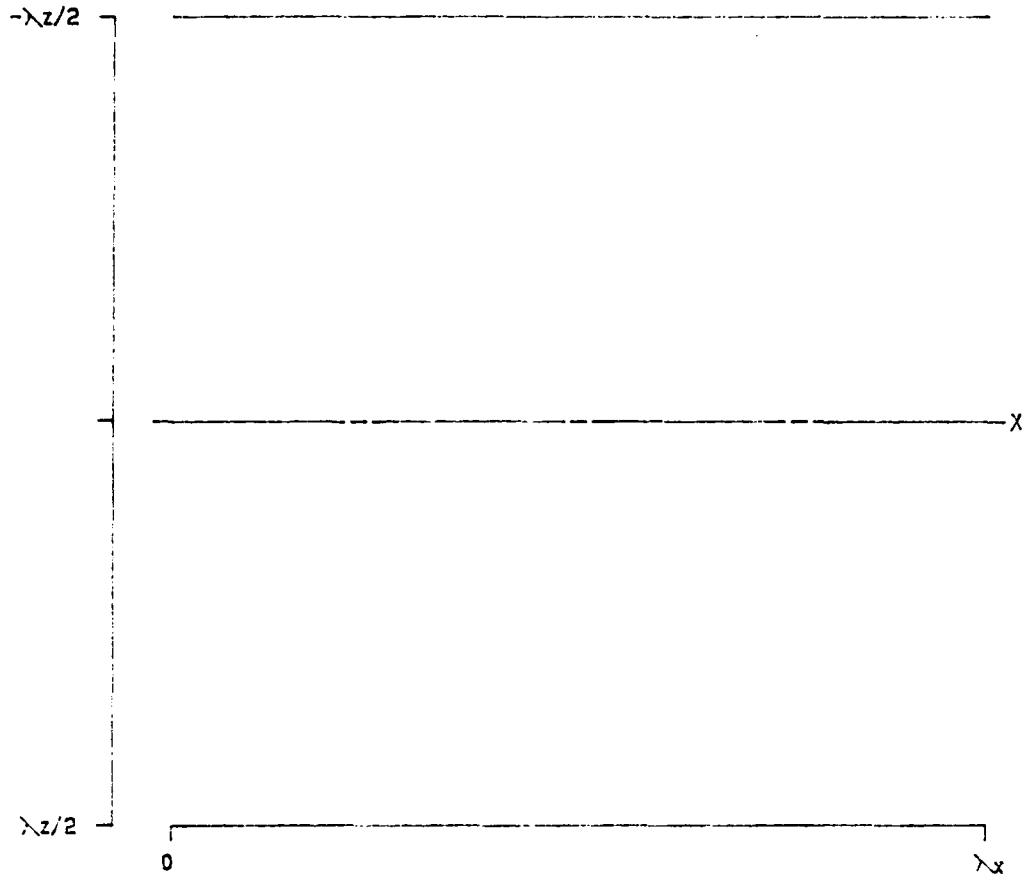

PPT 3-D F D3 (X, Y, Z)

RE	5000.0	LEVELS: MIN	-0.0005081
ALPHA	1.1200	DIF	0.0001016
BETA	2.0000	NO.	20
SIGMA	0.046326		
RMS	0.025000	Y =	0.799443
MAX	0.001474		
SYM	0		

Figure 3.40- $D^{(3)}$ as a function of x, y and z at a position of $y = 0.799443$ for $\mathbf{v}_f$, at $\alpha = 1.12$, $Re = 5000$, $\beta = 2.00$ and $A = 0.025$.

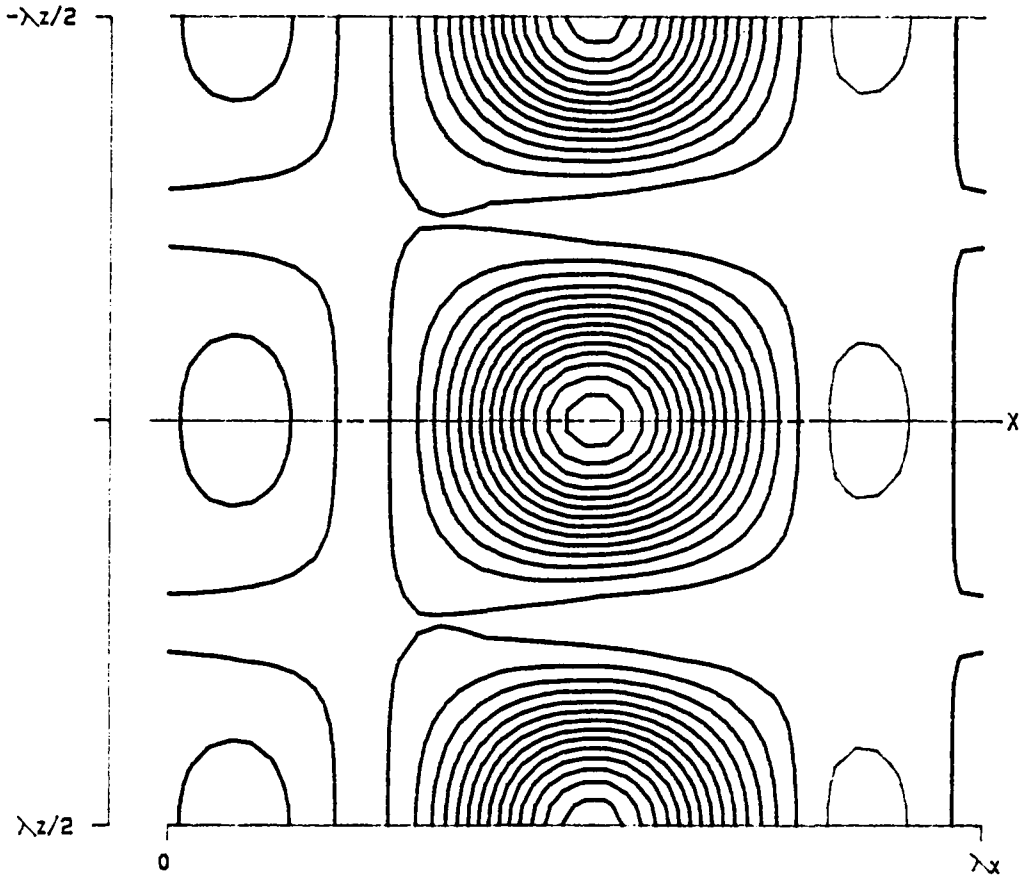

PPT 3-D F P3 (X, Y, Z)

RE	5000.0
ALPHA	1.1200
BETA	2.0000
SIGMA	0.046326
RMS	0.025000
MAX	0.001474
SYM	0

LEVELS:	MIN	-0.0005081
	DIF	0.0001016
	NO.	20
	Y =	0.799443

Figure 3.41- $P^{(3)}$ as a function of x, y and z at a position of $y = 0.799443$ for $\mathbf{v}_f$, at $\alpha = 1.12$, $Re = 5000$, $\beta = 2.00$ and $A = 0.025$.

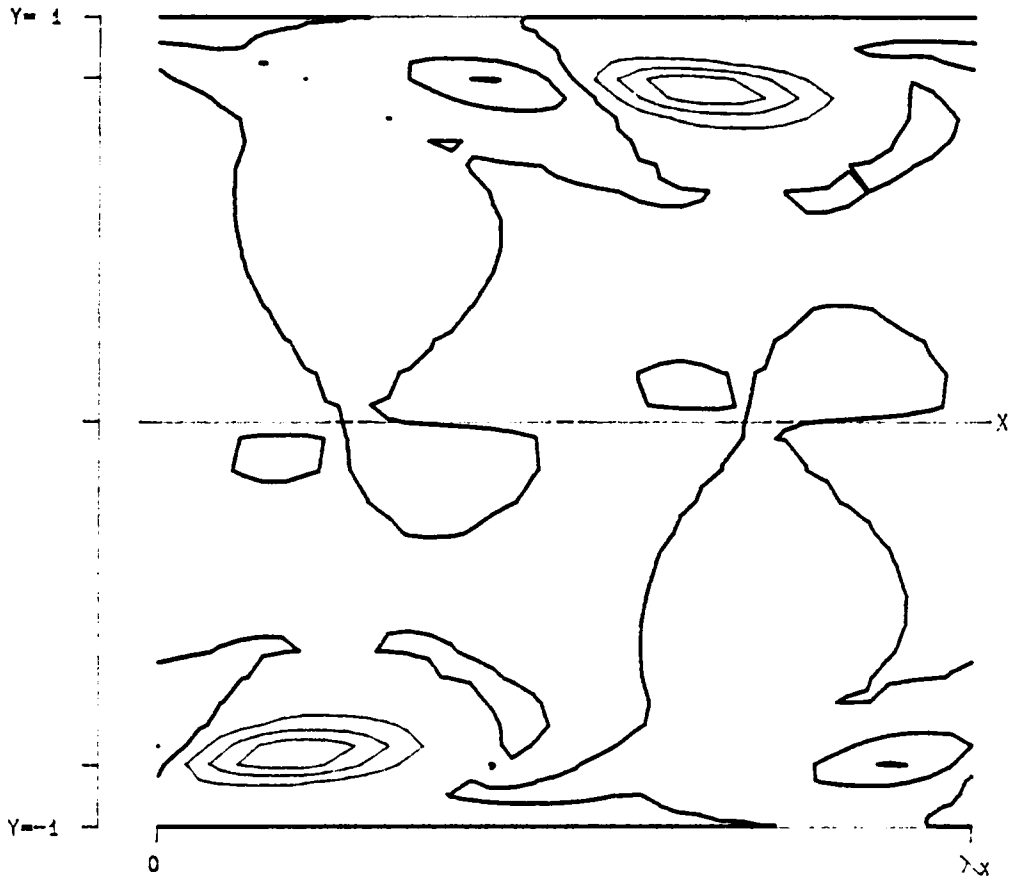

PPT 3-D F T31 (X, Y)

RE	5000.0	LEVELS: MIN	-0.0002541
ALPHA	1.1200	DIF	0.0000508
BETA	2.0000	NO.	20
SIGMA	0.046326		
RMS	0.025000		
MAX	0.000737		
SYM	0		

Figure 3.42- $T^{(31)}$ as a function of x and y for $\mathbf{v}_f$, at $\alpha = 1.12$, $Re = 5000$, $\beta = 2.00$ and $A = 0.025$.

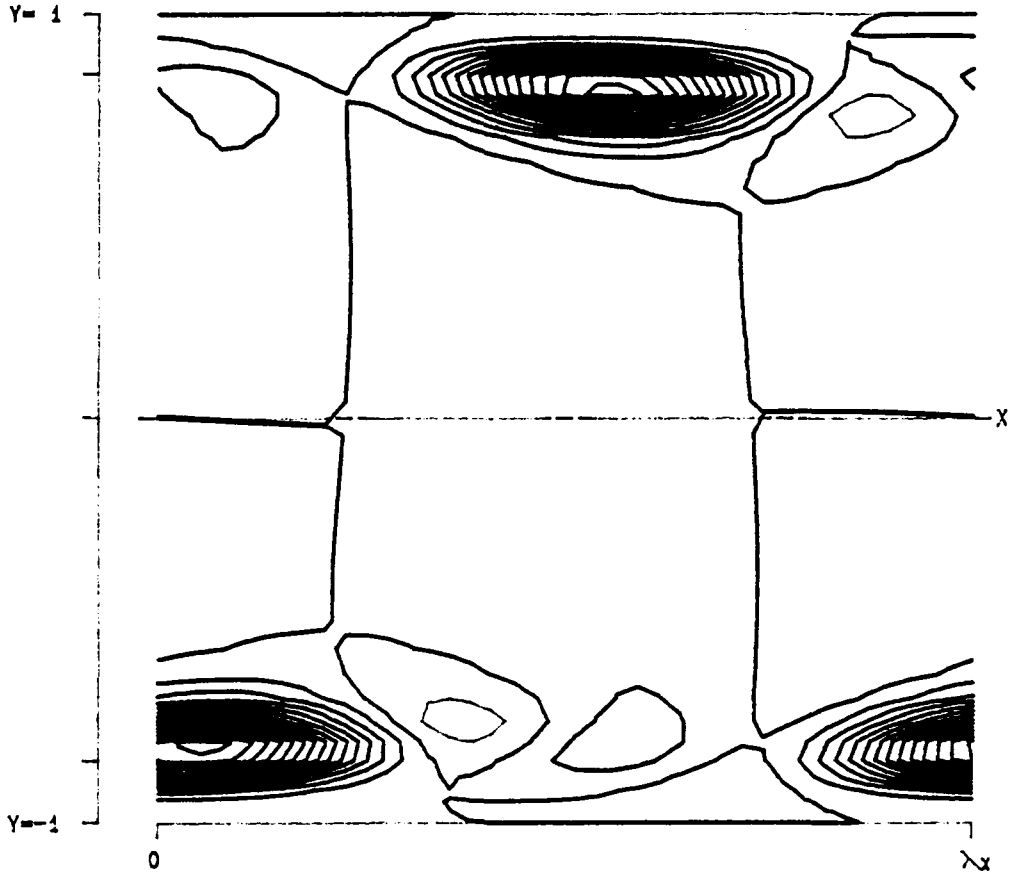

PPT 3-D F T30 (X, Y)

RE	5000.0
ALPHA	1.1200
BETA	2.0000
SIGMA	0.046326
RMS	0.025000
MAX	0.000737
SYM	0

LEVELS:	MIN	-0.0002541
	DIF	0.0000508
	NO.	20

Figure 3.43- $T^{(30)}$ as a function of x and y for $\mathbf{v}_{f_\theta}$ at $\alpha = 1.12$, $Re = 5000$, $\beta = 2.00$ and $A = 0.025$.

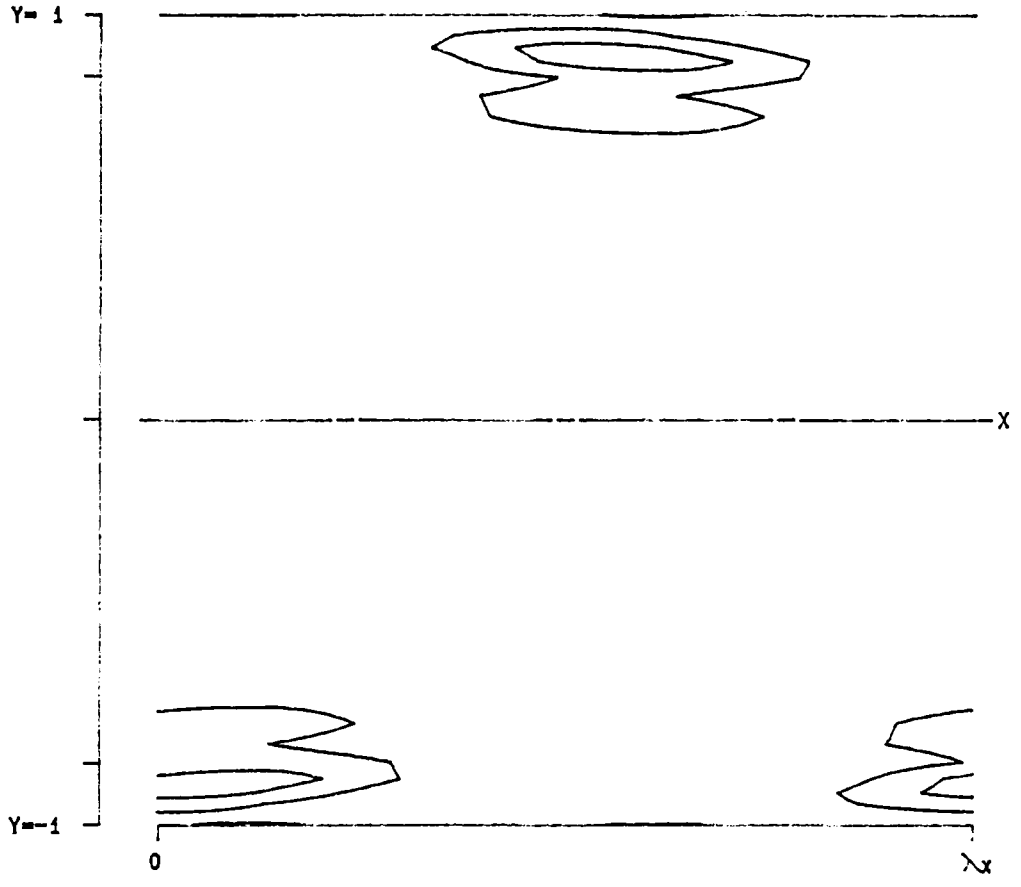

PPT 3-D F D3 (X, Y)

RE	5000.0
ALPHA	1.1200
BETA	2.0000
SIGMA	0.046326
RMS	0.025000
MAX	0.000737
SYM	0

LEVELS:	MIN	-0.0002541
	DIF	0.0000508
	NO.	20

Figure 3.44- $D^{(3)}$ as a function of x and y for $\mathbf{v}_f$ at $\alpha = 1.12$, $Re = 5000$, $\beta = 2.00$ and $A = 0.025$.

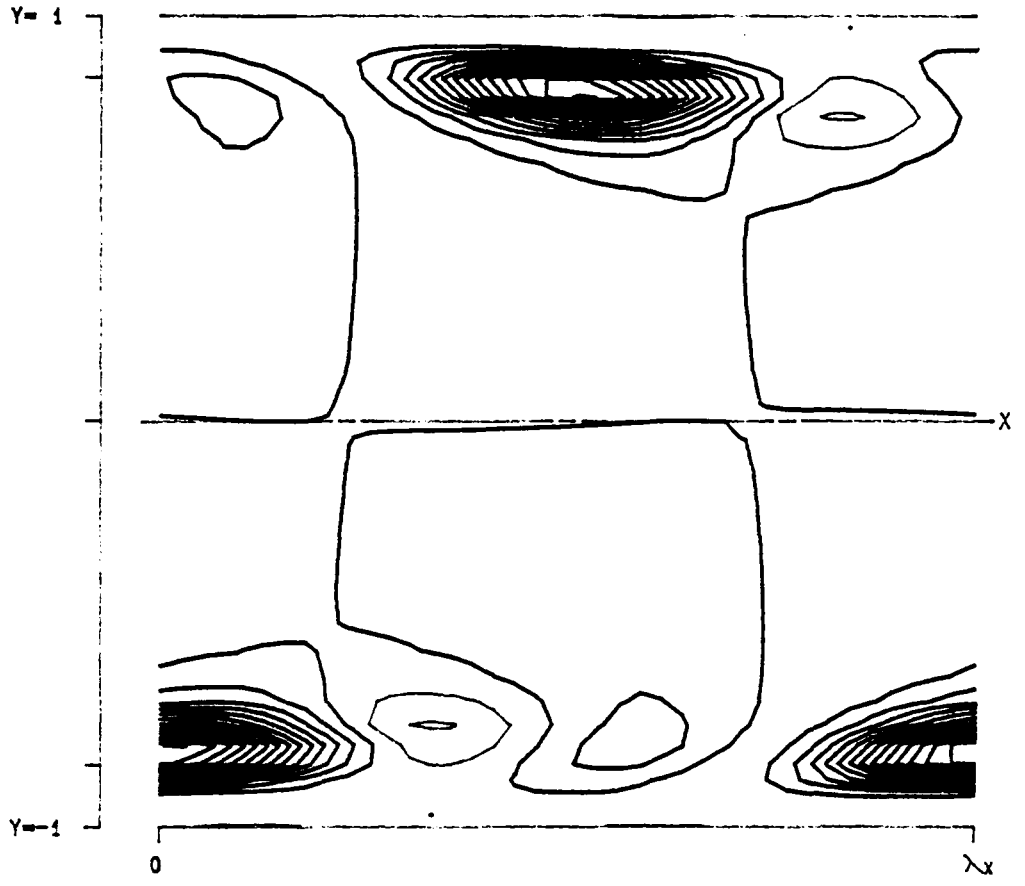

PPT 3-D F P3 (X, Y)

RE	5000.0
ALPHA	1.1200
BETA	2.0000
SIGMA	0.046326
RMS	0.025000
MAX	0.000737
SYM	0

LEVELS:	MIN	-0.0002541
	DIF	0.0000508
	NO.	20

Figure 3.45- $P^{(3)}$ as a function of x and y for $\mathbf{v}_f$, at $\alpha = 1.12$, $Re = 5000$, $\beta = 2.00$ and $A = 0.025$.

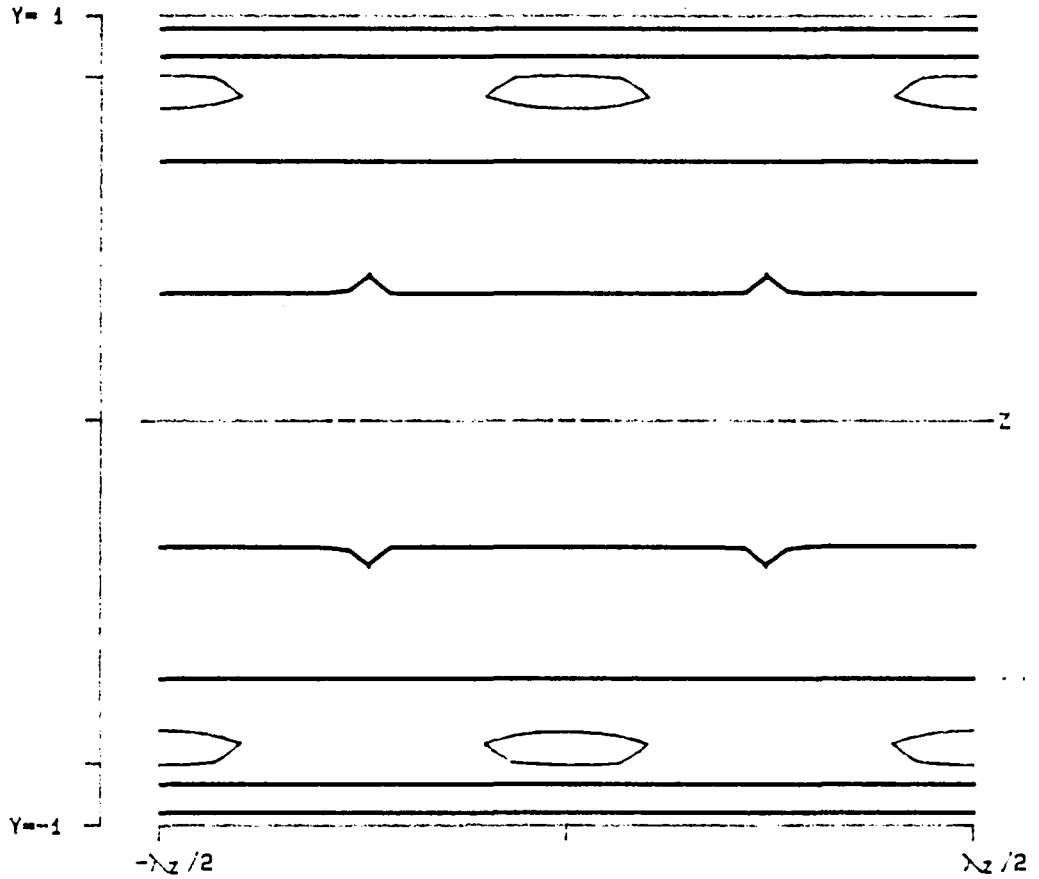

PPT 3-D F T31 (Y, Z)

RE	5000.0	LEVELS: MIN	-0.0001579
ALPHA	1.1200	DIF	0.0000316
BETA	2.0000	NO.	20
SIGMA	0.046326		
RMS	0.025000		
MAX	0.000458		
SYM	0		

Figure 3.46- $T^{(31)}$ as a function of y and z for $\mathbf{v}_f$, at $\alpha = 1.12$, $Re = 5000$, $\beta = 2.00$ and $A = 0.025$.

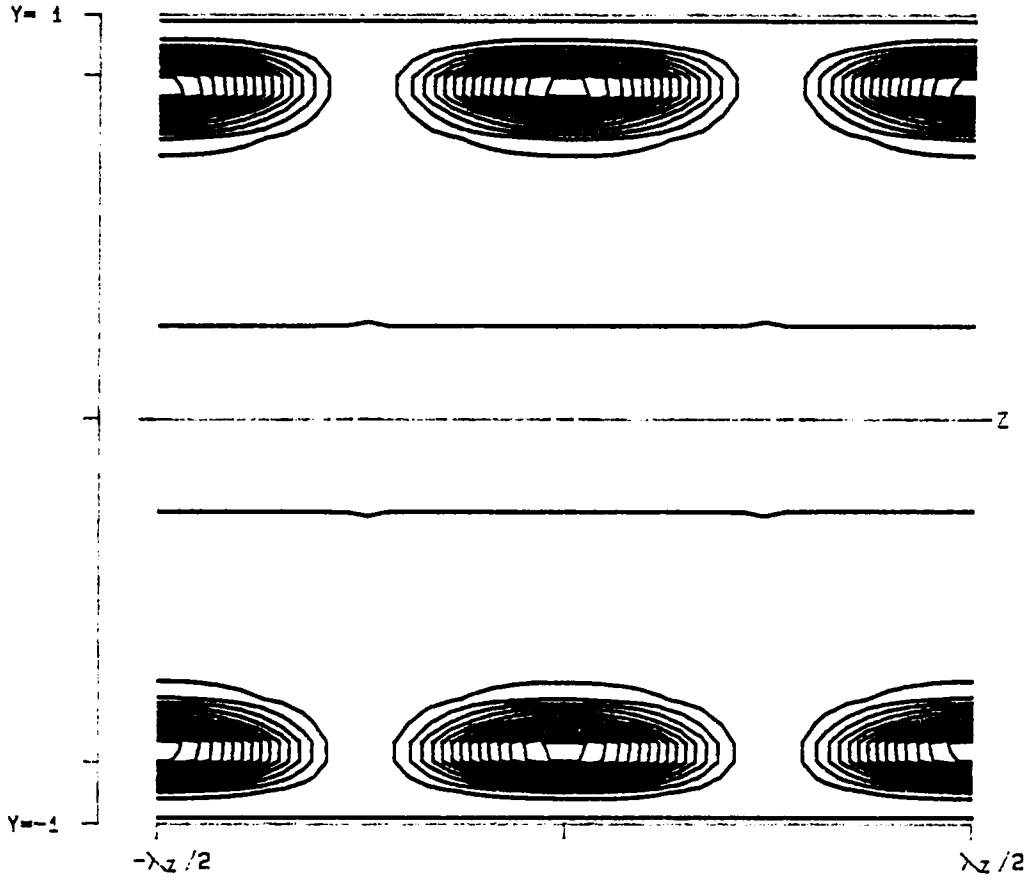

PPT 3-D F T30 (Y, Z)

RE	5000.0	LEVELS: MIN	-0.0001579
ALPHA	1.1200	DIF	0.0000316
BETA	2.0000	NO.	20
SIGMA	0.046326		
RMS	0.025000		
MAX	0.000458		
SYM	0		

Figure 3.47- $T^{(30)}$ as a function of y and z for $\mathbf{v}_{f_*}$ at $\alpha = 1.12$, $Re = 5000$, $\beta = 2.00$ and $A = 0.025$.

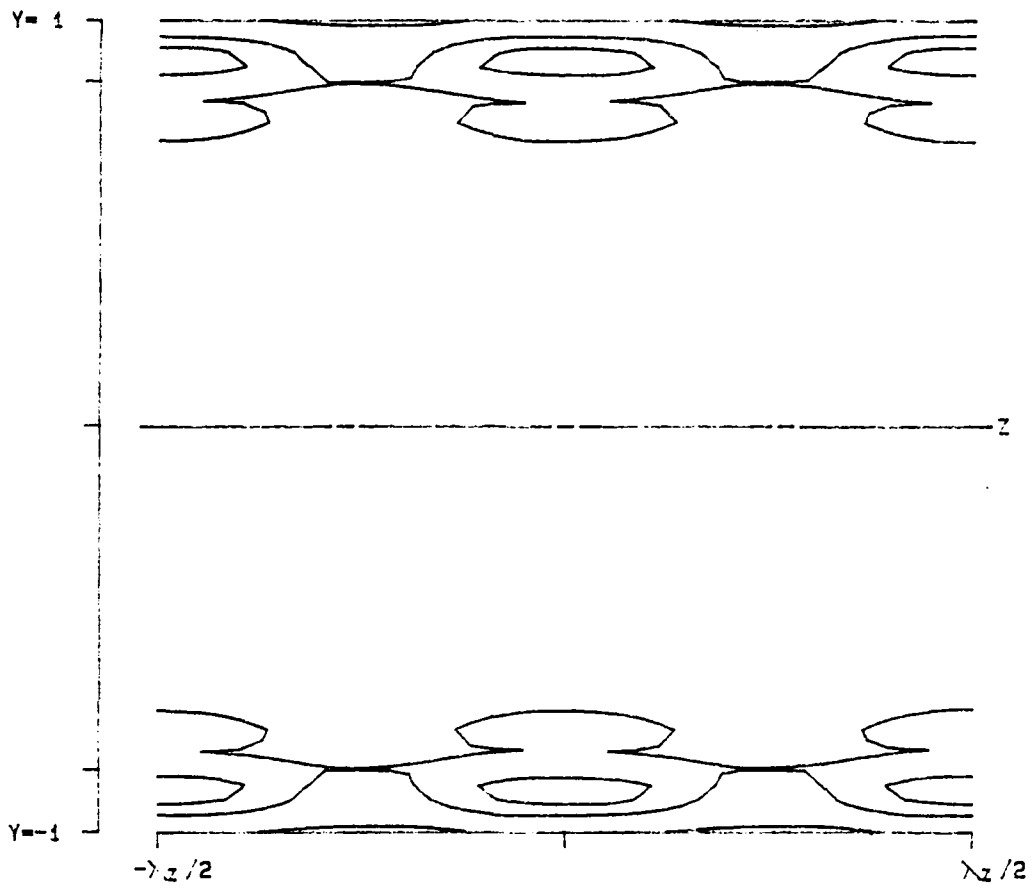

PPT 3-D F D3 (Y, Z)

RE	5000.0
ALPHA	1.1200
BETA	2.0000
SIGMA	0.046326
RMS	0.025000
MAX	0.000458
SYM	0

LEVELS:	MIN	-0.0001579
	DIF	0.0000316
	NO.	20

Figure 3.48- $D^{(3)}$ as a function of y and z for $\mathbf{v}_{f_\theta}$ at $\alpha = 1.12$, $Re = 5000$, $\beta = 2.00$ and $A = 0.025$.

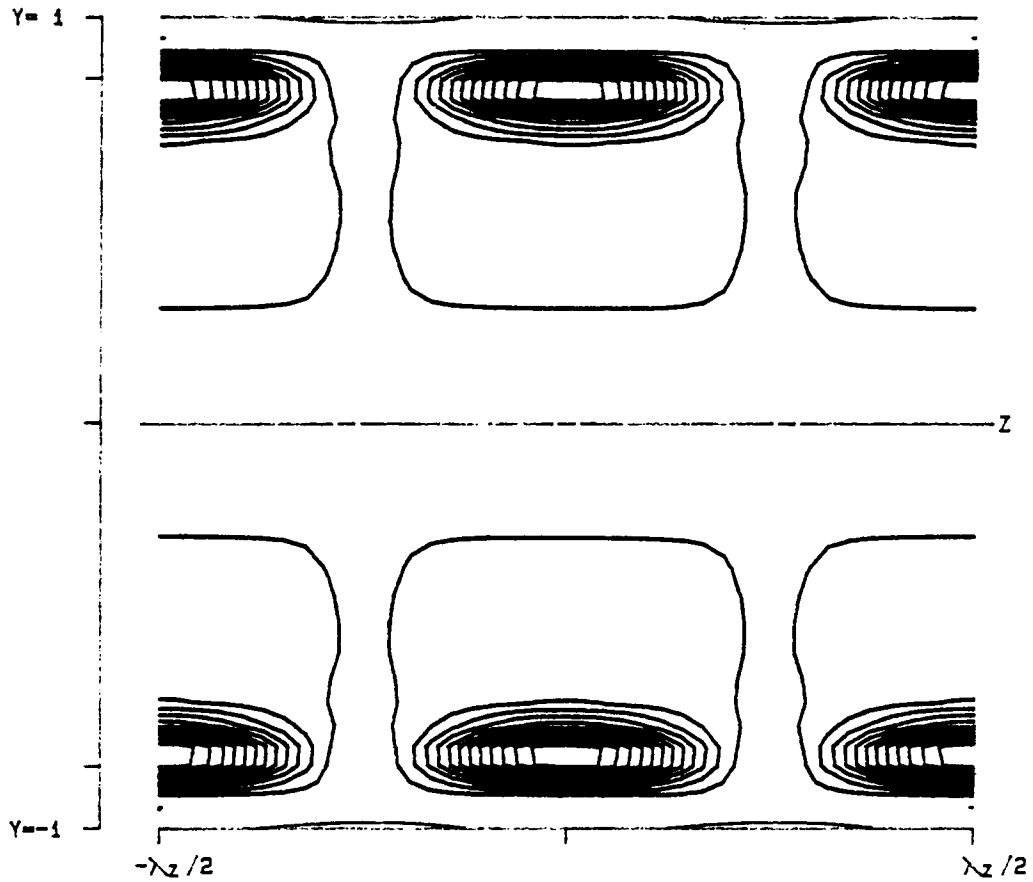

PPT 3-D F P3 (Y, Z)

RE	5000.0
ALPHA	1.1200
BETA	2.0000
SIGMA	0.046326
RMS	0.025000
MAX	0.000458
SYM	0

LEVELS:	MIN	-0.0001579
	DIF	0.0000316
	NO.	20

Figure 3.49- $P^{(3)}$ as a function of y and z for $\mathbf{v}_f$, at $\alpha = 1.12$, $Re = 5000$, $\beta = 2.00$ and $A = 0.025$.

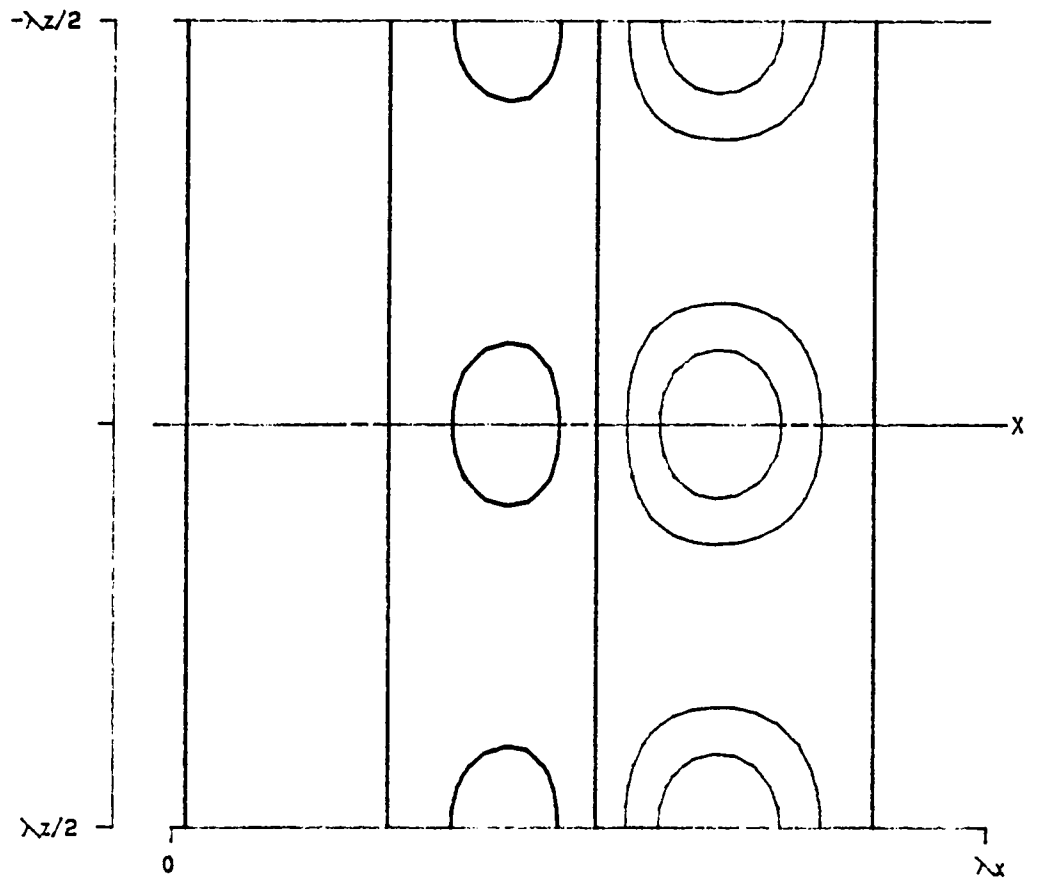

PPT 3-D F T31 (X, Z)

RE	5000.0
ALPHA	1.1200
BETA	2.0000
SIGMA	0.046326
RMS	0.025000
MAX	0.000196
SYM	0

LEVELS:	MIN	-0.0000676
	DIF	0.0000135
	NO.	20

Figure 3.50- $T^{(31)}$ as a function of x and z for $\mathbf{v}_f$, at $\alpha = 1.12$, $Re = 5000$, $\beta = 2.00$ and $A = 0.025$.

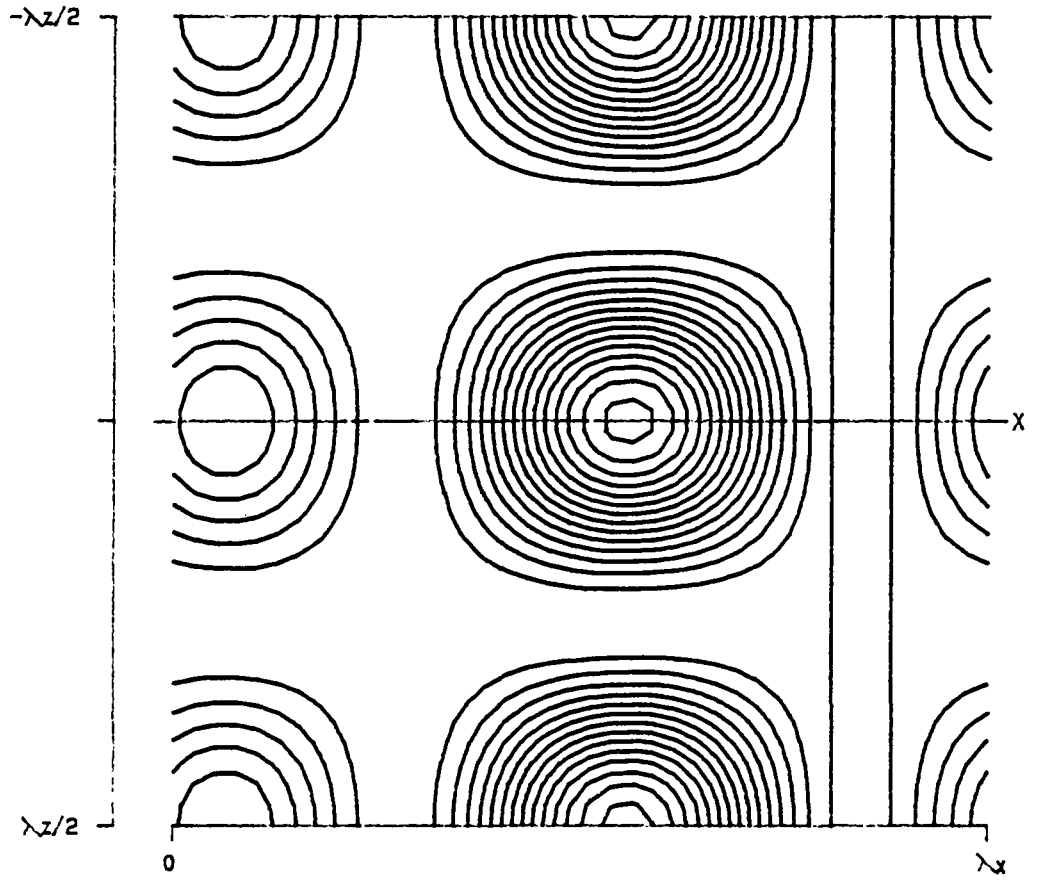

PPT 3-D F T30 (X, Z)

RE	5000.0
ALPHA	1.1200
BETA	2.0000
SIGMA	0.046326
RMS	0.025000
MAX	0.000196
SYM	0

LEVELS:	MIN	-0.0000676
	DIF	0.0000135
	NO.	20

Figure 3.51- $T^{(30)}$ as a function of x and z for $\mathbf{v}_f$, at $\alpha = 1.12$, $Re = 5000$, $\beta = 2.00$ and $A = 0.025$.

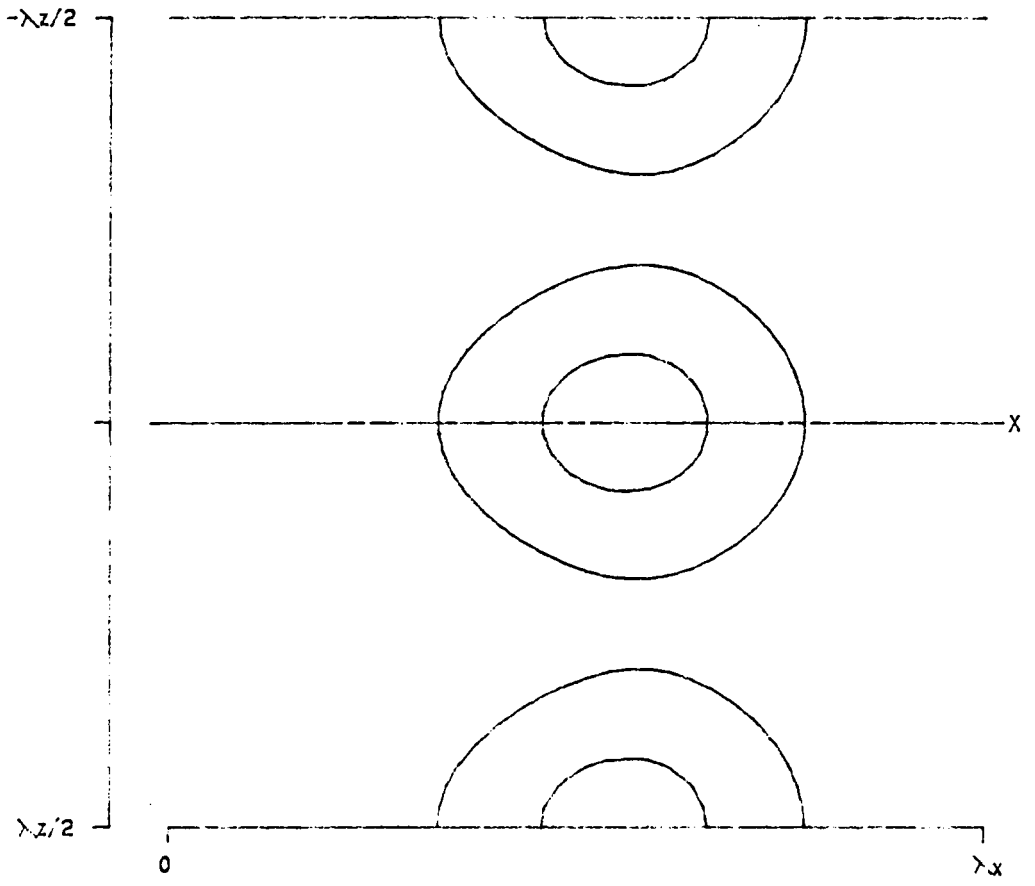

PPT 3-D F D3 (X, Z)

RE	5000.0
ALPHA	1.1200
BETA	2.0000
SIGMA	0.046326
RMS	0.025000
MAX	0.000196
SYM	0

LEVELS:	MIN	-0.0000676
	DIF	0.0000135
	NO.	20

Figure 3.52- $D^{(3)}$ as a function of x and z for $\mathbf{v}_{f_0}$ at $\alpha = 1.12$, $Re = 5000$, $\beta = 2.00$ and $A = 0.025$.

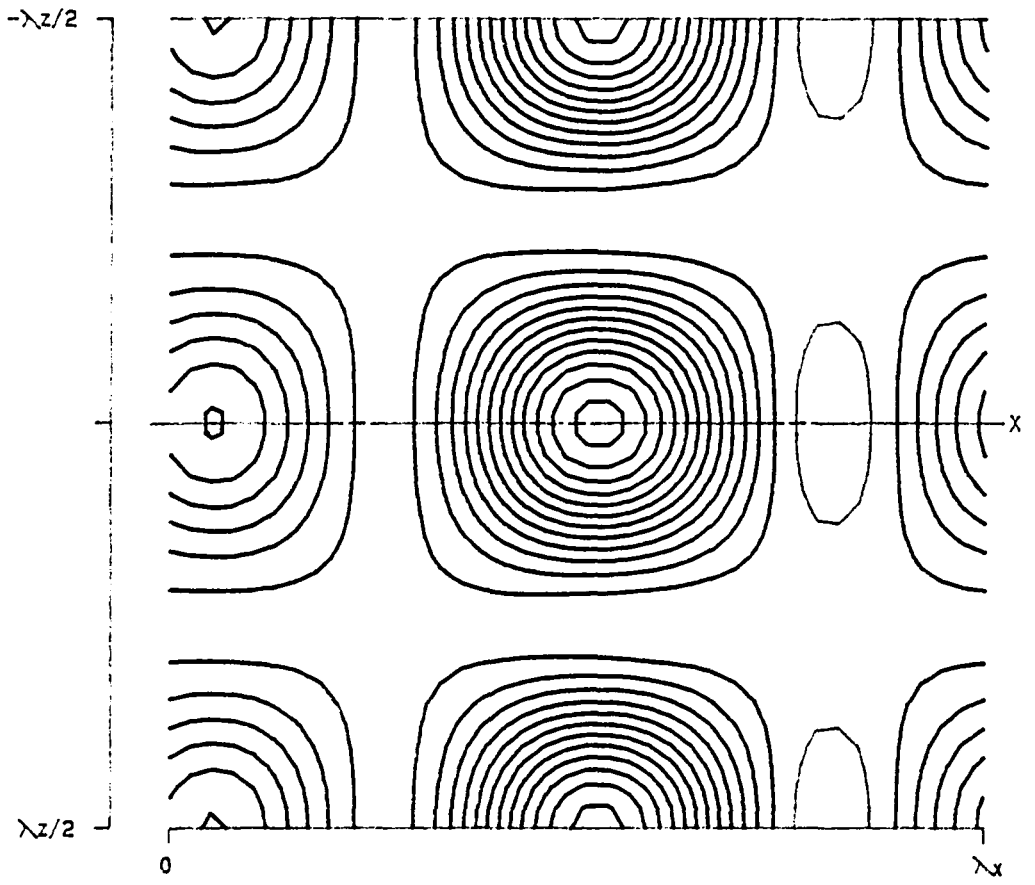

PPT 3-D F P3 (X, Z)

RE	5000.0
ALPHA	1.1200
BETA	2.0000
SIGMA	0.046326
RMS	0.025000
MAX	0.000196
SYM	0

LEVELS:	MIN	-0.0000676
	DIF	0.0000135
	NO.	20

Figure 3.53- $P^{(3)}$ as a function of x and z for $\mathbf{v}_{/\!/}$ at $\alpha = 1.12$, $Re = 5000$, $\beta = 2.00$ and $A = 0.025$.

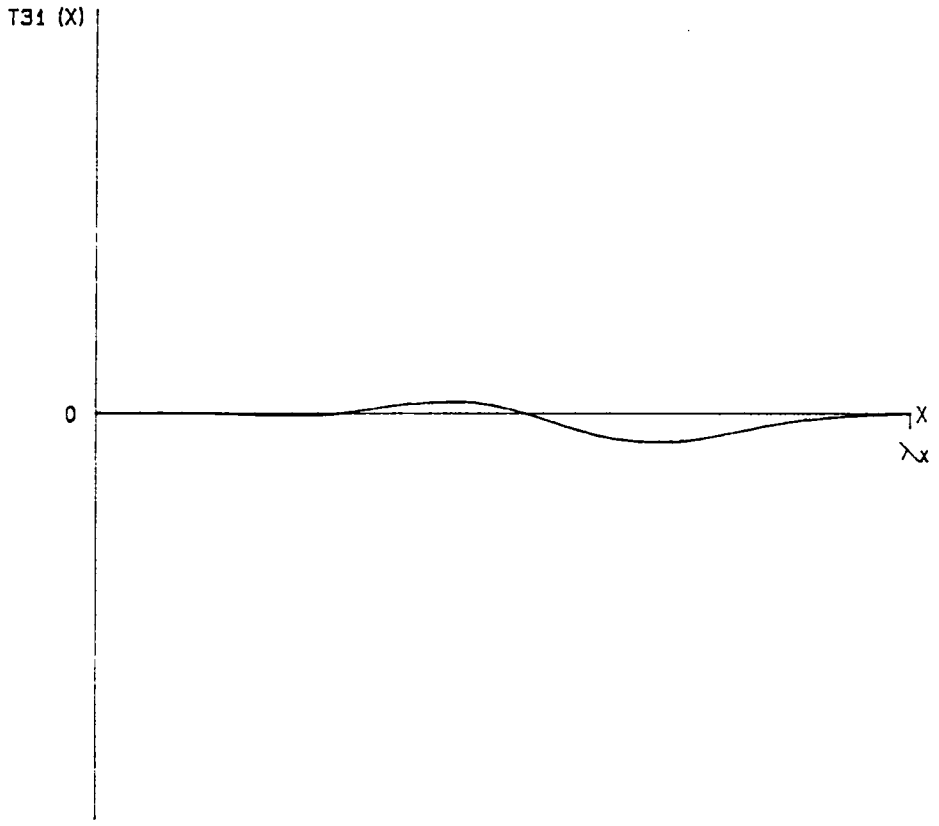

PPT 3-D F T31 (X)

RE	5000.0	SIGMA	0.046326
ALPHA	1.1200	CR	0.281755
BETA	2.0000	MAX	0.0000072
RMS	0.025000	MIN	-0.0000162
SYM	0		

Figure 3.54- $T^{(31)}$ as a function of x for $\mathbf{v}_{f_s}$ at $\alpha = 1.12$, $Re = 5000$, $\beta = 2.00$ and $A = 0.025$.

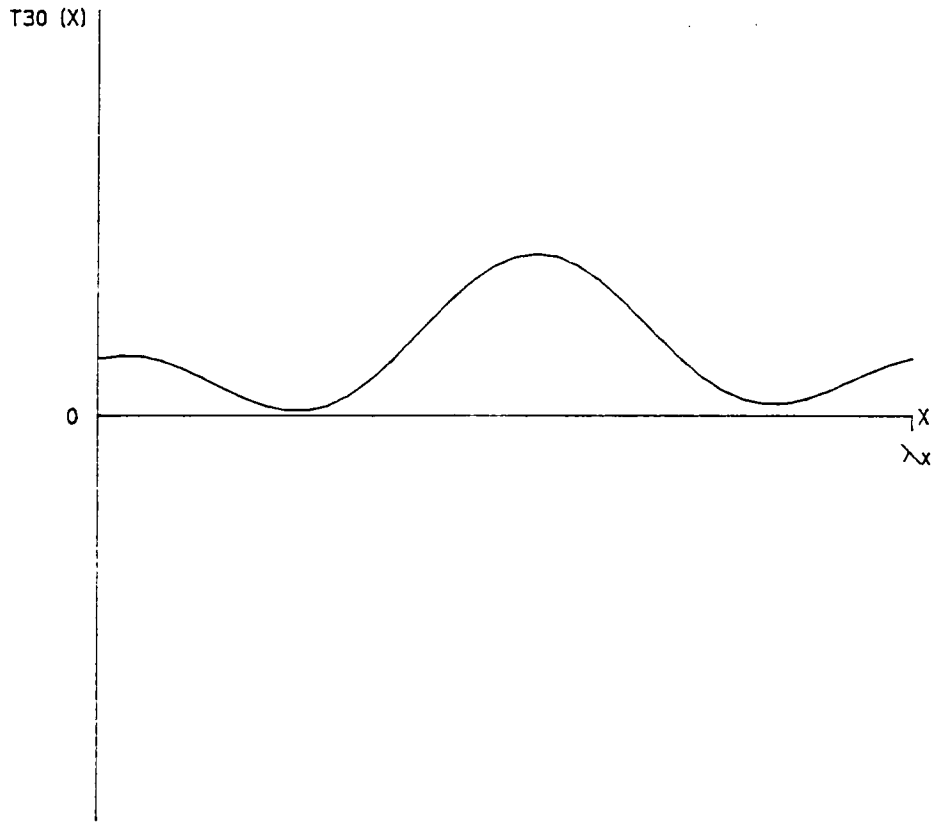

PPT 3-D F T30 (X)

RE	5000.0	SIGMA	0.046326
ALPHA	1.1200	CR	0.281755
BETA	2.0000	MAX	0.0000915
AMS	0.025000	MIN	0.0000029
SYM	0		

Figure 3.55- $T^{(30)}$ as a function of x for $\mathbf{v}_{f_1}$ at $\alpha = 1.12$, $Re = 5000$, $\beta = 2.00$ and $A = 0.025$.

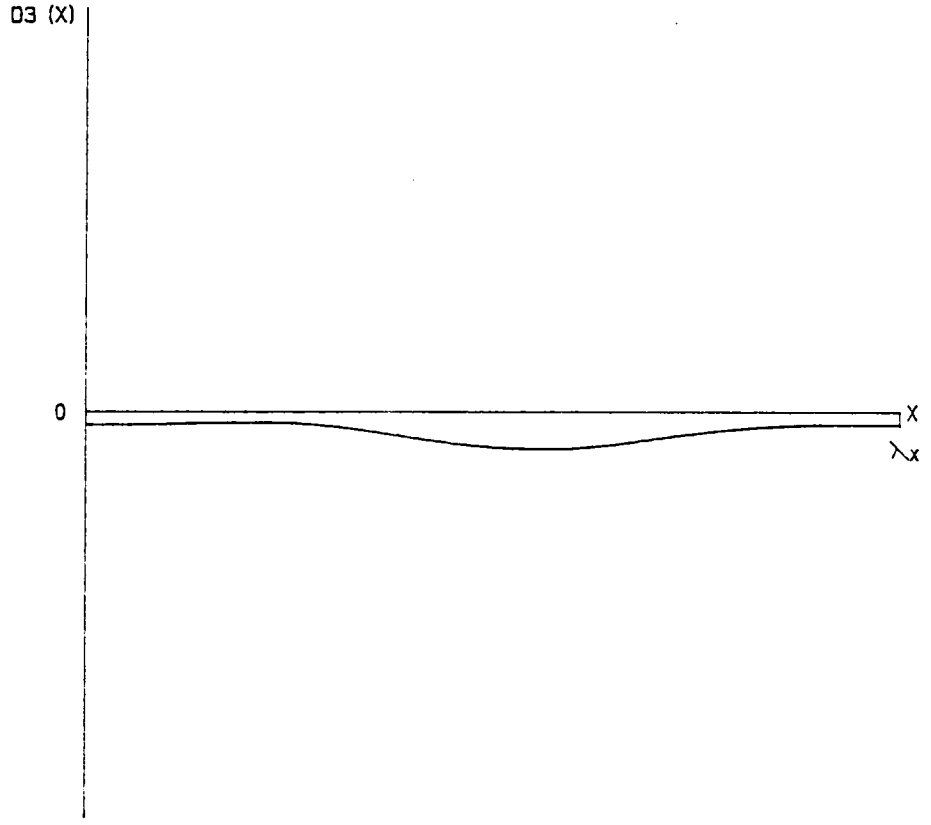

PPT 3-D F D3 (X)

RE	5000.0	SIGMA	0.046326
ALPHA	1.1200	CR	0.281755
BETA	2.0000	MAX	-0.0000055
RMS	0.025000	MIN	-0.0000210
SYM	0		

Figure 3.56- $D^{(3)}$ as a function of x for $\mathbf{v}_{f_\bullet}$ at $\alpha = 1.12$, $Re = 5000$, $\beta = 2.00$ and $A = 0.025$.

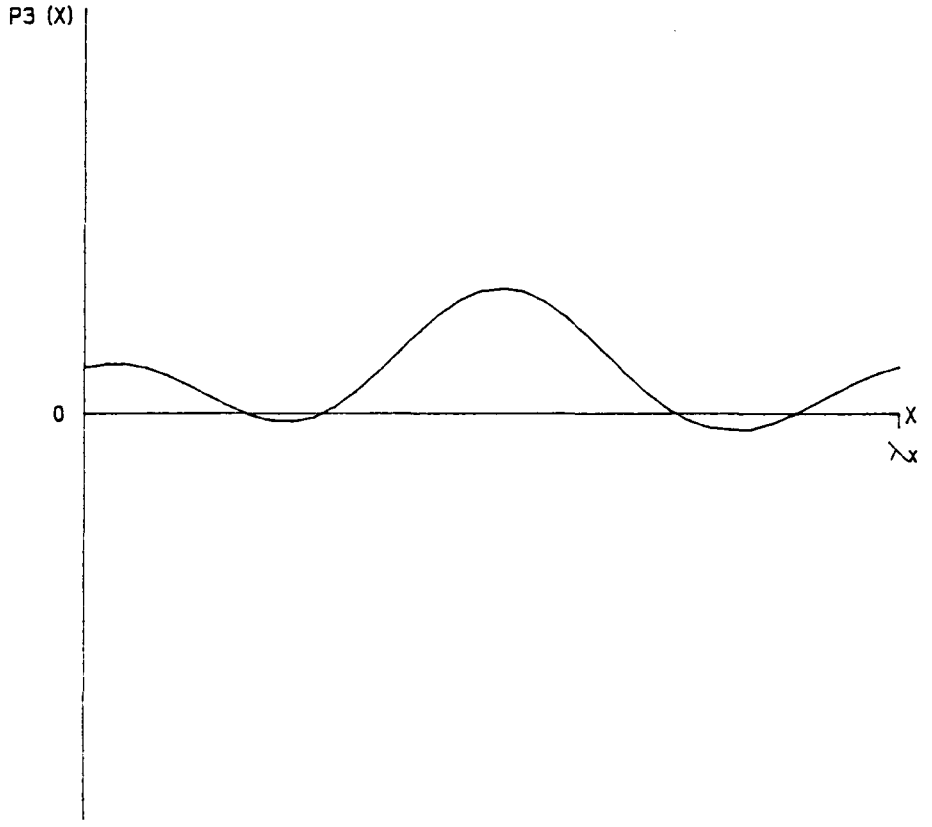

PPT 3-D F P3 (X)

RE	5000.0	SIGMA	0.046326
ALPHA	1.1200	CR	0.281755
BETA	2.0000	MAX	0.0000712
RMS	0.025000	MIN	-0.0000096
SYM	0		

Figure 3.57- $P^{(3)}$ as a function of x for $\mathbf{v}_f$, at $\alpha = 1.12$, $Re = 5000$, $\beta = 2.00$ and $A = 0.025$.

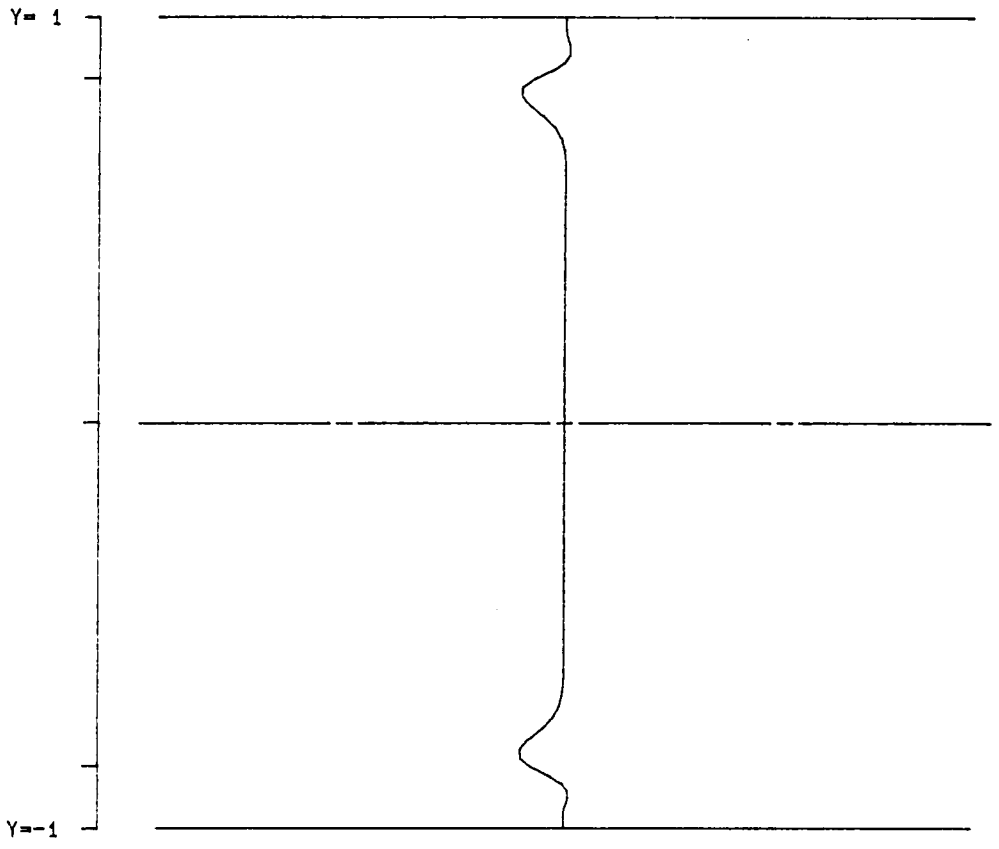

PPT 3-D F T31 (Y)

RE	5000.0	SIGMA	0.046326
ALPHA	1.1200	CR	0.281755
BETA	2.0000	MAX	0.0000027
AMS	0.025000	MIN	-0.0000241
SYM	0		

Figure 3.58- $T^{(31)}$ as a function of y for $\mathbf{v}_{f_\bullet}$ at $\alpha = 1.12$, $Re = 5000$, $\beta = 2.00$ and $A = 0.025$.

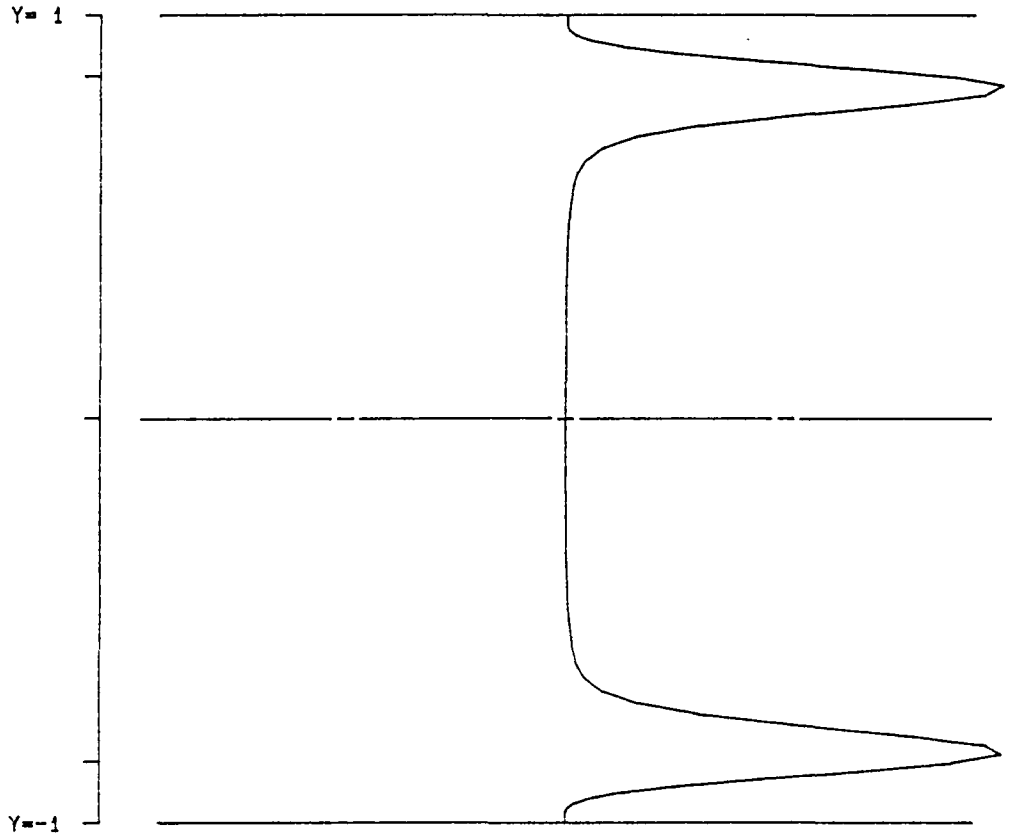

PPT 3-D F T30 (Y)

RE	5000.0	SIGMA	0.046326
ALPHA	1.1200	CR	0.281755
BETA	2.0000	MAX	0.0002290
AMS	0.025000	MIN	-0.0000000
SYM	0		

Figure 3.59- $T^{(30)}$ as a function of y for $\mathbf{v}_f$, at $\alpha = 1.12$, $Re = 5000$, $\beta = 2.00$ and $A = 0.025$.

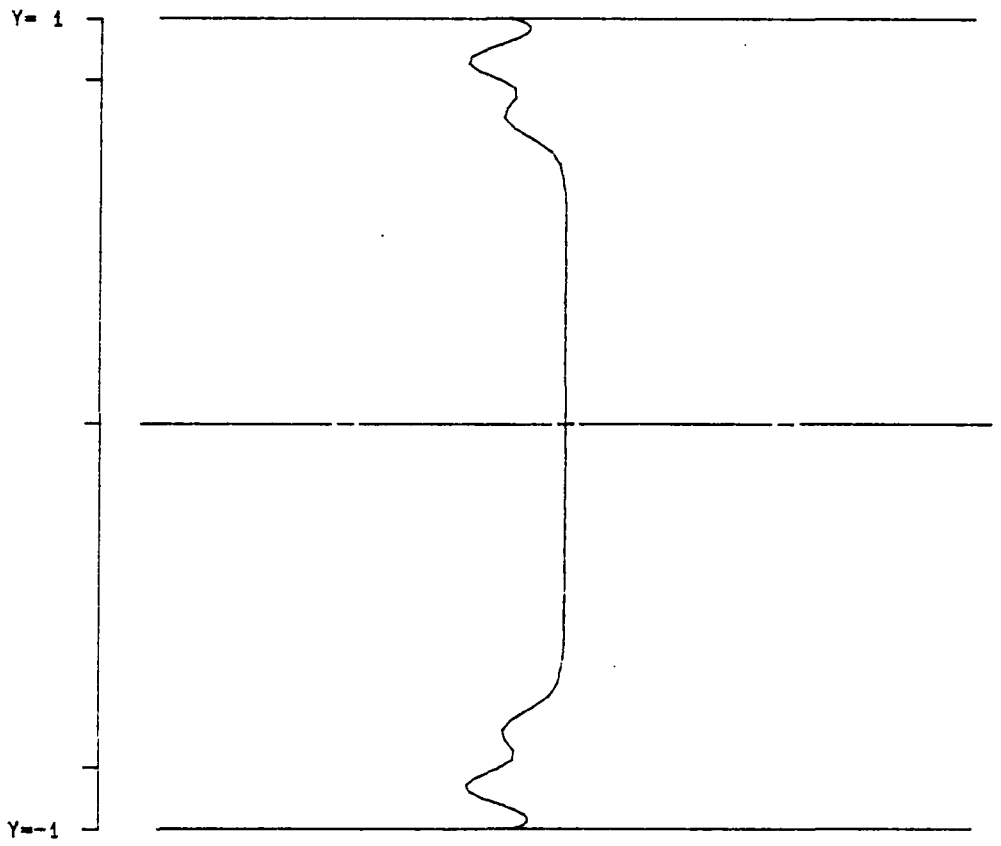

PPT 3-D F D3 (Y)

RE	5000.0	SIGMA	0.046326
ALPHA	1.1200	CR	0.281755
BETA	2.0000	MAX	-0.0000000
RMS	0.025000	MIN	-0.0000551
SYM	0		

Figure 3.60- $D^{(3)}$ as a function of y for $\mathbf{v}_{f_s}$ at $\alpha = 1.12$, $Re = 5000$, $\beta = 2.00$ and $A = 0.025$.

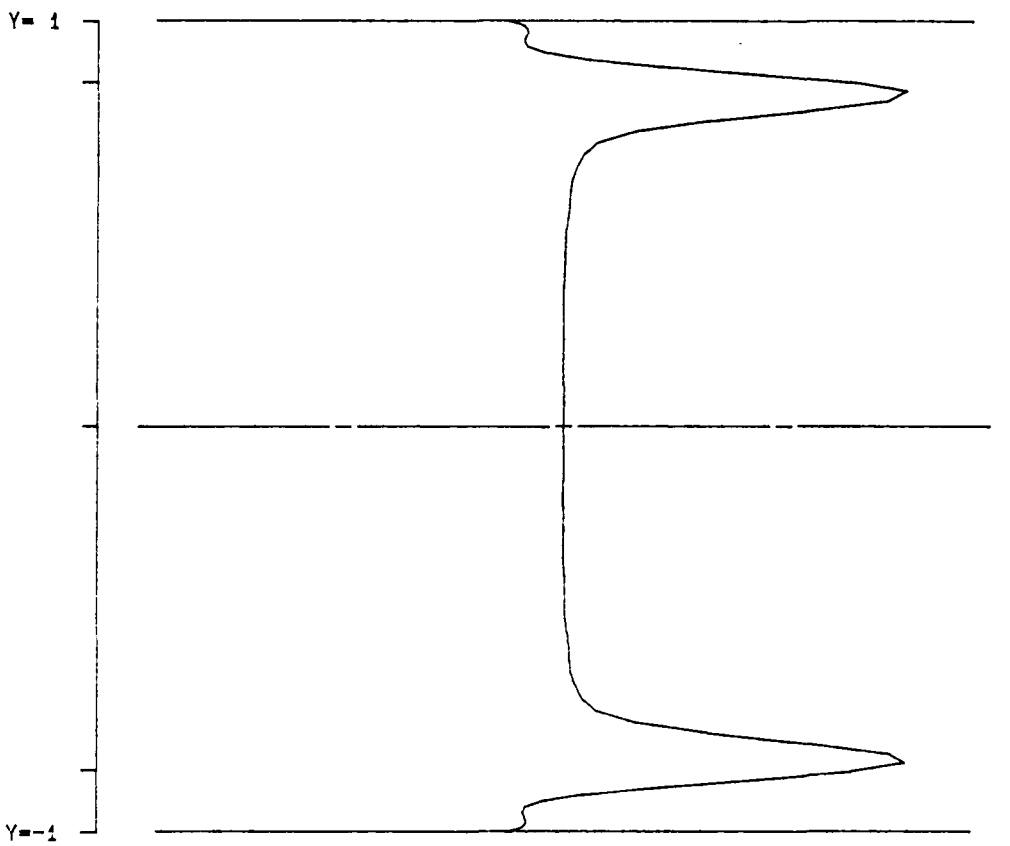

PPT 3-D F P3 (Y)

RE	5000.0	SIGMA	0.046326
ALPHA	1.1200	CR	0.281755
BETA	2.0000	MAX	0.0001754
RMS	0.025000	MIN	-0.0000319
SYM	0		

Figure 3.61- $P^{(3)}$ as a function of y for $\mathbf{v}_{f_s}$ at $\alpha = 1.12$, $Re = 5000$, $\beta = 2.00$ and $A = 0.025$.

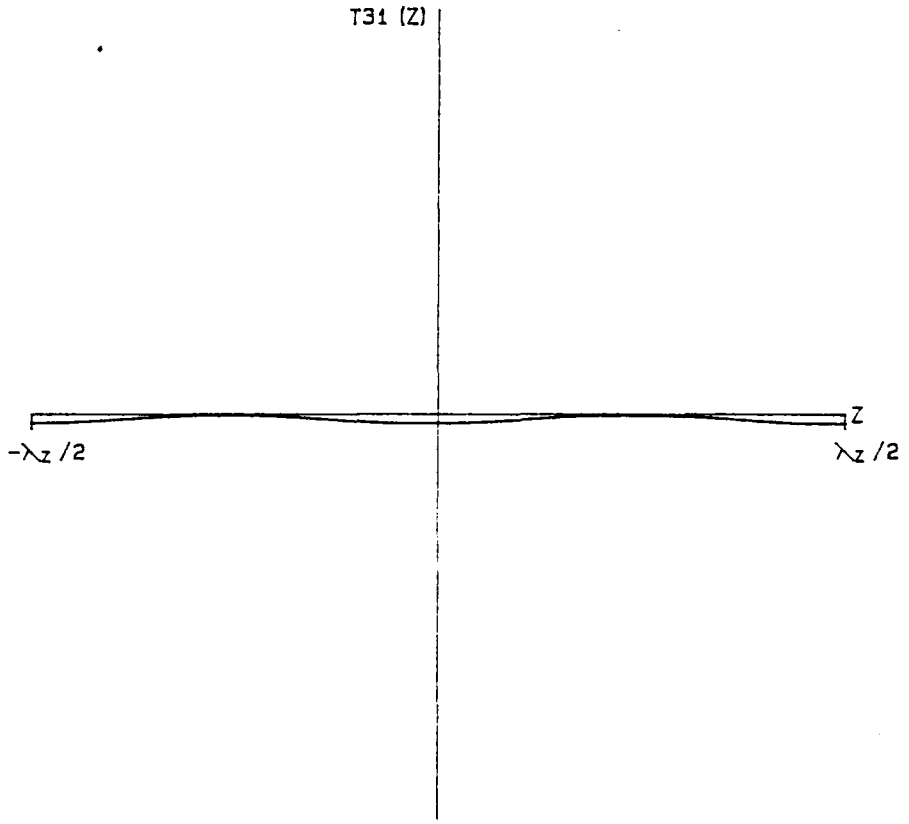

PPT 3-D F T31 (Z)

RE	5000.0	SIGMA	0.046326
ALPHA	1.1200	CR	0.281755
BETA	2.0000	MAX	-0.0000000
RMS	0.025000	MIN	-0.0000051
SYM	0		

Figure 3.62- $T^{(31)}$ as a function of z for $\mathbf{v}_{f_1}$ at $\alpha = 1.12$, $Re = 5000$, $\beta = 2.00$ and $A = 0.025$.

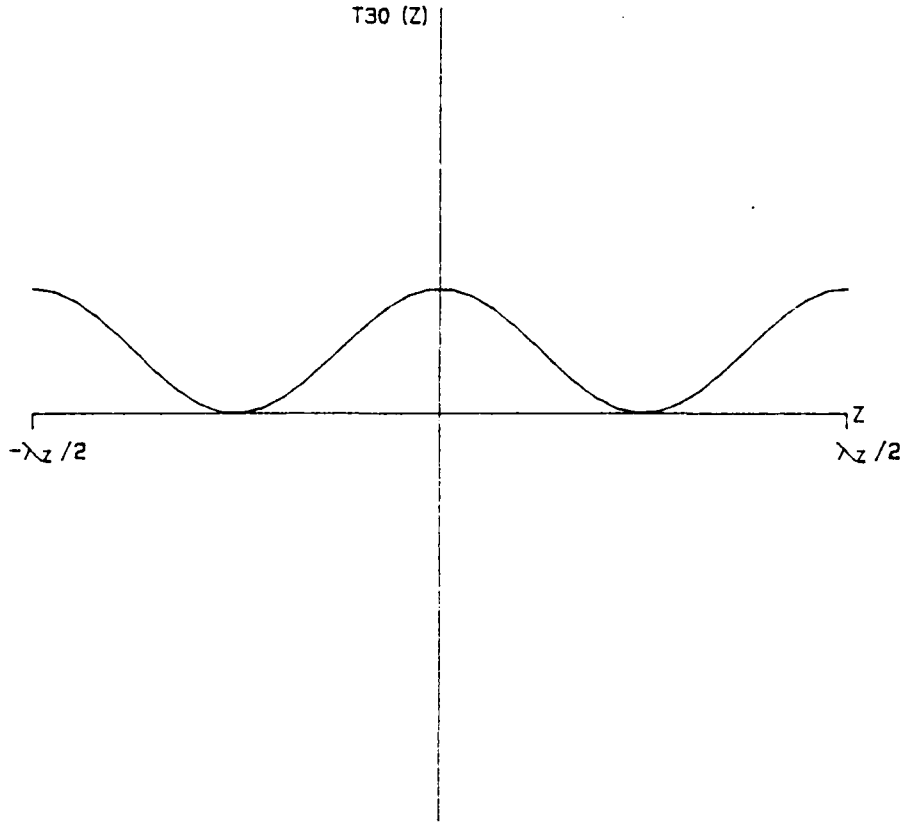

PPT 3-D F T30 (Z)

RE	5000.0	SIGMA	0.046326
ALPHA	1.1200	CR	0.281755
BETA	2.0000	MAX	0.0000711
RMS	0.025000	MIN	0.0000001
SYM	0		

Figure 3.63- $T^{(30)}$ as a function of z for $\mathbf{v}_{f_s}$ at $\alpha = 1.12$, $Re = 5000$, $\beta = 2.00$ and $A = 0.025$.

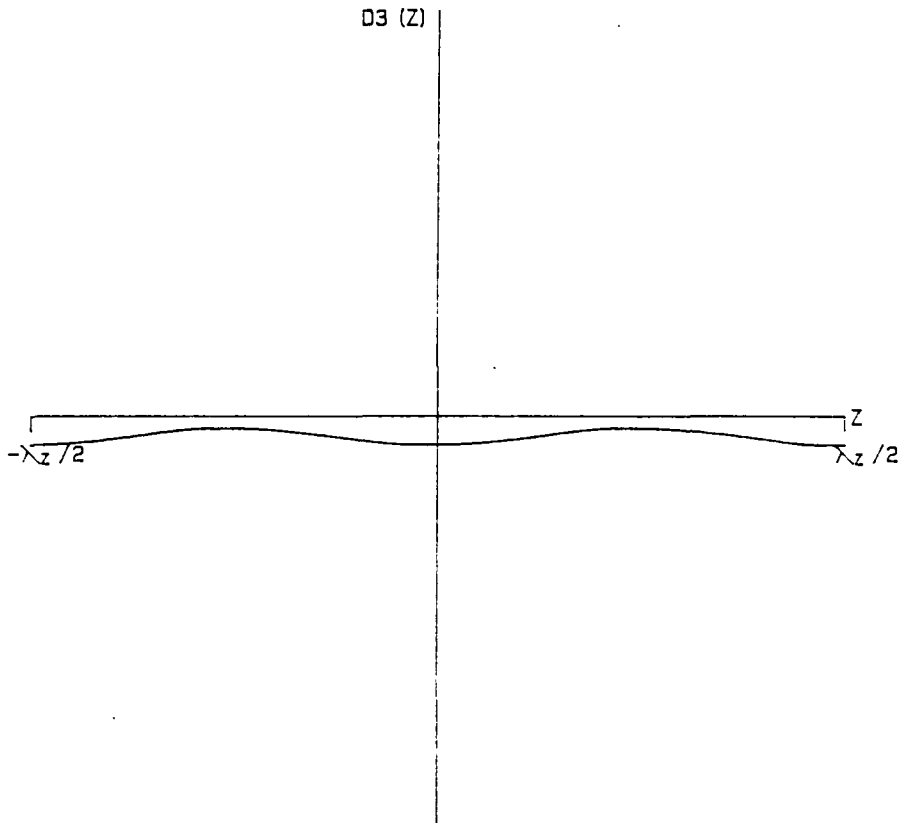

PPT 3-D F D3 (Z)

RE	5000.0	SIGMA	0.046325
ALPHA	1.1200	CR	0.281755
BETA	2.0000	MAX	-0.0000061
RMS	0.025000	MIN	-0.0000163
SYM	0		

Figure 3.64- $D^{(3)}$ as a function of z for $\mathbf{v}_f$, at $\alpha = 1.12$, $Re = 5000$, $\beta = 2.00$ and $A = 0.025$.

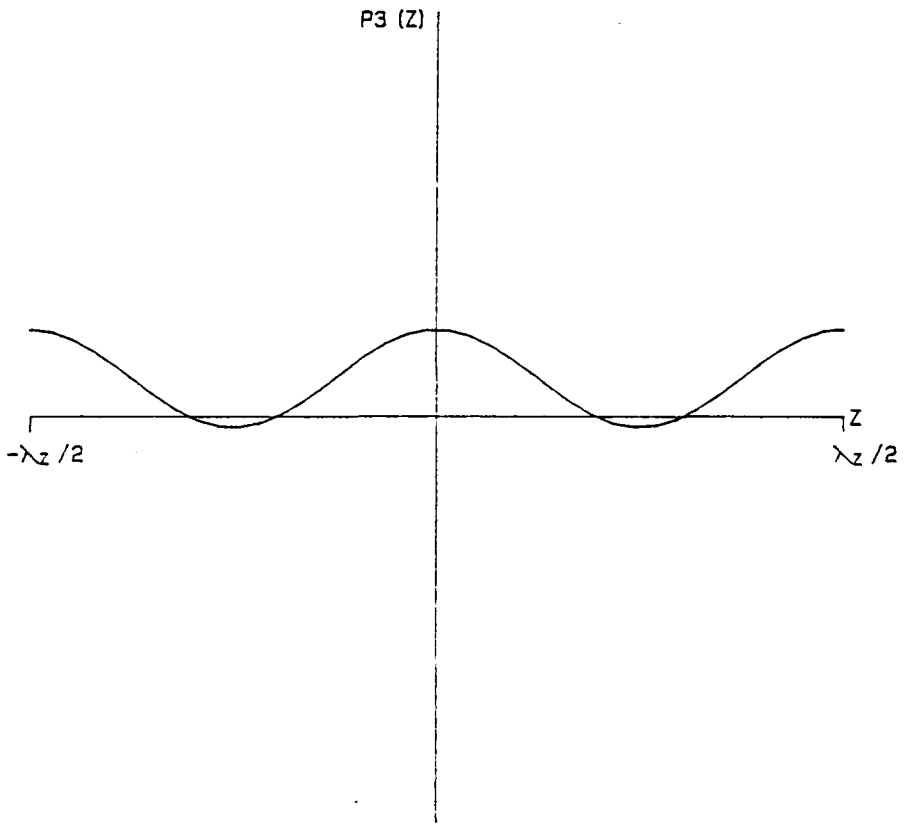

PPT 3-D F P3 (Z)

RE	5000.0	SIGMA	0.046326
ALPHA	1.1200	CR	0.281755
BETA	2.0000	MAX	0.0000497
RMS	0.025000	MIN	-0.0000060
SYM	0		

Figure 3.65- $P^{(3)}$ as a function of z for $\mathbf{v}_{f_3}$ at $\alpha = 1.12$, $Re = 5000$, $\beta = 2.00$ and $A = 0.025$.

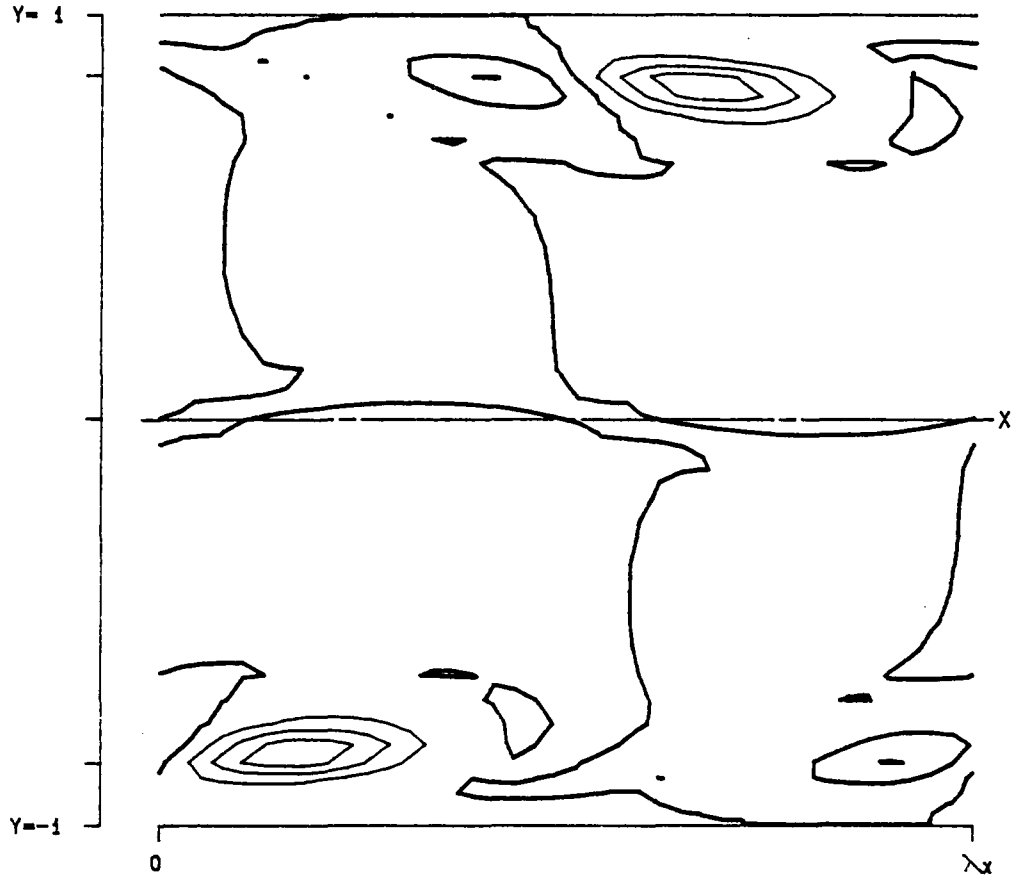

PPT 3-D F T31 (X, Y, Z)

RE	5000.0	LEVELS: MIN	-0.0004687
ALPHA	1.1200	DIF	0.0000937
BETA	2.0000	NO.	20
SIGMA	0.043798		
RMS	0.025000	Z =	-0.120831
MAX	0.001359		
SYM	1		

Figure 3.66- $T^{(31)}$ as a function of x, y and z at a position of $z = -0.120831$ for $\mathbf{v}_{fs}$ at $\alpha = 1.12$, $Re = 5000$, $\beta = 2.00$ and $A = 0.025$.

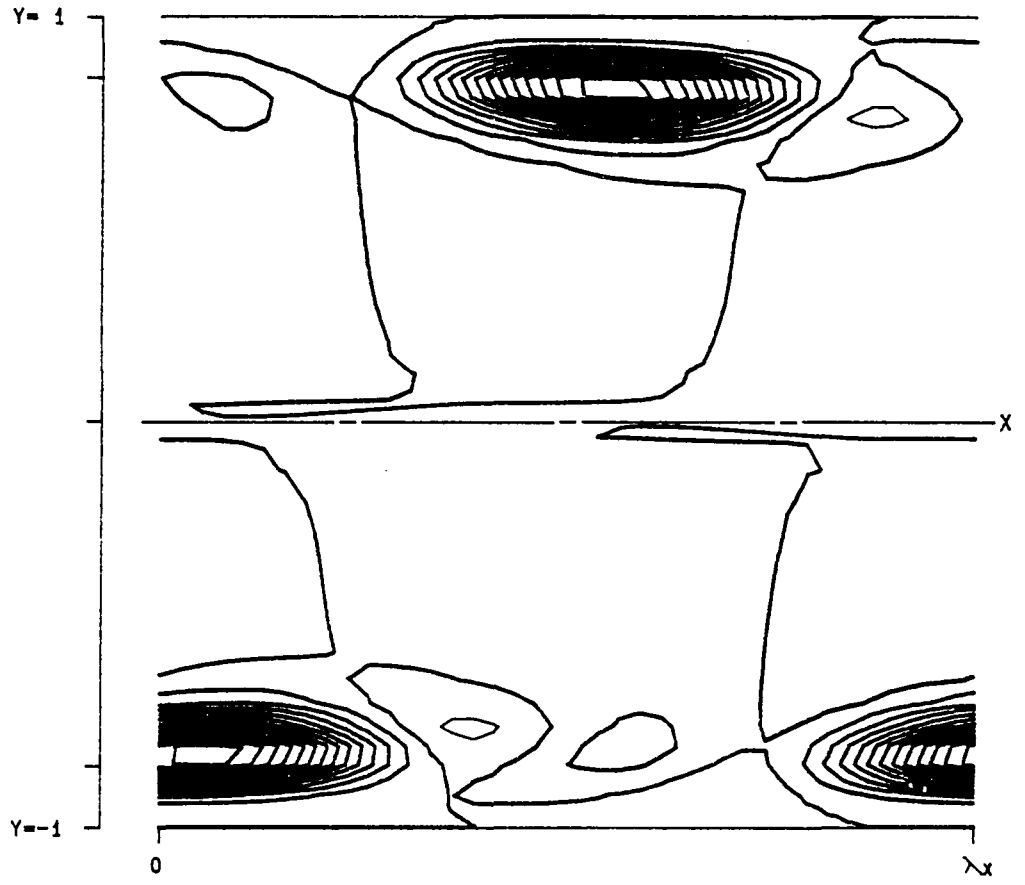

PPT 3-D F T30 (X, Y, Z)

RE	5000.0	LEVELS: MIN	-0.0004687
ALPHA	1.1200	DIF	0.0000937
BETA	2.0000	NO.	20
SIGMA	0.043798		
RMS	0.025000	Z =	-0.120831
MAX	0.001359		
SYM	1		

Figure 3.67- $T^{(30)}$ as a function of x, y and z at a position of $z = -0.120831$ for $\mathbf{v}_{fa}$ at $\alpha = 1.12$, $Re = 5000$, $\beta = 2.00$ and $A = 0.025$.

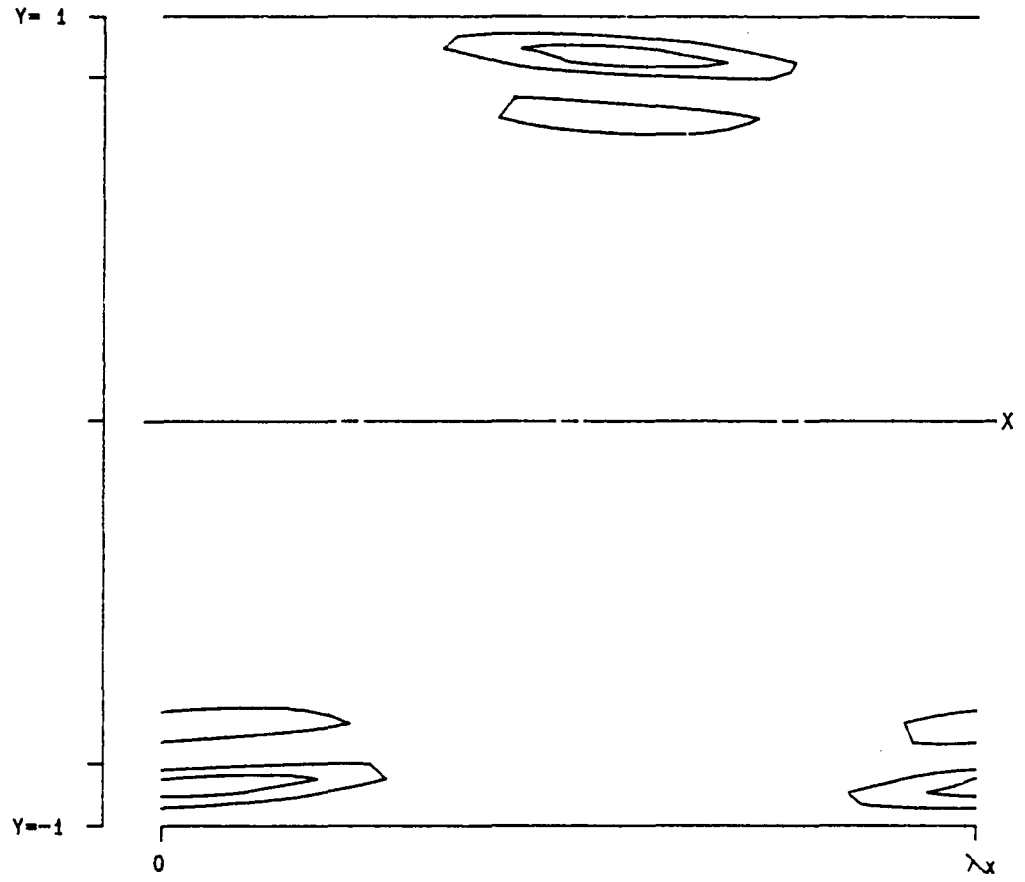

PPT 3-D F D3 (X, Y, Z)

RE	5000.0
ALPHA	1.1200
BETA	2.0000
SIGMA	0.043798
RMS	0.025000
MAX	0.001359
SYM	1

LEVELS:	MIN	-0.0004687
	DIF	0.0000937
	NO.	20
	Z =	-0.120831

Figure 3.68- $D^{(3)}$ as a function of x, y and z at a position of $z = -0.120831$ for $\mathbf{v}_{fa}$ at $\alpha = 1.12$, $Re = 5000$, $\beta = 2.00$ and $A = 0.025$.

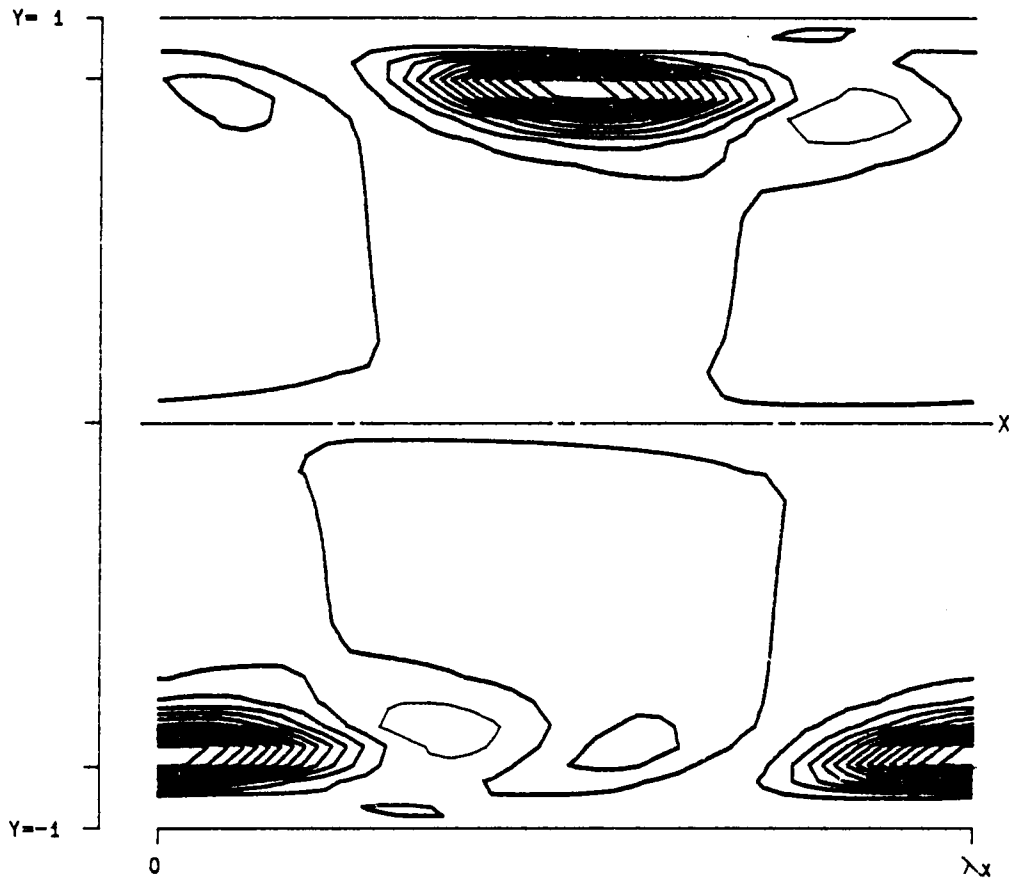

PPT 3-D F P3 (X, Y, Z)

RE	5000.0
ALPHA	1.1200
BETA	2.0000
SIGMA	0.043798
RMS	0.025000
MAX	0.001359
SYM	1

LEVELS:	MIN	-0.0004687
	DIF	0.0000937
	NO.	20
	Z =	-0.120831

Figure 3.69- $P^{(3)}$ as a function of x, y and z at a position of $z = -0.120831$ for $\mathbf{v}_{fa}$ at $\alpha = 1.12$, $Re = 5000$, $\beta = 2.00$ and $A = 0.025$.

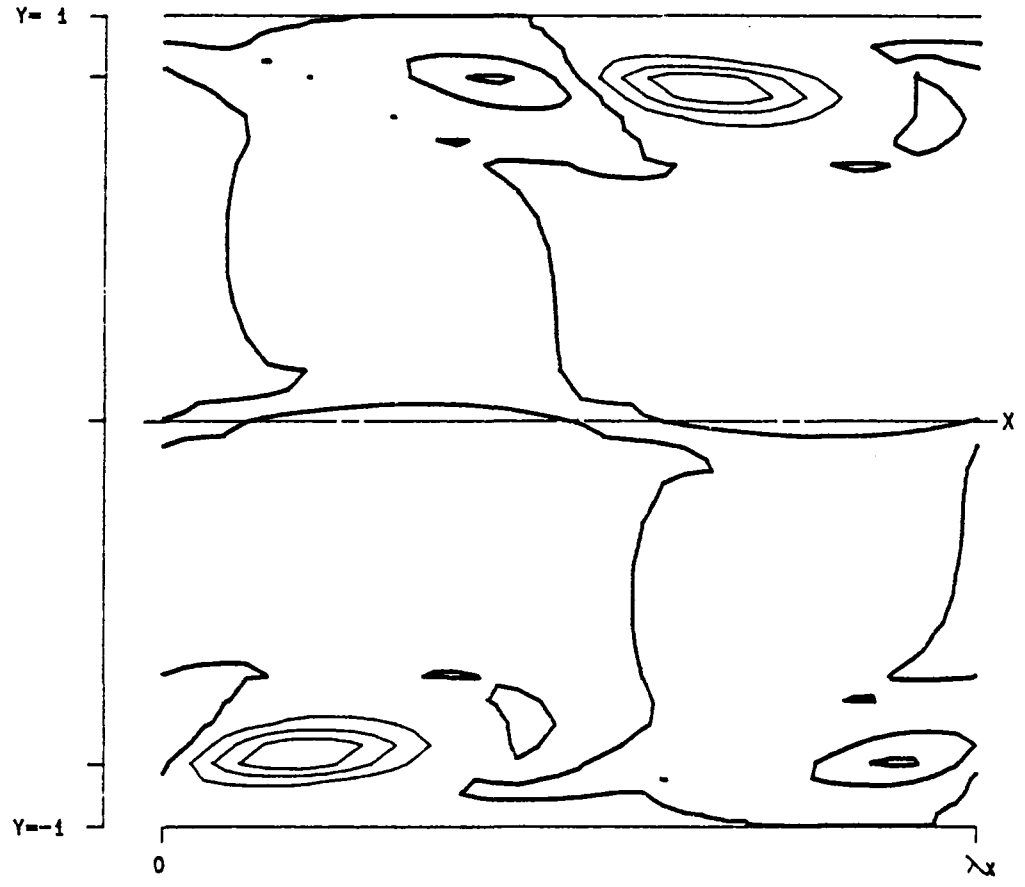

PPT 3-D F T31 (X, Y, Z)

RE	5000.0
ALPHA	1.1200
BETA	2.0000
SIGMA	0.043798
RMS	0.025000
MAX	0.001359
SYM	1

LEVELS: MIN	-0.0004687
DIF	0.0000937
NO.	20
Z =	-0.040277

Figure 3.70- $T^{(31)}$ as a function of x, y and z at a position of $z = -0.040277$ for $\mathbf{v}_{fa}$ at $\alpha = 1.12$, $Re = 5000$, $\beta = 2.00$ and $A = 0.025$.

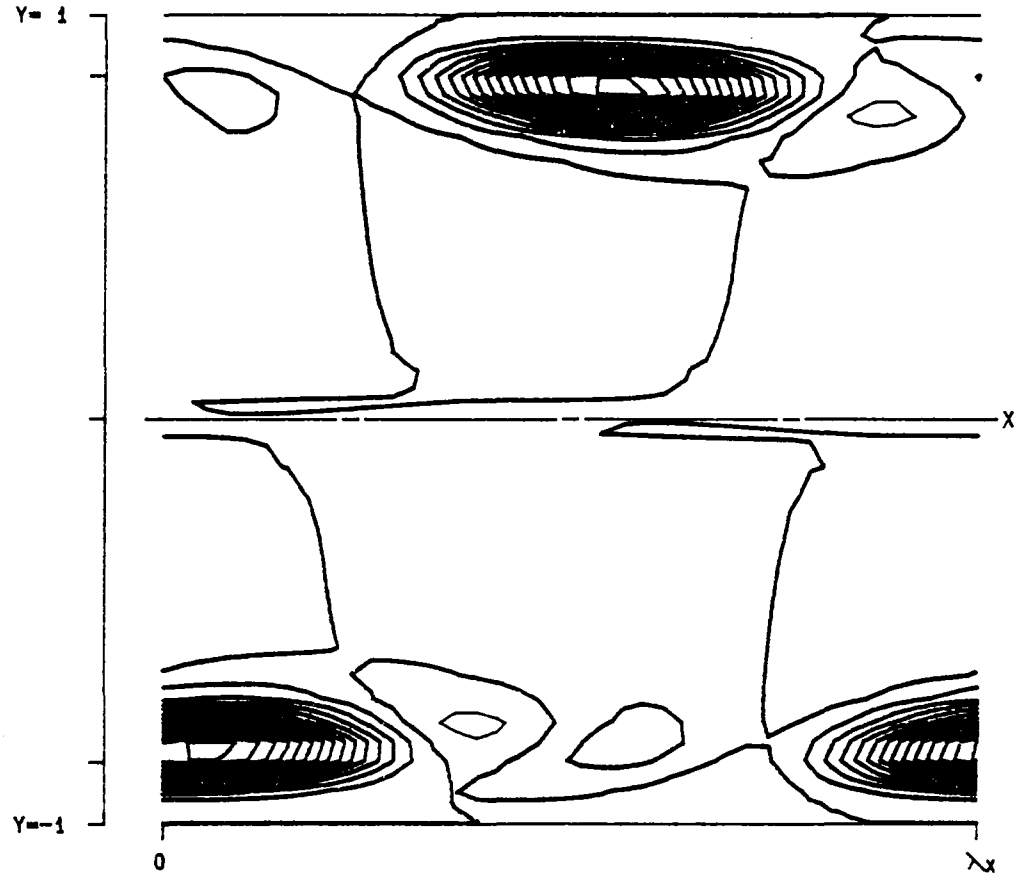

PPT 3-D F T30 (X, Y, Z)

RE	5000.0
ALPHA	1.1200
BETA	2.0000
SIGMA	0.043798
RMS	0.025000
MAX	0.001359
SYM	1

LEVELS:	MIN -0.0004687
	DIF 0.0000937
	NO. 20
	Z = -0.040277

Figure 3.71- $T^{(30)}$ as a function of x, y and z at a position of $z = -0.040277$ for $\mathbf{v}_{fa}$ at $\alpha = 1.12$, $Re = 5000$, $\beta = 2.00$ and $A = 0.025$.

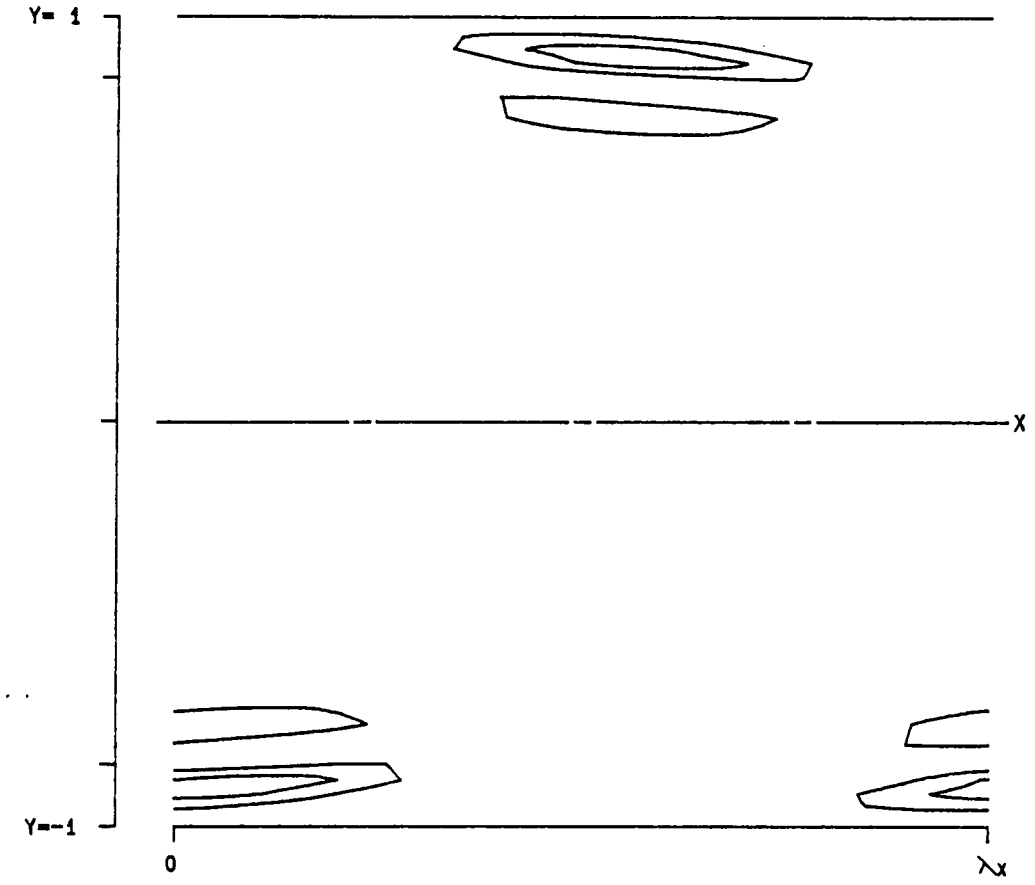

PPT 3-D F D3 (X, Y, Z)

RE	5000.0
ALPHA	1.1200
BETA	2.0000
SIGMA	0.043798
RMS	0.025000
MAX	0.001359
SYM	1

LEVELS:	MIN	-0.0004687
	DIF	0.0000937
	NO.	20
	Z =	-0.040277

Figure 3.72- $D^{(3)}$ as a function of x, y and z at a position of $z = -0.040277$ for $\mathbf{v}_{fa}$ at $\alpha = 1.12$, $Re = 5000$, $\beta = 2.00$ and $A = 0.025$.

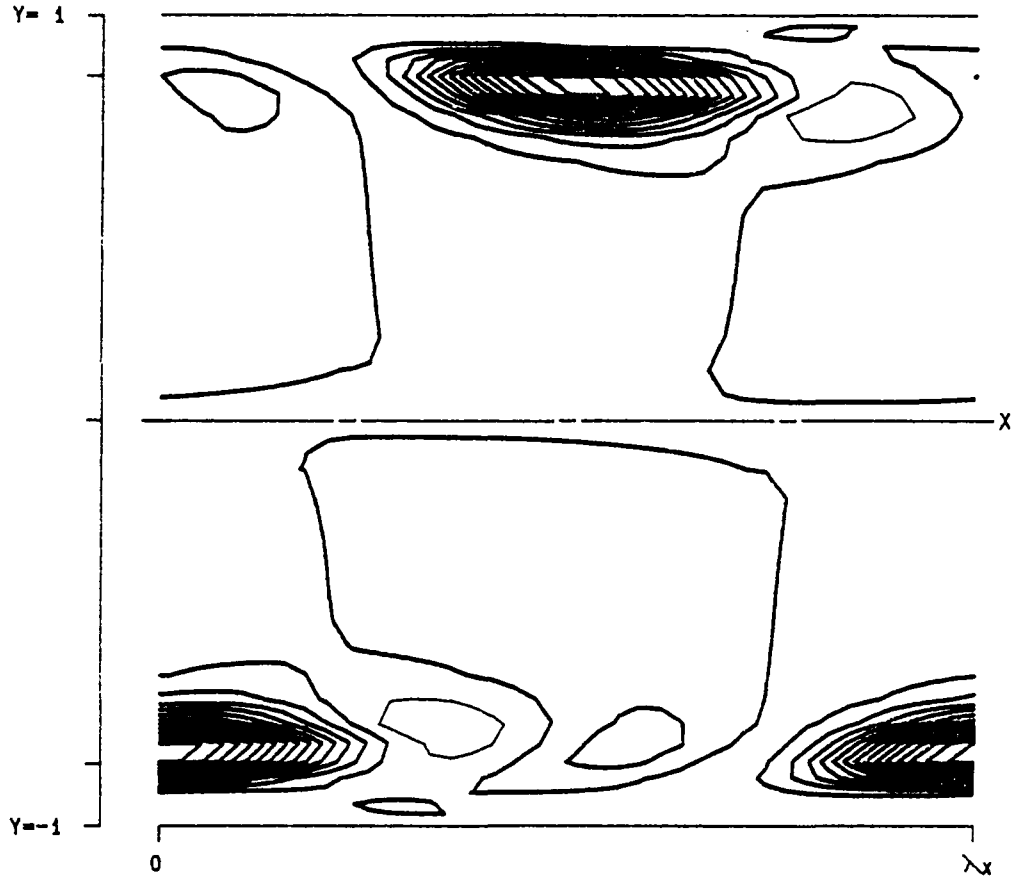

PPT 3-D F P3 (X, Y, Z)

RE	5000.0
ALPHA	1.1200
BETA	2.0000
SIGMA	0.043798
RMS	0.025000
MAX	0.001359
SYM	1

LEVELS:	MIN	-0.0004687
	DIF	0.0000937
	NO.	20
	Z =	-0.040277

Figure 3.73- $P^{(3)}$ as a function of x, y and z at a position of $z = -0.040277$ for $\mathbf{v}_{fa}$ at $\alpha = 1.12$, $Re = 5000$, $\beta = 2.00$ and $A = 0.025$.

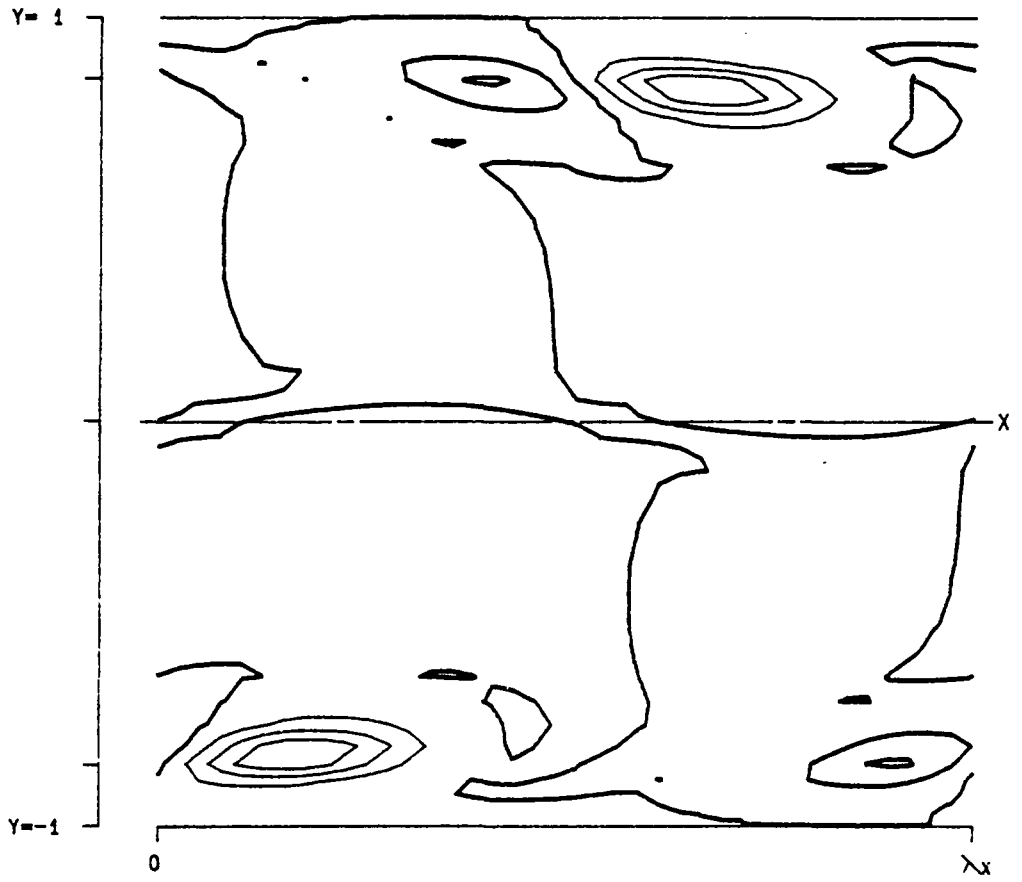

PPT 3-D F T31 (X, Y, Z)

RE	5000.0	LEVELS: MIN	-0.0004687
ALPHA	1.1200	DIF	0.0000937
BETA	2.0000	NO.	20
SIGMA	0.043798		
RMS	0.025000	Z =	0.040277
MAX	0.001359		
SYM	1		

Figure 3.74- $T^{(31)}$ as a function of x, y and z at a position of $z = 0.040277$ for $\mathbf{v}_{fa}$ at $\alpha = 1.12$, $Re = 5000$, $\beta = 2.00$ and $A = 0.025$.

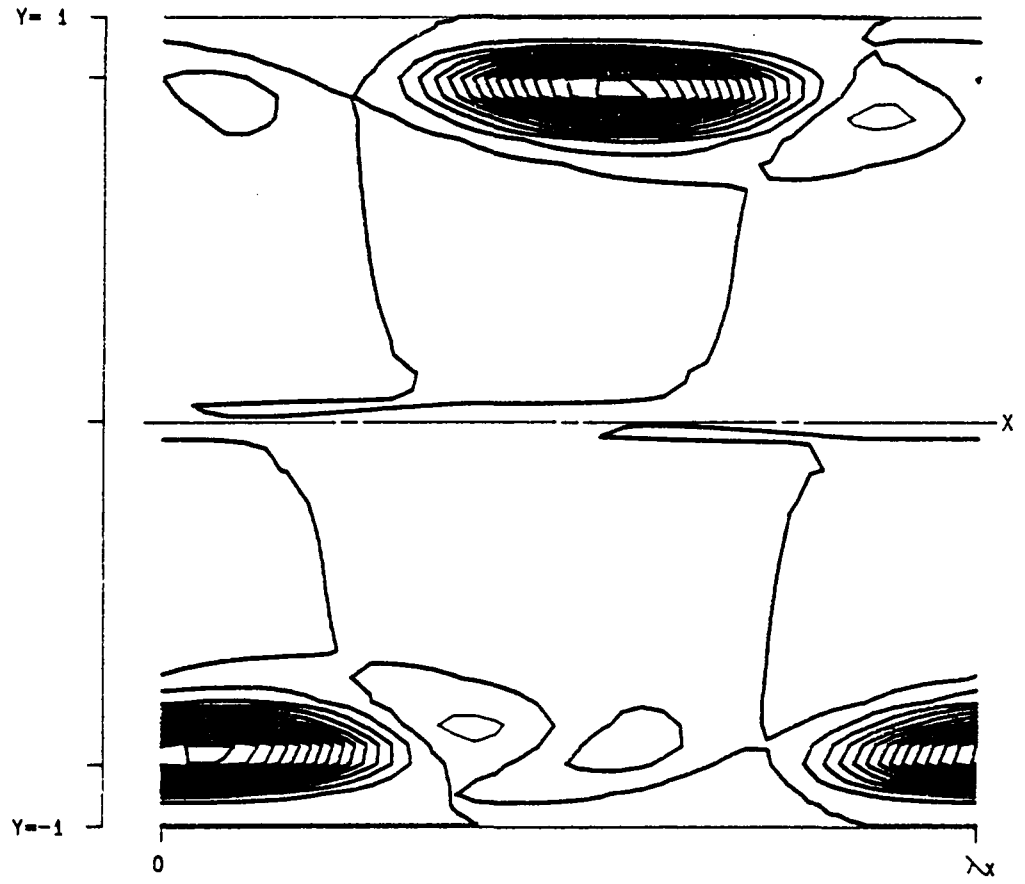

PPT 3-D F T30 (X, Y, Z)

RE	5000.0	LEVELS: MIN	-0.0004687
ALPHA	1.1200	DIF	0.0000937
BETA	2.0000	NO.	20
SIGMA	0.043798		
RMS	0.025000	Z =	0.040277
MAX	0.001359		
SYM	1		

Figure 3.75- $T^{(30)}$ as a function of x, y and z at a position of $z = 0.040277$ for $\mathbf{v}_{fa}$ at $\alpha = 1.12$, $Re = 5000$, $\beta = 2.00$ and $A = 0.025$.

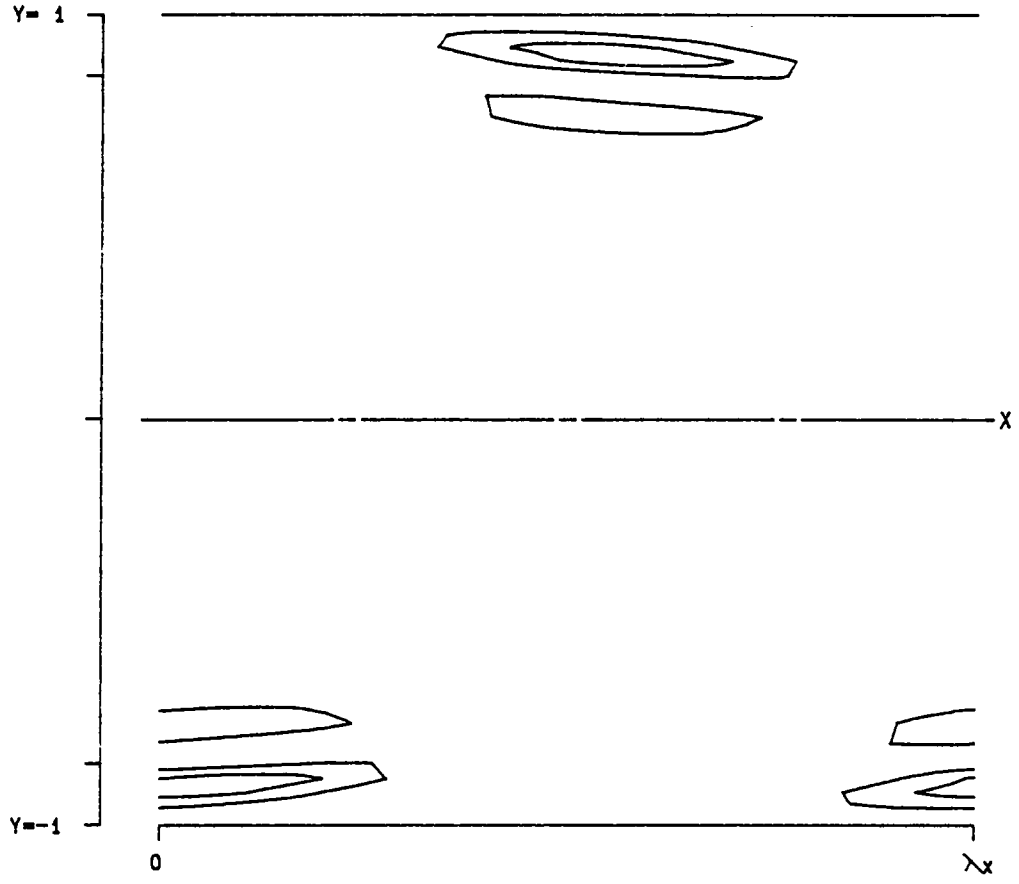

PPT 3-D F D3 (X, Y, Z)

RE	5000.0
ALPHA	1.1200
BETA	2.0000
SIGMA	0.043798
RMS	0.025000
MAX	0.001359
SYM	1

LEVELS: MIN	-0.0004687
DIF	0.0000937
NO.	20
Z =	0.040277

Figure 3.76- $D^{(3)}$ as a function of x, y and z at a position of $z = 0.040277$ for v_{f_a} at $\alpha = 1.12$, $Re = 5000$, $\beta = 2.00$ and $A = 0.025$.

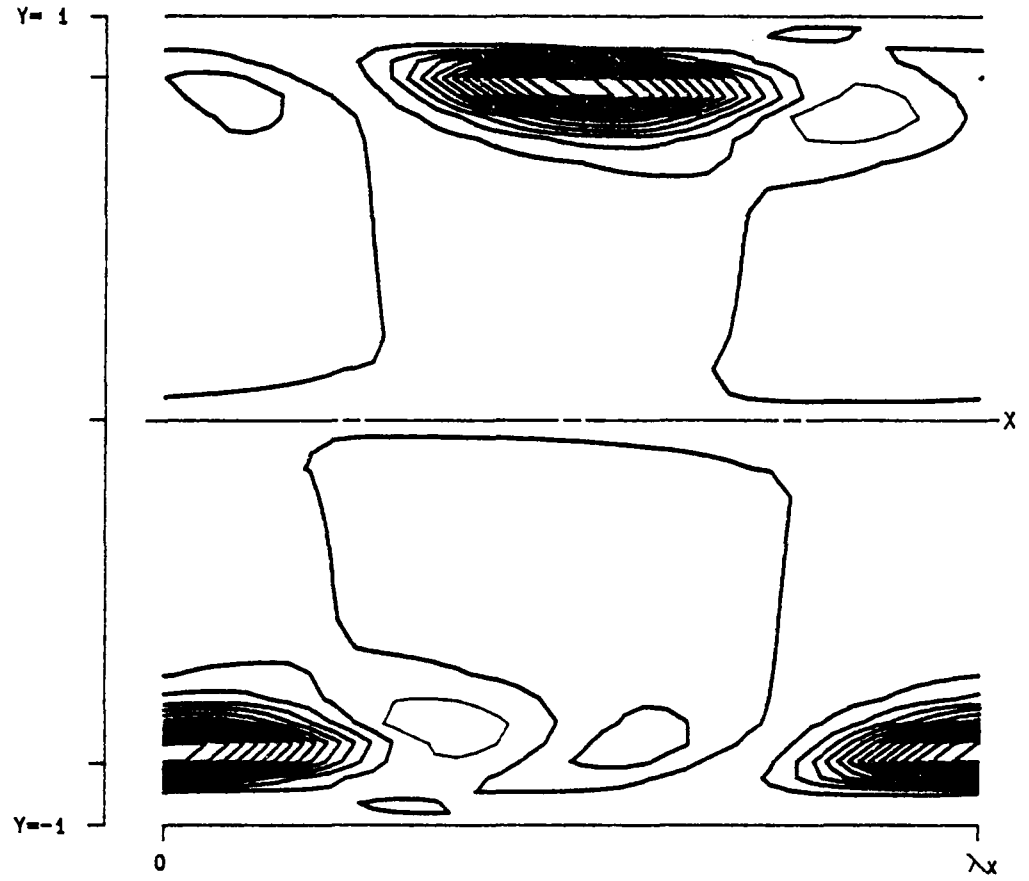

PPT 3-D F P3 (X, Y, Z)

RE	5000.0
ALPHA	1.1200
BETA	2.0000
SIGMA	0.043798
RMS	0.025000
MAX	0.001359
SYM	1

LEVELS: MIN	-0.0004687
DIF	0.0000937
NO.	20
Z =	0.040277

Figure 3.77- $P^{(3)}$ as a function of x, y and z at a position of $z = 0.040277$ for $\mathbf{v}_{f_a}$ at $\alpha = 1.12$, $Re = 5000$, $\beta = 2.00$ and $A = 0.025$.

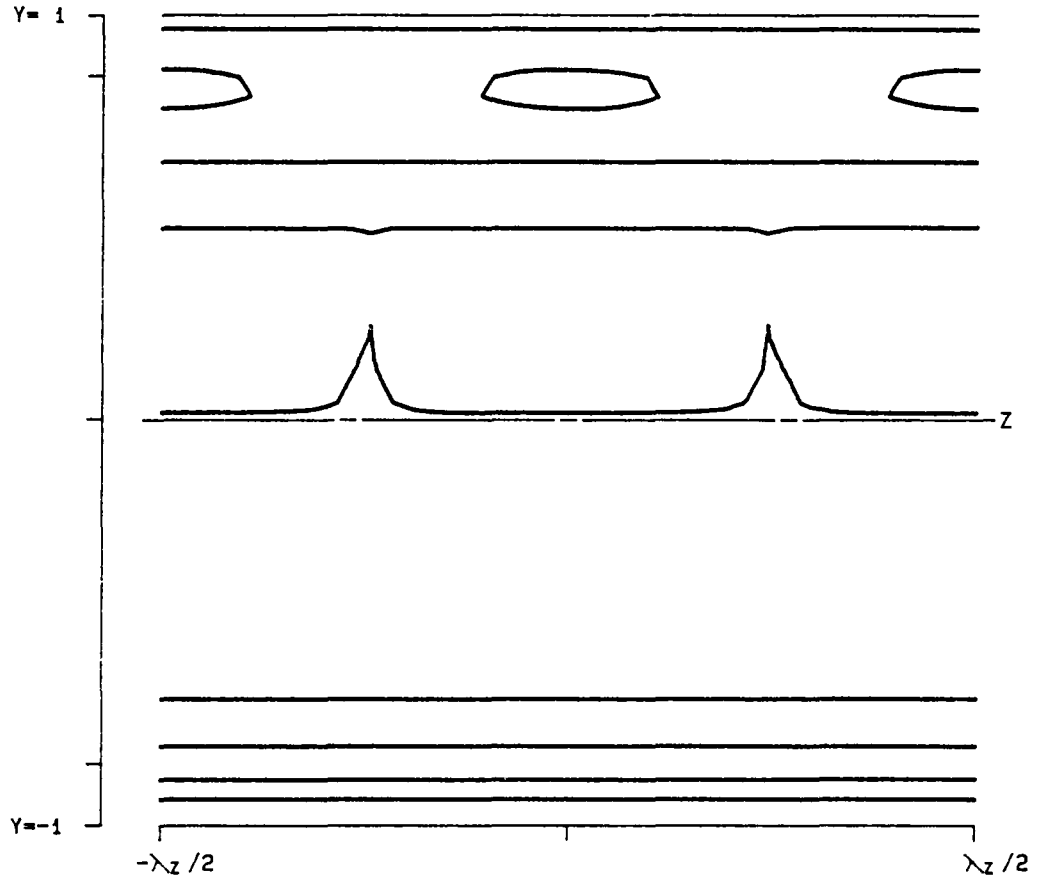

PPT 3-D F T31 (X, Y, Z)

RE	5000.0	LEVELS: MIN	-0.0004687
ALPHA	1.1200	DIF	0.0000937
BETA	2.0000	NO.	20
SIGMA	0.043798		
RMS	0.025000	X =	2.589225
MAX	0.001359		
SYM	1		

Figure 3.78- $T^{(31)}$ as a function of x, y and z at a position of $x = 2.589225$ for $\mathbf{v}_{fa}$ at $\alpha = 1.12$, $Re = 5000$, $\beta = 2.00$ and $A = 0.025$.

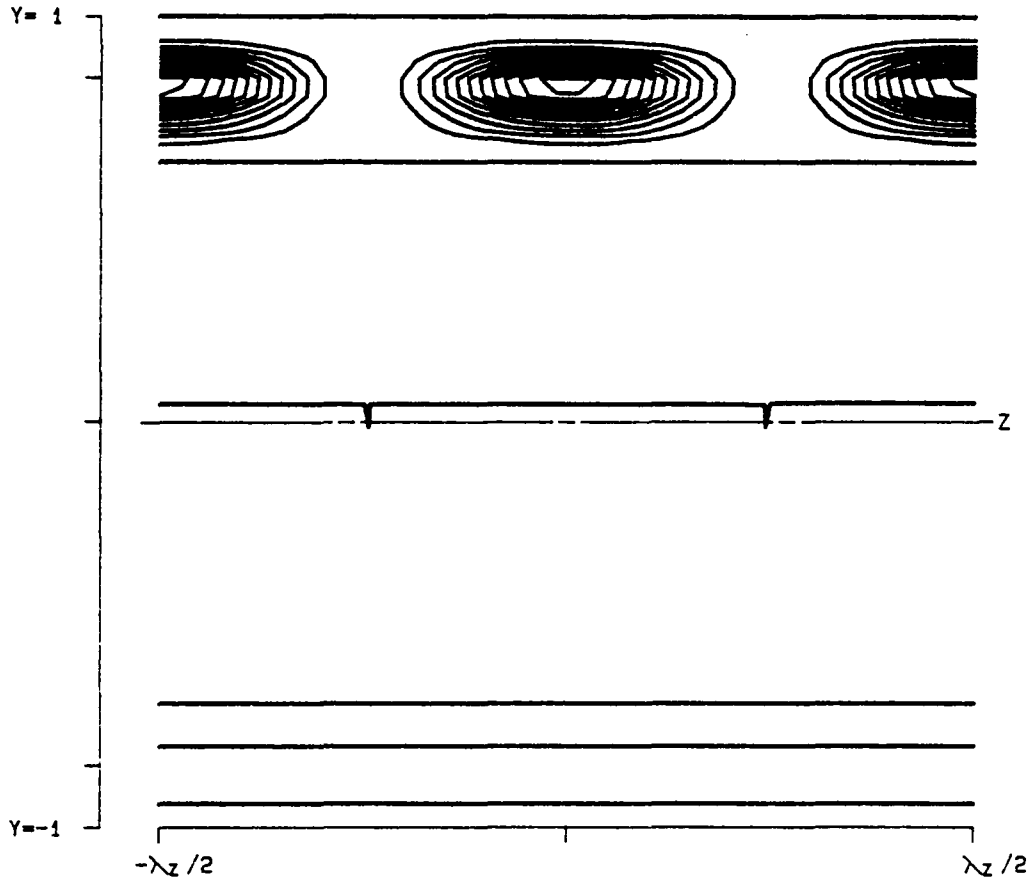

PPT 3-D F T30 (X, Y, Z)

RE	5000.0	LEVELS: MIN	-0.0004687
ALPHA	1.1200	DIF	0.0000937
BETA	2.0000	NO.	20
SIGMA	0.043798		
RMS	0.025000	X =	2.589225
MAX	0.001359		
SYM	1		

Figure 3.79- $T^{(30)}$ as a function of x, y and z at a position of $x = 2.589225$ for $\mathbf{v}_{fs}$ at $\alpha = 1.12$, $Re = 5000$, $\beta = 2.00$ and $A = 0.025$.

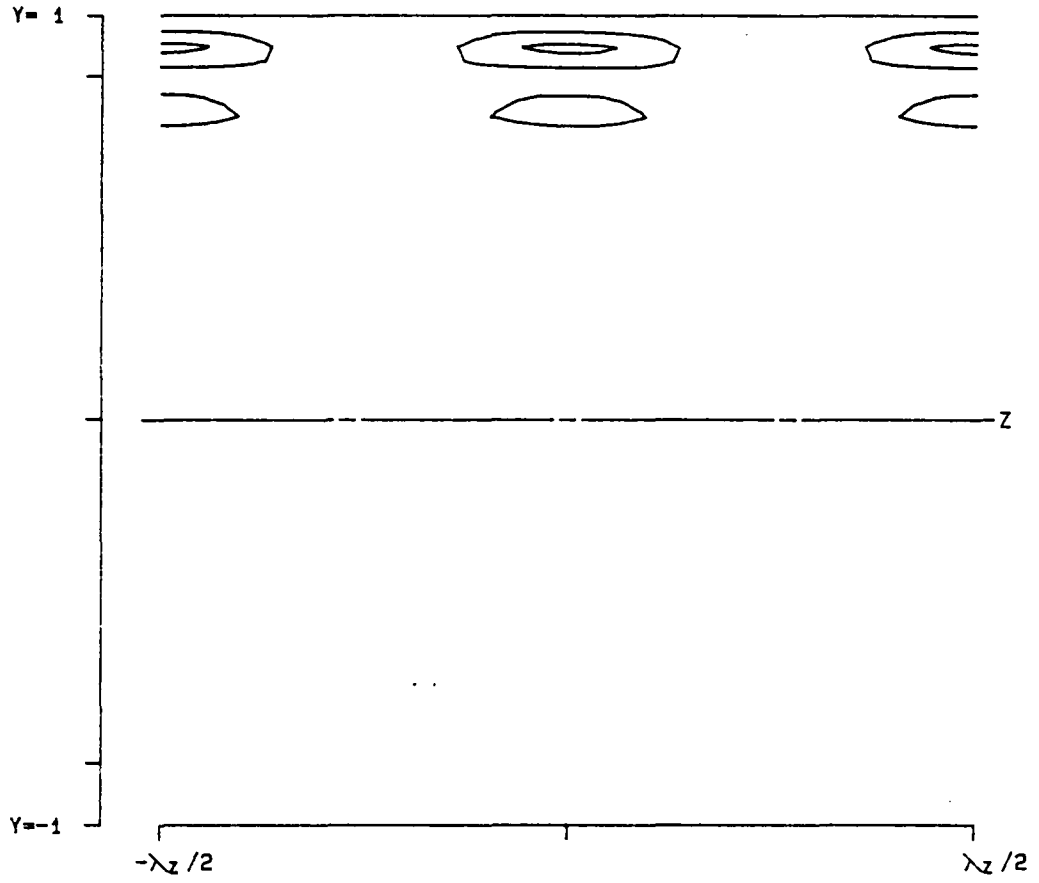

PPT 3-D F D3 (X, Y, Z)

RE	5000.0	LEVELS:	MIN -0.0004687
ALPHA	1.1200		DIF 0.0000937
BETA	2.0000		NO. 20
SIGMA	0.043798		
RMS	0.025000		X = 2.589225
MAX	0.001359		
SYM	1		

Figure 3.80- $D^{(3)}$ as a function of x, y and z at a position of $x = 2.589225$ for $\mathbf{v}_{f_6}$ at $\alpha = 1.12$, $Re = 5000$, $\beta = 2.00$ and $A = 0.025$.

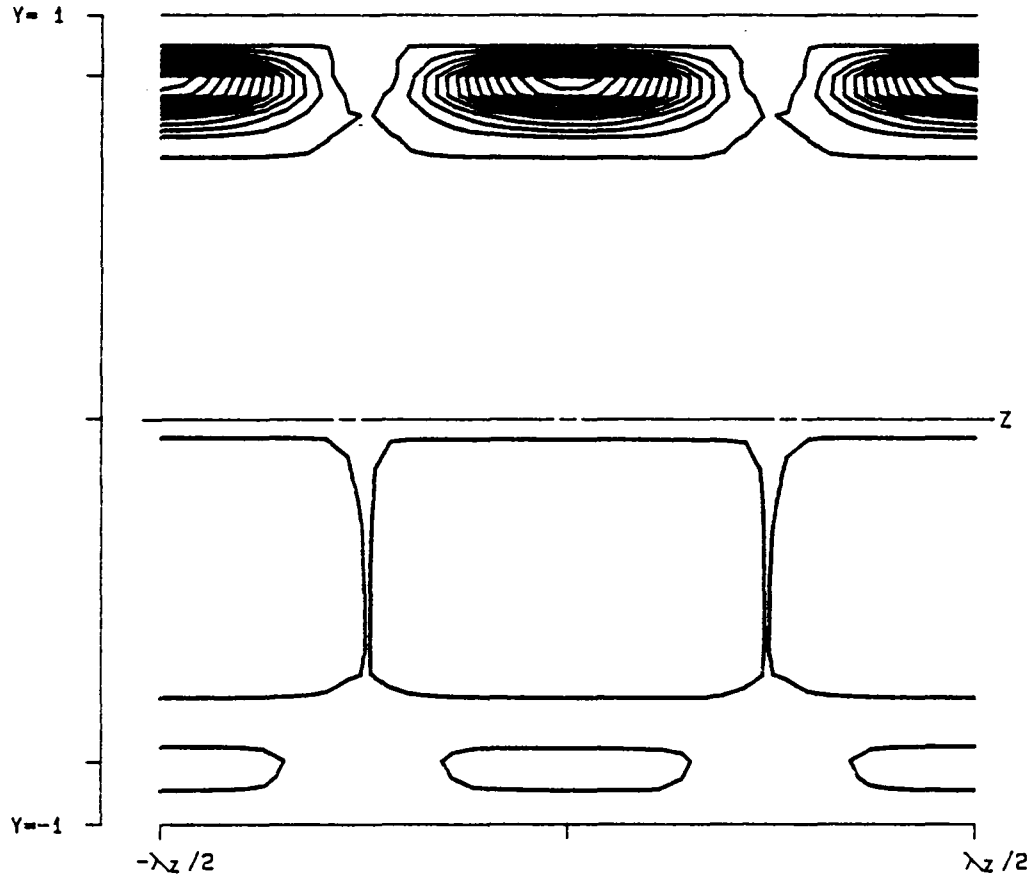

PPT 3-D F P3 (X, Y, Z)

RE	5000.0
ALPHA	1.1200
BETA	2.0000
SIGMA	0.043798
RMS	0.025000
MAX	0.001359
SYM	1

LEVELS:	MIN	-0.0004687
	DIF	0.0000937
	NO.	20
	X =	2.589225

Figure 3.81- $P^{(3)}$ as a function of x, y and z at a position of $x = 2.589225$ for $\mathbf{v}_{f_s}$ at $\alpha = 1.12$, $Re = 5000$, $\beta = 2.00$ and $A = 0.025$.

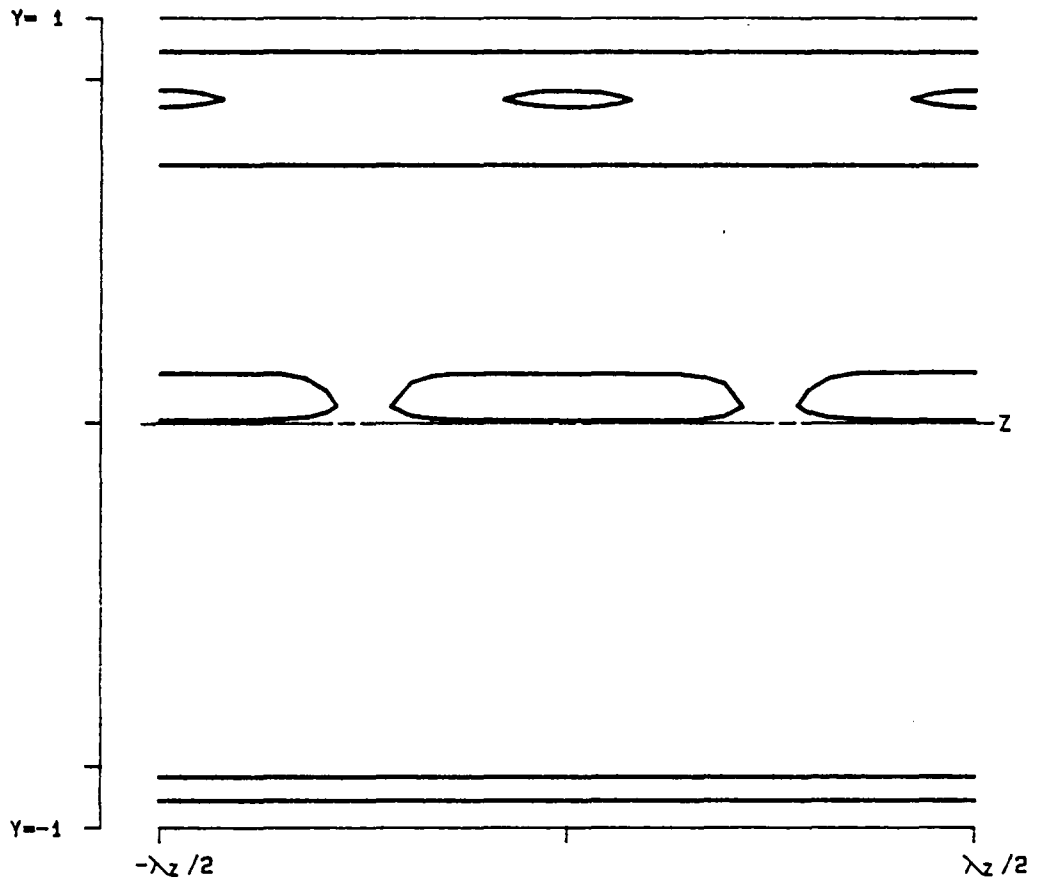

PPT 3-D F T31 (X, Y, Z)

RE	5000.0	LEVELS: MIN	-0.0004687
ALPHA	1.1200	DIF	0.0000937
BETA	2.0000	NO.	20
SIGMA	0.043798		
RMS	0.025000	X =	2.733071
MAX	0.001359		
SYM	1		

Figure 3.82- $T^{(31)}$ as a function of x, y and z at a position of $x = 2.733071$ for $\mathbf{v}_{fs}$ at $\alpha = 1.12$, $Re = 5000$, $\beta = 2.00$ and $A = 0.025$.

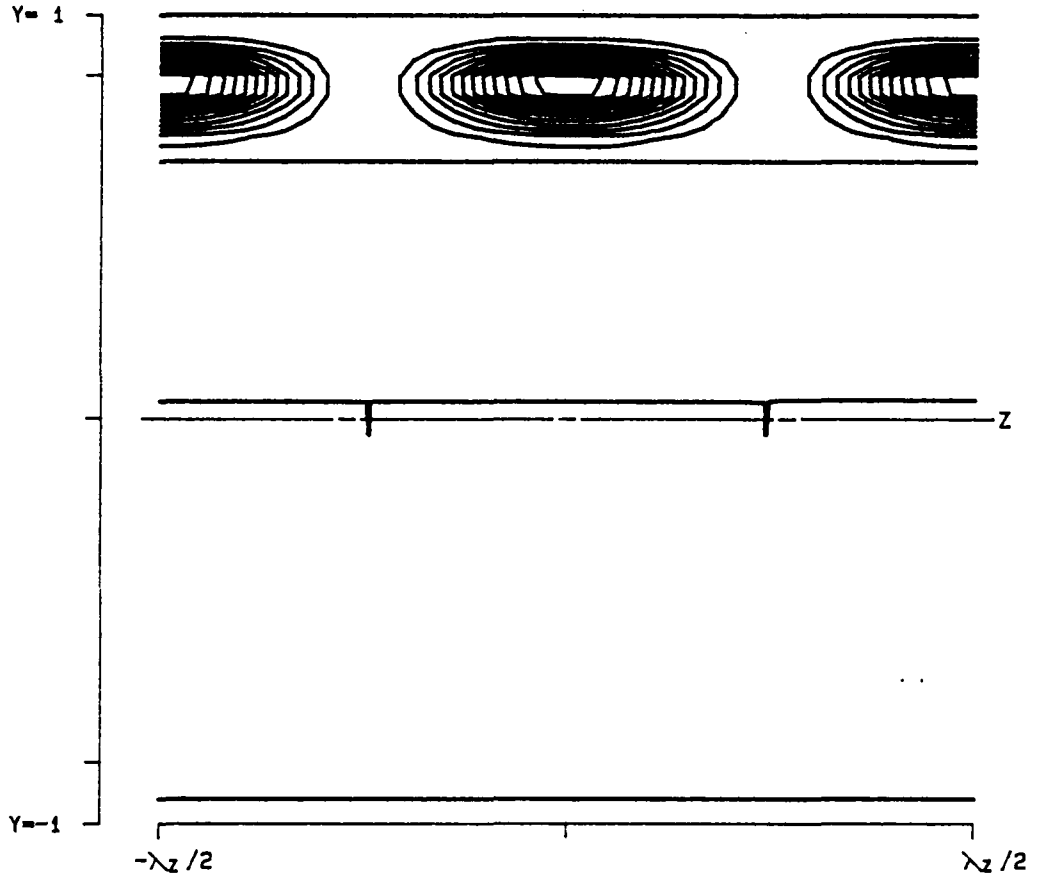

PPT 3-D F T30 (X, Y, Z)

RE	5000.0	LEVELS: MIN	-0.0004687
ALPHA	1.1200	DIF	0.0000937
BETA	2.0000	NO.	20
SIGMA	0.043798		
RMS	0.025000	X =	2.733071
MAX	0.001359		
SYM	1		

Figure 3.83- $T^{(30)}$ as a function of x, y and z at a position of $x = 2.733071$ for $\mathbf{v}_{f_4}$ at $\alpha = 1.12$, $Re = 5000$, $\beta = 2.00$ and $A = 0.025$.

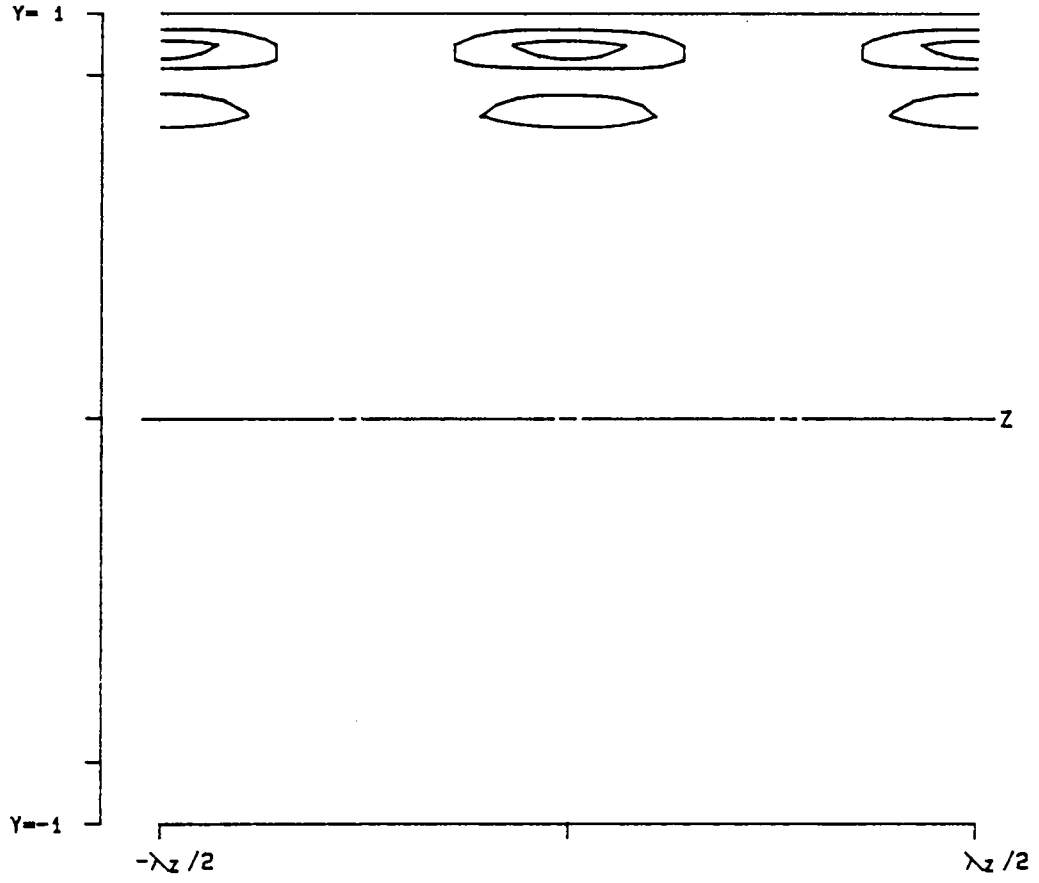

PPT 3-D F D3 (X, Y, Z)

RE	5000.0
ALPHA	1.1200
BETA	2.0000
SIGMA	0.043798
RMS	0.025000
MAX	0.001359
SYM	1

LEVELS:	MIN	-0.0004687
	DIF	0.0000937
	NO.	20
	X =	2.733071

Figure 3.85- $P^{(3)}$ as a function of x, y and z at a position of $x = 2.733071$ for $\mathbf{v}_{fa}$ at $\alpha = 1.12$, $Re = 5000$, $\beta = 2.00$ and $A = 0.025$.

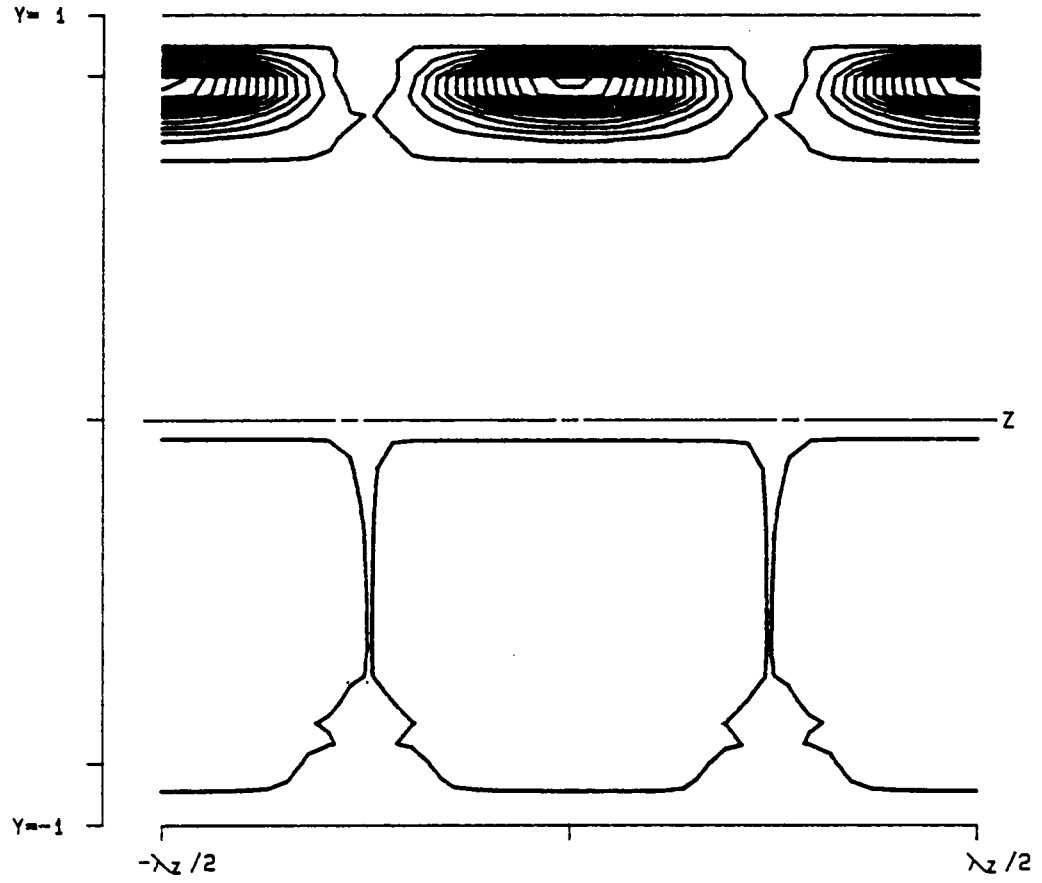

PPT 3-D F P3 (X, Y, Z)

RE	5000.0
ALPHA	1.1200
BETA	2.0000
SIGMA	0.043798
RMS	0.025000
MAX	0.001359
SYM	1

LEVELS:	MIN	-0.0004687
	DIF	0.0000937
	NO.	20
	X =	2.733071

Figure 3.84- $D^{(3)}$ as a function of x, y and z at a position of $x = 2.733071$ for $\mathbf{v}_{f_1}$ at $\alpha = 1.12$, $Re = 5000$, $\beta = 2.00$ and $A = 0.025$.

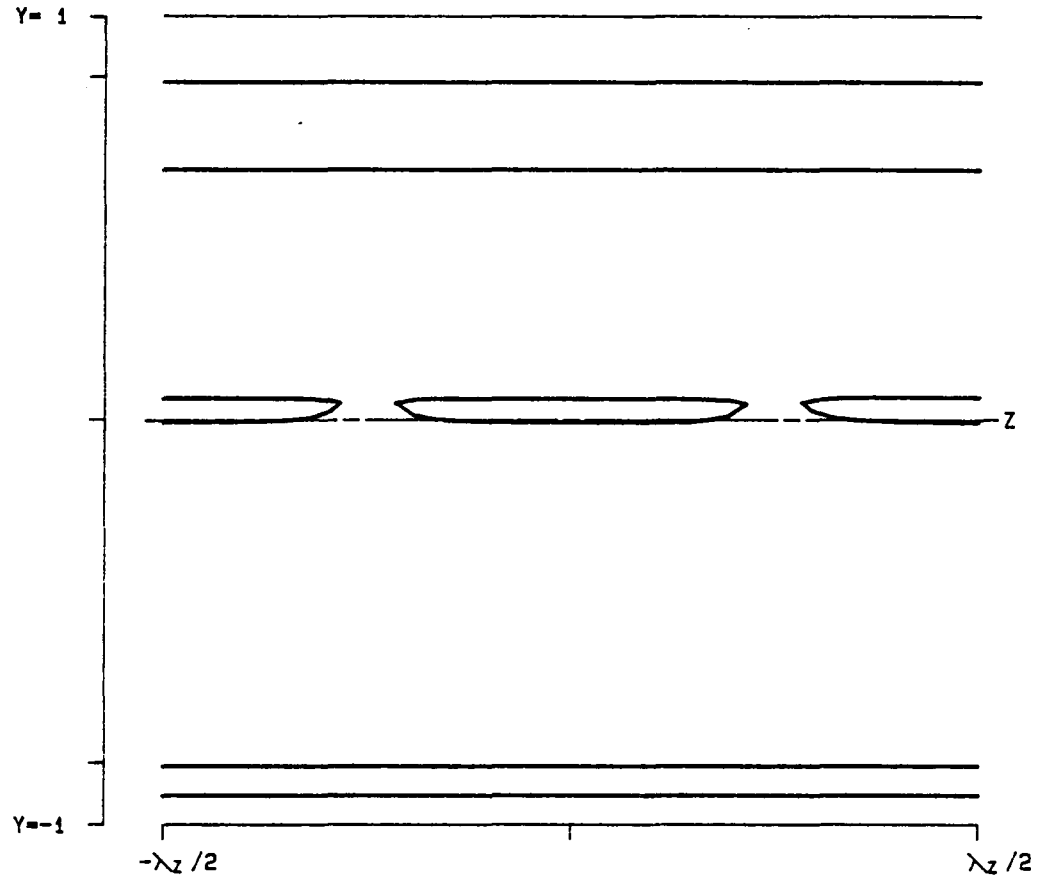

PPT 3-D F T31 (X, Y, Z)

RE	5000.0		LEVELS:	MIN	-0.0004687
ALPHA	1.1200			DIF	0.0000937
BETA	2.0000			NO.	20
SIGMA	0.043798				
RMS	0.025000			X =	2.876916
MAX	0.001359				
SYM	1				

Figure 3.86- $T^{(31)}$ as a function of x, y and z at a position of $x = 2.876916$ for $\mathbf{v}_{f_a}$ at $\alpha = 1.12$, $Re = 5000$, $\beta = 2.00$ and $A = 0.025$.

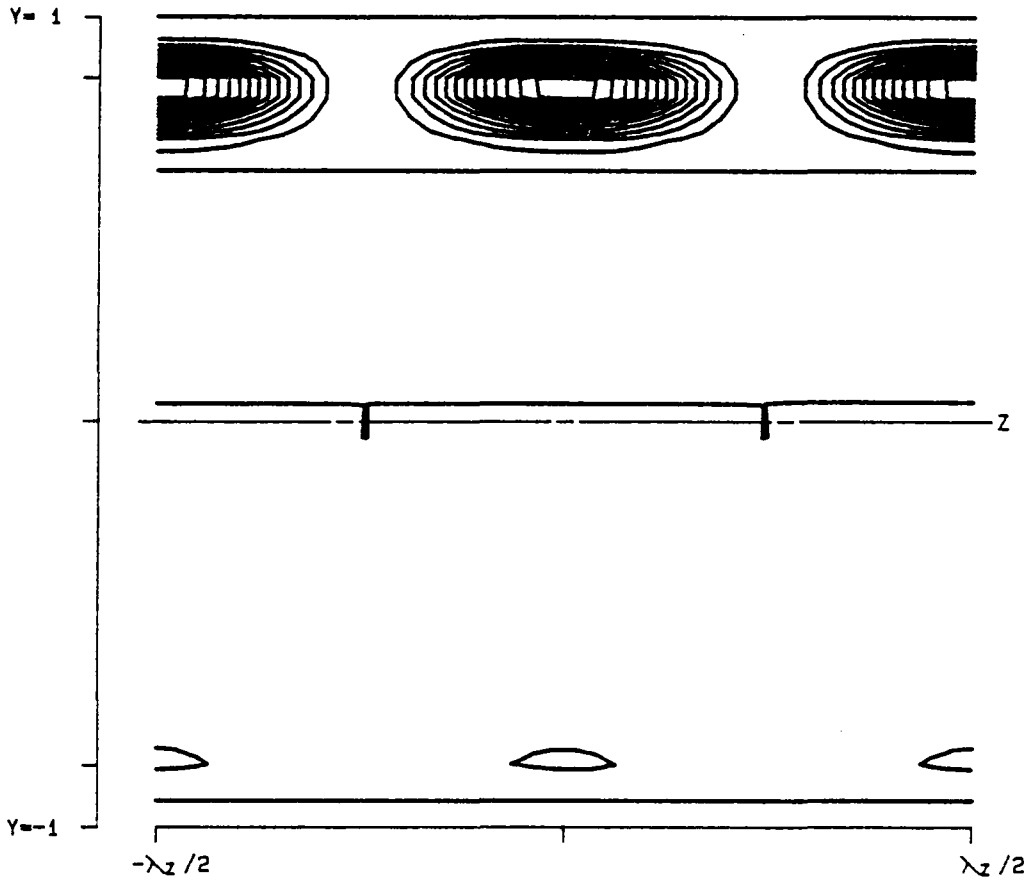

PPT 3-D F T30 (X, Y, Z)

RE	5000.0
ALPHA	1.1200
BETA	2.0000
SIGMA	0.043798
RMS	0.025000
MAX	0.001359
SYM	1

LEVELS:	MIN	-0.0004687
	DIF	0.0000937
	NO.	20
	X =	2.876916

Figure 3.87- $T^{(30)}$ as a function of x, y and z at a position of $x = 2.876916$ for $\mathbf{v}_{fa}$ at $\alpha = 1.12$, $Re = 5000$, $\beta = 2.00$ and $A = 0.025$.

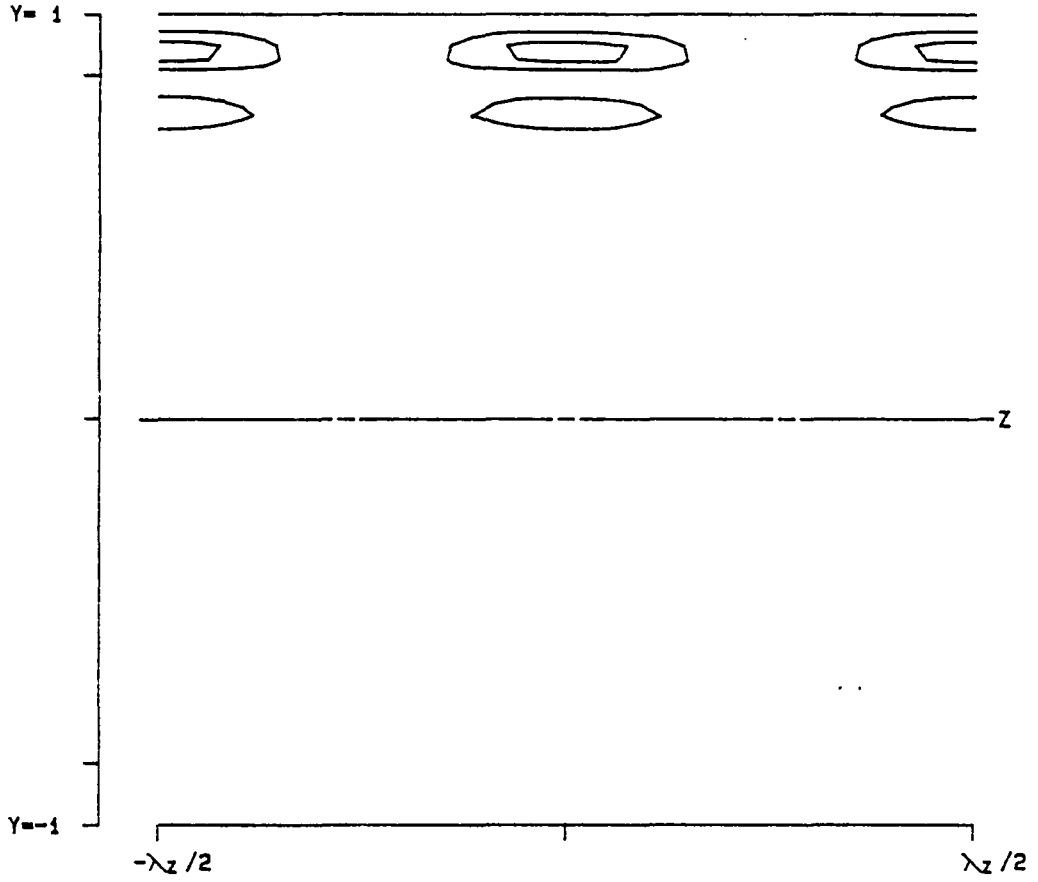

PPT 3-D F D3 (X, Y, Z)

RE	5000.0
ALPHA	1.1200
BETA	2.0000
SIGMA	0.043798
RMS	0.025000
MAX	0.001359
SYM	1

LEVELS:	MIN	-0.0004687
	DIF	0.0000937
	NO.	20
	X =	2.876916

Figure 3.88- $D^{(3)}$ as a function of x, y and z at a position of $x = 2.876916$ for $\mathbf{v}_{fs}$ at $\alpha = 1.12$, $Re = 5000$, $\beta = 2.00$ and $A = 0.025$.

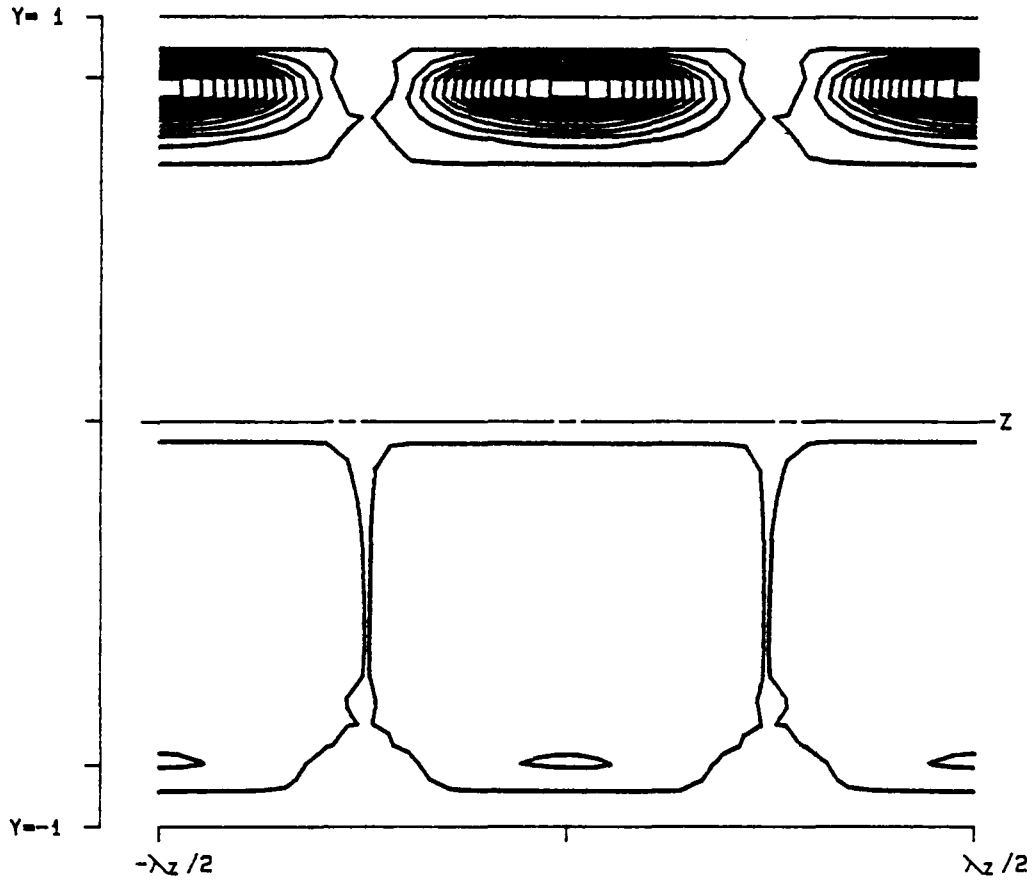

PPT 3-D F P3 (X, Y, Z)

RE	5000.0
ALPHA	1.1200
BETA	2.0000
SIGMA	0.043798
RMS	0.025000
MAX	0.001359
SYM	1

LEVELS:	MIN	-0.0004687
	DIF	0.0000937
	NO.	20
	X =	2.876916

Figure 3.89- $P^{(3)}$ as a function of x, y and z at a position of $x = 2.876916$ for $v_{/a}$ at $\alpha = 1.12$, $Re = 5000$, $\beta = 2.00$ and $A = 0.025$.

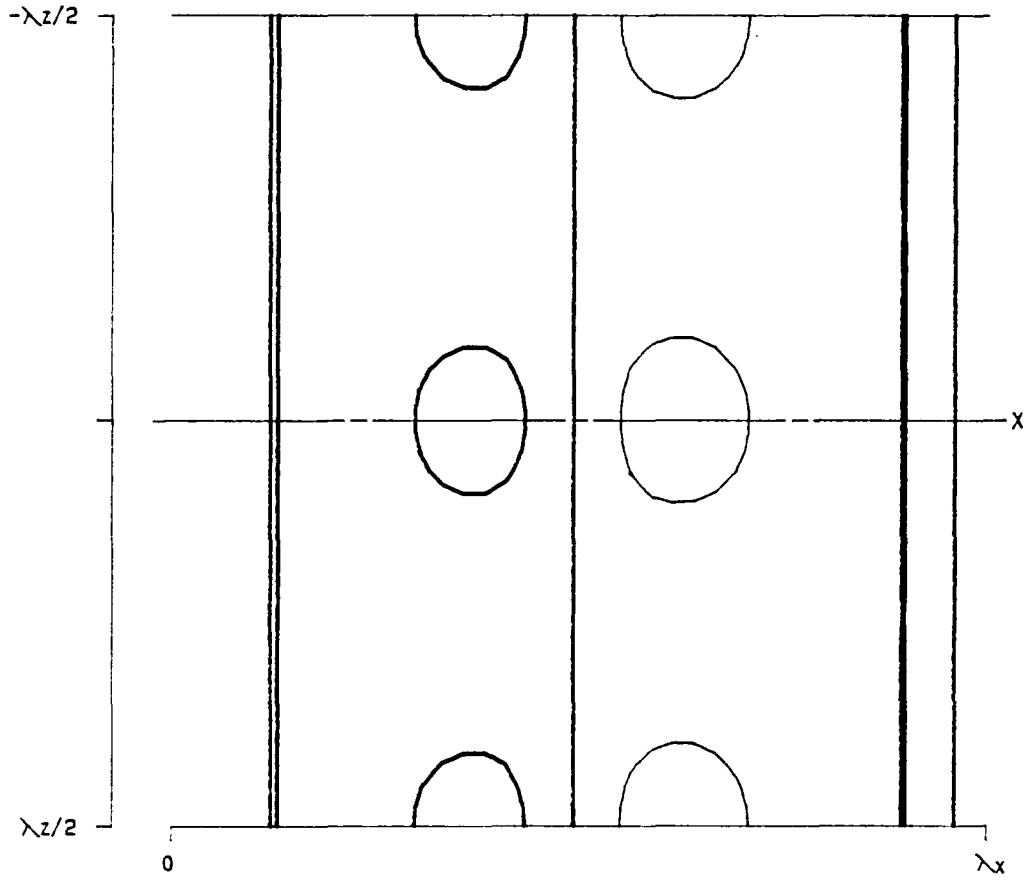

PPT 3-D F T31 (X, Y, Z)

RE	5000.0
ALPHA	1.1200
BETA	2.0000
SIGMA	0.043798
RMS	0.025000
MAX	0.001359
SYM	1

LEVELS:	MIN -0.0004687
	DIF 0.0000937
	NO. 20
	Y = 0.885456

Figure 3.90- $T^{(31)}$ as a function of x, y and z at a position of $y = 0.885456$ for $\mathbf{v}_{fa}$ at $\alpha = 1.12$, $Re = 5000$, $\beta = 2.00$ and $A = 0.025$.

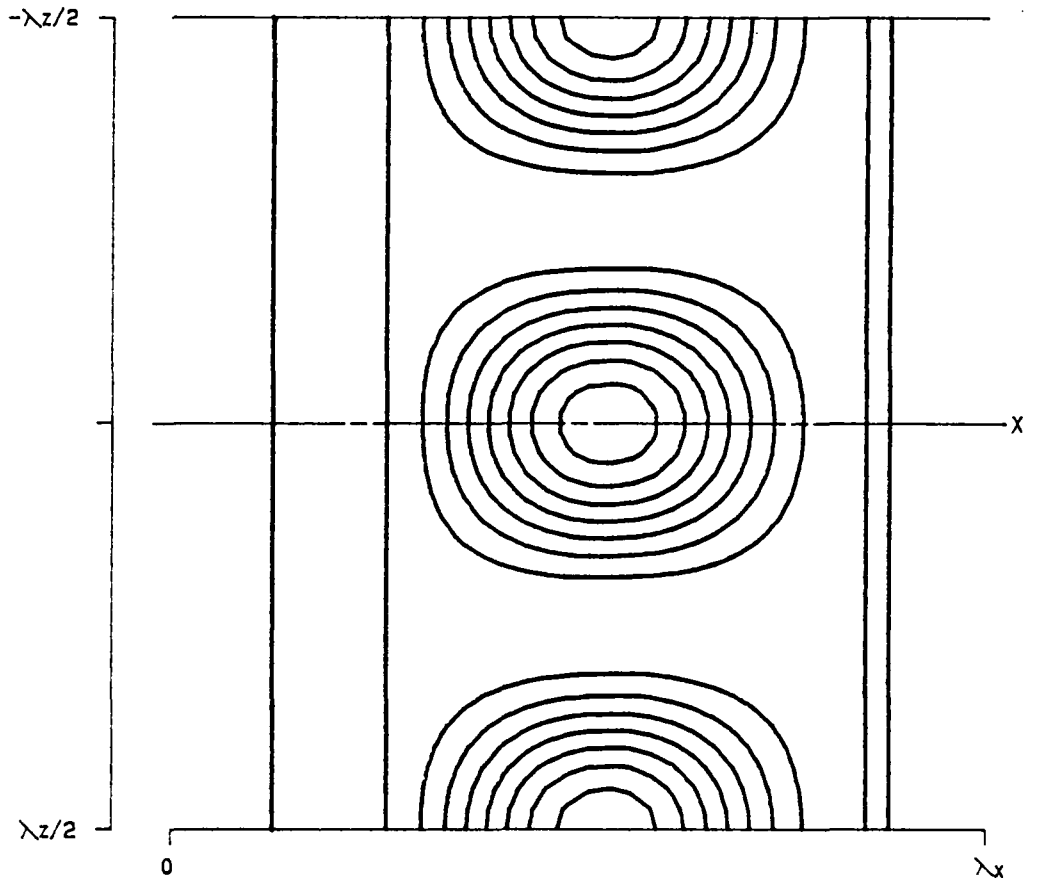

PPT 3-D F T30 (X, Y, Z)

RE	5000.0
ALPHA	1.1200
BETA	2.0000
SIGMA	0.043798
RMS	0.025000
MAX	0.001359
SYM	1

LEVELS:	MIN -0.0004687
	DIF 0.0000937
	NO. 20
	Y = 0.885456

Figure 3.91- $T^{(30)}$ as a function of x, y and z at a position of $y = 0.885456$ for $\mathbf{v}_{fa}$ at $\alpha = 1.12$, $Re = 5000$, $\beta = 2.00$ and $A = 0.025$.

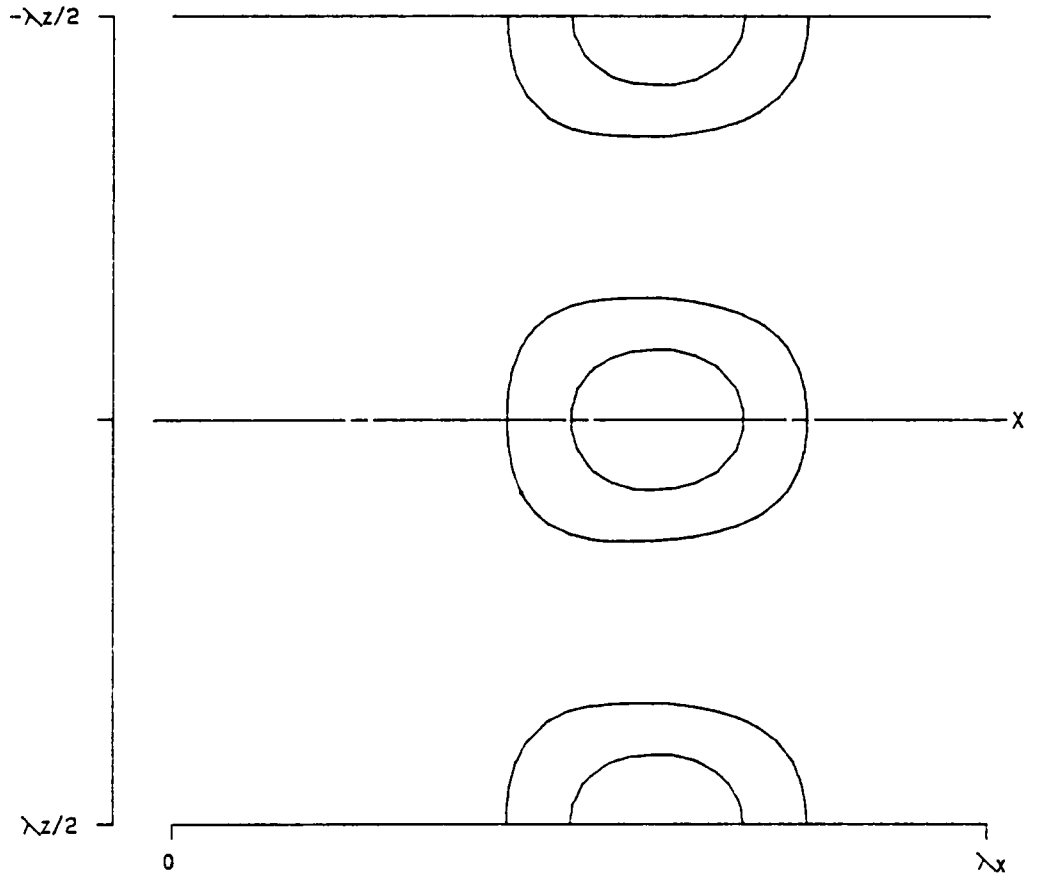

PPT 3-D F D3 (X, Y, Z)

RE	5000.0
ALPHA	1.1200
BETA	2.0000
SIGMA	0.043798
RMS	0.025000
MAX	0.001359
SYM	1

LEVELS:	MIN	-0.0004687
	DIF	0.0000937
	NO.	20
	Y =	0.885456

Figure 3.92- $D^{(3)}$ as a function of x, y and z at a position of $y = 0.885456$ for $\mathbf{v}_{fs}$ at $\alpha = 1.12$, $Re = 5000$, $\beta = 2.00$ and $A = 0.025$.

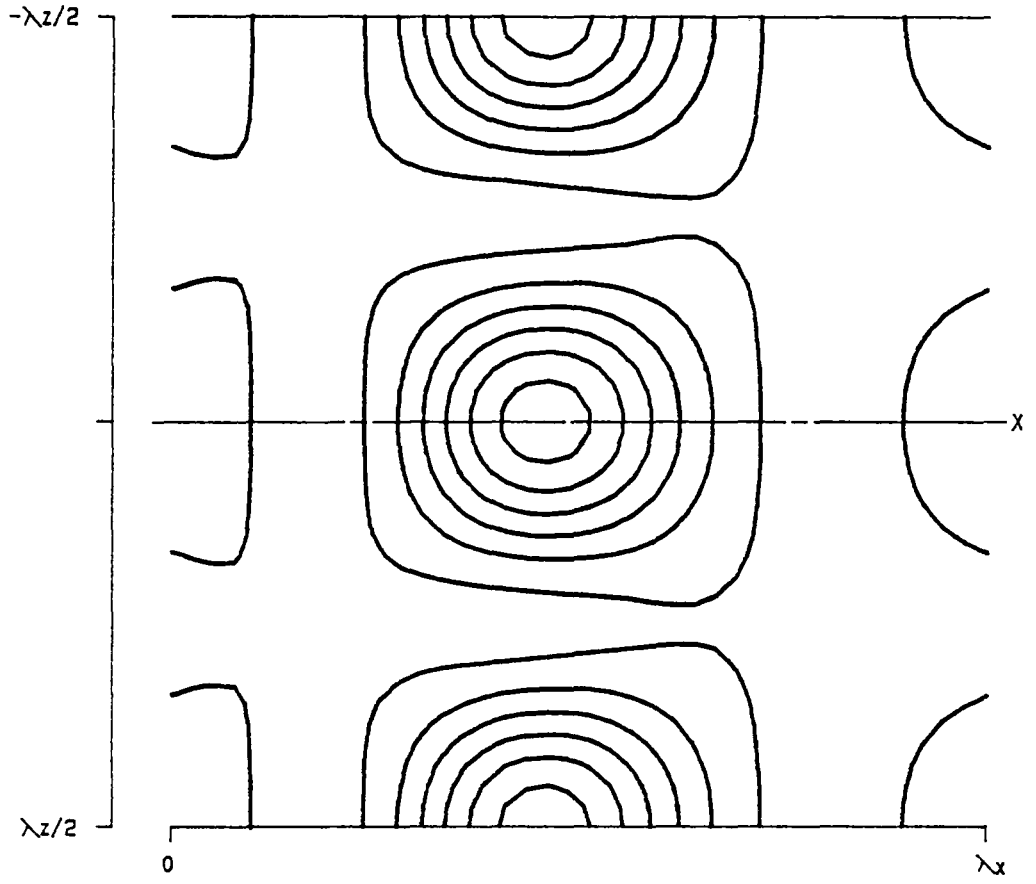

PPT 3-D F P3 (X, Y, Z)

RE	5000.0
ALPHA	1.1200
BETA	2.0000
SIGMA	0.043798
RMS	0.025000
MAX	0.001359
SYM	1

LEVELS:	MIN	-0.0004687
	DIF	0.0000937
	NO.	20
	Y =	0.885456

Figure 3.93- $P^{(3)}$ as a function of x, y and z at a position of $y = 0.885456$ for $\mathbf{v}_{fa}$ at $\alpha = 1.12$, $Re = 5000$, $\beta = 2.00$ and $A = 0.025$.

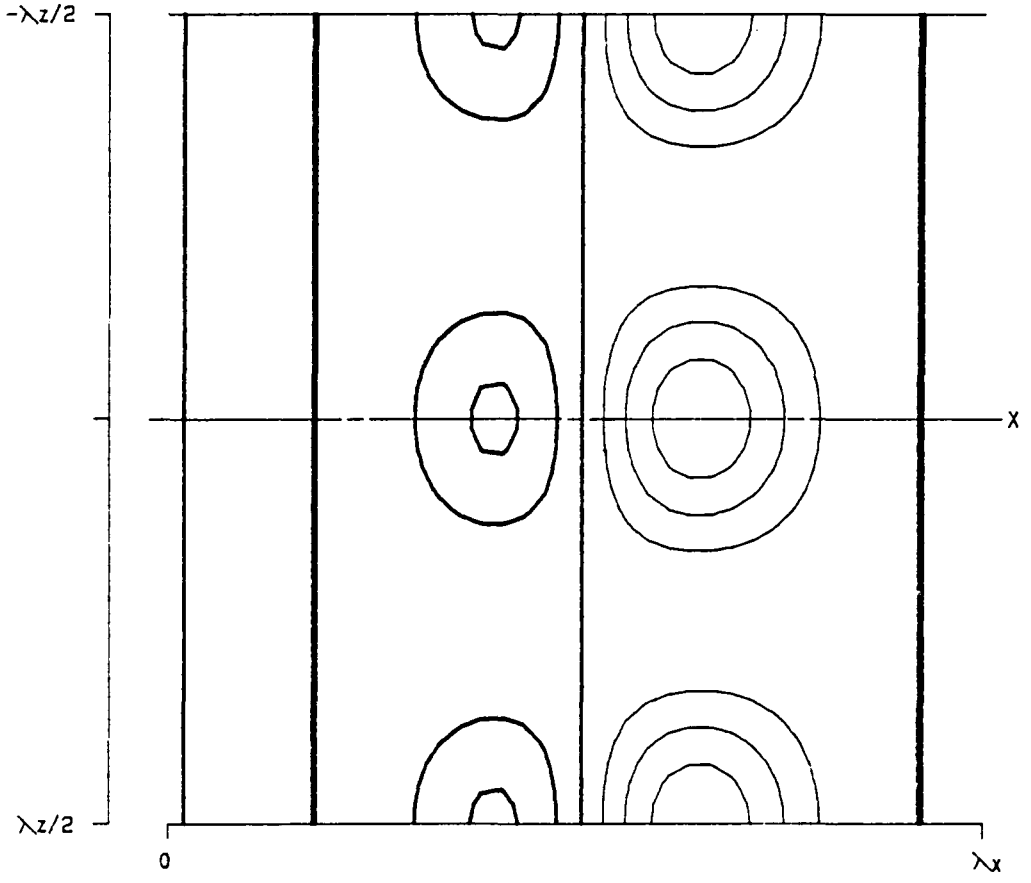

PPT 3-D F T31 (X, Y, Z)

RE	5000.0
ALPHA	1.1200
BETA	2.0000
SIGMA	0.043798
RMS	0.025000
MAX	0.001359
SYM	1

LEVELS: MIN	-0.0004687
DIF	0.0000937
NO.	20
Y =	0.845190

Figure 3.94- $T^{(31)}$ as a function of x, y and z at a position of $y = 0.845190$ for $\mathbf{v}_{fa}$ at $\alpha = 1.12$, $Re = 5000$, $\beta = 2.00$ and $A = 0.025$.

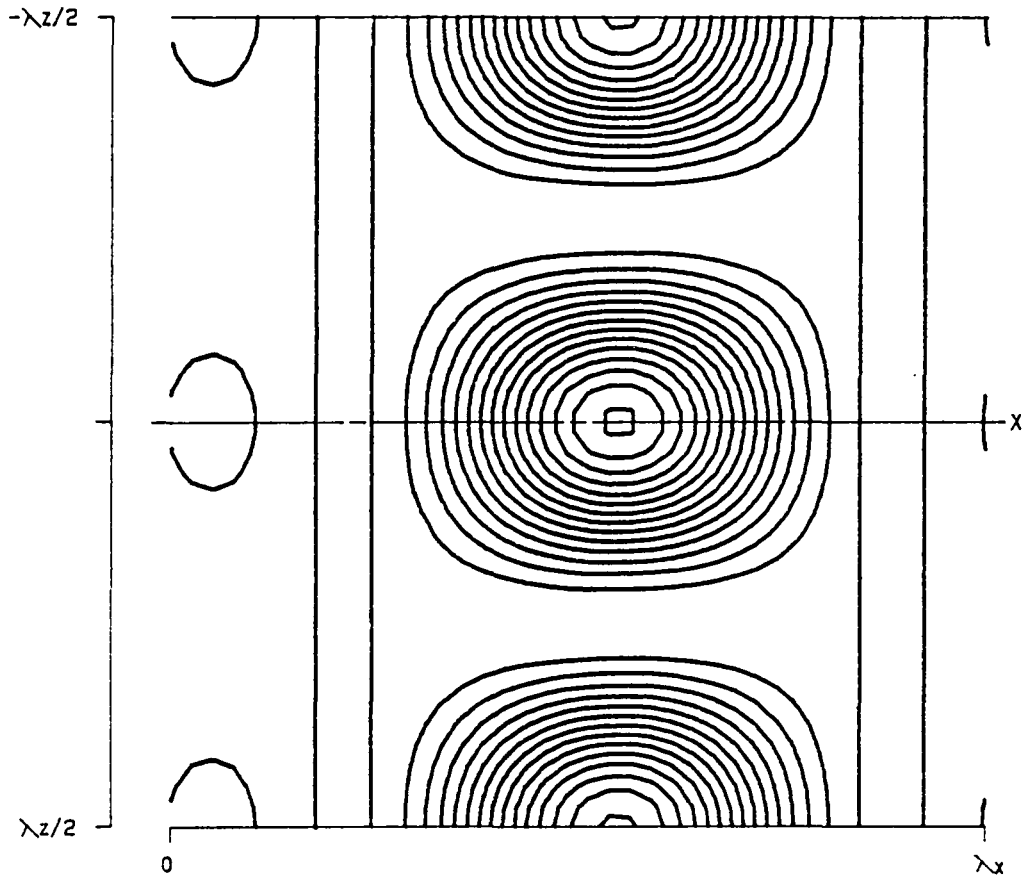

PPT 3-D F T30 (X, Y, Z)

RE	5000.0
ALPHA	1.1200
BETA	2.0000
SIGMA	0.043798
RMS	0.025000
MAX	0.001359
SYM	1

LEVELS:	MIN	-0.0004687
	DIF	0.0000937
	NO.	20
	Y =	0.845190

Figure 3.95- $T^{(30)}$ as a function of x, y and z at a position of $y = 0.845190$ for $\mathbf{v}_{f_d}$ at $\alpha = 1.12$, $Re = 5000$, $\beta = 2.00$ and $A = 0.025$.

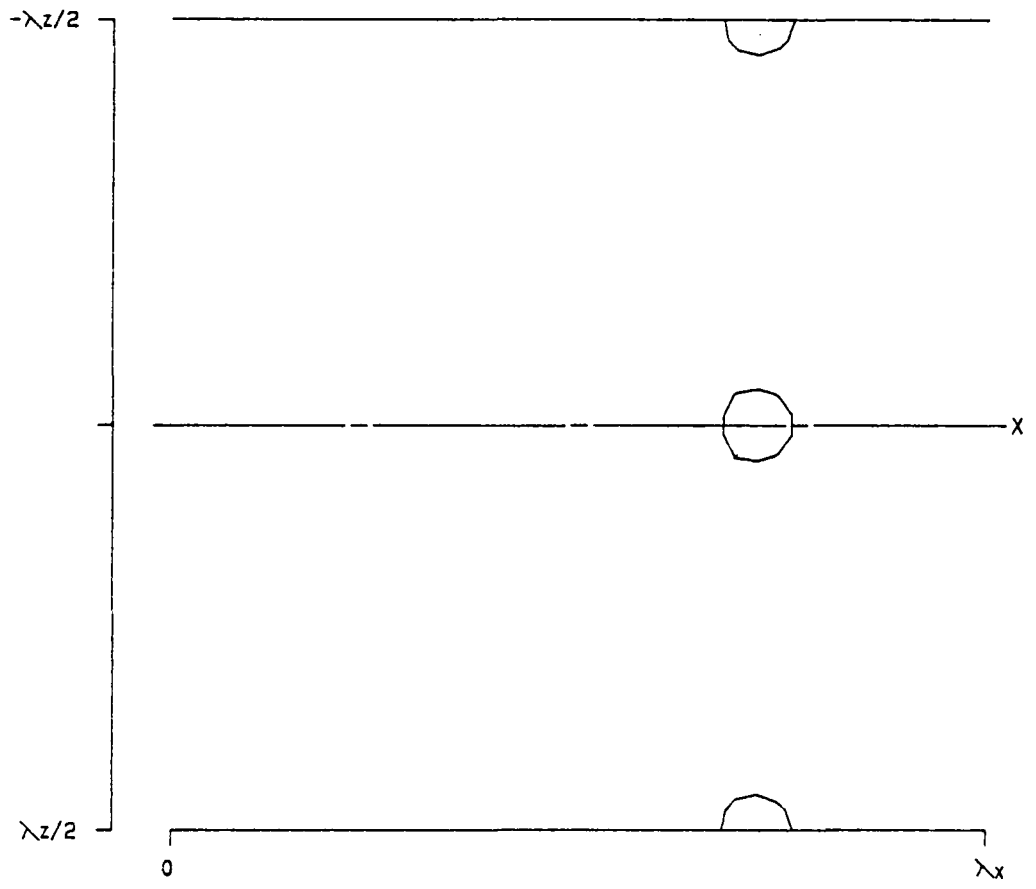

PPT 3-D F D3 (X, Y, Z)

RE	5000.0
ALPHA	1.1200
BETA	2.0000
SIGMA	0.043798
RMS	0.025000
MAX	0.001359
SYM	1

LEVELS:	MIN	-0.0004687
	DIF	0.0000937
	NO.	20
	Y =	0.845190

Figure 3.96- $D^{(3)}$ as a function of x, y and z at a position of $y = 0.845190$ for $\mathbf{v}_{f_a}$ at $\alpha = 1.12$, $Re = 5000$, $\beta = 2.00$ and $A = 0.025$.

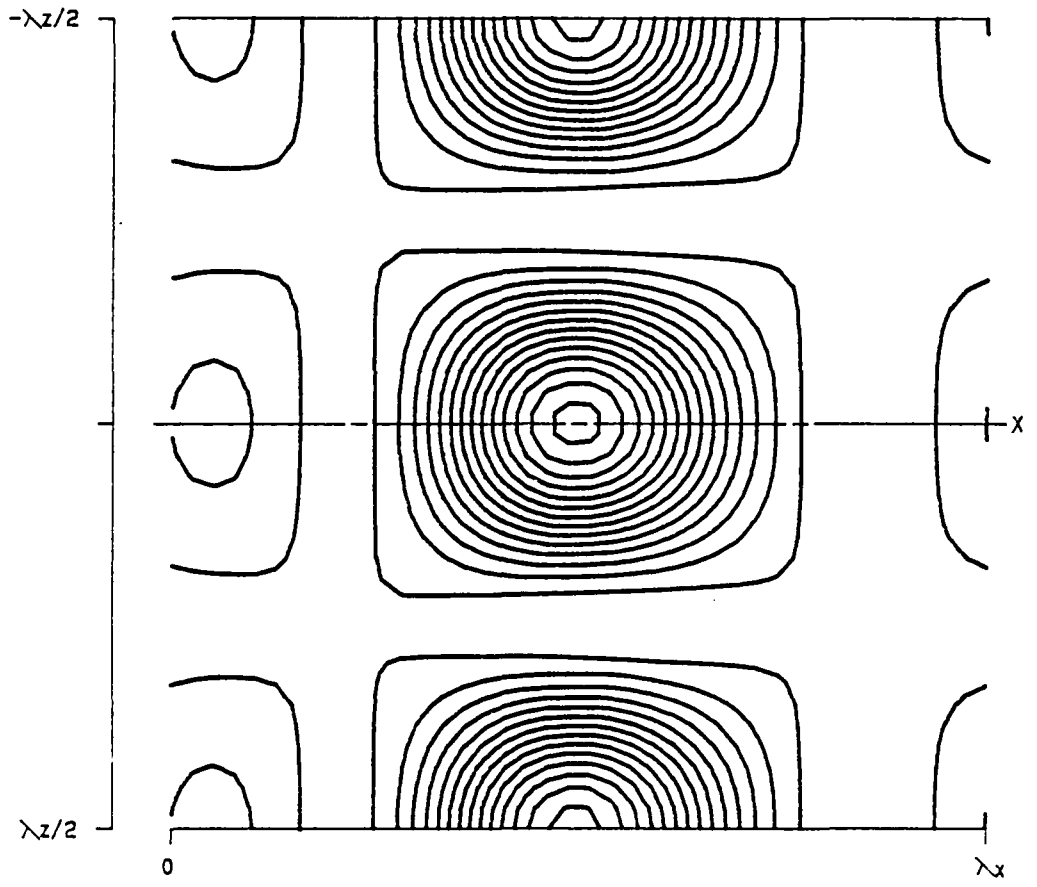

PPT 3-D F P3 (X, Y, Z)

RE	5000.0
ALPHA	1.1200
BETA	2.0000
SIGMA	0.043798
RMS	0.025000
MAX	0.001359
SYM	1

LEVELS:	MIN	-0.0004687
	DIF	0.0000937
	NO.	20
	Y =	0.845190

Figure 3.97- $P^{(3)}$ as a function of x, y and z at a position of $y = 0.845190$ for v_{fa} at $\alpha = 1.12$, $Re = 5000$, $\beta = 2.00$ and $A = 0.025$.

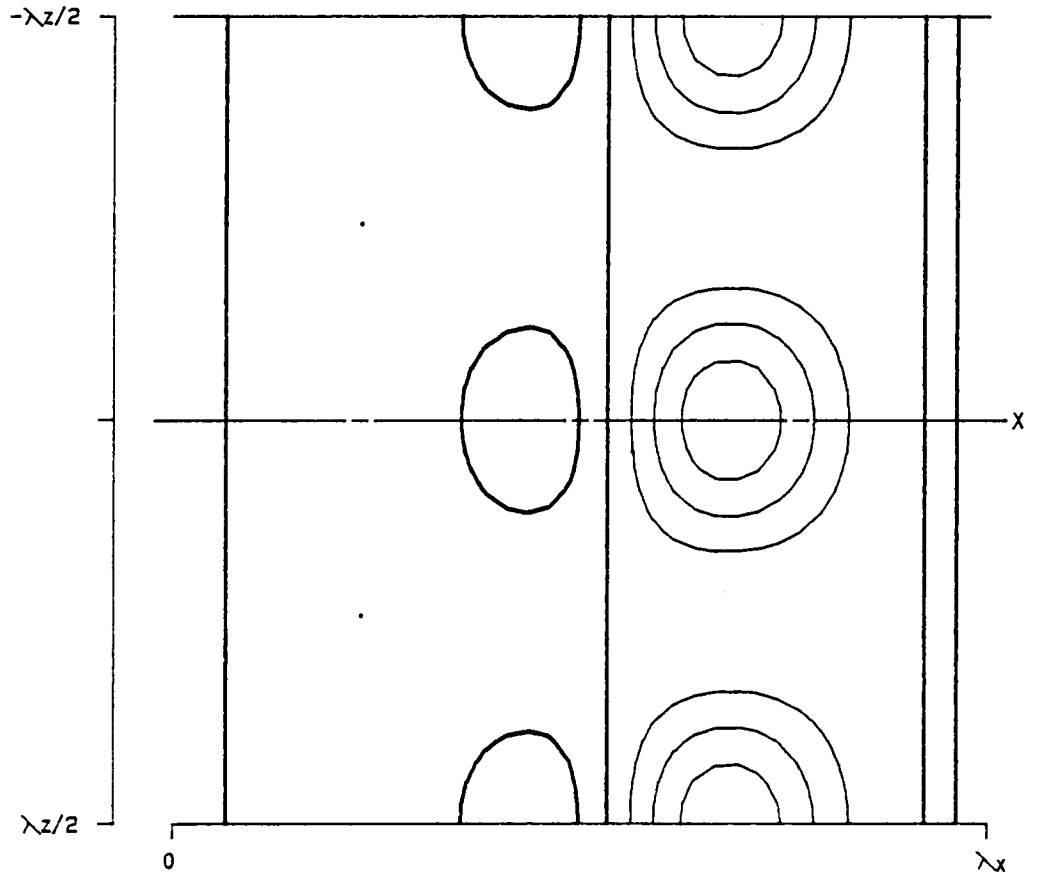

PPT 3-D F T31 (X, Y, Z)

RE	5000.0
ALPHA	1.1200
BETA	2.0000
SIGMA	0.043798
RMS	0.025000
MAX	0.001359
SYM	1

LEVELS:	MIN	-0.0004687
	DIF	0.0000937
	NO.	20
	Y =	0.799443

Figure 3.98- $T^{(31)}$ as a function of x, y and z at a position of $y = 0.799443$ for $\mathbf{v}_{fs}$ at $\alpha = 1.12$, $Re = 5000$, $\beta = 2.00$ and $A = 0.025$.

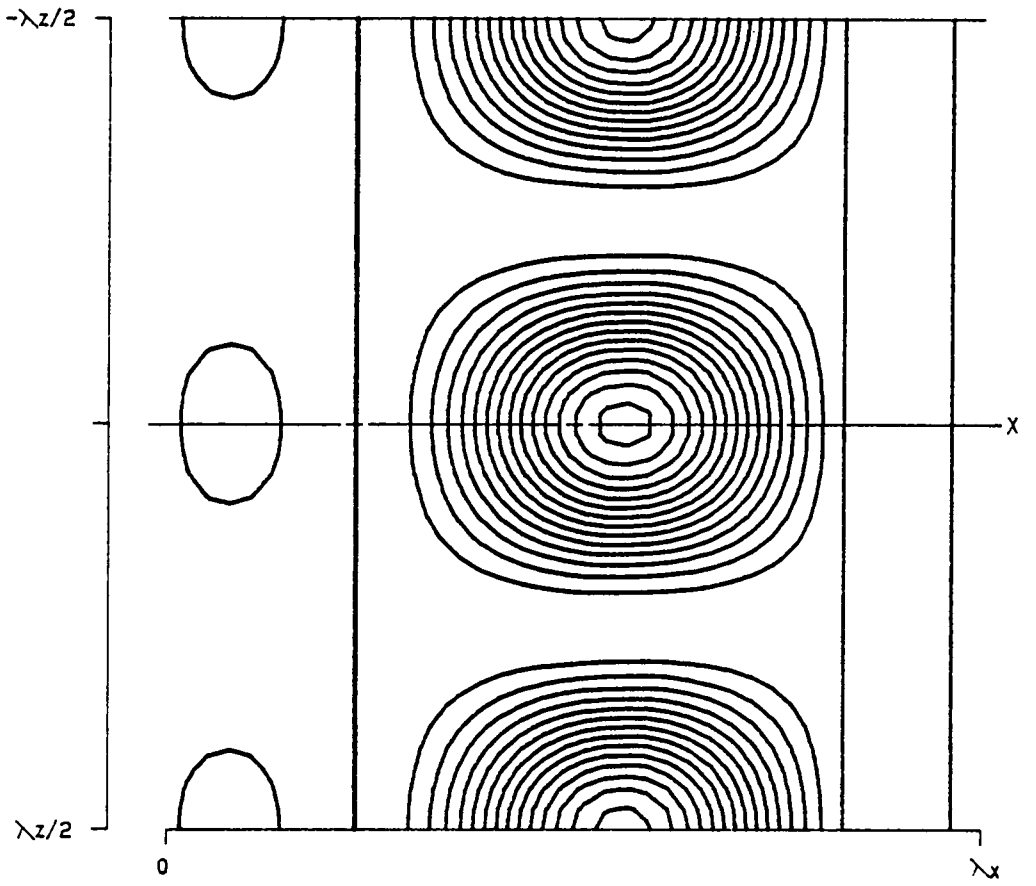

PPT 3-D F T30 (X, Y, Z)

RE	5000.0
ALPHA	1.1200
BETA	2.0000
SIGMA	0.043798
RMS	0.025000
MAX	0.001359
SYM	1

LEVELS:	MIN	-0.0004687
	DIF	0.0000937
	NO.	20
	Y =	0.799443

Figure 3.99- $T^{(30)}$ as a function of x, y and z at a position of $y = 0.799443$ for $\mathbf{v}_{fa}$ at $\alpha = 1.12$, $Re = 5000$, $\beta = 2.00$ and $A = 0.025$.

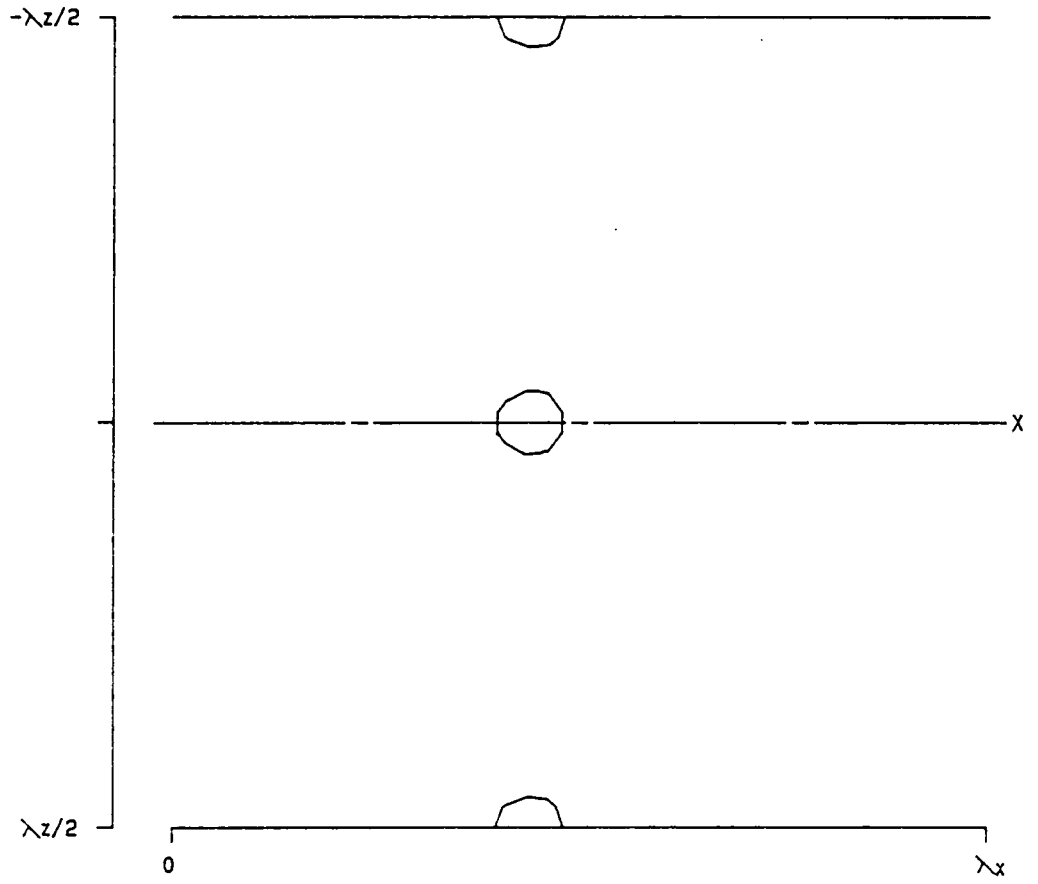

PPT 3-D F D3 (X, Y, Z)

RE	5000.0
ALPHA	1.1200
BETA	2.0000
SIGMA	0.043798
RMS	0.025000
MAX	0.001359
SYM	1

LEVELS:	MIN -0.0004687
	DIF 0.0000937
	NO. 20
	Y = 0.799443

Figure 3.100- $D^{(3)}$ as a function of x, y and z at a position of $y = 0.799443$ for $\mathbf{v}_{f_4}$ at $\alpha = 1.12$, $Re = 5000$, $\beta = 2.00$ and $A = 0.025$.

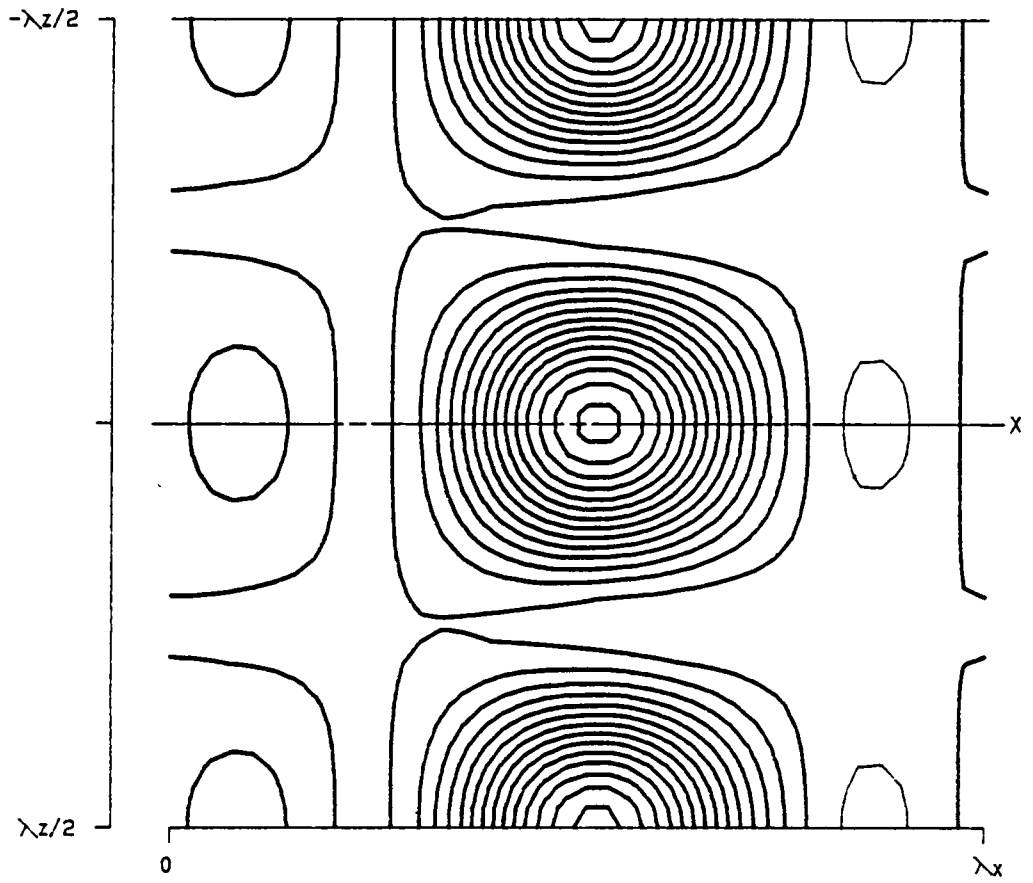

PPT 3-D F P3 (X, Y, Z)

RE	5000.0
ALPHA	1.1200
BETA	2.0000
SIGMA	0.043798
RMS	0.025000
MAX	0.001359
SYM	1

LEVELS:	MIN	-0.0004687
	DIF	0.0000937
	NO.	20
	Y =	0.799443

Figure 3.101- $P^{(3)}$ as a function of x, y and z at a position of $y = 0.799443$ for $\mathbf{v}_{fs}$ at $\alpha = 1.12$, $Re = 5000$, $\beta = 2.00$ and $A = 0.025$.

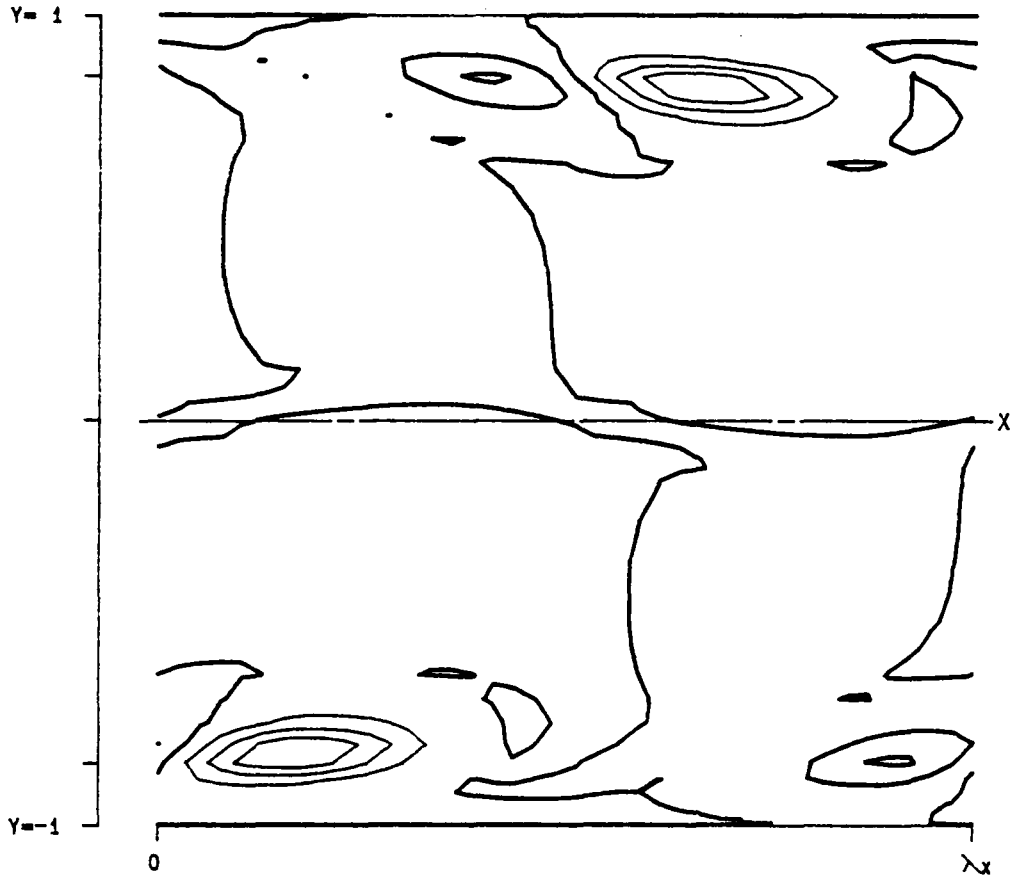

PPT 3-D F T31 (X, Y)

RE	5000.0
ALPHA	1.1200
BETA	2.0000
SIGMA	0.043798
RMS	0.025000
MAX	0.000680
SYM	1

LEVELS:	MIN	-0.0002343
	DIF	0.0000469
	NO.	20

Figure 3.102- $T^{(31)}$ as a function of x and y for $\mathbf{v}_{f_s}$ at $\alpha = 1.12$, $Re = 5000$, $\beta = 2.00$ and $A = 0.025$.

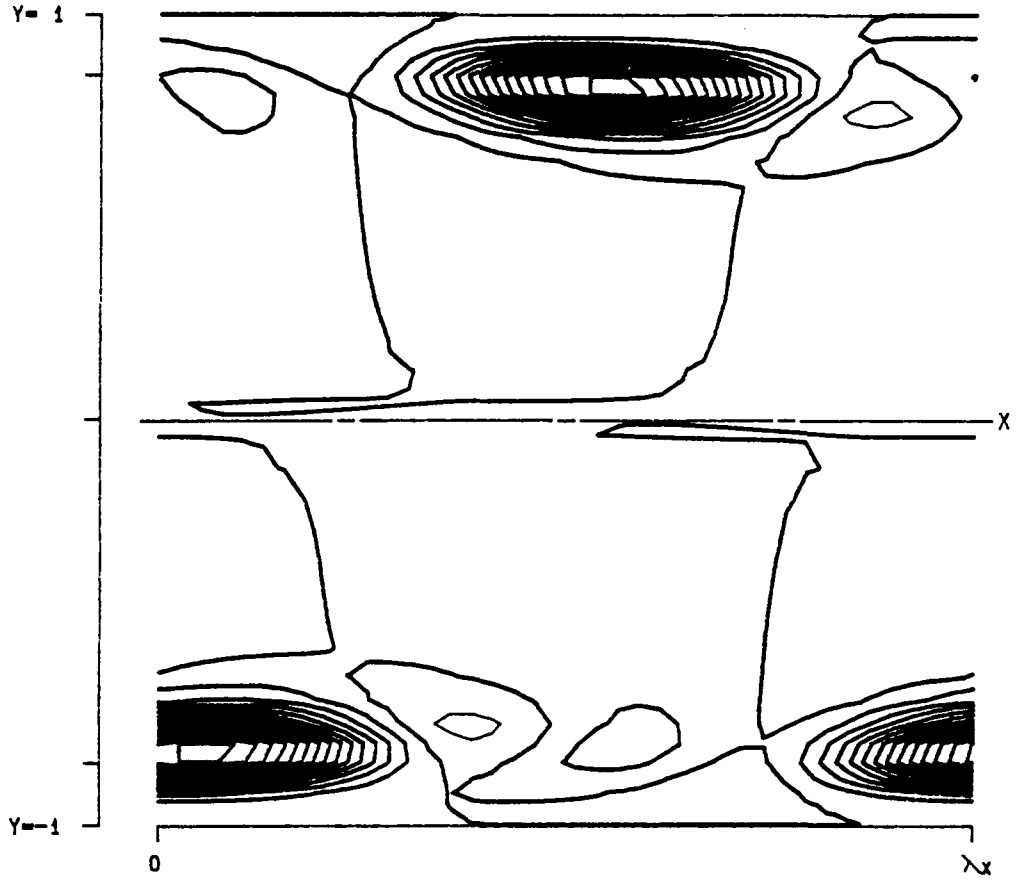

PPT 3-D F T30 (X, Y)

RE	5000.0	LEVELS: MIN	-0.0002343
ALPHA	1.1200	DIF	0.0000469
BETA	2.0000	NO.	20
SIGMA	0.043798		
RMS	0.025000		
MAX	0.000680		
SYM	1		

Figure 3.103- $T^{(30)}$ as a function of x and y for $\mathbf{v}_{f_a}$ at $\alpha = 1.12$, $Re = 5000$, $\beta = 2.00$ and $A = 0.025$.

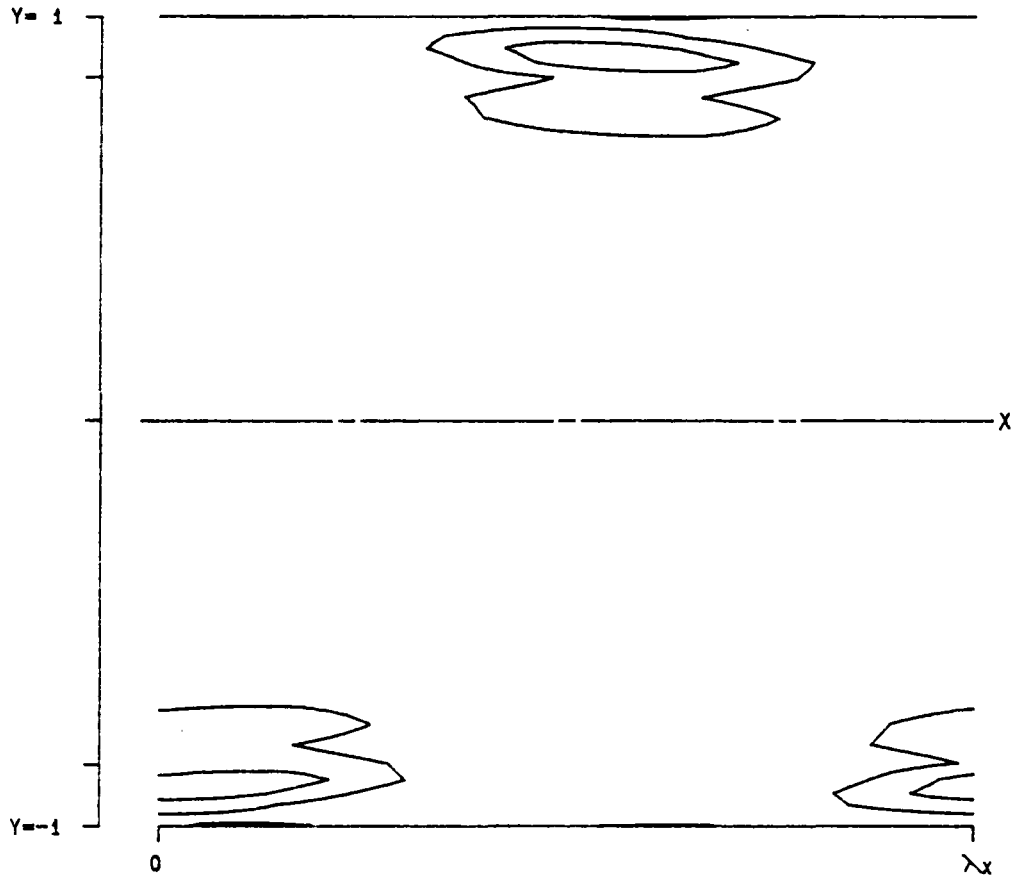

PPT 3-D F D3 (X, Y)

RE	5000.0
ALPHA	1.1200
BETA	2.0000
SIGMA	0.043798
RMS	0.025000
MAX	0.000680
SYM	1

LEVELS:	MIN	-0.0002343
	DIF	0.0000469
	NO.	20

Figure 3.104- $D^{(3)}$ as a function of x and y for $\mathbf{v}_{fa}$ at $\alpha = 1.12$, $Re = 5000$, $\beta = 2.00$ and $A = 0.025$.

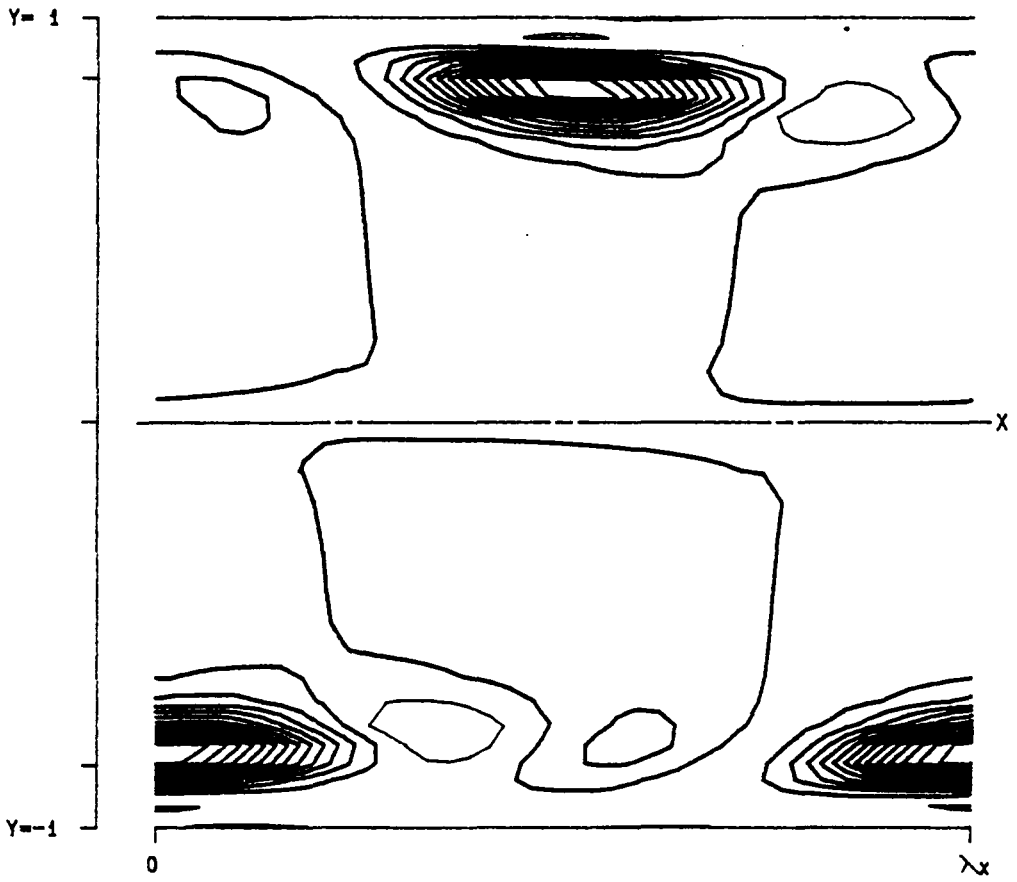

PPT 3-D F P3 (X, Y)

RE	5000.0
ALPHA	1.1200
BETA	2.0000
SIGMA	0.043798
RMS	0.025000
MAX	0.000680
SYM	1

LEVELS:	MIN	-0.0002343
	DIF	0.0000469
	NO.	20

Figure 3.105- $P^{(3)}$ as a function of x and y for $\mathbf{v}_{fa}$ at $\alpha = 1.12$, $Re = 5000$, $\beta = 2.00$ and $A = 0.025$.

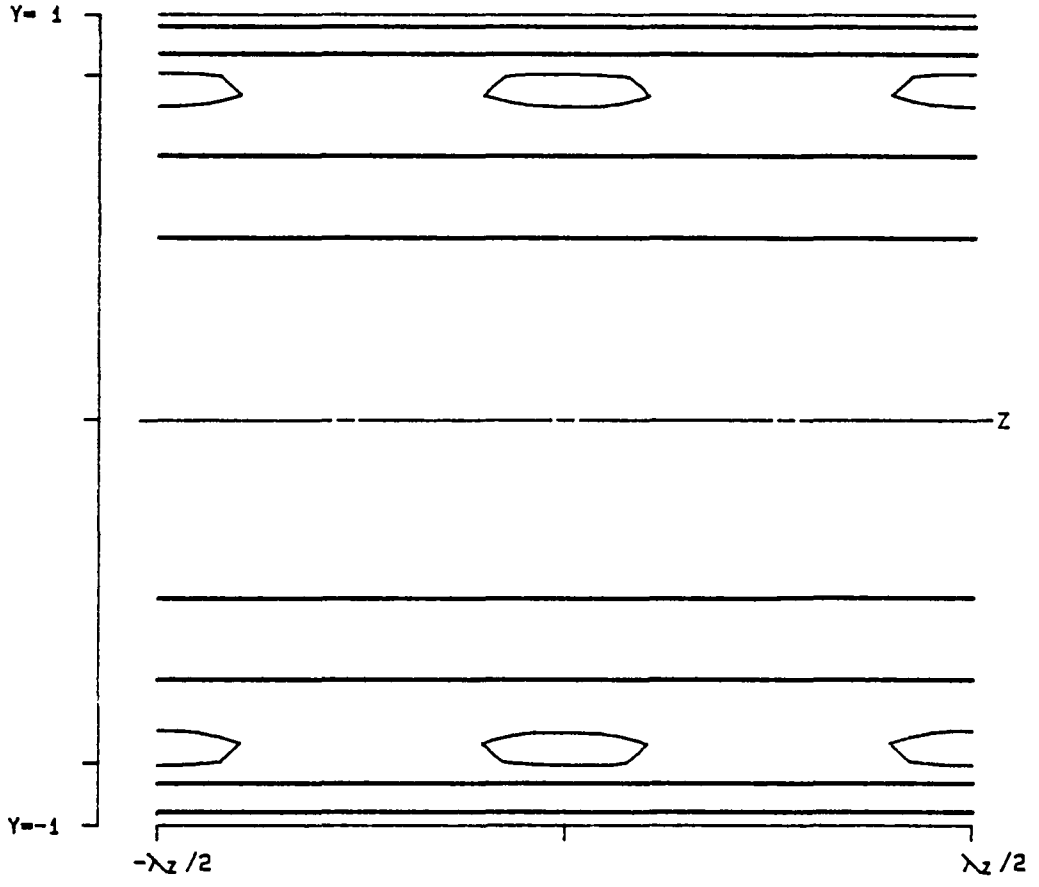

PPT 3-D F T31 (Y, Z)

RE	5000.0
ALPHA	1.1200
BETA	2.0000
SIGMA	0.043798
RMS	0.025000
MAX	0.000428
SYM	1

LEVELS:	MIN	-0.0001477
	DIF	0.0000295
	NO.	20

Figure 3.106- $T^{(31)}$ as a function of y and z for $\mathbf{v}_{f_a}$ at $\alpha = 1.12$, $Re = 5000$, $\beta = 2.00$ and $A = 0.025$.

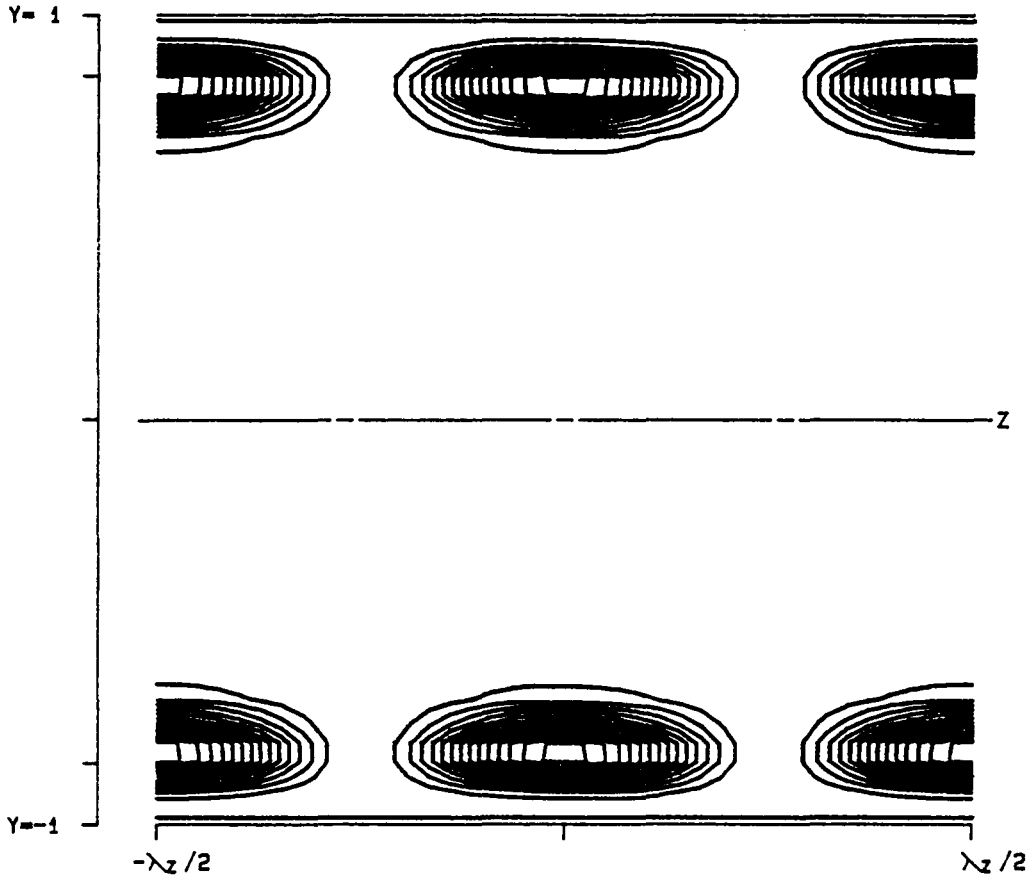

PPT 3-D F T30 (Y, Z)

RE	5000.0
ALPHA	1.1200
BETA	2.0000
SIGMA	0.043798
RMS	0.025000
MAX	0.000428
SYM	1

LEVELS:	MIN	-0.0001477
	DIF	0.0000295
	NO.	20

Figure 3.107- $T^{(30)}$ as a function of y and z for $\mathbf{v}_{f_4}$ at $\alpha = 1.12$, $Re = 5000$, $\beta = 2.00$ and $A = 0.025$.

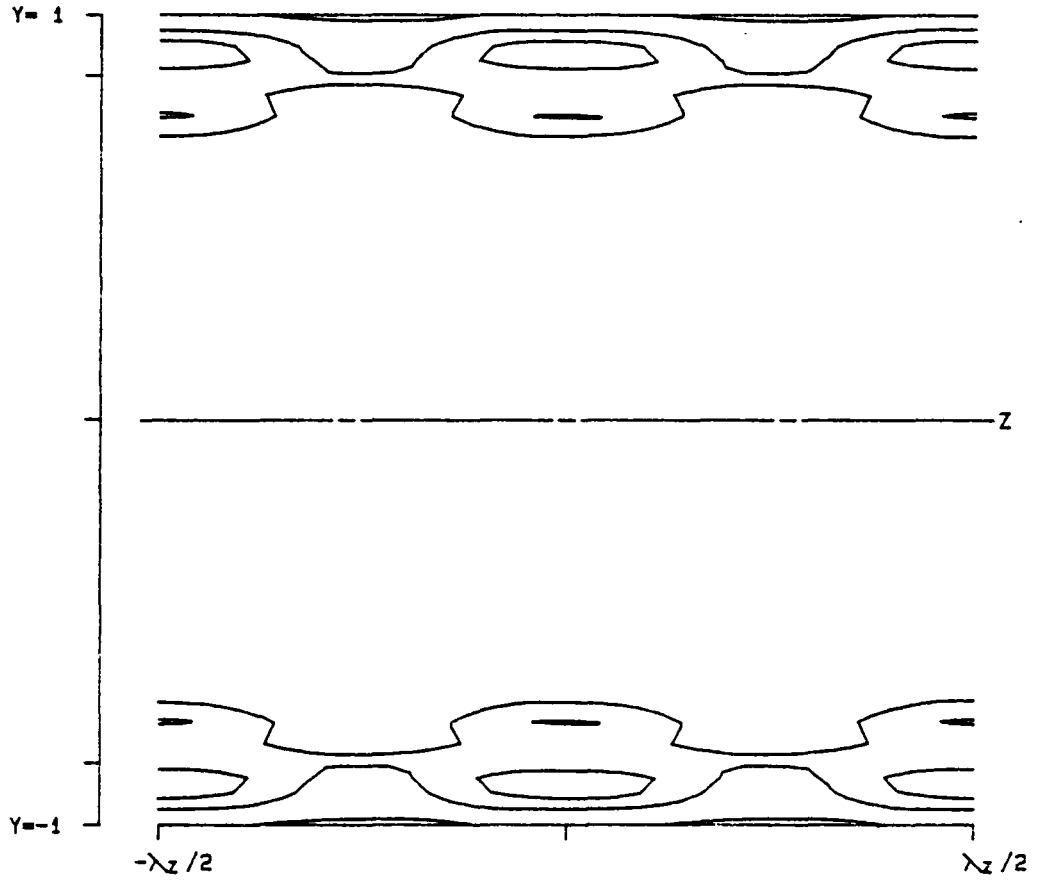

PPT 3-D F D3 (Y, Z)

RE	5000.0
ALPHA	1.1200
BETA	2.0000
SIGMA	0.043798
RMS	0.025000
MAX	0.000428
SYM	1

LEVELS:	MIN	-0.0001477
	DIF	0.0000295
	NO.	20

Figure 3.108- $D^{(3)}$ as a function of y and z for $\mathbf{v}_{f_s}$ at $\alpha = 1.12$, $Re = 5000$, $\beta = 2.00$ and $A = 0.025$.

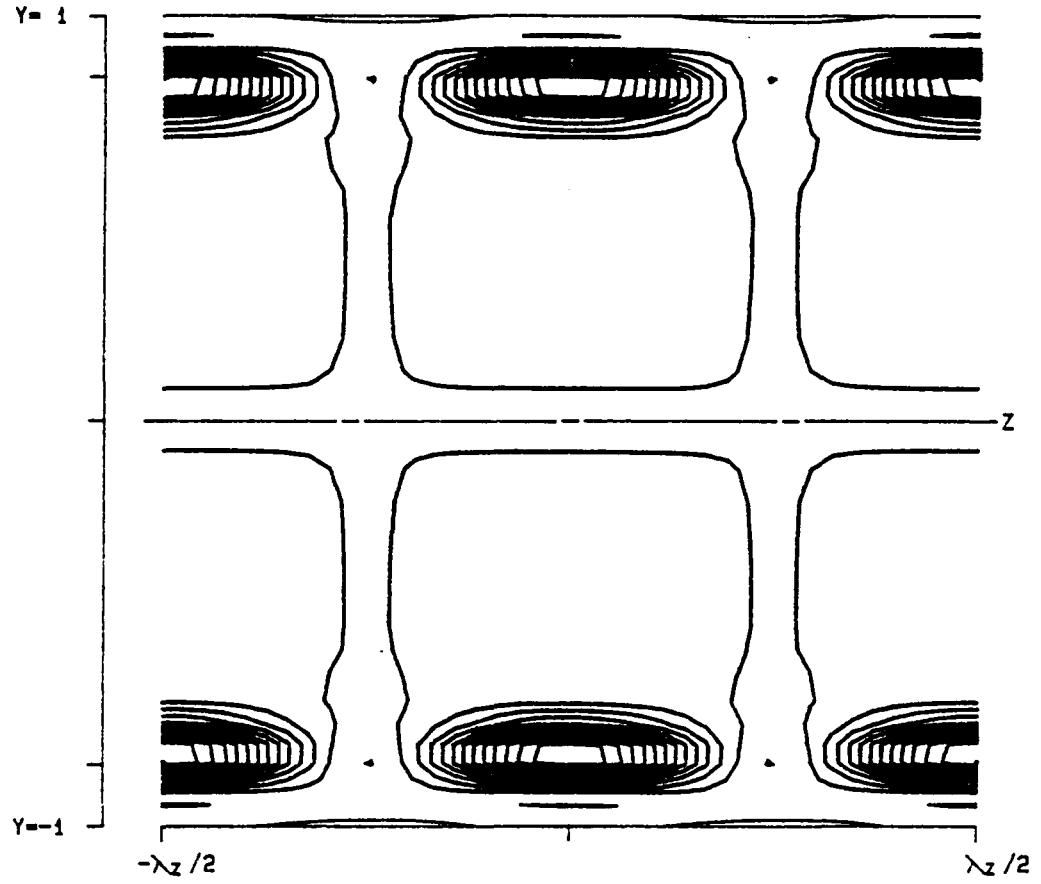

PPT 3-D F P3 (Y, Z)

RE	5000.0
ALPHA	1.1200
BETA	2.0000
SIGMA	0.043798
RMS	0.025000
MAX	0.000428
SYM	1

LEVELS: MIN	-0.0001477
DIF	0.0000295
NO.	20

Figure 3.109- $P^{(3)}$ as a function of y and z for $\mathbf{v}_{f_s}$ at $\alpha = 1.12$, $Re = 5000$, $\beta = 2.00$ and $A = 0.025$.

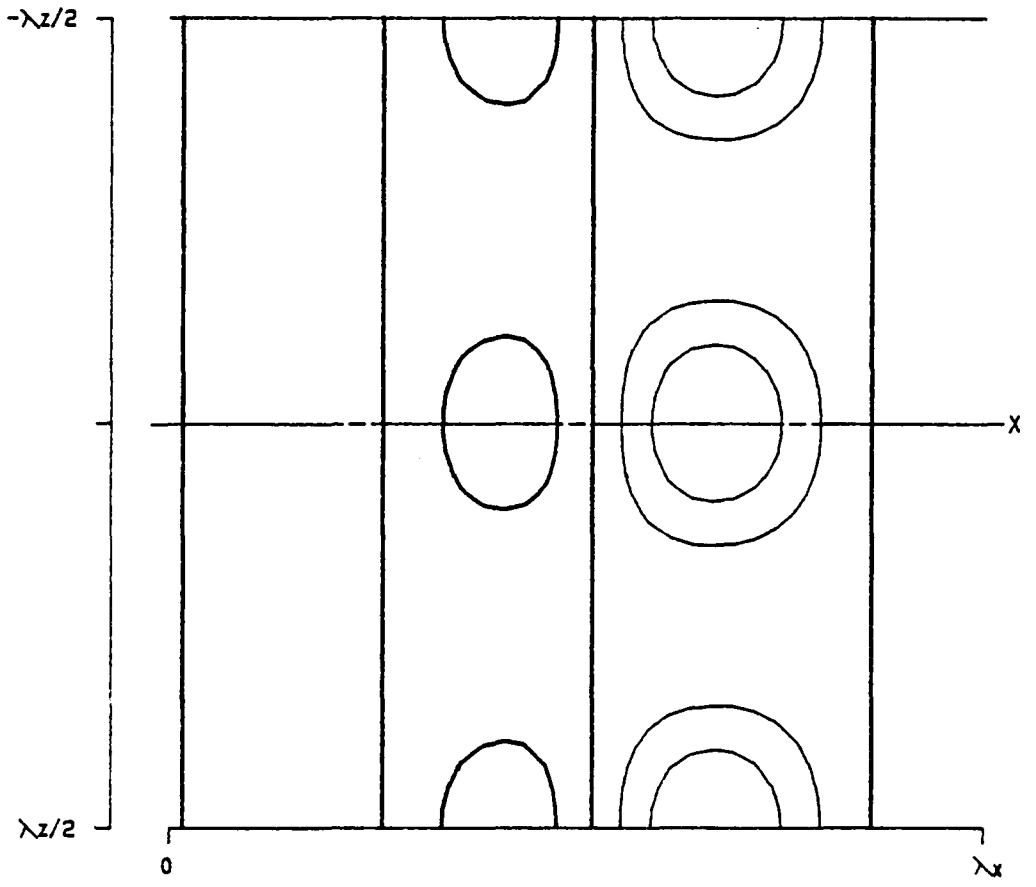

PPT 3-D F T31 (X, Z)

RE	5000.0
ALPHA	1.1200
BETA	2.0000
SIGMA	0.043798
RMS	0.025000
MAX	0.000176
SYM	1

LEVELS:	MIN	-0.0000607
	DIF	0.0000121
	NO.	20

Figure 3.110- $T^{(31)}$ as a function of x and z for $\mathbf{v}_{f_a}$ at $\alpha = 1.12$, $Re = 5000$, $\beta = 2.00$ and $A = 0.025$.

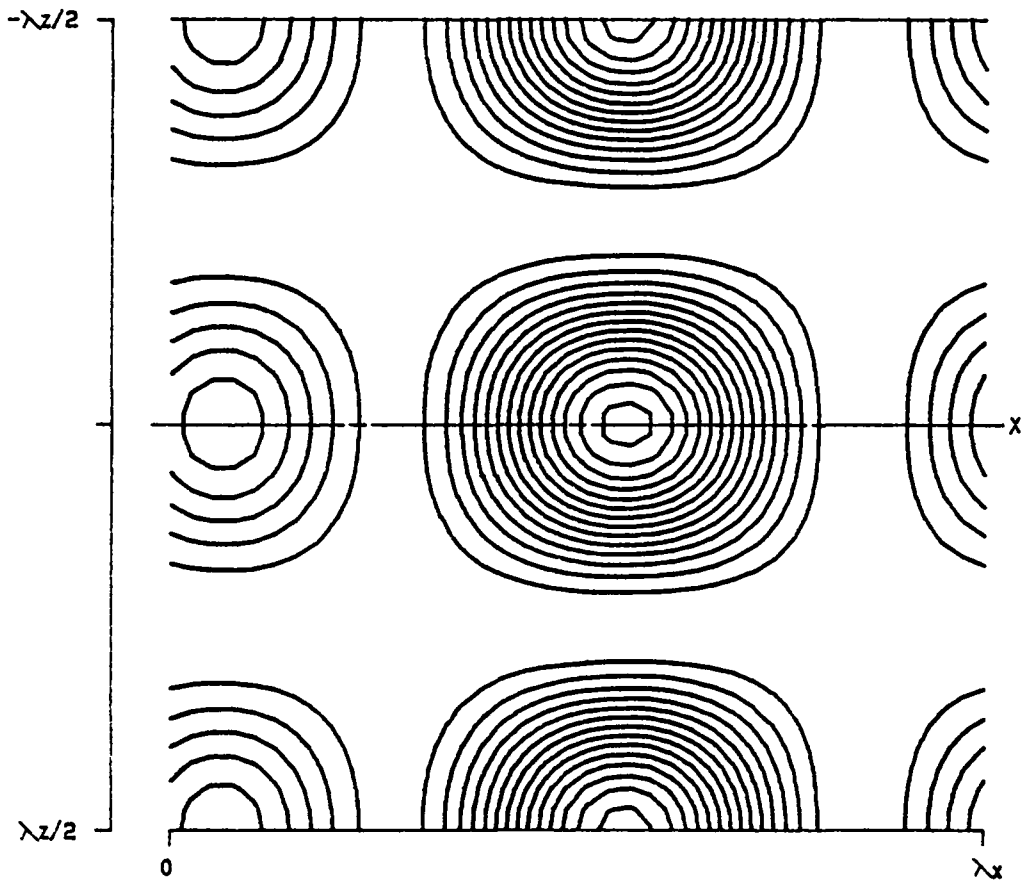

PPT 3-D F T30 (X, Z)

RE	5000.0
ALPHA	1.1200
BETA	2.0000
SIGMA	0.043798
RMS	0.025000
MAX	0.000176
SYM	1

LEVELS:	MIN	-0.0000607
	DIF	0.0000121
	NO.	20

Figure 3.111- $T^{(30)}$ as a function of x and z for $\mathbf{v}_{f_a}$ at $\alpha = 1.12$, $Re = 5000$, $\beta = 2.00$ and $A = 0.025$.

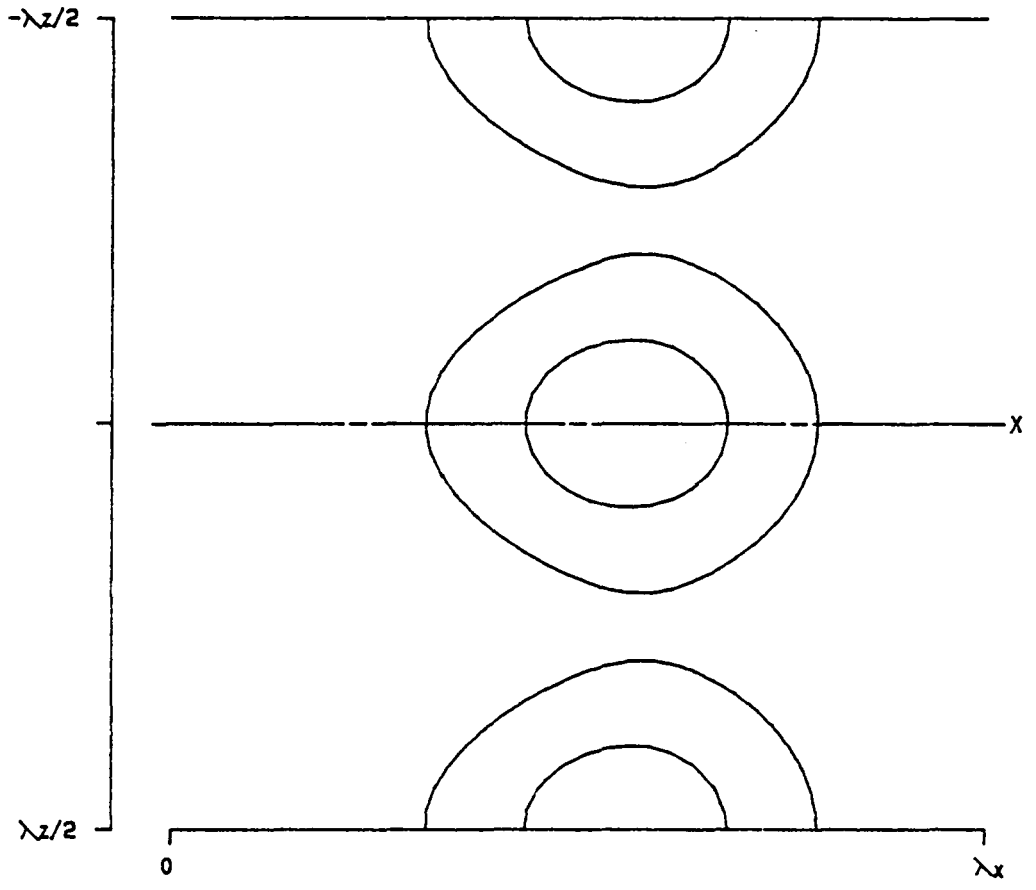

PPT 3-D F D3 (X, Z)

RE	5000.0
ALPHA	1.1200
BETA	2.0000
SIGMA	0.043798
RMS	0.025000
MAX	0.000176
SYM	1

LEVELS:	MIN	-0.0000607
	DIF	0.0000121
	NO.	20

Figure 3.112- $D^{(3)}$ as a function of x and z for $\mathbf{v}_{f_6}$ at $\alpha = 1.12$, $Re = 5000$, $\beta = 2.00$ and $A = 0.025$.

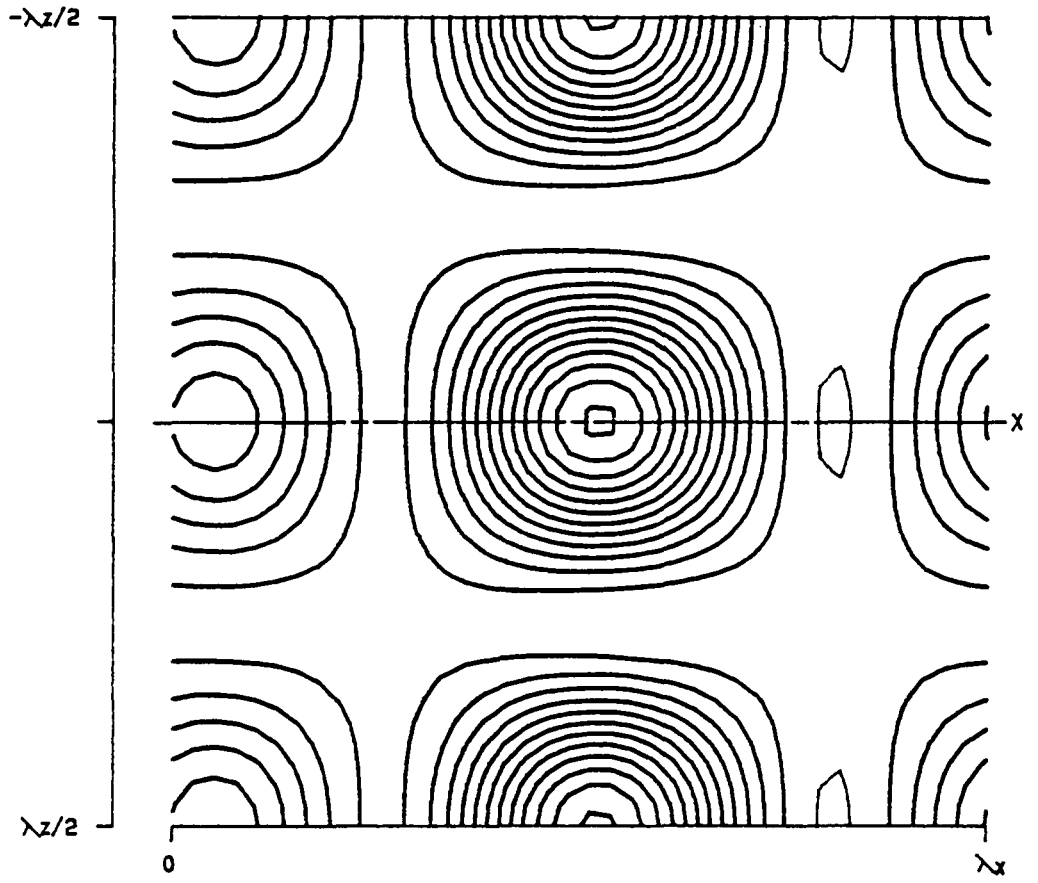

PPT 3-D F P3 (X, Z)

RE	5000.0
ALPHA	1.1200
BETA	2.0000
SIGMA	0.043798
RMS	0.025000
MAX	0.000176
SYM	1

LEVELS:	MIN	-0.0000607
	DIF	0.0000121
	NO.	20

Figure 3.113- $P^{(3)}$ as a function of x and z for $\mathbf{v}_{fa}$ at $\alpha = 1.12$, $Re = 5000$, $\beta = 2.00$ and $A = 0.025$.

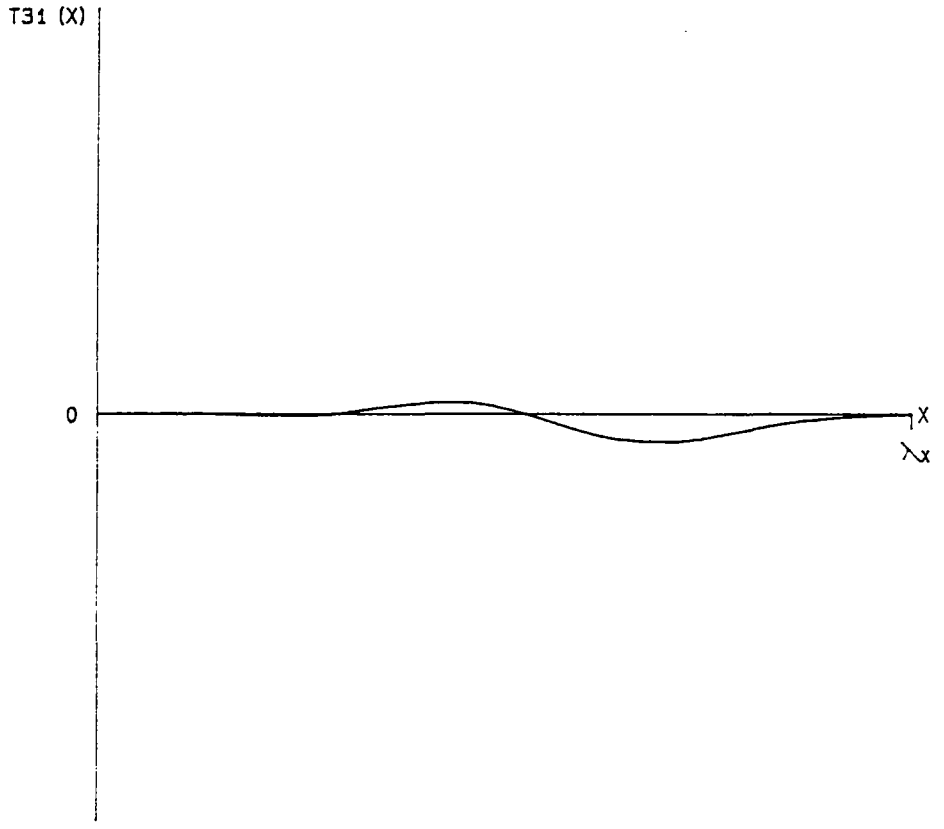

PPT 3-D F T31 (X)

RE	5000.0	SIGMA	0.043798
ALPHA	1.1200	CR	0.281755
BETA	2.0000	MAX	0.0000068
RMS	0.025000	MIN	-0.0000151
SYM	1		

Figure 3.114- $T^{(31)}$ as a function of x for $\mathbf{v}_{f_a}$ at $\alpha = 1.12$, $Re = 5000$, $\beta = 2.00$ and $A = 0.025$.

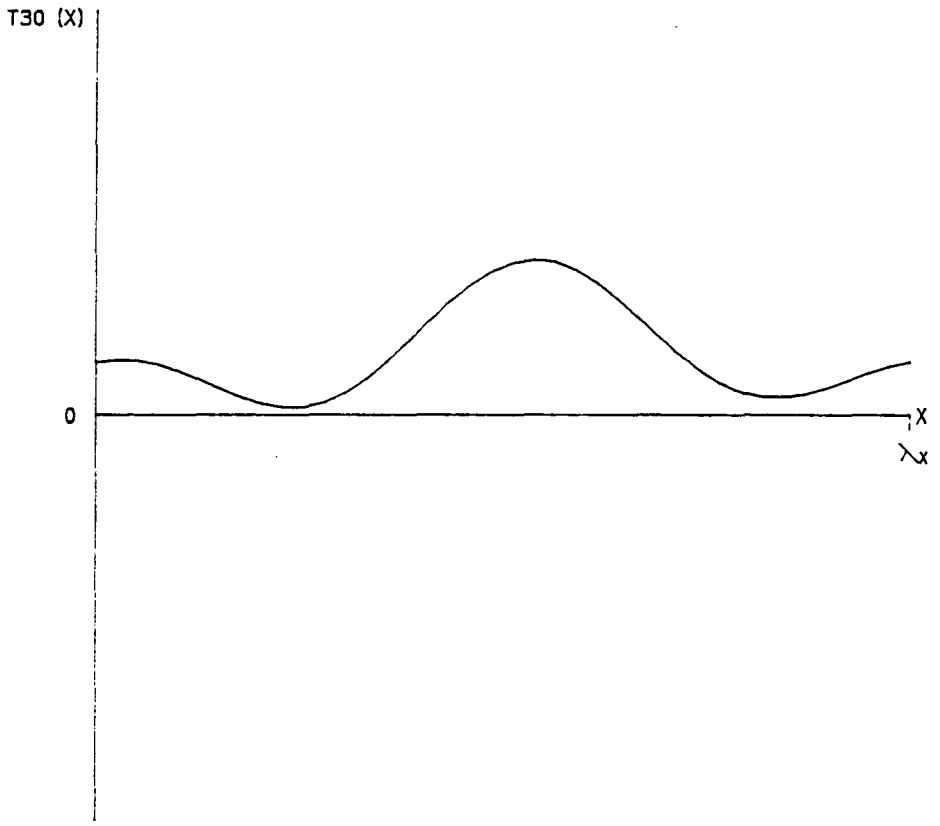

PPT 3-D F T30 (X)

RE	5000.0	SIGMA	0.043798
ALPHA	1.1200	CR	0.281755
BETA	2.0000	MAX	0.0000825
RMS	0.025000	MIN	0.0000038
SYM	1		

Figure 3.115- $T^{(30)}$ as a function of x for $\mathbf{v}_{f_a}$ at $\alpha = 1.12$, $Re = 5000$, $\beta = 2.00$ and $A = 0.025$.

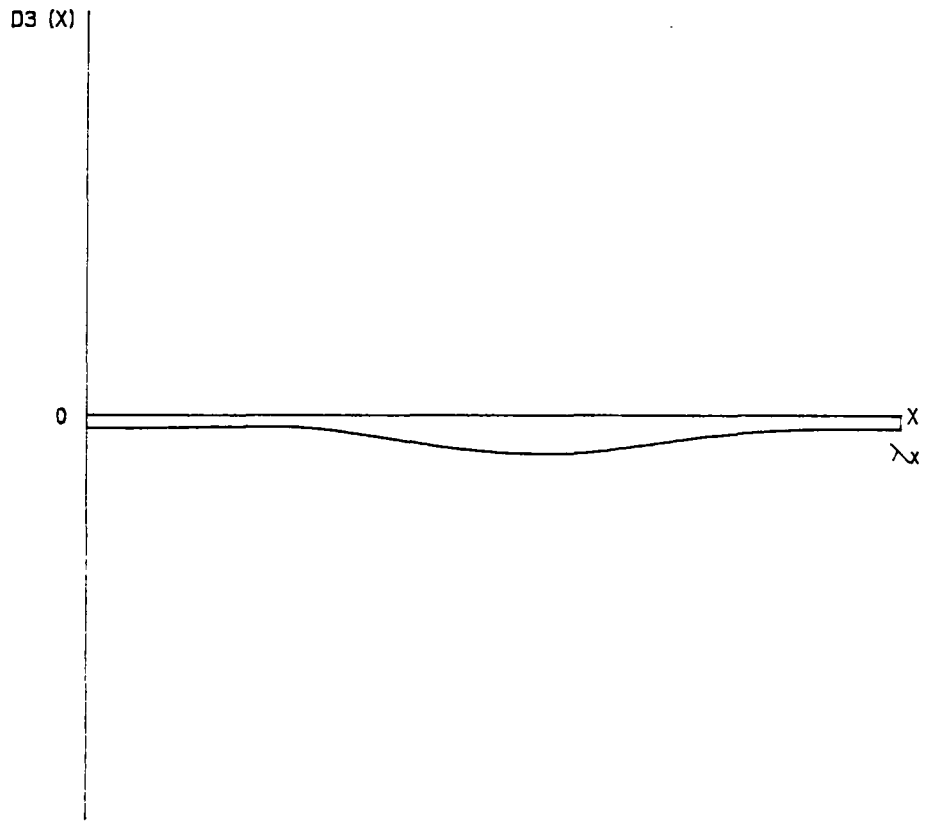

PPT 3-D F D3 (X)

RE	5000.0	SIGMA	0.043798
ALPHA	1.1200	CR	0.281755
BETA	2.0000	MAX	-0.0000054
RMS	0.025000	MIN	-0.0000206
SYM	1		

Figure 3.116- $D^{(3)}$ as a function of x for $\mathbf{v}_{f_s}$ at $\alpha = 1.12$, $Re = 5000$, $\beta = 2.00$ and $A = 0.025$.

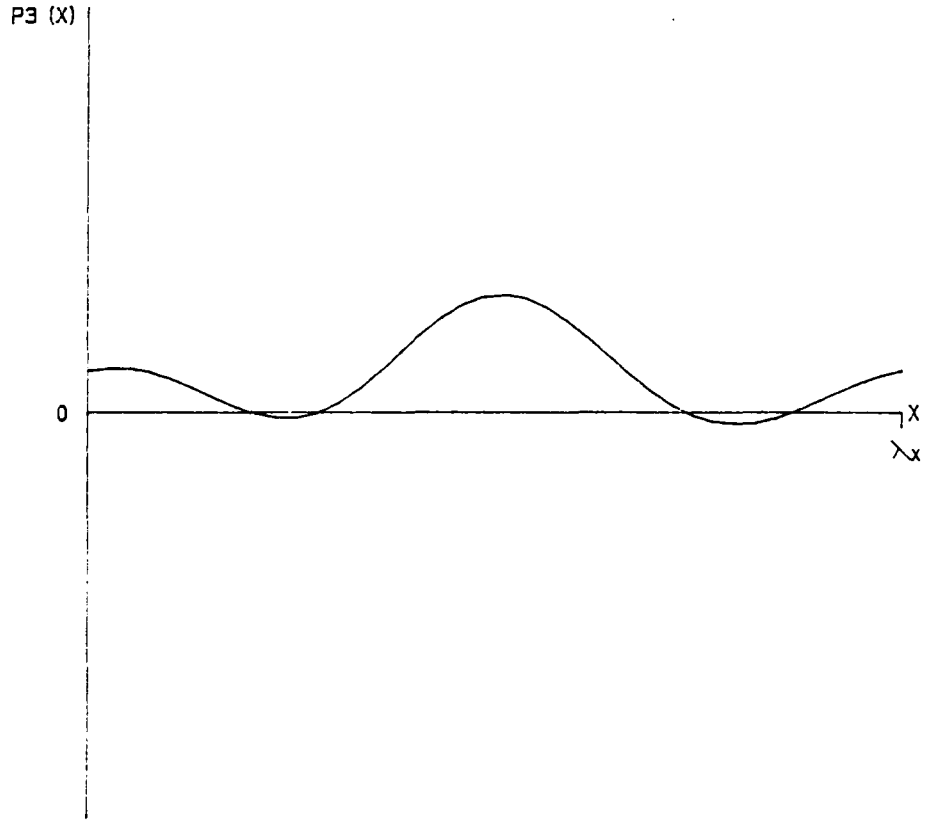

PPT 3-D F P3 (X)

RE	5000.0	SIGMA	0.043798
ALPHA	1.1200	CR	0.281755
BETA	2.0000	MAX	0.0000623
RMS	0.025000	MIN	-0.0000063
SYM	1		

Figure 3.117- $P^{(3)}$ as a function of x for $\mathbf{v}_{fa}$ at $\alpha = 1.12$, $Re = 5000$, $\beta = 2.00$ and $A = 0.025$.

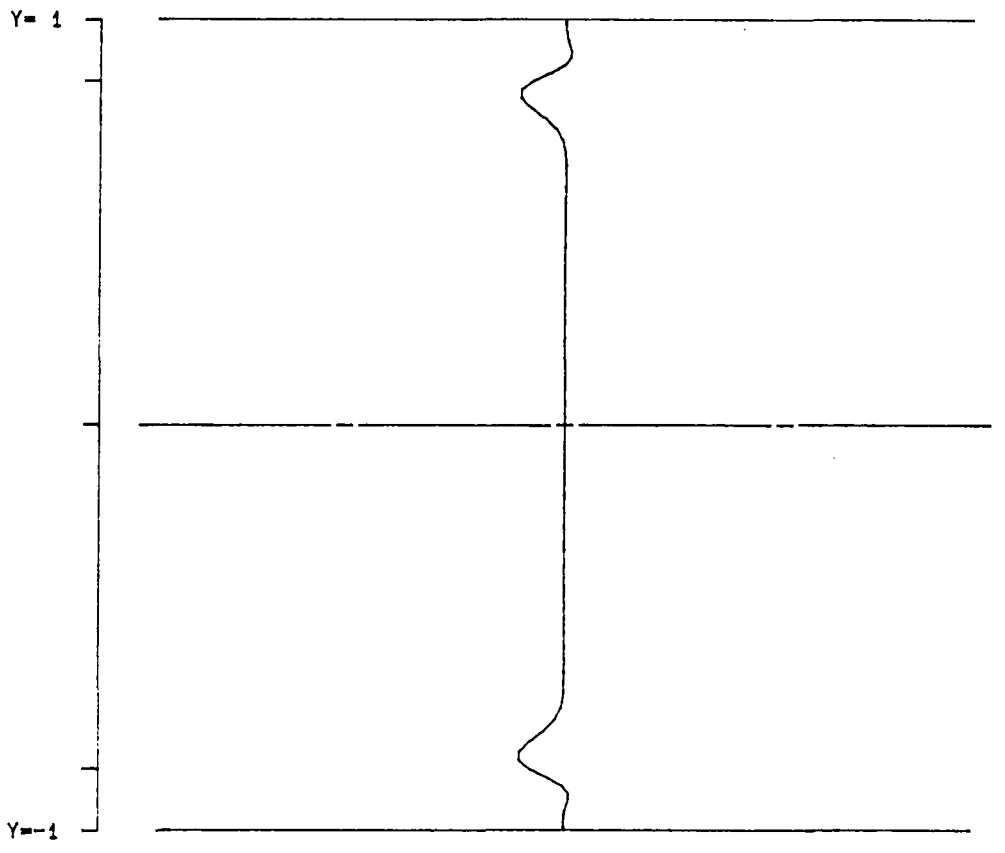

PPT 3-D F T31 (Y)

RE	5000.0	SIGMA	0.043798
ALPHA	1.1200	CR	0.281755
BETA	2.0000	MAX	0.0000029
RMS	0.025000	MIN	-0.0000228
SYM	1		

Figure 3.118- $T^{(31)}$ as a function of y for $\mathbf{v}_{f_4}$ at $\alpha = 1.12$, $Re = 5000$, $\beta = 2.00$ and $A = 0.025$.

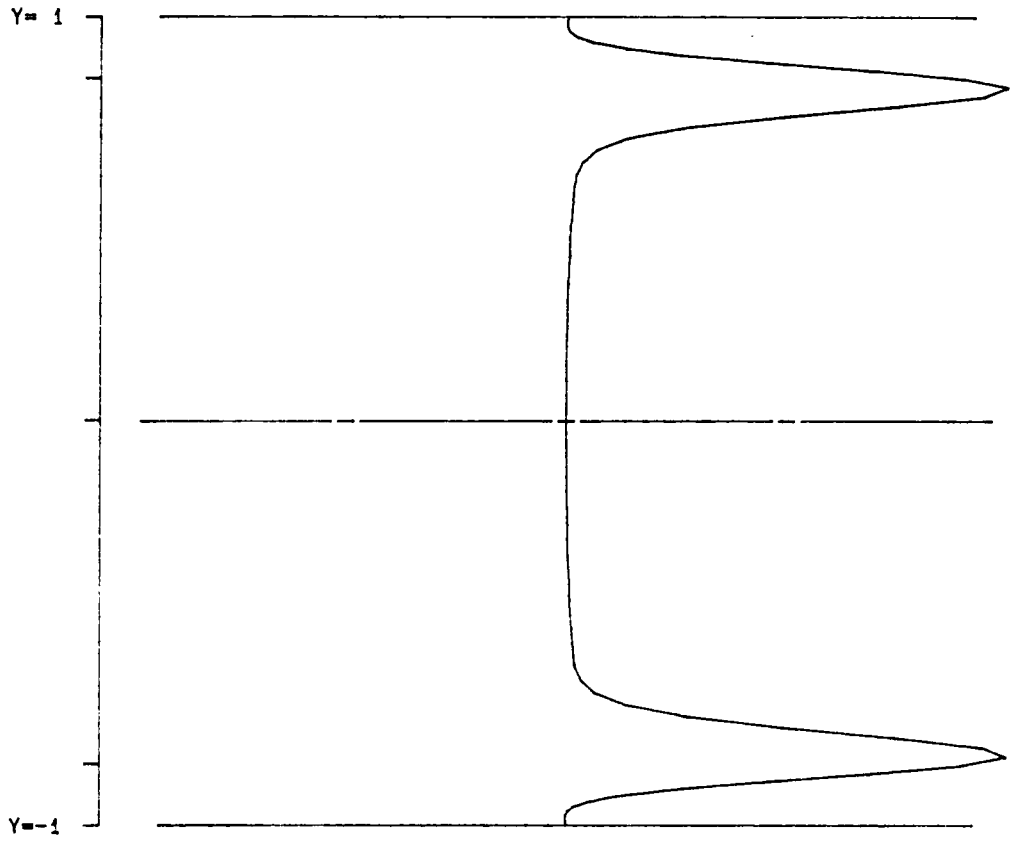

PPT 3-D F T30 (Y)

RE	5000.0	SIGMA	0.043798
ALPHA	1.1200	CR	0.281755
BETA	2.0000	MAX	0.0002142
RMS	0.025000	MIN	-0.0000000
SYM	1		

Figure 3.119- $T^{(30)}$ as a function of y for $\mathbf{v}_{f_4}$ at $\alpha = 1.12$, $Re = 5000$, $\beta = 2.00$ and $A = 0.025$.

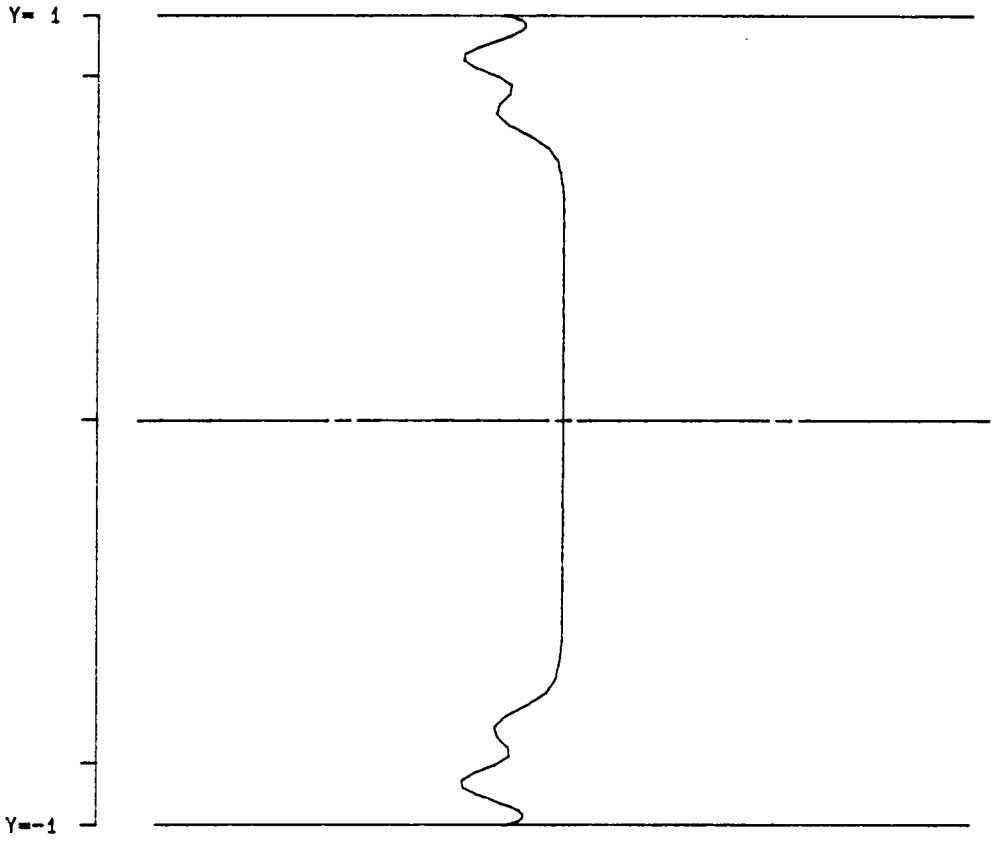

PPT 3-D F D3 (Y)

RE	5000.0	SIGMA	0.043798
ALPHA	1.1200	CR	0.281755
BETA	2.0000	MAX	-0.0000000
RMS	0.025000	MIN	-0.0000526
SYM	1		

Figure 3.120- $D^{(3)}$ as a function of y for $\mathbf{v}_{f_a}$ at $\alpha = 1.12$, $Re = 5000$, $\beta = 2.00$ and $A = 0.025$.

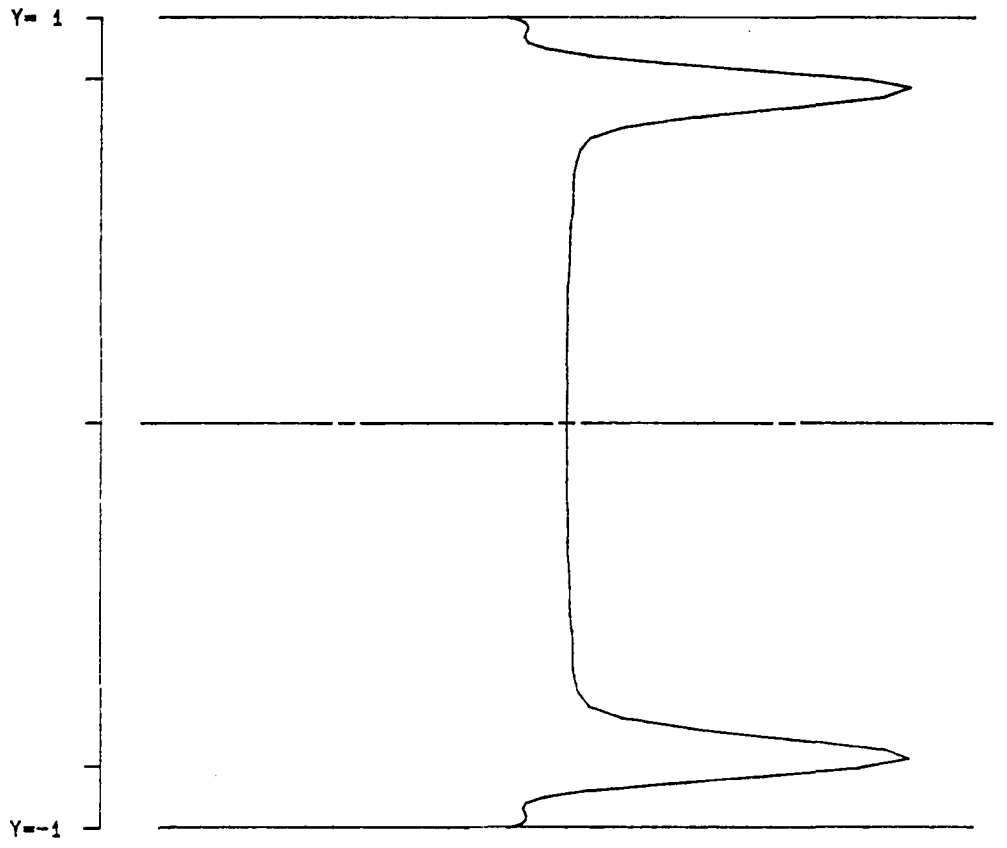

PPT 3-D F P3 (Y)

RE	5000.0	SIGMA	0.043798
ALPHA	1.1200	CR	0.281755
BETA	2.0000	MAX	0.0001619
RMS	0.025000	MIN	-0.0000313
SYM	1		

Figure 3.121- $P^{(3)}$ as a function of y for $\mathbf{v}_{f_4}$ at $\alpha = 1.12$, $Re = 5000$, $\beta = 2.00$ and $A = 0.025$.

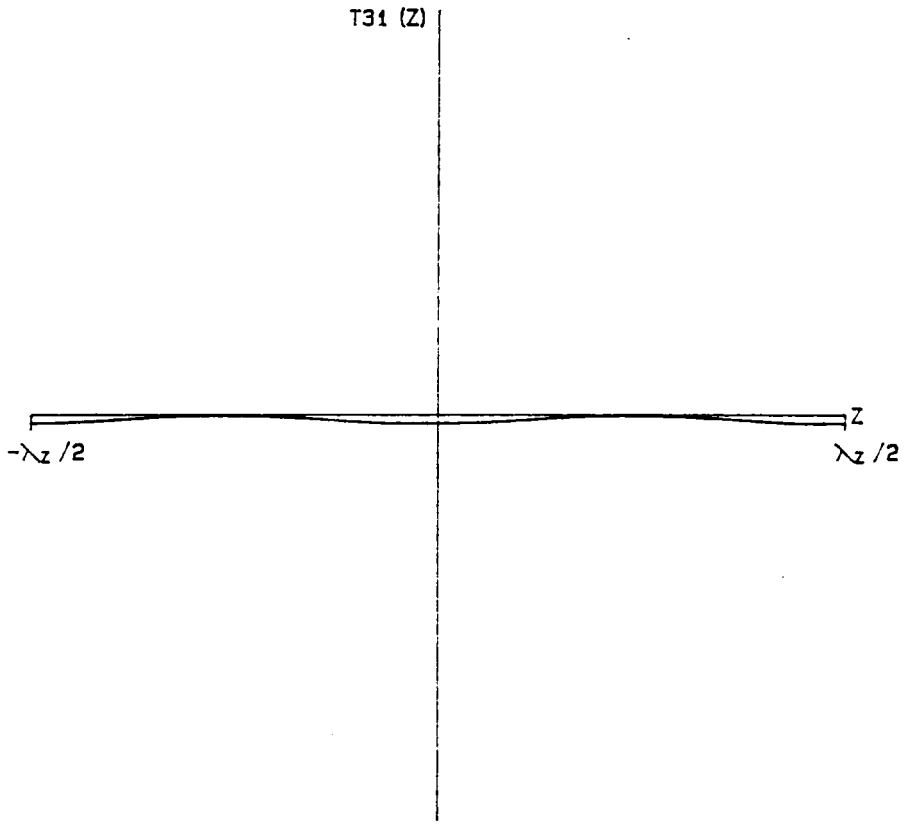

PPT 3-D F T31 (Z)

RE	5000.0	SIGMA	0.043798
ALPHA	1.1200	CR	0.281755
BETA	2.0000	MAX	-0.0000000
RMS	0.025000	MIN	-0.0000048
SYM	1		

Figure 3.122- $T^{(31)}$ as a function of z for $\mathbf{v}_{f_s}$ at $\alpha = 1.12$, $Re = 5000$, $\beta = 2.00$ and $A = 0.025$.

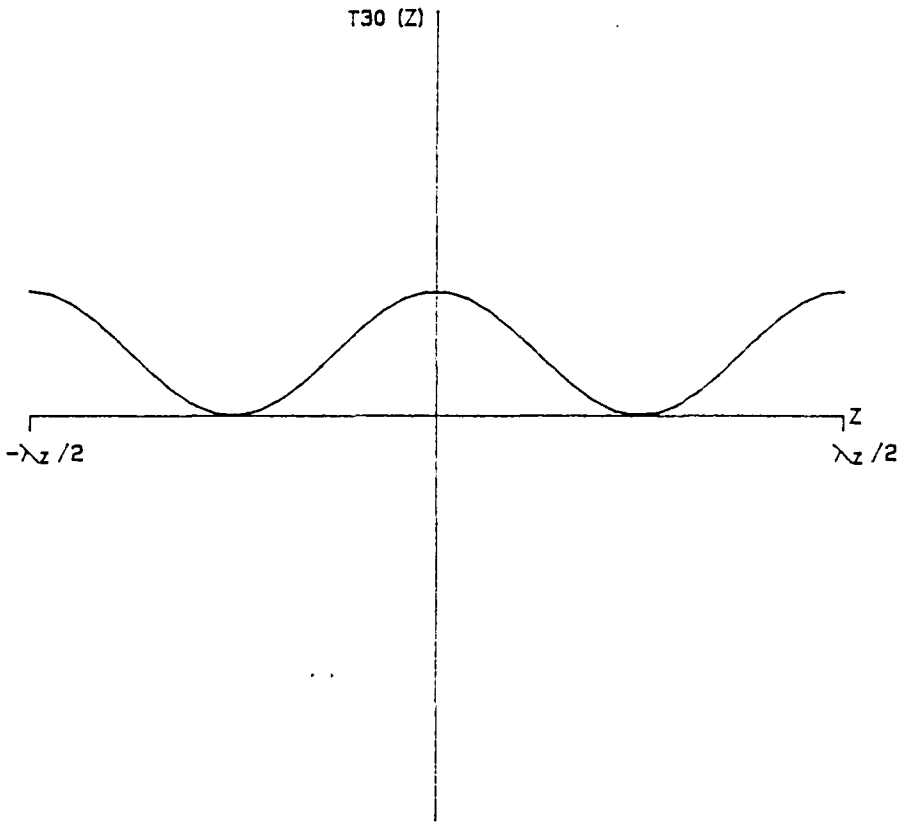

PPT 3-D F T30 (Z)

RE	5000.0	SIGMA	0.043798
ALPHA	1.1200	CR	0.281755
BETA	2.0000	MAX	0.0000661
RMS	0.025000	MIN	0.0000001
SYM	1		

Figure 3.123- $T^{(30)}$ as a function of z for $\mathbf{v}_{fs}$ at $\alpha = 1.12$, $Re = 5000$, $\beta = 2.00$ and $A = 0.025$.

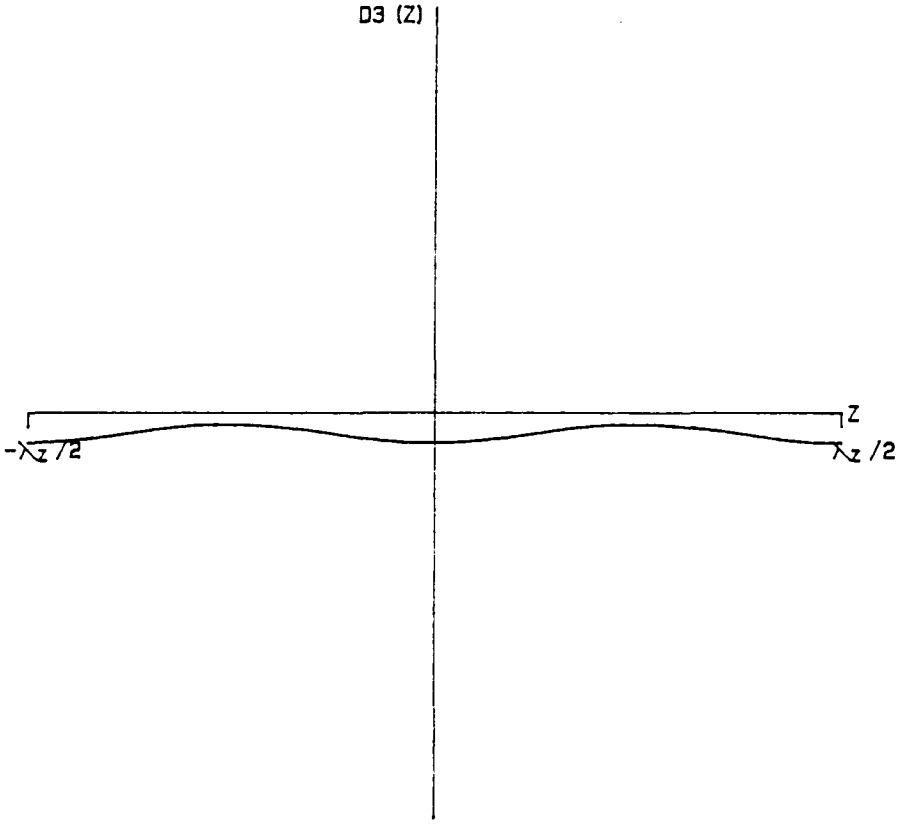

PPT 3-D F D3 (Z)

RE	5000.0	SIGMA	0.043798
ALPHA	1.1200	CR	0.281755
BETA	2.0000	MAX	-0.0000060
RMS	0.025000	MIN	-0.0000160
SYM	1		

Figure 3.124- $D^{(3)}$ as a function of z for $\mathbf{v}_{f_s}$ at $\alpha = 1.12$, $Re = 5000$, $\beta = 2.00$ and $A = 0.025$.

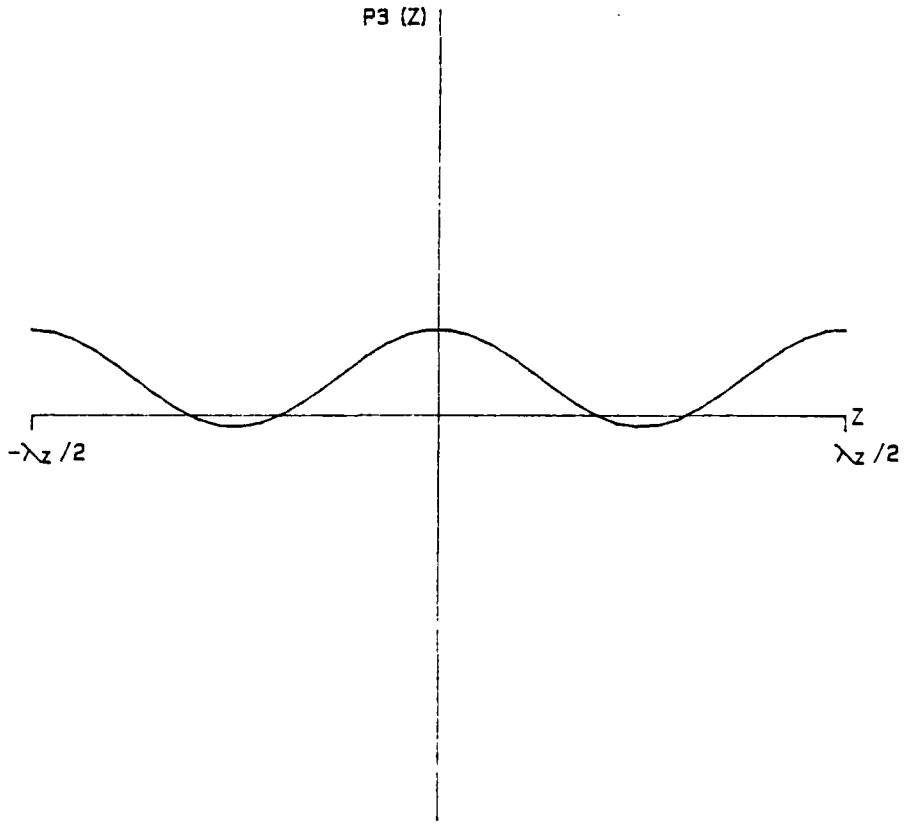

PPT 3-D F P3 (Z)

RE	5000.0	SIGMA	0.043798
ALPHA	1.1200	CR	0.281755
BETA	2.0000	MAX	0.0000452
RMS	0.025000	MIN	-0.0000059
SYM	1		

Figure 3.125- $P^{(3)}$ as a function of z for $\mathbf{v}_{f_4}$ at $\alpha = 1.12$, $Re = 5000$, $\beta = 2.00$ and $A = 0.025$.

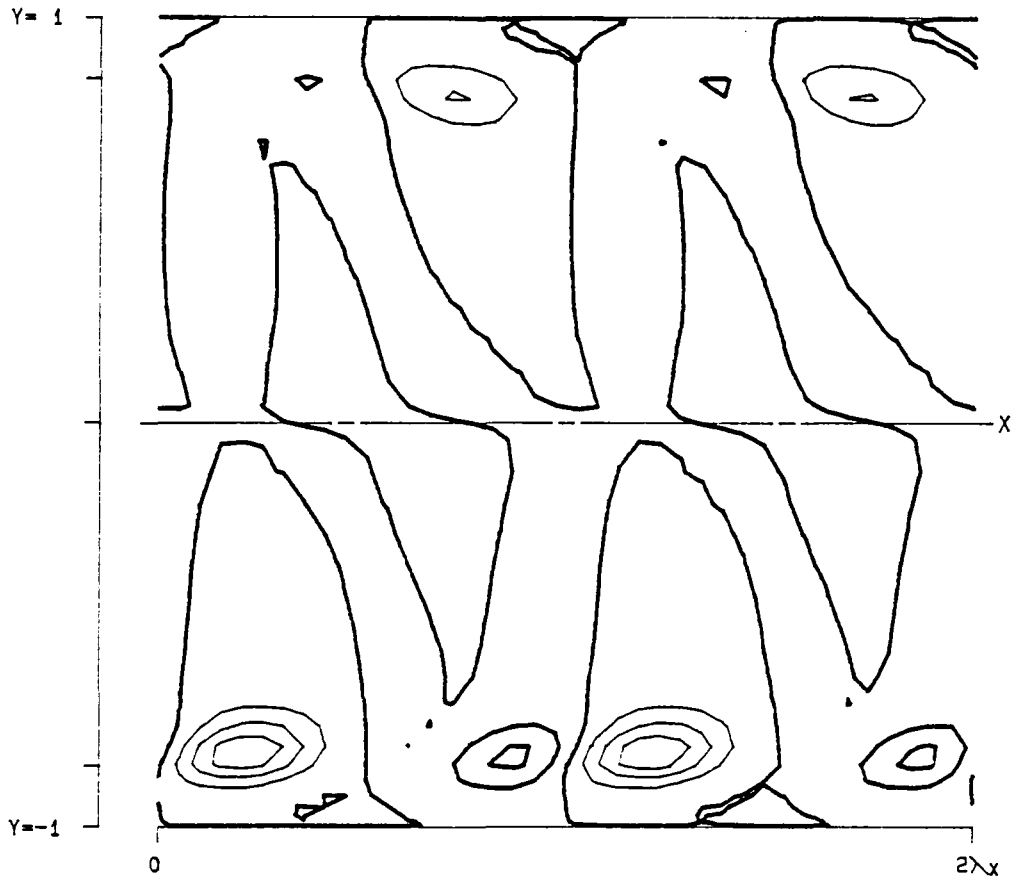

PPT 3-D S T31 (X, Y, Z)

RE	5000.0	LEVELS: MIN	-0.0002579
ALPHA	1.1200	DIF	0.0000516
BETA	2.0000	NO.	20
SIGMA	0.044449,-0.001926		
RMS	0.025000	Z =	-0.120830
MAX	0.000748		
SYM	1		

Figure 3.126- $T^{(31)}$ as a function of x, y and z at a position of $z = -0.120831$ for $\mathbf{v}$, at $\alpha = 1.12$, $Re = 5000$, $\beta = 2.00$ and $A = 0.025$.

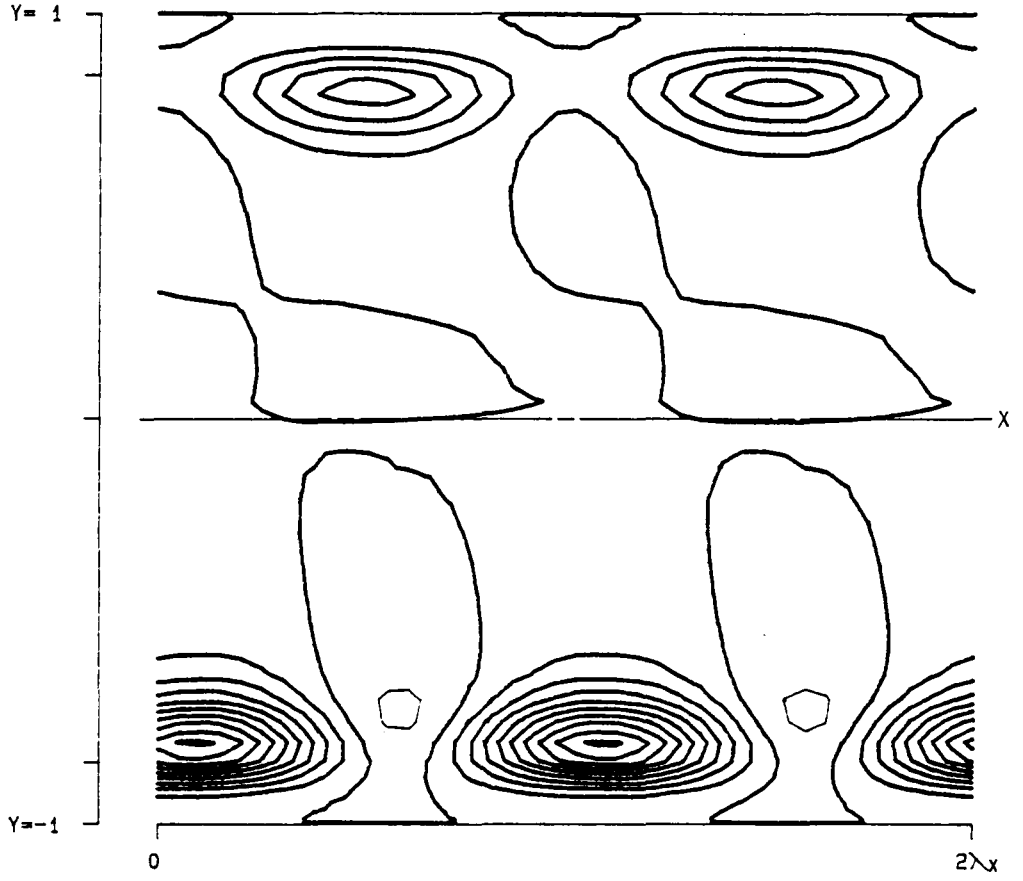

PPT 3-D S T30 (X, Y, Z)

RE	5000.0	LEVELS:	MIN -0.0002579
ALPHA	1.1200		DIF 0.0000516
BETA	2.0000		NO. 20
SIGMA	0.044449,-0.001926		
RMS	0.025000		Z = -0.120830
MAX	0.000748		
SYM	1		

Figure 3.127- $T^{(30)}$ as a function of x, y and z at a position of $z = -0.120831$ for **v**, at $\alpha = 1.12$, $Re = 5000$, $\beta = 2.00$ and $A = 0.025$.

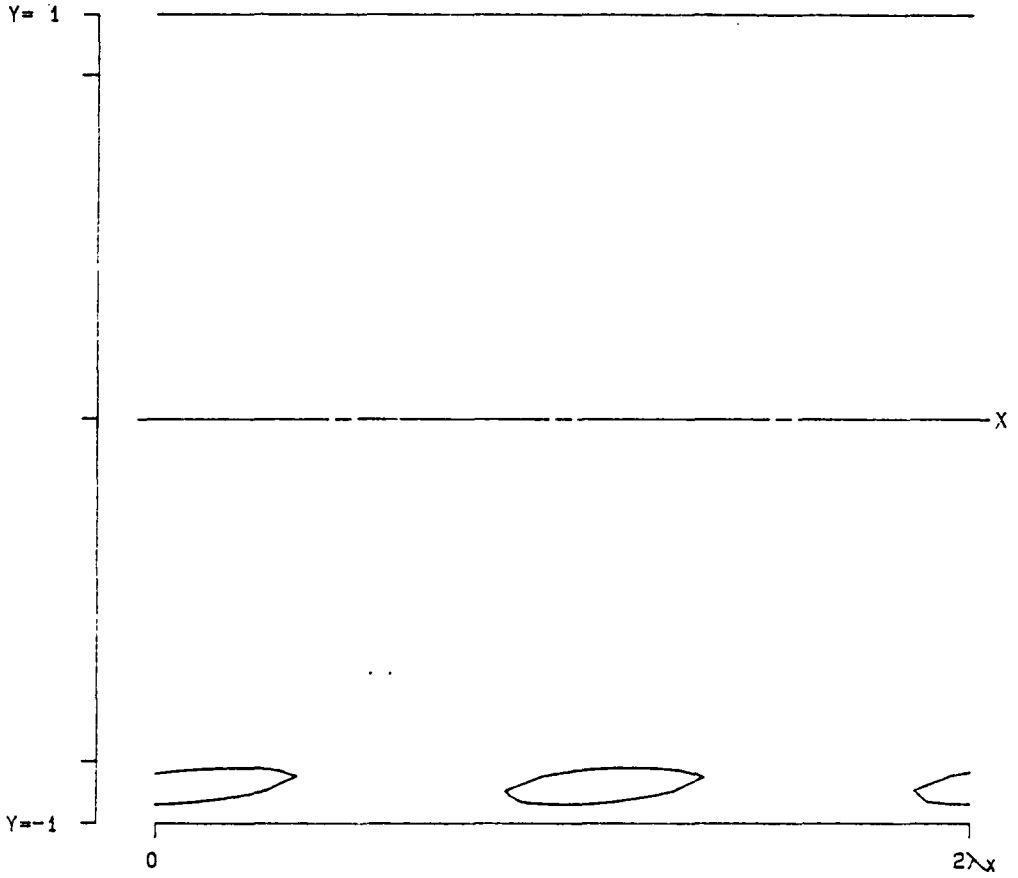

PPT 3-D S D3 (X, Y, Z)

RE	5000.0	LEVELS: MIN	-0.0002579
ALPHA	1.1200	DIF	0.0000516
BETA	2.0000	NO.	20
SIGMA	0.044449,-0.001926		
RMS	0.025000	Z =	-0.120830
MAX	0.000748		
SYM	1		

Figure 3.128- $D^{(3)}$ as a function of x, y and z at a position of $z = -0.120831$ for $\mathbf{v}_t$ at $\alpha = 1.12$, $Re = 5000$, $\beta = 2.00$ and $A = 0.025$.

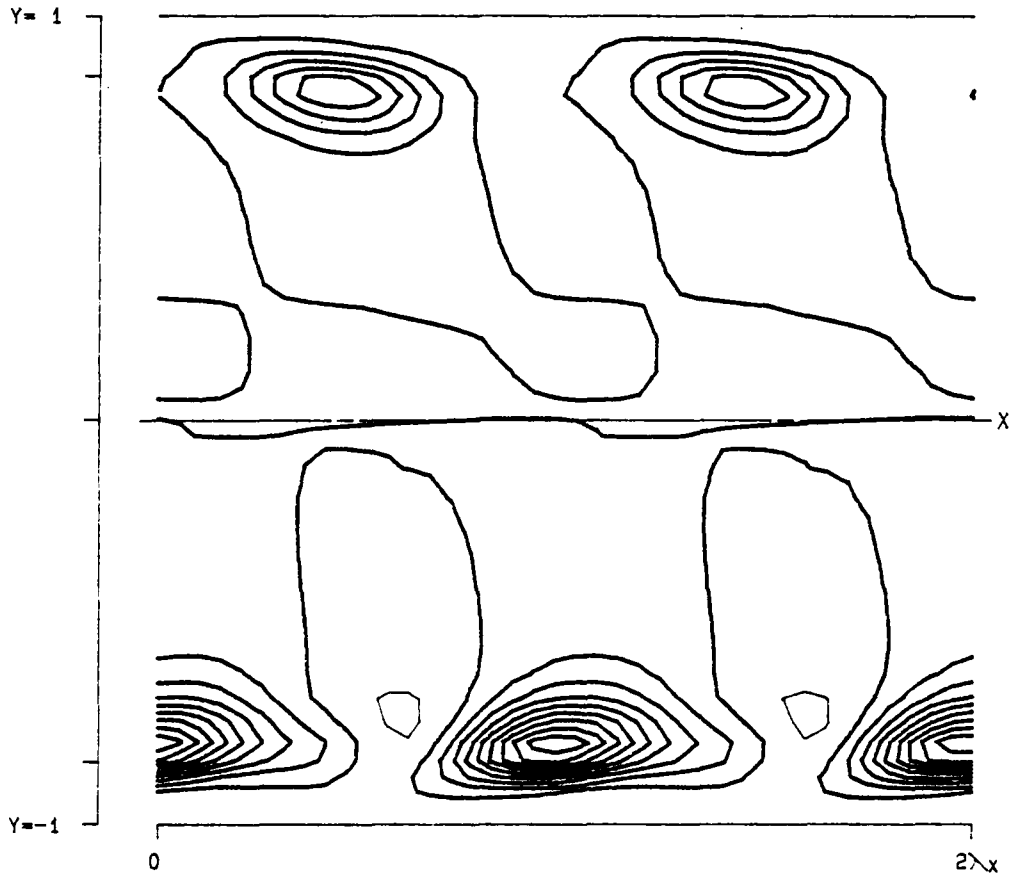

PPT 3-D S P3 (X, Y, Z)

RE	5000.0	LEVELS: MIN	-0.0002579
ALPHA	1.1200	DIF	0.0000516
BETA	2.0000	NO.	20
SIGMA	0.044449,-0.001926		
RMS	0.025000	Z =	-0.120830
MAX	0.000748		
SYM	1		

Figure 3.129- $P^{(3)}$ as a function of x, y and z at a position of $z = -0.120831$ for $\mathbf{v}_s$ at $\alpha = 1.12$, $Re = 5000$, $\beta = 2.00$ and $A = 0.025$.

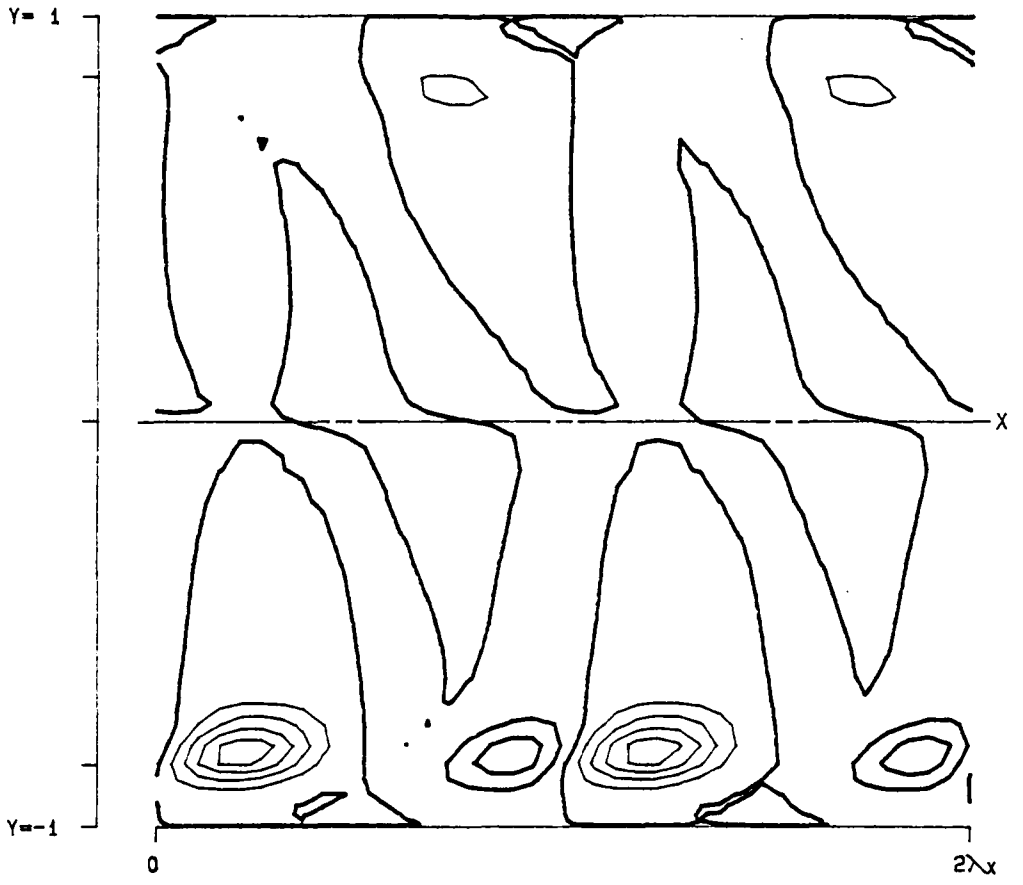

PPT 3-D S T31 (X, Y, Z)

RE	5000.0	LEVELS: MIN	-0.0002579
ALPHA	1.1200	DIF	0.0000516
BETA	2.0000	NO.	20
SIGMA	0.044449,-0.001926		
RMS	0.025000	Z =	-0.040277
MAX	0.000748		
SYM	1		

Figure 3.130- $T^{(31)}$ as a function of x, y and z at a position of $z = -0.040277$ for $\mathbf{v}_t$ at $\alpha = 1.12$, $Re = 5000$, $\beta = 2.00$ and $A = 0.025$.

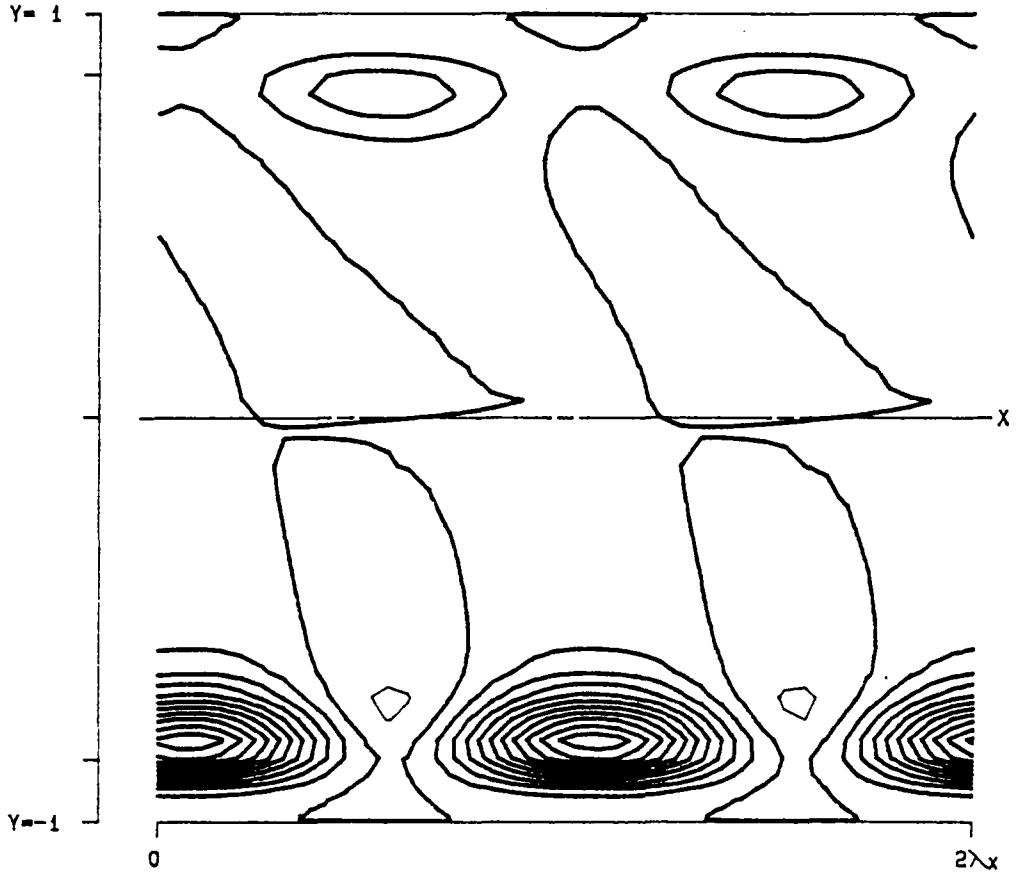

PPT 3-D S T30 (X, Y, Z)

RE	5000.0	LEVELS: MIN	-0.0002579
ALPHA	1.1200	DIF	0.0000516
BETA	2.0000	NO.	20
SIGMA	0.044449,-0.001926		
RMS	0.025000	Z =	-0.040277
MAX	0.000748		
SYM	1		

Figure 3.131- $T^{(30)}$ as a function of x, y and z at a position of $z = -0.040277$ for $\mathbf{v}$, at $\alpha = 1.12$, $Re = 5000$, $\beta = 2.00$ and $A = 0.025$.

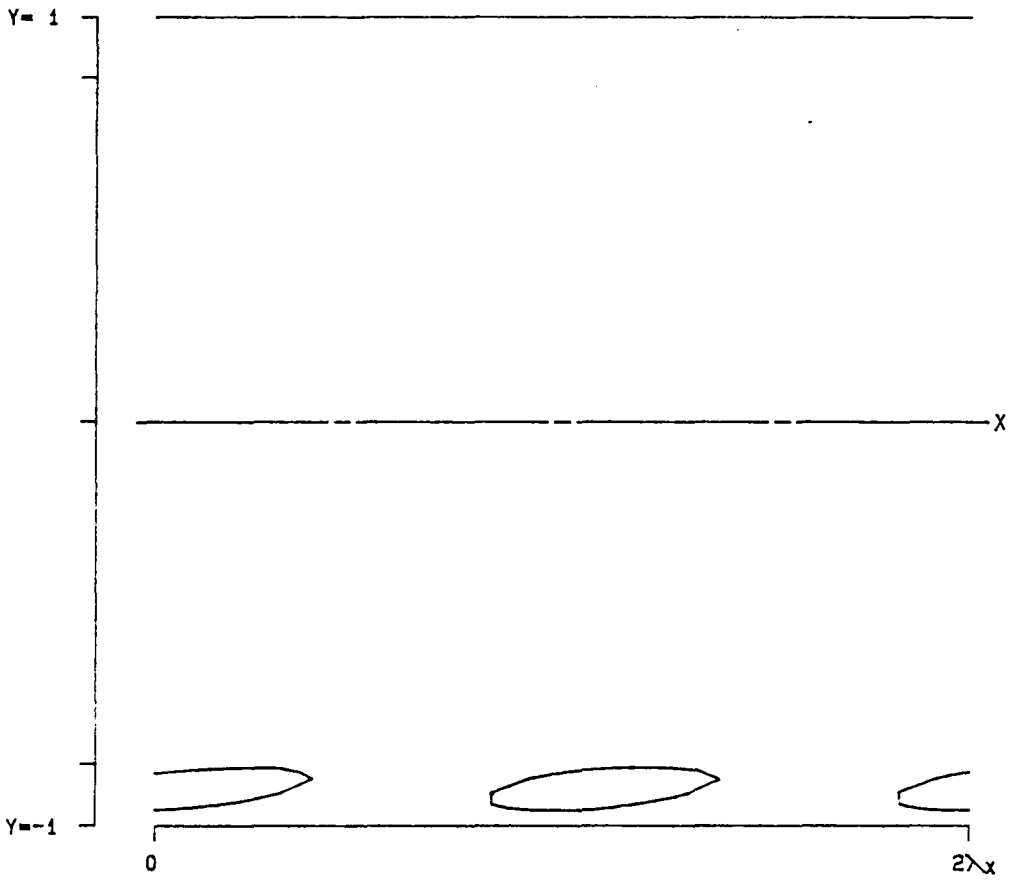

PPT 3-D S D3 (X, Y, Z)

RE	5000.0	LEVELS:	MIN	-0.0002579
ALPHA	1.1200		DIF	0.0000516
BETA	2.0000		NO.	20
SIGMA	0.044449,-0.001926			
RMS	0.025000		Z =	-0.040277
MAX	0.000748			
SYM	1			

Figure 3.132- $D^{(3)}$ as a function of x, y and z at a position of $z = -0.040277$ for $\mathbf{v}_s$ at $\alpha = 1.12$, $Re = 5000$, $\beta = 2.00$ and $A = 0.025$.

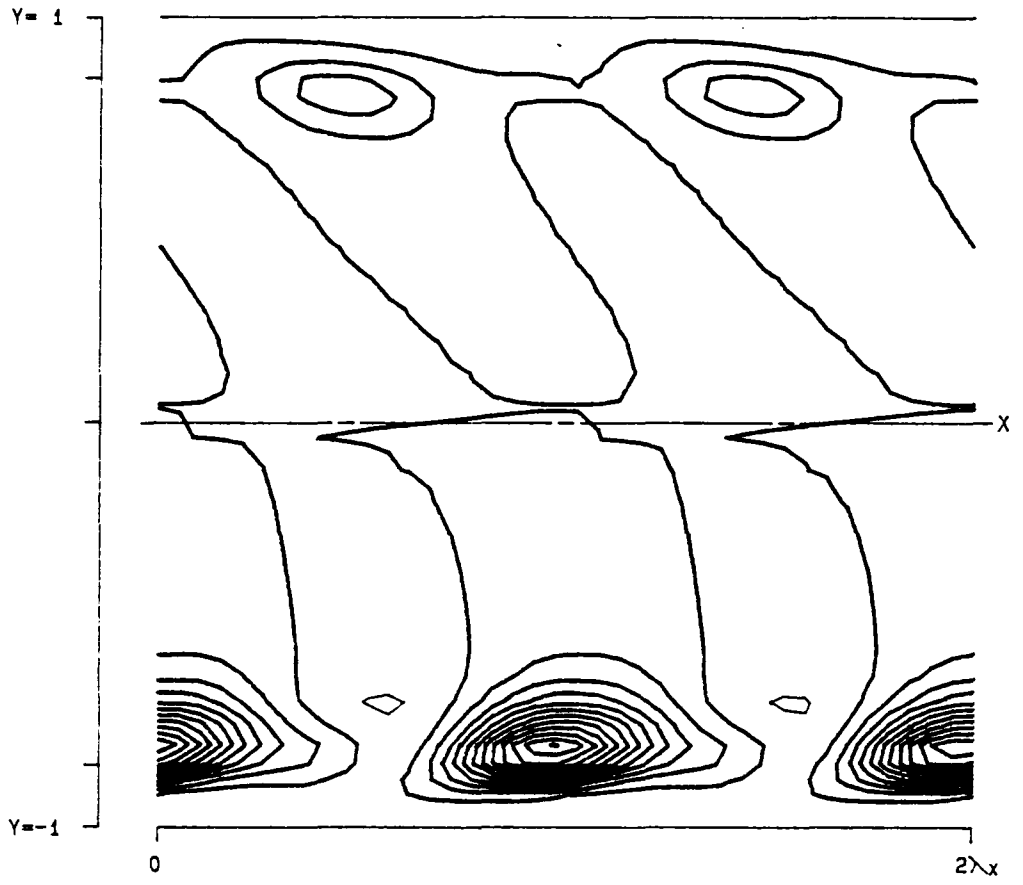

PPT 3-D S P3 (X, Y, Z)

RE	5000.0	LEVELS:	MIN -0.0002579
ALPHA	1.1200		DIF 0.0000516
BETA	2.0000		NO. 20
SIGMA	0.044449,-0.001926		
RMS	0.025000		Z = -0.040277
MAX	0.000748		
SYM	1		

Figure 3.133- $P^{(3)}$ as a function of x, y and z at a position of $z = -0.040277$ for $\mathbf{v}_s$ at $\alpha = 1.12$, $Re = 5000$, $\beta = 2.00$ and $A = 0.025$.

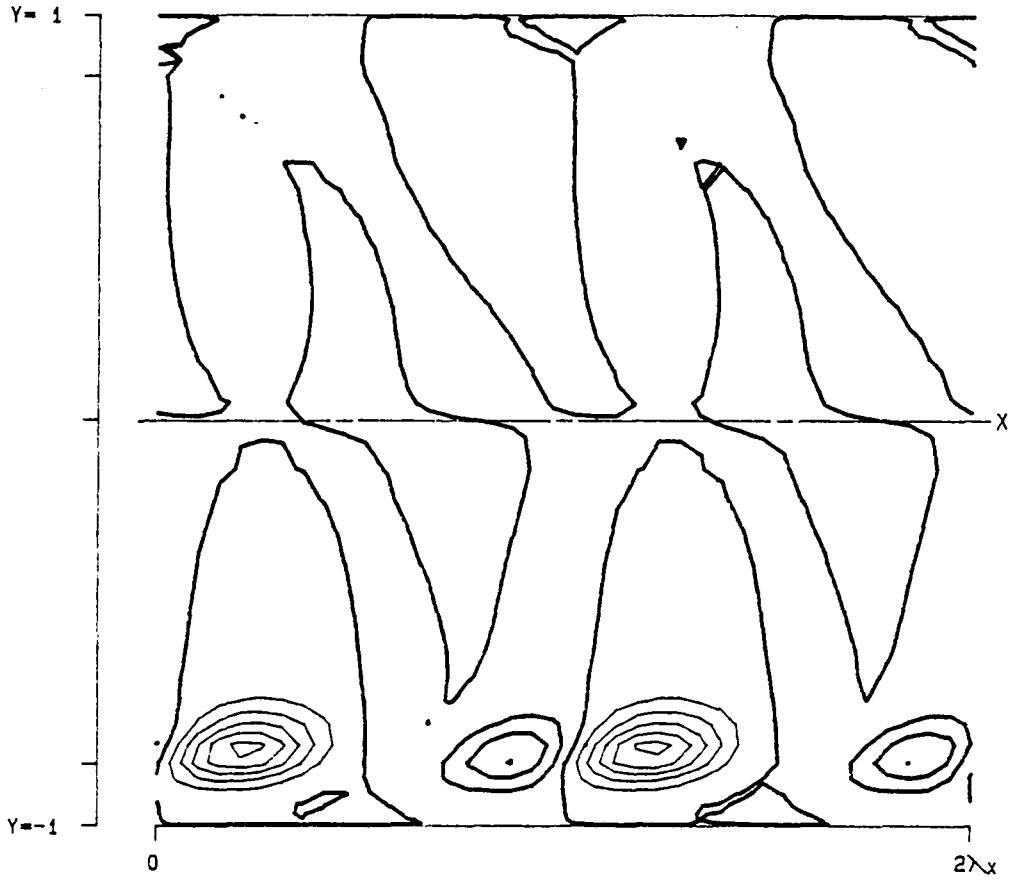

PPT 3-D S T31 (X, Y, Z)

RE	5000.0	LEVELS: MIN	-0.0002579
ALPHA	1.1200	DIF	0.0000516
BETA	2.0000	NO.	20
SIGMA	0.044449,-0.001926		
RMS	0.025000	Z =	0.040277
MAX	0.000748		
SYM	1		

Figure 3.134- $T^{(31)}$ as a function of x, y and z at a position of $z = 0.040277$ for $\mathbf{v}_s$ at $\alpha = 1.12$, $Re = 5000$, $\beta = 2.00$ and $A = 0.025$.

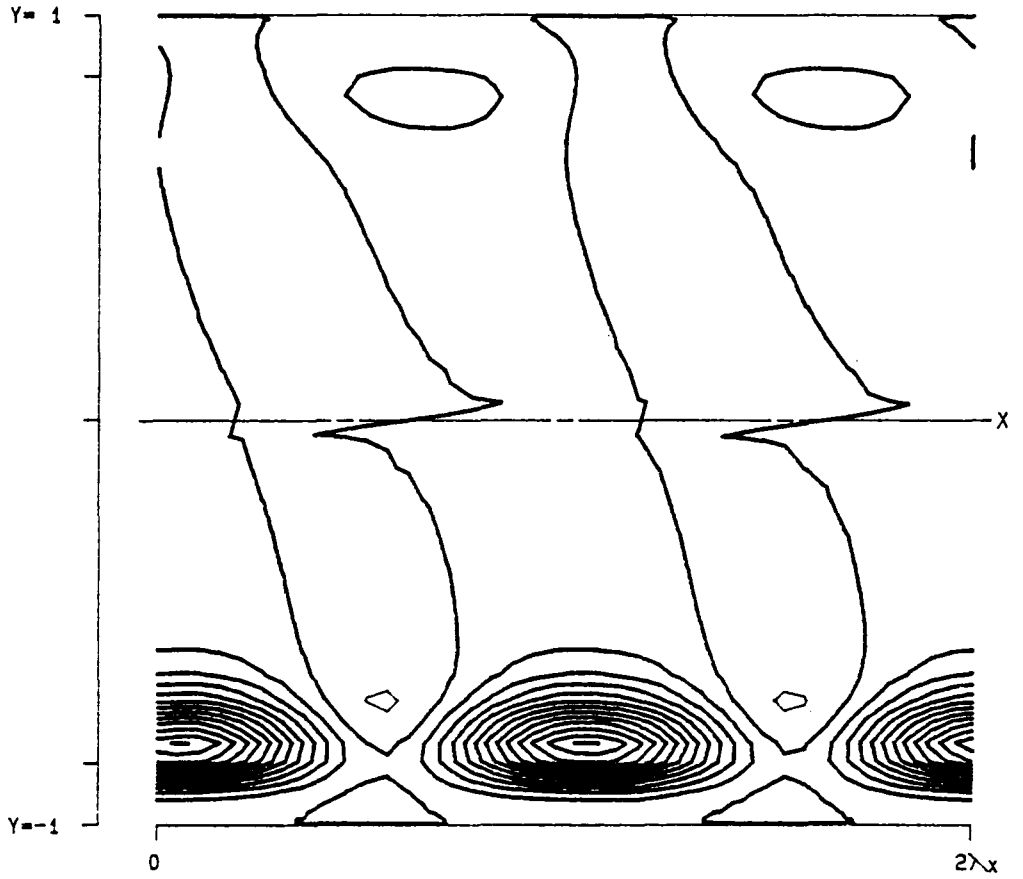

PPT 3-D S T30 (X, Y, Z)

RE	5000.0	LEVELS: MIN	-0.0002579
ALPHA	1.1200	DIF	0.0000516
BETA	2.0000	NO.	20
SIGMA	0.044449,-0.001926		
RMS	0.025000	Z =	0.040277
MAX	0.000748		
SYM	1		

Figure 3.135- $T^{(30)}$ as a function of x, y and z at a position of $z = 0.040277$ for $\mathbf{v}_s$ at $\alpha = 1.12$, $Re = 5000$, $\beta = 2.00$ and $A = 0.025$.

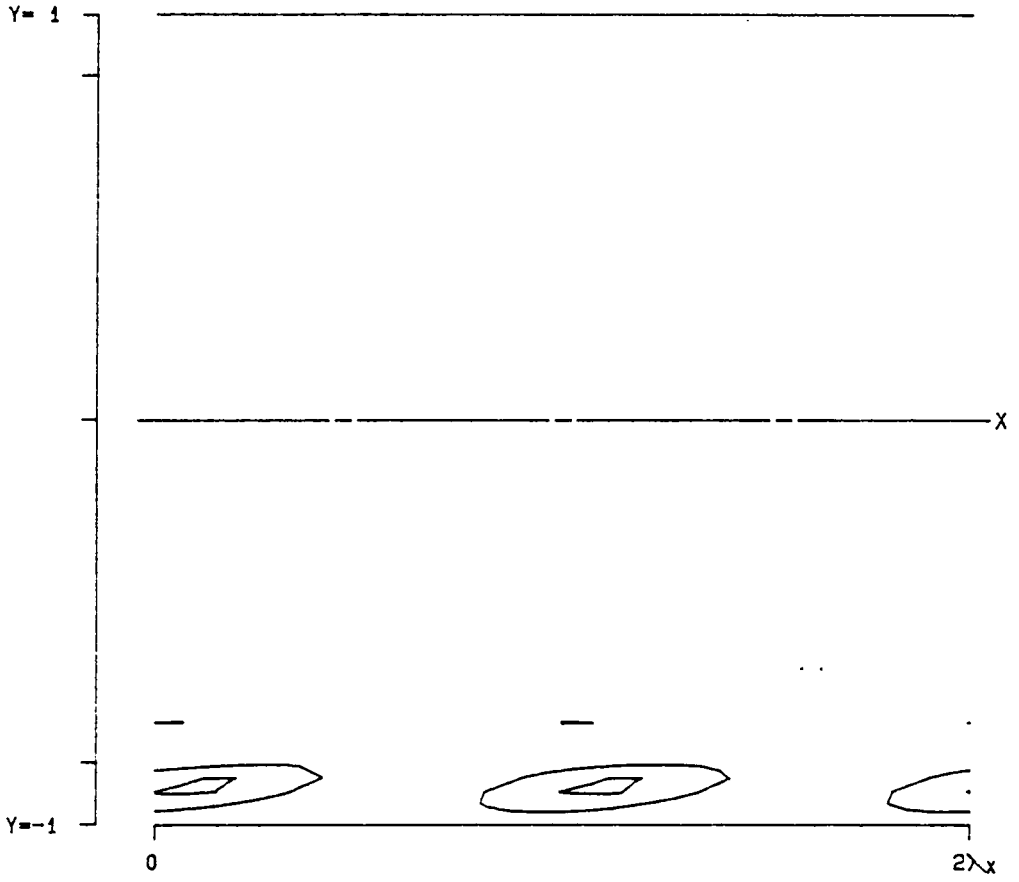

PPT 3-D S D3 (X, Y, Z)

RE	5000.0	LEVELS:	MIN -0.0002579
ALPHA	1.1200		DIF 0.0000516
BETA	2.0000		NO. 20
SIGMA	0.044449,-0.001926		
RMS	0.025000		Z = 0.040277
MAX	0.000748		
SYM	1		

Figure 3.136- $D^{(3)}$ as a function of x, y and z at a position of $z = 0.040277$ for $\mathbf{v}_s$ at $\alpha = 1.12$, $Re = 5000$, $\beta = 2.00$ and $A = 0.025$.

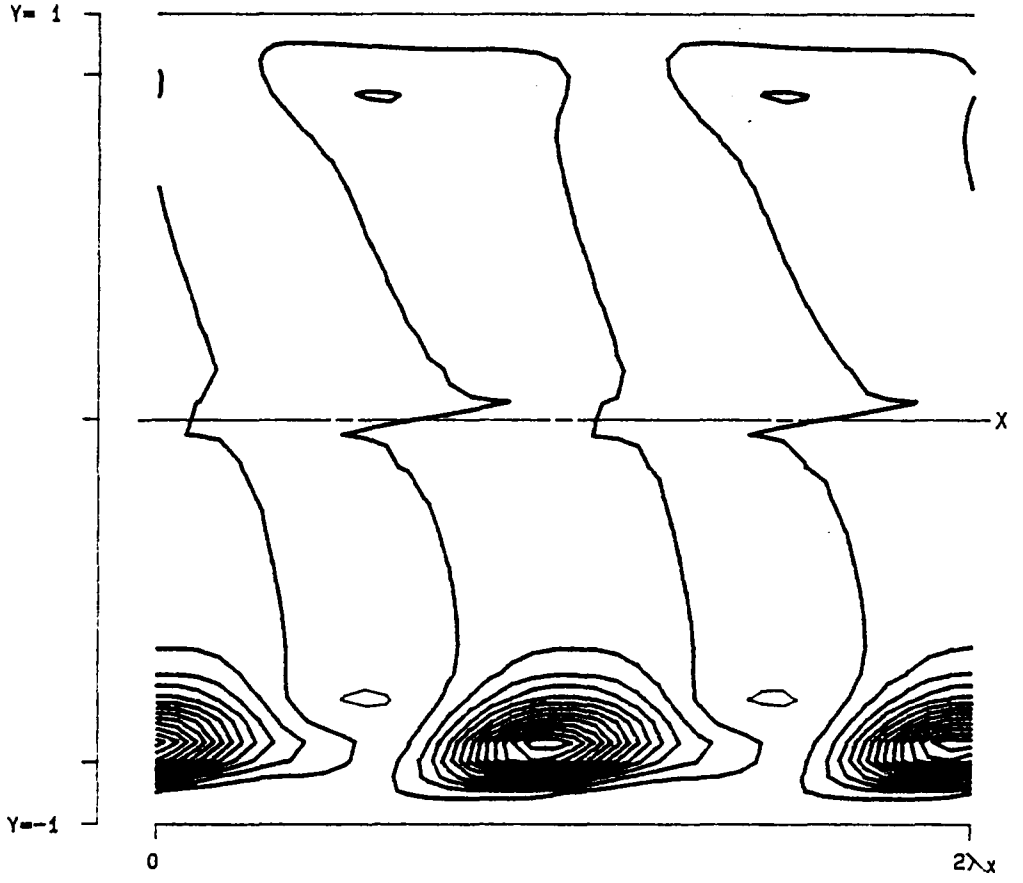

PPT 3-D S P3 (X, Y, Z)

RE	5000.0	LEVELS: MIN	-0.0002579
ALPHA	1.1200	DIF	0.0000516
BETA	2.0000	NO.	20
SIGMA	0.044449,-0.001926		
RMS	0.025000	Z =	0.040277
MAX	0.000748		
SYM	1		

Figure 3.137- $P^{(3)}$ as a function of x, y and z at a position of $z = 0.040277$ for $\mathbf{v}_s$ at $\alpha = 1.12$, $Re = 5000$, $\beta = 2.00$ and $A = 0.025$.

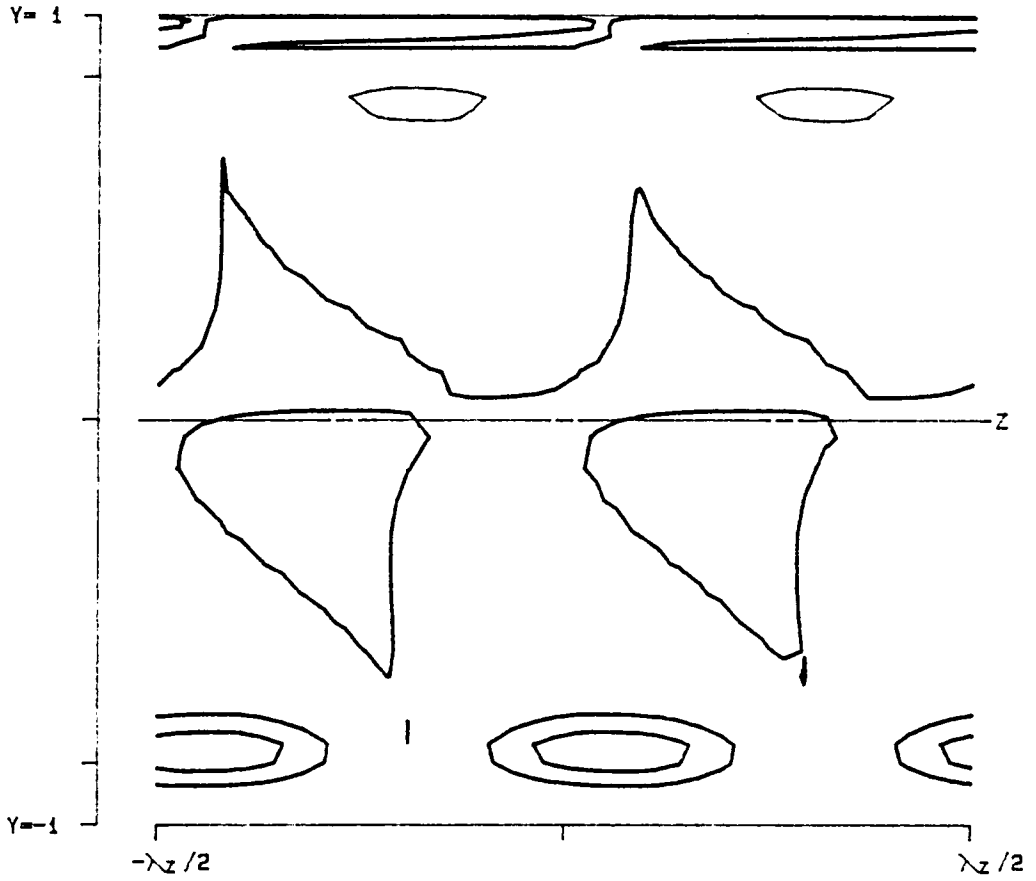

PPT 3-D S T31 (X, Y, Z)

RE	5000.0	LEVELS: MIN	-0.0002579
ALPHA	1.1200	DIF	0.0000516
BETA	2.0000	NO.	20
SIGMA	0.044449,-0.001926		
RMS	0.025000	X =	5.178450
MAX	0.000748		
SYM	1		

Figure 3.138- $T^{(31)}$ as a function of x, y and z at a position of $x = 2.589225$ for $\mathbf{v}_t$ at $\alpha = 1.12$, $Re = 5000$, $\beta = 2.00$ and $A = 0.025$.

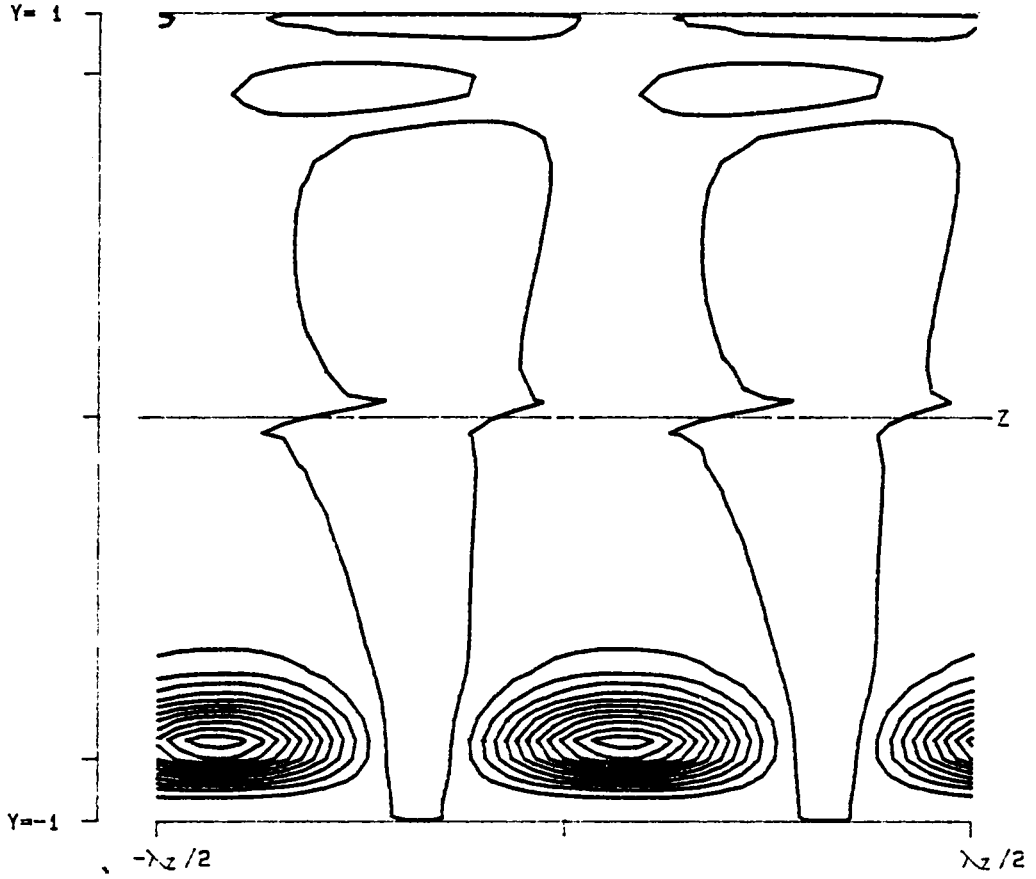

PPT 3-D S T30 (X, Y, Z)

RE	5000.0	LEVELS:	MIN -0.0002579
ALPHA	1.1200		DIF 0.0000516
BETA	2.0000		NO. 20
SIGMA	0.044449,-0.001926		
RMS	0.025000		X = 5.178450
MAX	0.000748		
SYM	1		

Figure 3.139- $T^{(30)}$ as a function of x, y and z at a position of $x = 2.589225$ for **v**, at $\alpha = 1.12$, $Re = 5000$, $\beta = 2.00$ and $A = 0.025$.

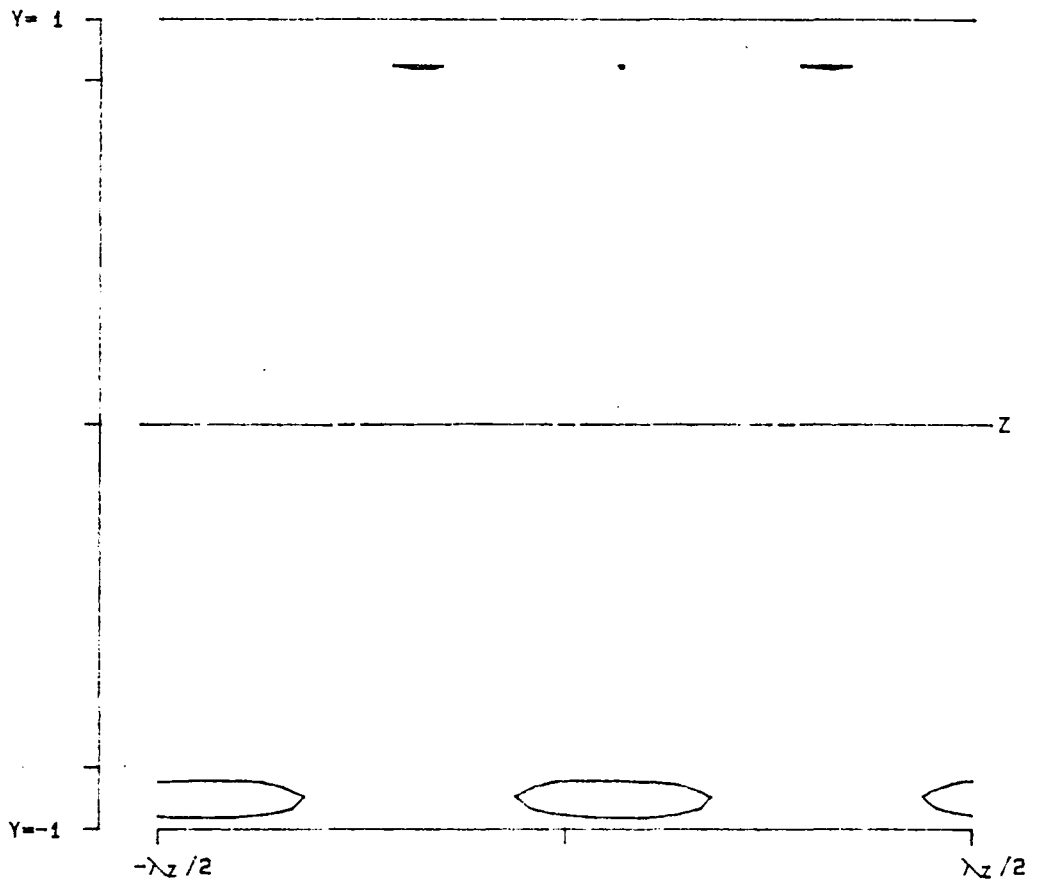

PPT 3-D S D3 (X, Y, Z)

RE	5000.0	LEVELS: MIN	-0.0002579
ALPHA	1.1200	DIF	0.0000516
BETA	2.0000	NO.	20
SIGMA	0.044449,-0.001926		
RMS	0.025000	X =	5.178450
MAX	0.000748		
SYM	1		

Figure 3.140- $D^{(3)}$ as a function of x, y and z at a position of $x = 2.589225$ for $\mathbf{v}$, at $\alpha = 1.12$, $Re = 5000$, $\beta = 2.00$ and $A = 0.025$.

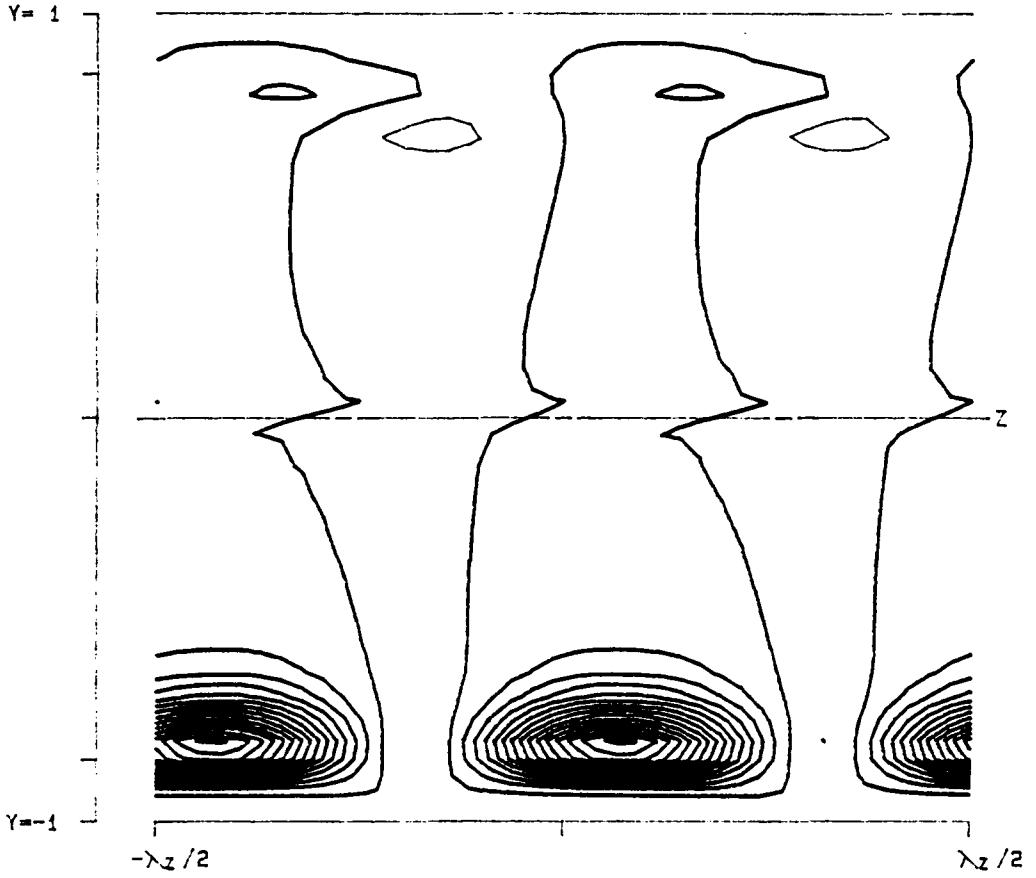

PPT 3-D S P3 (X, Y, Z)

RE	5000.0	LEVELS:	MIN -0.0002579
ALPHA	1.1200		DIF 0.0000516
BETA	2.0000		NO. 20
SIGMA	0.044449,-0.001926		
RMS	0.025000		X = 5.178450
MAX	0.000748		
SYM	1		

Figure 3.141- $P^{(3)}$ as a function of x, y and z at a position of $x = 2.589225$ for $\mathbf{v}_s$ at $\alpha = 1.12$, $Re = 5000$, $\beta = 2.00$ and $A = 0.025$.

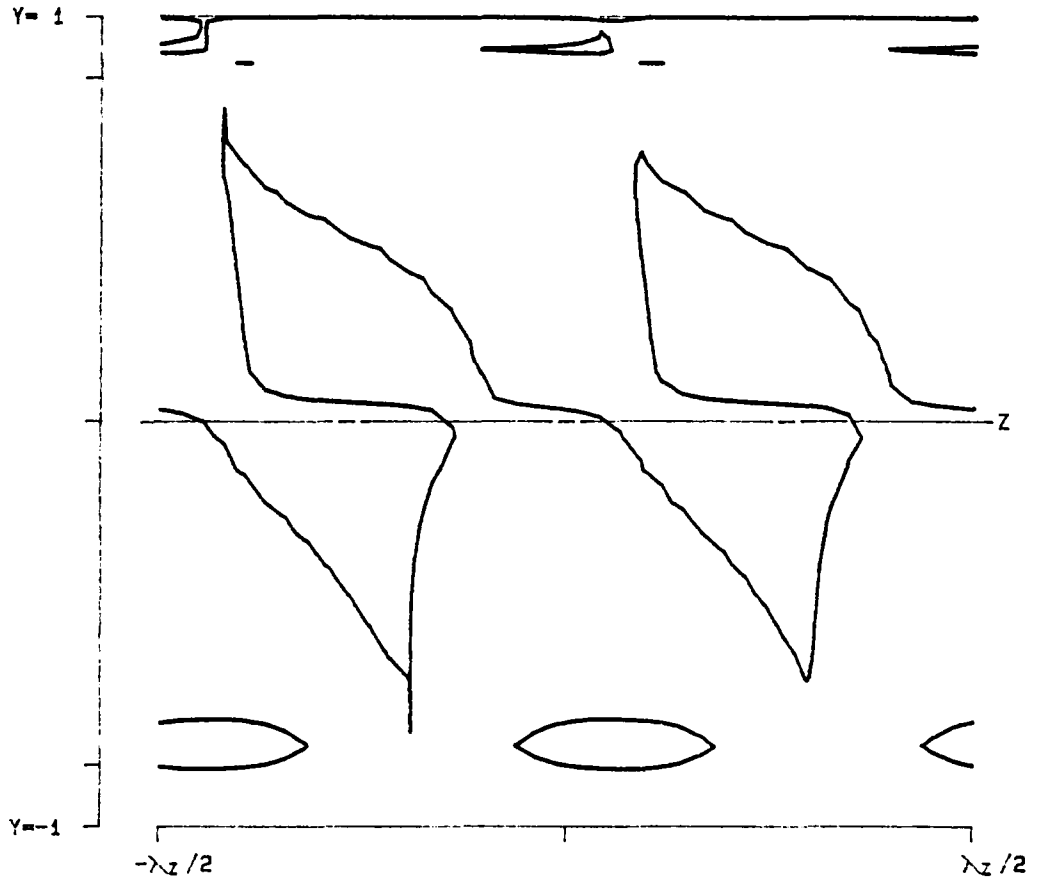

PPT 3-D S T31 (X, Y, Z)

RE	5000.0	LEVELS: MIN	-0.0002579
ALPHA	1.1200	DIF	0.0000516
BETA	2.0000	NO.	20
SIGMA	0.044449,-0.001926		
RMS	0.025000	X =	5.466141
MAX	0.000748		
SYM	1		

Figure 3.142- $T^{(31)}$ as a function of x, y and z at a position of $x = 2.733071$ for $\mathbf{v}_t$ at $\alpha = 1.12$, $Re = 5000$, $\beta = 2.00$ and $A = 0.025$.

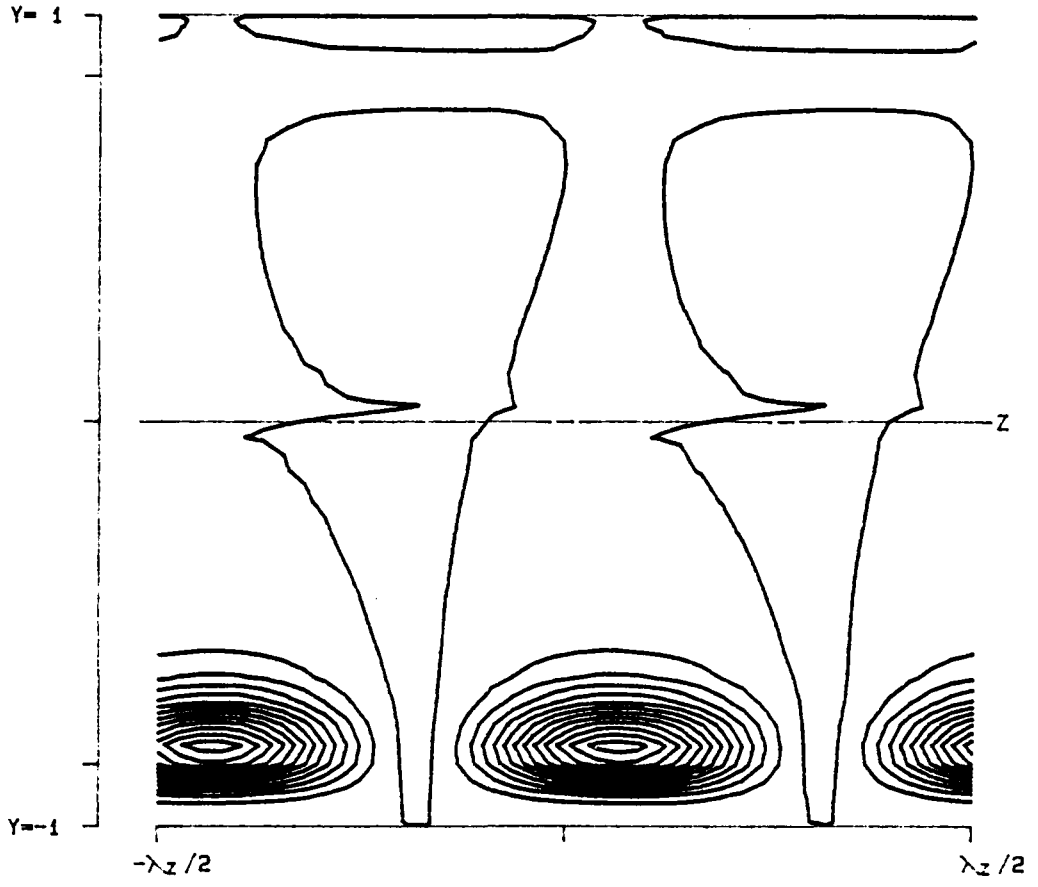

PPT 3-D S T30 (X, Y, Z)

RE	5000.0	LEVELS: MIN	-0.0002579
ALPHA	1.1200	DIF	0.0000516
BETA	2.0000	NO.	20
SIGMA	0.044449,-0.001926		
RMS	0.025000	X =	5.466141
MAX	0.000748		
SYM	1		

Figure 3.143- $T^{(30)}$ as a function of x, y and z at a position of $x = 2.733071$ for $\mathbf{v}_t$ at $\alpha = 1.12$, $Re = 5000$, $\beta = 2.00$ and $A = 0.025$.

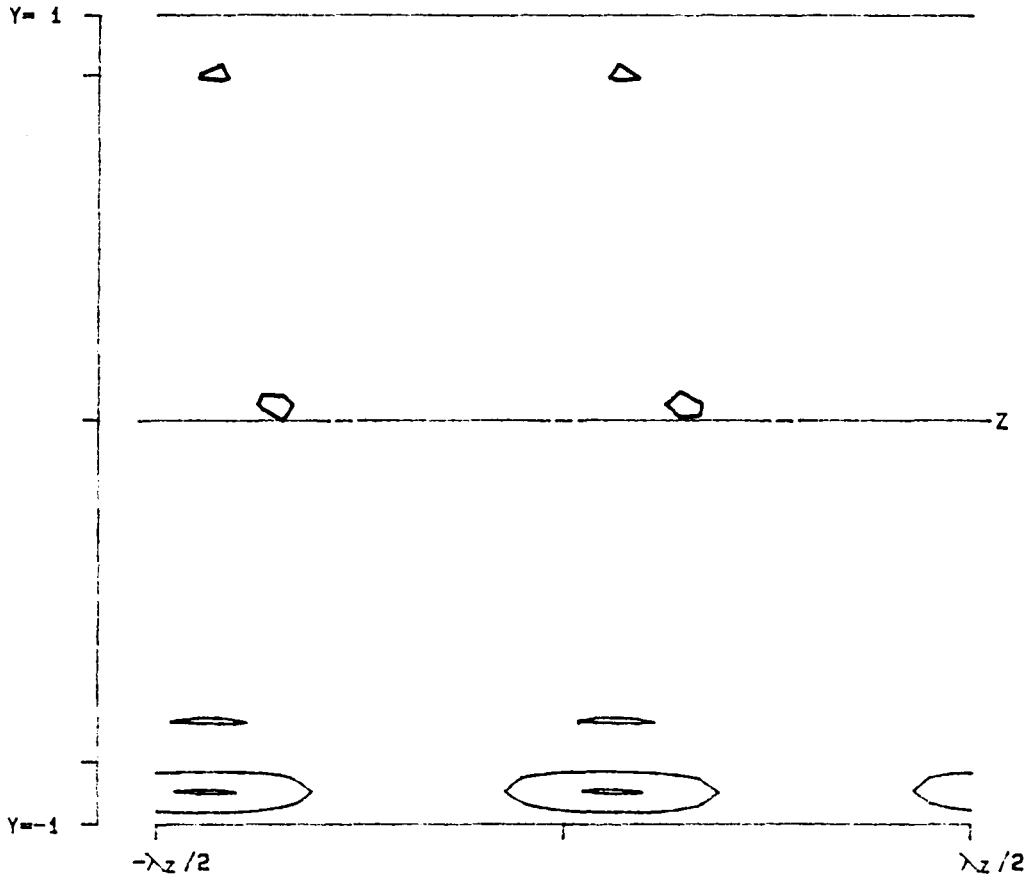

PPT 3-D S D3 (X, Y, Z)

RE	5000.0	LEVELS: MIN	-0.0002579
ALPHA	1.1200	DIF	0.0000516
BETA	2.0000	NO.	20
SIGMA	0.044449,-0.001926		
RMS	0.025000	X =	5.466141
MAX	0.000748		
SYM	1		

Figure 3.144- $D^{(3)}$ as a function of x, y and z at a position of $x = 2.733071$ for **v**, at $\alpha = 1.12$, $Re = 5000$, $\beta = 2.00$ and $A = 0.025$.

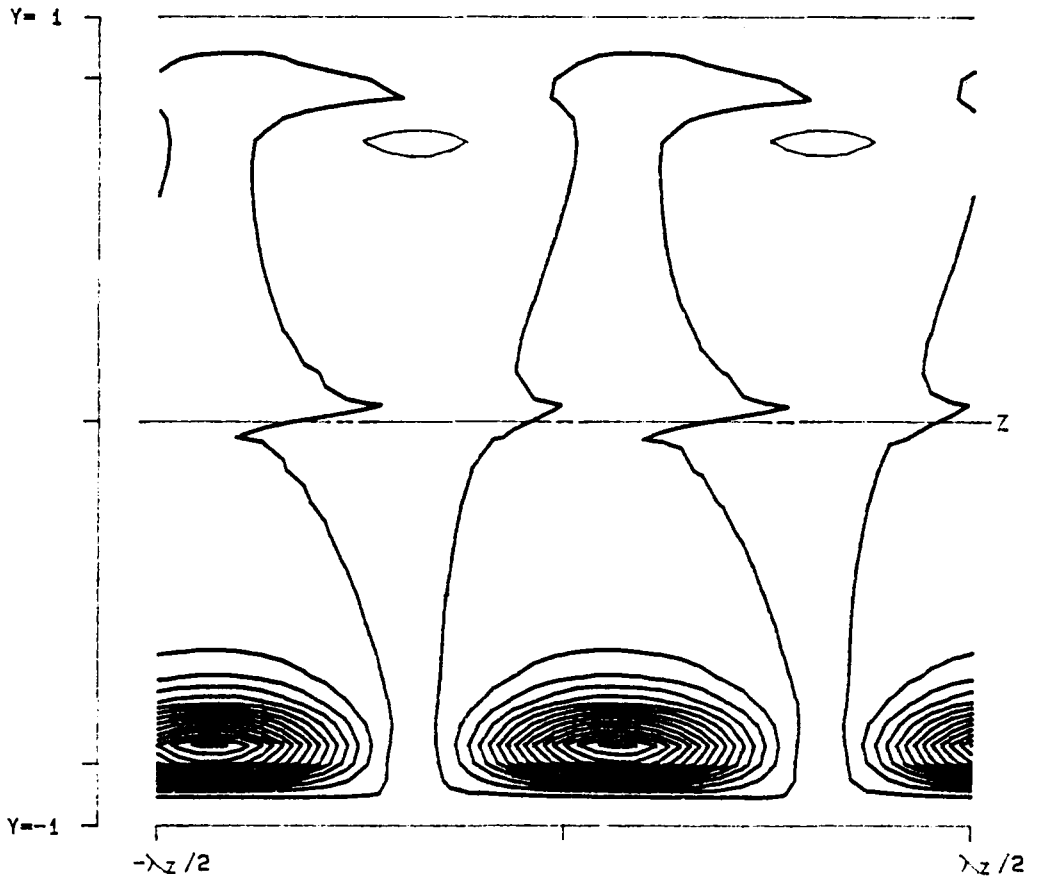

PPT 3-D S P3 (X, Y, Z)

RE	5000.0	LEVELS: MIN	-0.0002579
ALPHA	1.1200	DIF	0.0000516
BETA	2.0000	NO.	20
SIGMA	0.044449,-0.001926		
RMS	0.025000	X =	5.466141
MAX	0.000748		
SYM	1		

Figure 3.145- $P^{(3)}$ as a function of x, y and z at a position of $x = 2.733071$ for **v**, at $\alpha = 1.12$, $Re = 5000$, $\beta = 2.00$ and $A = 0.025$.

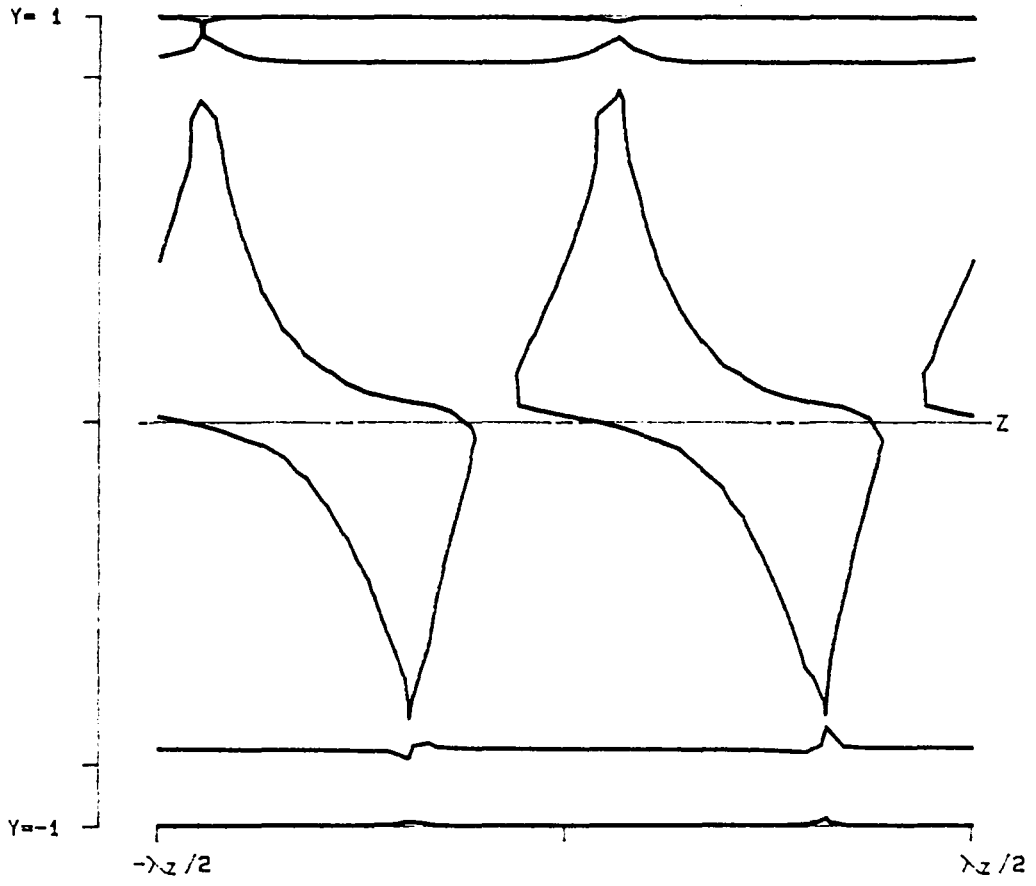

PPT 3-D S T31 (X, Y, Z)

RE	5000.0	LEVELS: MIN	-0.0002579
ALPHA	1.1200	DIF	0.0000516
BETA	2.0000	NO.	20
SIGMA	0.044449,-0.001926		
RMS	0.025000	X =	5.753833
MAX	0.000748		
SYM	1		

Figure 3.146- $T^{(31)}$ as a function of x, y and z at a position of $x = 2.876916$ for $\mathbf{v}_s$ at $\alpha = 1.12$, $Re = 5000$, $\beta = 2.00$ and $A = 0.025$.

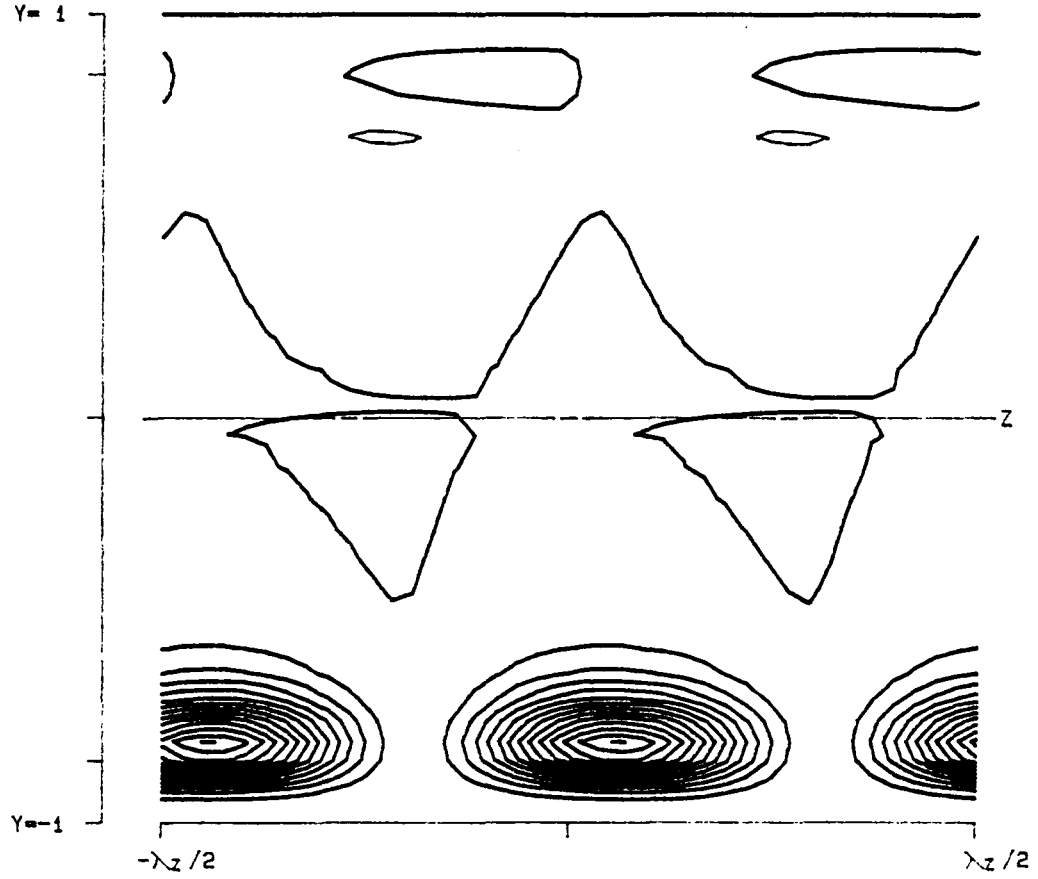

PPT 3-D S T30 (X, Y, Z)

RE	5000.0	LEVELS: MIN	-0.0002579
ALPHA	1.1200	DIF	0.0000516
BETA	2.0000	NO.	20
SIGMA	0.044449,-0.001926		
RMS	0.025000	X =	5.753833
MAX	0.000748		
SYM	1		

Figure 3.147- $T^{(30)}$ as a function of x, y and z at a position of $x = 2.876916$ for $\mathbf{v}_s$ at $\alpha = 1.12$, $Re = 5000$, $\beta = 2.00$ and $A = 0.025$.

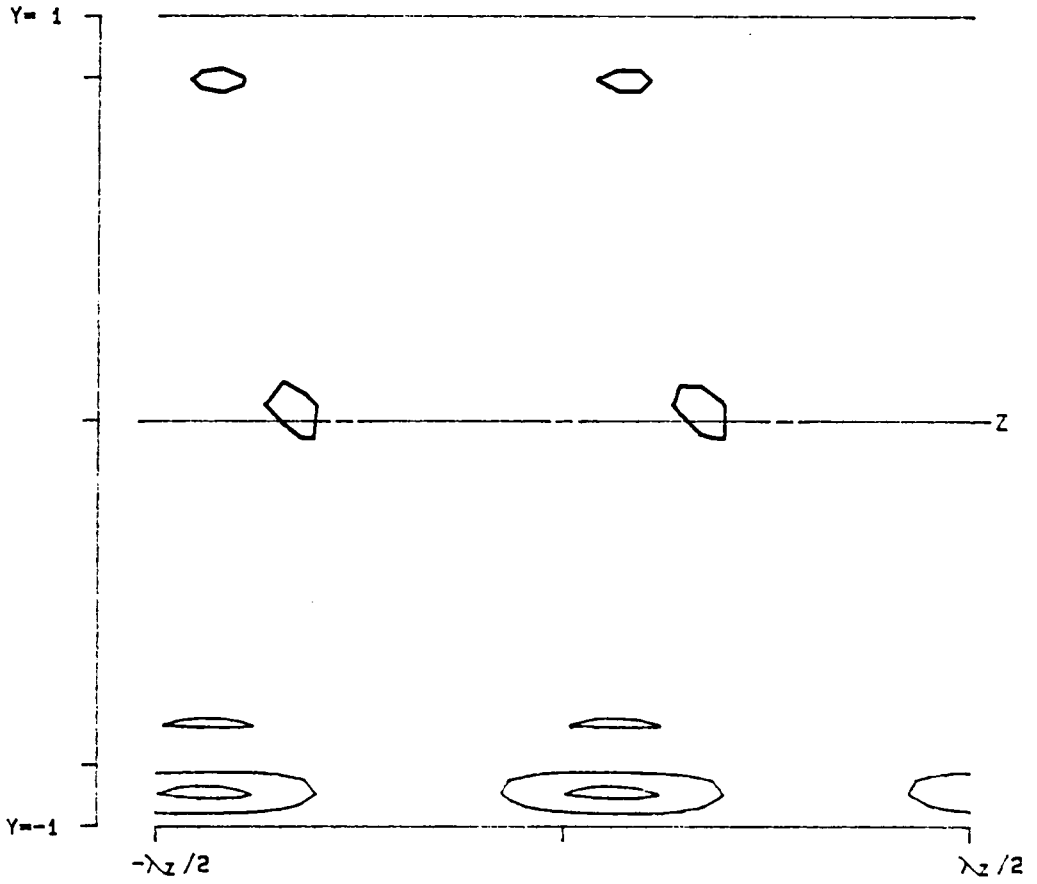

PPT 3-D S D3 (X, Y, Z)

RE	5000.0	LEVELS: MIN	-0.0002579
ALPHA	1.1200	DIF	0.0000516
BETA	2.0000	NO.	20
SIGMA	0.044449,-0.001926		
RMS	0.025000	X =	5.753833
MAX	0.000748		
SYM	1		

Figure 3.148- $D^{(3)}$ as a function of x, y and z at a position of $x = 2.876916$ for $\mathbf{v}_s$ at $\alpha = 1.12$, $Re = 5000$, $\beta = 2.00$ and $A = 0.025$.

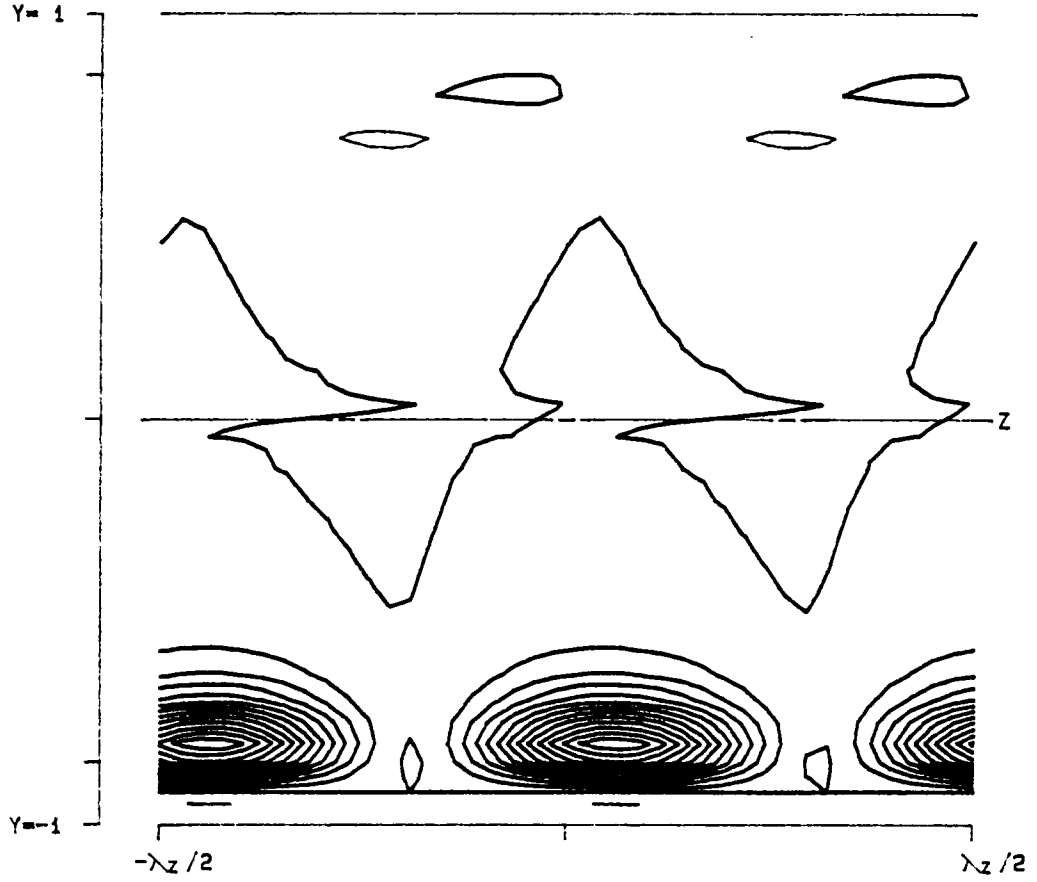

PPT 3-D S P3 (X, Y, Z)

RE	5000.0	LEVELS:	MIN -0.0002579
ALPHA	1.1200		DIF 0.0000516
BETA	2.0000		NO. 20
SIGMA	0.044449,-0.001926		
RMS	0.025000		X = 5.753833
MAX	0.000748		
SYM	1		

Figure 3.149- $P^{(3)}$ as a function of x, y and z at a position of $x = 2.876916$ for $\mathbf{v}$, at $\alpha = 1.12$, $Re = 5000$, $\beta = 2.00$ and $A = 0.025$.

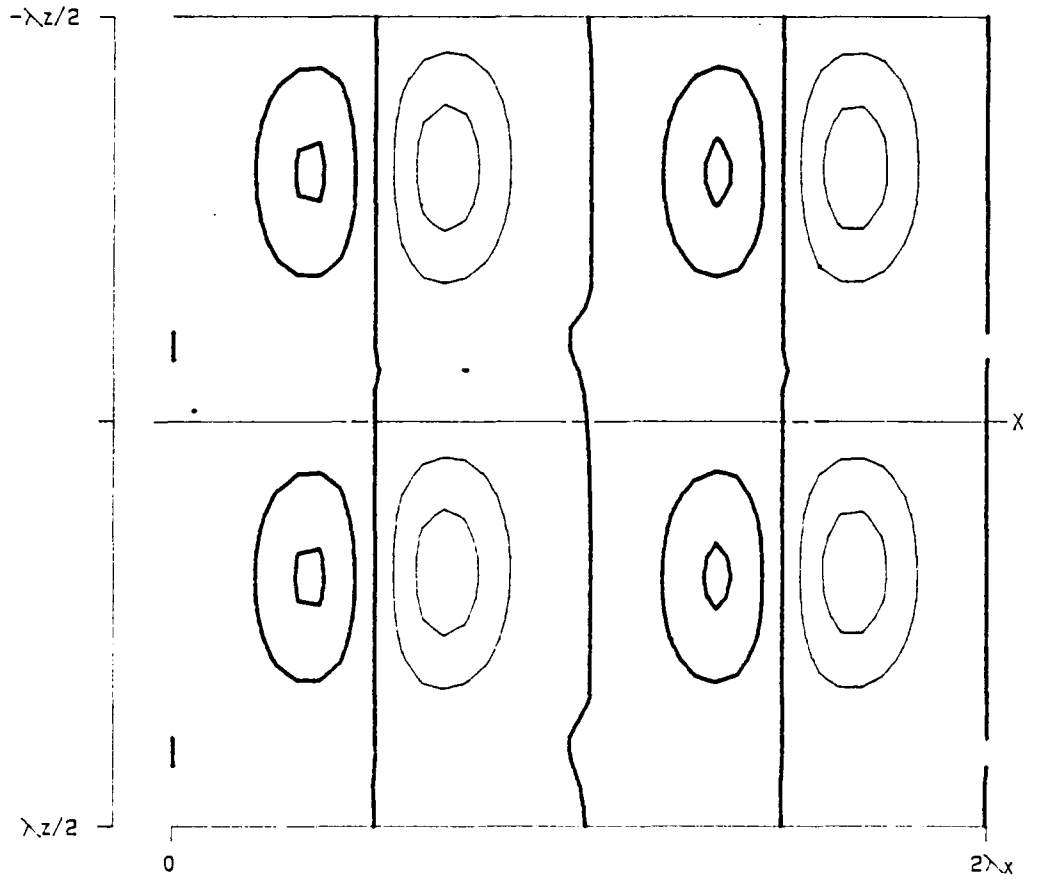

PPT 3-D S T31 (X, Y, Z)

RE	5000.0	LEVELS: MIN	-0.0002579
ALPHA	1.1200	DIF	0.0000516
BETA	2.0000	NO.	20
SIGMA	0.044449,-0.001925		
RMS	0.025000	Y =	0.885456
MAX	0.000748		
SYM	1		

Figure 3.150- $T^{(31)}$ as a function of x, y and z at a position of $y = 0.885456$ for $\mathbf{v}$, at $\alpha = 1.12$, $Re = 5000$, $\beta = 2.00$ and $A = 0.025$.

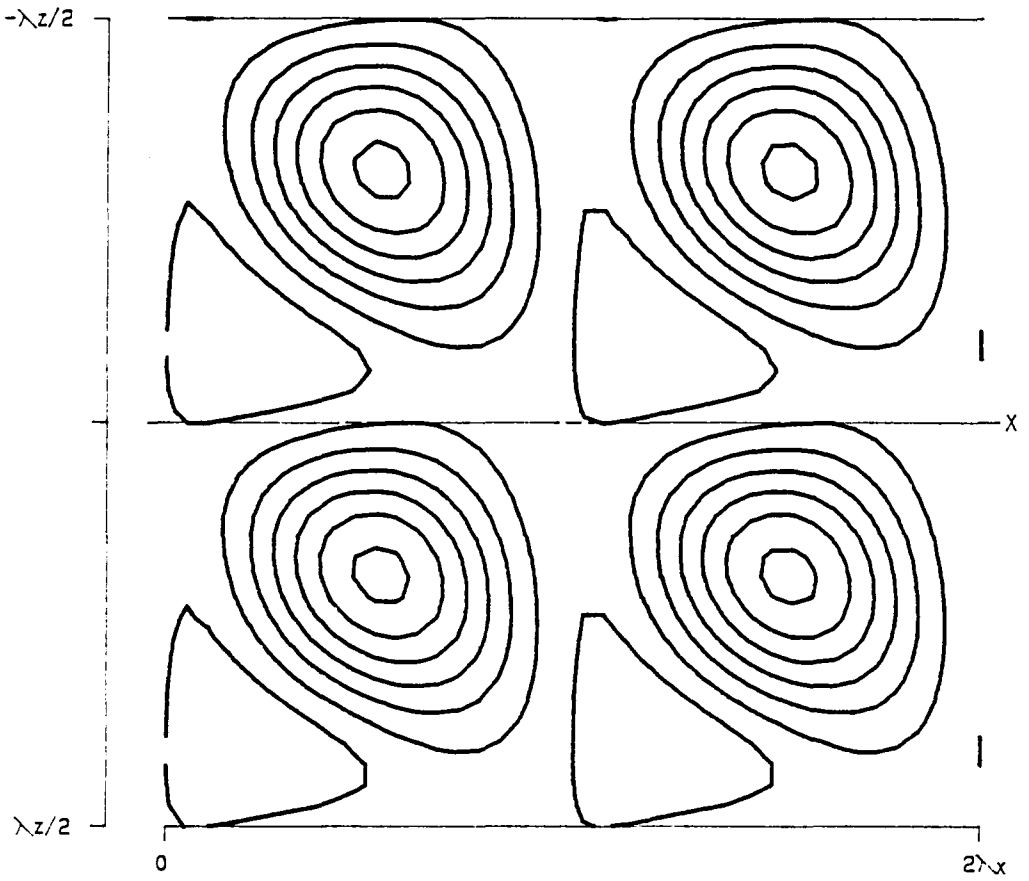

PPT 3-D S T30 (X, Y, Z)

RE	5000.0	LEVELS: MIN	-0.0002579
ALPHA	1.1200	DIF	0.0000516
BETA	2.0000	NO.	20
SIGMA	0.044449,-0.001926		
RMS	0.025000	Y =	0.885456
MAX	0.000748		
SYM	1		

Figure 3.151- $T^{(30)}$ as a function of x, y and z at a position of $y = 0.885456$ for **v**, at $\alpha = 1.12$, $Re = 5000$, $\beta = 2.00$ and $A = 0.025$.

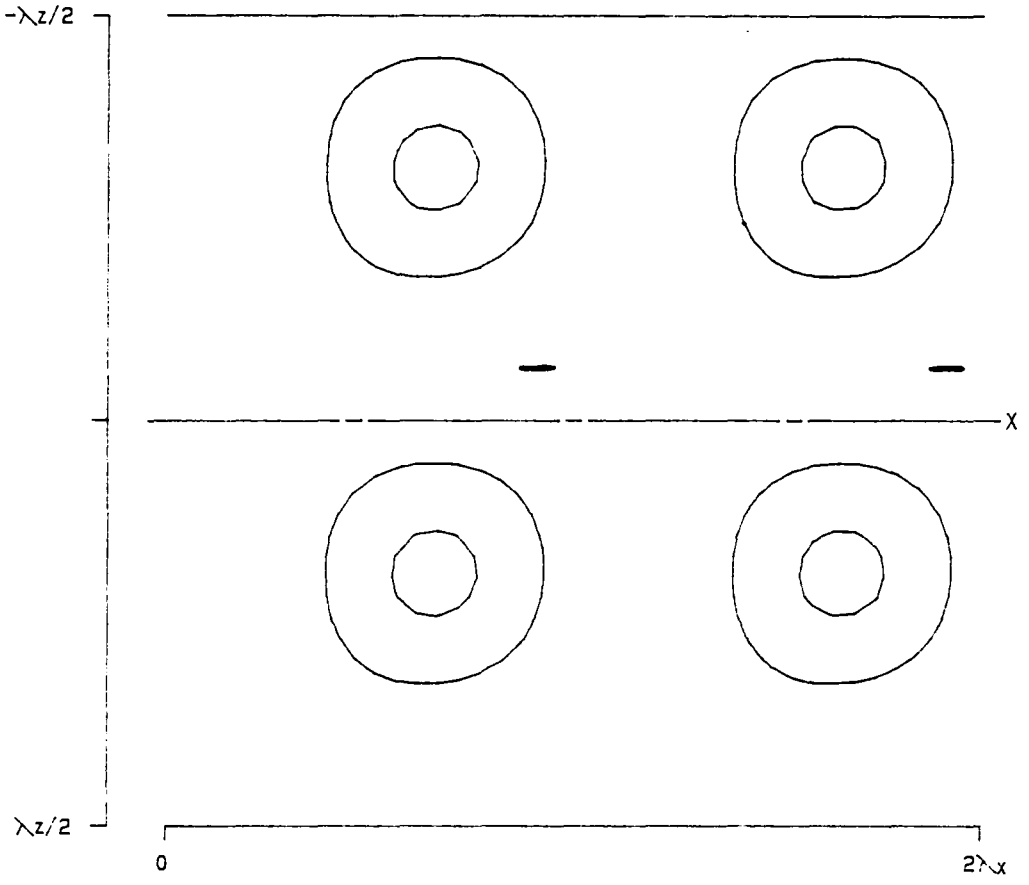

PPT 3-D S D3 (X, Y, Z)

RE	5000.0	LEVELS: MIN	-0.0002579
ALPHA	1.1200	DIF	0.0000516
BETA	2.0000	NC.	20
SIGMA	0.044449,-0.001926		
RMS	0.025000	Y =	0.885456
MAX	0.000748		
SYM	1		

Figure 3.152- $D^{(3)}$ as a function of x, y and z at a position of $y = 0.885456$ for $\mathbf{v}_s$ at $\alpha = 1.12$, $Re = 5000$, $\beta = 2.00$ and $A = 0.025$.

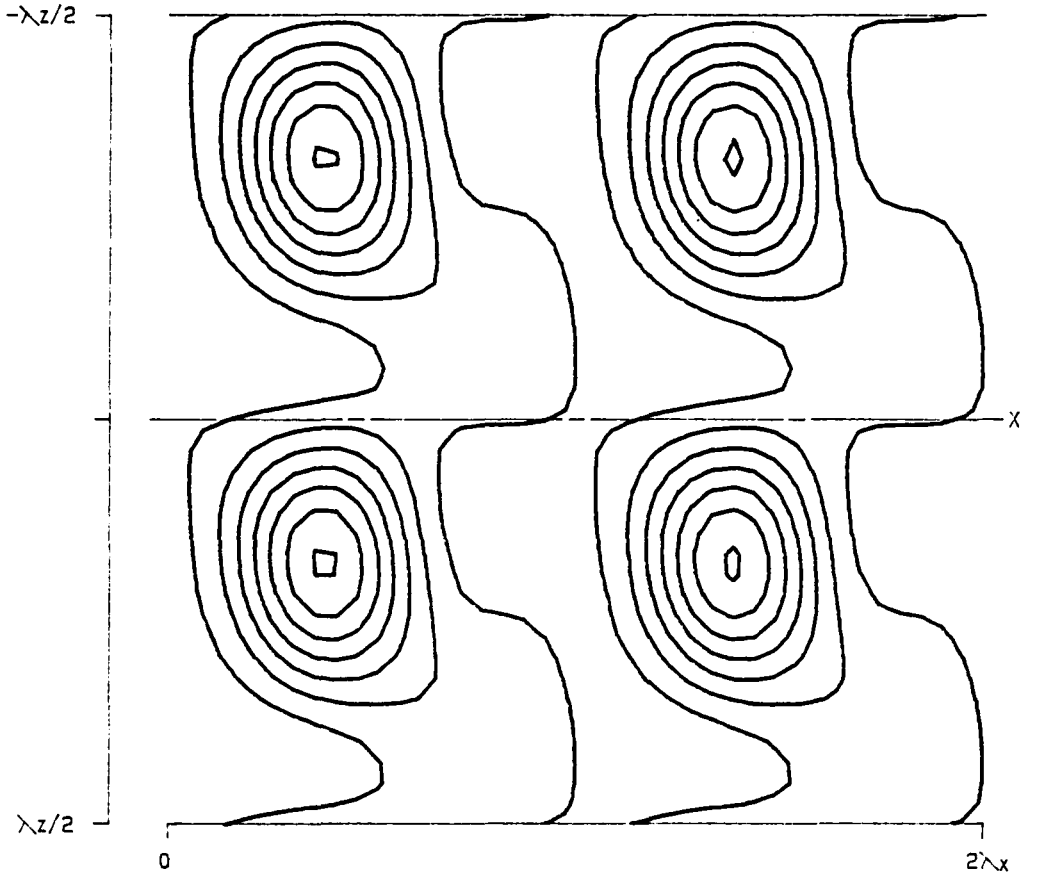

PPT 3-D S P3 (X, Y, Z)

RE	5000.0	LEVELS: MIN	-0.0002579
ALPHA	1.1200	DIF	0.0000516
BETA	2.0000	NO.	20
SIGMA	0.044449,-0.001926		
RMS	0.025000	Y =	0.885456
MAX	0.000748		
SYM	1		

Figure 3.153- $P^{(3)}$ as a function of x, y and z at a position of $y = 0.885456$ for $\mathbf{v}_s$ at $\alpha = 1.12$, $Re = 5000$, $\beta = 2.00$ and $A = 0.025$.

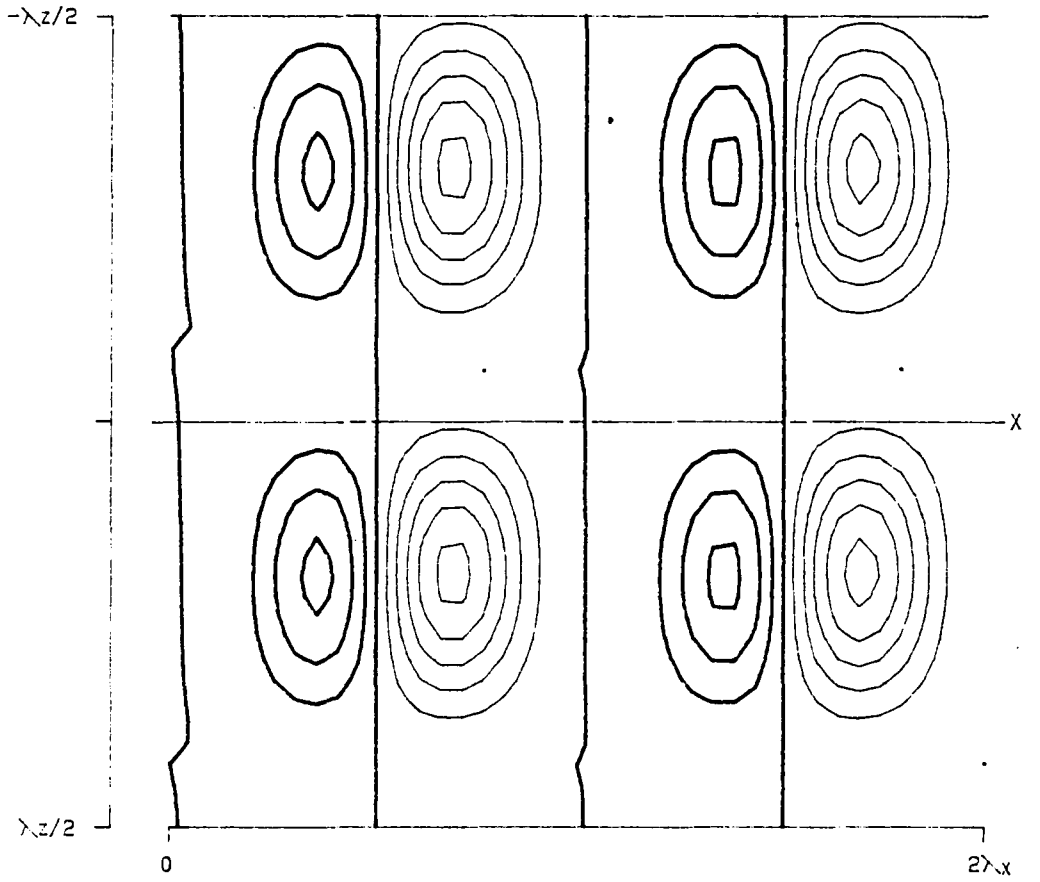

PPT 3-D S T31 (X, Y, Z)

RE	5000.0	LEVELS: MIN	-0.0002579
ALPHA	1.1200	DIF	0.0000516
BETA	2.0000	NO.	20
SIGMA	0.044449,-0.001926		
RMS	0.025000	Y =	0.845190
MAX	0.000748		
SYM	1		

Figure 3.154- $T^{(31)}$ as a function of x, y and z at a position of $y = 0.845190$ for $\mathbf{v}_s$ at $\alpha = 1.12$, $Re = 5000$, $\beta = 2.00$ and $A = 0.025$.

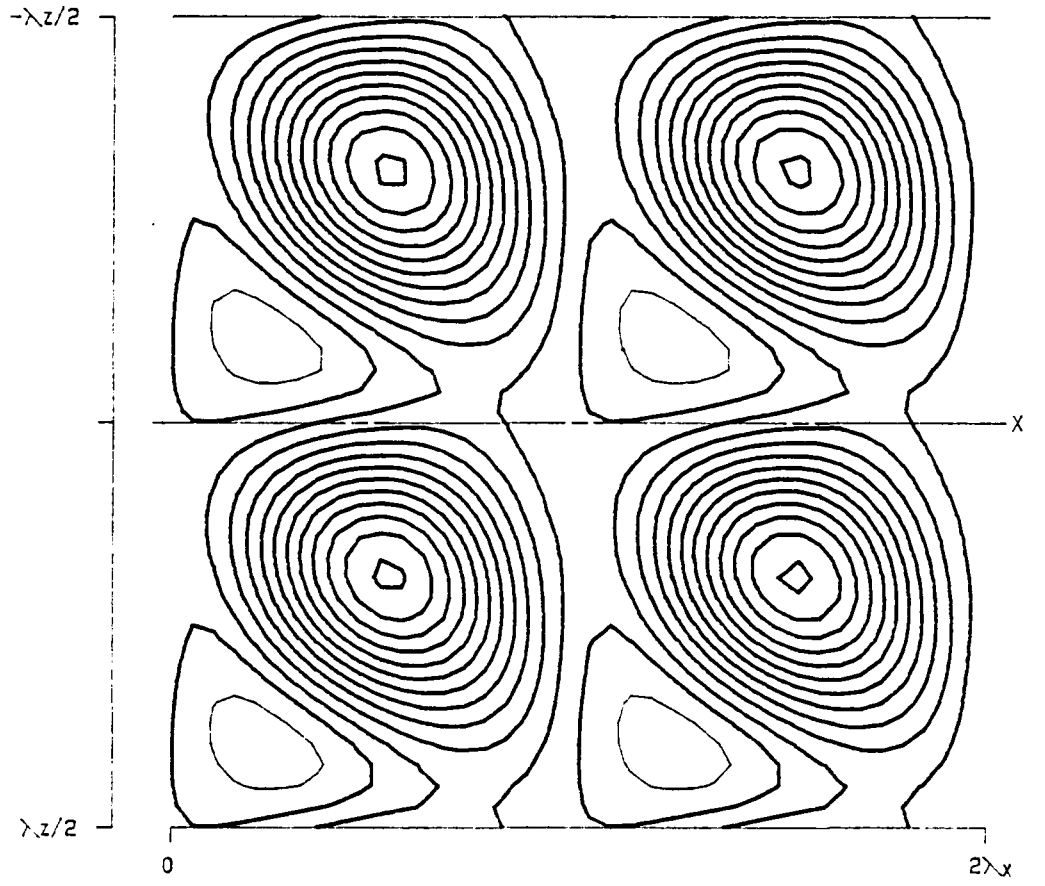

PPT 3-D S T30 (X, Y, Z)

RE	5000.0	LEVELS: MIN	-0.0002579
ALPHA	1.1200	DIF	0.0000516
BETA	2.0000	NO.	20
SIGMA	0.044449,-0.001925		
RMS	0.025000	Y =	0.845190
MAX	0.000748		
SYM	1		

Figure 3.155- $T^{(30)}$ as a function of x, y and z at a position of $y = 0.845190$ for $\mathbf{v}_s$ at $\alpha = 1.12$, $Re = 5000$, $\beta = 2.00$ and $A = 0.025$.

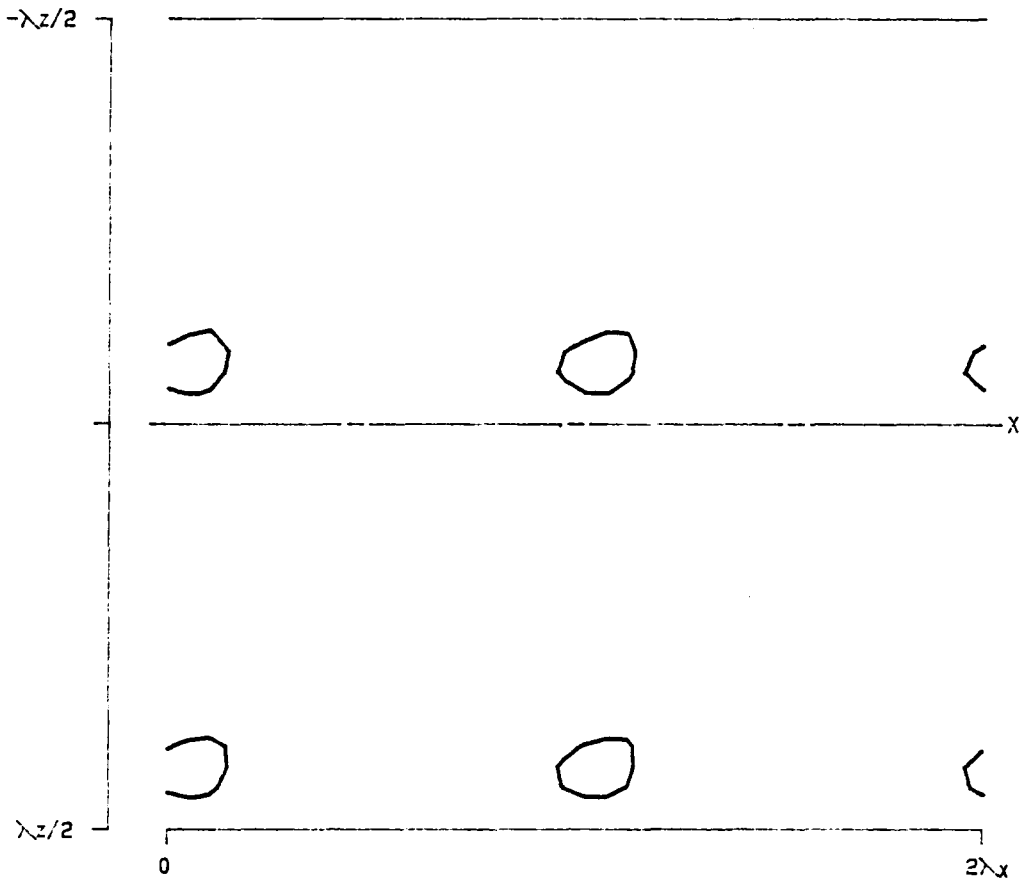

PPT 3-D S D3 (X, Y, Z)

RE	5000.0	LEVELS: MIN	-0.0002579
ALPHA	1.1200	DIF	0.0000516
BETA	2.0000	NO.	20
SIGMA	0.044449,-0.001926		
RMS	0.025000	Y =	0.845190
MAX	0.000748		
SYM	1		

Figure 3.156- $D^{(3)}$ as a function of x, y and z at a position of $y = 0.845190$ for $\mathbf{v}$, at $\alpha = 1.12$, $Re = 5000$, $\beta = 2.00$ and $A = 0.025$.

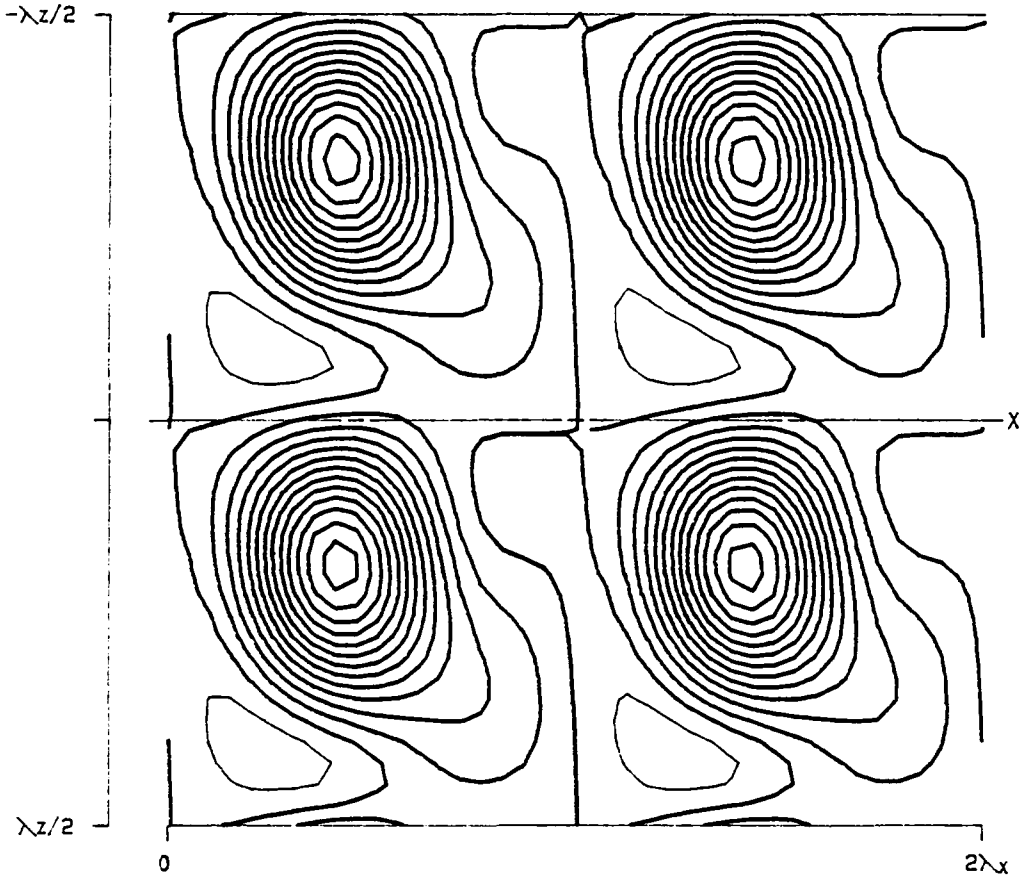

PPT 3-D S P3 (X, Y, Z)

RE	5000.0	LEVELS: MIN	-0.0002579
ALPHA	1.1200	DIF	0.0000516
BETA	2.0000	NO.	20
SIGMA	0.044449,-0.001926		
RMS	0.025000	Y =	0.845190
MAX	0.000748		
SYM	1		

Figure 3.157- $P^{(3)}$ as a function of x, y and z at a position of $y = 0.845190$ for $\mathbf{v}$, at $\alpha = 1.12$, $Re = 5000$, $\beta = 2.00$ and $A = 0.025$.

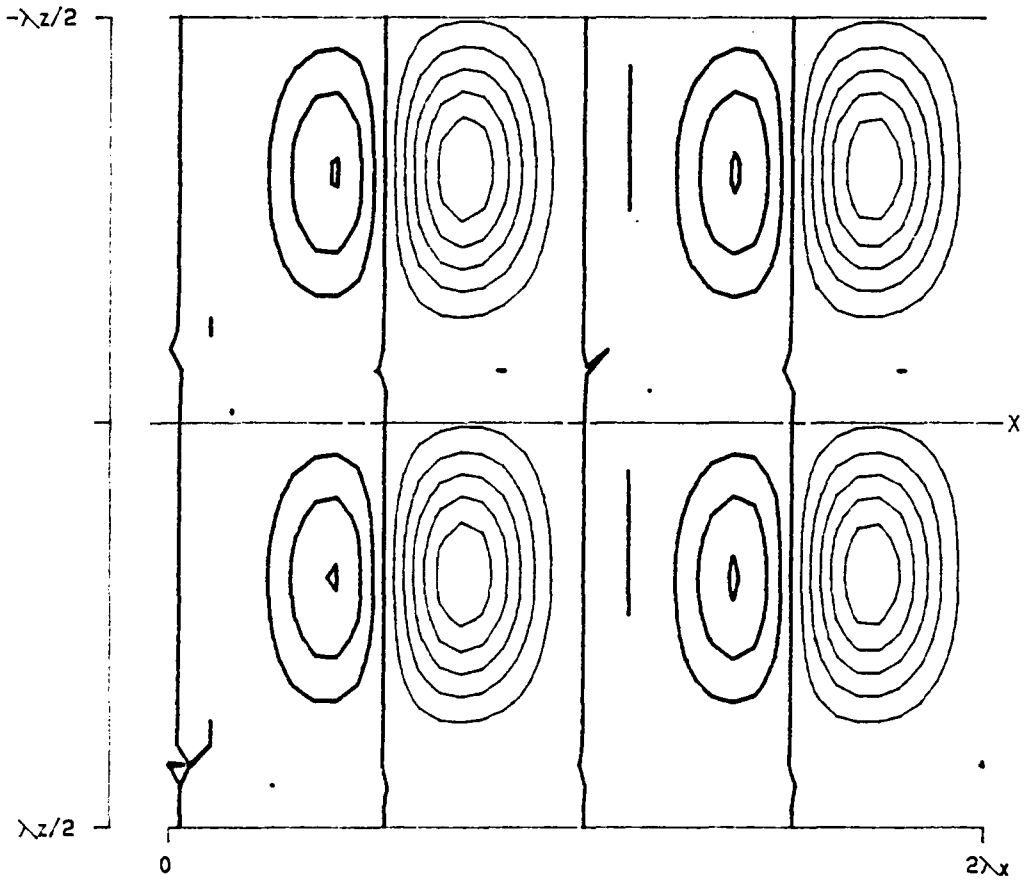

PPT 3-D S T31 (X, Y, Z)

RE	5000.0	LEVELS:	MIN -0.0002579
ALPHA	1.1200		DIF 0.0000516
BETA	2.0000		NO. 20
SIGMA	0.044449,-0.001926		
RMS	0.025000		Y = 0.799443
MAX	0.000748		
SYM	1		

Figure 3.158- $T^{(31)}$ as a function of x, y and z at a position of $y = 0.799443$ for $\mathbf{v}_t$ at $\alpha = 1.12$, $Re = 5000$, $\beta = 2.00$ and $A = 0.025$.

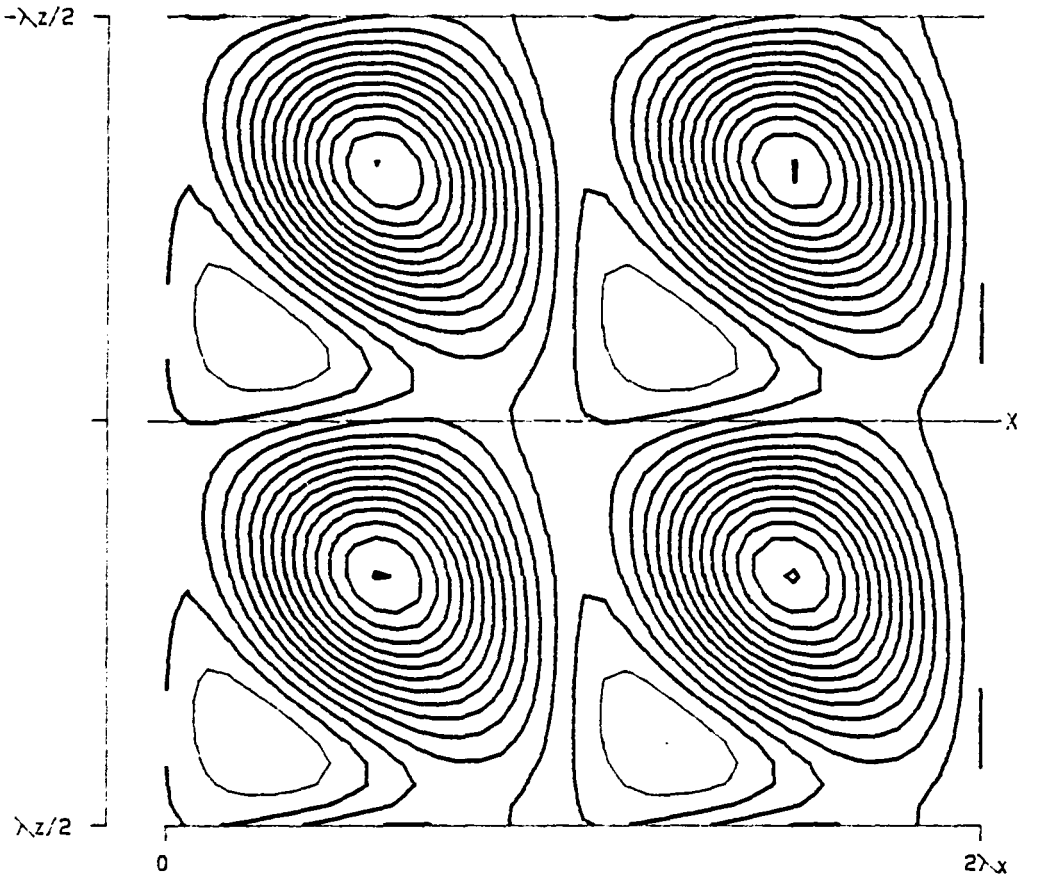

PPT 3-D S T30 (X, Y, Z)

RE	5000.0	LEVELS: MIN	-0.0002579
ALPHA	1.1200	DIF	0.0000516
BETA	2.0000	NO.	20
SIGMA	0.044449,-0.001926		
RMS	0.025000	Y =	0.799443
MAX	0.000748		
SYM	1		

Figure 3.159- $T^{(30)}$ as a function of x, y and z at a position of $y = 0.799443$ for $\mathbf{v}_s$ at $\alpha = 1.12$, $Re = 5000$, $\beta = 2.00$ and $A = 0.025$.

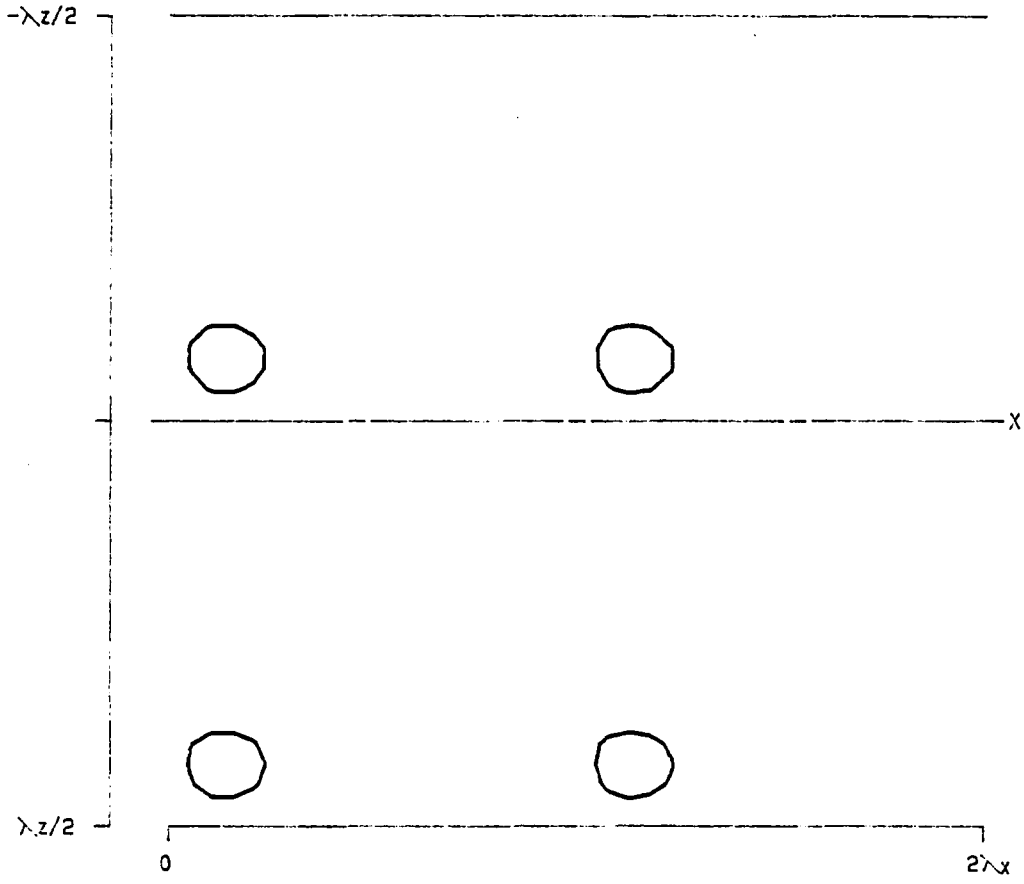

PPT 3-D S D3 (X, Y, Z)

RE	5000.0	LEVELS:	MIN -0.0002579
ALPHA	1.1200		DIF 0.0000516
BETA	2.0000		NO. 20
SIGMA	0.044449,-0.001926		
RMS	0.025000		Y = 0.799443
MAX	0.000748		
SYM	1		

Figure 3.160- $D^{(3)}$ as a function of x, y and z at a position of $y = 0.799443$ for $\mathbf{v}_s$ at $\alpha = 1.12$, $Re = 5000$, $\beta = 2.00$ and $A = 0.025$.

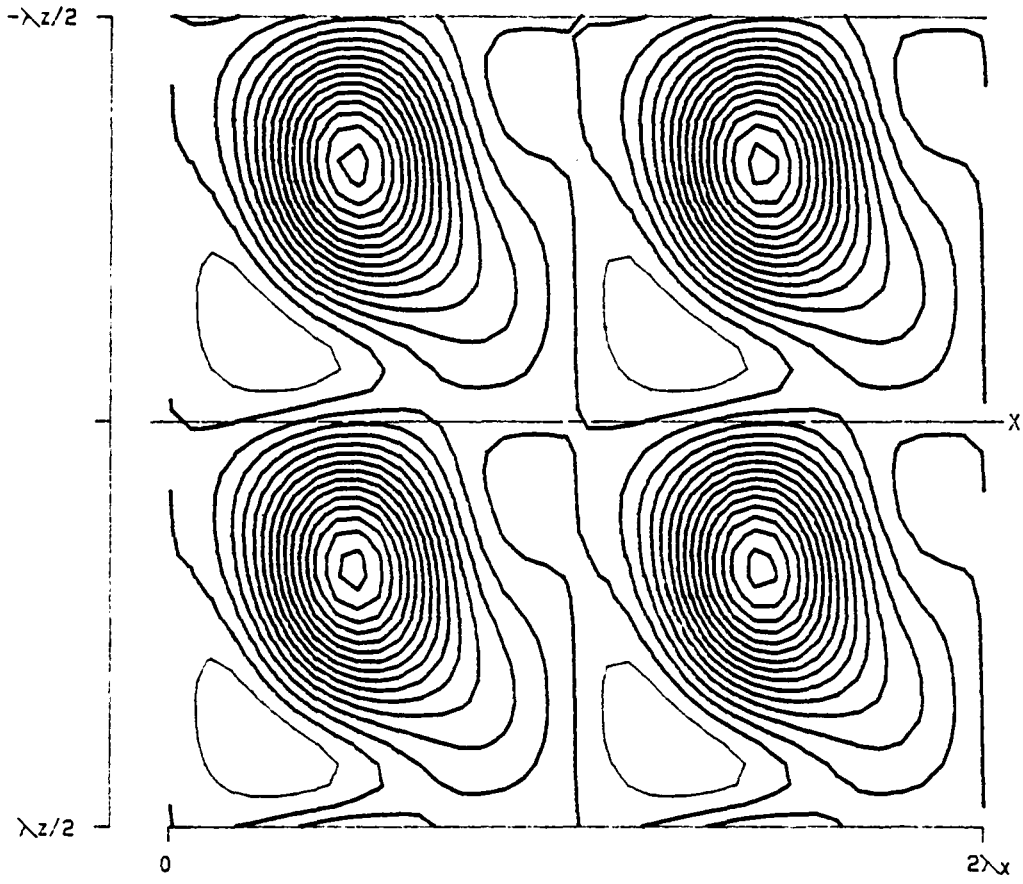

PPT 3-D S P3 (X, Y, Z)

RE	5000.0	LEVELS: MIN	-0.0002579
ALPHA	1.1200	DIF	0.0000516
BETA	2.0000	NO.	20
SIGMA	0.044449,-0.001926		
RMS	0.025000	Y =	0.799443
MAX	0.000748		
SYM	1		

Figure 3.161- $P^{(3)}$ as a function of x, y and z at a position of $y = 0.799443$ for $\mathbf{v}$, at $\alpha = 1.12$, $Re = 5000$, $\beta = 2.00$ and $A = 0.025$.

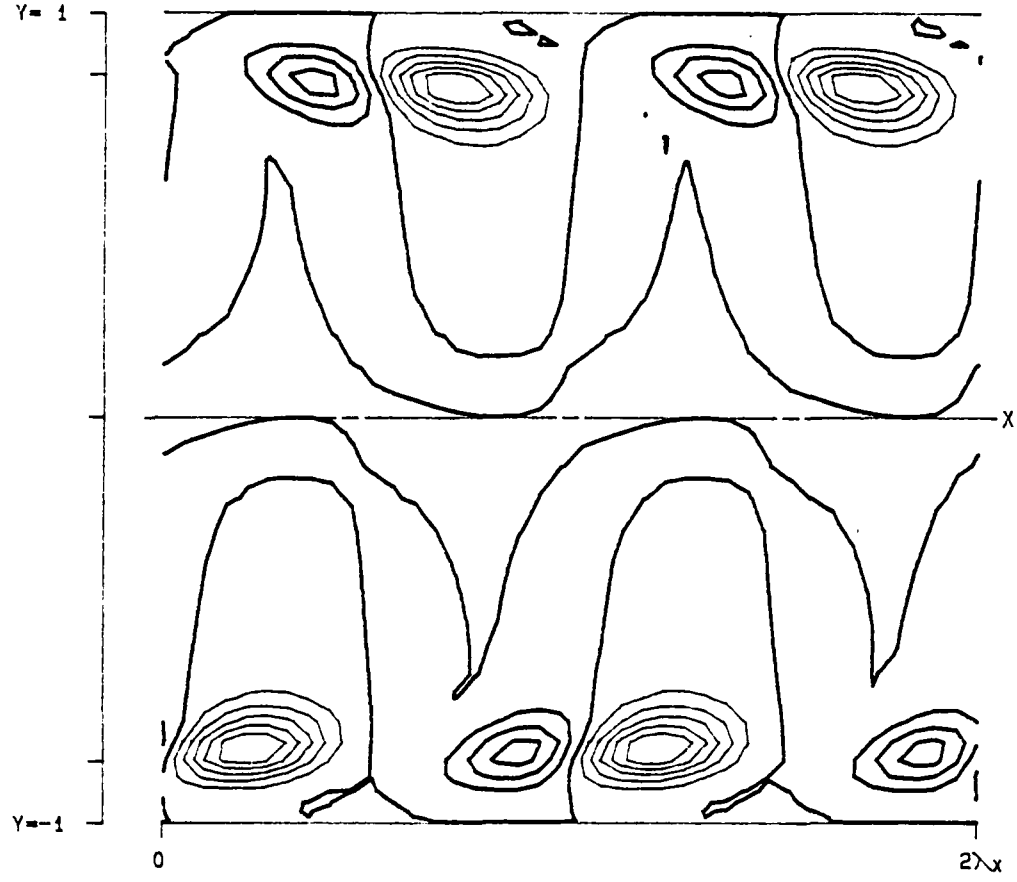

PPT 3-D S T31 (X, Y)

RE	5000.0	LEVELS:	MIN -0.0001229
ALPHA	1.1200		DIF 0.0000246
BETA	2.0000		NO. 20
SIGMA	0.044449,-0.001926		
RMS	0.025000		
MAX	0.000356		
SYM	1		

Figure 3.162- $T^{(31)}$ as a function of x and y for $\mathbf{v}$, at $\alpha = 1.12$, $Re = 5000$, $\beta = 2.00$ and $A = 0.025$.

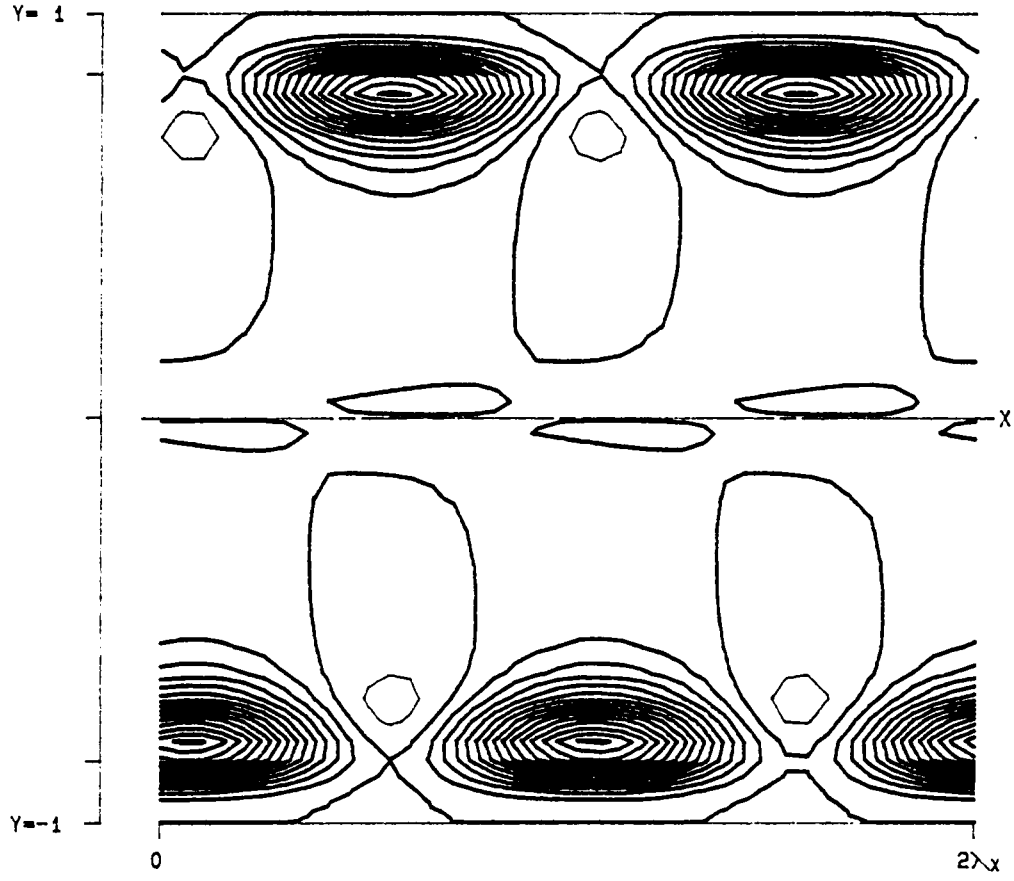

PPT 3-D S T30 (X, Y)

RE	5000.0	LEVELS: MIN	-0.0001229
ALPHA	1.1200	DIF	0.0000246
BETA	2.0000	NO.	20
SIGMA	0.044449,-0.001926		
RMS	0.025000		
MAX	0.000356		
SYM	1		

Figure 3.163- $T^{(30)}$ as a function of x and y for $\mathbf{v}_t$ at $\alpha = 1.12$, $Re = 5000$, $\beta = 2.00$ and $A = 0.025$.

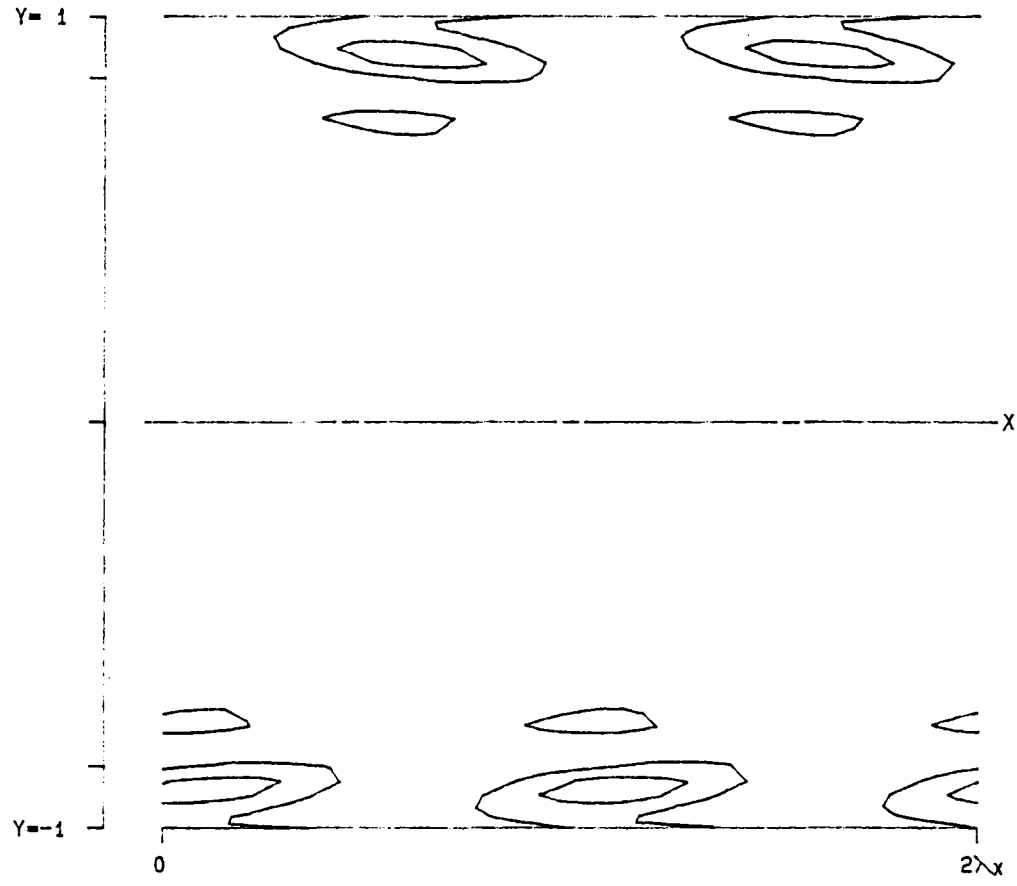

PPT 3-D S D3 (X, Y)

RE	5000.0	LEVELS: MIN	-0.0001229
ALPHA	1.1200	DIF	0.0000246
BETA	2.0000	NO.	20
SIGMA	0.044449,-0.001926		
RMS	0.025000		
MAX	0.000356		
SYM	1		

Figure 3.164- $D^{(3)}$ as a function of x and y for $\mathbf{v}$, at $\alpha = 1.12$, $Re = 5000$, $\beta = 2.00$ and $A = 0.025$.

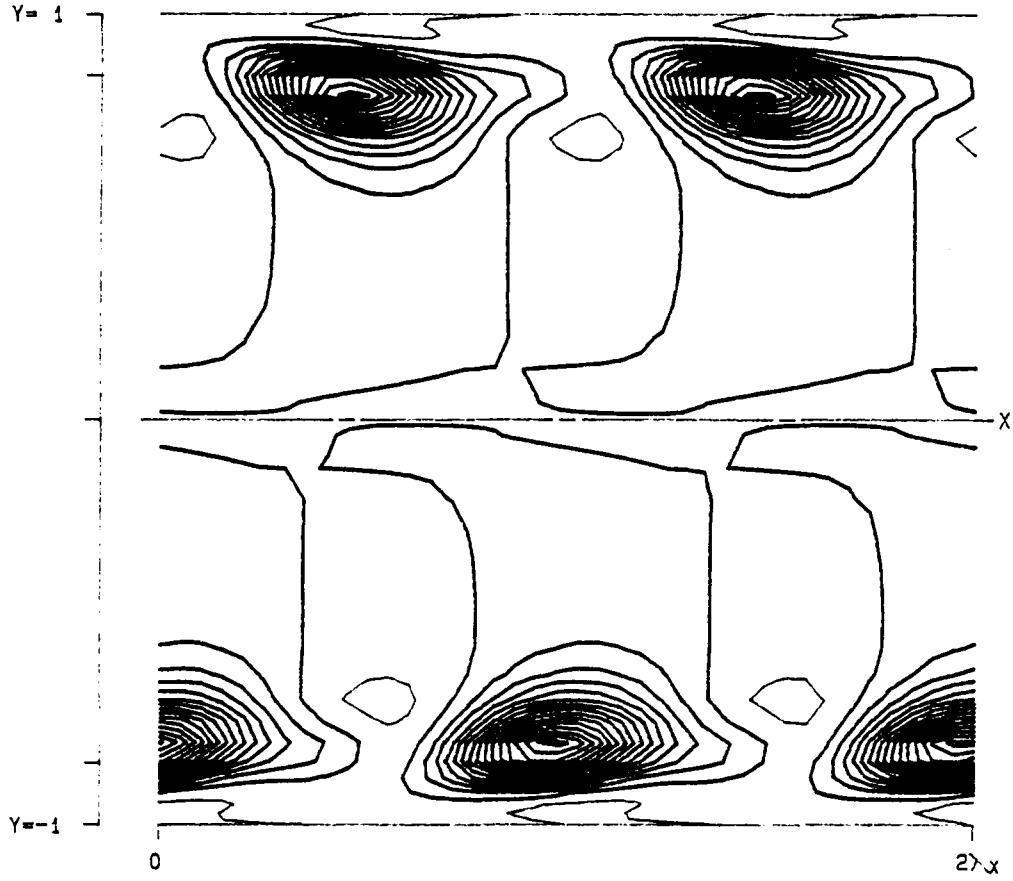

PPT 3-D S P3 (X, Y)

RE	5000.0	LEVELS:	MIN -0.0001229
ALPHA	1.1200		DIF 0.0000246
BETA	2.0000		NO. 20
SIGMA	0.044449,-0.001926		
RMS	0.025000		
MAX	0.000356		
SYM	1		

Figure 3.165- $P^{(3)}$ as a function of x and y for $\mathbf{v}_s$ at $\alpha = 1.12$, $Re = 5000$, $\beta = 2.00$ and $A = 0.025$.

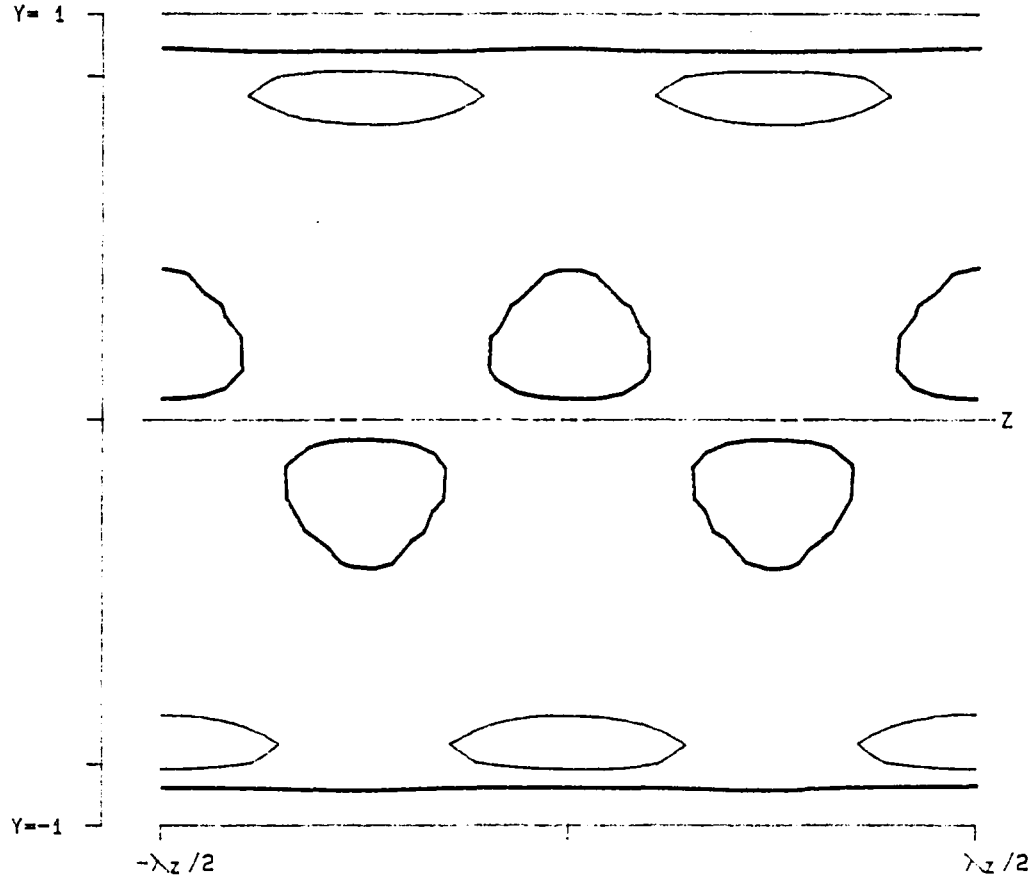

PPT 3-D S T31 (Y, Z)

RE	5000.0	LEVELS:	MIN -0.0000997
ALPHA	1.1200		DIF 0.0000199
BETA	2.0000		NO. 20
SIGMA	0.044449,-0.001926		
RMS	0.025000		
MAX	0.000289		
SYM	1		

Figure 3.166- $T^{(31)}$ as a function of y and z for $\mathbf{v}_s$ at $\alpha = 1.12$, $Re = 5000$, $\beta = 2.00$ and $A = 0.025$.

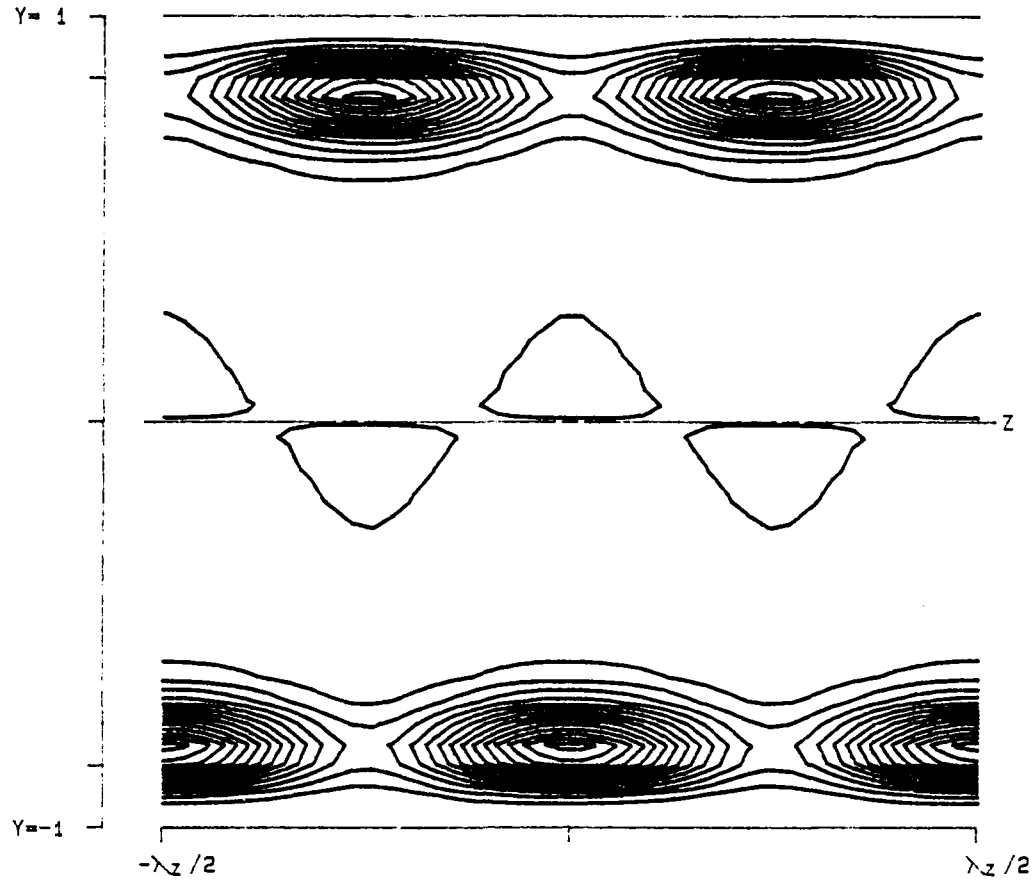

PPT 3-D S T30 (Y, Z)

RE	5000.0	LEVELS: MIN	-0.0000997
ALPHA	1.1200	DIF	0.0000199
BETA	2.0000	NO.	20
SIGMA	0.044449,-0.001926		
RMS	0.025000		
MAX	0.000289		
SYM	1		

Figure 3.167- $T^{(30)}$ as a function of y and z for $\mathbf{v}_s$ at $\alpha = 1.12$, $Re = 5000$, $\beta = 2.00$ and $A = 0.025$.

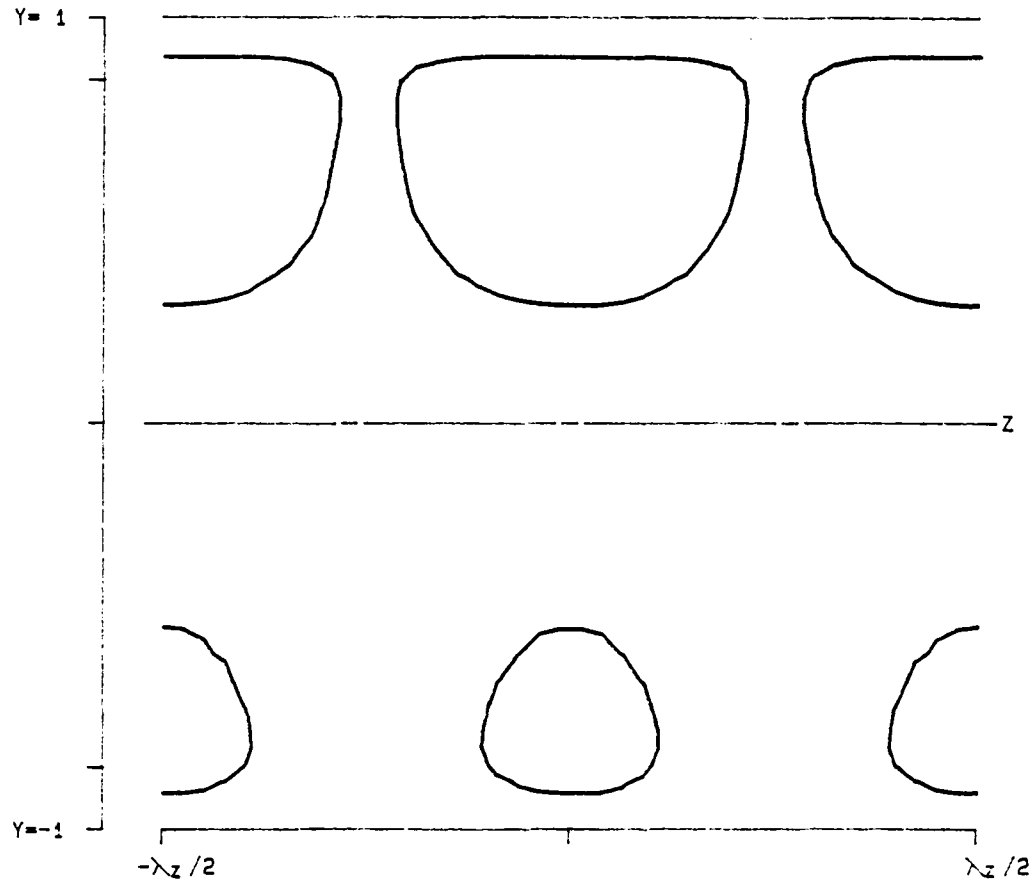

PPT 3-D S D3 (Y, Z)

RE	5000.0	LEVELS: MIN	-0.0000997
ALPHA	1.1200	DIF	0.0000199
BETA	2.0000	NO.	20
SIGMA	0.044449,-0.001926		
RMS	0.025000		
MAX	0.000289		
SYM	1		

Figure 3.168- $D^{(3)}$ as a function of y and z for $\mathbf{v}_s$ at $\alpha = 1.12$, $Re = 5000$, $\beta = 2.00$ and $A = 0.025$.

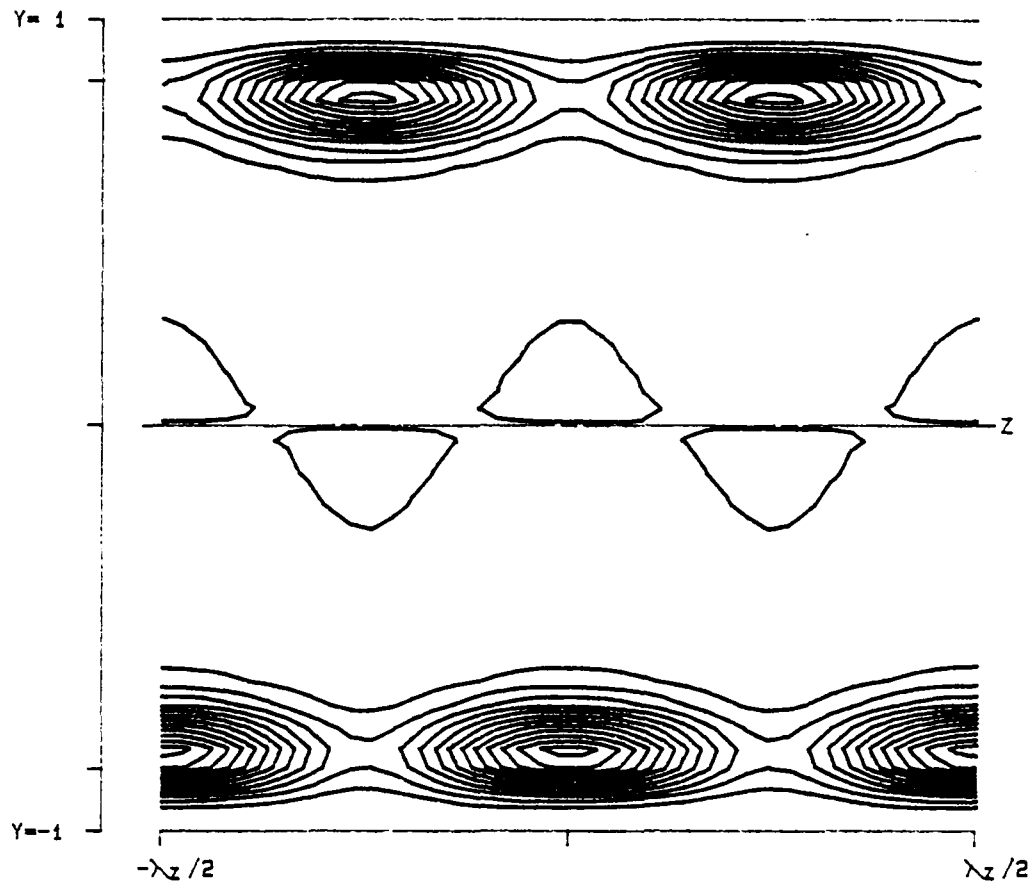

PPT 3-D S P3 (Y, Z)

RE	5000.0	LEVELS:	MIN -0.0000997
ALPHA	1.1200		DIF 0.0000199
BETA	2.0000		NO. 20
SIGMA	0.044449,-0.001926		
RMS	0.025000		
MAX	0.000289		
SYM	1		

Figure 3.169- $P^{(3)}$ as a function of y and z for $\mathbf{v}_s$ at $\alpha = 1.12$, $Re = 5000$, $\beta = 2.00$ and $A = 0.025$.

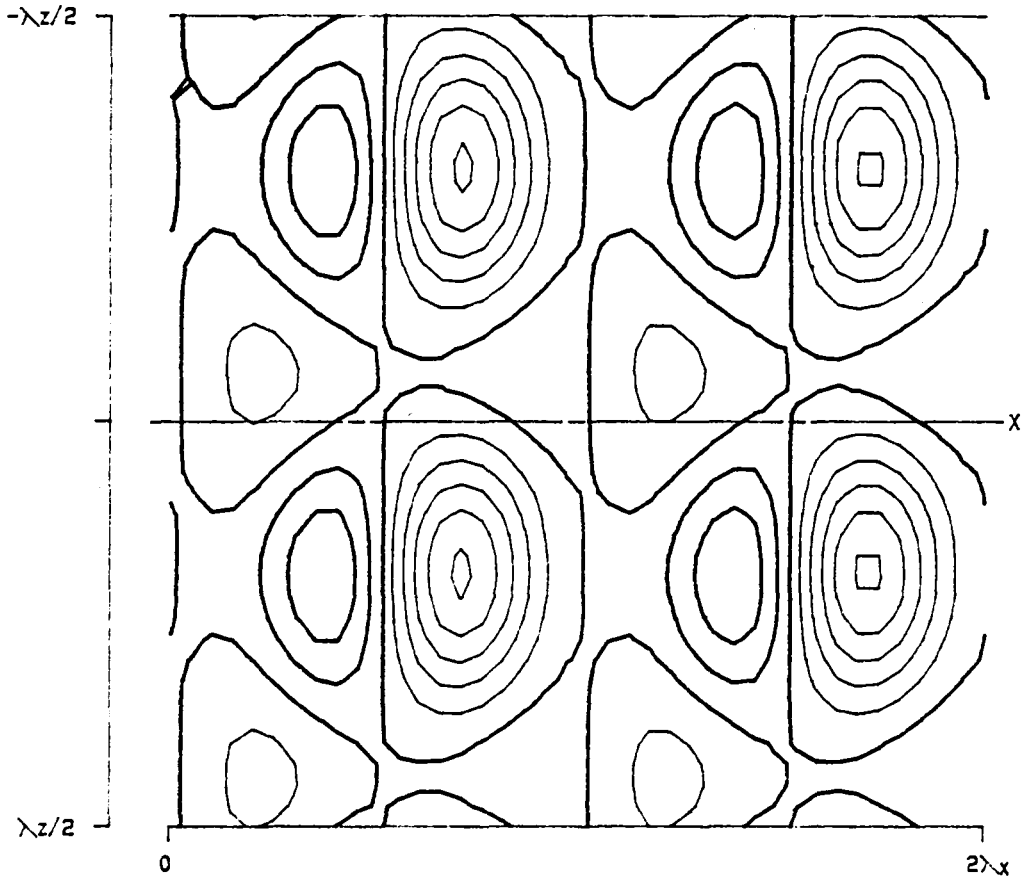

PPT 3-D S T31 (X, Z)

RE	5000.0	LEVELS:	MIN -0.0000357
ALPHA	1.1200		DIF 0.0000071
BETA	2.0000		NO. 20
SIGMA	0.044449,-0.001926		
RMS	0.025000		
MAX	0.000104		
SYM	1		

Figure 3.170- $T^{(31)}$ as a function of x and z for $\mathbf{v}$, at $\alpha = 1.12$, $Re = 5000$, $\beta = 2.00$ and $A = 0.025$.

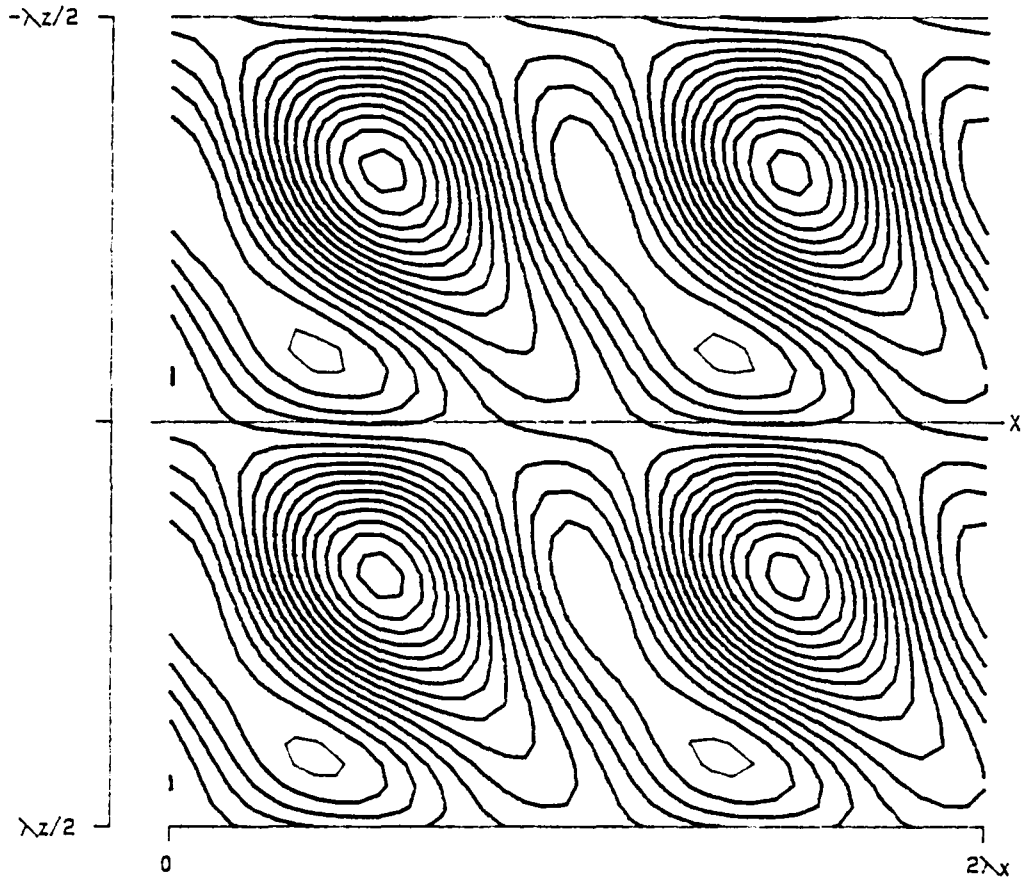

PPT 3-D S T30 (X, Z)

RE	5000.0	LEVELS:	MIN -0.0000357
ALPHA	1.1200		DIF 0.0000071
BETA	2.0000		NO. 20
SIGMA	0.044449,-0.001926		
RMS	0.025000		
MAX	0.000104		
SYM	1		

Figure 3.171- $T^{(30)}$ as a function of x and z for $\mathbf{v}_s$ at $\alpha = 1.12$, $Re = 5000$, $\beta = 2.00$ and $A = 0.025$.

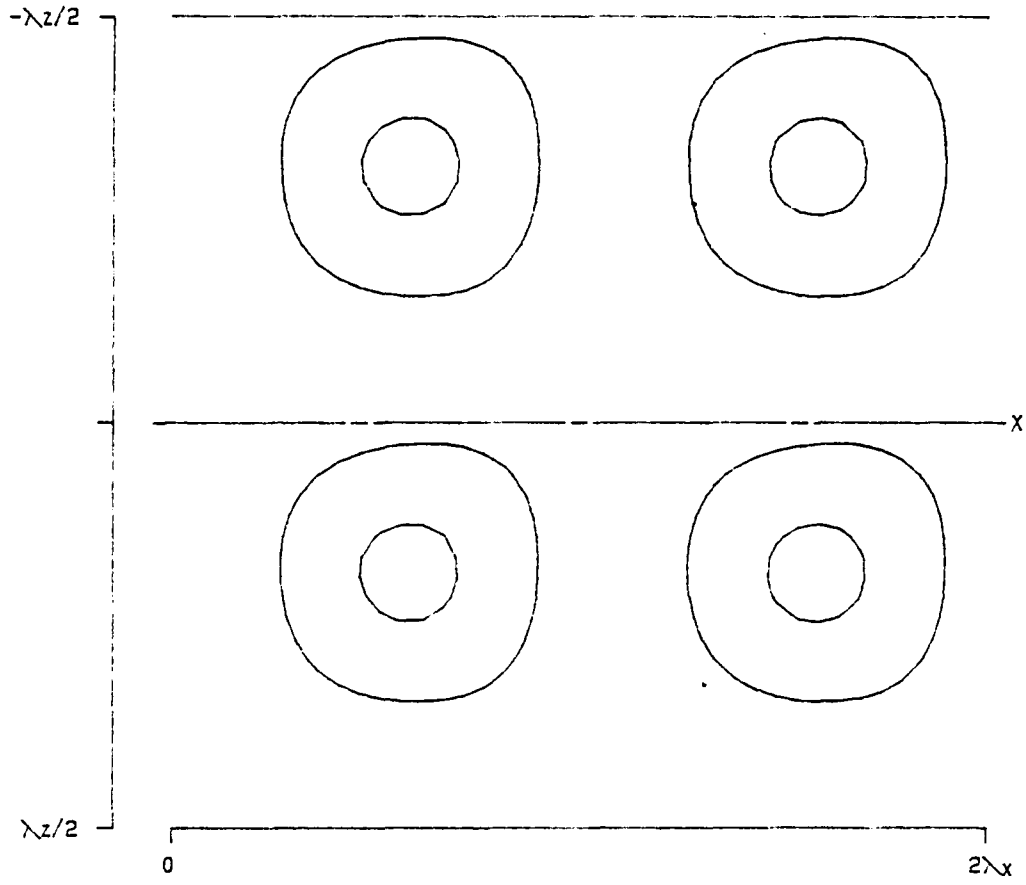

PPT 3-D S D3 (X, Z)

RE	5000.0	LEVELS: MIN	-0.0000357
ALPHA	1.1200	DIF	0.0000071
BETA	2.0000	NO.	20
SIGMA	0.044449,-0.001926		
RMS	0.025000		
MAX	0.000104		
SYM	1		

Figure 3.172- $D^{(3)}$ as a function of x and z for $\mathbf{v}_s$ at $\alpha = 1.12$, $Re = 5000$, $\beta = 2.00$ and $A = 0.025$.

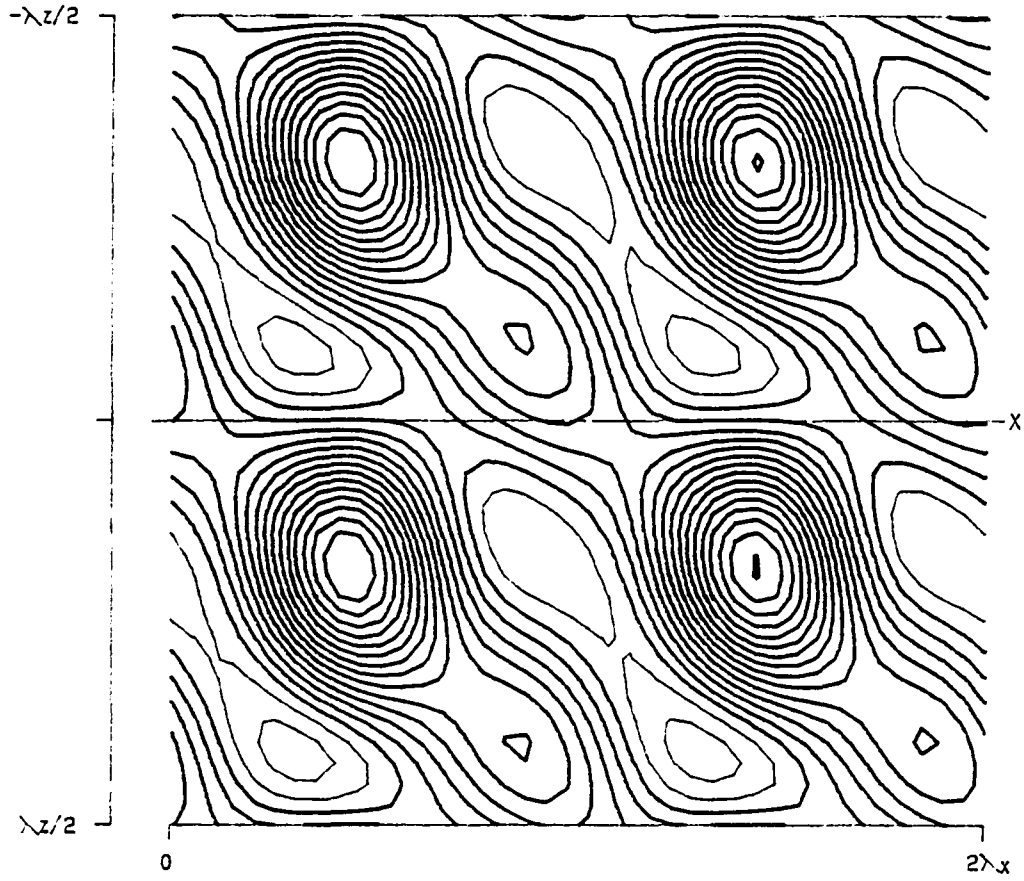

PPT 3-D S P3 (X, Z)

RE	5000.0	LEVELS: MIN	-0.0000357
ALPHA	1.1200	DIF	0.0000071
BETA	2.0000	NO.	20
SIGMA	0.044449,-0.001926		
RMS	0.025000		
MAX	0.000104		
SYM	1		

Figure 3.173- $P^{(3)}$ as a function of x and z for $\mathbf{v}_s$ at $\alpha = 1.12$, $Re = 5000$, $\beta = 2.00$ and $A = 0.025$.

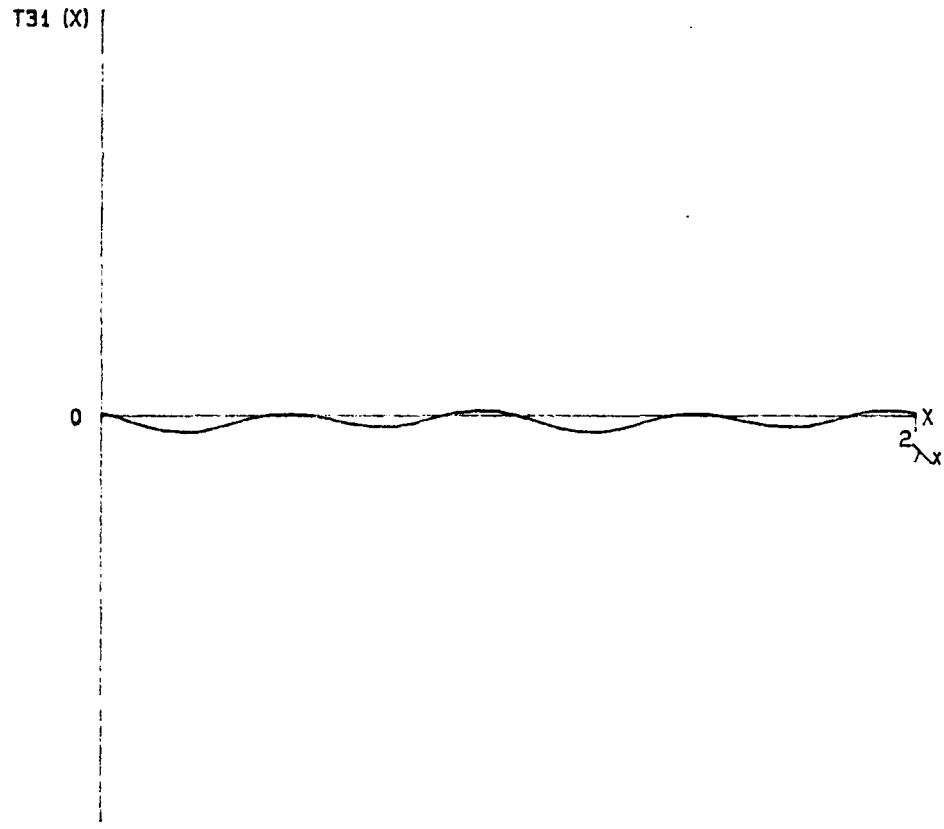

PPT 3-D S T31 (X)

RE	5000.0	SIGMA	0.044449,-0.001926
ALPHA	1.1200	CR	0.281755
BETA	2.0000	MAX	0.0000028
RMS	0.025000	MIN	-0.0000069
SYM	1		

Figure 3.174- $T^{(31)}$ as a function of x for $\mathbf{v}_s$ at $\alpha = 1.12$, $Re = 5000$, $\beta = 2.00$ and $A = 0.025$.

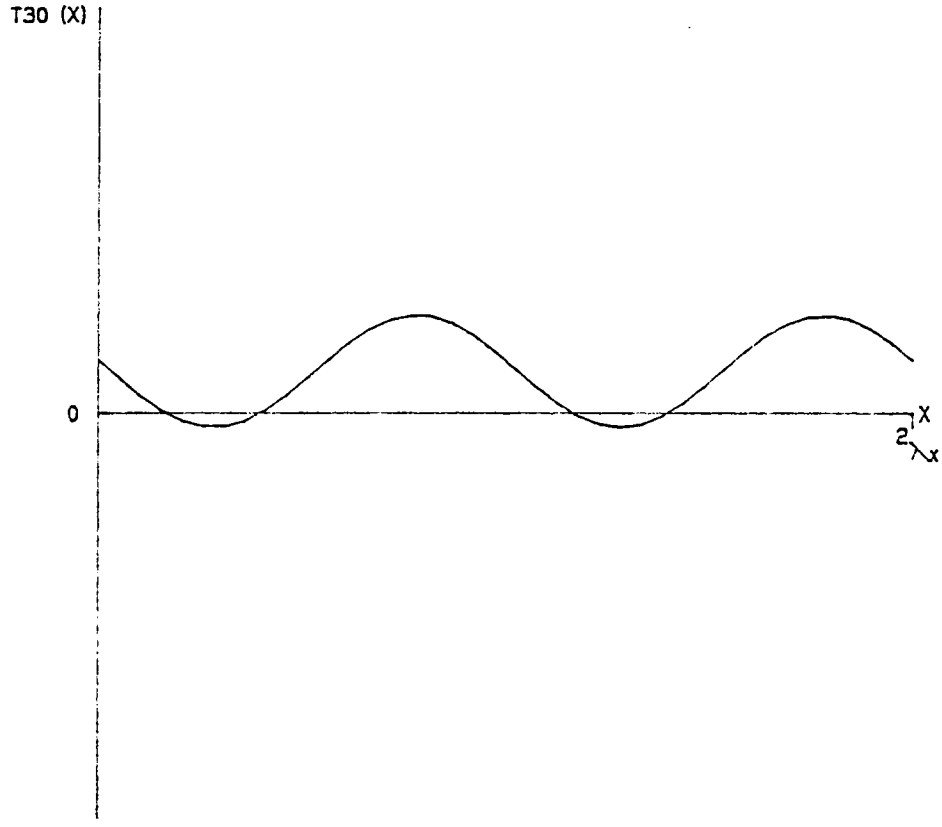

PPT 3-D S T30 (X)

RE	5000.0	SIGMA	0.044449,-0.001926
ALPHA	1.1200	CR	0.281755
BETA	2.0000	MAX	0.0000415
AMS	0.025000	MIN	-0.0000060
SYM	1		

Figure 3.175- $T^{(30)}$ as a function of x for $\mathbf{v}_s$ at $\alpha = 1.12$, $Re = 5000$, $\beta = 2.00$ and $A = 0.025$.

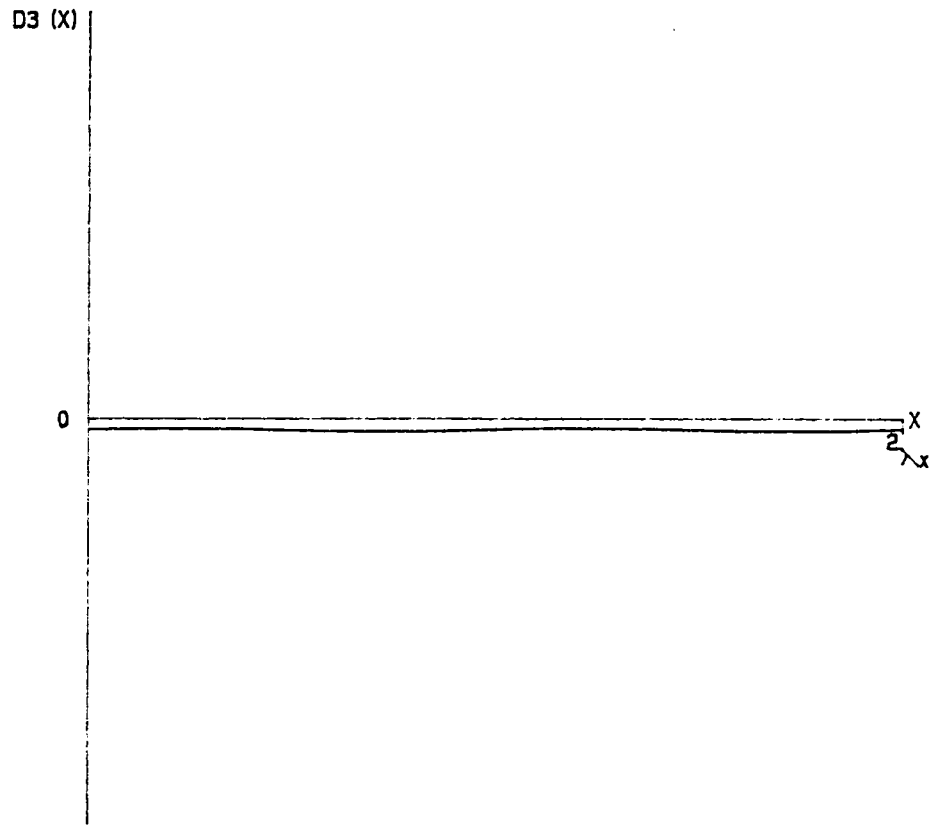

PPT 3-D S D3 (X)

RE	5000.0	SIGMA	0.044449,-0.001926
ALPHA	1.1200	CR	0.281755
BETA	2.0000	MAX	-0.0000035
RMS	0.025000	MIN	-0.0000053
SYM	1		

Figure 3.176- $D^{(3)}$ as a function of x for $\mathbf{v}$, at $\alpha = 1.12$, $Re = 5000$, $\beta = 2.00$ and $A = 0.025$.

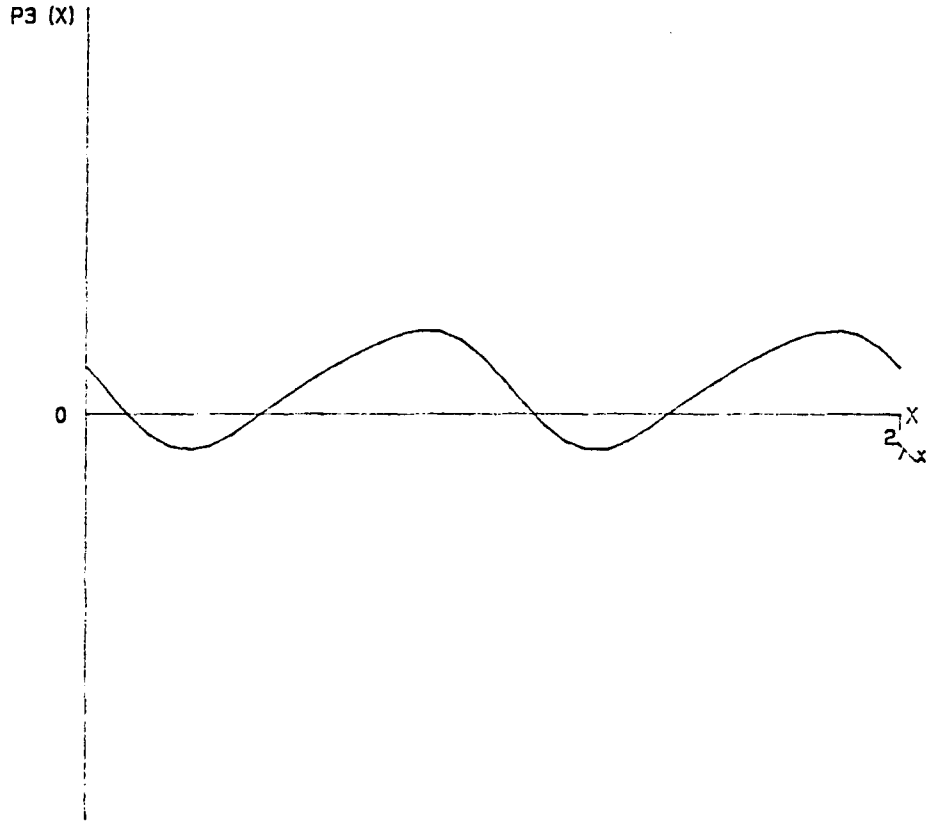

PPT 3-D S P3 (X)

RE	5000.0	SIGMA	0.044449,-0.001926
ALPHA	1.1200	CR	0.281755
BETA	2.0000	MAX	0.0000357
AMS	0.025000	MIN	-0.0000153
SYM	1		

Figure 3.177- $P^{(3)}$ as a function of x for $\mathbf{v}_s$ at $\alpha = 1.12$, $Re = 5000$, $\beta = 2.00$ and $A = 0.025$.

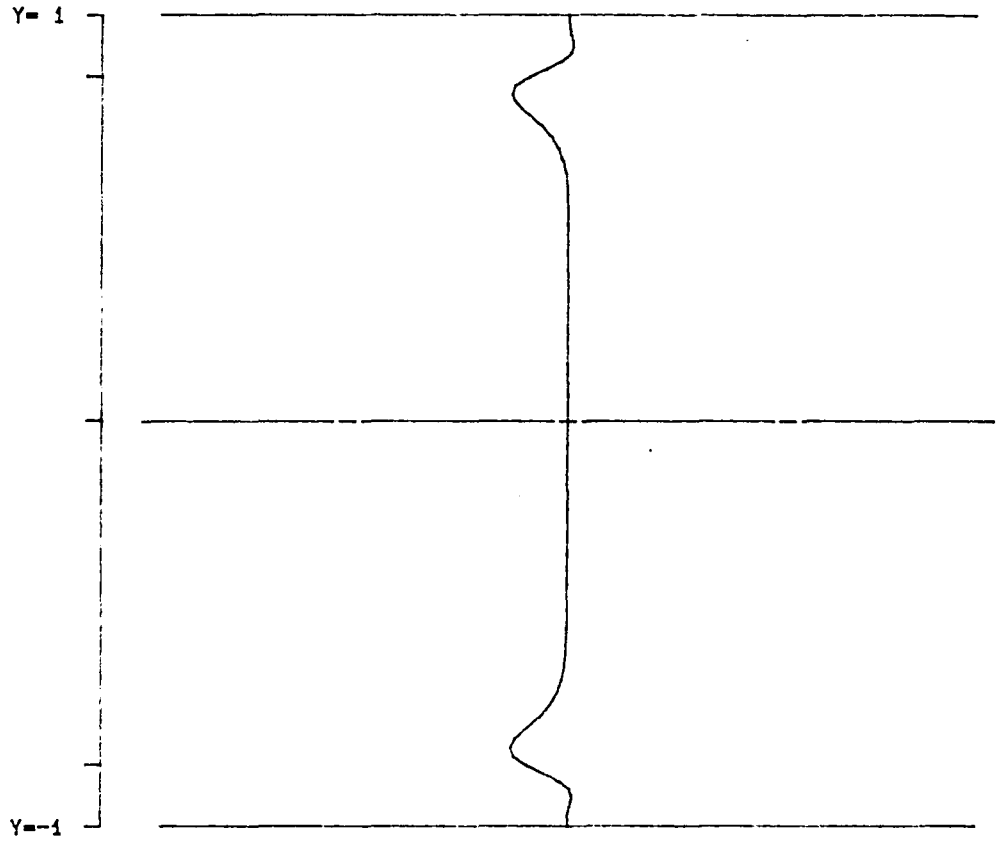

PPT 3-D S T31 (Y)

RE	5000.0	SIGMA	0.044449,-0.001926
ALPHA	1.1200	CR	0.281755
BETA	2.0000	MAX	0.0000020
AMS	0.025000	MIN	-0.0000238
SYM	1		

Figure 3.178- $T^{(31)}$ as a function of y for $\mathbf{v}_s$ at $\alpha = 1.12$, $Re = 5000$, $\beta = 2.00$ and $A = 0.025$.

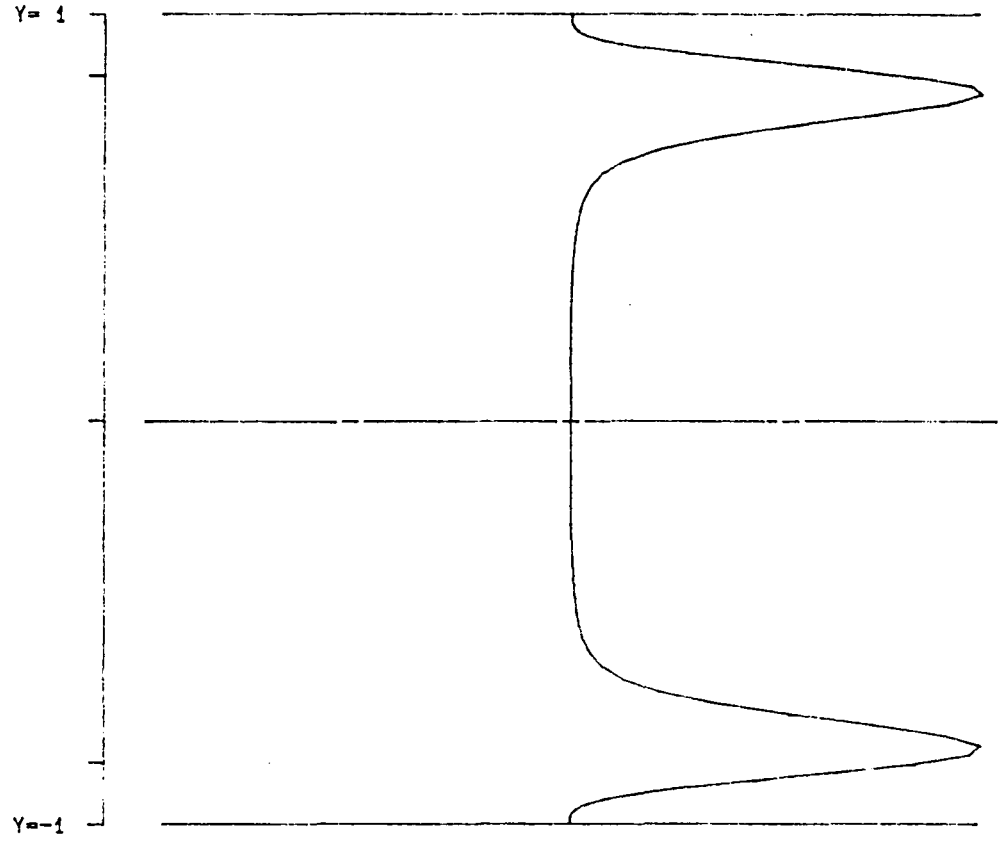

PPT 3-D S T30 (Y)

RE	5000.0	SIGMA	0.044449,-0.001926
ALPHA	1.1200	CR	0.281755
BETA	2.0000	MAX	0.0001706
AMS	0.025000	MIN	-0.0000000
SYM	1		

Figure 3.179- $T^{(30)}$ as a function of y for $\mathbf{v}$, at $\alpha = 1.12$, $Re = 5000$, $\beta = 2.00$ and $A = 0.025$.

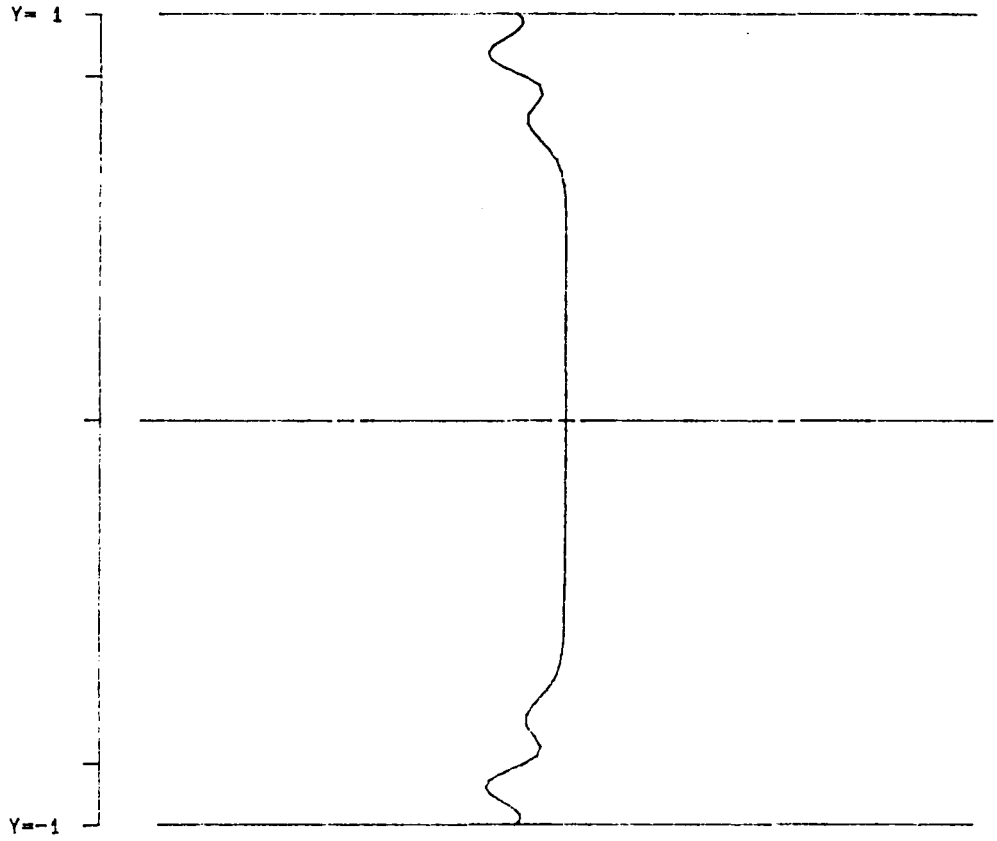

PPT 3-D S D3 (Y)

RE	5000.0	SIGMA	0.044449,-0.001926
ALPHA	1.1200	CR	0.281755
BETA	2.0000	MAX	-0.0000000
AMS	0.025000	MIN	-0.0000317
SYM	1		

Figure 3.180- $D^{(3)}$ as a function of y for $\mathbf{v}$, at $\alpha = 1.12$, $Re = 5000$, $\beta = 2.00$ and $A = 0.025$.

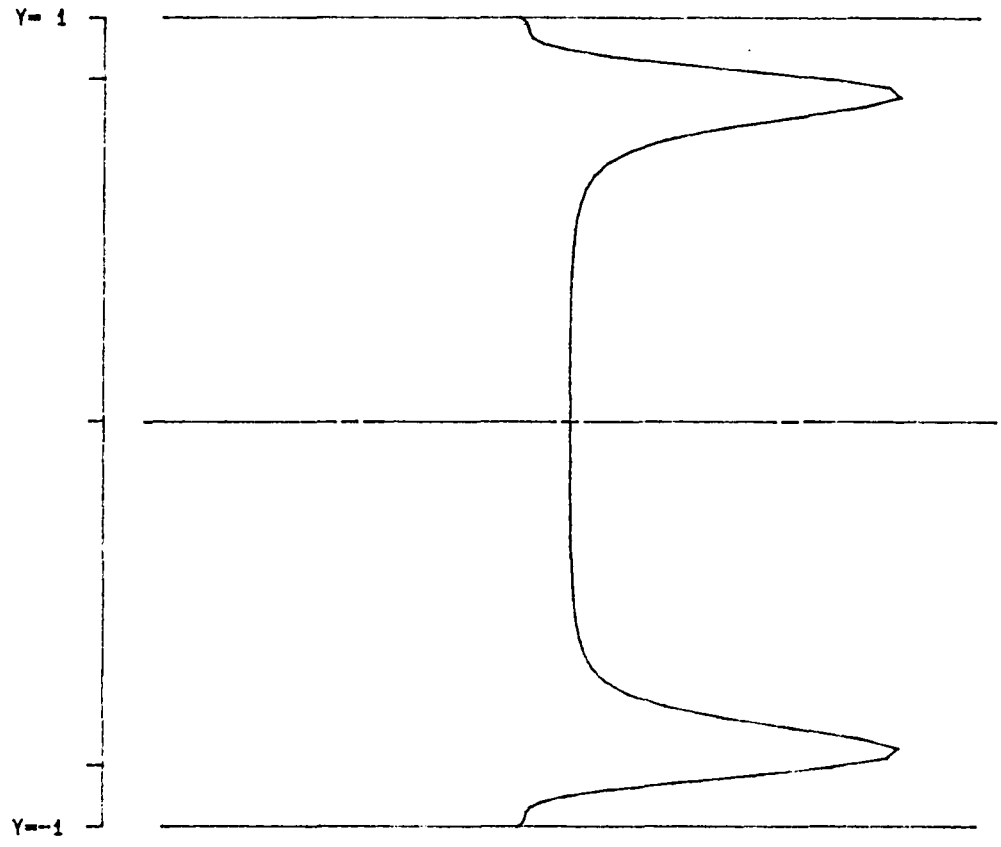

PPT 3-D S P3 (Y)

RE	5000.0	SIGMA	0.044449,-0.001926
ALPHA	1.1200	CR	0.281755
BETA	2.0000	MAX	0.0001364
RMS	0.025000	MIN	-0.0000215
SYM	1		

Figure 3.181- $P^{(3)}$ as a function of y for $\mathbf{v}_s$ at $\alpha = 1.12$, $Re = 5000$, $\beta = 2.00$ and $A = 0.025$.

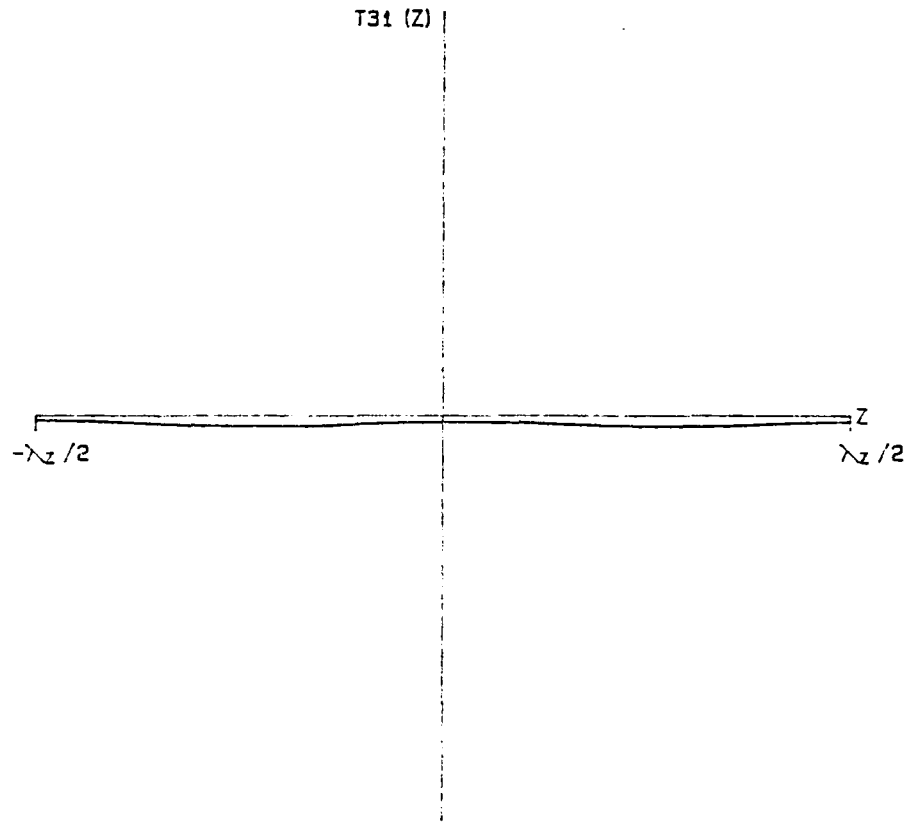

PPT 3-D S T31 (Z)

RE	5000.0	SIGMA	0.044449,-0.001926
ALPHA	1.1200	CR	0.281755
BETA	2.0000	MAX	-0.0000021
RMS	0.025000	MIN	-0.0000045
SYM	1		

Figure 3.182- $T^{(31)}$ as a function of z for $\mathbf{v}_*$ at $\alpha = 1.12$, $Re = 5000$, $\beta = 2.00$ and $A = 0.025$.

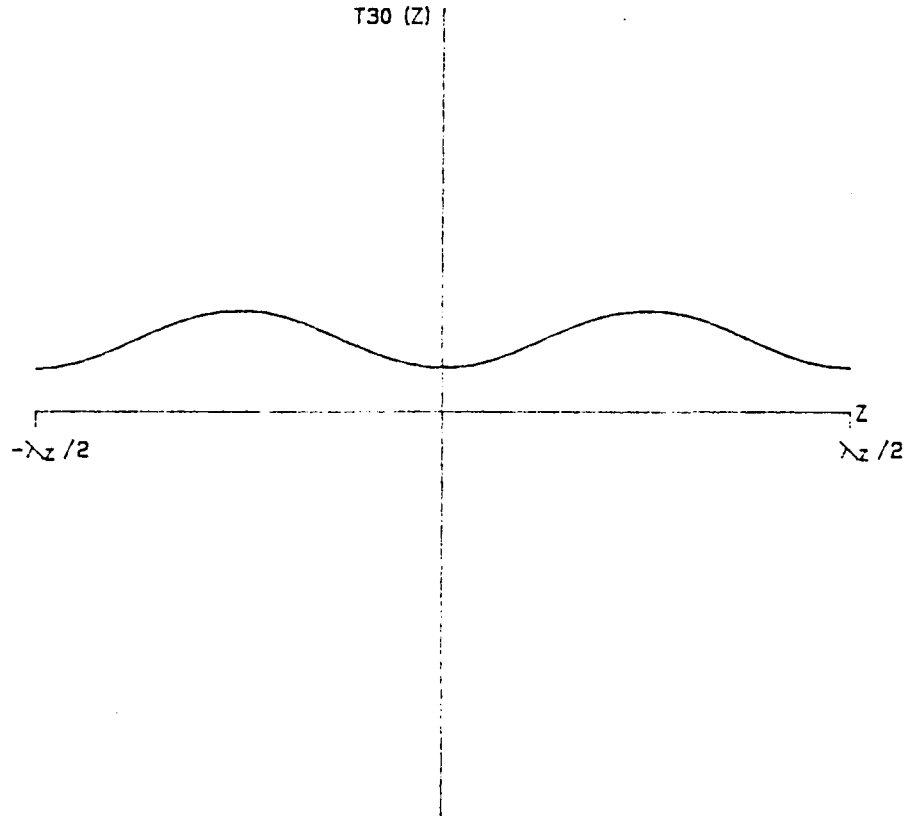

PPT 3-D S T30 (Z)

RE	5000.0	SIGMA	0.044449,-0.001926
ALPHA	1.1200	CR	0.281755
BETA	2.0000	MAX	0.0000429
RMS	0.025000	MIN	0.0000183
SYM	1		

Figure 3.183- $T^{(30)}$ as a function of z for $\mathbf{v}_s$ at $\alpha = 1.12$, $Re = 5000$, $\beta = 2.00$ and $A = 0.025$.

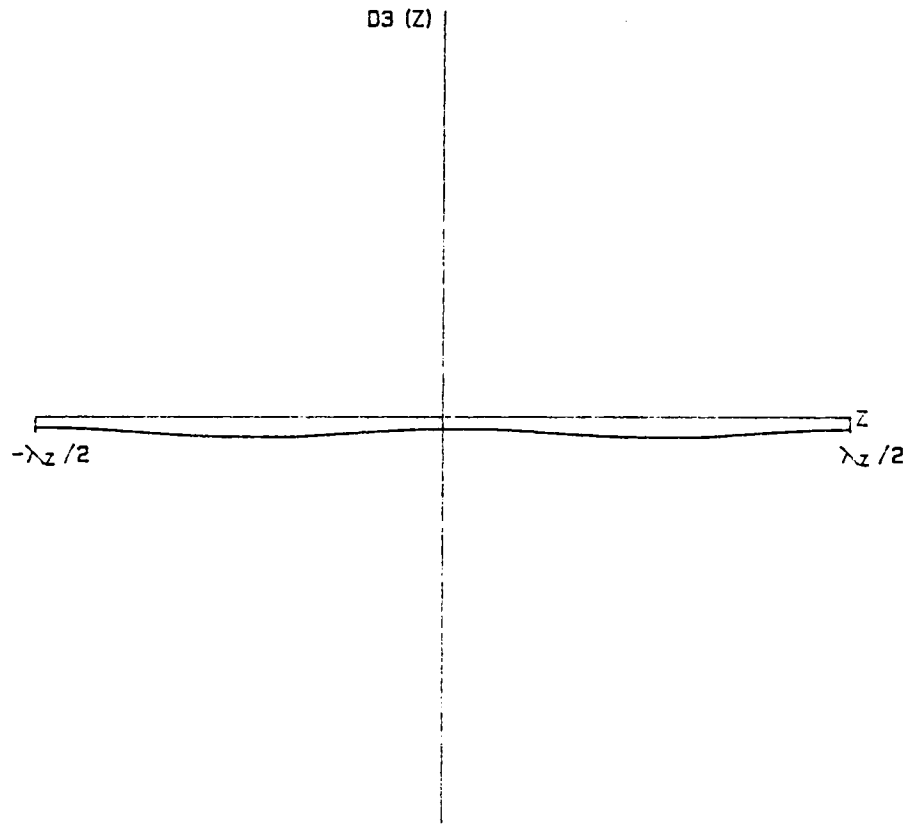

PPT 3-D S D3 (Z)

RE	5000.0	SIGMA	0.044449,-0.001926
ALPHA	1.1200	CR	0.281755
BETA	2.0000	MAX	-0.0000046
AMS	0.025000	MIN	-0.0000087
SYM	1		

Figure 3.184- $D^{(3)}$ as a function of z for $\mathbf{v}_s$ at $\alpha = 1.12$, $Re = 5000$, $\beta = 2.00$ and $A = 0.025$.

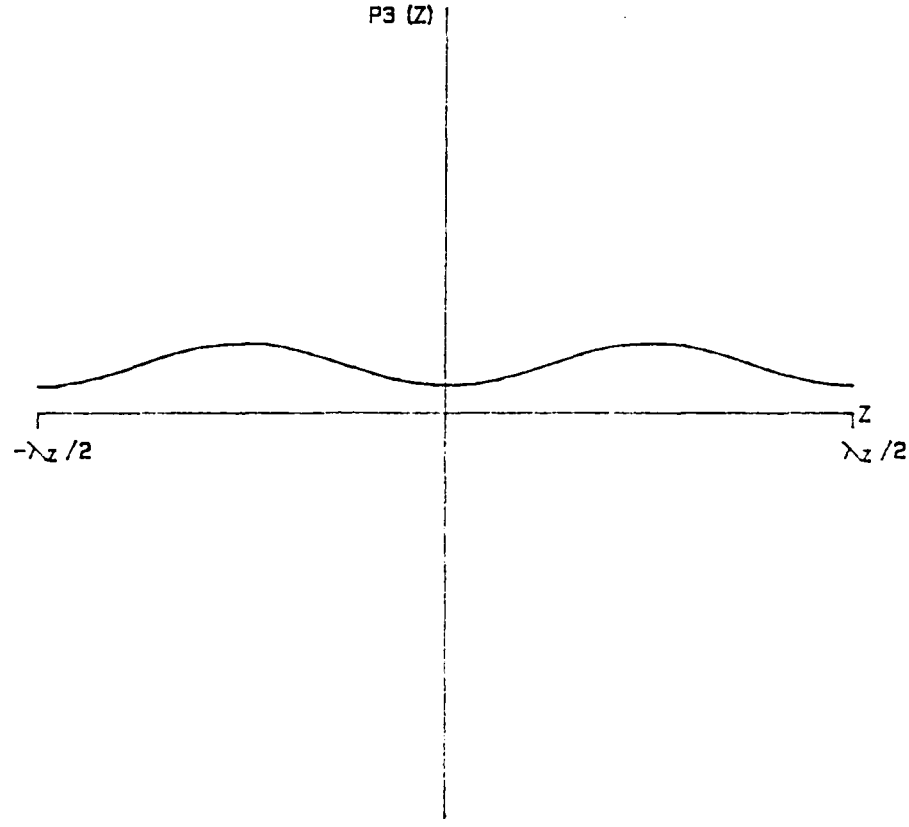

PPT.3-D S P3 (Z)

RE	5000.0	SIGMA	0.044449,-0.001926
ALPHA	1.1200	CR	0.281755
BETA	2.0000	MAX	0.0000296
AMS	0.025000	MIN	0.0000115
SYM	1		

Figure 3.185- $P^{(3)}$ as a function of z for $\mathbf{v}$, at $\alpha = 1.12$, $Re = 5000$, $\beta = 2.00$ and $A = 0.025$.

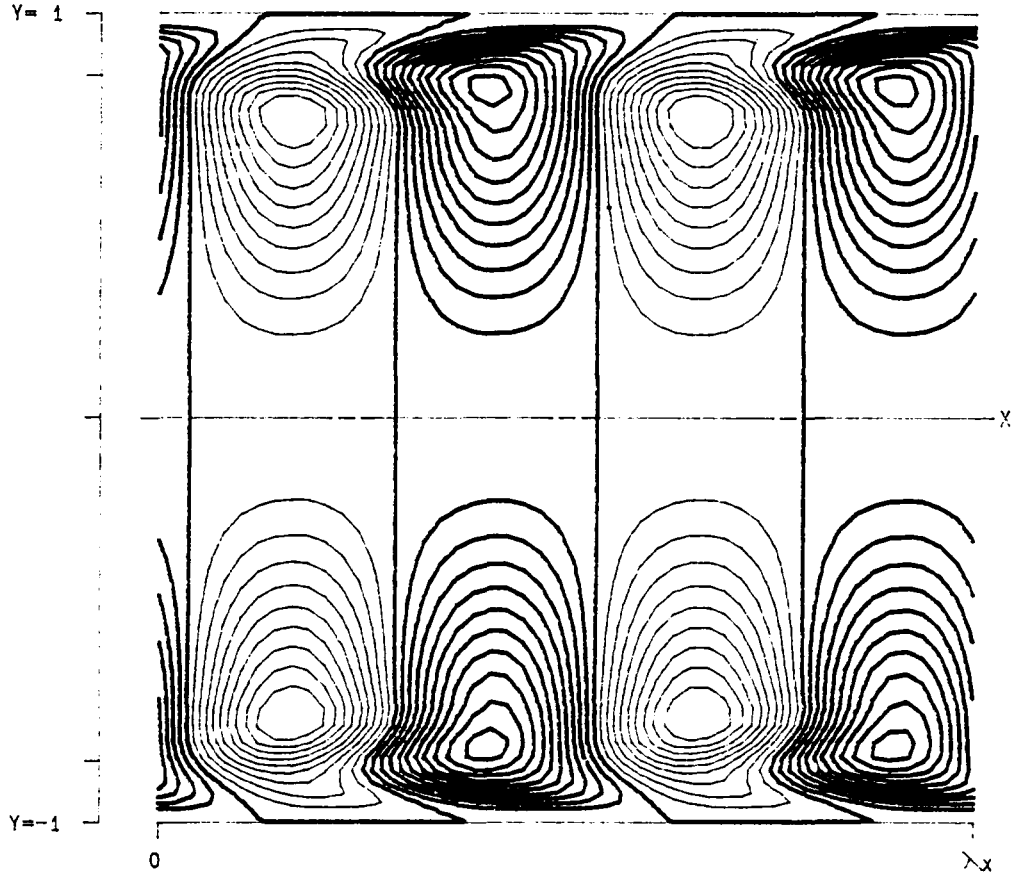

PPT 2-D T10 (X, Y)

RE	5000.0	LEVELS: MIN	-0.0000809
ALPHA	1.1200	DIF	0.0000090
RMS	0.025000	NO.	20
MAX	0.000094		

Figure 3.186- Reynolds stress as a function of x and y for $\alpha = 1.120$, $Re = 5000$.

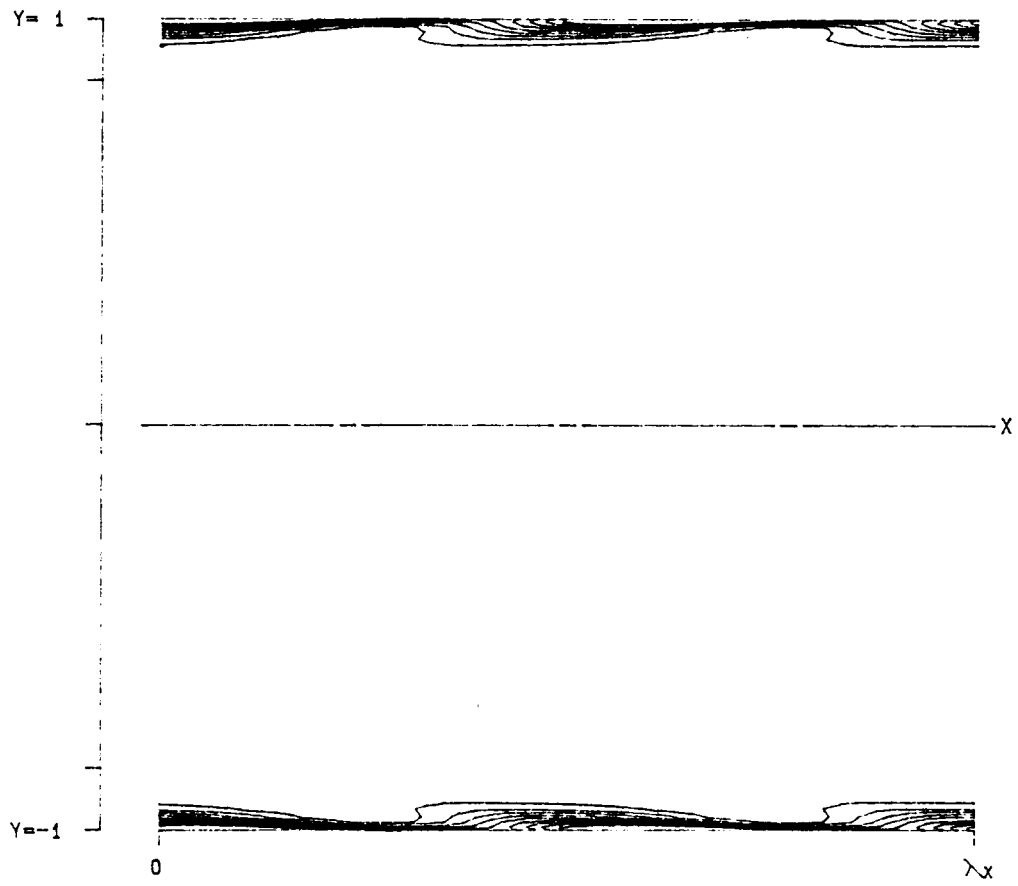

PPT 2-D D1 (X, Y)

RE	5000.0	LEVELS: MIN	-0.0000809
ALPHA	1.1200	DIF	0.0000090
RMS	0.025000	NO.	20
MAX	0.000094		

Figure 3.187- Dissipation as a function of x and y for $\alpha = 1.120$, $Re = 5000$.

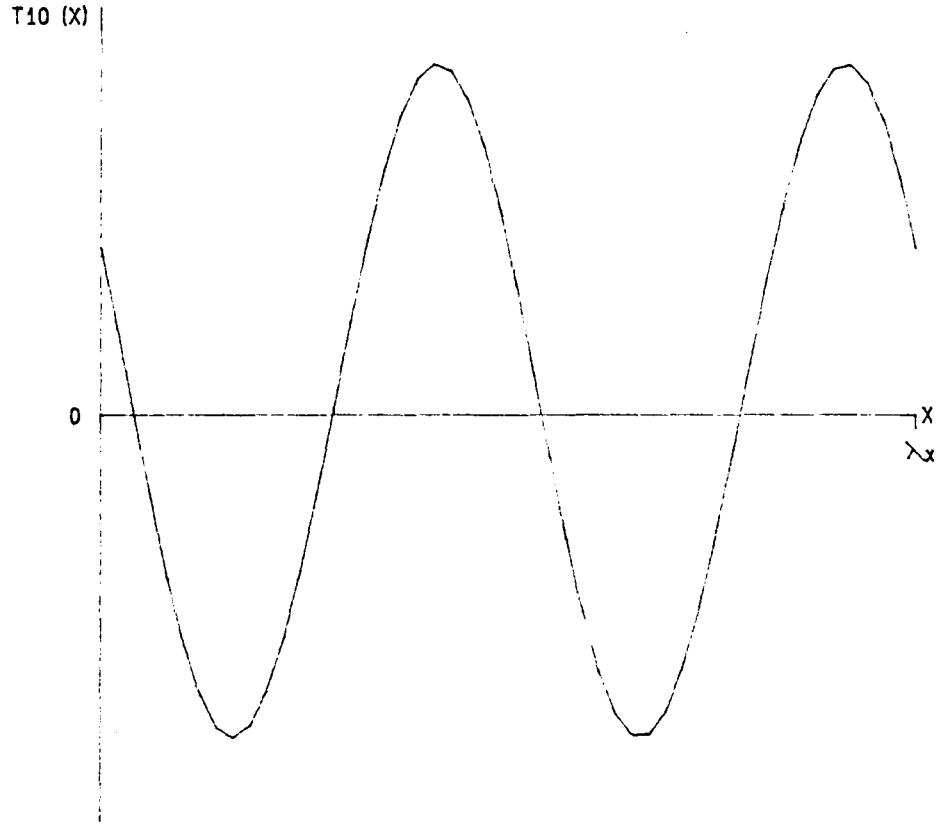

PPT 2-D T10 (X)

RE	5000.0	CR	0.281752
ALPHA	1.1200	MAX	0.0000830
AMS	0.025000	MIN	-0.0000763

Figure 3.188- Reynolds stress as a function of x for $\alpha = 1.120$, $Re = 5000$.

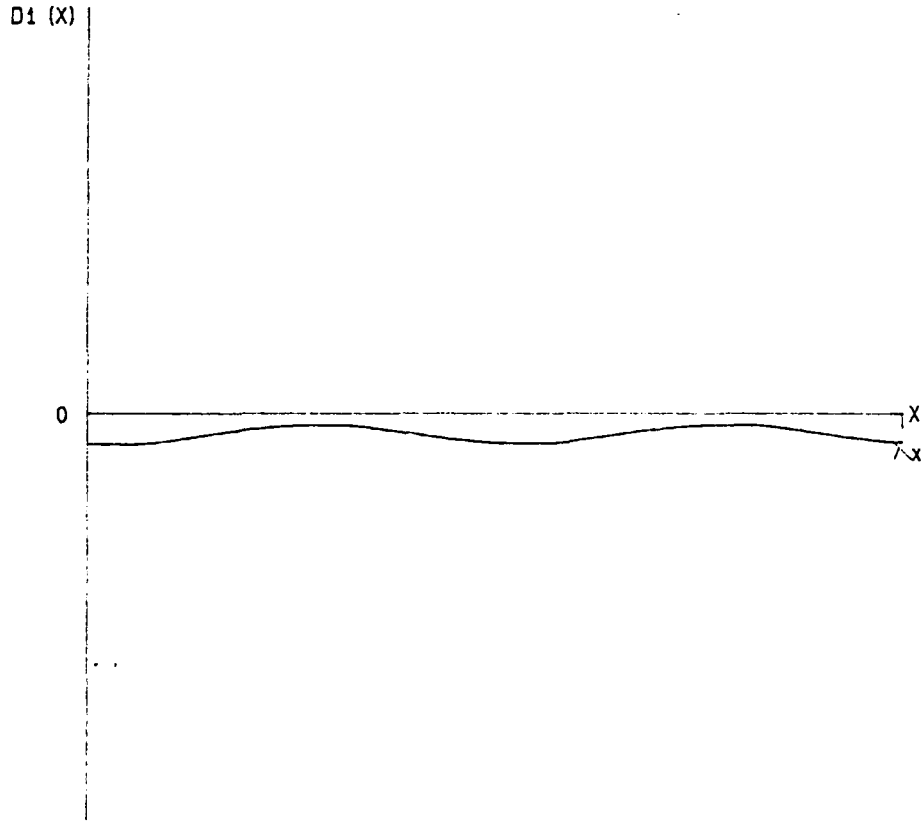

PPT 2-D D1 (X)

RE	5000.0	CR	0.281752
ALPHA	1.1200	MAX	-0.0000024
RMS	0.025000	MIN	-0.0000073

Figure 3.189- Dissipation as a function of x for $\alpha = 1.120$, $Re = 5000$.

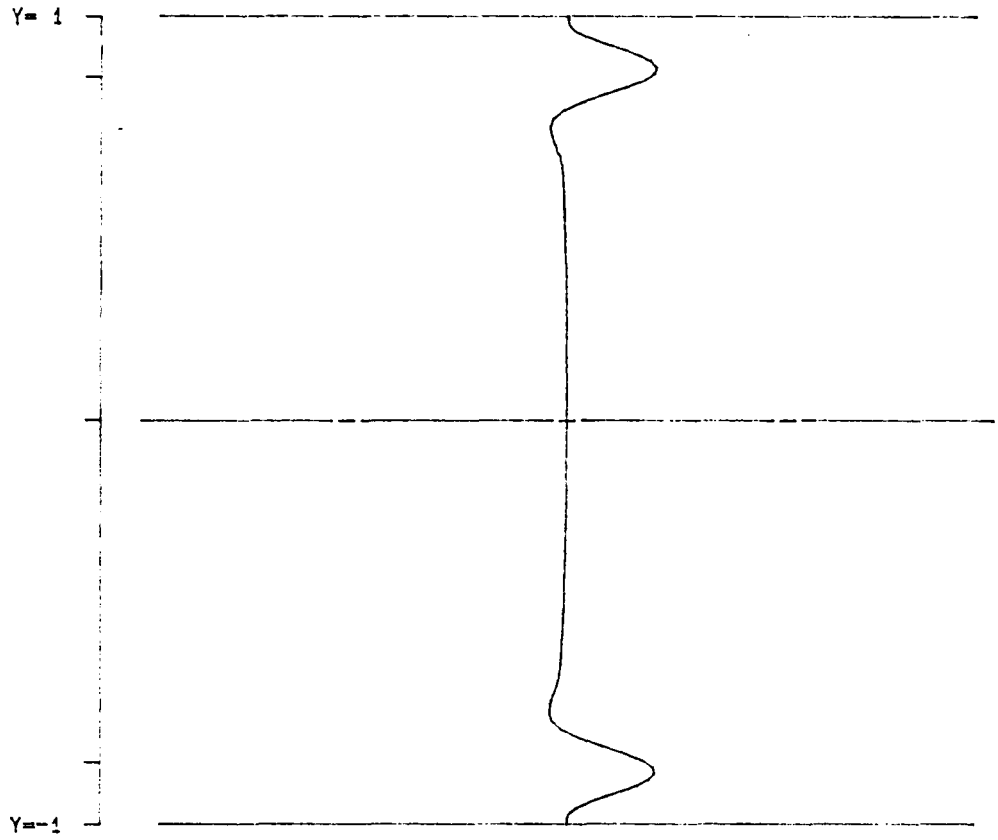

PPT 2-D T10 (Y)

RE	5000.0	CR	0.281752
ALPHA	1.1200	MAX	0.0000209
RMS	0.025000	MIN	-0.0000042

Figure 3.190- Reynolds stress as a function of y for $\alpha = 1.120$, $Re = 5000$.

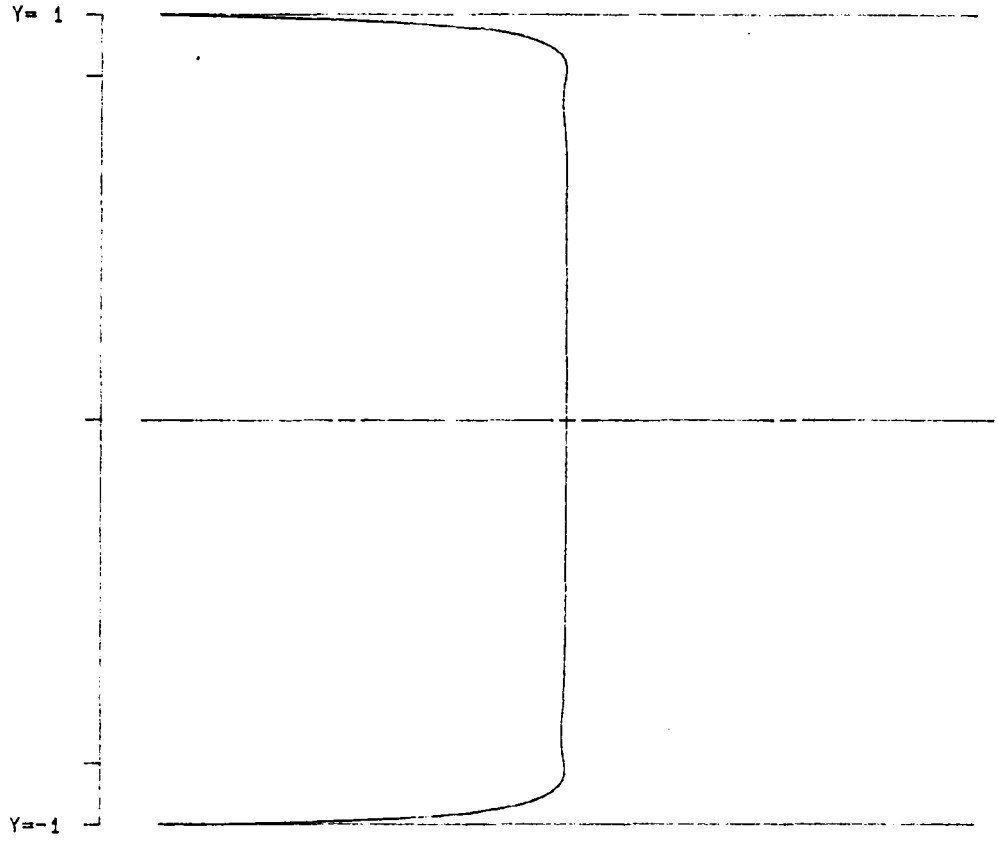

PPT 2-D D1 (Y)

RE	5000.0	CR	0.281752
ALPHA	1.1200	MAX	-0.0000001
RMS	0.025000	MIN	-0.0000960

Figure 3.191- Dissipation as a function of y for $\alpha = 1.120$, $Re = 5000$.

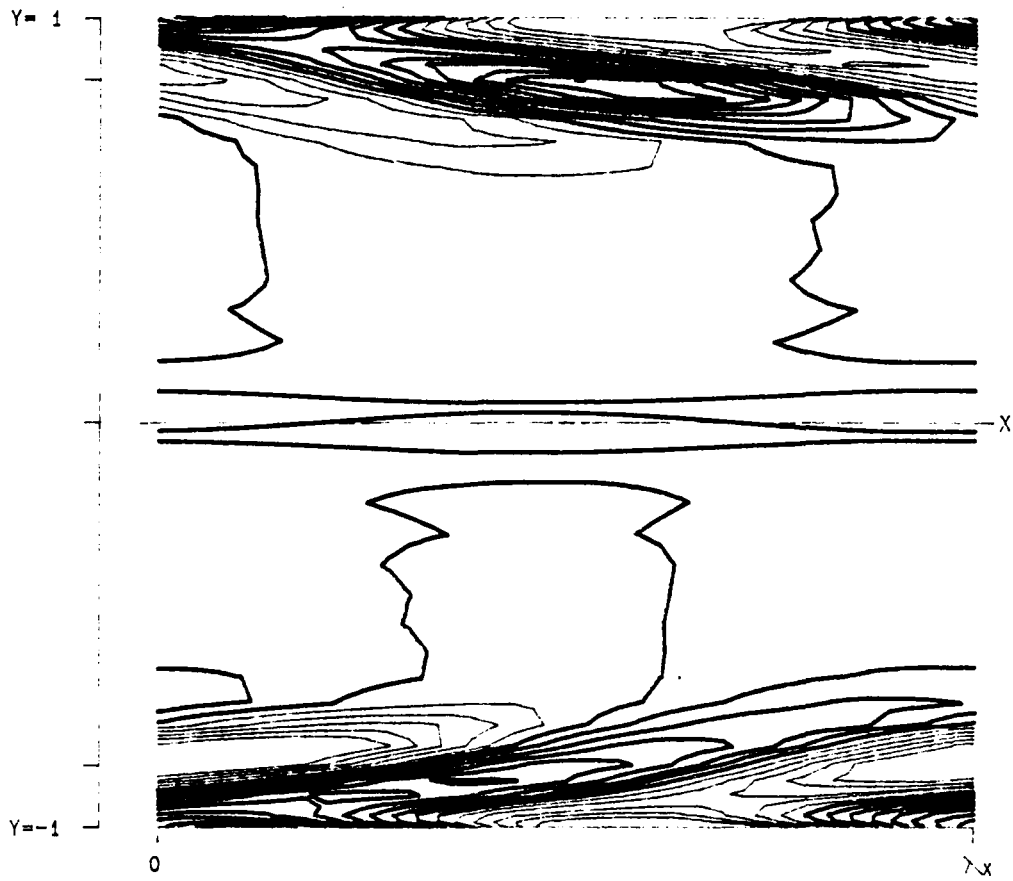

PPT 3-D F XI(X, Y, Z)

RE	5000.0
ALPHA	1.1200
BETA	2.0000
SIGMA	0.046326
RMS	0.025000
MAX	1.151704
SYM	0

LEVELS:	MIN	-0.3971385
	DIF	0.0794279
	NO.	20
	Z =	0.765260

Figure 3.192- ξ_3 as a function of x, y and z at a position of $z = 0.765260$ for $\mathbf{v}_f$, at $\alpha = 1.12$, $Re = 5000$, $\beta = 2.00$ and $A = 0.025$.

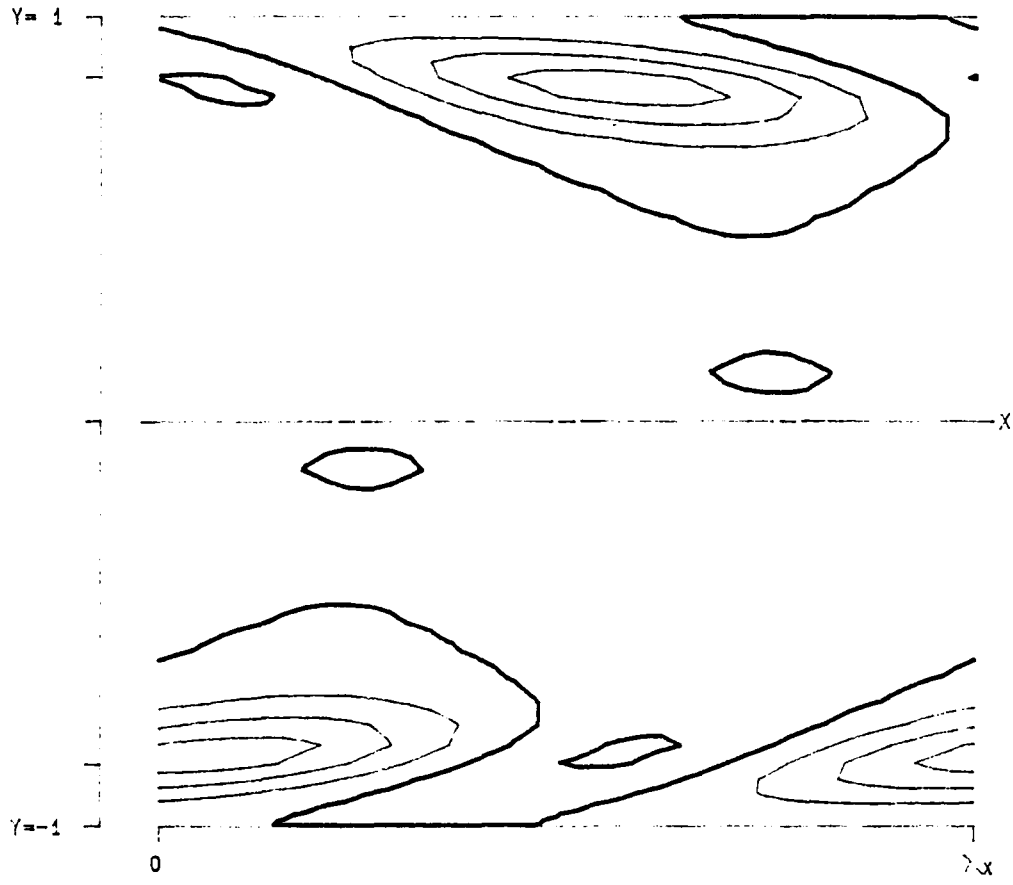

PPT 3-D F ETA(X, Y, Z)

RE	5000.0
ALPHA	1.1200
BETA	2.0000
SIGMA	0.046326
RMS	0.025000
MAX	1.151704
SYM	0

LEVELS:	MIN	-0.3971385
	DIF	0.0794279
	NO.	20
	Z =	0.765260

Figure 3.193- η_3 as a function of x, y and z at a position of $z = 0.765260$ for $\mathbf{v}_f$, at $\alpha = 1.12$, $Re = 5000$, $\beta = 2.00$ and $A = 0.025$.

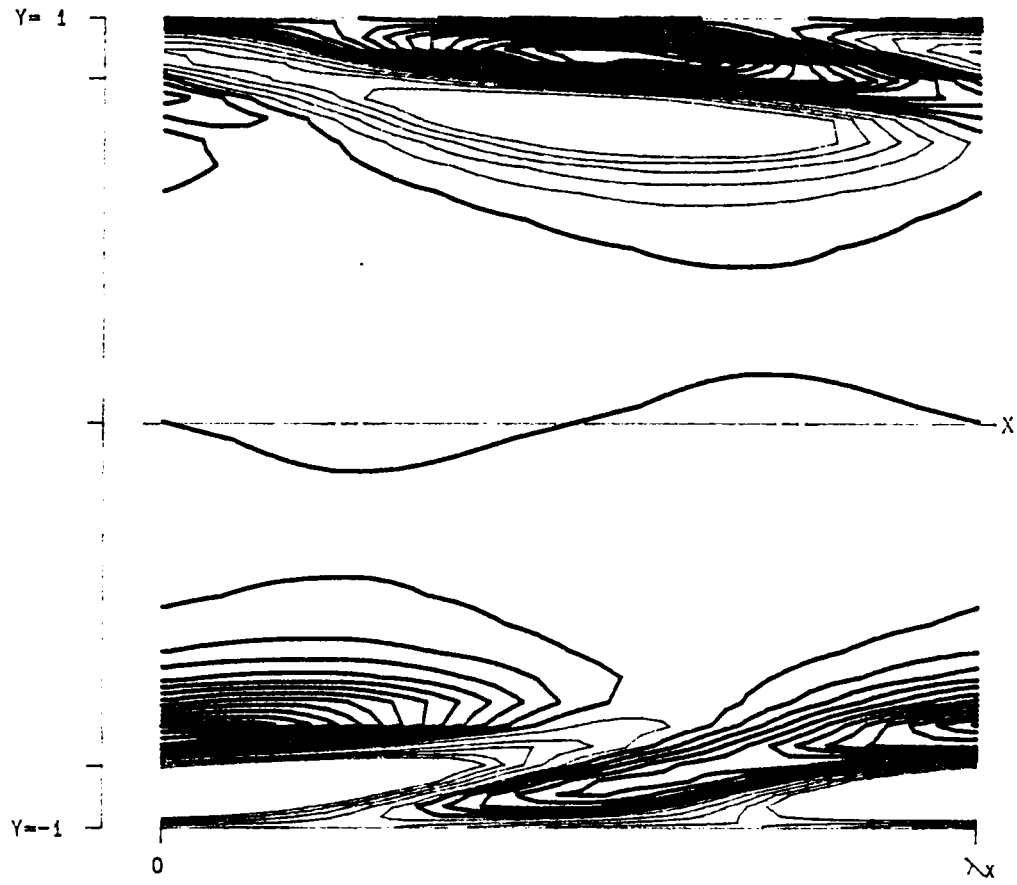

PPT 3-D F ZETA(X, Y, Z)

RE	5000.0	LEVELS: MIN	-0.3971385
ALPHA	1.1200	DIF	0.0794279
BETA	2.0000	NO.	20
SIGMA	0.046326		
RMS	0.025000	Z =	-0.040277
MAX	1.151704		
SYM	0		

Figure 3.194- ς_3 as a function of x, y and z at a position of $z = -0.040277$ for $\mathbf{v}_f$, at $\alpha = 1.12$, $Re = 5000$, $\beta = 2.00$ and $A = 0.025$.

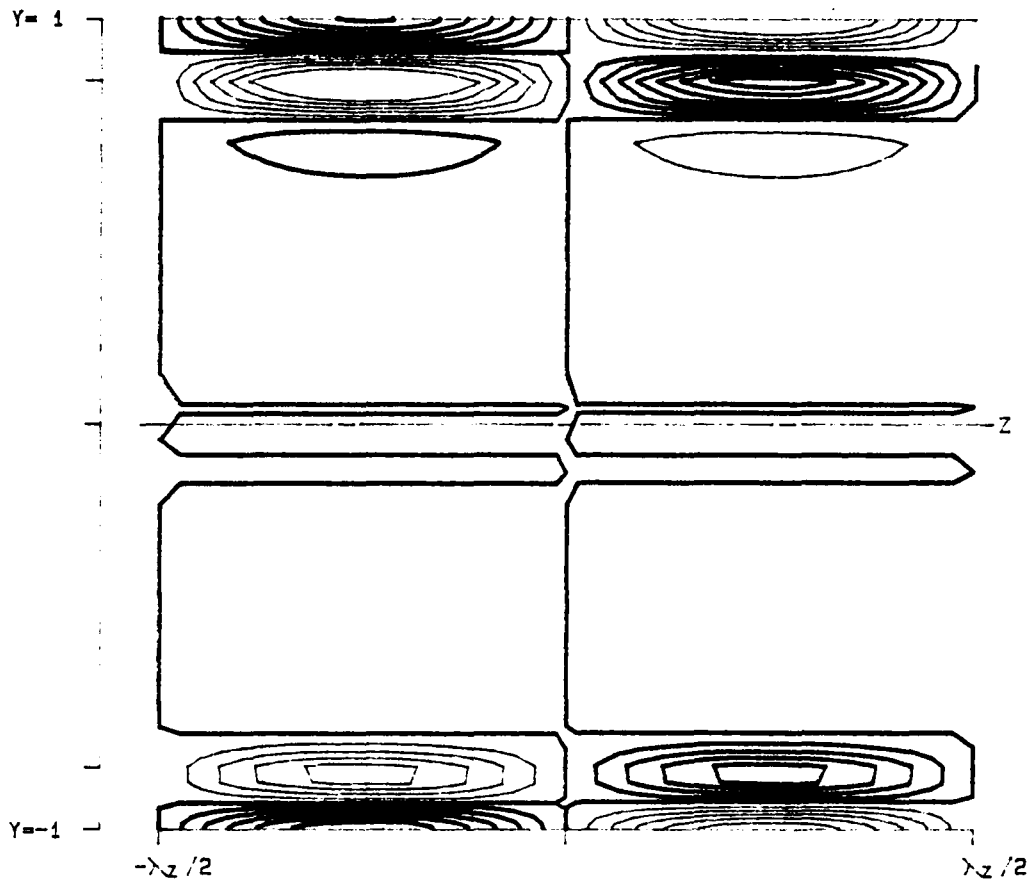

PPT 3-D F XI(X, Y, Z)

RE	5000.0
ALPHA	1.1200
BETA	2.0000
SIGMA	0.046326
RMS	0.025000
MAX	1.151704
SYM	0

LEVELS:	MIN	-0.3971385
	DIF	0.0794279
	NO.	20
	X =	2.733071

Figure 3.195- ξ_3 as a function of x, y and z at a position of $x = 2.733071$ for $\mathbf{v}_{f_s}$ at $\alpha = 1.12$, $Re = 5000$, $\beta = 2.00$ and $A = 0.025$.

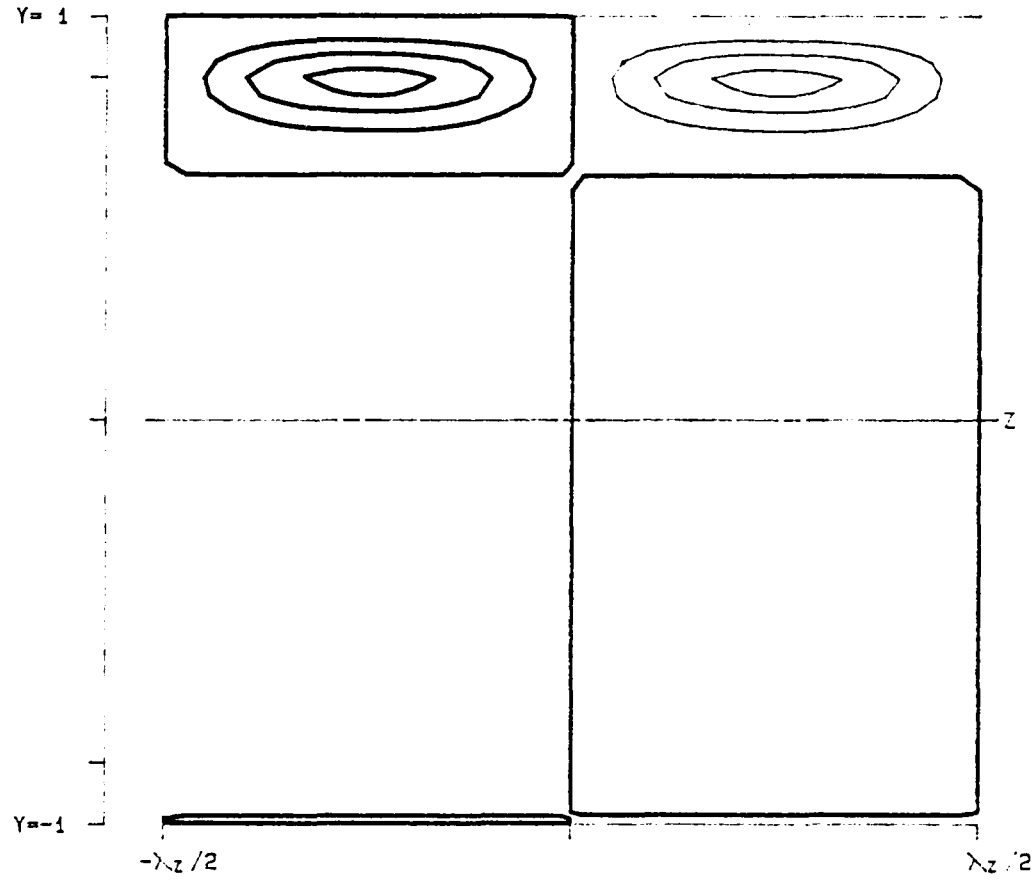

PPT 3-D F ETA(X, Y, Z)

RE	5000.0	LEVELS: MIN	-0.3971385
ALPHA	1.1200	DIF	0.0794279
BETA	2.0000	NO.	20
SIGMA	0.046326		
RMS	0.025000	X =	2.733071
MAX	1.151704		
SYM	0		

Figure 3.196- η_3 as a function of x, y and z at a position of $x = 2.733071$ for v_{fs} at $\alpha = 1.12$, $Re = 5000$, $\beta = 2.00$ and $A = 0.025$.

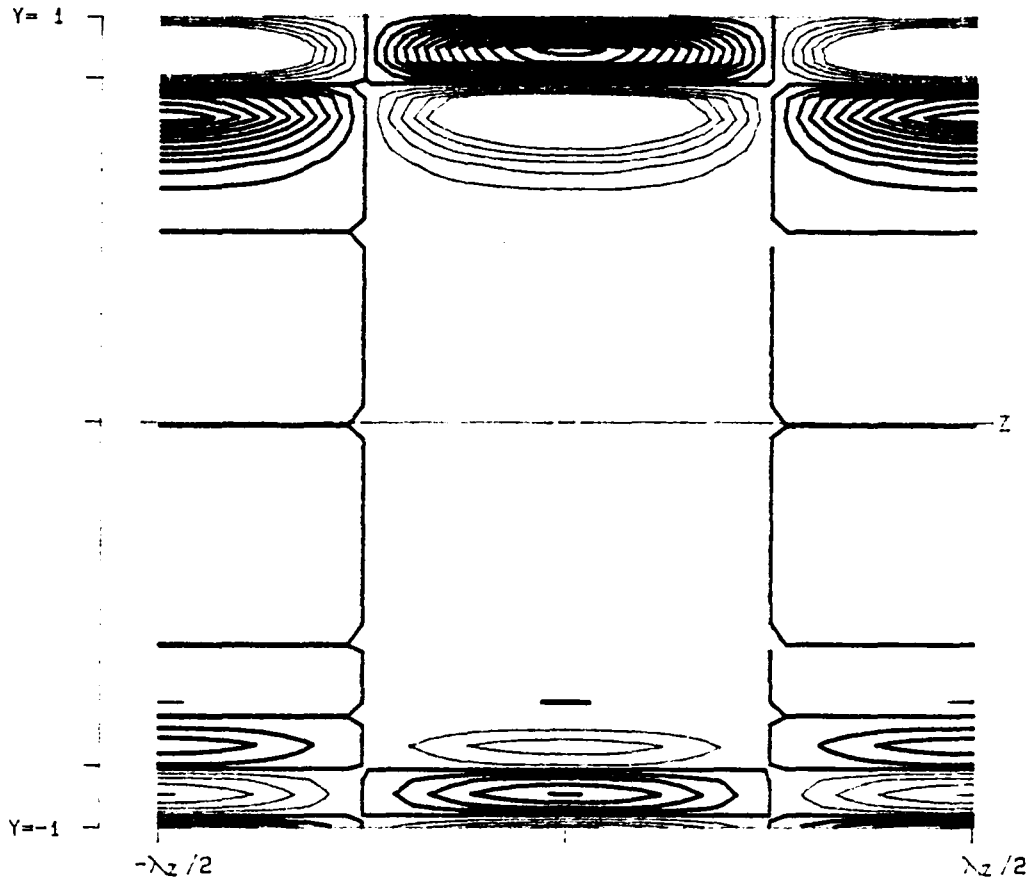

PPT 3-D F ZETA(X, Y, Z)

RE	5000.0	LEVELS: MIN	-0.3971385
ALPHA	1.1200	DIF	0.0794279
BETA	2.0000	NO.	20
SIGMA	0.046326		
RMS	0.025000	X =	2.733071
MAX	1.151704		
SYM	0		

Figure 3.197- ς_3 as a function of x, y and z at a position of $x = 2.733071$ for $\mathbf{v}_f$, at $\alpha = 1.12$, $Re = 5000$, $\beta = 2.00$ and $A = 0.025$.

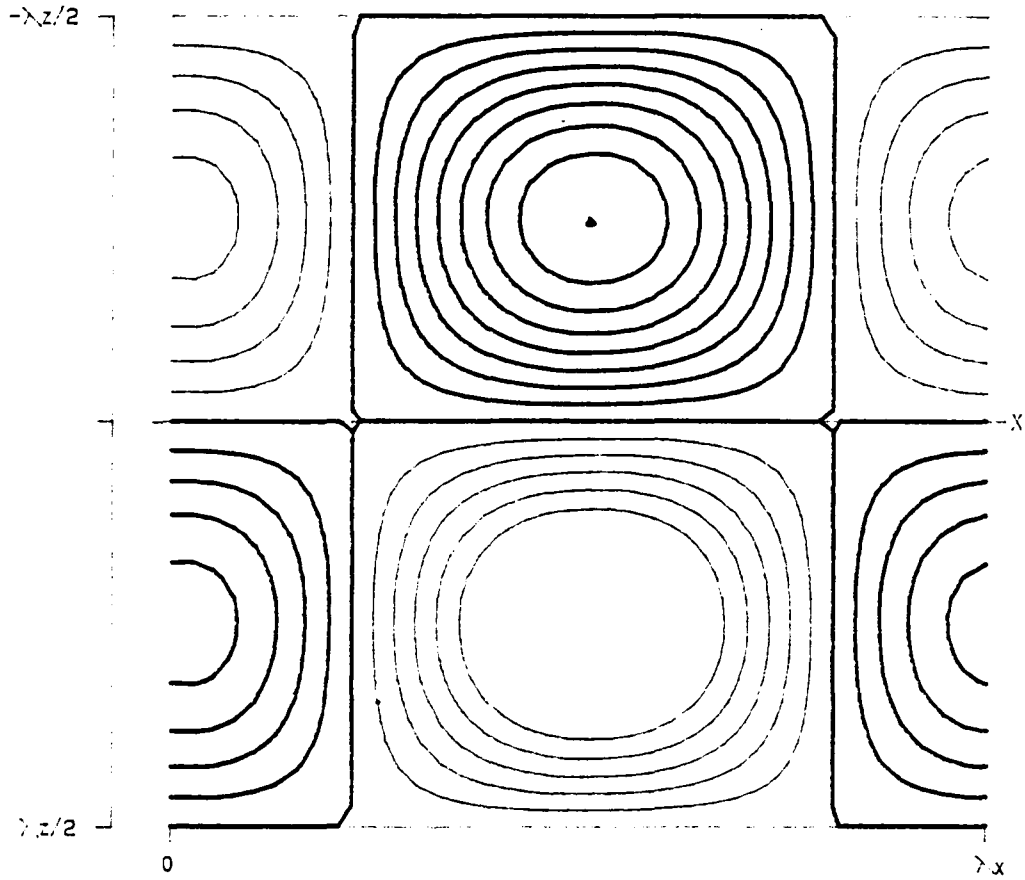

PPT 3-D F XI(X, Y, Z)

RE	5000.0
ALPHA	1.1200
BETA	2.0000
SIGMA	0.046326
RMS	0.025000
MAX	1.151704
SYM	0

LEVELS:	MIN	-0.3971385
	DIF	0.0794279
	NO.	20
	Y =	0.845190

Figure 3.198- ξ_3 as a function of x, y and z at a position of $y = 0.845190$ for v_{f_s} at $\alpha = 1.12$, $Re = 5000$, $\beta = 2.00$ and $A = 0.025$.

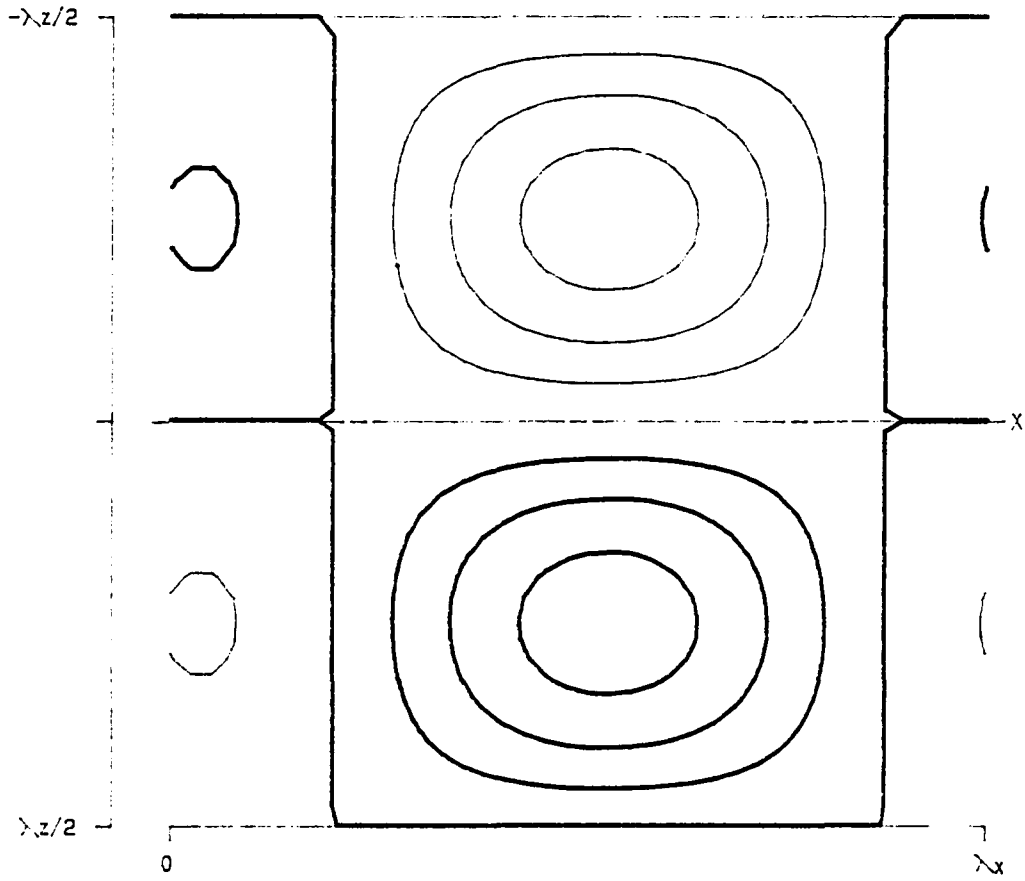

PPT 3-D F ETA(X, Y, Z)

RE	5000.0	LEVELS: MIN	-0.3971385
ALPHA	1.1200	DIF	0.0794279
BETA	2.0000	NO.	20
SIGMA	0.046326		
RMS	0.025000	Y =	0.845190
MAX	1.151704		
SYM	0		

Figure 3.199- η_3 as a function of x, y and z at a position of $y = 0.845190$ for $\mathbf{v}_{f_s}$ at $\alpha = 1.12$, $Re = 5000$, $\beta = 2.00$ and $A = 0.025$.

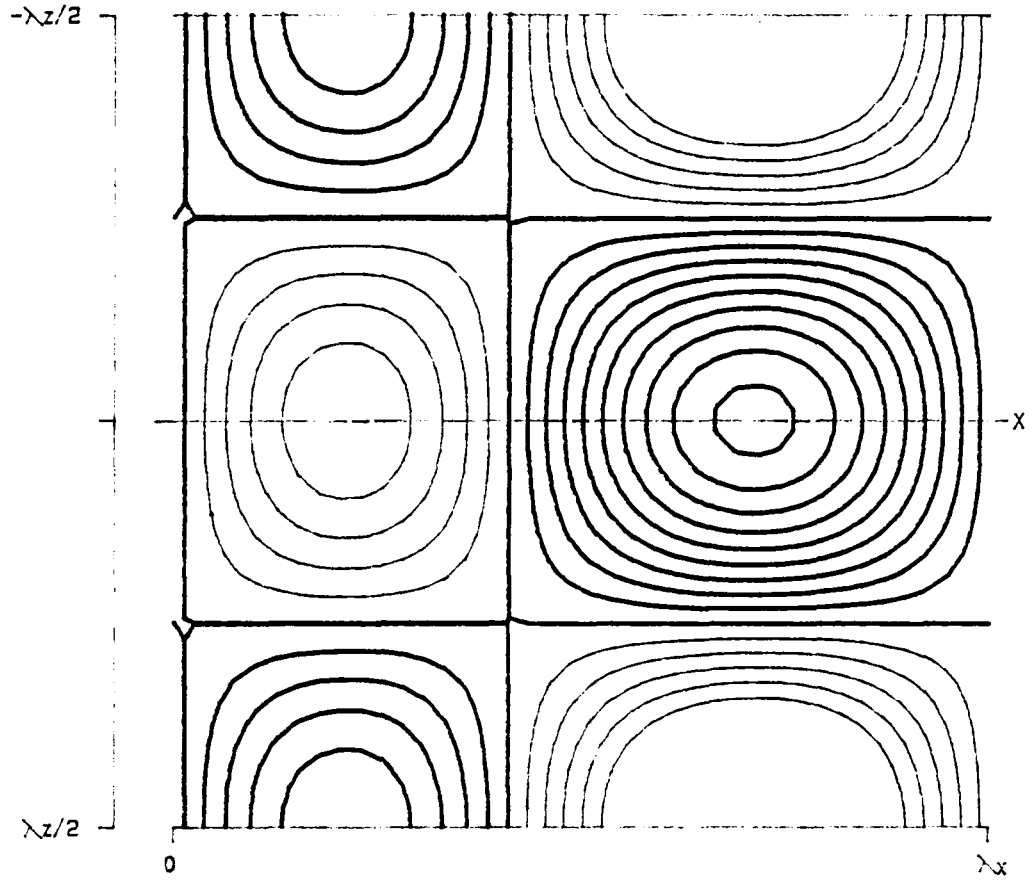

PPT 3-D F ZETA(X, Y, Z)

RE	5000.0
ALPHA	1.1200
BETA	2.0000
SIGMA	0.046326
RMS	0.025000
MAX	1.151704
SYM	0

LEVELS:	MIN	-0.3971385
	DIF	0.0794279
	NO.	20
	Y =	0.845190

Figure 3.200- ς_3 as a function of x, y and z at a position of $y = 0.845190$ for $\mathbf{v}_f$, at $\alpha = 1.12$, $Re = 5000$, $\beta = 2.00$ and $A = 0.025$.

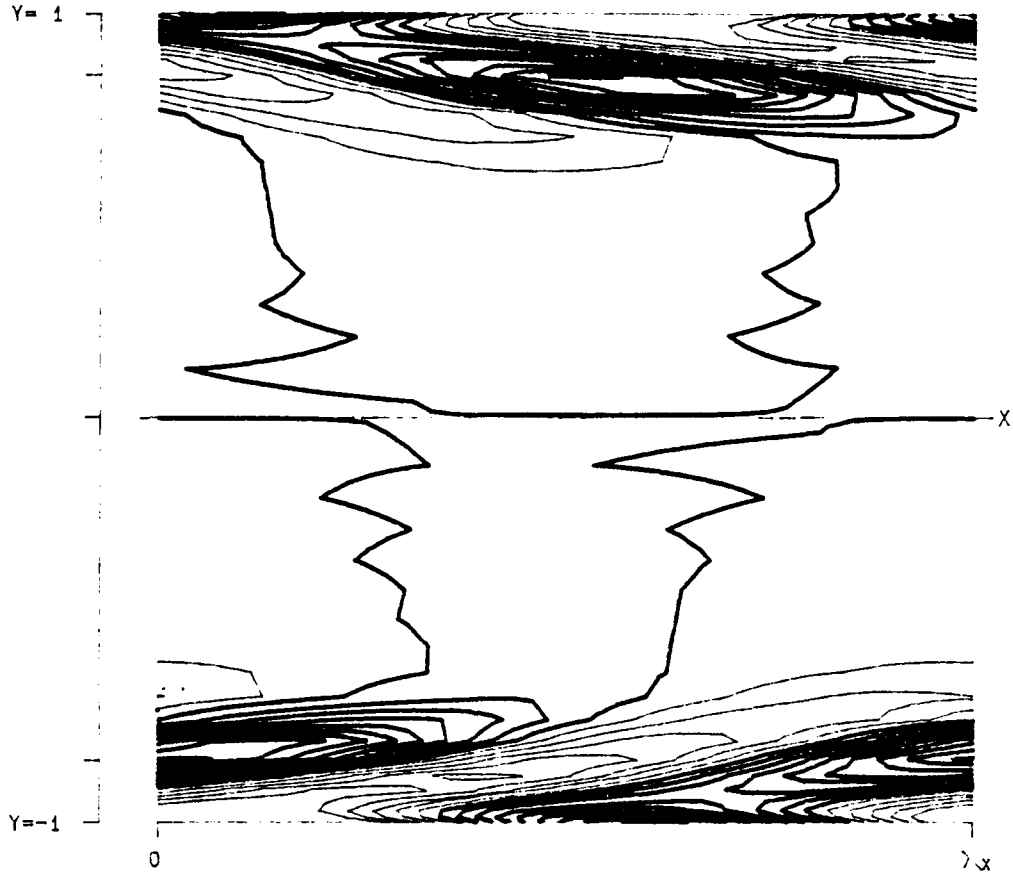

PPT 3-D F XI(X, Y, Z)

RE	5000.0
ALPHA	1.1200
BETA	2.0000
SIGMA	0.043798
AMS	0.025000
MAX	1.119222
SYM	1

LEVELS:	MIN	-0.3859390
	DIF	0.0771877
	NO.	20
	Z =	0.765260

Figure 3.201- ξ_3 as a function of x, y and z at a position of $z = 0.765260$ for $\mathbf{v}_{fa}$ at $\alpha = 1.12$, $Re = 5000$, $\beta = 2.00$ and $A = 0.025$.

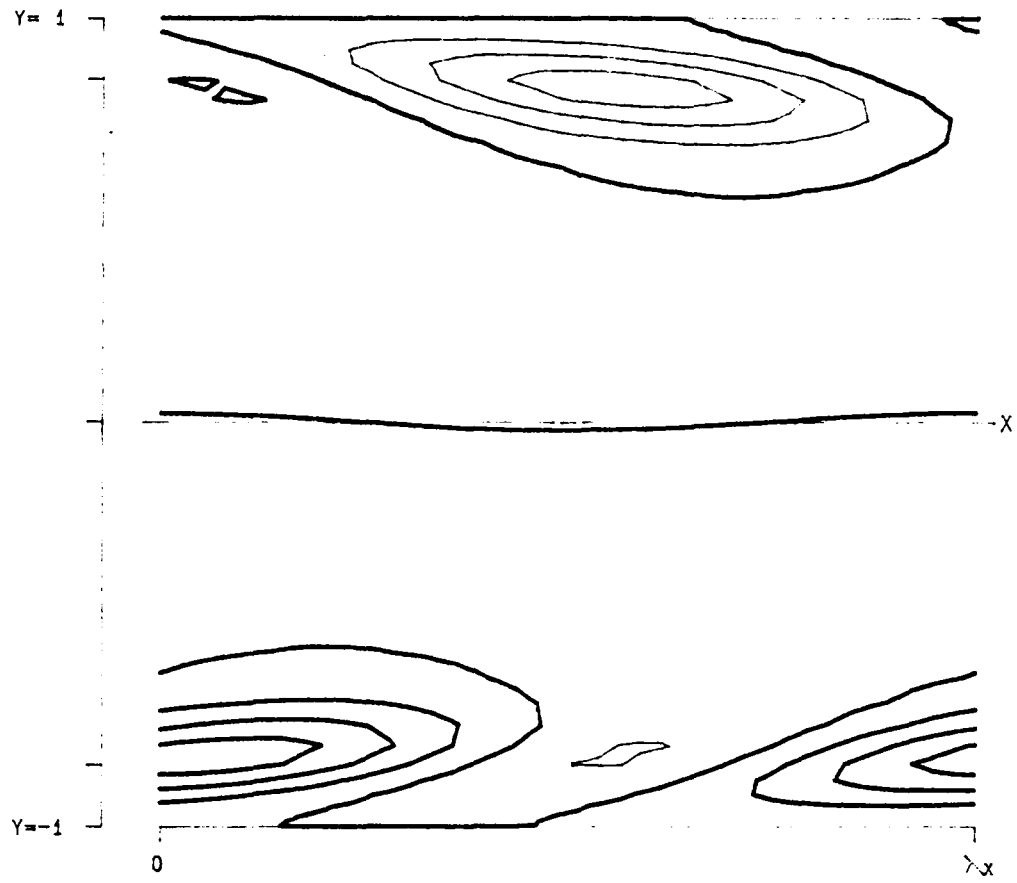

PPT 3-D F ETA(X, Y, Z)

RE	5000.0	LEVELS: MIN	-0.3859390
ALPHA	1.1200	DIF	0.0771877
BETA	2.0000	NO.	20
SIGMA	0.043798		
RMS	0.025000	Z =	0.765260
MAX	1.119222		
SYM	1		

Figure 3.202- η_3 as a function of x, y and z at a position of $z = 0.765260$ for $\mathbf{v}_{f_a}$ at $\alpha = 1.12$, $Re = 5000$, $\beta = 2.00$ and $A = 0.025$.

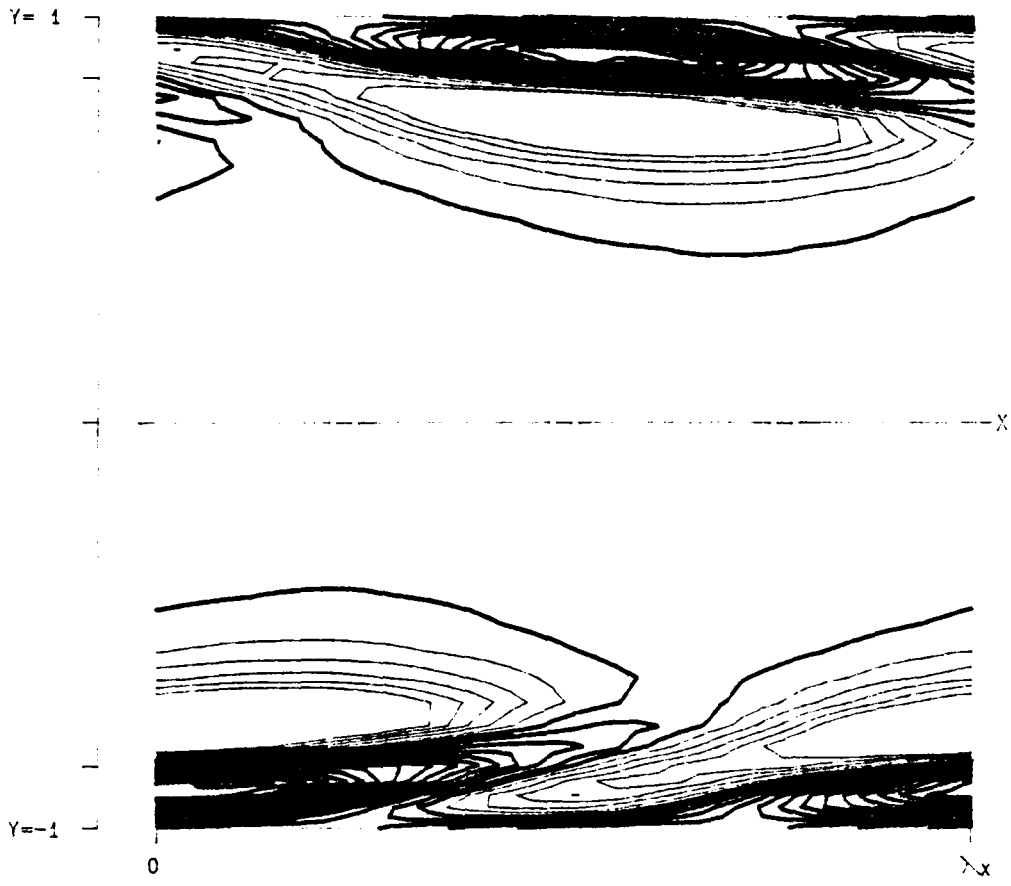

PPT 3-D F ZETA(X, Y, Z)

RE	5000.0	LEVELS:	MIN -0.3859390
ALPHA	1.1200		DIF 0.0771877
BETA	2.0000		NO. 20
SIGMA	0.043798		
RMS	0.025000		Z = -0.040277
MAX	1.119222		
SYM	1		

Figure 3.203- ς_3 as a function of x, y and z at a position of $z = -0.040277$ for $\mathbf{v}_{fa}$ at $\alpha = 1.12$, $Re = 5000$, $\beta = 2.00$ and $A = 0.025$.

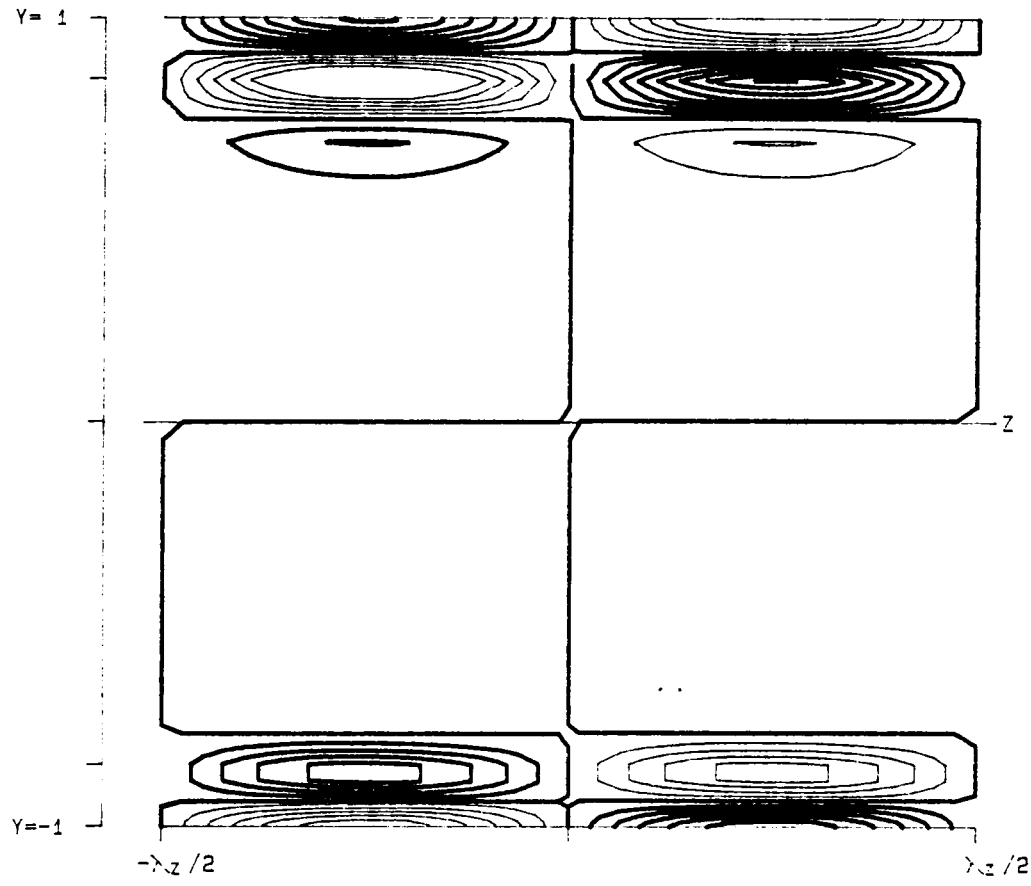

PPT 3-D F XI(X, Y, Z)

RE	5000.0
ALPHA	1.1200
BETA	2.0000
SIGMA	0.043798
RMS	0.025000
MAX	1.119222
SYM	1

LEVELS:	MIN	-0.3859390
	DIF	0.0771877
	NO.	20
	X =	2.733071

Figure 3.204- ξ_3 as a function of x, y and z at a position of $x = 2.733071$ for $\mathbf{v}_{fa}$ at $\alpha = 1.12$, $Re = 5000$, $\beta = 2.00$ and $A = 0.025$.

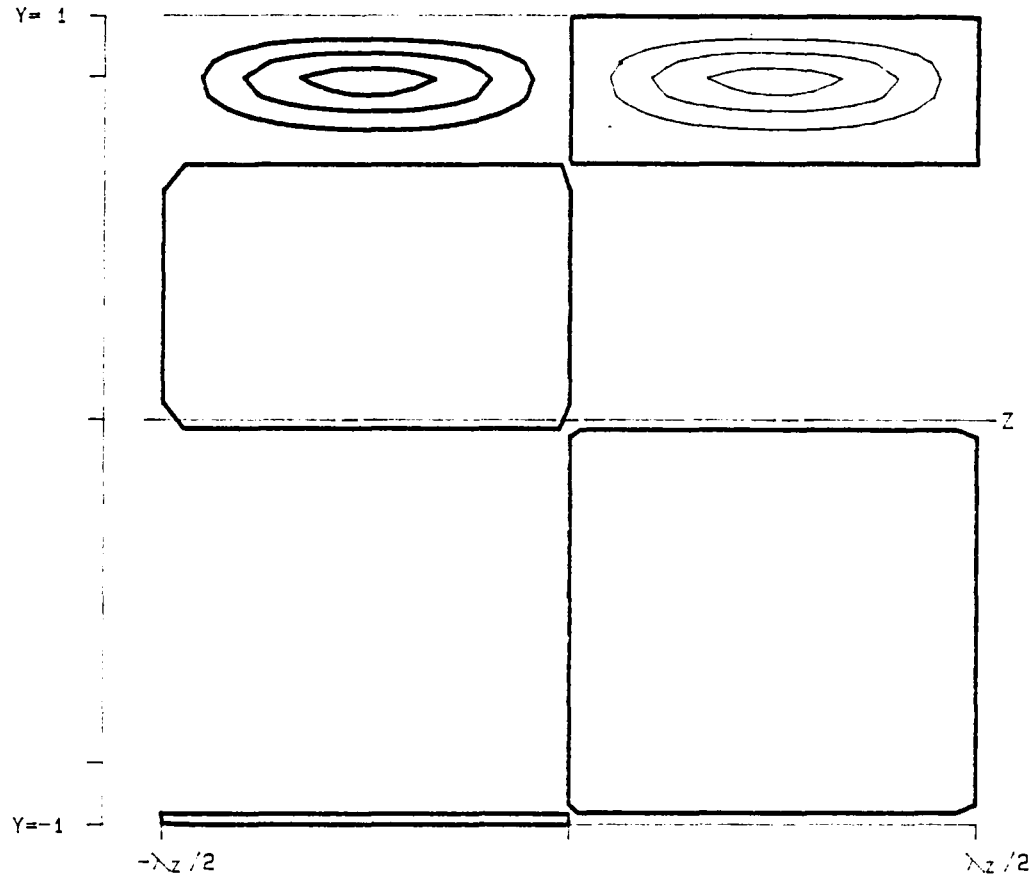

PPT 3-D F ETA(X, Y, Z)

RE	5000.0	LEVELS: MIN	-0.3859390
ALPHA	1.1200	DIF	0.0771877
BETA	2.0000	NO.	20
SIGMA	0.043798		
AMS	0.025000	X =	2.733071
MAX	1.119222		
SYM	1		

Figure 3.205- η_3 as a function of x, y and z at a position of $x = 2.733071$ for $\mathbf{v}_{fs}$ at $\alpha = 1.12$, $Re = 5000$, $\beta = 2.00$ and $A = 0.025$.

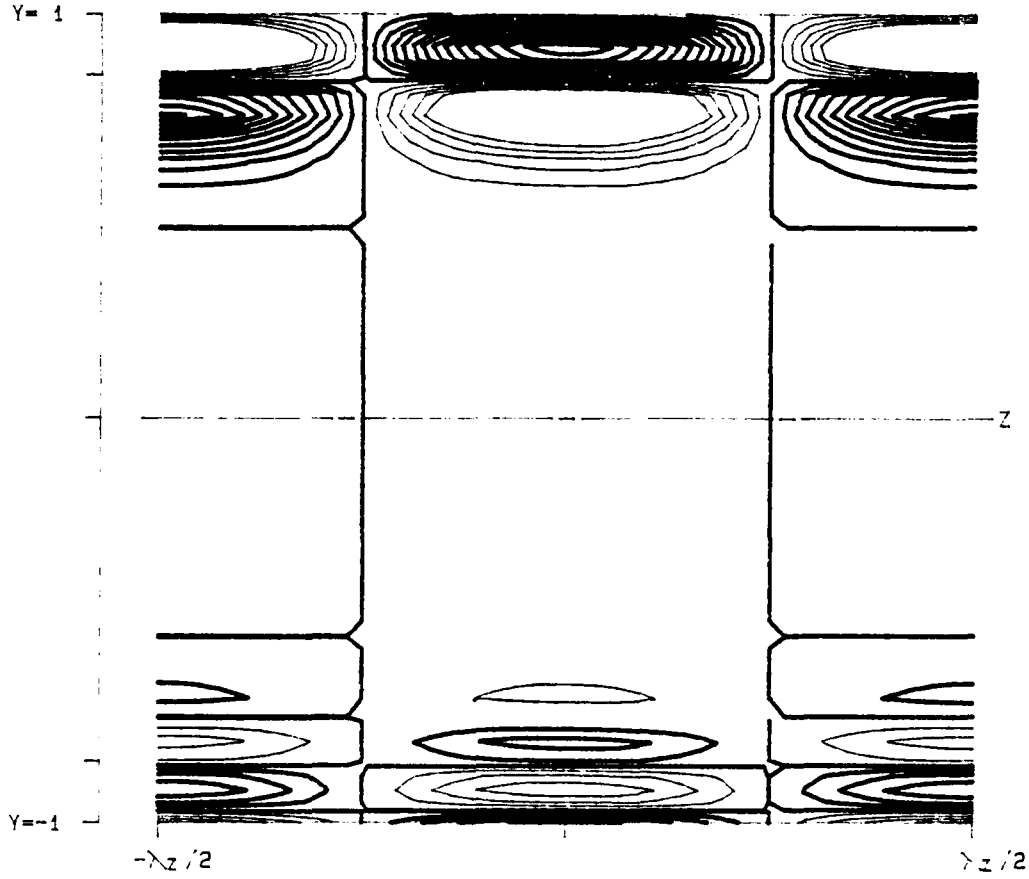

PPT 3-D F ZETA(X, Y, Z)

RE	5000.0	LEVELS: MIN	-0.3859390
ALPHA	1.1200	DIF	0.0771877
BETA	2.0000	NO.	20
SIGMA	0.043798		
RMS	0.025000	X =	2.733071
MAX	1.119222		
SYM	1		

Figure 3.206- ς_3 as a function of x, y and z at a position of $x = 2.733071$ for $\mathbf{v}_{f_a}$ at $\alpha = 1.12$, $Re = 5000$, $\beta = 2.00$ and $A = 0.025$.

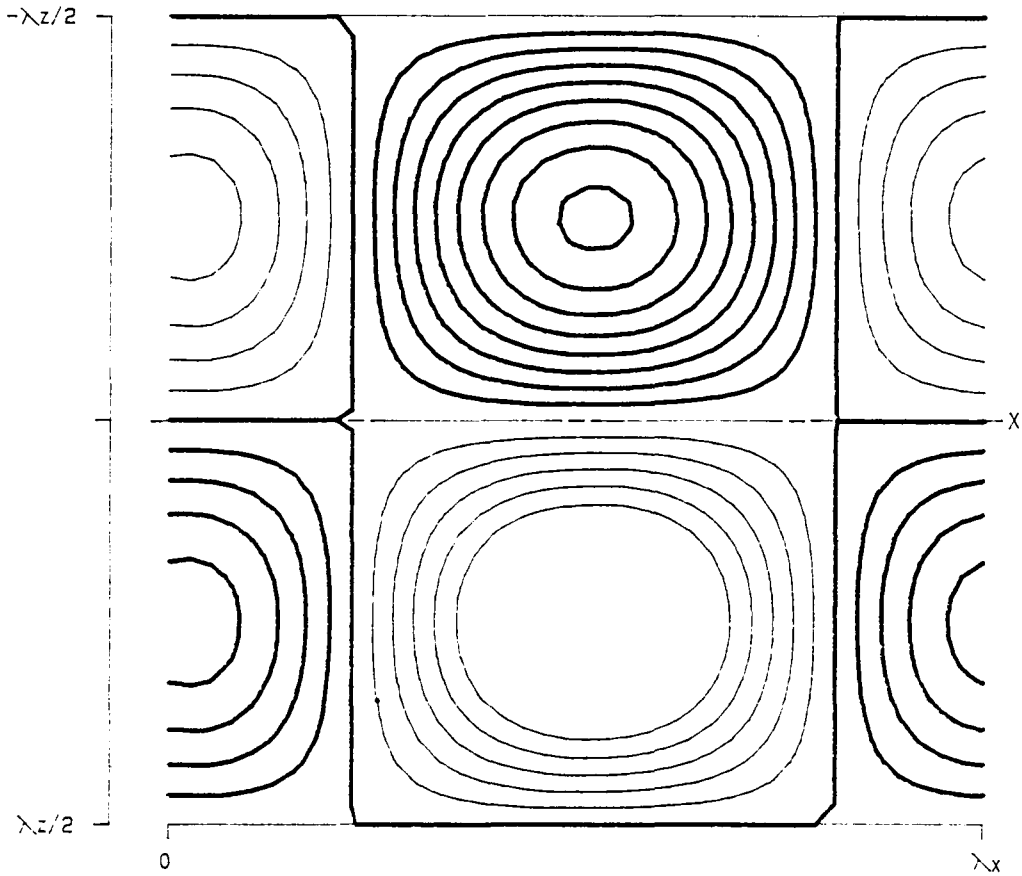

PPT 3-D F XI(X, Y, Z)

RE	5000.0
ALPHA	1.1200
BETA	2.0000
SIGMA	0.043798
RMS	0.025000
MAX	1.119222
SYM	1

LEVELS:	MIN	-0.3859390
	DIF	0.0771877
	NO.	20
	Y =	0.845190

Figure 3.207- ξ_3 as a function of x, y and z at a position of $y = 0.845190$ for $\mathbf{v}_{fa}$ at $\alpha = 1.12$, $Re = 5000$, $\beta = 2.00$ and $A = 0.025$.

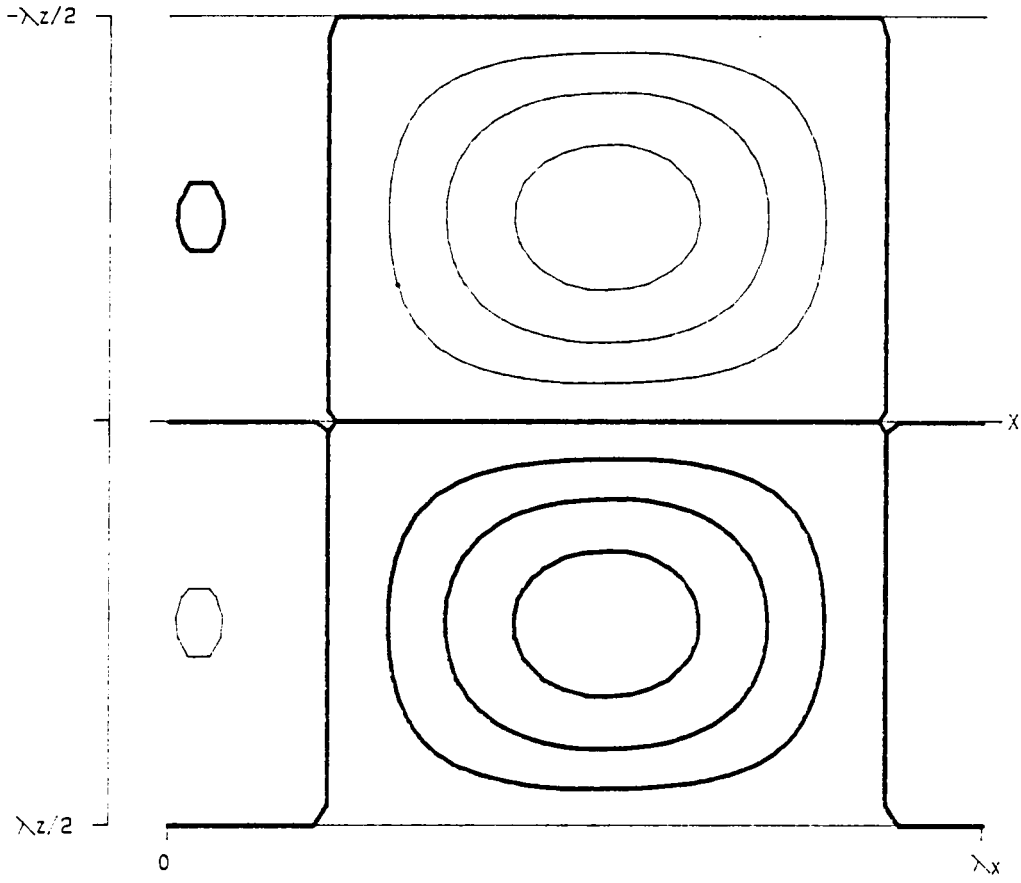

PPT 3-D F ETA(X, Y, Z)

RE	5000.0	LEVELS: MIN	-0.3859390
ALPHA	1.1200	DIF	0.0771877
BETA	2.0000	NO.	20
SIGMA	0.043798		
RMS	0.025000	Y =	0.845190
MAX	1.119222		
SYM	1		

Figure 3.208- η_3 as a function of x, y and z at a position of $y = 0.845190$ for $\mathbf{v}_{f_a}$ at $\alpha = 1.12$, $Re = 5000$, $\beta = 2.00$ and $A = 0.025$.

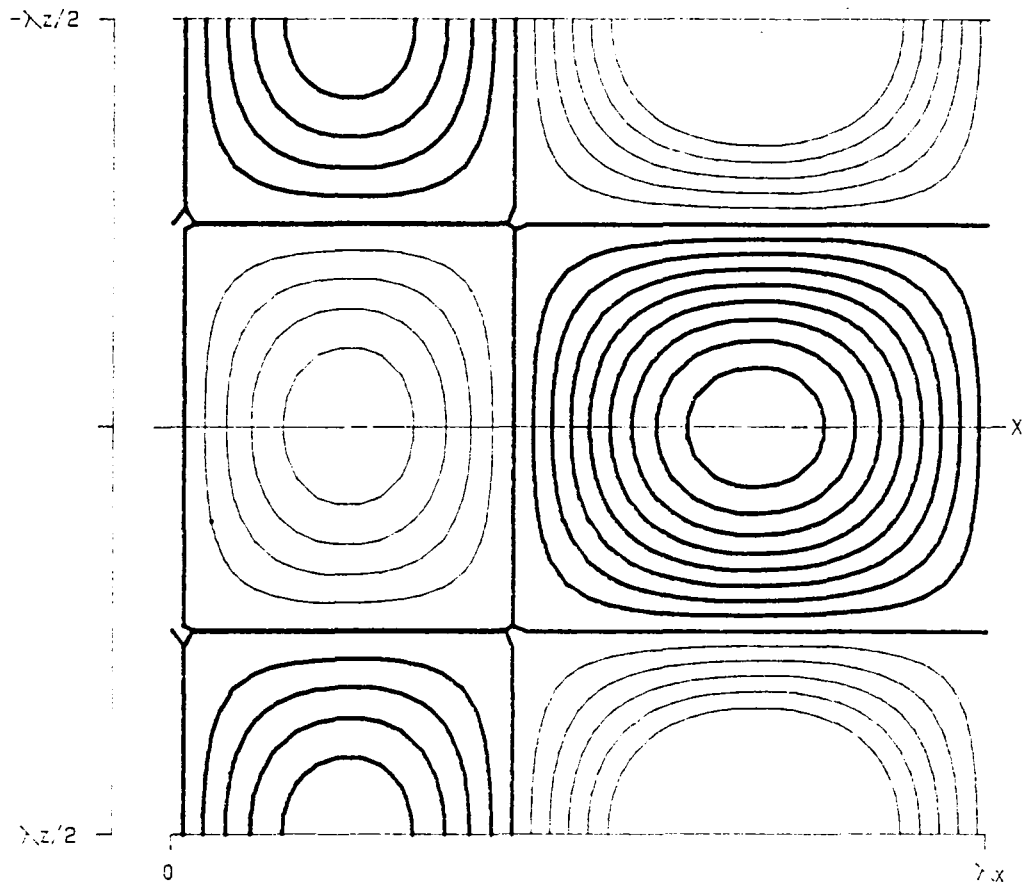

PPT 3-D F ZETA(X, Y, Z)

RE	5000.0
ALPHA	1.1200
BETA	2.0000
SIGMA	0.043798
RMS	0.025000
MAX	1.119222
SYM	1

LEVELS:	MIN	-0.3859390
	DIF	0.0771877
	NO.	20
	Y =	0.845190

Figure 3.209- ς_3 as a function of x, y and z at a position of $y = 0.845190$ for $\mathbf{v}_{fa}$ at $\alpha = 1.12$, $Re = 5000$, $\beta = 2.00$ and $A = 0.025$.

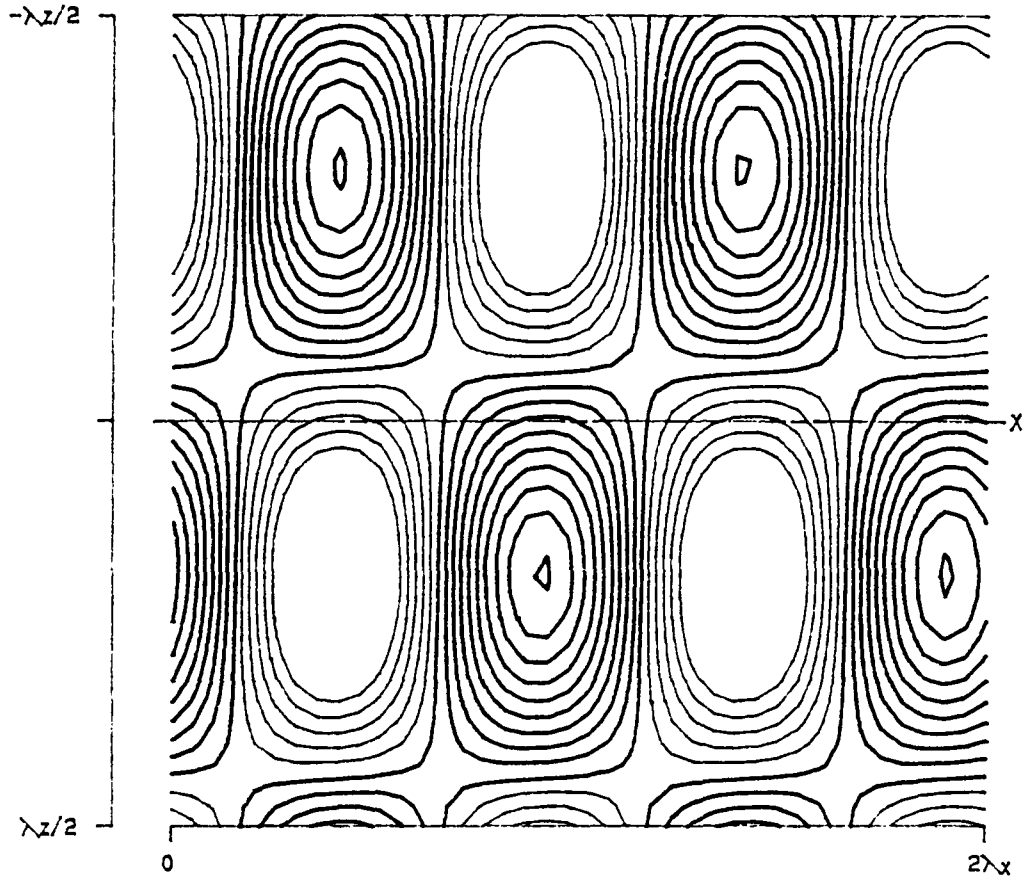

PPT 3-D S ZETA(X, Y, Z)

RE	5000.0	LEVELS: MIN	-0.2667158
ALPHA	1.1200	DIF	0.0533431
BETA	2.0000	NO.	20
SIGMA	0.044449,-0.001926		
RMS	0.025000	Y =	0.845190
MAX	0.773475		
SYM	1		

Figure 3.218- ς_3 as a function of x, y and z at a position of $y = 0.845190$ for $\mathbf{v}_s$ at $\alpha = 1.12$, $Re = 5000$, $\beta = 2.00$ and $A = 0.025$.

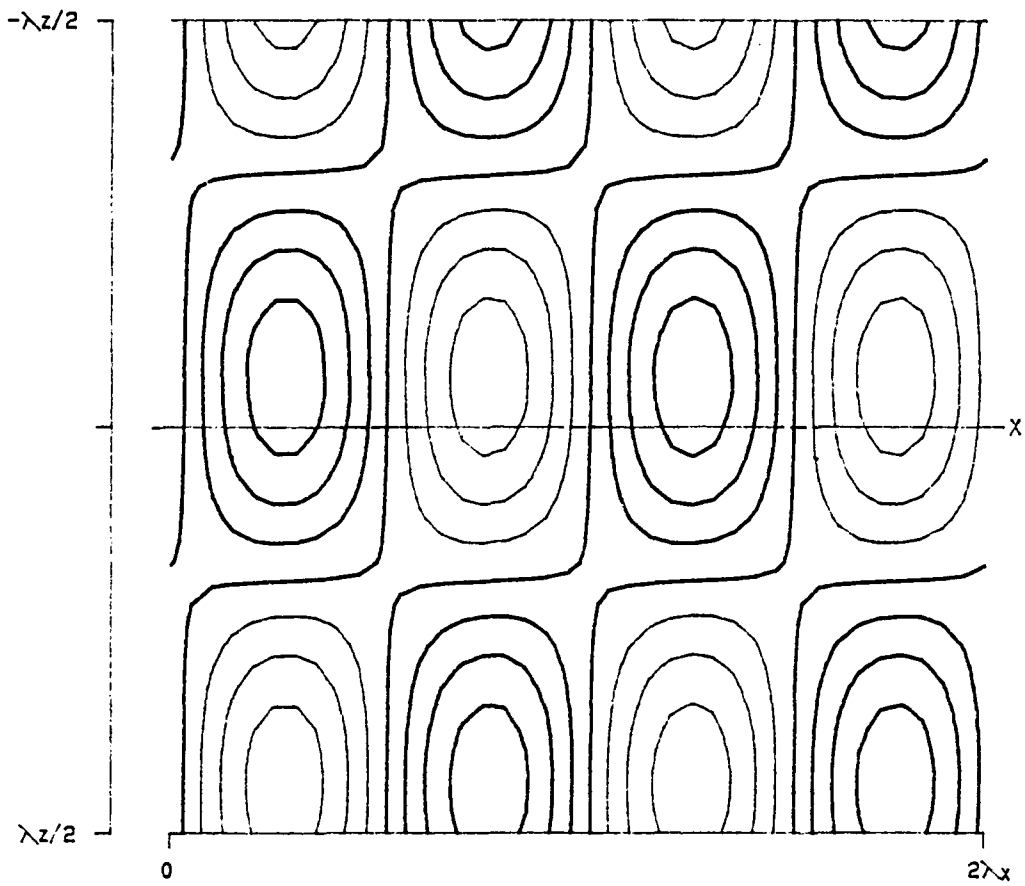

PPT 3-D S ETA(X, Y, Z)

RE	5000.0	LEVELS: MIN	-0.2667158
ALPHA	1.1200	DIF	0.0533431
BETA	2.0000	NO.	20
SIGMA	0.044449,-0.001926		
RMS	0.025000	Y =	0.845190
MAX	0.773475		
SYM	1		

Figure 3.217- η_3 as a function of x, y and z at a position of $y = 0.845190$ for $\mathbf{v}_s$ at $\alpha = 1.12$, $Re = 5000$, $\beta = 2.00$ and $A = 0.025$.

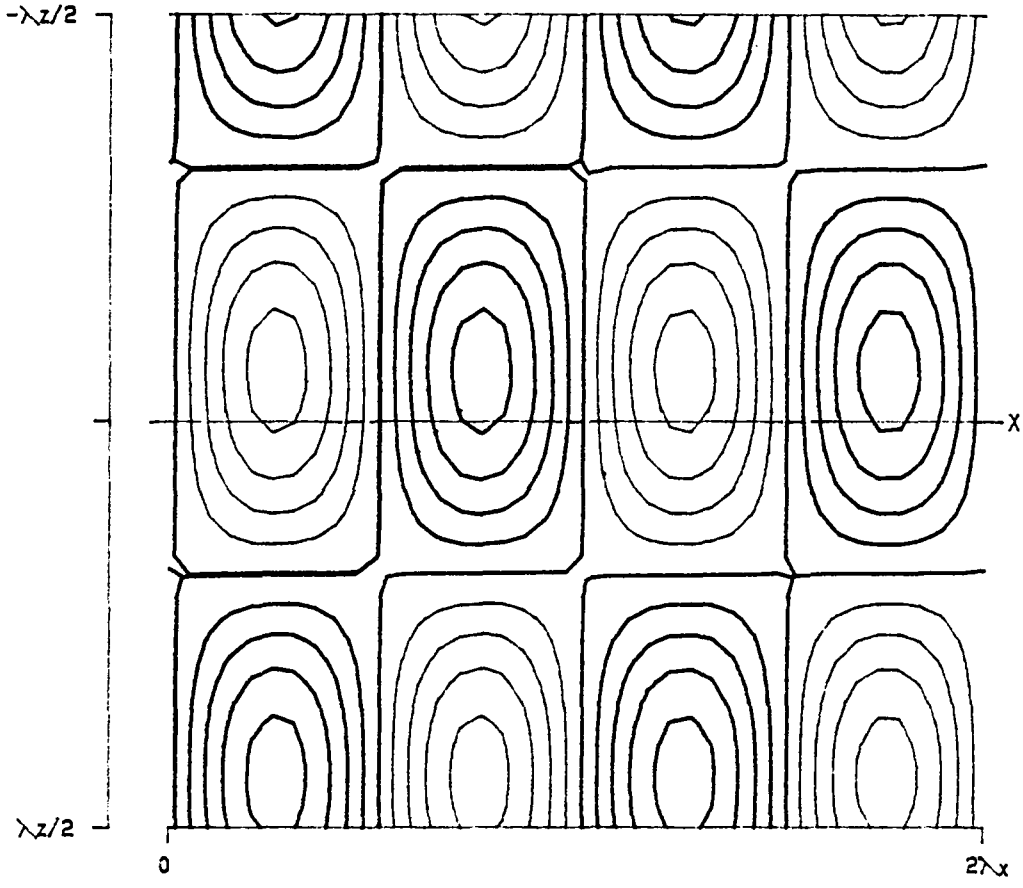

PPT 3-D S XI(X, Y, Z)

RE	5000.0	LEVELS:	MIN -0.2667158
ALPHA	1.1200		DIF 0.0533431
BETA	2.0000		NO. 20
SIGMA	0.044449,-0.001926		
RMS	0.025000		Y = 0.845190
MAX	0.773475		
SYM	1		

Figure 3.216- ξ_3 as a function of x, y and z at a position of $y = 0.845190$ for $\mathbf{v}_s$ at $\alpha = 1.12$, $Re = 5000$, $\beta = 2.00$ and $A = 0.025$.

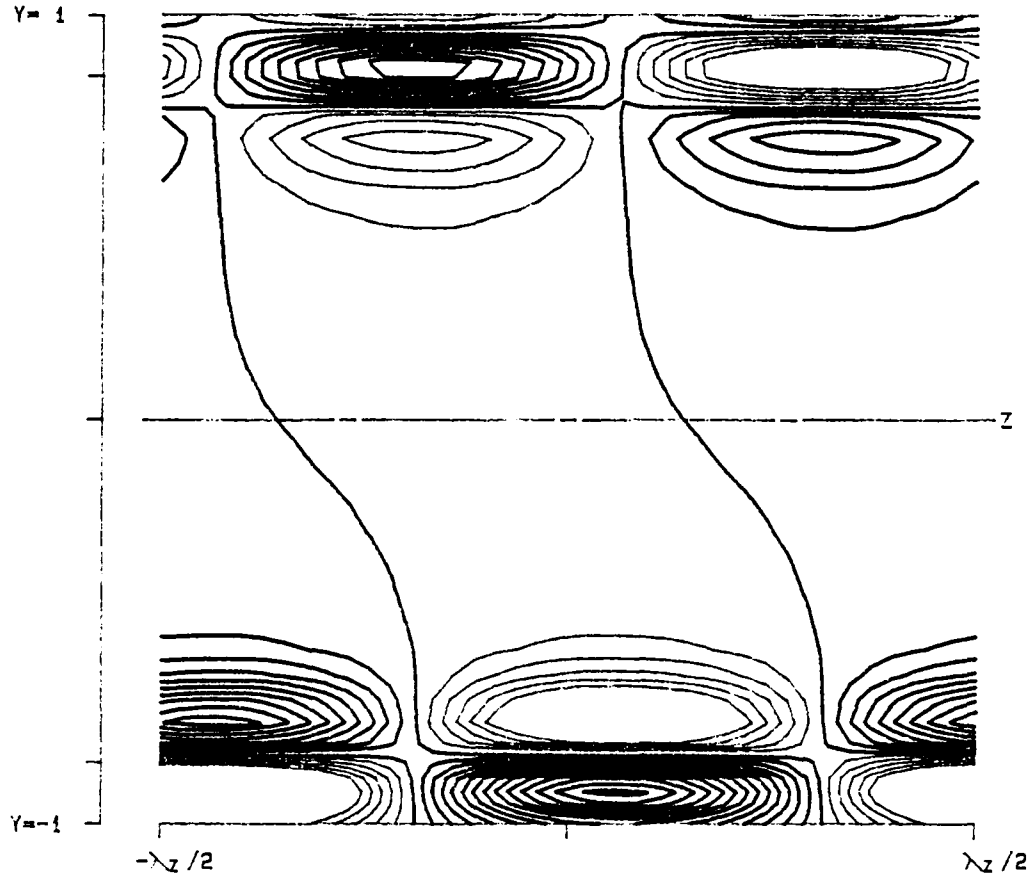

PPT 3-D S ZETA(X, Y, Z)

RE	5000.0	LEVELS: MIN	-0.2667158
ALPHA	1.1200	DIF	0.0533431
BETA	2.0000	NO.	20
SIGMA	0.044449,-0.001926		
RMS	0.025000	X =	5.466141
MAX	0.773475		
SYM	1		

Figure 3.215- ς_3 as a function of x, y and z at a position of $x = 5.466141$ for $\mathbf{v}_s$ at $\alpha = 1.12$, $Re = 5000$, $\beta = 2.00$ and $A = 0.025$.

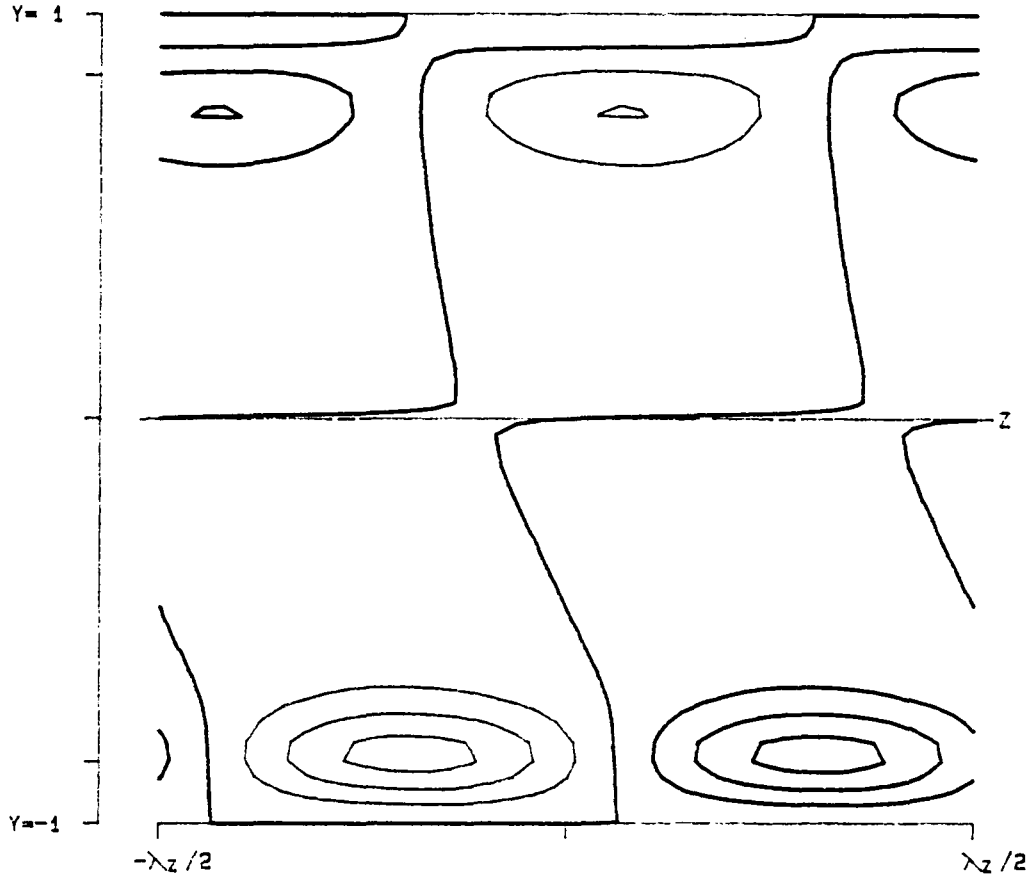

PPT 3-D S ETA(X, Y, Z)

RE	5000.0	LEVELS:	MIN -0.2667158
ALPHA	1.1200		DIF 0.0533431
BETA	2.0000		NO. 20
SIGMA	0.044449,-0.001926		
RMS	0.025000		X = 5.466141
MAX	0.773475		
SYM	1		

Figure 3.214- η_3 as a function of x, y and z at a position of $x = 5.466141$ for $\mathbf{v}_s$ at $\alpha = 1.12$, $Re = 5000$, $\beta = 2.00$ and $A = 0.025$.

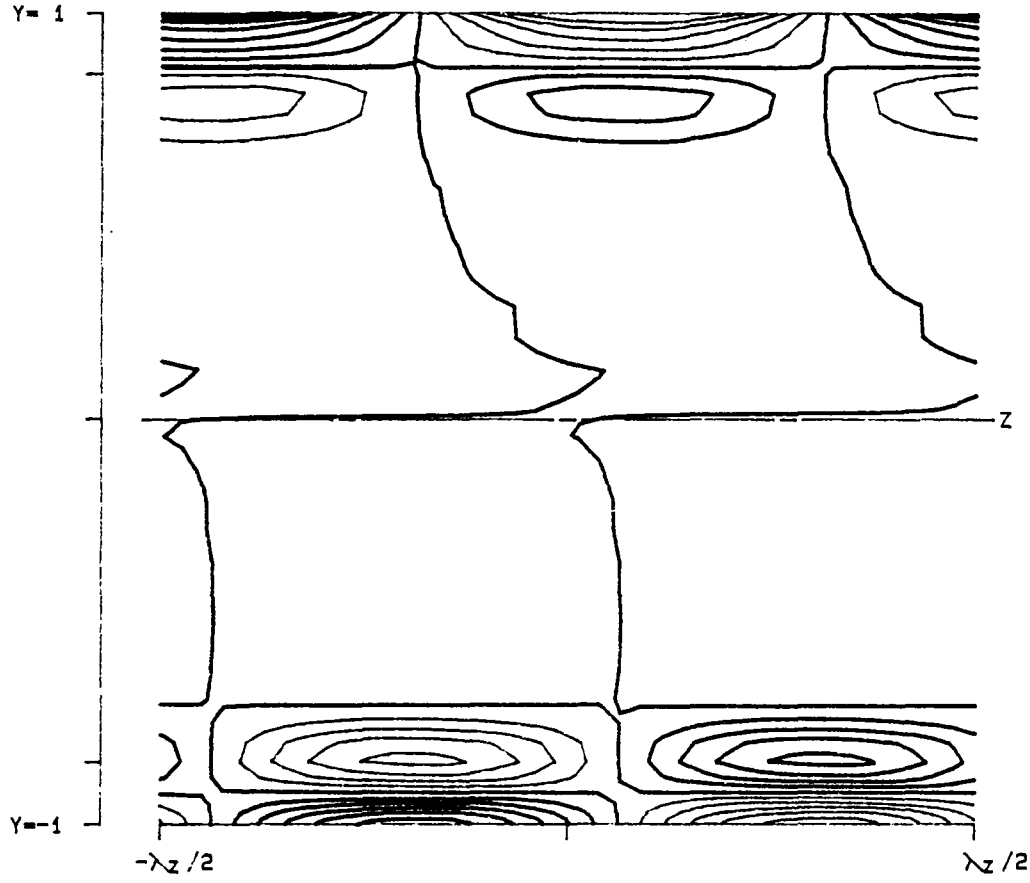

PPT 3-D S XI(X, Y, Z)

RE	5000.0	LEVELS: MIN	-0.2667158
ALPHA	1.1200	DIF	0.0533431
BETA	2.0000	NO.	20
SIGMA	0.044449,-0.001926		
RMS	0.025000	X =	5.466141
MAX	0.773475		
SYM	1		

Figure 3.213- ξ_3 as a function of x, y and z at a position of $x = 5.466141$ for $\mathbf{v}_s$ at $\alpha = 1.12$, $Re = 5000$, $\beta = 2.00$ and $A = 0.025$.

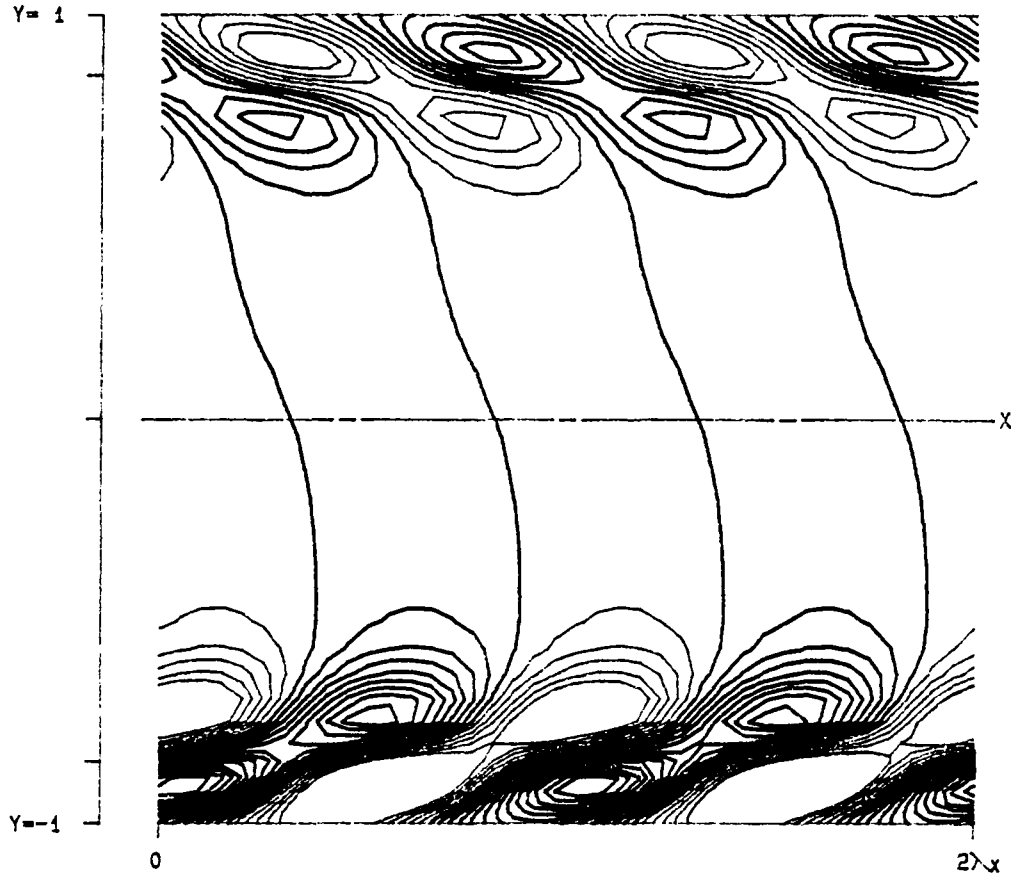

PPT 3-D S ZETA(X, Y, Z)

RE	5000.0	LEVELS: MIN	-0.2667158
ALPHA	1.1200	DIF	0.0533431
BETA	2.0000	NO.	20
SIGMA	0.044449,-0.001926		
RMS	0.025000	Z =	-0.040277
MAX	0.773475		
SYM	1		

Figure 3.212- ς_3 as a function of x, y and z at a position of $z = -0.040277$ for $\mathbf{v}_s$ at $\alpha = 1.12$, $Re = 5000$, $\beta = 2.00$ and $A = 0.025$.

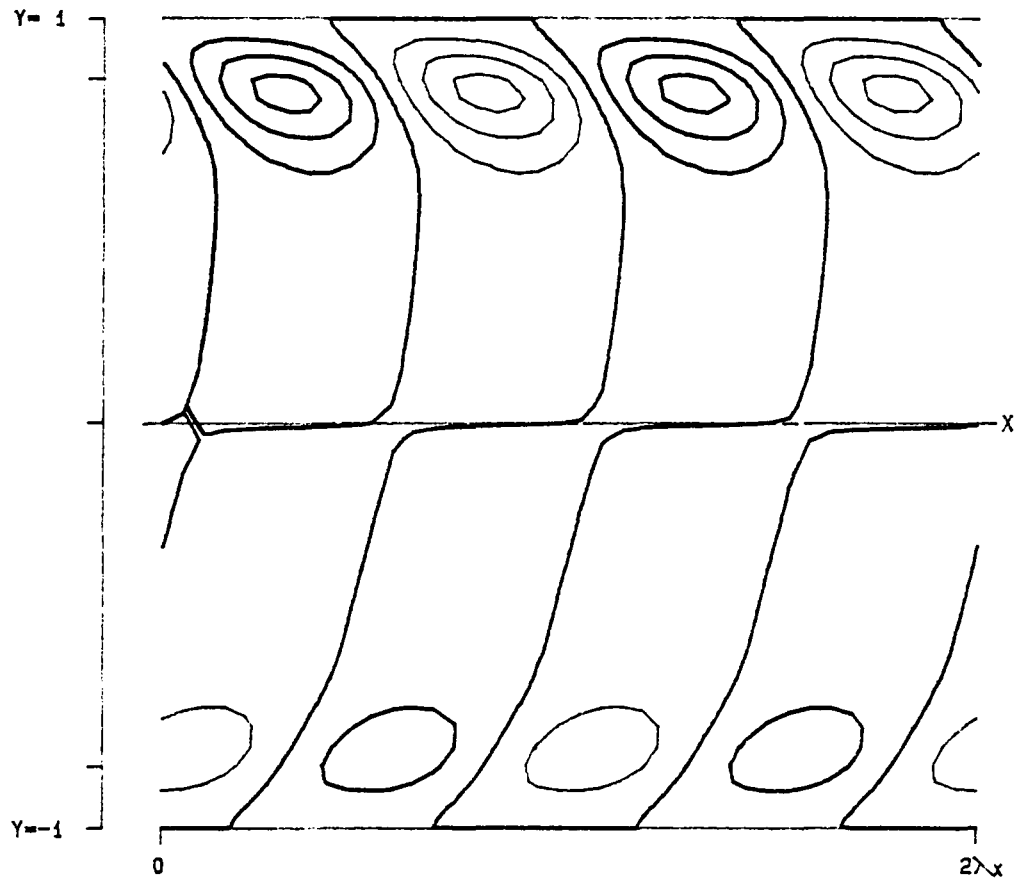

PPT 3-D S ETA(X, Y, Z)

RE	5000.0	LEVELS: MIN	-0.2667158
ALPHA	1.1200	DIF	0.0533431
BETA	2.0000	NO.	20
SIGMA	0.044449,-0.001926		
RMS	0.025000	Z =	-0.040277
MAX	0.773475		
SYM	1		

Figure 3.211- η_3 as a function of x, y and z at a position of $z = -0.040277$ for $\mathbf{v}_s$ at $\alpha = 1.12$, $Re = 5000$, $\beta = 2.00$ and $A = 0.025$.

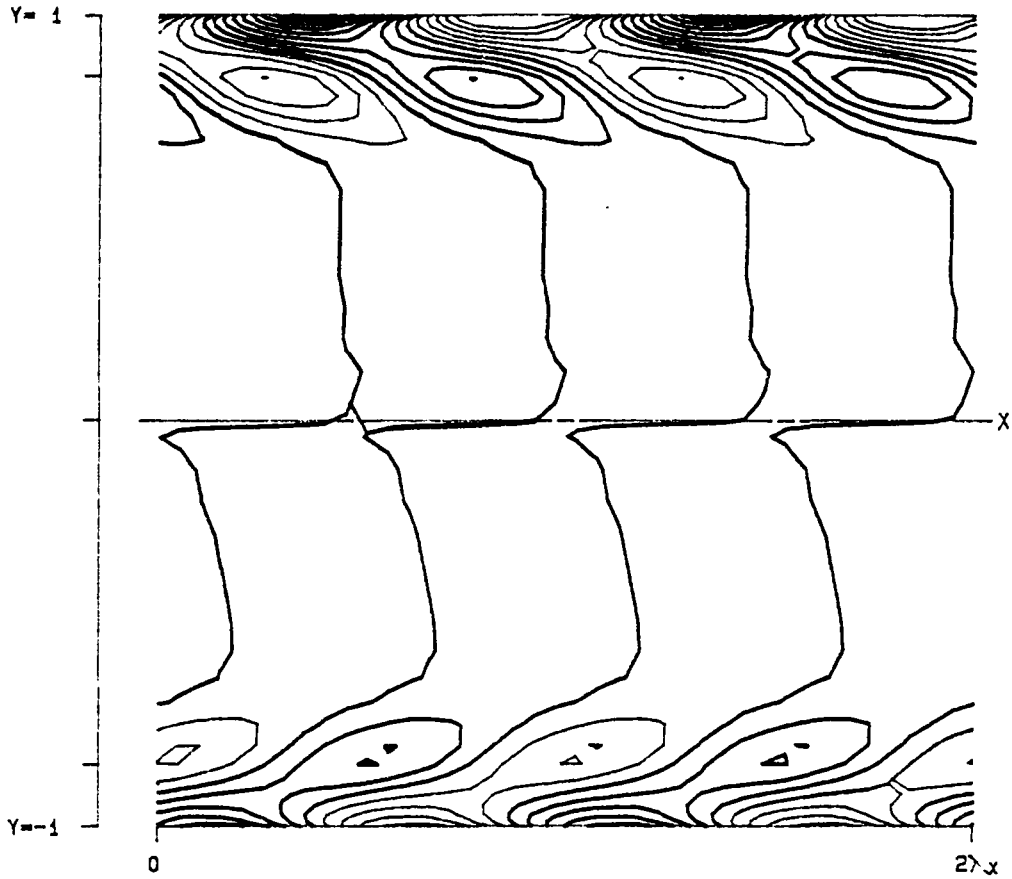

PPT 3-D S XI(X, Y, Z)

RE	5000.0	LEVELS: MIN	-0.2667158
ALPHA	1.1200	DIF	0.0533431
BETA	2.0000	NO.	20
SIGMA	0.044449,-0.001926		
RMS	0.025000	Z =	-0.040277
MAX	0.773475		
SYM	1		

Figure 3.210- ξ_3 as a function of x, y and z at a position of $z = -0.040277$ for $\mathbf{v}_s$ at $\alpha = 1.12$, $Re = 5000$, $\beta = 2.00$ and $A = 0.025$.

References

Benney, D.J. & Lin, C.C. 1960 On the secondary motion induced by oscillations in a shear flow. Phys. Fluids **3**, 656.

Busse, F.H. 1981 Transition to turbulence in Rayleigh-Bénard convection. In Hydrodynamic Instabilities and the Transition to Turbulence (eds. H.L. Swinney & J.P. Gollup), p.97, Springer -Verlag.

Coddington, E.A. & Levinson, N. 1955 Theory of Ordinary Differential Equations. McGraw-Hill.

Craik, A.D.D. 1971 Non-linear resonant instability in boundary layers. J. Fluid Mech. **50**, 393.

Davies, S.J. & White. C.M. 1928 An experimental study of the flow of water in pipes of rectangular section. Proc. R. Soc. Lond. A **119**, 92.

DiPrima, R.C. & Swinney, H.L. 1981 Instabilities and transition in flow between concentric rotating cylinders. In Hydrodynamic Instabilities and the Transition to Turbulence (eds. H.L. Swinney & J.P. Gollup), p.139, Springer -Verlag.

Drazin, P.G. & Reid, W.H. 1981 Hydrodynamic Instability. Cambridge University Press.

Heisenberg, W. 1924 Uber Stabilitt und Turbulenz von Flüssigkeitsströmung. Ann. d. Phys. **74**, 577.

Herbert, T. 1977 Finite-amplitude stability of plane parallel flows. AGARD Conf. Proc. CP-224, p.3/1.

Herbert, T. & Morkovin, M.V. 1980 Dialogue on bridging some gaps in stability and transition research. In Laminar-Turbulent Transition (eds. R. Eppler & H. Fasel), p.47, Springer -Verlag.

Herbert, T. 1981 A secondary stability mechanism in plane Poiseuille flow. Bull. Amer. Phys. Soc. **26**, 1257.

Herbert, T. 1983a Secondary instability of plane channel flow to subharmonic three-dimensional disturbances. Phys. Fluids **26**, 871.

Herbert, T. 1983b Modes of secondary instability in plane Poiseuille flow. Proc. IUTAM Symp., Turbulence and Chaotic Phenomena in Fluids, Kyoto, Japan.

Herbert, T. 1983c Subharmonic three-dimensional disturbances in unstable plane shear flows. AIAA Paper No. 83-1759.

Herbert, T. 1983d Stability of plane Poiseuille flow-theory and experiment. Fluid Dyn. Trans. **11**, 77.

Herbert, T. 1984 Stability and transition of laminar flows. Von Karmann Institute for Fluid Dynamics Special Course.

Kachanov, Y.S. & Levchenko, V.Y. 1982 Resonant interactions of disturbances in transition to turbulence in a boundary layer (in Russian). Preprint No. 10-82, I.T.A.M., USSR Academy of Sciences, Novosibirsk.

Kao, T.W. & Park, C. 1970 Experimental investigations of the stability of channel flows. Part 1. Flow of a single liquid in a rectangular channel. J. Fluid Mech. **43**, 145.

Klebanoff, P.S., Tidstrom, K.D. & Sargent, L.M. 1962 The three-dimensional nature of boundary layer instability. J. Fluid Mech. **12**, 1.

Meksyn, D. & Stuart, J.T. 1951 Stability of viscous motion between parallel planes for finite disturbances. Proc. R. Lon. Soc. A **208**, 517.

Nayfeh, A.H. & Mook, D.T. 1979 Non-linear Oscillations. Wiley.

Nishioka, M., Iida, S. & Ichikawa, Y. 1975 An experimental investigation of the stability of plane Poiseuille flow. J. Fluid Mech. **72**, 731.

Nishioka, M., Asai, M. & Iida, S. 1980 An experimental investigation of secondary instability. In Laminar-Turbulent Transition (eds. R. Eppler & H. Fasel), p.37, Springer-Verlag.

Nishioka, M., Asai, M. & Iida, S. 1981 Wall phenomena in the final stage of transition to turbulence. In Transition and Turbulence (ed. R.E. Meyer), p.113. Academic Press.

Orszag, S.A. 1971 Accurate solution to the Orr-Sommerfeld stability equation. J. Fluid Mech. **50**, 689.

Orszag, S.A. & Patera, A.T. 1980a Subcritical transition to turbulence in plane channel flows. Phys. Rev. Lett. **45**, 989.

Orszag, S.A. & Patera, A.T. 1980b Transition to turbulence in plane Poiseuille flow and plane Couette flow. J. Fluid Mech. **96**, 159.

Orszag, S.A. & Patera, A.T. 1981 Subcritical transition to turbulence in plane shear flows. In Transition and Turbulence (ed. R.E. Meyer). Academic Press.

Orszag, S.A. & Patera, A.T. 1983 Secondary instability of wall bounded shear flows. J. Fluid Mech. **128**, 347.

Radbill, J.R. & McCue, G.A. 1970 Quasilinearization and Non-linear Problems in Fluid and Orbital Mechanics. American Elsevier.

Rayleigh, Lord F.R.S. 1878 On the stability of jets. Proc. Lond. Math. Soc., Vol. 10, 4.

Rayleigh, Lord F.R.S. 1880 On the stability, or instability, of certain fluid motions. Proc. Lond Math. Soc., Vol 11, 57.

Rayleigh, Lord F.R.S. 1916 On the dynamics of revolving fluids. Proc. R. Soc. Lond. A **93**, 148.

Reynolds, W.C. & Potter, M.C. 1967 Finite-amplitude instability of parallel shear flows. J. Fluid Mech. **27**, 465.

Saric, W.S. & Thomas, A.S.W. 1981 Harmonic and subharmonic waves during boundary layer transition. Bull. Amer. Phys. Soc. **26**, 1252.

Schubauer, G.B. & Skramstad, H.K. 1947 Laminar boundary-layer oscillations and transition on a flat plate. J. Res. Nat. Bur. Stan., Vol 38, Nat. Bur. Stan.

Schlichting, H. 1933 Zur Entstehung der Turbulenz bei der Plattenströmung. Nachr. Ges. Wiss. Göttingen, Math. Phys. Klasse 182-208.

Squire, H.B. 1933 On the stability for three-dimensional disturbances of viscous fluid flow between parallel walls. Proc. R. Lond. Soc. A **142**, 621.

Stuart, J.T. 1958 On the non-linear mechanics of hydrodynamic stability. J. Fluid Mech. **4**, 1.

Stuart, J.T. 1960 On the non-linear mechanics of wave disturbances in stable and unstable parallel flows. J. Fluid Mech. **9**, 353.

Tollmien, W. 1929 Uber die Entstehung der Turbulenz. #1. Mitt., Nachr. Ges. Wiss. Göttingen, Math. Phys. Klasse, 21; Engl. transl. in NACA TM 609 (1931).

Appendix I

This appendix contains the detailed form of the vorticity and each of the terms in the energy equation for the disturbance (2.24). In addition, we show that the complimentary energy transfer terms $T^{(ij)}$ and $T^{(\bar{i}\bar{j})}$ are equal in magnitude, but opposite in sign. In Sectiion 2.1, we found a solution of the Orr-Sommerfeld equation could be written in real form as follows:

$$\begin{aligned} \mathbf{v}_1(x,y) &= \mathbf{v}_0(y) + A\mathbf{v}_1(x,y) \\ &= \mathbf{v}_0(y) + 2A[\ \mathbf{v}_1^+\cos\alpha x - \mathbf{v}_1^-\sin\alpha x\ ] \quad . \end{aligned} \tag{A1.1}$$

Substitution of (A1.1) into the expression for the vorticity of the disturbance (2.16) gives

$$\begin{aligned} \varsigma_1 &= A\left(\frac{\partial v_1}{\partial x} - \frac{\partial u_1}{\partial y}\right)\mathbf{k} \\ &= -2A\Big\{[\ Du_1^+ + \alpha v_1^-\ ]\cos\alpha x - [\ Du_1^- - \alpha v_1^+\ ]\sin\alpha x\Big\}\mathbf{k} \quad . \end{aligned} \tag{A1.2}$$

The energy transfer terms $T^{(01)}$, $T^{(10)}$ in Section 2 were defined as

$$\begin{aligned} T^{(01)} &= -\int_\Omega A^2\mathbf{v}_1\cdot\nabla\mathbf{v}_1\cdot\mathbf{v}_0\ d\Omega \\ T^{(10)} &= -\int_\Omega A^2\mathbf{v}_1\cdot\nabla\mathbf{v}_0\cdot\mathbf{v}_1\ d\Omega \end{aligned} \tag{A1.3}$$

Recall that the components of the velocity field are defined as

$$\mathbf{v}_0 = (U,0,0), \qquad \mathbf{v}_1 = (u_1,v_1,0) \tag{A1.4}$$

$$\mathbf{v}_0 = \mathbf{v}_0(y), \qquad \mathbf{v}_1(x,y) = \mathbf{v}_1(x+\lambda_x,y), \quad \lambda_x = \frac{2\pi}{\alpha} \quad .$$

Now consider the following vector identity:

(A1.5)

$$\int_{\Omega} \nabla[\mathbf{v}_1 \cdot \mathbf{v}_0] \, d\Omega = \int_{\Omega} \left\{ \nabla \mathbf{v}_1 \cdot \mathbf{v}_0 + \nabla \mathbf{v}_0 \cdot \mathbf{v}_1 + \mathbf{v}_0 \times (\nabla \times \mathbf{v}_1) + \mathbf{v}_1 \times (\nabla \times \mathbf{v}_0) \right\} d\Omega \quad .$$

Expanding the left hand side of (A1.5) gives.

$$\int_{\Omega} \nabla[\mathbf{v}_1 \cdot \mathbf{v}_0] \, d\Omega = \int_{\Omega} \left\{ \frac{\partial}{\partial x}(\mathbf{v}_1 \cdot \mathbf{v}_0)\, \mathbf{i} + \frac{\partial}{\partial y}(\mathbf{v}_1 \cdot \mathbf{v}_0)\, \mathbf{j} + \frac{\partial}{\partial z}(\mathbf{v}_1 \cdot \mathbf{v}_0)\, \mathbf{k} \right\} d\Omega \equiv 0$$

because of the periodicity of $\mathbf{v}_1$ over Ω. Continuing, the cross-product terms in (A1.5) become

$$\int_{\Omega} \mathbf{v}_0 \times (\nabla \times \mathbf{v}_1) \, d\Omega = \int_{\Omega} - \left(\frac{\partial \mathbf{v}_1}{\partial x} - \frac{\partial u_1}{\partial y} \right) U \mathbf{j} \, d\Omega = 0$$

$$\int_{\Omega} \mathbf{v}_1 \times (\nabla \times \mathbf{v}_0) \, d\Omega = \int_{\Omega} - (v_1 \, \mathbf{i} - u_1 \, \mathbf{j}) \frac{dU}{dy} \, d\Omega = 0$$

since $\mathbf{v}_1$ is periodic over Ω. Thus, (A1.5) reduces to

$$0 = \int_{\Omega} \nabla \mathbf{v}_1 \cdot \mathbf{v}_0 \, d\Omega + \int_{\Omega} \nabla \mathbf{v}_0 \cdot \mathbf{v}_1 \, d\Omega \quad . \tag{A1.6}$$

Multiplying (A1.6) by $A^2 \mathbf{v}_1$ gives

$$\int_{\Omega} A^2 \mathbf{v}_1 \cdot \nabla \mathbf{v}_1 \cdot \mathbf{v}_0 \, d\Omega = - \int_{\Omega} A^2 \mathbf{v}_1 \cdot \nabla \mathbf{v}_0 \cdot \mathbf{v}_1 \, d\Omega$$

or

$$T^{(01)} = - T^{(10)} \quad .$$

We can then rewrite the energy equations (2.23)-(2.24) as

$$\frac{dE^{(0)}}{dt} = - T^{(10)} + D^{(0)} \tag{A1.7}$$

$$\frac{dE^{(1)}}{dt} = T^{(10)} + D^{(1)} \tag{A1.8}$$

as in Section 2.

Substitution of solution (A1.1) into the disturbance energy equation (A1.8) gives

$$\frac{dE^{(1)}}{dt} = - \int_{\Omega} A^2 \mathbf{v}_1 \cdot \nabla \mathbf{v}_0 \cdot \mathbf{v}_1 \, d\Omega + \frac{1}{Re} \int_{\Omega} A^2 \nabla^2 \mathbf{v}_1 \cdot \mathbf{v}_1 \, d\Omega \tag{A1.9}$$

$$= - \int_{\Omega} 4A \left\{ u_1^+ v_1^+ \cos^2 \alpha x - (u_1^+ v_1^- + u_1^- v_1^+) \sin 2\alpha x + u_1^- v_1^- \sin^2 \alpha x \right\} \frac{dU}{dy} \, d\Omega$$

$$- \frac{1}{R} e \int_{\Omega} 4A^2 \left\{ [D\mathbf{v}_1^+ \cdot D\mathbf{v}_1^+ + \alpha^2 \mathbf{v}_1^- \cdot \mathbf{v}_1^-] \cos^2 \alpha x - [D\mathbf{v}_1^+ \cdot D\mathbf{v}_1^- - \alpha^2 \mathbf{v}_1^+ \cdot \mathbf{v}_1^-] \sin 2\alpha x \right.$$

$$\left. + [D\mathbf{v}_1^- \cdot D\mathbf{v}_1^- + \alpha^2 \mathbf{v}_1^+ \cdot \mathbf{v}_1^+] \sin^2 \alpha x \right\} d\Omega \quad .$$

The results of integrating equation (A1.9) appear in Section 2.2.

Appendix II

This appendix contains the detailed form of the three-dimensional disturbance vorticity and each of the terms in the energy equation (3.37). In addition, we also have a similar treatment to that in Appendix I to show that the complimentary energy transfer terms $T^{(ij)}$ and $T^{(\bar{i}\bar{j})}$, involving the fundamental and subharmonic modes, are equal in magnitude but opposite in sign. To begin, recall that in Section 3, a real formulation of the fundamental and subharmonic modes was obtained by adding a complex conjugate solution ($\hat{\mathbf{v}}_f$ and $\hat{\mathbf{v}}_s$) to (3.13) and (3.14), respectively, resulting in

$$\mathbf{v}_f(x,y,z,t) = \hat{\mathbf{v}}_f(x,y,z) + \tilde{\mathbf{v}}_f(x,y,z) \tag{A2.1}$$

$$\begin{aligned} &= 2e^{\sigma t}\Big\{ \big[\, u_0^+ + 2(u_2^+ \cos\alpha x - u_2^- \sin\alpha x)\,\big]\cos\beta z\ \mathbf{i} \\ &\quad + \big[\, v_0^+ + 2(v_2^+ \cos\alpha x - v_2^- \sin\alpha x)\,\big]\cos\beta z\ \mathbf{j} \\ &\quad - \big[\, w_0^- + 2(w_2^+ \cos\alpha x - w_2^- \sin\alpha x)\,\big]\sin\beta z\ \mathbf{k}\Big\} \end{aligned}$$

and

$$\mathbf{v}_s(x,y,z,t) = \hat{\mathbf{v}}_s(x,y,z) + \tilde{\mathbf{v}}_s(x,y,z) \tag{A2.2}$$

$$\begin{aligned} &= 4e^{\sigma t}\Big\{ \big[\, u_{11}^+ \cos\frac{\alpha}{2}x - u_{11}^- \sin\frac{\alpha}{2}x\,\big]\cos\nu\ \mathbf{i} - \big[\, u_{12}^+ \cos\frac{\alpha}{2}x - u_{12}^- \sin\frac{\alpha}{2}x\,\big]\sin\nu\ \mathbf{i} \\ &\quad + \big[\, v_{11}^+ \cos\frac{\alpha}{2}x - v_{11}^- \sin\frac{\alpha}{2}x\,\big]\cos\nu\ \mathbf{j} - \big[\, v_{12}^+ \cos\frac{\alpha}{2}x - v_{12}^- \sin\frac{\alpha}{2}x\,\big]\sin\nu\ \mathbf{j} \\ &\quad - \big[\, w_{11}^- \cos\frac{\alpha}{2}x - w_{11}^- \sin\frac{\alpha}{2}x\,\big]\cos\nu\ \mathbf{k} - \big[\, w_{12}^+ \cos\frac{\alpha}{2}x - w_{12}^- \sin\frac{\alpha}{2}x\,\big]\sin\nu\ \mathbf{k}\Big\} \end{aligned}$$

The vorticity generated by the disturbance is given by (3.19)

$$\omega_3 = \nabla \times \mathbf{v}_3 = B(\xi_3, \eta_3, \zeta_3) \tag{A2.3}$$
$$= B\left\{ \left[\frac{\partial w_3}{\partial y} - \frac{\partial v_3}{\partial z} \right] \mathbf{i} - \left[\frac{\partial w_3}{\partial x} - \frac{\partial u_3}{\partial z} \right] \mathbf{j} + \left[\frac{\partial v_3}{\partial x} - \frac{\partial u_3}{\partial y} \right] \mathbf{k} \right\}$$

with the amplitude of the disturbance defined by $B = B_0 e^{\sigma_r t}$. Substitution of (A2.1) and (A2.2) into (A2.3) gives, for the fundamental

$$\omega_f = \nabla \times B\mathbf{v}_f \tag{A2.4}$$
$$= -2B\Big[\{ [Dw_0^- - \beta v_0^-] + 2[Dw_2^+ - \beta v_2^+]\cos\alpha x - 2[Dw_2^- - \beta v_2^-]\sin\alpha x \} \sin\beta z \mathbf{i}$$
$$- \{ \beta u_0^+ + 2[\beta u_2^+ + \alpha w_2^-]\cos\alpha x - 2[\beta u_2^- - \alpha w_2^+]\sin\alpha x \} \sin\beta z \mathbf{j}$$
$$- \{ Du_0^+ + 2[Du_2^+ + \alpha v_2^-]\cos\alpha x - 2[Du_2^- - \alpha v_2^+]\sin\alpha x \} \cos\beta z \mathbf{k} \Big] .$$

The expression for the subharmonic is given by

$$\omega_s = \nabla \times B\mathbf{v}_s \tag{A2.5}$$
$$= 4B\Big[\{ [(Dw_{11}^+ + \beta v_{12}^+)\cos\hat{\alpha}x - (Dw_{11}^- + \beta v_{12}^-)\sin\hat{\alpha}x] \cos\nu$$
$$- [(Dw_{12}^+ - \beta v_{11}^+)\cos\hat{\alpha}x - (Dw_{12}^- - \beta v_{11}^-)\sin\hat{\alpha}x] \sin\nu \} \mathbf{i}$$

$$+ \{ [(\hat{\alpha} w_{11}^- - \beta u_{12}^+)\cos\hat{\alpha}x + (\hat{\alpha} w_{11}^+ + \beta u_{12}^-)\sin\hat{\alpha}x] \cos\nu$$
$$- [(\hat{\alpha} w_{12}^- + \beta u_{11}^+)\cos\hat{\alpha}x + (\hat{\alpha} w_{12}^+ - \beta u_{11}^-)\sin\hat{\alpha}x] \sin\nu \} \mathbf{j}$$

$$+ \{ [-(Du_{11}^+ + \hat{\alpha} v_{11}^-)\cos\hat{\alpha}x + (Du_{11}^- - \hat{\alpha} v_{11}^+)\sin\hat{\alpha}x] \cos\nu$$
$$+ [(Du_{12}^+ + \hat{\alpha} v_{12}^-)\cos\hat{\alpha}x - (Du_{12}^- - \hat{\alpha} v_{12}^-)\sin\hat{\alpha}x] \sin\nu \} \mathbf{i} \Big]$$

where $\nu = \beta z + \sigma_i$ and $\hat{\alpha} = \alpha/2$. The result of (A2.4) and (A2.5) can be found in Section 3. The energy equations in Section 3 contain terms which transfer energy between the system of equations (3.35)-(3.37). It was shown in Appendix I that

$$T^{(01)} = -T^{(10)} .$$

We use a similar procedure for the pair

$$T^{(13)} = -\int_{\Omega} A^2 \mathbf{v}_3 \cdot \nabla \mathbf{v}_3 \cdot \mathbf{v}_1 \, d\Omega \qquad \text{(A2.7)}$$
$$T^{(31)} = -\int_{\Omega} A^2 \mathbf{v}_3 \cdot \nabla \mathbf{v}_1 \cdot \mathbf{v}_3 \, d\Omega$$

and

$$T^{(03)} = -\int_{\Omega} A^2 \mathbf{v}_3 \cdot \nabla \mathbf{v}_3 \cdot \mathbf{v}_0 \, d\Omega \qquad \text{(A2.8)}$$
$$T^{(30)} = -\int_{\Omega} A^2 \mathbf{v}_3 \cdot \nabla \mathbf{v}_0 \cdot \mathbf{v}_3 \, d\Omega \quad .$$

Recall that from Section 3, we defined the components of the flow as

$$\mathbf{v}_0 = (U,0,0), \qquad \mathbf{v}_1 = (u_1, v_1, 0), \qquad \mathbf{v}_3 = (u_3, v_3, w_3) \qquad \text{(A2.9)}$$
$$\mathbf{v}_0 = \mathbf{v}_0(y), \qquad \mathbf{v}_1(x,y) = \mathbf{v}_1(x+\lambda_x, y), \quad \lambda_x = \frac{2\pi}{\alpha}$$
$$\mathbf{v}_3(x,y,z,t) = \mathbf{v}_3(x+\lambda_x, y, z, t), \quad \lambda_x = \frac{2\pi}{\alpha}$$
$$\mathbf{v}_3(x,y,z,t) = \mathbf{v}_3(x, y, z+\lambda_z, t), \quad \lambda_z = \frac{2\pi}{\beta} \quad .$$

Considering the form of (A2.7) and (A2.8), we have the vector identity

$$\int_{\Omega} \nabla [\mathbf{v}_i \cdot \mathbf{v}_3] \, d\Omega = \int_{\Omega} \left\{ \nabla \mathbf{v}_i \cdot \mathbf{v}_3 + \nabla \mathbf{v}_3 \cdot \mathbf{v}_i + \mathbf{v}_3 \times (\nabla \times \mathbf{v}_i) + \mathbf{v}_i \times (\nabla \times \mathbf{v}_3) \right\} d\Omega \qquad \text{(A2.10)}$$

for $i = 0,1$. Expanding the left hand side of (A2.10) gives

$$\int_{\Omega} \nabla [\mathbf{v}_i \cdot \mathbf{v}_3] \, d\Omega = \int_{\Omega} \left\{ \frac{\partial}{\partial x}(\mathbf{v}_i \cdot \mathbf{v}_3)\, \mathbf{i} + \frac{\partial}{\partial y}(\mathbf{v}_i \cdot \mathbf{v}_3)\, \mathbf{j} + \frac{\partial}{\partial z}(\mathbf{v}_i \cdot \mathbf{v}_3)\, \mathbf{k} \right\} d\Omega \equiv 0 \, , i = 0,1$$

because of the periodicity of $\mathbf{v}_3$ over Ω. Continuing, the cross-product terms in (A2.10) become

$$\int_{\Omega} \mathbf{v}_3 \times (\nabla \times \mathbf{v}_i)\, d\Omega = \int_{\Omega} \Big\{ v_i \Big[\frac{\partial v_3}{\partial x} - \frac{\partial u_3}{\partial y}\Big]\, \mathbf{i} - u_i \Big[\frac{\partial v_3}{\partial x} - \frac{\partial u_3}{\partial y}\Big]\, \mathbf{j}$$

$$- u_i \Big[\frac{\partial w_3}{\partial x} - \frac{\partial u_3}{\partial y}\Big]\, \mathbf{k} - v_i \Big[\frac{\partial w_3}{\partial x} - \frac{\partial v_3}{\partial y}\Big]\, \mathbf{k} \Big\}\, d\Omega = 0 \,, i = 0,1$$

$$\int_{\Omega} \mathbf{v}_3 \times (\nabla \times \mathbf{v}_i)\, d\Omega = \int_{\Omega} -\Big\{ v_3 \Big[\frac{\partial v_i}{\partial x} - \frac{\partial u_i}{\partial y}\Big]\, \mathbf{i} - u_3 \Big[\frac{\partial w_i}{\partial x} - \frac{\partial u_i}{\partial y}\Big]\, \mathbf{j} \Big\}\, d\Omega = 0 \,, i = 0,1$$

since $\mathbf{v}_3$ is periodic over Ω . Then, (A2.10) reduces to

$$0 = \int_{\Omega} \nabla \mathbf{v}_3 \cdot \mathbf{v}_i \, d\Omega + \int_{\Omega} \nabla \mathbf{v}_i \cdot \mathbf{v}_3 \, d\Omega \,, i = 0,1 \quad . \tag{A2.11}$$

Multiplying (A2.11) by $B^2 \mathbf{v}_3$ gives

$$\int_{\Omega} A^2 \mathbf{v}_3 \cdot \nabla \mathbf{v}_3 \cdot \mathbf{v}_i \, d\Omega = - \int_{\Omega} A^2 \mathbf{v}_3 \cdot \nabla \mathbf{v}_i \cdot \mathbf{v}_3 \, d\Omega$$

or

$$T^{(i3)} = - T^{(3i)} \,, i = 0,1 \quad . \tag{A2.12}$$

With these simplifications, we can rewrite equations (3.35)-(3.37) as

$$\begin{aligned} \frac{dE^{(0)}}{dt} &= - T^{(10)} - T^{(30)} + D^{(0)} \\ \frac{dE^{(1)}}{dt} &= T^{(10)} - T^{(31)} + D^{(1)} \\ \frac{dE^{(3)}}{dt} &= T^{(31)} + T^{(30)} + D^{(3)} \quad . \end{aligned} \tag{A2.13}$$

Substitution of solutions (A2.1) and (A2.2) into the energy equations in (A2.13) gives expressions for $T^{(ij)}$ and the $D^{(i)}$, as defined by (A1.3), (A2.7) and (A2.8), in terms of the eigenfunctions calculated for the linear secondary stability analysis. The detailed form

of $T^{(10)}$ and $D^{(1)}$ have been given in Appendix I. Similarly, the form of solutions (A2.1) and (A2.2) gives rise to periodic (P_i) and aperiodic (AP_i) terms multiplied by trigonometric functions in x and z in the energy equations (A2.13). Substitution of the fundmental solution (A2.1) into the energy equation (3.37) gives, for the first term:

$$T^{(31)} = -\int_{\Omega} AB^2\left\{ u_3 u_3 \frac{\partial u_1}{\partial x} + u_3 v_3 \left(\frac{\partial v_1}{\partial x} + \frac{\partial u_1}{\partial y}\right) + v_3 v_3 \frac{\partial v_1}{\partial y} \right\} d\Omega \qquad \text{(A2.14)}$$

$$= -\int_{\Omega} 8AB^2\Big\{ P_1\cos\alpha x + P_2\sin\alpha x + AP_1\cos^2\alpha x$$

$$+ P_3\sin 2\alpha x + AP_2\sin^2\alpha x + P_4\cos^3\alpha x + P_5\sin\alpha x\cos^2\alpha x$$

$$+ P_6\sin^2\alpha x\cos\alpha x + P_7\sin^3\alpha x \Big\}\cos^2\beta z \; d\Omega$$

where the P_i 's are given by

$$P_1 = \; v_0\mathbf{v}_0\cdot D\mathbf{v}_1^+ - \alpha u_0\mathbf{v}_0\cdot\mathbf{v}_1^-$$

$$P_2 = -\left(v_0\mathbf{v}_0\cdot D\mathbf{v}_1^- + \alpha u_0\mathbf{v}_0\cdot\mathbf{v}_1^+ \right)$$

$$P_3 = -\left[v_2^+\mathbf{v}_0\cdot D\mathbf{v}_1^- + v_2^-\,\mathbf{v}_0\cdot D\mathbf{v}_1^+ + v_0(\mathbf{v}_2^+\cdot D\mathbf{v}_1^- + \mathbf{v}_2^-\cdot D\mathbf{v}_1^+) + \alpha(u_2^+\mathbf{v}_0\cdot\mathbf{v}_1^+ - u_2\mathbf{v}_0\cdot\mathbf{v}_1^- + u_0(\mathbf{v}_2^+\mathbf{v}_1^+ - \mathbf{v}_2^-\cdot\mathbf{v}_1^-)) \right]$$

$$P_4 = \; 4\left[v_2^+\mathbf{v}_2^+\cdot D\mathbf{v}_1^+ - \alpha u_2^+\mathbf{v}_2^+\cdot\mathbf{v}_1^- \right]$$

$$P_5 = -4\left[v_2^+(\mathbf{v}_2^+\cdot D\mathbf{v}_1^- + \mathbf{v}_2^-\cdot D\mathbf{v}_1^+) + v_2^-\,\mathbf{v}_2^+\cdot D\mathbf{v}_1^+ + \alpha(u_2^+(\mathbf{v}_2^+\cdot\mathbf{v}_1^+ - \mathbf{v}_2^-\cdot\mathbf{v}_1^-) - u_2^-\,\mathbf{v}_2^+\cdot\mathbf{v}_1^-) \right]$$

$$P_6 = \; 4\left[v_2^-(\mathbf{v}_2^+\cdot D\mathbf{v}_1^- + \mathbf{v}_2^-\cdot D\mathbf{v}_1^+) + v_2^+\mathbf{v}_2^-\cdot D\mathbf{v}_1^- + \alpha(u_2^-(\mathbf{v}_2^+\cdot\mathbf{v}_1^+ - \mathbf{v}_2^-\cdot\mathbf{v}_1^-) + u_2^+\mathbf{v}_2^-\cdot\mathbf{v}_1^+) \right]$$

$$P_7 = -4[v_2^- \mathbf{v}_2^- \cdot D\mathbf{v}_1^- - \alpha u_2^- \mathbf{v}_2^- \cdot \mathbf{v}_1^+]$$

and the AP_i 's are

$$AP_1 = 2[\, v_2^+ \mathbf{v}_0 \cdot D\mathbf{v}_1^+ + v_0 \mathbf{v}_2^+ \cdot D\mathbf{v}_1^+ - \alpha(u_2^+ \mathbf{v}_0 \cdot \mathbf{v}_1^- + u_0 \mathbf{v}_2^+ \cdot \mathbf{v}_1^-)\,]$$

$$AP_2 = 2[\, v_2^- \mathbf{v}_0 \cdot D\mathbf{v}_1^- + v_0 \mathbf{v}_2^- \cdot D\mathbf{v}_1^- + \alpha(u_2^- \mathbf{v}_0 \cdot \mathbf{v}_1^+ + u_0 \mathbf{v}_2^- \cdot \mathbf{v}_1^+)\,] \quad .$$

The second term is:

$$T^{(30)} = -\int_\Omega B^2 u_3 v_3 \frac{dU}{dy}\, d\Omega$$

$$= -\int_\Omega 4B^2 \Big\{ AP_{13} + P_8 \cos\alpha x + P_9 \sin\alpha x + AP_3 \cos^2\alpha x + P_{10} \sin 2\alpha x + AP_4 \sin^2\alpha x \Big\} \cos^2\beta z\, d\Omega$$

where the P_i 's are given by

$$P_8 = 2(\, v_0 u_2^+ + u_0 v_2^+\,) \frac{dU}{dy}$$

$$P_9 = -2(\, v_0 u_2^- + u_0 v_2^-\,) \frac{dU}{dy}$$

$$P_{10} = -2(\, u_2^+ v_2^- + u_2^- v_2^+\,) \frac{dU}{dy}$$

and the AP_i 's are

$$AP_{13} = u_0 v_0 \frac{dU}{dy}$$

$$AP_3 = 4 u_2^+ v_2^- \frac{dU}{dy}$$

$$AP_4 = \; 4u_2^- v_2^- \frac{dU}{dy}$$

The dissipation is:

$$D^{(3)} = -\frac{1}{Re}\int_\Omega B^2\Big\{(\frac{\partial u_3}{\partial x})^2+(\frac{\partial u_3}{\partial y})^2+(\frac{\partial u_3}{\partial z})^2+(\frac{\partial v_3}{\partial x})^2+(\frac{\partial v_3}{\partial y})^2+(\frac{\partial v_3}{\partial z})^2+$$
$$(\frac{\partial w_3}{\partial x})^2+(\frac{\partial w_3}{\partial y})^2+(\frac{\partial w_3}{\partial z})^2\Big\}\, d\Omega$$

$$= -\frac{4B^2}{Re}\int_\Omega \Big\{ (AP_{14} + P_{11}\cos\alpha x + P_{12}\sin\alpha x$$
$$+ AP_5\cos^2\alpha x + P_{13}\sin 2\alpha x + AP_6\sin^2\alpha x)\, \cos^2\beta z$$
$$+ (AP_{15} + P_{14}\cos\alpha x + P_{15}\sin\alpha x$$
$$+ AP_7\cos^2\alpha x + P_{16}\sin 2\alpha x + AP_8\sin^2\alpha x)\, \sin^2\beta z \Big\}\, d\Omega$$

where the P_i 's are given by

$$P_{11} = \; 4[\; D\mathbf{v}_0 \cdot D\mathbf{v}_2^- + \beta^2 w_0^- w_2^+ \;]$$

$$P_{12} = -4[\; D\mathbf{v}_0 \cdot D\mathbf{v}_2^- + \beta^2 w_0^- w_2^- \;]$$

$$P_{13} = \; 4[\; -D\mathbf{v}_2^+ \cdot D\mathbf{v}_2^- + \alpha^2 \mathbf{v}_2^+ \cdot \mathbf{v}_2^- - \beta^2 w_2^+ w_2^- \;]$$

$$P_{14} = \; 4[\; Dw_0^- Dw_2^+ + \beta^2 \mathbf{v}_0 \cdot \mathbf{v}_2^+ \;]$$

$$P_{15} = -4[\; Dw_0^- Dw_2^- + \beta^2 \mathbf{v}_0 \cdot \mathbf{v}_2^- \;]$$

$$P_{16} = -4[\; Dw_2^+ \cdot Dw_2^- - \alpha^2 w_2^+ w_2^- + \beta^2 \mathbf{v}_2^+ \mathbf{v}_2^- \;]$$

and the AP_i's are

$$AP_{14} = [\, D\mathbf{v}_0 \cdot D\mathbf{v}_0 + \beta^2 w_0^- w_0^- \,]$$

$$AP_5 = 4[\, D\mathbf{v}_2^+ \cdot D\mathbf{v}_2^+ + \alpha^2 \mathbf{v}_2^- \cdot \mathbf{v}_2^- + \beta^2 w_2^+ w_2^+ \,]$$

$$AP_6 = 4[\, D\mathbf{v}_2^- \cdot D\mathbf{v}_2^- + \alpha^2 \mathbf{v}_2^+ \cdot \mathbf{v}_2^+ + \beta^2 w_2^- w_2^- \,]$$

$$AP_{15} = 4[\, Dw_0^- Dw_0^- + \beta^2 \mathbf{v}_0 \cdot \mathbf{v}_0]$$

$$AP_7 = 4[\, Dw_2^+ Dw_2^+ + \alpha^2 w_2^- w_2^- + \beta^2 \mathbf{v}_2^+ \cdot \mathbf{v}_2^+ \,]$$

$$AP_8 = 4[\, Dw_2^- Dw_2^- + \alpha^2 w_2^+ w_2^+ + \beta^2 \mathbf{v}_2^- \cdot \mathbf{v}_2^- \,] \quad .$$

where the dot product terms omit the z-components in this instance.

Substitution of the subharmonic solution (A2.2) into the energy equation (3.37) results in the following terms, beginning with the first term:

$$T^{(31)} = -\int_{\Omega} 16AB^2 \Big\{ [\, P_1\cos\hat{\alpha}x + P_2\sin\hat{\alpha}x + AP_1\cos^2\hat{\alpha}x$$

$$+ P_3\sin\hat{\alpha}x\cos\hat{\alpha}x + AP_2\sin^2\hat{\alpha}x \,]\cos^2\nu$$

$$+ [\, P_4\cos\hat{\alpha}x + P_5\sin\hat{\alpha}x + P_6\cos^2\hat{\alpha}x$$

$$+ P_7\sin\hat{\alpha}x\cos\hat{\alpha}x + P_8\sin^2\hat{\alpha}x \,]\sin\nu\cos\nu$$

$$+ [\, P_9\cos\hat{\alpha}x + P_{10}\sin\hat{\alpha}x + AP_3\cos^2\hat{\alpha}x$$

$$+ P_{11}\sin\hat{\alpha}x\cos\hat{\alpha}x + AP_4\sin^2\hat{\alpha}x \,]\sin^2\nu \Big\}\, d\Omega$$

where the P_i 's are given by

$$P_1 = v_{11}^{+}\mathbf{v}_{11}^{+}\cdot D\mathbf{v}_1^{+} + v_{\bar{1}1}\mathbf{v}_{\bar{1}1}\cdot D\mathbf{v}_1^{+} - \alpha(\, u_{11}^{+}\mathbf{v}_{11}^{+}\cdot\mathbf{v}_1^{-} + u_{\bar{1}1}\mathbf{v}_{\bar{1}1}\cdot\mathbf{v}_1^{-} \,)$$

$$P_2 = -v_{11}^{+}\mathbf{v}_{11}^{+}\cdot D\mathbf{v}_1^{-} - v_{\bar{1}1}\mathbf{v}_{\bar{1}1}\cdot D\mathbf{v}_1^{-} - \alpha(\, u_{11}^{+}\mathbf{v}_{11}^{+}\cdot\mathbf{v}_1^{+} + u_{\bar{1}1}\mathbf{v}_{\bar{1}1}\cdot\mathbf{v}_1^{+} \,)$$

$$P_3 = -v_{11}^{+}(\, \mathbf{v}_{11}^{+}\cdot D\mathbf{v}_1^{-} + \mathbf{v}_{\bar{1}1}\cdot D\mathbf{v}_1^{+} \,) - v_{\bar{1}1}(\, \mathbf{v}_{11}^{+}\cdot D\mathbf{v}_1^{+} - \mathbf{v}_{\bar{1}1}\cdot D\mathbf{v}_1^{-} \,)$$
$$- \alpha[\, u_{11}^{+}(\, \mathbf{v}_{11}^{+}\cdot\mathbf{v}_1^{+} - \mathbf{v}_{\bar{1}1}\cdot\mathbf{v}_1^{-} \,) - u_{\bar{1}1}\,(\mathbf{v}_{11}^{+}\cdot\mathbf{v}_1^{-} + \mathbf{v}_{\bar{1}1}\cdot\mathbf{v}_1^{+}) \,]$$

$$P_4 = -v_{11}^{+}\mathbf{v}_{12}^{+}\cdot D\mathbf{v}_1^{+} - v_{\bar{1}1}\mathbf{v}_{\bar{1}2}\cdot D\mathbf{v}_1^{+} - v_{12}^{+}\mathbf{v}_{11}^{+}\cdot D\mathbf{v}_1^{+} - v_{\bar{1}2}\mathbf{v}_{\bar{1}1}\cdot D\mathbf{v}_1^{+}$$
$$+ \alpha[\, u_{11}^{+}\mathbf{v}_{12}^{+}\cdot\mathbf{v}_1^{-} + u_{\bar{1}1}\mathbf{v}_{\bar{1}2}\cdot\mathbf{v}_1^{-} + u_{12}^{+}\mathbf{v}_{11}^{+}\cdot\mathbf{v}_1^{-} + u_{\bar{1}2}\mathbf{v}_{\bar{1}1}\cdot\mathbf{v}_1^{-} \,]$$

$$P_5 = v_{11}^{+}\mathbf{v}_{12}^{+}\cdot D\mathbf{v}_1^{-} + v_{\bar{1}1}\mathbf{v}_{\bar{1}2}\cdot D\mathbf{v}_1^{-} + v_{12}^{+}\mathbf{v}_{11}^{+}\cdot D\mathbf{v}_1^{-} + v_{\bar{1}2}\mathbf{v}_{\bar{1}1}\cdot D\mathbf{v}_1^{-}$$
$$+ \alpha[\, u_{11}^{+}\mathbf{v}_{12}^{+}\cdot\mathbf{v}_1^{+} + u_{\bar{1}1}\mathbf{v}_{\bar{1}2}\cdot\mathbf{v}_1^{+} + u_{\bar{1}2}\mathbf{v}_{\bar{1}1}\cdot\mathbf{v}_1^{+} + u_{\bar{1}2}\mathbf{v}_{\bar{1}1}\cdot\mathbf{v}_1^{+} \,]$$

$$P_6 = -v_{11}^{+}\mathbf{v}_{12}^{+}\cdot D\mathbf{v}_1^{+} + v_{\bar{1}1}\mathbf{v}_{\bar{1}2}\cdot D\mathbf{v}_1^{+} - v_{12}^{+}\mathbf{v}_{11}^{+}\cdot D\mathbf{v}_1^{+} + v_{\bar{1}2}\mathbf{v}_{\bar{1}1}\cdot D\mathbf{v}_1^{+}$$
$$+ \alpha[\, u_{11}^{+}\mathbf{v}_{12}^{+}\cdot\mathbf{v}_1^{-} - u_{\bar{1}1}\mathbf{v}_{\bar{1}2}\cdot\mathbf{v}_1^{-} + u_{\bar{1}2}\mathbf{v}_{11}^{+}\cdot\mathbf{v}_1^{-} - u_{\bar{1}2}\mathbf{v}_{\bar{1}1}\cdot\mathbf{v}_1^{-} \,]$$

$$P_7 = v_{11}^{+}(\mathbf{v}_{12}^{+}\cdot D\mathbf{v}_1^{-} + \mathbf{v}_{\bar{1}2}^{-}\cdot D\mathbf{v}_1^{+}) + v_{\bar{1}1}^{-}(\mathbf{v}_{12}^{+}\cdot D\mathbf{v}_1^{+} - \mathbf{v}_{\bar{1}2}^{-}\cdot D\mathbf{v}_1^{-})$$
$$+ v_{12}^{+}(\mathbf{v}_{11}^{+}\cdot D\mathbf{v}_1^{-} + \mathbf{v}_{\bar{1}1}^{-}\cdot D\mathbf{v}_1^{+}) + v_{\bar{1}2}^{-}(\mathbf{v}_{11}^{+}\cdot D\mathbf{v}_1^{+} - \mathbf{v}_{\bar{1}1}^{-}\cdot D\mathbf{v}_1^{-})$$
$$+ \alpha[u_{11}^{+}(\mathbf{v}_{12}^{+}\cdot\mathbf{v}_1^{+} - \mathbf{v}_{\bar{1}2}^{-}\cdot\mathbf{v}_1^{-}) - u_{\bar{1}1}^{-}(\mathbf{v}_{12}^{+}\cdot\mathbf{v}_1^{-} + \mathbf{v}_{\bar{1}2}^{-}\cdot\mathbf{v}_1^{+})$$
$$+ u_{12}^{+}(\mathbf{v}_{11}^{+}\cdot\mathbf{v}_1^{+} - \mathbf{v}_{\bar{1}1}^{-}\cdot\mathbf{v}_1^{-}) - u_{\bar{1}2}^{-}(\mathbf{v}_{11}^{+}\cdot\mathbf{v}_1^{-} + \mathbf{v}_{\bar{1}1}^{-}\cdot\mathbf{v}_1^{+})]$$

$$P_8 = - v_{11}^{+}\mathbf{v}_{\bar{1}2}^{-}\cdot D\mathbf{v}_1^{-} - v_{\bar{1}1}^{-}\mathbf{v}_{12}^{+}\cdot D\mathbf{v}_1^{-} - v_{12}^{+}\mathbf{v}_{\bar{1}1}^{-}\cdot D\mathbf{v}_1^{-} - v_{\bar{1}2}^{-}\mathbf{v}_{11}^{+}\cdot D\mathbf{v}_1^{-}$$
$$- \alpha[u_{11}^{+}\mathbf{v}_{\bar{1}2}^{-}\cdot\mathbf{v}_1^{+} + u_{\bar{1}1}^{-}\mathbf{v}_{12}^{+}\cdot\mathbf{v}_1^{+} + u_{12}^{+}\mathbf{v}_{\bar{1}1}^{-}\cdot\mathbf{v}_1^{+} + u_{\bar{1}2}^{-}\mathbf{v}_{11}^{+}\cdot\mathbf{v}_1^{+}]$$

$$P_9 = v_{12}^{+}\mathbf{v}_{12}^{+}\cdot D\mathbf{v}_1^{+} + v_{\bar{1}2}^{-}\mathbf{v}_{\bar{1}2}^{-}\cdot D\mathbf{v}_1^{+} - \alpha(u_{12}^{+}\mathbf{v}_{12}^{+}\cdot\mathbf{v}_1^{-} + u_{\bar{1}2}^{-}\mathbf{v}_{\bar{1}2}^{-}\cdot\mathbf{v}_1^{-})$$

$$P_{10} = - v_{12}^{+}\mathbf{v}_{12}^{+}\cdot D\mathbf{v}_1^{-} - v_{\bar{1}2}^{-}\mathbf{v}_{\bar{1}2}^{-}\cdot D\mathbf{v}_1^{-} - \alpha(u_{12}^{+}\mathbf{v}_{12}^{+}\cdot\mathbf{v}_1^{+} + u_{\bar{1}2}^{-}\mathbf{v}_{\bar{1}2}^{-}\cdot\mathbf{v}_1^{+})$$

$$P_{11} = - v_{12}^{+}(\mathbf{v}_{12}^{+}\cdot D\mathbf{v}_1^{-} + \mathbf{v}_{\bar{1}2}^{-}\cdot D\mathbf{v}_1^{+}) - v_{\bar{1}2}^{-}(\mathbf{v}_{12}^{+}\cdot D\mathbf{v}_1^{+} - \mathbf{v}_{\bar{1}2}^{-}\cdot D\mathbf{v}_1^{-})$$
$$- \alpha[u_{12}^{+}(\mathbf{v}_{12}^{+}\cdot\mathbf{v}_1^{+} - \mathbf{v}_{\bar{1}2}^{-}\cdot\mathbf{v}_1^{-}) - u_{\bar{1}2}^{-}(\mathbf{v}_{12}^{+}\cdot\mathbf{v}_1^{-} + \mathbf{v}_{\bar{1}2}^{-}\cdot\mathbf{v}_1^{+})]$$

and the AP_i's are

$$AP_1 = v_{11}^{+}\mathbf{v}_{11}^{+}\cdot D\mathbf{v}_1^{+} - v_{\bar{1}1}^{-}\mathbf{v}_{\bar{1}1}^{-}\cdot D\mathbf{v}_1^{+} - \alpha(u_{11}^{+}\mathbf{v}_{11}^{+}\cdot\mathbf{v}_1^{-} - u_{\bar{1}1}^{-}\mathbf{v}_{\bar{1}1}^{-}\cdot\mathbf{v}_1^{-})$$

$$AP_2 = v_{11}^{+}\mathbf{v}_{\bar{1}1}^{-}\cdot D\mathbf{v}_1^{-} + v_{\bar{1}1}^{-}\mathbf{v}_{11}^{+}\cdot D\mathbf{v}_1^{-} + \alpha(u_{11}^{+}\mathbf{v}_{\bar{1}1}^{-}\cdot\mathbf{v}_1^{+} + u_{\bar{1}1}^{-}\mathbf{v}_{11}^{+}\cdot\mathbf{v}_1^{+})$$

$$AP_3 = v_{12}^{+}\mathbf{v}_{12}^{+}\cdot D\mathbf{v}_1^{+} - v_{\bar{1}2}^{-}\mathbf{v}_{\bar{1}2}^{-}\cdot D\mathbf{v}_1^{+} - \alpha(u_{12}^{+}\mathbf{v}_{12}^{+}\cdot\mathbf{v}_1^{-} - u_{\bar{1}2}^{-}\mathbf{v}_{\bar{1}2}^{-}\cdot\mathbf{v}_1^{-})$$

$$AP_4 = v_{12}^{+}\mathbf{v}_{\bar{1}2}^{-}\cdot D\mathbf{v}_1^{-} + v_{\bar{1}2}^{-}\mathbf{v}_{12}^{+}\cdot D\mathbf{v}_1^{-} + \alpha(u_{12}^{+}\mathbf{v}_{\bar{1}2}^{-}\cdot\mathbf{v}_1^{+} + u_{\bar{1}2}^{-}\mathbf{v}_{12}^{+}\cdot\mathbf{v}_1^{+}) \quad .$$

The second term is:

$$T^{(30)} = -\int_{\Omega} 8AB^2 \Big\{ [\ AP_5 + P_{12}\cos\hat{\alpha}x + P_{13}\sin\hat{\alpha}x + \ ]\cos^2\nu$$

$$+ [\ P_{14} + P_{15}\sin\hat{\alpha}x + P_{16}\cos\hat{\alpha}x\ ]\sin\nu\cos\nu$$

$$+ [\ AP_6 + P_{17}\cos\hat{\alpha}x + P_{18}\sin\hat{\alpha}x + \ ]\sin^2\nu \Big\}\, d\Omega$$

where the P_i 's are given by

$$P_{12} = (\ u_{11}^{+}v_{11}^{+} - u_{\bar{1}1}^{-}v_{\bar{1}1}^{-}\ )\ dU/dy$$

$$P_{13} = -(\ u_{11}^{+}v_{\bar{1}1}^{-} + u_{\bar{1}1}^{-}v_{11}^{+}\ )\ dU/dy$$

$$P_{14} = -(\ u_{11}^{+}v_{12}^{+} + u_{12}^{+}v_{11}^{+} + u_{\bar{1}1}^{-}v_{\bar{1}2}^{-} + u_{\bar{1}2}^{-}v_{\bar{1}1}^{-}\ )\ dU/dy$$

$$P_{15} = -(\ u_{11}^{+}v_{12}^{+} + u_{12}^{+}v_{11}^{+} - u_{\bar{1}1}^{-}v_{\bar{1}2}^{-} - u_{\bar{1}2}^{-}v_{\bar{1}1}^{-}\ )\ dU/dy$$

$$P_{16} = -(\ u_{11}^{+}v_{\bar{1}2}^{-} + u_{\bar{1}2}^{-}v_{11}^{+} + u_{\bar{1}1}^{-}v_{12}^{+} + u_{12}^{+}v_{\bar{1}1}^{-}\ )\, dU/dy$$

$$P_{17} = (\ u_{12}^{+}v_{12}^{+} - u_{\bar{1}2}^{-}v_{\bar{1}2}^{-}\ )\ dU/dy$$

$$P_{18} = -(\ u_{12}^{+}v_{\bar{1}2}^{-} + u_{\bar{1}2}^{-}v_{12}^{+}\ )\ dU/dy$$

and the AP_i's are

$$AP_5 = (\ u_{11}^{+}v_{\bar{1}1}^{-} + u_{\bar{1}1}^{-}v_{11}^{+}\ )\ dU/dy$$

$$AP_6 = (\ u_{12}^{+}v_{\bar{1}2}^{-} + u_{\bar{1}2}^{-}v_{12}^{+}\ )\ dU/dy \quad .$$

The dissipation is:

$$D^{(3)} = -\int_{\Omega} \frac{8AB^2}{Re}\Big\{ [\ AP_7 + P_{19}\cos\hat{\alpha}x + P_{20}\sin\hat{\alpha}x + \ ]\cos^2\nu$$

$$+ [\ P_{21} + P_{22}\sin\hat{\alpha}x + P_{23}\cos\hat{\alpha}x\ ]\sin\nu\cos\nu$$

$$+ [\ AP_8 + P_{24}\cos\hat{\alpha}x + P_{25}\sin\hat{\alpha}x + \ ]\sin^2\nu \Big\}\, d\Omega$$

where the P_i 's are given by

$$P_{19} = \ (D\mathbf{v}_{11}^{+}\cdot D\mathbf{v}_{11}^{+} - D\mathbf{v}_{1\bar{1}}\cdot D\mathbf{v}_{1\bar{1}}) - \hat{\alpha}^2(\mathbf{v}_{11}^{+}\cdot\mathbf{v}_{11}^{+} - \mathbf{v}_{1\bar{1}}\cdot\mathbf{v}_{1\bar{1}}) + \beta^2(\mathbf{v}_{12}^{+}\cdot\mathbf{v}_{12}^{+} - \mathbf{v}_{1\bar{2}}\cdot\mathbf{v}_{1\bar{2}})$$

$$P_{20} = -2[\ D\mathbf{v}_{11}^{+}\cdot D\mathbf{v}_{1\bar{1}} - \hat{\alpha}^2\mathbf{v}_{11}^{+}\cdot\mathbf{v}_{1\bar{1}} + \beta^2\mathbf{v}_{12}^{+}\cdot\mathbf{v}_{1\bar{2}}\ ]$$

$$P_{21} = -2[\ (D\mathbf{v}_{11}^{+}\cdot D\mathbf{v}_{12}^{+} + D\mathbf{v}_{1\bar{1}}\cdot D\mathbf{v}_{1\bar{2}}) + \hat{\alpha}^2(\mathbf{v}_{11}^{+}\cdot\mathbf{v}_{12}^{+} + \mathbf{v}_{1\bar{1}}\cdot\mathbf{v}_{1\bar{2}}) - \beta^2(\mathbf{v}_{11}^{+}\cdot\mathbf{v}_{12}^{+} - \mathbf{v}_{1\bar{1}}\cdot\mathbf{v}_{1\bar{2}})\ ]$$

$$P_{22} = -2[\ (D\mathbf{v}_{11}^{+}\cdot D\mathbf{v}_{12}^{+} - D\mathbf{v}_{1\bar{1}}\cdot D\mathbf{v}_{1\bar{2}}) - \hat{\alpha}^2(\mathbf{v}_{11}^{+}\cdot\mathbf{v}_{12}^{+} - \mathbf{v}_{1\bar{1}}\cdot\mathbf{v}_{1\bar{2}}) - \beta^2(\mathbf{v}_{11}^{+}\cdot\mathbf{v}_{12}^{+} - \mathbf{v}_{1\bar{1}}\cdot\mathbf{v}_{1\bar{2}})\ ]$$

$$P_{23} = \ 2[\ (D\mathbf{v}_{11}^{+}\cdot D\mathbf{v}_{1\bar{2}} + D\mathbf{v}_{1\bar{1}}\cdot D\mathbf{v}_{12}^{+}) - \hat{\alpha}^2(\mathbf{v}_{11}^{+}\cdot\mathbf{v}_{1\bar{2}} + \mathbf{v}_{1\bar{1}}\cdot\mathbf{v}_{12}^{+}) - \beta^2(\mathbf{v}_{11}^{+}\cdot\mathbf{v}_{1\bar{2}} + \mathbf{v}_{1\bar{1}}\cdot\mathbf{v}_{12}^{+})\ ]$$

$$P_{24} = \ (D\mathbf{v}_{12}^{+}\cdot D\mathbf{v}_{12}^{+} - D\mathbf{v}_{1\bar{2}}\cdot D\mathbf{v}_{1\bar{2}}) - \hat{\alpha}^2(\mathbf{v}_{12}^{+}\cdot\mathbf{v}_{12}^{+} - \mathbf{v}_{1\bar{2}}\cdot\mathbf{v}_{1\bar{2}}) + \beta^2(\mathbf{v}_{11}^{+}\cdot\mathbf{v}_{11}^{+} - \mathbf{v}_{1\bar{1}}\cdot\mathbf{v}_{1\bar{1}})$$

$$P_{25} = -2[\ D\mathbf{v}_{12}^{+}\cdot D\mathbf{v}_{1\bar{2}} - \hat{\alpha}^2\mathbf{v}_{12}^{+}\cdot\mathbf{v}_{1\bar{2}} + \beta^2\mathbf{v}_{11}^{+}\cdot\mathbf{v}_{1\bar{1}}\ ]$$

and the AP_i's are

$$AP_7 = \left(D\mathbf{v}_{11}^{+}\cdot D\mathbf{v}_{11}^{+} + D\mathbf{v}_{1\bar{1}}^{-}\cdot D\mathbf{v}_{1\bar{1}}^{-} \right) + \hat{\alpha}^2\left(\mathbf{v}_{11}^{+}\cdot\mathbf{v}_{11}^{+} + \mathbf{v}_{1\bar{1}}^{-}\cdot\mathbf{v}_{1\bar{1}}^{-} \right) + \beta^2\left(\mathbf{v}_{12}^{+}\cdot\mathbf{v}_{12}^{+} + \mathbf{v}_{1\bar{2}}^{-}\cdot\mathbf{v}_{1\bar{2}}^{-} \right)$$

$$AP_8 = \left(D\mathbf{v}_{12}^{+}\cdot D\mathbf{v}_{12}^{+} + D\mathbf{v}_{1\bar{2}}^{-}\cdot D\mathbf{v}_{1\bar{2}}^{-} \right) + \hat{\alpha}^2\left(\mathbf{v}_{12}^{+}\cdot\mathbf{v}_{12}^{+} + \mathbf{v}_{1\bar{2}}^{-}\cdot\mathbf{v}_{1\bar{2}}^{-} \right) + \beta^2\left(\mathbf{v}_{11}^{+}\cdot\mathbf{v}_{11}^{+} + \mathbf{v}_{1\bar{1}}^{-}\cdot\mathbf{v}_{1\bar{1}}^{-} \right) .$$

Numerical and graphical results for the fundamental and subharmonic modes appear in Section 3.

The vita has been removed from the scanned document